

THE JOURNAL OF PHYSICAL CHEMISTRY

(Registered in U. S. Patent Office)

CONTENTS

V. C. F. Holm, G. C. Bailey and Alfred Clark: Acidity Studies of Silica-Alumina Catalysts.....	129
P. L. Walker, Jr., J. F. Rakszawski and G. R. Imperial: Carbon Formation from Carbon Monoxide-Hydrogen Mixtures over Iron Catalysts. I. Properties of Carbon Formed.....	133
P. L. Walker, Jr., J. F. Rakszawski and G. R. Imperial: Carbon Formation from Carbon Monoxide-Hydrogen Mixture over Iron Catalysts. II. Rates of Carbon Formation.....	140
Henry E. Wirth, John H. Wood and John W. Droegge: Low Temperature Heat Capacities and Thermodynamic Functions of Hydrated Sodium Palmitate.....	149
Henry E. Wirth, John W. Droegge and John H. Wood: Heat Capacities and Thermodynamic Functions for δ - and ω -Sodium Palmitate.....	152
A. K. Fischer, F. A. Cotton and G. Wilkinson: Heats of Combustion and Formation of Bis-benzenechromium.....	154
Wiktor Kemula and Henryk Buchowski: The Effect of Acidity and Concentration of Buffers on Partition Coefficients of Dilute Solution of Acids and Bases and on Selectivity of a Liquid-Liquid System.....	155
Peter Cannon: Adsorption of Fluorinated Methanes by Linde Molecular Sieves.....	160
G. P. Rutledge and W. Davis Jr.: Solid-Liquid and Liquid-Liquid Equilibria of the Ternary System Uranium Hexafluoride-Chlorine Trifluoride-Hydrogen Fluoride.....	166
J. Hermans Jr., and J. J. Hermans: Solution Properties of Desoxyribonucleic Acid (DNA). I. Hydrodynamic Behavior.....	170
J. Hermans, Jr.: Solution Properties of Desoxyribonucleic Acid (DNA). II. Light Scattering.....	175
H. A. Benesi and A. C. Jones: An Infrared Study of the Water-Silica Gel System.....	179
M. Folman and D. J. C. Yates: Infrared Studies of Physically Adsorbed Polar Molecules and of the Surface of a Silica Adsorbent Containing Hydroxyl Groups.....	183
S. J. Stephens: Surface Reactions on Evaporated Palladium Films.....	188
C. W. Freeark and R. Hardwick: Long Range Energy Transfer and Self Absorption in Fluorescent Solutions.....	194
W. D. Johnston, R. C. Miller and R. Mazelsky: A Study of Several Systems of the Type $Li_2[Co_xNi_{(1-x)}](1-x)O$	198
Roger S. Porter and Julian F. Johnson: Laminar Flow Degradation of Polyisobutene.....	202
Julian B. Andelman, Guenther K. Hoeschele and Harry P. Gregor: Metal-Polyelectrolyte Complexes. VI. Preparation and Properties of a New Polychelate-Polyvinylmethylglyoxime.....	206
John R. Cann: Effect of Binding of Ions and Other Small Molecules on Protein Structure. V. On the Interpretation of the Electrophoretic Patterns of Proteins in Acidic Media.....	210
Donald C. Kaufman, J. West Loveland and Philip J. Elving: An Improved Apparatus for Oscillographic Observation of Polarographic Phenomena. Oxidation-Reduction Pattern of Cd(II): Effects of Oxygen and Gelatin.....	217
Roy L. Allen and Walter J. Moore: Diffusion of Silver in Silver Sulfide.....	223
Hurley D. Cook and Herman E. Ries, Jr.: Adsorption of Radiostearic Acid and Radiostearyl Alcohol from n -Hexadecane onto Solid Surfaces.....	226
S. J. Yosim, A. J. Darnell, W. G. Gehman and S. W. Mayer: The Bismuth-Bismuth Trichloride System.....	230
Edward A. Sullivan and Sidney Johnson: The Lithium Borohydride-Ammonia System: P - C - T Relationships and Densities.....	233
C. M. Huggins and D. R. Carpenter: A Proton Magnetic Resonance Comparison of Silicichloroform and Chloroform in Basic Solvents.....	238
Hiroshi Fujita: Evaluation of Diffusion Coefficients from Sedimentation Velocity Measurements.....	242
Stanley M. Ohlberg: The Stable Crystal Structures of Pure n -Paraffins Containing an Even Number of Carbon Atoms in the Range C_{20} to C_{28}	248
Henry Freiser, Quintus Fernando and Graeme E. Cheney: A New Approach to the Comparison of Metal Chelate Stability Constants.....	250
J. R. Thomas and L. deVries: Sonically Induced Heterolytic Cleavage of Polymethylsiloxane.....	252
K. Bril, S. Bril and P. Krumholz: Separation of Metal Ions by Means of Ion-exchange Membranes. I. Separation of Rare Earth Mixtures, and of Thorium-Rare Earth Mixtures Using Ethylenediaminetetraacetic Acid.....	256
David Fleischer and Henry Freiser: The Calorimetric Determination of the Heats of Coordination Reactions.....	260
L. Rheume and G. Parravano: Decomposition Kinetics of Nitrous Oxide on α -Manganese Sesquioxide.....	264
J. P. Dux and J. Steigman: Tracer Diffusion Coefficients of Strontium Ion in Aqueous Polystyrenesulfonic Acid Solutions.....	269
Gordon G. Hammes and Robert A. Alberty: The Influence of the Net Protein Charge on the Rate of Formation of Enzyme-Substrate Complexes.....	274
Frederick S. Lee and Gene B. Carpenter: The Crystal Structure of Perchloric Acid Monohydrate.....	279
T. A. Orofino and P. J. Flory: The Second Virial Coefficient for Polyelectrolytes. Theory and Experiment.....	283
Lloyd E. Line, Jr., Harold A. Rhodes and Thomas E. Gilmer, Jr.: The Spark Ignition of Dust Clouds.....	290
Daniel Cubicciotti and F. J. Kenesha, Jr.: The Vapor Pressures of BiI_3 over Liquid Bi - BiI_3 Solutions.....	295
Hartland Schmidt, George Jura and Joel H. Hildebrand: The Heat Capacity of the System Carbon Tetrachloride-Perfluoromethylcyclohexane through the Critical Region.....	296
NOTES	
W. E. Bell: Effect of Micellar Behavior on Adsorption Characteristics of Two Surfactants.....	299
Harold F. Mason and Farrington Daniels: The Reaction of Reciprocal Salt Pairs during Crystallization from the Gaseous Phase.....	300
R. G. Rinker, T. P. Gordon, D. M. Mason and W. H. Corcoran: The Presence of the SO_3 Radical Ion in Aqueous Solutions of Sodium Dithionite.....	302
G. V. D. Tiers and F. A. Bovey: Proton N.S.R. Spectroscopy. III. Annihilation of Nitrogen Quadrupole Broadening by Means of Strong Molecular Electric Field Gradients.....	302
Reynold T. Iwamoto: Chronopotentiometric Study of the Disproportionation of Uranium(V).....	303
Robert F. Adamsky: Oxidation of Silicon Carbide in the Temperature Range 1200 to 1500°.....	305
Robert Earl Davis: Temperature as a Variable during a Klett Experiment.....	307
Thomas R. Harkins and Henry Freiser: The Chelating Tendency of Riboflavin.....	309
Claude P. Talley: Thermal Conductivity of Polycrystalline Boron.....	311
K. S. Howard and F. P. Pike: The Desiccation and Density of Acetone.....	311
Edward B. Dismukes: The Effect of Drop Size on the Accuracy of Surface Tension Determinations by the Sessile Drop Method.....	312
J. A. Friend and P. W. Smith: The Polarographic Behavior of Chromamines and Chromium(III) Salts in an Acetate Buffer.....	314
Jack Allen Campbell and Frederick L. Marsh: The System Magnesium Bromide, Ammonium Bromide and Water at 25°.....	316
S. P. Harold: The Effect of Excess Salt on Minima Observed in γ -Ray Curves for Surface Active Agents.....	317
R. F. Trimble, Jr.: Solubilities in 2-Methoxyethanol. I. 1-1, Aqueous Metal Salts.....	318
J. J. Hemley: Hydrolysis of K-Feldspar and Microcline at Elevated Temperatures and Pressures.....	320

THE JOURNAL OF PHYSICAL CHEMISTRY

(Registered in U. S. Patent Office)

W. ALBERT NOYES, JR., EDITOR

ALLEN D. BLISS

ASSISTANT EDITORS

A. B. F. DUNCAN

EDITORIAL BOARD

C. E. H. BAWN

S. C. LIND

G. B. B. M. SUTHERLAND

R. W. DODSON

R. G. W. NORRISH

A. R. UBBELOHDE

JOHN D. FERRY

W. H. STOCKMAYER

E. R. VAN ARTSDALEN

G. D. HALSEY, JR.

EDGAR F. WESTRUM, JR.

Published monthly by the American Chemical Society at 20th and Northampton Sts., Easton, Pa.

Second-class mail privileges authorized at Easton, Pa.

The *Journal of Physical Chemistry* is devoted to the publication of selected symposia in the broad field of physical chemistry and to other contributed papers.

Manuscripts originating in the British Isles, Europe and Africa should be sent to F. C. Tompkins, The Faraday Society, 6 Gray's Inn Square, London W. C. 1, England.

Manuscripts originating elsewhere should be sent to W. Albert Noyes, Jr., Department of Chemistry, University of Rochester, Rochester 20, N. Y.

Correspondence regarding accepted papers, proofs and reprints should be directed to Assistant Editor, Allen D. Bliss, Department of Chemistry, Simmons College, 300 the Fenway, Boston 15, Mass.

Business Office: Alden H. Emery, Executive Secretary, American Chemical Society, 1155 Sixteenth St., N. W., Washington 6, D. C.

Advertising Office: Reinhold Publishing Corporation, 430 Park Avenue, New York 22, N. Y.

Articles must be submitted in duplicate, typed and double spaced. They should have at the beginning a brief Abstract, in no case exceeding 300 words. Original drawings should accompany the manuscript. Lettering at the sides of graphs (black on white or blue) may be pencilled in and will be typeset. Figures and tables should be held to a minimum consistent with adequate presentation of information. Photographs will not be printed on glossy paper except by special arrangement. All footnotes and references to the literature should be numbered consecutively and placed in the manuscript at the proper places. Initials of authors referred to in citations should be given. Nomenclature should conform to that used in *Chemical Abstracts*, mathematical characters marked for italic, Greek letters carefully made or annotated, and subscripts and superscripts clearly shown. Articles should be written as briefly as possible consistent with clarity and should avoid historical background unnecessary for specialists.

Notes describe fragmentary or incomplete studies but do not otherwise differ fundamentally from articles and are subjected to the same editorial appraisal as are articles. In their preparation particular attention should be paid to brevity and conciseness. Material included in Notes must be definitive and may not be republished subsequently.

Communications to the Editor are designed to afford prompt preliminary publication of observations or discoveries whose value to science is so great that immediate publication is imperative. The appearance of related work from other

laboratories is in itself not considered sufficient justification for the publication of a Communication, which must in addition meet special requirements of timeliness and significance. Their total length may in no case exceed 500 words or their equivalent. They differ from Articles and Notes in that their subject matter may be republished.

Symposium papers should be sent in all cases to Secretaries of Divisions sponsoring the symposium, who will be responsible for their transmittal to the Editor. The Secretary of the Division by agreement with the Editor will specify a time after which symposium papers cannot be accepted. The Editor reserves the right to refuse to publish symposium articles, for valid scientific reasons. Each symposium paper may not exceed four printed pages (about sixteen double spaced typewritten pages) in length except by prior arrangement with the Editor.

Remittances and orders for subscriptions and for single copies, notices of changes of address and new professional connections, and claims for missing numbers should be sent to the American Chemical Society, 1155 Sixteenth St., N. W., Washington 6, D. C. Changes of address for the *Journal of Physical Chemistry* must be received on or before the 30th of the preceding month.

Claims for missing numbers will not be allowed (1) if received more than sixty days from date of issue (because of delivery hazards, no claims can be honored from subscribers in Central Europe, Asia, or Pacific Islands other than Hawaii), (2) if loss was due to failure of notice of change of address to be received before the date specified in the preceding paragraph, or (3) if the reason for the claim is "missing from files."

Subscription Rates (1959): members of American Chemical Society, \$8.00 for 1 year; to non-members, \$16.00 for 1 year. Postage free to countries in the Pan American Union; Canada, \$0.40; all other countries, \$1.20. Single copies, current volume, \$1.35; foreign postage, \$0.15; Canadian postage \$0.05. Back volumes (Vol. 56-59) \$15.00 per volume; (starting with Vol. 60) \$18.00 per volume; foreign postage, per volume \$1.20; Canadian, \$0.15; Pan-American Union, \$0.25. Single copies: back issues, \$1.75; for current year, \$1.35; postage, single copies: foreign, \$0.15; Canadian, \$0.05; Pan-American Union, \$0.05.

The American Chemical Society and the Editors of the *Journal of Physical Chemistry* assume no responsibility for the statements and opinions advanced by contributors to THIS JOURNAL.

The American Chemical Society also publishes *Journal of the American Chemical Society*, *Chemical Abstracts*, *Industrial and Engineering Chemistry*, *Chemical and Engineering News*, *Analytical Chemistry*, *Journal of Agricultural and Food Chemistry*, *Journal of Organic Chemistry* and *Journal of Chemical and Engineering Data*. Rates on request.

THE JOURNAL OF PHYSICAL CHEMISTRY

(Registered in U. S. Patent Office) (© Copyright, 1959, by the American Chemical Society)

VOLUME 63

FEBRUARY 18, 1959

NUMBER 2

ACIDITY STUDIES OF SILICA-ALUMINA CATALYSTS

BY V. C. F. HOLM, G. C. BAILEY AND ALFRED CLARK

Research Division, Phillips Petroleum Co., Bartlesville, Oklahoma

Received March 24, 1958

The protonic acid content of some acid-type solid catalysts was determined by base exchange with 0.1 *N* ammonium acetate solution followed by *pH* measurement. This procedure also permitted evaluation of the relative acid strengths of the catalysts. Measurements were made on silica-alumina catalysts of various compositions after heat treatments ranging from 100 to 900° and were compared with data from non-aqueous butylamine titrations and propylene polymerization tests. Polymerization activity correlated better with protonic acid content than with total acids determined by butylamine titration for the entire composition range from pure silica to pure alumina. The results are consistent with the view that protons on the catalyst surface are necessary for acid catalysis such as propylene polymerization. Catalytic activity destroyed by heat treatment at 900° was regained by rehydration.

Introduction

The importance of acid-type catalysts in petroleum processing as well as the interest in similar materials for other applications has stimulated a considerable amount of research on the measurement of the acidity of solid surfaces and the correlation of acidity tests with catalytic activity.¹⁻¹⁶ The present investigation was conducted to obtain further information on this subject by a study of a series of silica-alumina catalysts using two selected methods for measurement of acid content. Catalytic studies provided data for correlation of acid properties with catalytic activity.

The catalyst protonic acid was evaluated by a base-exchange procedure using an ammonium ace-

tate solution, similar to methods used by Plank,⁷ Maehl,⁶ and Trambouze, *et al.*¹⁵ Since this procedure involves the development of an equilibrium between H⁺ and NH₄⁺ ions in solution and those attached to the catalyst surface, it is possible to obtain an index of the strength of the solid acid from the equilibrium constant. The other method of measuring catalyst acid was titration of the finely divided catalyst suspended in dry benzene with a solution of *n*-butylamine, using *p*-dimethylaminoazobenzene as an indicator according to a procedure described initially by Tamele.⁴ This method determines both protonic and Lewis acid content.

The catalytic activity of the silica-alumina catalysts was evaluated by a propylene polymerization test and by a hydrogen-transfer reaction with Decalin as donor and isobutene as acceptor.

Experimental

Materials.—The principal catalysts studied in this investigation were various compositions of silica-alumina prepared by coprecipitation, using appropriate solutions of sodium silicate and sodium aluminate. The gels were base-exchanged with NH₄Cl solutions until the sodium content was less than 0.02%. After washing and drying, the gels were heat treated for 16 hours at 550° in dry air except when special tests required other heat treatments. The alumina gel was made by precipitation from an Al(NO₃)₃ solution with NH₄OH.

Propylene Polymerization Activity.—The method of evaluating polymerization activity has been described previously.¹⁷ It consisted of passing Phillips Research Grade

- (1) A. G. Oblad, T. H. Milliken, Jr., and G. A. Mills, "Advances in Catalysis, III," Academic Press Inc., New York, N. Y., 1951, p. 199.
- (2) C. L. Thomas, *Ind. Eng. Chem.*, **41**, 2565 (1949).
- (3) O. Johnson, *THIS JOURNAL*, **59**, 827 (1955).
- (4) M. W. Tamele, *Disc. Faraday Soc.*, **8**, 270 (1950).
- (5) Y. Trambouze, *Compt. rend.*, **233**, 648 (1951).
- (6) K. A. Maehl, *Ind. Eng. Chem., Anal. Ed.*, **12**, 24 (1940).
- (7) C. J. Plank, *Anal. Chem.*, **24**, 1304 (1952).
- (8) Y. Trambouze, L. de Mourgues and M. Perrin, *J. chim. phys.*, **51**, 723 (1954).
- (9) P. Stright and J. D. Danforth, *THIS JOURNAL*, **57**, 448 (1953).
- (10) J. E. Mapes and R. P. Eischens, *ibid.*, **58**, 1059 (1954).
- (11) R. C. Hansford, *Ind. Eng. Chem.*, **39**, 849 (1947).
- (12) S. G. Hindin, A. G. Oblad and G. A. Mills, *J. Am. Chem. Soc.*, **77**, 535, 538 (1955).
- (13) A. G. Oblad, S. G. Hindin and G. A. Mills, *ibid.*, **75**, 4096 (1953).
- (14) J. D. Danforth, *THIS JOURNAL*, **59**, 564 (1955).
- (15) Y. Trambouze, L. de Mourgues and M. Perrin, *Compt. rend.*, **234**, 1770 (1952).
- (16) C. J. Plank, *THIS JOURNAL*, **57**, 284 (1953).

- (17) V. C. F. Holm, G. C. Bailey and A. Clark, *Ind. Eng. Chem.*, **49**, 250 (1957).

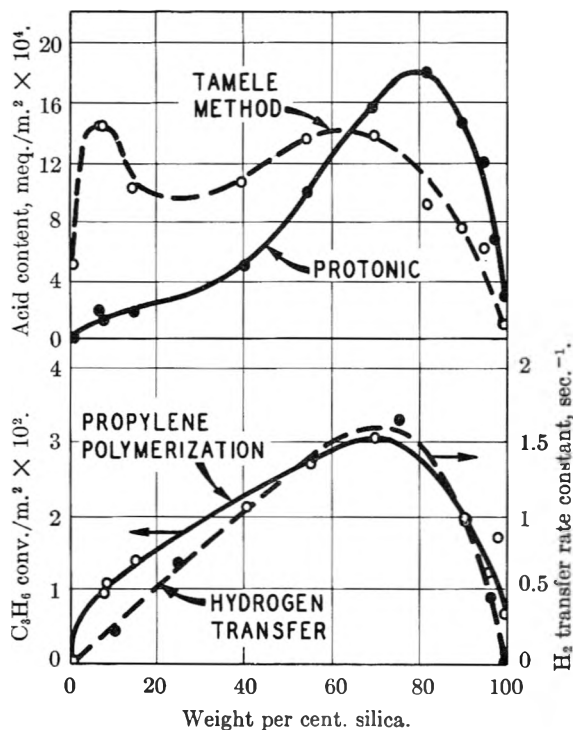


Fig. 1.—Relationship between acid content and catalytic properties for various compositions of silica-alumina.

propylene over the catalyst while the temperature was increased steadily from 30 to 300° in the course of two hours. Metering the propylene feed and effluent provided a continual measure of conversion. The maximum conversion obtained for each catalyst was considered as indicative of the polymerization activity.

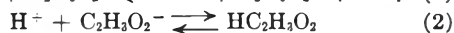
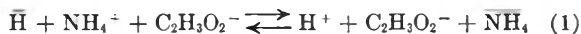
Determination of Total Acids.—Measurements of acid content by the Tamele method were made essentially by the procedures described in the literature.^{3,4} It was found that the time required for titration was reduced if the samples were ground to pass a 200-mesh sieve. However, in spite of this, titrations required three hours or more. Ground samples were heat-treated at 450° prior to the determination except when it was desired to test a catalyst condition resulting from activation at a lower temperature.

Base-exchange Procedure for Protonic Acid.—Approximately 0.1-g. samples of the granular or powdered catalysts were weighed into 50-ml. glass-stoppered erlenmeyer flasks. After addition of exactly 25 ml. of 0.1 *N* ammonium acetate solution (pH 7.00 ± 0.02) and occasional agitation in the course of a 24-hour contact at 25 ± 2°, a portion of the supernatant solution was decanted and the pH determined. The acid concentration was obtained from a calibration curve for the addition of acetic acid to the ammonium acetate solution, and the milliequivalents of acid per gram of catalyst calculated. Tests made on catalyst in the form of granules up to 16 mesh were in good agreement with those on powdered samples, indicating that it was not necessary to control granule size within close limits.

The effect of varying the weight of sample used with 25 ml. of solution also was studied. In tests on a catalyst containing 40% silica the values for protonic acid content increased from 0.06 to 0.19 meq. per gram as the sample size decreased from 1.6 to 0.1 g. In the case of a 70% silica catalyst the values for acid content increased from 0.22 to 0.45 meq. per gram for a similar change in sample size. In each instance a plot of the data showed a typical equilibrium reaction in which the proportion of acid released in the solution increased with decreasing sample size. As the sample size was reduced below 0.1 g. the increase was negligible so sample weights of 0.1 g. were used for subsequent tests. The difference in the degree to which the acid content varied with sample size, suggested that this variation could be used to study relative strengths of the surface acids.

Estimation of Acid Strength.—A few investigators have considered means of evaluating the acid strengths of solid catalysts. One approach⁴ was based on measuring the vapor pressure of ammonia from an ammonium salt of the protonic acid or the energy of chemisorption for a Lewis acid. Another method^{3,18} involved the use of indicators that gave color changes at different *pK* values in non-aqueous systems. Both of the above procedures appear applicable in classifying materials that exhibit considerable differences in acid strength but neither method has thus far shown promise in demonstrating differences within a group of similar materials such as silica-alumina catalysts of various compositions.

The reaction between ammonium acetate solution and a solid acid catalyst may be described by the equations



where \bar{H} and $\bar{\text{NH}}_4$ represent hydrogen and ammonium ions bound to the catalyst surface. Most of the protons set free by base exchange combine with acetate ions to form undissociated acetic acid and this tendency is increased by the presence of excess acetate ions.

The essential reaction, therefore, is



and the base exchange equilibrium constant may be expressed

$$K = \frac{(\text{H}^+) \times (\bar{\text{NH}}_4)}{(\bar{H}) \times (\text{NH}_4^+)}$$

Since the driving force in this reaction is the product of the activity of the hydrogen ion in the catalyst phase and that of the ammonium ion in the solution phase, a high activity of hydrogen ions in the catalyst (high acid strength) should be reflected by a high value for the base-exchange equilibrium constant.

If the acid content of a given catalyst is determined first with a 0.1-g. sample and then with a larger sample, for example 1.0-g., the value of the constant *K* may be calculated. The milliequivalents of each reactant in the 25-ml. equilibrium mixture for the one-gram sample is obtained as

(H^+)—from pH measurement

(NH_4^+)—equal to the meq. of acid formed by base exchange (from calibration curve)

(\bar{H})—equal to the total available acid of the 1-g. sample (from measurement on 0.1-g. sample) minus the value for $\bar{\text{NH}}_4$

(NH_4^+)—equal to the initial amount of NH_4^+ in the 0.1 *N* soln. minus the value for $\bar{\text{NH}}_4$

Equilibrium constants calculated for a large number of catalysts were in good agreement over a range of sample weights for each catalyst, showing that this method of computation was valid and that a definite characteristic of the catalyst was being measured. For example, a silica-alumina catalyst yielded values of *K* ranging from 9.8 to 11 × 10⁻⁶ for four samples weighing from 0.44 to 2.6 g. Usually equilibrium constants on samples of a given catalyst showed a deviation of less than 10% from the mean value.

Results and Discussion

Effect of Varying the Composition of Silica-Alumina.—The data obtained on silica-alumina catalysts of various compositions are given in Table I. The results are compared more easily in Fig. 1 where the acid content and polymerization activity are plotted per unit of surface area. The rate constants for the hydrogen-transfer reaction between Decalin and isobutene on a similar series of catalysts tested previously in this Laboratory¹⁹ also are shown. The similarity between the curves for propylene polymerization, hydrogen transfer and protonic acid content suggests a direct correlation between these properties. A correla-

(18) C. Walling, *J. Am. Chem. Soc.*, **72**, 1164 (1950).

(19) R. W. Blue and C. J. Engle, *Ind. Eng. Chem.*, **43**, 494 (1951).

tion between acid determined by butylamine titration and catalyst activity has been reported in the literature.^{3,4} However, that work covered only the range of high silica content and our data show that the correlation does not extend to the high alumina compositions. It appears, therefore, that butylamine titration measures Lewis acid sites in the high alumina catalysts which are not effective for catalyzing the reactions studied. The protonic acid test does not distinguish between acid protons present on the catalyst before the test and those formed by the interaction of Lewis acid sites and water, but data will be presented later to support the view that protons on the catalyst are necessary for catalytic activity.

TABLE I
RESULTS OF TESTS ON SILICA-ALUMINA CATALYSTS HEAT TREATED AT 550°

Nominal SiO ₂ content, wt. %	Surface area, m. ² /g.	Acid content, meq./g.		Propylene polym., max. % conv.	Acid-strength index, K
		Protonic	Tamele meth.		
0	274	0.0	0.14	0
7.5	298	.06	.43	20
8	286	.04	.41	15
15	383	.07	.34	25	2.3×10^{-7}
40	400	.19	.42	49	4.7×10^{-6}
55	345	.34	.46	48	1.1×10^{-5}
70	292	.45	.40	44	3.9×10^{-5}
82	450	.80	.40	56	6.1×10^{-5}
90	530	.77	.40	55	1.4×10^{-4}
95	516	.61	.31	36	2.4×10^{-4}
98	608	.38	34	2.5×10^{-4}
100	478	.13	.03 app.	13	1.1×10^{-5}

It appears inconsistent that for some of the catalysts tested the total acid determined by butylamine titration was lower than the protonic acid. This was true particularly for catalysts containing large amounts of silica. This may be due to the occurrence of more small pores as the surface area increases in which the surface may not be available to the large molecules of butylamine but is accessible to the smaller ammonium ions of the ammonium acetate solution used for the base-exchange determination of protonic acid.

The values for acid-strength index in Table I show that the acid strength reaches a maximum at 95 to 98% silica whereas the concentration of protonic acid sites reaches a maximum at about 82% silica. Catalysts with 55 and 95% silica have about the same quantity of acid per unit area whereas the acid-strength index of the latter is 20 times greater. By referring to Fig. 1, it is apparent that the polymerization activity per unit area for the 55% catalyst was almost twice that of the catalyst with 95% silica. This suggests that the acid sites of lower acid strength are more effective in propylene polymerization than sites of high strength. Additional evidence for this is indicated in Fig. 2 where the ratio of the polymerization activity to the protonic acid per unit area for several catalysts is plotted against the acid-strength index. Although the points are somewhat scattered, there is an unmistakable trend toward a more effective utilization of acid sites that have a lower acid-strength index.

Effect of Varying Temperature of Heat Treat-

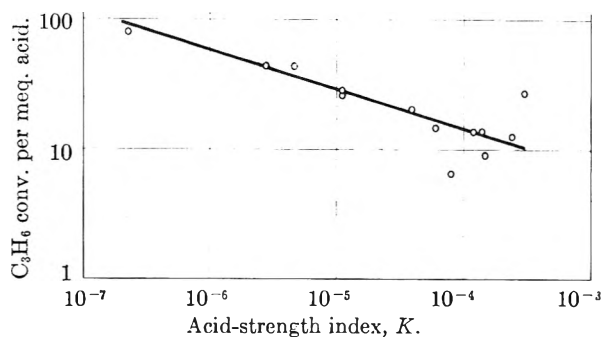


Fig. 2.—Effectiveness of protonic acid for propylene polymerization as a function of the acid-strength index.

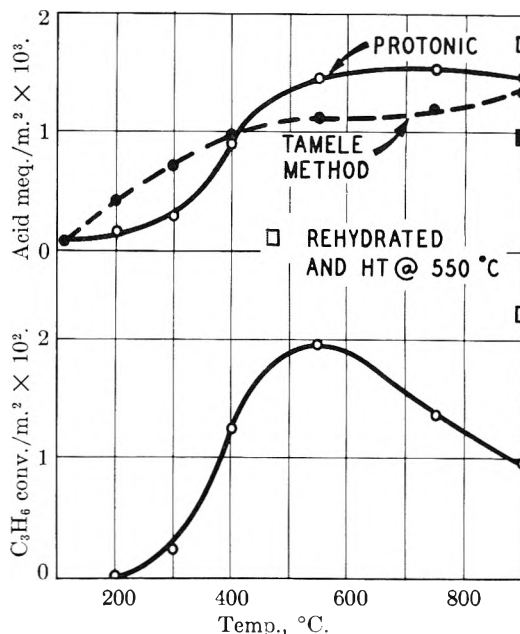


Fig. 3.—Effect of temperature of heat treatment on acid content and polymerization activity of silica-alumina containing 90% silica.

ment.—A study of the effect of variation in the temperature of heat treatment was of interest particularly in view of the results of Traumbouze⁸ which indicated that the sum of the Lewis and protonic acids of a silica-alumina catalyst was practically constant after various heat treatments but that the protonic acid, predominant at the low temperatures, was gradually converted to Lewis acid at the higher temperatures (700°). These results are logical if one considers the Lewis acid as an anhydride formed by the elimination of water from the protonic acid. However, the data of Traumbouze suggest that the conversion to a Lewis acid at the high temperature is irreversible and a protonic acid is not regenerated on contact with water during the determination of protonic acidity by base exchange.

The results obtained on a catalyst containing 90% silica heat treated under various conditions are presented in Table II. The surface areas tend to decrease with increasing temperatures of heat treatment but the values for catalysts after heating at 900° are surprisingly high considering the severity of this treatment. Apparently heating in an atmosphere of dried air prevented the usual drastic

TABLE II
RESULTS FOR A CATALYST CONTAINING 90% SILICA, HEAT TREATED AT VARIOUS TEMPERATURES

Treatment	Surface area, m. ² /g.	Acid content, meq./g.		% Propylene polym., max. conv.	Acid-strength index, K
		Protonic	Tamele meth. ^a		
110°	(600)	0.05	0.04
200	(600)	.09	.25	0
300	597	.17	.43	6	1.8×10^{-4}
400	577	.53	.59	32	1.2×10^{-4}
550	530	.77	.60	55	1.4×10^{-4}
750	475	.72	.56	29	1.5×10^{-4}
900	424	.62	.58	21	$.8 \times 10^{-4}$
900° rehydrated and HT at 550°	381	.67	.36	43	$.7 \times 10^{-4}$
Original catalyst, base exchanged with HOAc, washed, dried at 110°	(600)	.52	.56	13	1.7×10^{-4}

^a Butylamine titrations were performed on catalysts as described without the usual prior grinding and heat treatment.

TABLE III
RESULTS FOR A CATALYST CONTAINING 40% SILICA, HEAT TREATED AT VARIOUS TEMPERATURES

Treatment	Surface area, m. ² /g.	Acid content				% Propylene polym.		Acid-strength index K
		Protonic meq./m. ² $\times 10^3$	Tamele meth. meq./m. ² $\times 10^3$	meq./m. ² $\times 10^3$	meq./m. ² $\times 10^3$	max. conv.	max. conv./m. ² $\times 10^2$	
110°	...	0.0	0.0	0.0	0.0
200	(360)	.02	.06	.16	.45	0	0
300	357	.10	.28	.42	1.18	7	0.34	2.9×10^{-6}
400	380	.19	.50	.48	1.27	48	2.2	2.8×10^{-6}
550	400	.19	.47	.42	1.05	49	2.1	4.7×10^{-6}
900	302	.20	.66	.36	1.19	26	1.4
900° rehydrated and HT at 550°	275	.19	.69	.45	1.64	35	2.04	4.9×10^{-6}
Original catalyst, base exchanged with HOAc, washed, dried at 110°	(360)	.16	.44	.11	0.31	5.9×10^{-6}

effects obtained on catalysts subjected to this high temperature. The results indicate that the acid-strength index is not changed appreciably except at the highest temperature. The fact that the catalysts heat-treated at 300 and 400° have the same acid-strength index as the acid base-exchanged catalyst dried at only 110° and the one heat-treated at 550° suggests that the acid sites still occupied by NH₃ in the 300 and 400° catalysts are the same strength as the free sites. The low polymerization activity of the base-exchanged catalyst, dried only at 110°, is attributed to excess water present which could be attached to acid sites as oxonium ions, H₃O⁺, and which might be considered similar to NH₄⁺ in modifying the behavior of the protonic acid.

The relative effect of heat treatments at various temperatures is shown more clearly in Fig. 3, where the acid content and polymerization activity are plotted on the basis of unit surface area. The quantity of acid determined by both methods as well as polymerization activity increase with the temperature of heat treatment up to 550° but the curve for polymerization activity correlates a little better with the protonic acid curve. The protonic acid content remains relatively constant and the total acid content increases slightly with further increases in temperature but the polymerization activity decreases and reaches a value of approximately one-half the maximum value when the catalyst is heated at 900° for five hours in dry air. This suggests that protons on the catalyst are necessary for polymerization activity and that heating at temperatures higher than 550° results in the gradual loss of protons as water with the

formation of Lewis acid sites. This change from protonic acid to Lewis acid on the catalyst would not be detected by the butylamine titration which measures both types. Neither would the protonic acid test detect this if the Lewis acid sites so produced react with water to form protonic acid. To obtain information on this point a catalyst which had been heated at 900° was contacted with water, dried and heat treated at 550°. The polymerization activity per unit area then was slightly higher than the sample treated only at 550°. This result supports the proposed mechanism. Reversibility of Lewis acid sites is not found for all compositions in this catalyst system because an alumina gel, which showed measurable Lewis acid, did not show protonic acidity and was not active for propylene polymerization. Whether or not a protonic acid is formed by reaction of a Lewis acid with water probably is dependent on the strength of the Lewis acid.

Results of a similar study on the effect of temperature of heat treatment are shown for a catalyst with 40% silica in Table III. The results are somewhat different than for the catalyst with 90% silica in that the amount of protonic acid is lower and there is a wider spread between the acid determined by base exchange and that obtained by butylamine titration with the latter considerably the greater. The results are similar in that the highest temperature heat treatment decreased the propylene polymerization activity but this was regained by rehydration. The maximum polymerization activity for the 40% catalyst is obtained by heat treatment at 400° whereas the 90% catalyst shows the greatest activity when heated at

550°. This is presumably connected with the greater retention of ammonia acquired in the treatment with ammonium chloride during the preparation and reflects the higher acid-strength index of the catalyst with 90% silica.

It is evident for both catalysts that the acid determined by butylamine titration reaches a high value at a lower temperature of heat treat-

ment than that required for developing maximum polymerization activity. The latter reaches a maximum only when the temperature of heat treatment is adequate to develop the greatest quantity of protonic acid. This provides additional evidence that the protonic acid is of greater significance in the polymerization of propylene than total acids or Lewis acid alone.

CARBON FORMATION FROM CARBON MONOXIDE-HYDROGEN MIXTURES OVER IRON CATALYSTS.^{1,2} I. PROPERTIES OF CARBON FORMED

BY P. L. WALKER, JR., J. F. RAKSZAWSKI AND G. R. IMPERIAL

Department of Fuel Technology

The Pennsylvania State University, University Park, Pennsylvania

Received April 8, 1958

The properties of carbons formed from various carbon monoxide-hydrogen mixtures in a flow system over iron catalysts at temperatures from 450 to 700° and atmospheric pressure have been investigated. The crystallite height, surface area, C-H ratio and electrical resistivity of the carbons are found to be markedly affected by formation temperature, gas composition and amount of carbon formed over the catalyst. The carbons have an unusually well developed crystalline character, considering the relatively low formation temperatures, with crystallite heights in most cases being above 100 Å. and interlayer spacings indicating substantial three-dimensional ordering.

Introduction

The majority of research on the reaction $2\text{CO} \rightarrow \text{C} + \text{CO}_2$ has been prompted by its highly deleterious effects on currently or potentially important industrial processes. Ceramic brick linings containing iron undergo physical disintegration when exposed to carbon monoxide under certain conditions, because of carbon formation within the porous material. The Fischer-Tropsch process used for the synthesis of hydrocarbons is subject to carbon deposition, which may lead to blockage of the reaction vessel and to deactivation and disintegration of the catalyst. The reaction has become of concern in nuclear reactors, when graphite is used as the moderator and carbon dioxide as the coolant. The extent of carbon transfer by the combined reactions of carbon monoxide formation by carbon gasification in the high temperature reactor zone and carbon monoxide decomposition to carbon in the low temperature reactor zone must be understood.

Recently there has been interest shown in using the carbon monoxide deposition reaction to produce carbons of commercial utility. During World War II, the Germans used the reaction to produce a substitute for carbon black.³ A French patent describes a process and equipment for producing carbon in a falling-bed reactor using a finely divided iron catalyst.⁴ A recent American patent describes an apparatus for the production of carbon black at conditions between 700 to 1035° and

10 to 40 atm., where a metallic catalyst is not necessary.⁵ An excellent, annotated bibliography of the literature and patents related to the production of carbon by the decomposition of carbon monoxide has been compiled.⁶

This research had two main objectives: (1) to investigate in detail the structure of carbon produced by the decomposition of carbon monoxide over an iron catalyst, as a function of temperature and inlet carbon monoxide-hydrogen composition, and (2) to investigate the effect of temperature and inlet carbon monoxide-hydrogen composition on the rate and amount of carbon formation before deactivation of the iron catalyst occurs. All reactions were conducted at atmospheric pressure. This first paper discusses the properties of the carbons formed.

Experimental

Reactor.—The reactor consisted of a Vycor combustion tube 600 mm. long, 25 mm. i.d., and 31 mm. o.d., heated by a conventional split-tube furnace. The catalyst was held in a Coors porcelain micro combustion boat, glazed inside and outside, size 0000, having a volume of 0.2 cc. A Vycor thermocouple protection tube, 7 mm. o.d. and 5 mm. i.d., extended halfway into the reactor tube and housed a chromel-alumel thermocouple for measuring reaction temperature. A second chromel-alumel thermocouple, located between the reactor and the furnace windings, was connected to a Phen-Trols Electronic Temperature Controller, which held the reactor temperature within $\pm 5^\circ$. Auxiliary equipment included wet test meters, before and after the reactor, to determine cumulative gas flow; a rotameter to measure instantaneous helium, hydrogen or carbon monoxide flow into the reactor; water saturators immediately before the wet test meters; Ascarite towers before and after the reactor to remove carbon dioxide; and magnesium perchlorate towers before and after the reactor to remove water.

Catalysts.—The iron catalyst used for the majority of the

(1) Based, in part, on an M.S. thesis submitted by G. R. Imperial to the Graduate School of the Pennsylvania State University, August, 1957.

(2) At different stages, this work was supported by the Reading Anthracite Company and the Atomic Energy Commission under Contract No. AT(30-1)-1710.

(3) B.I.O.S. Final Report No. 1399, Item No. 22.

(4) French Patent No. 874,681 (August 18, 1942).

(5) U. S. Patent No. 2,716,053 (August 23, 1955).

(6) An Annotated Bibliography. H. Jack Donald, Mellon Institute of Industrial Research, 1956.

work was a Baker Analyzed reagent grade iron powder produced by reducing iron carbonyl in hydrogen (called carbonyl iron, for convenience). The powder consisted of spherical particles having an average diameter on a weight basis of *ca.* 10 μ . Following reduction of the powder in hydrogen for 24 hours at 400° the material had a B.E.T. surface area of 0.99 m.²/g., as given by nitrogen adsorption. The powder packed to a bulk density of *ca.* 2.7 g./cc. in the porcelain boat prior to reaction. Additional information on the catalyst is available from a recent publication.⁷

Because of interest in a cheap, successful catalyst for the carbon monoxide deposition reaction, some runs were made using "Sinter B," which is an iron typical of the sintered by-product made from iron-containing fines blowing from the top of open hearths and blast furnaces.⁸ Morton⁹ presents detailed physical and chemical properties of a "Sinter B." X-Ray diffraction analysis of the "Sinter B" used in this research yielded lines for Fe₂O₃ and SiO₂ as the main constituents. The B.E.T. surface areas of an 80 \times 100 and a -100 mesh fraction of "Sinter B" heated to 528° was 0.41 and 0.46 m.²/g., respectively, as given by nitrogen adsorption.

The iron catalysts used in this research have a negligible surface area compared to conventional catalysts used commercially for the ammonia synthesis and Fischer-Tropsch processes. Therefore, initially (prior to significant catalyst disintegration) they will be found to be much less active than commercial catalysts.

Reactants.—All gases were obtained from the Matheson Company. Helium and hydrogen, used for pretreatment, were guaranteed at 99.8 and 99.9% purity, respectively. The carbon monoxide-hydrogen mixtures were analyzed by the Matheson Company by either an Orsat apparatus or a mass spectrometer. In addition to the two main constituents, the mixtures contained up to 0.3% carbon dioxide (removed prior to entering the reactor), traces of iron pentacarbonyl (removed by decomposition in the entering end of the reactor), and small amounts of oxygen and nitrogen. A maximum of 0.3 mg. of sulfur per liter of gas was found.

X-Ray Diffraction Apparatus.—A 164° (2 θ) General Electric X-ray diffraction unit, XRD-3, was employed to determine interlayer spacings and average crystallite heights of the carbons produced. Copper radiation was used except when analyzing samples containing high concentrations of iron and/or iron carbide. In those cases, iron radiation was substituted because of the excessive absorption of the copper radiation by iron compounds. Standard X-ray procedures and subsequent calculations for graphitic specimens, as discussed in detail in a recent paper,¹⁰ were adopted. Three separate X-ray samples for each carbon were analyzed. With a few exceptions, the interlayer spacing and average crystallite height data varied less than ± 0.003 Å. and $\pm 5\%$, respectively, on a given carbon.

Electrical Resistivity Apparatus.—The apparatus and procedure employed in this determination has been described.¹¹ Essentially the electrical resistivity of a sample was determined by comparing the voltage drop across a known sample length with that across a fixed resistance, both carrying the same total current. Electrical resistivities could be duplicated within $\pm 2.5\%$ on a given sample.

Low Temperature Gas Adsorption Apparatus.—A standard gas adsorption apparatus¹² was employed to obtain adsorption isotherms, using nitrogen as the adsorbate. Specific surface areas, calculated from the isotherms by the B.E.T. equation, could be duplicated within $\pm 2.5\%$. An equilibration time of one-half hour for each adsorption point proved more than ample.

Acid Treatment of Raw Carbon.—Some of the raw carbons were treated separately with 12 *N* HCl, 15 *N* HNO₃ and 50% by weight of HF to remove compounds of iron. The procedure for HCl and HNO₃ treatment consisted of boiling 0.63 g. of raw carbon with 50 cc. of acid for a designated period of time, washing the purified carbon with hot water in a Morton bacteria filtering apparatus (containing a fritted disc with openings of less than 2 μ), and drying at 120° in a vac-

uum oven. The procedure for HF treatment was similar, except that in the initial step 0.63 g. of raw carbon and 10 cc. of acid were held in a platinum crucible and the contents evaporated to dryness.

Typical Carbon-deposition Run.—An iron sample of desired weight was placed in the porcelain boat, which in turn was centered in the Vycor reactor tube. Prior to a run, helium was passed through the entire system (5.8 cc./sec., STP) for one-half hour, during which time the volume of gas passing through the two wet test meters was recorded to check for leaks. Then, with helium flow continuing, the reactor was brought to reaction temperature and allowed to equilibrate during a second half-hour period. After the period of helium flow, the catalyst usually was pretreated by reducing in hydrogen (11.0 cc./sec.), for one hour. In other runs, the catalyst was pretreated by carbiding with carbon monoxide (5.8 cc./sec.) at 359° for varying lengths of time. In some runs, no pretreatment of the catalyst was employed.

In runs using hydrogen pretreatment, the carbon monoxide-hydrogen mixture was passed into the reactor (5.8 cc./sec., unless otherwise specified) immediately following the pretreatment. Following the carbiding pretreatment and prior to the introduction of the carbon monoxide-hydrogen mixtures, helium was passed through the reactor while the catalyst was being brought to reaction temperature. During the passage of the carbon monoxide-hydrogen mixture, the cumulative volumes of gas passing through the wet test meters, before and after the reactor, were recorded. Before the gas entered the exit wet test meter, it was passed through an Ascarite tower, where the carbon dioxide which was formed during the reaction was removed.

At the end of a run, helium was passed (30 cc./sec.) through the reactor while it was cooled to room temperature. Cooling was greatly accelerated by opening of the split-tube furnace and directing a stream of compressed air against the reactor tube. After cooling, the contents of the reactor tube were removed, the weight of free carbon being taken as the difference between the total weight of material removed and the initial weight of catalyst employed.^{13,14}

Results and Discussion

Electron Micrographs of Carbon.—Electron micrographs of the carbon produced from the decomposition of carbon monoxide at different temperatures, from different carbon monoxide-hydrogen mixtures, and after varying amounts of carbon formed per weight of catalyst were obtained. The nature of the carbon formed agrees with that shown in previously published electron micrographs of carbon deposited over iron, cobalt and nickel.¹⁵⁻¹⁷ The most characteristic growth consisted of two carbon filaments tightly twisted into a rope over 1 μ in length and between 0.1 and 0.5 μ in diameter. Much bifilamentary growth also was observed, where the carbon threads did not become twisted. It was not possible, however, to associate a particular type of growth with variations in operating conditions.

At the end of the carbon growths, there invariably was located a particle of iron and/or iron carbide, which presumably was the catalyst for the growth of the particular filament. Figure 1 presents a dark-field micrograph of a carbon (78%

(13) The increase in weight actually represents closely the total carbon (free carbon plus carbidic carbon); but the maximum carbidic carbon present, for all runs reported, represents less than one per cent. of this weight and can be ignored. Therefore, in the future discussion free carbon and carbidic carbon will not be distinguished.

(14) The actual weights of carbon were less than computed values because of competing reactions producing hydrocarbons.

(15) L. V. Radushkevich and V. M. Luk'yanovich, *Zhur. Fiz. Khim.*, **26**, 88 (1952).

(16) L. J. E. Hofer, E. Sterling and J. T. McCartney, *THIS JOURNAL*, **59**, 1153 (1955).

(17) W. R. Davis, R. J. Slawson and G. R. Rigby, *Trans. Brit. Ceram. Soc.*, **56**, 67 (1957).

(7) P. L. Walker, Jr., and F. Rusinko, Jr., *THIS JOURNAL*, **59**, 1106 (1955).

(8) C. B. Bigelow, *Am. Inst. Mining Met. Engrs.*, **10**, 103 (1951).

(9) R. J. Morton, *ibid.*, **10**, 122 (1951).

(10) P. L. Walker, Jr., H. A. McKinstry and J. V. Pustinger, *Ind. Eng. Chem.*, **46**, 1651 (1954).

(11) P. L. Walker, Jr., and F. Rusinko, Jr., *Fuel*, **36**, 43 (1957).

(12) P. H. Emmett, A.S.T.M. Tech. Publ. No. 51, 95 (1941).

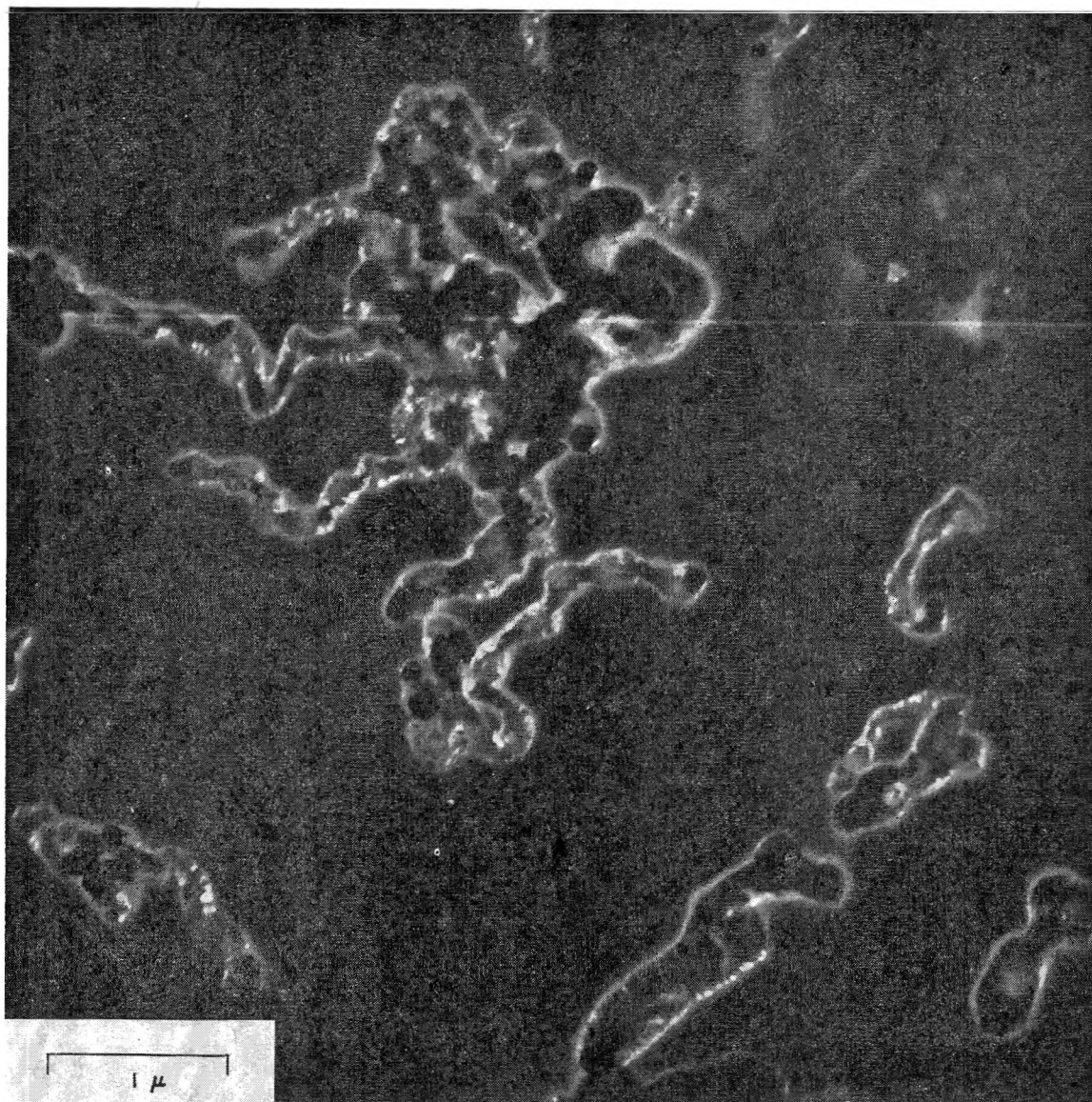


Fig. 1.—Dark-field electron micrograph of raw carbon (78% C-22% Fe) formed at 528° from a 98.6% CO-1.4% H₂ mixture over carbonyl iron.

C-22% Fe) formed at 528° from a 98.6% CO-1.4% H₂ mixture over carbonyl iron. The micrograph clearly shows the location of the iron-containing material. The particle size of this material is markedly less than that of the original carbonyl iron, agreeing with the findings of Tenenbaum and Joseph¹⁸ that carbon monoxide deposition on and within iron disintegrates the material.

Under dark-field conditions, crystalline areas of the solid diffract the electron beam and sharp, light lines are produced. Such diffraction from the carbon filaments is observed in Fig. 1, indicating the crystalline nature of the carbon formed. This has been confirmed by X-ray diffraction studies, to be discussed.

Properties of the Carbon Produced by Decomposition of Carbon Monoxide-Hydrogen Mixtures over Carbonyl Iron.—Initially, it was desired to investigate only the effect of temperature and

carbon monoxide-hydrogen composition on the character of the carbon formed. To do this, other factors (total gas flow rate, amount of carbon formed per starting weight of iron, and pretreatment of the iron), were held constant. A 0.1-g. sample of iron was used from which *ca.* 0.9 g. of carbon was produced, meaning that the final carbon had *ca.* 10% iron (primarily Fe and Fe₃C) present. Table I presents the data on the average crystallite height and interlayer spacing of the carbon produced.¹⁹ To the authors' knowledge, the crystallite heights (L_c) of the majority of the carbons produced are considerably larger than those reported for other carbonaceous materials having seen comparable maximum temperatures. For example, typical carbon blacks,²⁰ carbons pro-

(19) Data presented in an accompanying paper show that for the 34.1% CO-65.9% H₂ mixture more of the carbon was formed by the reaction $\text{CO} + \text{H}_2 \rightarrow \text{C} + \text{H}_2\text{O}$ than by the reaction $2\text{CO} \rightarrow \text{C} + \text{CO}_2$. This suggests that as the hydrogen content of the gas mixture is increased the former reaction becomes of increasing significance.

(18) M. Tenenbaum and T. L. Joseph, *Trans. Am. Inst. Mining Met. Engrs.*, **140**, 106 (1940).

TABLE I

EFFECT OF CARBON MONOXIDE-HYDROGEN COMPOSITION AND TEMPERATURE ON THE AVERAGE CRYSTALLITE HEIGHT AND INTERLAYER SPACING OF CARBONS FORMED BY CARBON MONOXIDE DECOMPOSITION OVER CARBONYL IRON

Formation temp., °C.	Av. crystallite height and interlayer spacing of carbons produced from various carbon monoxide-hydrogen mixtures													
	0.8% H ₂		2.2		5.2		9.0		19.9		39.8		65.9	
	L _c , Å	d-spacing, Å	L _c	d-spacing	L _c	d-spacing	L _c	d-spacing	L _c	d-spacing	L _c	d-spacing	L _c	d-spacing
450	38	3.416
470	67	3.408	53	3.418	62	3.410
500	97	3.384	98	3.388	66	3.394	79	3.404	40	3.443	132	3.436
528	124	3.377	132	3.372	149	3.373	118	3.377	76	3.398	54	3.431	102	3.430
576	127	3.369	175	3.367	231	3.364	195	3.359	211	3.363	154	3.365	170	3.398
585	141	3.369
602	101	3.380	134	3.372	130	3.369	253	3.361	282	3.360	191	3.360	248	3.364
630	114	3.374	168	3.368	192	3.363	280	3.359	263	3.359
700	128	3.380	137	3.378

duced from high molecular weight aromatic compounds,²¹ and heat-treated coals²² have crystallite heights in the range of only 10 to 35 Å. Likewise, the interlayer spacings of all the carbons produced from the carbon monoxide-hydrogen mixtures are significantly less than those of other carbons formed at similar temperatures.²⁰⁻²² For these other carbons, spacings are always greater than 3.44 Å, the lower interlayer spacing limit of completely amorphous carbons, according to Franklin.²³ The lowest interlayer spacing seen in Table I, 3.359 Å, is indicative of a carbon having ca. 85% three-dimensional ordering, according to the Franklin correlation.²³ For the carbons produced by conventional treatment of carbon-containing raw materials, a heat treatment temperature above 2000° is necessary before the high degree of three-dimensional ordering found for most of the carbon samples in Table I is achieved.^{21,24} Indeed, for the majority of commercial carbon blacks, it is not possible to produce as high a degree of three-dimensional ordering even after heat treatment to 3200°.²⁰

From Table I it is seen that for each carbon monoxide-hydrogen mixture used the crystalline character of the carbon increases with increasing temperature of formation to a maximum and then decreases with further temperature rise. Further, the temperature at which the maximum crystalline character is attained gradually increases with increasing hydrogen content in the gas mixture. The maximum crystallite size attained also increases as the hydrogen content in the gas mixture is increased, at least up to the 19.9% H₂-containing mixture.

The change in surface area of the carbon as a function of temperature of formation and carbon monoxide-hydrogen composition is presented in Table II. The surface area values indicate that the carbon has a high degree of internal porosity and surface roughness; for if a typical particle size is taken to be 0.1 μ in diameter and 1 μ long, the specific surface area of a non-porous particle is

calculated to be only 15 m.²/g. The surface areas are considerably larger than those for carbons which are easily graphitized,²⁵ smaller than the areas for typical active carbons,²⁶ and comparable to the areas of intermediate grades of carbon black.²⁷

TABLE II

EFFECT OF CARBON MONOXIDE-HYDROGEN COMPOSITION AND TEMPERATURE ON THE SPECIFIC SURFACE AREA OF CARBONS FORMED BY CARBON MONOXIDE DECOMPOSITION OVER CARBONYL IRON

Formation temp., °C.	Specific surface area, m. ² /g., of carbons produced from various carbon monoxide-hydrogen mixtures						
	0.8% H ₂	2.2	5.2	9.0	19.9	39.8	65.9
450	44
470	106	116	125
500	113	131	132	125	161	152	99
528	111	121	157	132	134	156	170
576	87	97	93	61	91	105	172
602	71	76	95	82	77	65	104
630	35	84	82	89	87
700	42	52	...

TABLE III

EFFECT OF CARBON MONOXIDE-HYDROGEN COMPOSITION AND TEMPERATURE ON THE ATOMIC CARBON-HYDROGEN RATIO OF CARBONS FORMED BY CARBON MONOXIDE DECOMPOSITION OVER CARBONYL IRON

Formation temp., °C.	Atomic carbon-hydrogen ratio of carbons produced from various carbon monoxide-hydrogen mixtures						
	0.8% H ₂	2.2	5.2	9.0	19.9	39.8	65.9
470	14.4	13.1	11.4
500	21.5	16.4	14.1	9.6	11.4	7.3	9.0
528	25.3	15.4	19.5	10.8	13.3	10.1	9.6
576	27.3	21.1	21.6	23.2	17.3	14.3	12.2
602	..	27.4	26.2	27.4	28.1	16.4	20.4
630	34.2	34.5	35.2	..	34.6
700	52.7	53.0	..

It is also seen from Table II that the specific surface areas of the carbons exhibit an over-all trend similar to the crystallographic data, despite some scattered inconsistencies. They increase in area

(20) W. D. Schaeffer, W. R. Smith and M. H. Polley, *Ind. Eng. Chem.*, **45**, 1721 (1953).

(21) C. R. Kinney, *Proceedings of the Conferences on Carbon*, U. of Buffalo, 1956, p. 83.

(22) H. E. Blayden, H. L. Riley and A. Taylor, *J. Am. Chem. Soc.*, **62**, 180 (1940).

(23) R. E. Franklin, *Acta Cryst.*, **4**, 253 (1951).

(24) A. E. Austin and W. A. Hedden, *Ind. Eng. Chem.*, **46**, 1520 (1954).

(25) "Some Factors Affecting the Reactivity of Sized Particle Carbons to Carbon Dioxide." P. L. Walker, Jr., and J. R. Nichols, *Proceedings of the Conference on Industrial Carbon and Graphite*, London, 1957, in press.

(26) J. W. Hassler, "Encyclopedia of Chemical Technology," Vol. 2, The Interscience Encyclopedia, Inc., New York, N. Y., 1949, pp. 881-897.

(27) "Cabot Carbon Blacks Under the Electron Microscope," 2nd Edition, Godfrey L. Cabot, Inc., Boston, Mass.

with increasing deposition temperature to a maximum and then decrease with a further temperature increase. The temperature at which the surface area reaches its maximum value for a particular carbon monoxide-hydrogen mixture is less than the temperature at which the crystallite height of the carbon reaches its maximum value. It is seen that the maximum specific surface area obtained generally increases with an increase in the percentage of hydrogen in the carbon monoxide, but the effect is not as marked as in the case of the crystallite height data.

Table III presents data on the effect of temperature of formation and carbon monoxide-hydrogen composition on the atomic carbon-hydrogen ratio of the carbon produced. For a given gas mixture, the amount of hydrogen in the carbon²⁸ markedly decreases as the formation temperature increases. At lower formation temperatures, the amount of hydrogen in the carbon also increases with an increase in the amount of hydrogen in the inlet gas mixture; but this effect becomes small at temperatures above 602°. If the hydrogen were chemisorbing on the edges of the carbon crystallites, it would be predicted that the hydrogen content in the carbon would decrease with increasing crystallite size. Qualitatively, this fact is suggested at formation temperatures below 576° by comparing the data in Tables I and III; but the correlation doubtless is complicated by the effect of temperature and hydrogen concentration on the extent of hydrogen chemisorption on carbon. Assuming that the fraction of edge atoms on the carbon crystallite which will be occupied by hydrogen is a maximum at the lowest carbon formation temperature, 470°, and taking a crystallite size of $L_c = 62 \text{ \AA}$. and $L_a = 124 \text{ \AA}$.³⁰ an atomic C-H ratio of 12.5 is calculated, if two atoms of hydrogen are assumed, on the average, to occupy an edge carbon atom.³¹ This is in good agreement with the experimental atomic C-H ratios for the carbons produced at 470°.

Table IV presents data on the effect of temperature of formation and carbon monoxide-hydrogen composition on the electrical resistivity of the carbons under a pressure of 2500 p.s.i.a. The effect of formation temperature on the electrical resistivity of the carbon is seen to be a function of the hydrogen content in the gas mixture. For hydrogen contents below 5.2%, the electrical resistivity is seen to decrease monotonically with increasing temperature of formation. For the carbons produced from gas mixtures containing 39.8 and 65.9% H₂, the electrical resistivity is clearly seen to go through a maximum at a formation temperature of ca. 528°. At a particular formation temperature, the electrical resistivity is seen to increase, with a few exceptions, with increasing

hydrogen content in the gas mixture to a maximum at 39.8% H₂ and then to decrease.

TABLE IV

EFFECT OF CARBON MONOXIDE-HYDROGEN COMPOSITION AND TEMPERATURE ON THE ELECTRICAL RESISTIVITY OF CARBONS FORMED BY CARBON MONOXIDE DECOMPOSITION OVER CARBONYL IRON

Formation temp., °C.	Electrical resistivities, ohm cm. $\times 10^3$, of carbons under a pressure of 2500 p.s.i.a. produced from various carbon monoxide-hydrogen mixtures						
	0.8% H ₂	2.2	5.2	9.0	19.9	39.8	65.9
470	8.90	14.0	17.3
500	8.54	13.3	16.9	..	22.3	21.6	12.6
528	..	12.0	.. ^a	15.4	..	27.5	22.4
576	5.71	6.9	12.7	12.3	15.9	23.0	18.9
602	5.67	4.1	8.0	..	11.4	18.4	12.3
630	5.3	6.1	9.1	7.4
700	4.9	7.3	..

TABLE V

CHANGE OF PROPERTIES OF CARBONS WITH WEIGHT FORMED FROM A 99.2% CO-0.8% H₂ MIXTURE AT 528° OVER 0.1 GRAM OF CARBONYL IRON

Carbon formed, g.	L_c , Å.	Interlayer spacing, Å.	Surface area, m. ² /g.	C/H	Electrical resistivity, ohm cm. $\times 10^3$ at 2500 p.s.i.a.
0.09	145	3.365	83	8.5	<i>a</i>
0.92	124	3.370	110	25.3	10.3
2.05	110	3.374	117	18.5	11.6
3.39	94	3.383	131	16.3	10.5
4.63	97	3.384	143	17.3	9.1
6.87	87	3.384	144	18.2	8.7

^a Insufficient sample.

The electrical resistivities of these carbons are considerably less than that of a widely used channel black, Spheron 6 (resistivity of 2.4 ohm cm. and a surface area of 95 m.²/g.), somewhat less than that of a second channel black, Excelsior (resistivity of 0.25 ohm cm. and a surface area of 210 m.²/g.), and comparable to that of acetylene black (resistivity of 0.09 ohm cm. and a surface area of 64 m.²/g.)

The electrical resistivity of the carbon would be expected to increase with an increase in surface area, a decrease in size and orientation of the crystallites, and an increase in hydrogen content.³² Comparing these properties with the resistivity data, it is seen that for carbons produced at different temperatures from gas mixtures containing less than 9.0% H₂, variations in the hydrogen content of the carbons appear to have the dominant effect on the electrical resistivity. Both the surface area and crystallite size data go through maximum values with increasing formation temperature—a trend which is not found for the resistivity data. For the carbons produced from the gas mixture containing 19.9% H₂, both the change in surface area and C-H ratio are in the proper direction to explain the electrical resistivity data. For carbons produced from gas mixtures containing 39.8 and 65.9% H₂, the resistivity appears to be primarily determined by the surface area of the carbon, the electrical resistivity and surface area reaching their maximum values at the same temperature.

(28) It is calculated²⁸ that the amount of hydrogen chemisorbed on the catalyst constitutes a negligible part of the hydrogen present.

(29) H. H. Podgurski and P. H. Emmett, *THIS JOURNAL*, **57**, 159 (1953).

(30) It was approximated from the (112) X-ray diffraction peak of the carbons that the crystallite diameter is roughly twice the crystallite height.

(31) R. H. Savage, *Ann. N. Y. Acad. Sci.*, **63**, 862 (1951).

(32) H. T. Pinnick, *Proceedings of the Conferences on Carbon*, U. of Buffalo, 1956, p. 3.

For carbons produced at the same formation temperature up to 576°, the increase of electrical resistivity with increase in hydrogen content in the gas mixture primarily parallels the decrease in the C-H ratio. However, at formation temperatures of 602, 630 and 700°, a change in electrical resistivity with an increase in hydrogen content in the inlet gas mixture occurs in spite of the relative constancy of the surface area and C-H ratio data. This suggests that the crystallite size of the carbon also is affecting its electrical resistivity, even though its effect is masked by variations in C-H ratio and surface area for many of the other data.

If the electrical resistivity were determined primarily by scattering of electrons at crystallite boundaries, it would be expected that the electrical resistivities of the carbons would decrease with increase in crystallite size. That this is not the case is best seen by two examples. At a temperature of 630°, carbons formed from gas mixtures containing 9.0% or more hydrogen have very similar surface areas and C-H ratios. For these carbons, electrical resistivity increases as crystallite size increases. The carbons prepared at 470° from a gas mixture containing 0.8% H₂ and at 576° from a gas mixture containing 39.8% H₂ have almost identical C-H ratios and surface areas, and yet the electrical resistivity of the carbon prepared at 576° is 2.6 times that of the carbon prepared at 470°. The crystallite height of the carbon prepared at 576° is 2.3 times as great as that prepared at 470°. It is suggested, therefore, that the crystallite size of the carbon is not affecting the resistivity primarily by scattering of electrons at crystallite boundaries but is determining the number of positive holes formed by π electrons jumping from the π band into the σ state, forming a spin pair at the edge of the crystallite.³² For equal C-H ratios, the percentage of edge carbon atoms having their unshared electrons satisfied by the formation of a spin pair would increase as the crystallite size decreases. This in turn would increase the positive hole concentration within the crystallite and result in a decrease in electrical resistivity with a decrease in crystallite size, as is found in the two examples cited above. In conclusion, then, it can be said that the electrical resistivities of the carbons appear to be a complex function of surface area, C-H ratio, and crystallite size, with variations in C-H ratio having the dominant effect on the electrical resistivities of most of the carbons produced.

Table V presents data on the change of properties of the carbon with weight formed from a 99.2% CO-0.8% H₂ mixture at 528° over 0.1 g. of carbonyl iron. The maximum amount of carbon formed, 6.879 g., represents that formed under the above conditions before the catalyst was completely deactivated. It is seen from the crystallite size and interlayer spacing data that there is a marked decrease in crystalline character of the carbon during the early stages of carbon formation. When the concentration of iron in the carbon becomes less than ca. 3%, there is little further change in crystalline character observed.

With increasing amounts of carbon formed, the specific surface area increases, becoming essentially

constant when the iron concentration in the carbon becomes less than ca. 2%. Some of the sharp, initial rise in surface area probably is caused by the decrease in percentage of iron (with its lower specific surface area) in the sample; but with the decrease in particle size of the iron during carbon formation, the extent to which the iron affects the over-all surface area is not known. A close parallel between the decrease in crystallite size and increase in surface area is found, suggesting that a significant part of the crystallite area is available to the adsorbate. This is confirmed, for example, for the 6.87-g. carbon sample (Table V) where the surface area of a crystallite 87 Å. in height and 174 Å. in diameter is ca. 200 m.²/g., as compared to the B.E.T. area of 144 m.²/g., or an area ratio of only 1.39. In comparison to this, a non-porous commercial carbon black, such as P-33 has a crystallite area ($L_c = 17$ Å. and $L_a = 28$ Å.²⁰) of ca. 1300 m.²/g. and a B.E.T. area of 15 m.²/g.,²⁰ or an area ratio of 87, indicating the small extent to which the crystallite surfaces are available to the adsorbate.

The C-H data, in Table V, for small amounts of carbon formed are not understood, but are seen to reach an essentially constant value when the iron concentration in the carbon becomes less than ca. 5%. The electrical resistivities of the carbon, as a function of amount produced, show relatively little change, suggesting that the effects which surface area and crystallite size changes may have on electrical resistivity are counterbalancing each other.

The effect of several other operating variables on the properties of the carbon produced by carbon monoxide decomposition were investigated. It was found that varying pretreatment times in hydrogen at 528°, no pretreatment, or precarbiting with carbon monoxide at 359° had minor effects on the crystallite size of an equal weight of carbon produced at 528°. A 20-fold decrease in the carbon monoxide volume flow rate, from that which was usually used, resulted in an increase in the crystallite size, a decrease in the surface area, little change in the C-H ratio, and an increase in the electrical resistivity of the carbon formed.

Properties of the Carbon Produced by Decomposition of a Carbon Monoxide-Hydrogen Mixture over "Sinter B."—Carbon was produced by the decomposition of a 99.2% CO-0.8% H₂ mixture at 528° over 0.1-g. samples of the raw and reduced (H₂ pretreatment for one hour at 528°) "Sinter B." Table VI presents data on the crystallite size and interlayer spacing of the carbon formed over two particle sizes of "Sinter B," with the weight of carbon reported being the amount produced before complete deactivation of the catalyst in each case. For equal weights of carbon formed, the crystallite height of the carbon produced over the reduced "Sinter B" catalyst compares closely with that of the carbon (105 Å.) produced over the reduced carbonyl iron. The interlayer spacings of the carbon formed over the reduced "Sinter B" are slightly higher than that of the carbon formed over the reduced carbonyl iron, indicating a smaller degree of three-dimensional ordering in the carbon.²³ The crystallite heights of the carbons formed over the raw "Sinter B," are substantially

smaller than that of the carbon (120 Å.) formed over the reduced carbonyl iron catalyst, for the same weight of carbon produced. The interlayer spacings of the carbon formed over the raw "Sinter B" are substantially higher than that of the carbon formed over the reduced carbonyl iron. It is seen that for either the raw or reduced "Sinter B" catalyst, reduction in catalyst particle size, within limits, has essentially no effect on the crystallite size or interlayer spacing of the carbon produced.

It is apparent from the results given in Table VI that reduction of an iron catalyst, high in oxygen, prior to carbon deposition can affect the crystalline character of the carbon formed. On the other hand, for iron catalysts low in oxygen, such as carbonyl iron, use of a raw or reduced catalyst has been found to have a minor effect on crystalline character of the carbon, as previously discussed.

TABLE VI

AVERAGE CRYSTALLITE HEIGHT AND INTERLAYER SPACING OF CARBONS FORMED FROM A 99.2% CO-0.8% H₂ MIXTURE AT 528° OVER 0.1-GRAM SAMPLES OF RAW AND REDUCED "SINTER B" CATALYST

Mesh size of "Sinter B"	Catalyst treatment	Carbon produced, g.	L _c , Å.	d-spacing, Å.
80-100	Reduced	2.42	100	3.382
-100	Reduced	2.24	91	3.387
80-100	Raw	1.15	84	3.390
-100	Raw	1.23	81	3.392

TABLE VII

CHANGE IN CHEMICAL COMPOSITION OF A CARBON PRODUCED AT 528° FROM A 98.6% CO-1.4% H₂ MIXTURE AFTER ACID TREATMENTS

Treatment	Purif. time, hr.	C	Anal. of carbon, wt. %		Diff.
			H	Fe	
None ^a	None	94.24	0.29	5.40	0.07
HCl	2.8	97.39	.57	0.40	1.64
HCl	8.0	97.34	.53	.35	1.78
HNO ₃	8.0	88.60	.84	.24	10.32
HF	2.0	97.57	.45	.38	1.60

^a Original material.

TABLE VIII

EFFECT OF HEAT TREATMENT ON A TYPICAL PETROLEUM COKE AND A CARBON PRODUCED AT 528° FROM A 98.6% CO-1.4% H₂ MIXTURE OVER CARBONYL IRON

Sample	Temp., °C.	L _c , Å.	d-spacing, Å.	Ash content
CO carbon	528	144	3.373	5.40
CO carbon	2500	217	3.373	0.15
CO carbon	3000	269	3.371	0.08
Petroleum coke	ca. 1000	34	3.482	0.32
Petroleum coke	3000	840	3.362	0.03

Acid Treatment of Raw Carbons.—The carbon made by the decomposition of carbon monoxide over iron has a certain percentage of iron impurity present depending upon the extent of carbon formation. It was desirable to investigate the ease with which the iron and/or iron compounds could be removed by acid treatment and the effect of such treatment on the properties of the carbon formed over carbonyl iron powder. In all cases, the amount of acid added to the carbon represented a considerable excess over that required to com-

bine with the iron present. Table VII presents data on the change in chemical composition of a carbon produced at 528° from a 98.6% CO-1.4% H₂ mixture upon acid treatment. The percentage iron reported was obtained by weighing the ash (Fe₂O₃) at the end of an analysis and converting it back to iron. It is seen that the raw carbon essentially contains only carbon, hydrogen and iron. Acid treatment substantially reduces the percentage of iron in the carbon, but even the rather severe treatments used are found not to remove the iron completely.³³ Electron micrographs of the acid-treated carbon almost invariably show the removal of iron and/or iron compounds from the tip of the carbon filaments. X-Ray diffraction patterns of the above carbon clearly show the complete removal of strong Fe₃C peaks after acid treatment.

Concurrent with the removal of iron from raw carbon it is seen from Table VII that acid treatment increases the percentage of hydrogen and other elements present in the carbon. To be particularly noted is the 10% of other elements present in the carbon after nitric acid treatment—probably existing primarily as peripheral carboxyl, carbonyl and hydroxyl groups. Considering the extensive washing of the acid-treated carbons, it is not likely that the increase in other elements after HCl and HF purification is caused primarily by adsorption of these species (HCl or HF) on the carbon surface, but probably is caused by formation of chlorine and fluorine surface complexes. After purification with HCl or HF, the carbon was washed easily in the filtering apparatus, with the water flowing through the fritted disc at a good rate. By comparison, after purification with HNO₃, the water flowed through the fritted disc extremely slowly. Qualitatively, purification with HCl or HF did not change the appearance or texture of the carbons, whereas, after HNO₃ purification, the carbon had agglomerated considerably and had changed from a soft to an extremely hard material. X-Ray diffraction studies showed that there was no appreciable change in crystallite size or interlayer spacing of the carbon following purification with any of the acids used.

Heat Treatment of the Carbon.—It was of interest to investigate the effect of heat treatment of the carbon on the extent of its purification and crystallite size growth. Samples of carbon produced at 528° from a 98.6% CO-1.4% H₂ mixture were heat treated at 2500 and 3000°. For comparison, a sample of petroleum coke, produced by conventional delayed coking procedures,³⁴ also was heat treated, at the same time, to 3000°. Table VIII shows that the petroleum coke is considerably more graphitizable than the carbon produced from the carbon monoxide-hydrogen mixture despite its much poorer crystalline character in the raw state. The superior graphitizing character of the petroleum coke is in line with its low

(33) In other runs not reported, it is found that there is always a small amount of residual iron left after acid treatment which cannot be removed, independent of the percentage of iron in the raw carbon.

(34) H. W. Abbott, "Encyclopedia of Chemical Technology," Vol. 3, The Interscience Encyclopedia, Inc., New York, N. Y., 1949, pp. 1-23.

surface area (0.8 m.²/g.) as compared to that of the carbon from the carbon monoxide-hydrogen mixture (120 m.²/g.), agreeing with the findings of Schaeffer and co-workers²⁰ on the effect of surface area on graphitizability for a series of carbon blacks. As expected, heat treatment to 2500° and above is effective in removing the majority of the impurities from the carbons.

Conclusions

Carbons formed from various carbon monoxide-hydrogen mixtures over iron catalysts are highly crystalline, considering the relatively low formation temperatures at which they can be produced. For each carbon monoxide-hydrogen mixture used, the crystallinity of the carbon shows a maximum in the temperature range of ca. 576 to 630°. The

maximum crystallite height of the carbon increases with increasing hydrogen content in the gas mixture, at least up to 19.9% H₂. The specific surface areas of the carbons show a maximum in the temperature range of ca. 500 to 576°. The atomic C-H ratio of the carbons is found to increase monotonically with increasing formation temperatures over the entire temperature range for each carbon monoxide-hydrogen mixture investigated and to decrease with increasing amounts of hydrogen in the gas mixture up to formation temperatures of ca. 600°. The electrical resistivity of the carbons is found to be a complex function of their crystallinity, surface area and C-H ratio. The properties of the carbon are found to be affected by the amount formed over the iron catalyst; in particular the crystallinity decreases markedly with increasing amount formed.

CARBON FORMATION FROM CARBON MONOXIDE-HYDROGEN MIXTURES OVER IRON CATALYSTS.^{1,2} II. RATES OF CARBON FORMATION

BY P. L. WALKER, JR., J. F. RAKSZAWSKI AND G. R. IMPERIAL

*Department of Fuel Technology
The Pennsylvania State University, University Park, Pennsylvania*

Received April 8, 1968

The effect of temperature and inlet carbon monoxide-hydrogen composition on the rate of carbon formation and amount of carbon which can be formed over iron catalysts before the catalysts are deactivated has been investigated. As the hydrogen content of the gas mixture is increased, the temperature at which the maximum rate of carbon deposition occurs also increases, this temperature ranging from ca. 528° for a 99.2% CO-0.8% H₂ mixture to ca. 630° for a 80.1% CO-19.9% H₂ mixture. Change in mixture composition has a relatively small effect on rate of carbon deposition or total amount of carbon which can be formed from a given catalyst weight at lower temperatures (470 to 528°) but has a major effect at higher temperatures (above ca. 576°). At the higher temperatures, the maximum rate of carbon formation increases with increasing hydrogen content in the gas up to a point and then decreases. Also, increases in hydrogen content in the gas markedly increase the total amount of carbon which can be formed before catalyst deactivation occurs. The type of catalyst pretreatment and nature of catalyst used is also seen to affect carbon deposition. A spent catalyst consists primarily of cementite. Upon hydrogen treatment the cementite is converted to iron and the spent catalyst is reactivated for additional carbon production. It is proposed that iron, on which carbon monoxide can chemisorb and dissociate, is the active catalyst for carbon deposition and that complete conversion of iron to cementite, on which carbon monoxide cannot chemisorb at elevated temperatures, is responsible for stopping carbon deposition.

Introduction

There is general agreement in the literature that the rate of carbon formation from carbon monoxide decomposition over iron catalysts is significant between ca. 400 and 750°, with the maximum rate occurring between 500 and 600°.³⁻⁸ Considerable uncertainty exists, however, as to why the rate of carbon deposition decreases above ca. 600°, but it is known not to be caused by equilibrium in the

reaction $2\text{CO} \rightleftharpoons \text{C} + \text{CO}_2$. Some explanations offered for this diminution in rate are decreasing chemisorption of carbon monoxide on the catalyst,³ beginning of appreciable catalyst sintering,^{4,7} and absence of carbide formation.⁸ There is some suggestion that the rate of carbon formation increases again at higher temperatures (850°),⁹ but this has not been well confirmed.

It has been shown that the addition of small amounts of sulfur compounds to carbon monoxide greatly retards the decomposition of the latter over iron.^{5,8,10-13} Also, selected nitrogen compounds, particularly cyanogen and ammonia, have been shown to be powerful retarders of carbon deposition.^{8,11,12} On the other hand, hydro-

(1) Based, in part, on an M.S. thesis submitted by G. R. Imperial to the Graduate School of the Pennsylvania State University, August, 1957.

(2) At different stages, this work was supported by the Reading Anthracite Company and the Atomic Energy Commission under Contract No. AT(30-1)-1710.

(3) W. Baukloh and B. Edwin, *Arch. Eisenhuttene.*, **16**, 197 (1942).

(4) Francois Olmer, *THIS JOURNAL*, **46**, 405 (1942).

(5) G. I. Chufarov and M. F. Antonova, *Bull. acad. sci. U.R.S.S., Classe sci. tech.*, 381 (1947).

(6) W. Baukloh, B. Chatterjee and P. P. Das, *Trans. Indian Inst. Metals*, **4**, 271 (1950).

(7) B. Fleureau and A. Sancelme, *Compt. rend.*, **235**, 801 (1952).

(8) T. F. Berry, R. N. Ames and R. B. Snow, *J. Am. Ceram. Soc.*, **39**, 308 (1956).

(9) J. Taylor, *J. Iron Steel Inst. (London)*, **184**, 1 (1956).

(10) T. Watanabe, *Bull. Inst. Phys. Chem. Research (Tokyo)*, **7**, 1078 (1928).

(11) W. Baukloh and G. Henke, *Metallwirtschaft*, **19**, 463 (1940).

(12) S. Klemantaski, *J. Iron Steel Inst. (London)*, **171**, 176 (1952).

(13) B. Chatterjee and P. P. Das, *J. Sci. Ind. Research (India)*, **15B**, 412 (1956).

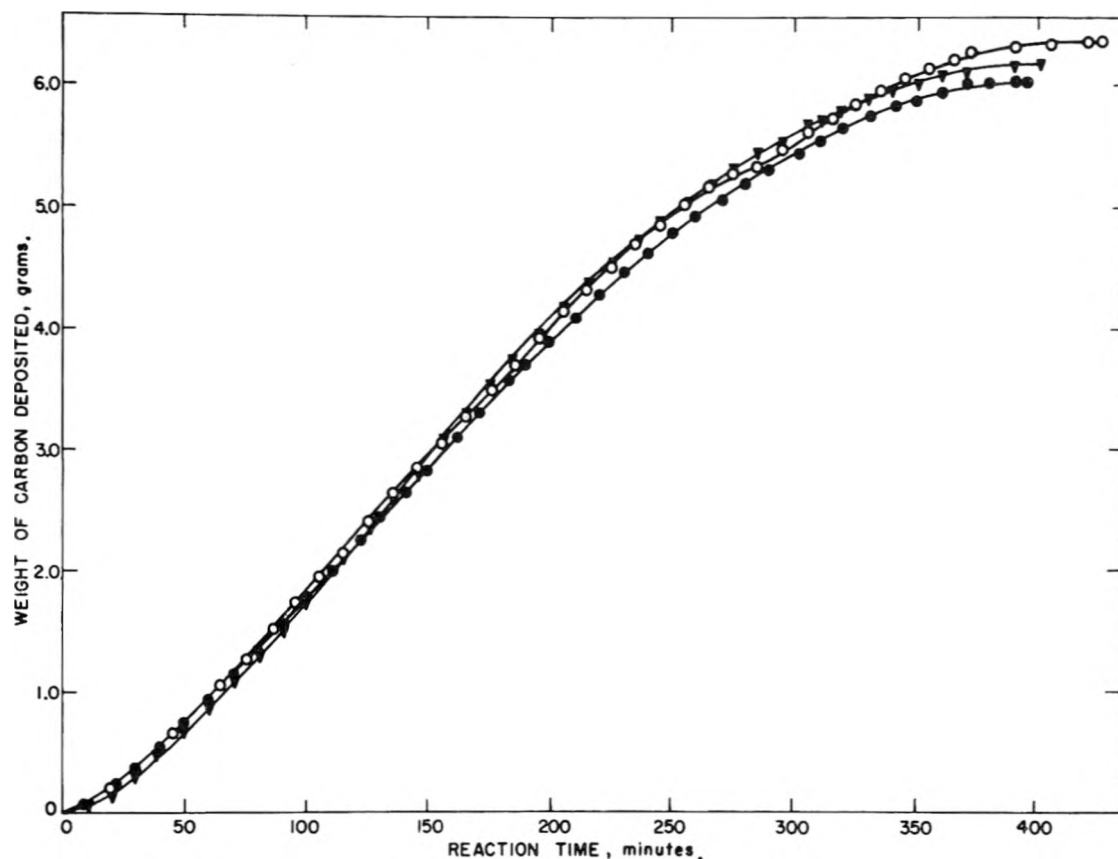


Fig. 1.—Three typical rate curves showing carbon formation from a 98.6% CO-1.4% H₂ mixture over 0.10 g. of reduced carbonyl iron at 576°.

gen has been shown to be an accelerator of carbon monoxide decomposition over iron catalysts.^{8,12,14,15} Water vapor has been found to both accelerate^{8,14} and retard¹¹ carbon monoxide decomposition.

There is considerable disagreement as to what the active form of the iron catalyst is in the decomposition of carbon monoxide, but it is generally agreed that an oxide of iron alone is not the active catalyst. Various investigators have attributed the catalytic activity to one or more of the carbides of iron (Fe₂C, Fe₃C, Fe₂₀C₉),^{8,16-18} to metallic iron,^{6,19,20} or to the iron-iron oxide interface.⁹ This disagreement as to the active catalyst is caused primarily by the concurrent production of free carbon and carbidic carbon, which raises the question as to whether or not the carbidic carbon is a precursor of the free carbon.

In this research, a detailed investigation of the effect of hydrogen on the rate of carbon deposition from carbon monoxide-hydrogen mixtures was conducted. This involved, in many cases, the obtaining of rate data until the deposition of carbon

ceased, since it was of interest to know not only the maximum rate of carbon deposition but also the amount of carbon which could be formed from a starting catalyst weight. Other factors affecting the rate of carbon deposition which were investigated include catalyst pretreatment, gas flow rate past the catalyst, different starting catalyst materials and reactivation of a spent catalyst. Experimental details describing the apparatus, the catalysts used, and operating procedures have been included in an accompanying paper,²¹ which presents the properties of the carbons formed from the carbon monoxide-hydrogen mixtures used in this paper.

Results

Determination of Carbon Deposition Rate.—As was discussed,²¹ the cumulative weight of carbon formed during a run was determined from the cumulative volumes of gas passing through the wet test meters before and after the reactor. Before the gas entered the exit wet test meter, it was passed through an Ascarite tower to remove carbon dioxide. The gas was saturated with water prior to entering both wet test meters. From the difference in gas volumes between the entering and exit wet test meters, the amount of carbon formed was calculated (predicted), assuming the difference in volumes to be caused by only two reactions, $2\text{CO} \rightarrow \text{C} + \text{CO}_2$ and $\text{CO} + \text{H}_2 \rightarrow \text{C} + \text{H}_2\text{O}$. For both of these reactions, the wet-test-meter readings indicate a decrease of two moles of gas for each mole of carbon formed. For this calculation the extent of the water-gas shift reaction, $\text{CO} + \text{H}_2\text{O} \rightleftharpoons \text{H}_2 + \text{CO}_2$, is unimportant.

This simplified approach to determining the carbon deposition rate is incorrect insofar as reactions producing hydro-

(14) W. A. Bone, H. L. Saunders and H. J. Tress, *J. Iron Steel Inst. (London)*, **137**, 85 (1938).

(15) W. Baukloh and E. Spetzler, *Arch. Eisenhüttenw.*, **13**, 223 (1939).

(16) H. Tutiya, *Sci. Papers Inst. Phys. Chem. Research (Tokyo)*, **10**, 69 (1929).

(17) U. Hofmann and E. Groll, *Z. anorg. allgem. Chem.*, **191**, 414 (1930).

(18) W. R. Davia, R. J. Slawson and G. R. Rigby, *Trans. Brit. Ceram. Soc.*, **56**, 67 (1957).

(19) A. P. Lyuban, *Stal*, **7**, 199 (1947).

(20) B. Chatterjee and P. P. Das, *Nature*, **173**, 1046 (1954).

(21) P. L. Walker, Jr., J. F. Rakszawski and G. R. Imperial, *This Journal*, **63**, 133 (1959).

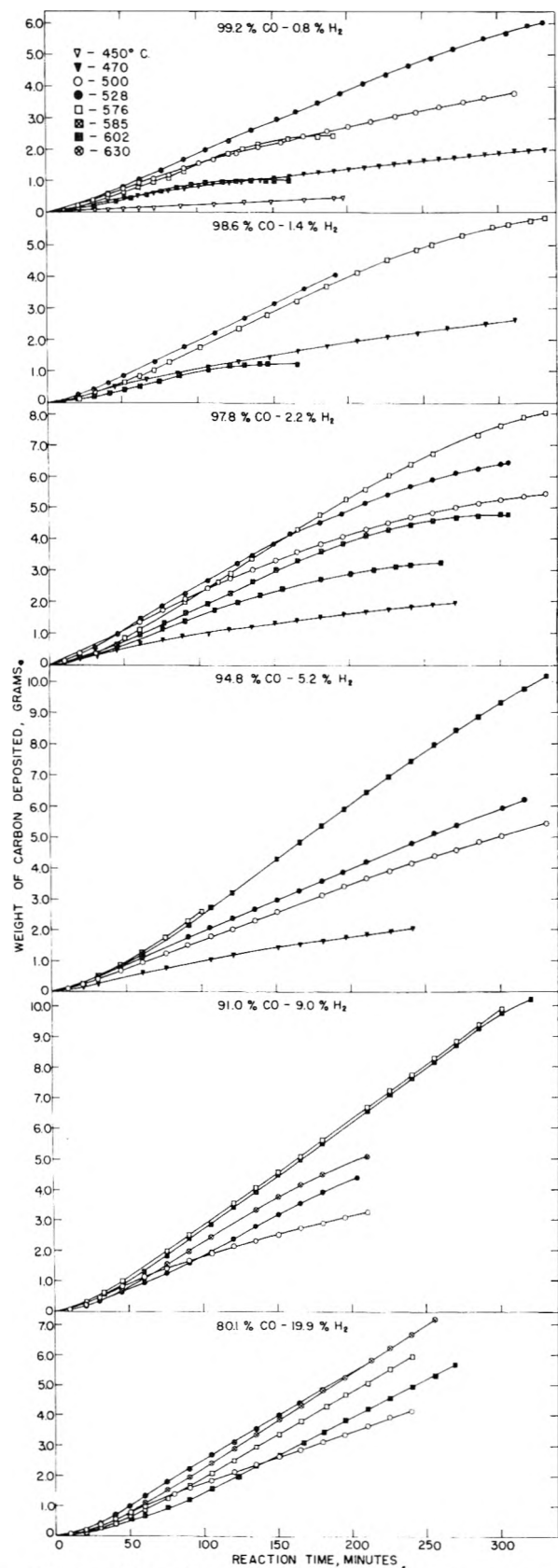


Fig. 2.—Effect of variation in temperature on carbon deposition for different CO-H₂ mixtures over 0.10 g. of carbonyl iron.

carbons cause errors in the predicted amount of carbon formed. The reaction of hydrogen with free and carbidic

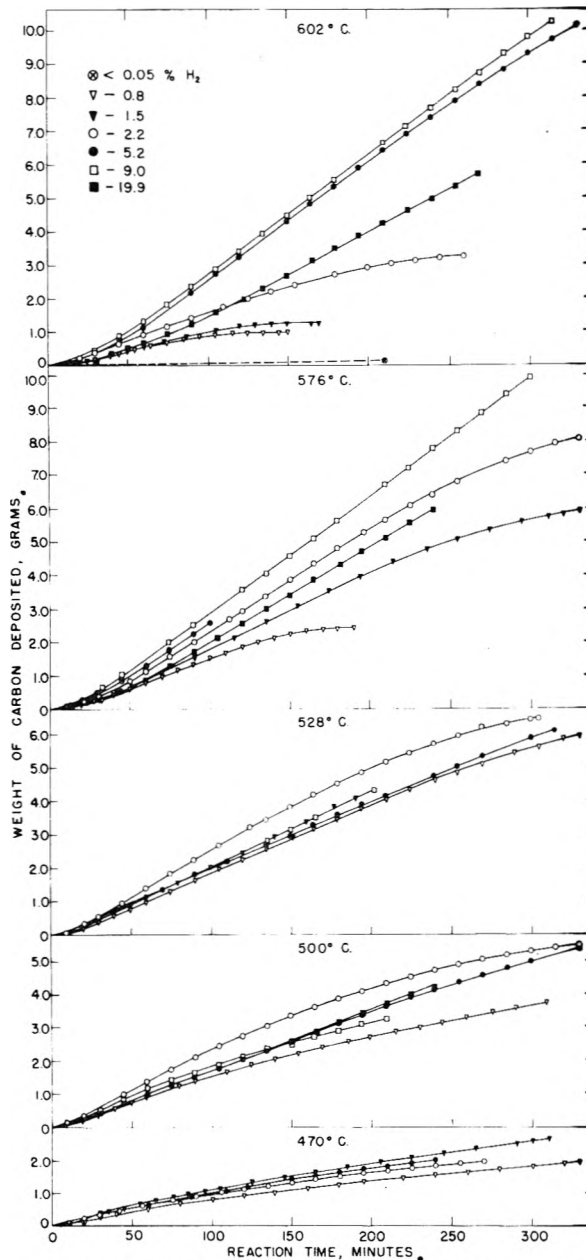


Fig. 3.—Effect of variation in carbon monoxide-hydrogen composition on carbon deposition at different temperatures over 0.10 g. of carbonyl iron.

carbon to produce methane ($C + 2H_2 \rightarrow CH_4$) and the reaction $CO + 3H_2 \rightarrow CH_4 + H_2O$ are the most likely to produce errors. In addition, the chemisorption of hydrogen at the edges of the carbon crystallites will produce a decrease in gas volume which is not attributable to carbon formation. Results show, however, that for gas mixtures containing less than 40% hydrogen, extraneous reactions have relatively little effect on distorting the true picture of carbon deposition, with agreement between predicted and actual amounts of carbon formed invariably being within 10%. Considering the large variations in carbon deposition rates found for different gas mixtures, temperatures and catalysts, the above agreement is quite satisfactory to allow major conclusions to be made.

Figure 1 presents data for the rate of carbon deposition from a 98.6% CO-1.4% H₂ mixture over 0.10 g. of carbonyl iron²¹ at 576°. The gas flow rate was 5.8 cc./sec. (STP) and the catalyst was pretreated in hydrogen, as previously described.^{21,22} The shape of the deposition curves is typical

(22) These conditions were used throughout the work unless otherwise specified.

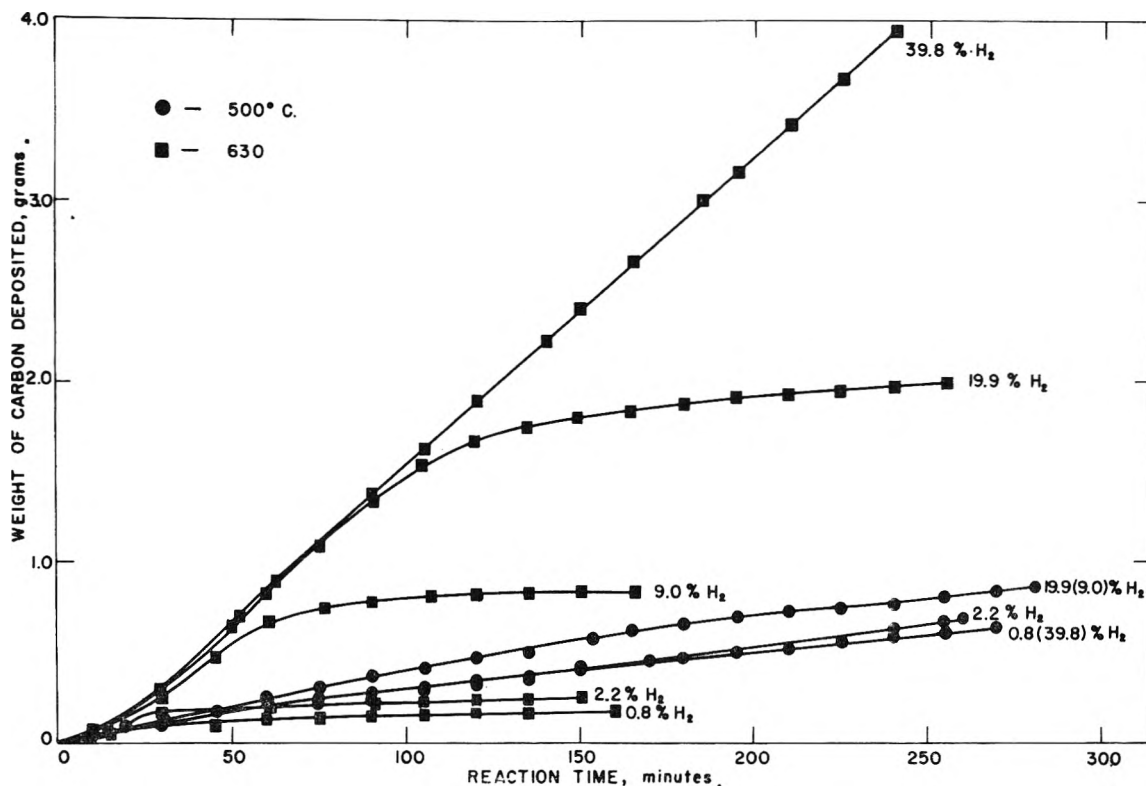


Fig. 4.—Effect of variation in carbon monoxide-hydrogen composition on carbon deposition at 500 and 630° over 0.02 g. of carbonyl iron.

of those usually found—an initial induction period, a period of essentially constant rate of carbon deposition and a period of decreasing rate of carbon deposition until deposition completely stops. The agreement between runs, as shown in Fig. 1, is also fairly typical, with the maximum deposition rates varying by *ca.* $\pm 3\%$. The predicted weights of carbon formed in the runs, 6.05, 6.15 and 6.47 g., can be compared with the weights actually obtained, 5.94, 6.18 and 6.27 g., respectively. The final carbons contain *ca.* 2% iron by weight.

Effect of Variation in Carbon Monoxide-Hydrogen Composition on Carbon Deposition at Different Temperatures.—Figures 2 and 3 present the results of carbon deposition as a function of gas composition and temperature. From Fig. 2, it is seen that as the hydrogen content of the gas mixture is increased, the temperature at which the maximum rate of carbon deposition occurs also increases, it ranging from *ca.* 528° for the 0.8% H_2 mixture to *ca.* 630° for the 19.9% H_2 mixture. Also, the deposition temperature is seen to affect markedly the total amount of carbon which can be produced from a starting catalyst weight. For example, for the gas mixture containing 0.8% H_2 , carbon deposition has stopped after formation of 2.4 and 1.0 g. of carbon at 576 and 602°, respectively; whereas at the temperature of 528°, 6.0 g. of carbon has been deposited with deposition still continuing. It is seen that increasing the hydrogen content of the gas mixture markedly increases the amount of carbon which can be formed from a given catalyst weight, particularly at the higher temperatures. For hydrogen contents of 5.2% or greater, the reaction at all temperatures had to be discontinued before carbon deposition had ceased because of either plugging of the reactor with carbon or undue duration of a reaction run.

Figure 3 clearly shows the effect of increasing the hydrogen content in the gas mixture on carbon deposition rates at particular temperatures. It is seen that a change in gas composition has a relatively small effect on maximum rate of carbon deposition or amount of carbon which can be formed at the lower temperatures (470 to 528°) but has a major effect at the higher temperatures (above 576°). At the higher temperatures it is seen that the maximum rate of carbon formation increases with increasing hydrogen content in the gas up to a point and then decreases. Also at the higher temperatures, increasing additions of hydrogen to the gas markedly increase the total amount of carbon which can be formed.

Of particular interest in Fig. 3 is the run made with a gas mixture containing less than 0.05% H_2 , which clearly shows the relatively high stability of carbon monoxide which is dry and low in hydrogen, even over iron.

In order to show more clearly the effect of change in mixture composition and temperature on the total amount of carbon which can be formed from a given catalyst weight, a series of runs were made using a starting weight of carbonyl iron of only 0.02 g. From Fig. 4, it is again seen that at a relatively low temperature (500°) variations in gas composition have little effect on the extent of carbon deposition and that the catalyst remains active to catalyze carbon deposition for extended periods.²³ Even for the gas mixture containing

(23) The deposition curves at 500° for 9.0 and 39.8% H_2 -containing mixtures are very similar to those for 19.9 and 0.8% H_2 -containing mixtures, respectively. The experimental points have been omitted from Fig. 4 to avoid confusion.

TABLE I

PREDICTION OF TOTAL AMOUNT OF CARBON FORMED FROM A 34.1% CO-65.9% H₂ MIXTURE USING DATA FOR THE AMOUNT OF WATER AND CARBON DIOXIDE ABSORBED FROM THE PRODUCT GAS

Reaction temp., °C.	Wt. H ₂ O absorbed, g.	Equiv. wt. C, g.	Wt. CO ₂ absorbed, g.	Equiv. wt. C, g.	Total pred. C wt., g.	Total exp. C wt., g.
528	1.165	0.777	0.443	0.121	0.898	0.779
576	1.988	1.325	3.158	.861	2.186	2.091
600	2.447	1.631	3.038	.828	2.459	2.370
630	1.462	0.975	1.597	.436	1.411	1.426

only 0.8% H₂, there is no indication of a decrease in rate of carbon deposition after 270 minutes. On the other hand, at a relatively high temperature (630°) increases in hydrogen content in the gas mixture are seen to have a major effect on the amount of carbon which can be formed. For example, the mixture containing 0.8% H₂ can produce only 0.16 g. of carbon, whereas the mixture containing 39.8% H₂ can produce more than 3.94 g. of carbon. Incidentally, for the 39.8% H₂ mixture the amount of carbon recovered after the run was 3.73 g. or only 5.6% less than predicted, which indicates the relative unimportance of side reactions of hydrogen in distorting the carbon formation picture.

For the mixture containing 65.9% H₂, agreement between the predicted and actual amounts of carbon formed was relatively poor, undoubtedly because of the reactions of hydrogen previously discussed. In this case the total weight of carbon formed was compared with the weight predicted from the amounts of water and carbon dioxide absorbed from the product gas stream, as shown in Table I. It is seen that the agreement in the weights is good at deposition temperatures of 576, 600 and 630°, indicating that the reaction $\text{CO} + 3\text{H}_2 \rightarrow \text{CH}_4 + \text{H}_2\text{O}$ is not occurring to a significant extent. On the other hand, agreement is less satisfactory at 528°, suggesting that the above reaction becomes a factor at the lower temperature.

If the reaction $\text{CO}_2 + \text{H}_2 \rightarrow \text{CO} + \text{H}_2\text{O}$ is not a significant factor in determining the composition of the product gas leaving the reactor, it is concluded, from Table I, that a larger portion of the carbon is formed as a result of the reaction $\text{CO} + \text{H}_2 \rightarrow \text{C} + \text{H}_2\text{O}$ rather than the reaction $2\text{CO} \rightarrow \text{C} + \text{CO}_2$ for the 34.1% CO-65.9% H₂ mixture. Unfortunately, for the other gas mixtures studied, the amounts of water and carbon dioxide absorbed from the product gas were not determined; but undoubtedly the relative amounts of carbon formed by the above two reactions is a function of the partial pressures of hydrogen and carbon monoxide and the extent of their chemisorption on the catalyst.

Effect of Operating Variables on the Deposition of Carbon from Carbon Monoxide-Hydrogen Mixtures. Catalyst Pretreatment.—The effect of catalyst pretreatment on the subsequent deposition of carbon at 576° from a 99.2% CO-0.8% H₂ mixture over 0.10 g. of carbonyl iron was studied briefly. Carbon deposition after reduction of the catalyst for one hour in hydrogen at 576° was compared with deposition over the unreduced catalyst and a catalyst which had been partially precarbided using carbon monoxide for three hours at 359°. ²⁴

Figure 5 presents the data with each deposition curve representing the average of two experimental runs. It is seen that pretreatment affects the three main regions of the deposition curve. Carbon deposition over the reduced catalyst is the most rapid during the early stages of the run. The maximum rate of carbon deposition occurs over the precarbided catalyst from ca. 30 to 50 minutes after the reaction has started. The maximum rate of carbon deposition over the reduced and unreduced catalysts is essentially the same. Pretreatment has a marked effect on the amount of carbon which can be produced from a given weight of catalyst, with the reduced catalyst producing ca. 30% more carbon than the unreduced catalyst and ca. 38% more carbon than the precarbided catalyst.

Carbon Monoxide-Hydrogen Mixture Flow Rate.—Figure 6 presents results on the effect of flow rate of a 97.8% CO-2.2% H₂ mixture on the deposition of carbon at 528° over 0.10 g. of carbonyl iron. From the rate of carbon formation in the region of constant deposition rate, it is calculated that the CO₂-CO ratio in the product gas ranged from ca. 2.5 to 12.5% of the equilibrium value as the flow rate was decreased from 5.80 to 0.29 cc./sec.

A plot of reaction rate, expressed as grams of carbon deposited per hour per atmosphere of average carbon monoxide pressure in the reactor, ²⁶ versus the gas flow rate shows a decreasing positive slope with increasing flow rate. This is the usual relation for a heterogeneous reaction which is being controlled to a significant extent by both chemical and mass-transport resistances. With increasing flow rate, the extent of rate control by mass transport resistance continuously decreases, until at a sufficiently high flow rate the reaction rate is independent of further increases in flow rate.

As seen in Fig. 6, changes in gas flow rate over the catalyst can affect not only the maximum rate of carbon formation but also the total amount of

(24) X-Ray diffraction studies of the carbided catalyst showed high concentrations of Fe₃C and Fe₂C (Hagg carbide). The amount of free carbon formed was negligible. During the time taken to heat the precarbided catalyst from 359° to reaction temperature in helium, the reactions $\text{Fe} + \text{Fe}_3\text{C} \rightarrow \text{Fe}_5\text{C}_3$ or $3\text{Fe}_3\text{C} \rightarrow 2\text{Fe}_5\text{C}_3 + \text{C}$ undoubtedly occurred. ²⁵ Furthermore, some decomposition of Fe₃C back to α-Fe and C would be expected. For example, after carbiding another sample of iron at 359° for 3 hours, heating it in helium to 600° and holding for one hour resulted in the conversion of the carbide back to α-Fe, as revealed by X-ray diffraction studies. Unfortunately an X-ray diffraction pattern was not taken after heating the precarbided catalyst to 576° prior to making the carbon deposition runs.

(25) H. H. Podgurski, J. T. Kummer, T. W. DeWitt and P. H. Emmett, *J. Am. Chem. Soc.*, **72**, 5382 (1950).

(26) The average concentration of carbon monoxide is calculated assuming all the carbon to be formed from the reaction $2\text{CO} \rightarrow \text{C} + \text{CO}_2$. This should be a reasonably good approximation, since the amount of hydrogen in the inlet gas mixture is low.

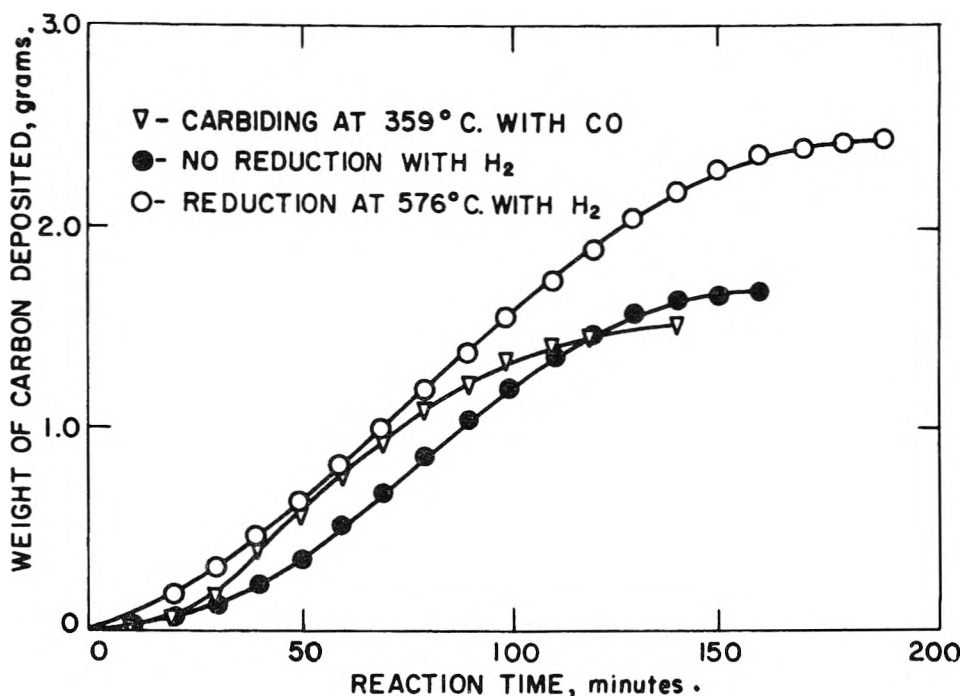


Fig. 5.—Effect of pretreatment of 0.10 g. of carbonyl iron samples on subsequent carbon deposition from a 99.2% CO-0.8% H₂ mixture at 576°.

carbon which can be formed. For a flow rate of 5.80 cc./sec., the rate of carbon deposition progressively decreases after production of *ca.* 3.5 g. of carbon and undoubtedly stops after formation of *ca.* 7 g. On the other hand, for a flow rate of 2.08 cc./sec., carbon deposition remains at a maximum rate up to *ca.* 7 g. of carbon formed and then decreases in rate very slowly, with the total amount of carbon which can be formed being considerably above 12 g.

Catalyst Type.—The rate of carbon deposition from a 99.2% CO-0.8% H₂ mixture at 528° over 0.10 g. of "Sinter B" catalyst was investigated. "Sinter B" is a sinter of fine iron-containing powder which comes from the top of open hearths and blast furnaces, as previously described.²¹ The carbon deposition rate was investigated over both the reduced (the same reduction procedure being used as for carbonyl iron) and the raw catalyst for two different particle sizes. As was found for carbon deposition over carbonyl iron, the initial rate of carbon deposition and the total amount of carbon which can be formed is appreciably greater over the reduced than over the raw catalyst. Also, in this case, the maximum deposition rate over the reduced catalyst is considerably greater than that over the raw catalyst. Change in particle size (representing a change in initial B.E.T. surface area from only 0.41 to 0.46 m.²/g.) is found to have a minor effect on rate of carbon deposition.

Comparison of carbon deposition over reduced "Sinter B" with that over reduced carbonyl iron under the same experimental conditions shows that the maximum carbon deposition rate over the carbonyl iron is *ca.* 25% higher. However, since the specific surface area of carbonyl iron²¹ is *ca.* twice that of the "Sinter B," the specific activity of "Sinter B," at the maximum carbon deposition rate, is higher. Total carbon production over

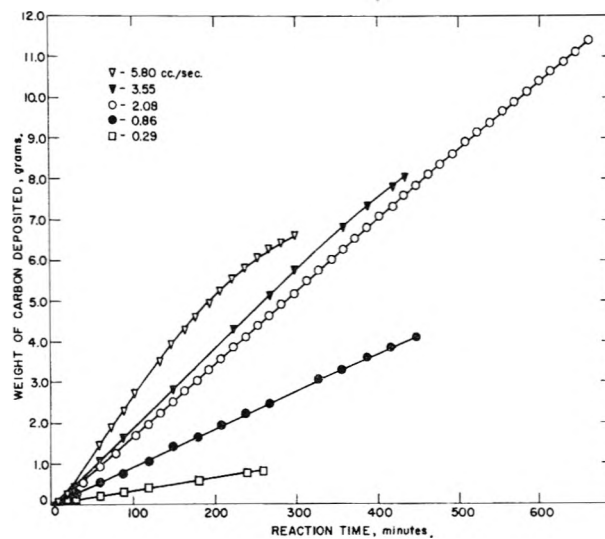


Fig. 6.—Effect of gas flow rate through reactor on carbon deposition from a 97.8% CO-2.2% H₂ mixture at 528° over 0.10 g. of carbonyl iron.

reduced "Sinter B" (2.3 g.) is found to be considerably less than over reduced carbonyl iron (greater than 6.0 g.).

The importance of a major difference in state of subdivision of the starting catalyst on its activity to formation of carbon from carbon monoxide-hydrogen mixtures has been brought out by using an iron rod, containing only 0.02% nickel as a major impurity, as a catalyst. The rod had an apparent density of 7.85 g./cc., agreeing well with the true density of iron, 7.86 g./cc., indicating negligible internal porosity. Following hydrogen reduction, a 98.6% CO-1.4% H₂ mixture was passed (5.80 cc./sec.) over a piece of the iron rod (5.1 mm. in diameter and 1 mm. long) for 230 minutes at 576°. A total weight increase of

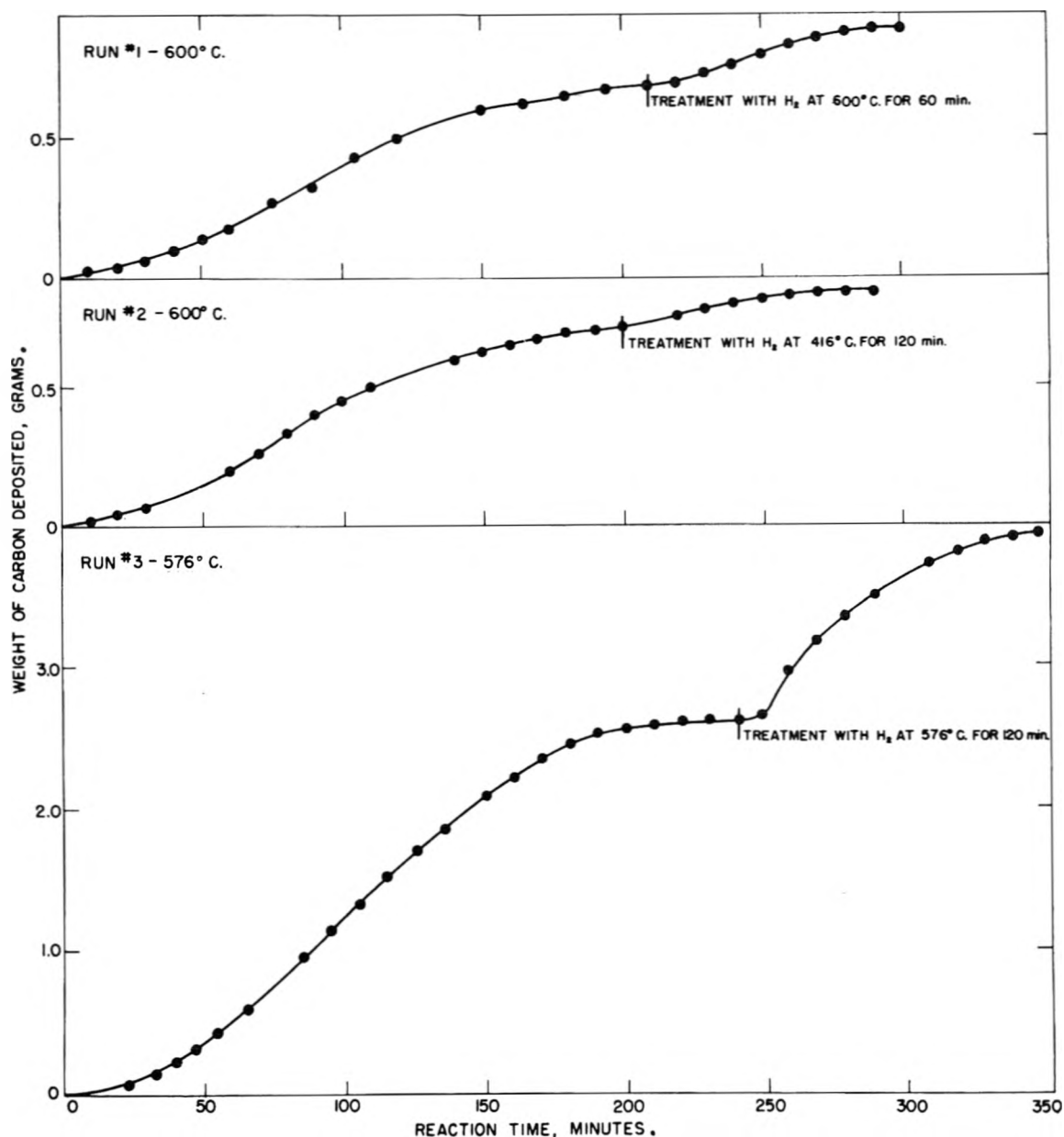


Fig. 7.—Reactivation runs on spent carbonyl iron catalyst using hydrogen following carbon deposition from 99.2% CO-0.8% H₂ mixture over 0.10 g. samples of carbonyl iron.

0.124 g., which would include both free and carbidic carbon, was found. The carbon, which was in the form of a thin film deposited over the rod, had a similar appearance in electron micrographs to that formed over carbonyl iron. Also, sub-micron particles of iron were located at the ends of the carbon filaments. The rate of carbon formation over the reduced iron rod, expressed as grams of carbon formed per 230 minutes per gram of starting catalyst weight, is 0.0305 in comparison to a carbon formation rate of 46.5 over the reduced carbonyl iron (Fig. 2). On the basis of activity per square meter of starting catalyst surface, however, if the surface area of the iron rod is taken as its geometric area, the rates of carbon formation are 304 and 47 over the iron rod and carbonyl iron, respectively. The greater specific activity of the iron rod is probably primarily a result of the reaction

being controlled to a lesser extent by mass transport resistance for the rod than for the carbonyl iron.²⁷

Reactivation of Spent Catalyst.—In an attempt to find the true catalyst for the carbon-deposition reactions, possible reactivation of the spent catalyst once carbon deposition had stopped was investigated. Figure 7 presents the results for three different runs in which the deposition of carbon from a 99.2% CO-0.8% H₂ mixture over an initial weight of 0.10 g. of reduced iron was studied. For runs 1 and 2, 0.39 and 0.25 g. of material were removed from the reactor for X-ray diffraction analysis after reaction times of 210 and 200 minutes, respectively. After these periods of reaction, it is seen that carbon deposition had practically stopped.

(27) A. Wheeler, "Advances in Catalysis," Vol. 3, Academic Press, Inc., New York, N. Y., 1951, pp. 249-327.

X-Ray diffraction patterns of the products, in both cases, showed strong peaks for cementite (Fe_3C) and carbon. No diffraction peaks were found for Fe_3O_4 , Fe_2O_3 or $\alpha\text{-Fe}$.²⁸ Since it is known that hydrogen readily converts Fe_3C to $\alpha\text{-Fe}$,^{29,30} possible reactivation of the spent catalyst by passing 6.5 cc./sec. of hydrogen through the reactor at different temperatures and for different times was attempted. For run 1, an additional 0.05 g. of the product was taken for X-ray diffraction analysis after hydrogen treatment. Analysis showed that the cementite present before treatment with hydrogen had been completely converted to $\alpha\text{-Fe}$. From Fig. 7, it is evident that hydrogen treatment reactivates the catalyst to a marked extent. Indeed, in run 3 the maximum rate of carbon formation after reactivation of the catalyst with hydrogen is greater than in the first carbon deposition cycle. It is seen for each run, however, that the reaction time which elapses before carbon deposition again stops is much less than in the initial cycle. X-Ray diffraction patterns of the product taken at the end of runs 1 and 2 once again show strong cementite peaks and no Fe_3O_4 , Fe_2O_3 or $\alpha\text{-Fe}$ peaks. No X-ray diffraction patterns were taken of the carbon during run 3, but similar results are expected.

For runs 1 and 3, where hydrogen reactivation was conducted at the relatively high temperatures of 600 and 576°, respectively, wet-test-meter readings indicated that hydrogen was reacting to a considerable extent with the free carbon. If it is assumed that the cumulative increase in difference between the wet-test-meter readings was caused by the reaction $\text{C} + 2\text{H}_2 \rightarrow \text{CH}_4$, it is calculated that 0.50 and 0.49 g. of carbon had reacted in runs 1 and 3, respectively. The addition of these weights to the amounts of carbon recovered from runs 1 and 3 give total weights of carbon formed of 0.89 and 3.91 g.—in excellent agreement with 0.89 and 3.94 g., the weights predicted from the reactions $2\text{CO} \rightarrow \text{C} + \text{CO}_2$ and $\text{H}_2 + \text{CO} \rightarrow \text{C} + \text{H}_2\text{O}$.

For run 2, where hydrogen treatment was conducted at 416°, there was no detectable difference in cumulative wet-test-meter readings during the treatment. If, prior to treatment, all of the iron existed as cementite, total conversion of it to $\alpha\text{-Fe}$ and methane would result in a difference of only 0.0004 ft.³ in the wet-test-meter readings. This difference could not be detected. Unfortunately an X-ray diffraction analysis was not made on a sample after hydrogen treatment in run 2, but conversion of cementite to $\alpha\text{-Fe}$ is suggested because of the subsequent significant increase in carbon deposition rate over the rate just prior to hydrogen treatment. Since the maximum rate of carbon deposition and the amount of carbon formed following hydrogen treatment in run 2 is seen to be not as great as that for run 1, probably decarburization was not complete.

(28) This does not necessarily mean that these substances were not present in small concentrations, since it is usually not possible to pick up peaks for constituents present in concentrations of less than 5% by X-ray diffraction.

(29) H. Pichler and H. Merkel, U. S. Bureau of Mines Tech. Paper 718, 1949.

(30) L. C. Browning, T. W. DeWitt and P. H. Emmett, *J. Am. Chem. Soc.*, **72**, 4211 (1950).

Discussion

On the basis of results presented in this and an accompanying paper,²¹ in addition to key findings by other workers, a qualitative mechanism for carbon formation from carbon monoxide-hydrogen mixtures over iron catalysts is proposed. First, Fischer and Bahr³¹ appear to have adequately explained how the iron catalyst is able to permeate the carbon formed. They report that an iron-copper catalyst, when heated with carbon monoxide at 500° results in the formation of a carbon which contains copper as well as iron, well separated from the main catalyst mass. They conclude that if the iron were carried into the carbon phase as volatile carbonyls of iron, the copper, which forms no carbonyl, would be left behind. The copper and presumably the iron, therefore, must be carried into the carbon phase by some other method, probably mechanical. The key point in the mechanism is the supposition that carbon monoxide chemisorbs on iron but not on cementite, at the temperatures employed in this research. Emmett and co-workers²⁵ find that iron chemisorbs carbon monoxide extensively at 100° but at 150° the iron begins to carbide with carbon monoxide rapidly enough so as to make adsorption measurements on pure iron difficult. They find that at 200° pure carbon monoxide does not chemisorb on Hägg carbide (Fe_2C). As Hägg carbide and cementite have essentially the same ferro-magnetic moment, it is expected that their capacities for chemisorption are essentially the same.³² Therefore, carbon monoxide is not expected to chemisorb on cementite at elevated temperatures.

Consider the case of the passage of a carbon monoxide-hydrogen mixture over reduced carbonyl iron. After reduction, the carbonyl iron contains chemisorbed hydrogen, probably in atomic form.³³ Since chemisorption of carbon monoxide on iron is only slightly inhibited by chemisorbed hydrogen,³³ carbon monoxide will adsorb on iron atoms occupied by hydrogen, as well as on free iron atoms. A fraction of the chemisorbed carbon monoxide will react with chemisorbed hydrogen by the reactions $\text{CO} + \text{H}_2 \rightarrow \text{C} + \text{H}_2\text{O}$ and $\text{CO} + 3\text{H}_2 \rightarrow \text{CH}_4 + \text{H}_2\text{O}$, decreasing the amount of hydrogen chemisorbed on the surface, the extent of the decrease being a function of the hydrogen content in the carbon monoxide-hydrogen mixture and the changing nature of the surface. Another fraction of the chemisorbed carbon monoxide will dissociate into carbon and oxygen atoms (the amount and the rate of dissociation depending upon the temperature and the crystallographic plane of iron on which chemisorption takes place,³⁴ among other factors). The majority of the oxygen atoms produced by the decomposition of carbon monoxide will react rapidly with additional undecomposed carbon monoxide to produce carbon dioxide or with hydrogen to produce water, which leave the iron surface.

(31) F. Fischer and H. A. Bahr, *Ges. Abhandl. Kenntnis Kohle*, **8**, 225 (1928).

(32) Private communication from R. B. Anderson.

(33) S. Brunauer and P. H. Emmett, *J. Am. Chem. Soc.*, **62**, 1732 (1940).

(34) V. J. Kehrler, Jr., and H. Leidheiser, Jr., *THIS JOURNAL*, **58**, 550 (1954).

The carbon atoms produced from carbon monoxide dissociation have a high mobility and the majority of them (some react with hydrogen to form methane) migrate across the surface to a nucleating center (probably a dislocation), where they begin forming concurrently both free carbon and carbidic carbon (cementite). The production of free carbon will stop when the catalyst has been completely carbided to cementite, since the necessary chemisorption of carbon monoxide also will stop.

This general picture of carbon deposition from carbon monoxide-hydrogen mixtures is consistent with the major findings reported in this research. X-Ray diffraction studies clearly show that the major constituent in a spent catalyst is cementite. Following reduction of the cementite to α -Fe by hydrogen, the activity of the catalyst for carbon deposition is restored.

As was seen in Figs. 2, 3 and 4, hydrogen addition to carbon monoxide can also result in marked increases in maximum carbon deposition rate and total amount of carbon formed. At 630°, the rate of production of carbidic carbon is high and relatively little free carbon can be produced from a carbon monoxide-hydrogen mixture low in hydrogen (0.8% H₂, for example) before the catalyst is completely carbided. As the hydrogen content in the gas mixture is increased, the rate of conversion of cementite back to iron is increased; and this results in an increasing rate of free carbon formation and a prolonging, or perhaps removing, of the time of complete conversion of the iron to cementite. The optimum hydrogen content to produce a maximum amount of free carbon is a balance between the fraction of surface which is iron and the concentration of carbon monoxide in the inlet gas. Obviously, in the limit, the complete absence of carbon monoxide will result in the production of no free nor carbidic carbon. That the addition of hydrogen, up to a point, can result in an increase in the net amount of free carbon recovered is a consequence of the considerably higher reactivity of carbidic carbon than free carbon with hydrogen.^{29,30}

From Fig. 4, it was seen that additions of hydrogen to carbon monoxide have little effect on the carbon deposition rate at 500°. At this relatively low deposition temperature, the rate of formation of carbidic carbon is low and, therefore, the presence of a large amount of hydrogen to prevent early catalyst deactivation is not necessary. The fact that the carbon deposition rate at 500° is so insensitive to gas composition also indicates that the reactions $2\text{CO} \rightarrow \text{C} + \text{CO}_2$ and $\text{CO} + \text{H}_2 \rightarrow \text{C} + \text{H}_2\text{O}$ have very similar rates; this primarily implies similar rates for the reactions of carbon monoxide and hydrogen with an oxygen atom to produce carbon dioxide and water, respectively.

The fact that in many runs extended periods of constant carbon deposition rates are found in spite of a probable build-up of carbidic carbon content in the catalyst should be noted. It is suggested that during these periods, disintegration of the catalyst into smaller particle sizes is taking place. This can result in the total surface area of the iron remaining constant, even though the percentage of

the total surface which is iron continues to decrease. At some point, probably when the crystallite size of the catalyst equals the particle size, disintegration of the particles stops and a gradual reduction in carbon deposition rate is noted, as conversion of iron to cementite continues.

The effect which reduction of particle size (greater specific surface area) of the catalyst can have on carbon deposition rate is perhaps best seen in the reactivation runs, shown in Fig. 7. For run 3, following reactivation, the maximum rate of carbon deposition is considerably higher than in the initial deposition cycle. Furthermore, the time for deactivation of the catalyst following its reactivation is considerably less than in the initial cycle. This is consistent with a catalyst of greater surface area on which greater rates of production of both free and carbidic carbon occur. Runs 2 and 3 in Fig. 7 also show a very much shorter catalyst deactivation-time following reactivation. They do not show a greater maximum carbon deposition rate following catalyst reactivation because of the removal of part of the catalyst for X-ray diffraction analysis and/or lack of complete reactivation.

Partially precarbiting a carbonyl iron catalyst was shown in Fig. 5 to decrease the time for catalyst deactivation, when using a gas mixture low in hydrogen. This is consistent with the overall picture. The fact that an unreduced catalyst also is deactivated in a shorter time than a reduced catalyst, resulting in less free carbon formation should be noted. This is possibly a result of the stabilizing influence of oxygen on cementite, as noted by Emmett and co-workers.²⁵

It is interesting to compare the qualitative mechanism proposed by the authors for the formation of free carbon over an iron catalyst with that proposed by Hofer³⁵ and Hofer, Peebles and Bean³⁶ for the formation of free carbon over a cobalt-thoria-kieselguhr catalyst. Hofer³⁵ proposes that free carbon formation follows two routes, one a surface process and the other process passing through a carbide intermediate. He bases his statement on the findings of the latter workers³⁶ who studied carbon formation over two identical catalyst specimens, except that the cobalt in one had been converted to Co₃C by carburization with carbon monoxide. These two specimens were then carburized with carbon monoxide at 285° for 22 hours. Carbon deposition initially was 20 times faster on the metallic catalyst than on the carbided catalyst. During the carburization process, the rate of carbon deposition on the metallic specimen decreased markedly, whereas the rate on the carbided catalyst remained constant. It is concluded that the carbide inhibits the deposition of free carbon in line with the conclusion expressed in this paper; but, unlike the present conclusions, a completely carbided catalyst is still considered partially active to carbon formation. Because of the complexity and possible differences in these

(35) L. J. E. Hofer, "Catalysis," Vol. 4, Reinhold Publ. Corp., New York, N. Y., 1956, pp. 373-441.

(36) L. J. E. Hofer, W. C. Peebles and E. H. Bean, *J. Am. Chem. Soc.*, **72**, 2698 (1950).

two systems, however, it is difficult to rationalize completely these two viewpoints at present.

Alternate explanations for the final termination of carbon formation which were considered are (a) blocking of the catalyst by carbon, (b) possibility of a minimum catalyst crystallite size being required and (c) sulfur poisoning.

The first explanation was ruled out for two reasons. First, the carbon produced is highly porous, and, therefore, its ability to block reacting gas molecules from reaching the catalyst is doubtful. Second, the final termination of carbon formation was not dependent upon the amount of carbon formed. If physical blockage of the catalyst by carbon was significant, it is difficult to understand, for example, why the reaction was terminated after the production of only one gram of carbon at 602° and still not terminated after

the production of 6 g. of carbon at 528° (see Fig. 2 for the 98.6% CO-1.4% H₂ mixture).

The second explanation was ruled out because of the experimental fact that the catalyst can be reactivated with hydrogen. It would not be expected that significant, if any, growth in catalyst crystallite size would be possible during hydrogen reactivation. This is particularly true where the reactivation temperature is even lower than the carbon deposition temperature.

The third explanation, sulfur poisoning, was ruled out because of the marked effect of the hydrogen content in the carbon monoxide in determining the rate of catalyst reactivation. That is, to the authors' knowledge, it has not been reported that hydrogen addition to a gas stream reduces the extent of poisoning of iron catalysts by sulfur compounds.

LOW TEMPERATURE HEAT CAPACITIES AND THERMODYNAMIC FUNCTIONS OF HYDROUS SODIUM PALMITATE

BY HENRY E. WIRTH, JOHN H. WOOD AND JOHN W. DROEGE

Contribution from the Cryogenic Laboratory and the Department of Chemistry, The Ohio State University, Columbus, Ohio, and the Department of Chemistry, Syracuse University, Syracuse, New York

Received April 28, 1958

The heat capacities of β -sodium palmitate (NaP) containing 0.064% H₂O and 2.56% H₂O and of ϵ -NaP containing 4.48% H₂O were determined in the temperature range 15-300°K. The heat capacity of ϵ -NaP (3.02% H₂O) was determined in the range 60-300°K. The calculated entropies at 298.16°K. are 113.0 \pm 0.5 e.u. (β -NaP-0.010H₂O), 119.3 \pm 0.5 e.u. (β -NaP-0.409 H₂O) 119.7 \pm 0.5 e.u. (ϵ -NaP-0.482H₂O), and 123.9 \pm 0.5 e.u. (ϵ -NaP-0.715H₂O). The first half mole of water per mole of NaP is strongly bound to the soap, and its heat capacity in the temperature range 270-300°K. is strong evidence for the assumption that this water is present as a hydrate. The additional water is adsorbed on the surface of the soap.

Introduction

The water present in sodium palmitate (NaP) containing 0-3.1% H₂O has been shown^{1,2} to be strongly bound to the soap. Above 3.1% H₂O the water is probably weakly adsorbed on the surface of soap crystallites. The upper limit of 3.1% for the strongly bound water suggested a definite hydrate, NaP·1/2H₂O (3.14% H₂O), but other interpretations were not excluded by the experimental results.

To obtain further information on the nature of the strongly bound water, heat capacities of NaP containing 0-4.5% H₂O were determined. The original intention was to make all determinations on the same phase of the soap, but it was found subsequently that the phase chosen, the β -phase,³ undergoes an irreversible transition to the ϵ -phase when cooled to low temperature and when the moisture content is greater than 3%. Data were therefore obtained on two samples of low moisture β -NaP (0.064 and 2.56% H₂O) and on two samples of ϵ -NaP (3.02 and 4.48% H₂O).

Experimental

Materials.—Palmitic acid (99.8%), from the same sample used for heat capacity determinations,⁴ was dissolved in 85%

C₂H₅OH and less than the theoretical amount of carbonate-free NaOH was added to the hot solution. The solution was evaporated, the recovered soap was ground to a fine powder and heated to 180° under vacuum for 12 hours to remove excess palmitic acid. This treatment gave the anhydrous ω -phase.

A mixture of 65 parts of ω -NaP and 35 parts of H₂O was converted to neat soap by holding it at a temperature of 100° for 1 hour. The neat soap was cooled to 67° and held at this temperature for 24 hours to give "tempered" β -NaP. This material was cooled to room temperature and dried over 60% H₂SO₄ until its moisture content was reduced to 4.5%. Portions of this sample were dried over 65% H₂SO₄ and over P₂O₅ in a vacuum desiccator to obtain samples containing 2.56 and 0.064% H₂O, respectively. All samples were equilibrated for several months in closed containers before use. Water content was determined with an average deviation of \pm 0.05% by loss of weight at 105° for six hours under vacuum.

All solutions and high-moisture soaps were protected from atmospheric CO₂ by keeping them under a blanket of N₂. Tests for carbonate in the final samples were negative.

A fourth sample containing 3.02% H₂O was from the lot used for dielectric constant measurements¹. The palmitic acid regenerated from this sample was 98% pure, but the experimentally determined equivalent weight indicated the impurities to be about equally divided between higher and lower molecular weight fatty acids.

The molecular weight of NaP was taken as 278.42.

X-Ray powder patterns of samples before and after the heat capacity runs were taken and interpreted for us by Dr. F. B. Rosevear of the Procter and Gamble Co.

Procedure.—Measurements were made in a copper calorimeter (laboratory designation No. 5) using procedures described previously.⁵ All samples had a low bulk density and

(1) H. E. Wirth and W. W. Wellman, *THIS JOURNAL*, **60**, 919 (1956). This article gives references to other work in this field.

(2) H. E. Wirth and W. L. Kosiba, *ibid.*, **60**, 923 (1956).

(3) The phase designations used are discussed in reference 2.

(4) H. E. Wirth, J. W. Droegge and J. H. Wood, *THIS JOURNAL*, **60**, 917 (1956).

(5) H. L. Johnston and E. C. Kerr, *J. Am. Chem. Soc.*, **72**, 4733 (1950).

TABLE I
HEAT CAPACITIES (CAL./DEG. MOLE)

T , °K.	C_p	T , °K.	C_p	T , °K.	C_p	T , °K.	C_p
β -NaP·0.010H ₂ O							
14.66	1.89 ^a	56.80	26.90 ^a	117.94	51.54 ^a	231.99	83.00
15.69	3.12 ^a	60.82	28.59	121.62	52.89	240.52	85.50
17.87	3.70 ^a	62.28	29.48 ^a	129.15	55.29	248.60	88.82
20.53	4.62 ^a	65.60	30.90	137.49	58.02	254.19	90.99
23.10	5.99 ^a	68.37	32.35 ^a	146.07	60.50	262.40	94.05
25.51	7.27 ^a	71.24	33.77	154.07	62.34	269.08	97.34
27.83	8.49 ^a	77.19	36.64	163.02	64.23	277.57	101.40
30.21	9.77 ^a	83.54	39.59	173.25	66.46	277.87	100.96 ^a
32.93	11.53 ^a	90.01	42.15	183.46	69.30	285.95	105.16
36.07	13.06 ^a	96.22	45.30	185.93	69.99	286.17	104.71 ^a
39.56	15.81 ^a	101.32	46.05 ^a	194.89	72.58	292.03	107.89
43.32	18.01 ^a	102.90	46.80	204.64	74.87	293.83	107.94 ^a
47.57	20.55 ^a	109.58	48.95 ^a	214.43	78.40	299.78	112.93
52.02	23.89 ^a	109.98	49.14	223.70	80.38	301.33	112.43 ^a
β -NaP·0.409H ₂ O							
14.53	2.37 ^a	56.51	27.56 ^a	145.22	62.12	246.39	95.69 ^a
16.41	3.70 ^a	61.37	30.24 ^a	156.37	65.82	255.28	97.47
18.40	3.87 ^a	64.46	31.60	167.33	68.88	255.74	97.50 ^a
20.58	5.07 ^a	70.28	34.72	177.97	71.89	262.77	99.12
23.09	6.46 ^a	76.75	38.28	188.86	75.45	263.68	99.95 ^a
27.25	8.77 ^a	84.17	41.65	198.73	78.74	272.46	102.32
27.39	8.46 ^a	92.97	45.33	198.79	78.12	272.90	103.85 ^a
30.55	10.83 ^a	102.15	48.67	208.18	81.91	281.47	106.50
34.20	13.31 ^a	103.93	49.84	217.79	85.25	281.56	107.94 ^a
38.37	15.95 ^a	112.11	52.37	226.32	88.54	289.68	110.59 ^a
42.62	18.77 ^a	113.05	52.70	235.72	90.74	296.53	114.32 ^a
46.95	21.61 ^a	123.72	55.91	237.05	90.96 ^a		
51.20	24.28 ^a	134.21	58.72	245.42	95.02		
ϵ -NaP·0.482H ₂ O							
61.60	30.18	125.14	56.57	217.37	85.92 ^a	271.11	103.60 ^a
66.41	32.46	134.76	58.91	219.19	87.45 ^b	272.22	101.48
71.60	35.61	143.04	61.92	223.94	90.93	277.16	105.13 ^a
77.94	39.01	153.13	65.21	225.17	88.04 ^a	277.40	104.24
84.03	41.85	155.21	65.96 ^a	227.29	91.38 ^b	282.98	107.30
90.66	44.49	163.24	68.27	235.47	92.80 ^b	283.82	107.58 ^a
97.34	46.69	164.98	68.57 ^a	243.00	95.44 ^b	286.70	108.58
101.37	48.89 ^b	172.96	70.64	250.06	99.40 ^b	290.64	110.34 ^a
105.93	50.23 ^a	174.88	71.16 ^a	250.77	97.42 ^a	291.98	112.65
108.17	51.20 ^b	183.20	73.73	257.09	99.51 ^b	296.66	113.01 ^a
115.02	53.23 ^b	192.97	77.18	257.28	99.28 ^a	296.87	113.87
116.23	54.01	199.80	79.63	263.63	99.62 ^a	301.57	114.88
121.93	55.16 ^b	208.56	82.55	264.30	101.01 ^b		
125.09	56.60	216.80	86.48	270.59	102.10 ^a		
ϵ -NaP·0.715H ₂ O							
13.82	2.26 ^a	68.88	34.64 ^a	185.16	76.73	269.11	135.15 ^a
15.67	3.03 ^a	69.43	35.33	194.46	80.35	271.53	133.47
17.53	3.76 ^a	75.56	38.20	203.72	84.14	273.37	125.48 ^a
19.89	4.79 ^a	82.16	41.07	213.19	87.93	274.59	110.23 ^b
22.16	5.96 ^a	89.32	44.52	222.45	91.82	276.41	110.45 ^b
24.69	7.41 ^a	97.25	47.41	229.23	95.00 ^a	279.00	111.23 ^a
27.32	9.30 ^a	106.80	50.81	232.43	95.61	280.46	111.67 ^b
30.14	10.97 ^a	116.99	54.90	239.32	97.34 ^a	280.91	112.73
33.52	12.75 ^a	127.01	58.41	242.60	99.17	286.00	113.99 ^a
37.10	15.20 ^a	137.46	61.75	249.19	103.13 ^a	286.50	114.35 ^b
41.12	17.82 ^a	148.79	65.09	252.61	104.66	292.79	117.02 ^a
51.21	24.61 ^a	154.58	67.02	258.68	108.11 ^a	293.13	116.83 ^b
56.43	28.12 ^a	165.70	70.41	262.32	113.57	299.58	121.08 ^a
62.28	31.32 ^a	175.37	73.22	266.51	122.20 ^b		

^a Series 2. ^b Series 3.

only 0.1 mole of NaP could be loaded in the calorimeter. The heat capacity of the sample plus calorimeter was only twice that of the empty calorimeter, and the estimated uncertainty of a single observation of the heat capacity was $\pm 10\%$ at the lowest temperatures (15–25°K.), $\pm 0.5\%$ at intermediate temperatures and $\pm 1\%$ at room temperature. With samples of intermediate water content additional uncertainty was introduced by the slow attainment of equilibrium in the range 180–280°K.

One defined calorie was taken equal to 4.1833 international joules, and the ice point at 273.16°K.

Results

Heat capacities were determined for β -NaP·0.010H₂O, β -NaP·0.409H₂O and ϵ -NaP·0.715H₂O in the temperature range 14–300°K., and for ϵ -NaP·0.482H₂O in the range 60–300°K. (Table I). Heat capacities for the latter sample at temperatures below 60°K. were estimated to be 0.3% lower than the corresponding values for β -NaP·0.409H₂O. A smooth curve on a large scale plot of C_p vs. T was used to obtain preliminary values of C_p for each degree in the range 30–300°K. A smooth curve on a large scale plot of C_p/T vs. T in the temperature range 14–40°K. was extrapolated to 0°K. to give preliminary values of C_p below 30°K. The tabulated values of C_p were smoothed, and the thermodynamic functions given in Table II were obtained from these smoothed values by tabular methods.

Discussion

Only ϵ -NaP·0.715H₂O exhibits a first-order transition (Fig. 1). The difference between the heat contents of ϵ -NaP·0.715H₂O and ϵ -NaP·0.482H₂O in the temperature interval 250–273.16°K. is 370 cal. This agrees within the experimental error with the value 356 cal. calculated for the heat content change of 0.215 mole of pure water in the same temperature range. The transition is due therefore to the melting of adsorbed water.

If it is assumed that the water present in ϵ -NaP·0.48H₂O is liquid above 270°K., then the curve (dashed curve 2, Fig. 1) drawn by subtracting the difference between the heat capacity of water and of ice above 270°K. from the experimental curve and extrapolating back to 180°K. would represent the heat capacity of an ice-soap mixture. The difference in heat content in the temperature range 180–270°K. between this reference curve and the experimental curve is 300 cal., or 620 cal. per mole of H₂O present. Since the heat of fusion of ice is 1,436 cal., the anomaly cannot be due to the melting of ice.

The difference in heat content between the smooth curve (dashed curve 1, Fig. 1) and the experimental curve is 130 cal., or 270 cal. per mole of water. The entropy difference is 0.55 e.u., corresponding to 1.1 e.u. per mole of water.

A similar anomaly is present in β -NaP·0.409H₂O in the temperature range 200–270°K. The heat effect was estimated to be 74 cal., or 180 cal. per mole of water. The heat capacity curve for β -NaP·0.010H₂O is smooth in the temperature

(6) In the extrapolation of C_p/T vs. T to 0°K., the curve approached 0°K. with a finite slope. This corresponds to $n = 2$ in the empirical equation $C_p = aT^n$. The values of n obtained from the slope of $\log C_p$ vs. $\log T$ were 1.7, 2.2 and 2.3 for NaP·0.010H₂O, NaP·0.409H₂O and NaP·0.716H₂O, respectively. If C_p/T is assumed to approach 0°K. with zero slope, the calculated entropies would be reduced by approximately 0.3 e.u.

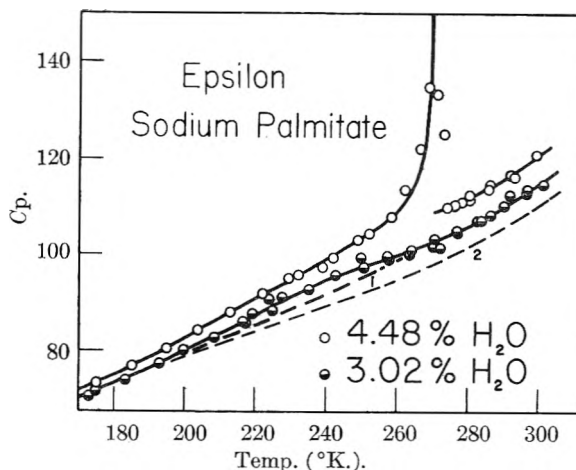


Fig. 1.—Heat capacity of ϵ -NaP·0.715H₂O (4.48% H₂O) and of ϵ -NaP·0.482H₂O (3.02% H₂O). See text for the significance of dashed curves 1 and 2.

range 200–270°K., but a small anomaly may be present between 120 and 175°K.

TABLE II
THERMODYNAMIC FUNCTIONS

T , °K.	C_p , cal. (mole degree) ⁻¹	$S^\circ - S_0^\circ$ e.u.	$H^\circ - H_0^\circ$, cal. mole ⁻¹	$-(F^\circ - H_0^\circ)/T$ cal. (mole degree) ⁻¹
β -NaP·0.010H ₂ O				
50	22.29	13.09	420.3	4.69
100	45.75	36.56	2,181	14.76
150	61.45	58.21	4,876	25.70
200	73.91	77.48	8,240	36.27
250	89.31	95.51	12,290	46.33
273.16	99.07	103.8	14,480	50.85
298.16	110.6	113.0	17,090	55.68
β -NaP·0.409H ₂ O				
50	23.53	13.93	449.5	4.91
100	48.12	38.47	2,291	15.57
150	63.84	61.07	5,104	27.05
200	79.15	81.47	8,668	38.14
250	96.31	101.0	13,060	48.76
273.16	102.9	109.8	15,360	53.57
298.16	115.0	119.3	18,080	58.68
ϵ -NaP·0.482H ₂ O				
50	23.46	13.89	448.1	4.93
100	48.15	38.43	2,290	15.53
150	64.07	61.08	5,109	27.02
200	79.55	81.58	8,691	38.13
250	97.23	101.4	13,140	48.80
273.16	103.6	110.3	15,460	53.63
298.16	113.9	119.7	18,170	58.78
ϵ -NaP·0.715H ₂ O				
50	23.83	14.06	452.4	5.01
100	48.48	38.94	2,318	15.76
150	65.60	61.99	5,189	27.40
200	82.55	83.02	8,865	38.70
250	103.3	103.6	13,510	49.63
273.16	109.7	113.9	16,203	54.63
298.16	119.9	123.9	19,058	60.02

It is not certain that these anomalies should be attributed to the water present in the soap, as δ -NaP with 0.79% H₂O did not exhibit this behavior.⁷ The effects may be due to reversible phase transitions in the substrate.

Insofar as the entropy of hydrate water is the same as that of ice^{8,9} the heat capacity should also

(7) H. E. Wirth, J. W. Droegge and J. H. Wood, *THIS JOURNAL*, **63** 152 (1959).

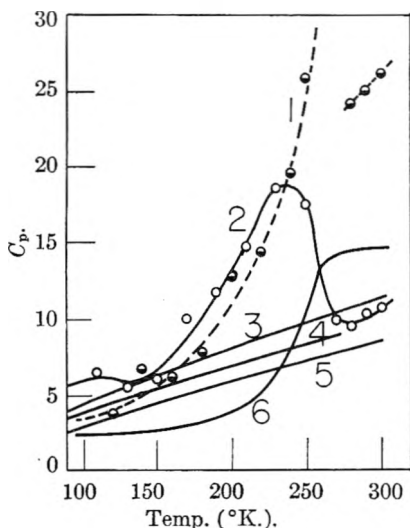


Fig. 2.—Molal heat capacity of water in: (1) ϵ -NaP, $[(C_{pNaP \cdot 0.715 H_2O} - C_{pNaP \cdot 0.409 H_2O})/0.233]$; (2) β -NaP, $[(C_{pNaP \cdot 0.409 H_2O} - C_{pNaP \cdot 0.010 H_2O})/0.399]$; (3) $CdSO_4 \cdot 8/3 H_2O$ $[(C_{pCdSO_4 \cdot 8/3 H_2O} - C_{pCdSO_4 \cdot H_2O})/3/5]$; (4) ice; (5) $CdSO_4 \cdot H_2O$ $[C_{pCdSO_4 \cdot H_2O} - C_{pCdSO_4}]$; (6) in a gelatin gel containing 12.5% H_2O .

parallel that of ice and should permit conclusions to be drawn as to the nature of the binding of water with the substrate.

In Fig. 2 the molal heat capacities are given in the range 90–300°K. for ice (curve 4), for the water present in $CdSO_4 \cdot H_2O$ ¹⁰ (curve 5), and for the additional water present in $CdSO_4 \cdot 8/3 H_2O$ ¹⁰ (curve 3). The heat capacity of the hydrate water present in most of the hydrates reported in the literature lies between curves 3 and 5. The only values in the literature for the heat capacity of "bound" water in the temperature range 90–300°K. are those of Hampton and Mennie¹¹ who deter-

(8) K. K. Kelley and G. E. Moore, *J. Am. Chem. Soc.*, **65**, 2340 (1943).

(9) V. A. Koreev, *Zhur. Fiz. Khim.*, **22**, 847 (1948).

(10) M. N. Papadopoulos and W. F. Giaque, *J. Am. Chem. Soc.*, **77**, 2740 (1955).

(11) W. F. Hampton and J. H. Mennie, *Can. J. Research*, **10**, 452 (1934).

mined the heat capacity of gelatin gels containing 0–91% H_2O by a drop calorimeter method. The molal heat capacity of the water present in a gel containing 12.5% H_2O as calculated from the data of Hampton and Mennie is given in curve 6, Fig. 2. Free water (water melting near 0°) was not present in gels containing less than 33% H_2O .

Curve 2, Fig. 2 gives the molal heat capacity of water as calculated from the heat capacities of the two samples of β -NaP. This curve resembles neither a typical hydrate curve nor the "bound" water curve. The minimum at 140°K. is associated with the small anomaly in β -NaP·0.010 H_2O and part, but not all of the maximum at 240°K. is due to the anomaly in the heat capacity of β -NaP·0.409 H_2O .

The most significant feature of curve 2 is that the heat capacity corresponds to that of hydrate water in the range 270–300°K.

Curve 1, Fig. 2, for the molal heat capacity of the water present in ϵ -NaP is that expected for adsorbed water. The heat capacity of the adsorbed water (270–300°K.) is greater than that of free water. This is in agreement with the results of Hampton and Mennie¹¹ who found the average specific heat of water to be as high as 1.24 in a gel containing 54.7% H_2O even though this included the water between 0 and 12.5% H_2O which had an average specific heat of 0.80.

Conclusions.—This work has verified the previous conclusions that the first half mole of water per mole of NaP is strongly bound to the soap, and that any additional water is adsorbed on the surface. The fact that the heat capacity of the water present in β -NaP lies within the range expected for hydrates in the temperature range 270–300°K. is strong evidence for the existence of a hydrate, $NaP \cdot 1/2 H_2O$.

Acknowledgment.—The authors wish to express their sincere gratitude to Prof. Herrick L. Johnston for his full cooperation in the use of facilities of the Cryogenic Laboratory, and to the Procter and Gamble Co. for a fellowship which partially supported this work.

HEAT CAPACITIES AND THERMODYNAMIC FUNCTIONS FOR δ - AND ω -SODIUM PALMITATE

BY HENRY E. WIRTH, JOHN W. DROEGE AND JOHN H. WOOD

Contribution from the Cryogenic Laboratory and the Department of Chemistry, The Ohio State University, Columbus, Ohio and from the Department of Chemistry, Syracuse University, Syracuse, N. Y.

Received April 28, 1958

The entropies of δ -sodium palmitate (NaP) (0.79% H_2O) and ω -NaP (0.11% H_2O) at 298.16°K. are 113.4 ± 0.4 e.u. and 113.8 ± 0.4 e.u., respectively. The entropies of completely anhydrous NaP at 298.16°K. are estimated to be 112.2, 113.6 and 112.9 for the δ -, ω - and β -phases, respectively.

Introduction

The present work extends the study of the thermodynamic properties of palmitic acid and its derivatives^{1,2} to the δ - and ω -phases of sodium palmitate (NaP).

(1) H. E. Wirth, J. W. Droegge and J. H. Wood, *THIS JOURNAL*, **60**, 917 (1956).

Experimental

Materials.—A portion of the sample of ω -NaP obtained in the course of the preparation of hydrous β -NaP² was used. The sample contained 0.08% H_2O before and 0.14% H_2O after the heat capacity determination, so was essentially anhydrous.

(2) H. E. Wirth, J. H. Wood and J. W. Droegge, *ibid.*, **63**, 149 (1959).

TABLE I

HEAT CAPACITIES (CAL./DEG. MOLE)							
T , °K.	C_p	T , °K.	C_p	T , °K.	C_p	T , °K.	C_p
ω -Sodium palmitate							
58.37	27.16 ^b	104.18	47.12	174.71	67.55	247.82	91.00 ^a
64.01	30.00 ^b	110.84	49.26	182.04	69.62	250.10	91.43 ^a
65.77	30.35	118.30	51.98	190.37	72.16	236.82	94.46 ^b
69.52	32.44 ^b	125.60	54.08	198.80	74.54	263.16	97.73 ^b
72.13	33.97	133.27	56.32	206.82	77.18	269.73	101.58 ^b
77.32	36.66	141.54	58.64	214.57	79.40	276.11	105.95 ^b
84.50	39.74	149.60	60.79	223.58	82.28	281.15	107.86 ^b
88.67	41.15	157.62	63.37	224.68	82.25 ^a	286.90	112.35 ^b
95.21	43.98	158.74	63.29	232.67	84.44 ^a	292.33	114.82 ^b
97.50	44.76	166.58	65.63	240.22	87.54 ^a	297.44	117.61 ^b
δ -Sodium palmitate							
58.25	27.73	111.01	50.18	180.81	68.48	248.95	88.73 ^a
64.25	30.61	122.15	53.55	190.95	71.37	256.96	91.19 ^a
70.94	34.14	132.12	56.54	201.05	74.50 ^a	266.01	94.67 ^a
78.51	37.89	142.37	59.25	210.95	77.13 ^a	274.75	98.50 ^a
85.96	41.16	152.04	62.02	220.51	79.90 ^a	282.02	100.52 ^a
93.81	44.04	162.03	64.52	230.56	82.92 ^a	290.40	104.22 ^a
100.52	46.62	171.06	66.50	238.26	85.69 ^a	298.21	107.42 ^a

^a Series 2. ^b Series 3.

A solution of 90 g. of NaP in 2.5 l. of H₂O was heated to boiling, filtered and allowed to cool. The water was removed by slow evaporation at temperatures between 35 and 40°; the final dehydration was carried out under the vacuum of a mechanical pump. The sample was protected from atmospheric CO₂ at all times. The final product was δ -NaP containing 0.79% H₂O.

The phase present in each sample was checked by X-ray powder diffraction before and after the calorimetric runs by Dr. F. B. Rosevear of the Procter and Gamble Co. No phase changes occurred as a result of the thermal treatment.

The reported results are based on 278.42 as the molecular weight of NaP, and on one defined calorie = 4.1833 joules.

Results

The experimental heat capacities obtained between 60 and 300°K. are given in Table I. Smooth curves through a large scale plot of C_p vs. T were used to obtain preliminary values of C_p at each degree, and these tabular values were further smoothed to give the final "best" values.

The heat capacity of ω -NaP and of δ -NaP closely paralleled that of β -NaP·0.010H₂O between 60 and 100°K. Heat capacities in the range 0–60°K. were estimated on the assumption that the heat capacity of ω -NaP was 1.85% less, and that of δ -NaP was 0.77% greater, than the corresponding values for β -NaP.

The thermodynamic functions given in Table II were obtained by tabular methods from the smoothed tables of heat capacities.

Discussion

Despite the fact that the sample of δ -NaP contained 0.12 mole water per mole of NaP, no anomalies similar to those found with β -NaP containing 0.010 or 0.409 mole of water were observed.² This may indicate that the anomalies in the latter samples were associated with reversible phase transitions in the substrate soap and did not involve the water.

The entropies at 298.16°K. for all the anhydrous phases of sodium palmitate which have been studied are summarized in Table III. In correcting the

 TABLE II
THERMODYNAMIC FUNCTIONS

T , °K.	C_p , cal. degree mole ⁻¹	S_p^0 , cal. (degree mole ⁻¹) ⁻¹	H_0 , cal. mole ⁻¹	$-(F^0 - H_0^0)/T$, cal. (degree mole ⁻¹) ⁻¹
(NaP·0.017H ₂ O)				
50	21.88	12.85	412.4	4.60
100	45.70	36.13	2,160	14.53
150	61.02	57.70	4,846	25.40
200	74.91	77.12	8,238	35.93
250	91.52	95.50	12,370	46.02
273.16	103.3	104.1	14,620	50.58
298.16	118.3	113.8	17,390	55.47
(NaP·0.12H ₂ O)				
50	22.46	13.19	423.6	4.72
100	46.42	36.96	2,206	14.90
150	61.32	58.77	4,921	25.96
200	73.94	78.09	8,294	36.62
250	89.07	96.18	12,360	46.74
273.16	97.25	104.4	14,510	51.28
298.16	107.4	113.4	17,070	56.11

TABLE III

Phase	ENTROPY PER MOLE OF ANHYDROUS SODIUM PALMITATE $S_{298.16K}^0$, e.u. (obsd.)	Cor. for H ₂ O content, e.u.	$S_{298.16K}^0$ (anhyd.), e.u.
β	113.0	0.1	112.9
δ	113.4	1.2	112.2
ω	113.8	0.2	113.6

observed entropies the assumption was made that the entropy of the water present was equal to that of ice.² While this assumption may be in error by as much as $\pm 50\%$, the order of the phases would not be changed. No conclusions can be drawn as to which phase is thermodynamically stable at room temperature until data on heats of solution are available.

Acknowledgment.—The authors wish to express their sincere gratitude to Prof. Herrick L. Johnston for his full cooperation in the use of facilities of the Cryogenic Laboratory, and to the Procter and Gamble Co. for a fellowship which partially supported this work.

HEATS OF COMBUSTION AND FORMATION OF BIS-BENZENECHROMIUM

By A. K. FISCHER, F. A. COTTON AND G. WILKINSON

Contribution from the Departments of Chemistry of Harvard University, Cambridge, Mass. Massachusetts Institute of Technology, Cambridge, Mass., and Imperial College, London, England

Received May 1, 1958

The enthalpy change (ΔH_{298}^0) for the reaction $(C_6H_6)_2Cr(s) + 63/4 O_2(g) = 1/2 Cr_2O_3(s) + 12CO_2(g) + 6H_2O(l)$ was found to be -1696 ± 8 kcal./mole. From this the standard heat of formation (ΔH_{298}^0) was calculated to be 21 ± 8 kcal./mole and an estimate of the metal-ring bond energy was obtained. The metal-ring bond appears to be weaker than in the structurally analogous and isoelectronic $(C_5H_5)_2Fe$ which is in accord with the known thermal stabilities of the two compounds.

Introduction

That bis-benzenechromium(0) and its derivatives have sandwich-like structures analogous to those found in ferrocene, $(C_5H_5)_2Fe$, and other biscyclopentadienylmetal compounds is now well established.¹ Moreover, the bond in the two classes of compounds is doubtless similar in principle although there must be slight differences in detail due to the differing symmetry. In view of the qualitative similarities in the nature of the structures and in the type of bonding, a comparison of the strengths of the metal-to-ring bonds in the isoelectronic compounds $(C_6H_6)_2Cr$ and $(C_5H_5)_2Fe$ is of interest.

Experimental

The product obtained from Fischer and Hafner's procedure² was reworked five times with deaerated anhydrous ethyl ether in an argon atmosphere using a pump-out dry-box and then was fractionally sublimed twice *in vacuo*. Subsequent manipulations and material transfers were performed in a polyethylene dry-bag flushed with nitrogen.

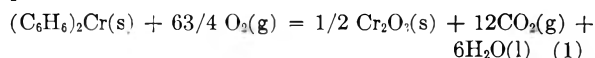
Since $(C_6H_6)_2Cr$ is a moderately oxygen-sensitive material, it must be protected from premature oxidation in the bomb. This was accomplished by melting thymol over the samples in the combustion cup under an inert atmosphere by means of an infrared heat lamp. Thymol has certain advantages over wax which had been previously used for a similar purpose; it is a definite and reproducible material and by virtue of its crystallinity has a higher mechanical resistance to collapse over empty interior pockets when under high pressures of oxygen in the bomb. Also, it is apparently a poorer solvent for $(C_6H_6)_2Cr$ than is paraffin wax and it has a conveniently low melting point (51.5°). The literature value of -1349.7 kcal./mole for the heat of combustion is rather old³ and it seemed advisable that it be re-determined. The value obtained and used in subsequent calculations was -1342.9 ± 2.3 kcal./mole for ΔE_{298}^0 (comb.).

The equipment and procedures have for the most part been described elsewhere.^{4,5} Again, in this case the combustion conditions were the same as the standard conditions for benzoic acid calibration runs except that no water was added to the bomb in order to minimize any possible hydration of oxide combustion products. The appearance of the solid combustion products was essentially the same as in the work on chromium hexacarbonyl.⁴ X-Ray powder patterns of these solids indicated that only Cr_2O_3 and metallic chromium were present. The bomb gases after combustion were analyzed for carbon dioxide by methods described in detail elsewhere.^{5,6} In all runs, deficiencies from the amount expected for complete combustion of all carbon to CO_2 were found. Several runs were made for the purpose of determining the fate of this carbon which did not appear as CO_2 . In these the solid combustion products were carefully removed from the bomb, dried, weighed and

briefly ignited and reweighed. Since no changes in weight were observed, the presence of unburned carbon or carbonaceous material is ruled out. Nor did the X-ray powder patterns give any evidence of the presence of chromium carbide. Hence it was concluded that the CO_2 deficiencies were attributable to CO , and corrections were made accordingly.^{4,6} Analyses and corrections for unburned chromium metal were made as previously described.⁴

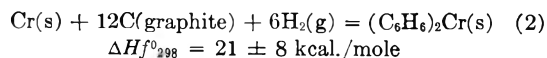
Results

The experimental data are recorded in Table I together with computed values of ΔE_{298}^0 for the process



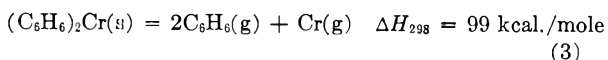
The average value of ΔE_{298}^0 is -1694.0 kcal./mole with an average deviation of ± 7.7 kcal./mole and a standard deviation of a single measurement of ± 8.1 kcal./mole. The expected maximum random error is estimated to be ± 9.8 kcal./mole. Uncertainties in the water equivalent of the bomb and calorimeter (which contribute heavily because of the large total heat of combustion of the $(C_6H_6)_2Cr$ and thymol) and in the analyses of the combustion products account for most of this error.

From the value of ΔE_{298}^0 for the combustion described by equation 1, the standard enthalpy of combustion ΔH_{298}^0 (comb.), is found to be -1696 ± 8 kcal./mole. The standard enthalpy of formation according to equation 2 has been computed using auxiliary data from the Bureau of Standards Tables.⁷ The quoted uncertainties are those due to present combustion data only; uncertainties in the auxiliary data are so small by comparison as to be negligible.



Discussion

Using the known heat of formation of benzene and the heats of vaporization of benzene and metallic chromium⁷ together with the heat of formation of $(C_6H_6)_2Cr$ given above, the enthalpy of process (3) was computed



This may be compared with the estimate previously given⁸ for the corresponding dissociation of ferrocene, *viz.*

(7) (a) "Selected Values of Chemical Thermodynamic Properties," U. S. National Bureau of Standards Circular No. 500, Washington, D. C., 1952. (b) "Selected Values of Chemical Thermodynamic Properties, Series III," U. S. Department of Commerce and National Bureau of Standards, Washington, D. C., 1947.

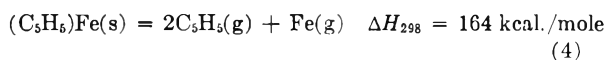
(8) F. A. Cotton and G. Wilkinson, *J. Am. Chem. Soc.*, **74**, 5764 (1952).

- (1) (a) E. Weiss and E. O. Fischer, *Z. anorg. Chem.*, **286**, 142 (1956); (b) H. Zeiss and M. Tsutsui, *J. Am. Chem. Soc.*, **79**, 3062 (1957).
 (2) E. O. Fischer and W. Hafner, *Z. anorg. Chem.*, **286**, 146 (1956).
 (3) F. Stohman, P. Rodatz and H. Herzberg, *J. prakt. Chem.* [2], **33**, 464 (1886).
 (4) F. A. Cotton, A. K. Fischer and G. Wilkinson, *J. Am. Chem. Soc.*, **78**, 5168 (1956).
 (5) F. A. Cotton, A. K. Fischer and G. Wilkinson, *ibid.*, **81**, in press (1959).
 (6) A. K. Fischer, Ph.D. Thesis, Harvard University, 1958.

TABLE I
DATA FOR COMBUSTION OF $(C_6H_6)_2Cr$

Vac. wt. of sample, g.	Cor. temp. rise, °C.	Uncor. ΔE_{298} comb., kcal./mole ^a	Cor. for thymol, kcal./mole	Cor. for Cr metal, kcal./mole	Cor. for CO, kcal./mole	Washburn cor., kcal./mole ^b	Fully cor. ΔE_{298} (comb), kcal./mole
0.4798	4.9761	-4993.6					
.4434	4.4035	-4784.3					
.4669	3.2723	-3375.9					
.9212	7.6146	-3981.2					
.5519	4.4617	-3894.3					
3365.8	-6.1	-49.4	-3.37				-1686.7
3126.0	-14.6	-23.1	-2.67				-1698.7
1727.3	-20.7	-11.0	-1.88				-1682.2
2299.6	-3.2	-11.3	-3.62				-1699.7
2201.3	-3.1	-5.2	-1.61				-1702.9

^a Mass of water plus water equivalent of bomb and calorimeter = 2316.9 ± 5.0 g. ^b Includes reduction to standard temperature, 25°, as well as the correction for the energy change of the gases.



Comparison between (3) and (4) indicates stronger bonding in ferrocene than in bis-benzenechromium, which is in accord with the observations that $(C_6H_6)_2Cr$ decomposes rapidly at about 300° into benzene and metallic chromium² whereas ferrocene

is stable up to at least 400°.⁹ While a comparison of processes similar to (3) and (4) but involving the gaseous compounds would be more appropriate, this cannot at present be done since the heat of vaporization of $(C_6H_6)_2Cr$ is not yet known. However, it is improbable that the qualitative conclusion would be altered since the heat of vaporization of $(C_6H_6)_2Cr$ is not likely to be too different from that of ferrocene, *viz.*, 16.8 kcal./mole.⁹

It is apparent that because of the high heat of combustion of bis-benzenechromium plus that of the necessary protective material and the numerous corrections necessary in converting the measured energy changes to that for a well-defined process, combustion calorimetry does not lead to as precise a value for the heat of formation as might be desired. Perhaps a more precise value could be obtained from measurements of other reactions such as the decomposition at elevated temperatures or hydrogenation to chromium and cyclohexane, if such reactions can be carried out stoichiometrically.

Acknowledgments.—We are grateful to the Mallinckrodt Chemical Company for a grant defraying some of the research expenses and to Professor G. B. Kistiakowsky for the loan of the Mueller resistance bridge.

(9) L. Kaplan, W. L. Kester and J. J. Katz, *ibid.*, **74**, 5531 (1952).

THE EFFECT OF ACIDITY AND CONCENTRATION OF BUFFERS ON PARTITION COEFFICIENTS OF DILUTE SOLUTIONS OF ACIDS AND BASES AND ON SELECTIVITY OF A LIQUID-LIQUID SYSTEM¹

BY WIKTOR KEMULA AND HENRYK BUCHOWSKI

Contribution from the Department of Inorganic Chemistry of the University, Warsaw, Poland

Received May 13, 1968

The partition coefficients of eight basic and acidic nitro compounds between organic solvents and buffer solutions of various acidities have been measured. The observed changes in partition coefficients are related to the acidity functions H_- or H_0 of the polar phase. The appropriate equations are presented. A method is described for the determination of the ionization constants and partition coefficients of un-ionized molecules from the partition data. The effect of concentrated acids on partition coefficients and the relation between acidity and selectivity are discussed.

The influence of the *pH* of the aqueous phase on partition coefficients of weak acids and bases is well known,² and equations have been derived which are applicable to dilute buffer solutions. However, we have investigated the partition of aromatic nitro compounds in highly acidic media to which these equations cannot be applied. Therefore, a more general theory, which would be valid for solutions in concentrated acids, is needed.

If the acidity of the polar phase is expressed in terms of the acidity function³ H_0 or H_- , the relationship between the partition coefficient and

acidity is given by expression (1) for bases and (2) for acids.

$$k = k^0 / (1 + 10(pK^a - H_0)) \quad (1)$$

$$k = k^0 / (1 + 10(H_- - pK)) \quad (2)$$

where k^0 denotes the partition coefficient of un-ionized molecules, and K and K^a the thermodynamic ionization constants.

In solutions of low acidity, *pH* may be substituted for H_0 or H_- in equations 1 and 2. Then K and K^a must be replaced by the ionization constants at given ionic strength, defined as

$$pK'^a = pK^a - \log(f_{BH^+}/f_B) \quad (3)$$

$$pK' = pK + \log(f_A/f_{HA}) \quad (4)$$

where f 's are activity coefficients. The resulting modifications are only for solutions of constant ionic strength.

(1) The preliminary report of the part of this communication was presented on the Polarographic Conference, Warsaw, 1956.

(2) (a) C. D. Murray, *J. Biol. Chem.*, **56**, 569 (1923); (b) C. Golumbic, M. Orchin and S. Weller, *J. Am. Chem. Soc.*, **71**, 2624 (1949); (c) C. Golumbic and N. Orchin, *ibid.*, **72**, 4145 (1950); (d) C. Golumbic and G. Goldbach, *ibid.*, **73**, 3966 (1951); (e) H. Irving, S. J. Cooke, S. C. Woodger and R. J. P. Williams, *J. Chem. Soc.*, 1847 (1949).

(3) L. P. Hammett and A. J. P. Deyrup, *J. Am. Chem. Soc.*, **54**, 2721 (1932).

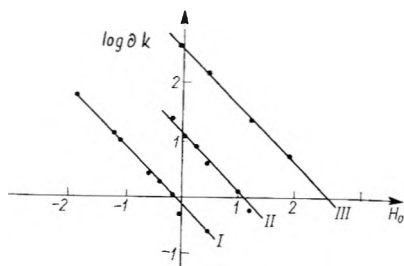


Fig. 1.—Log δk of nitroanilines in toluene-water-sulfuric acid: I, *o*-nitroaniline; II, *p*-nitroaniline; III, *m*-nitroaniline.

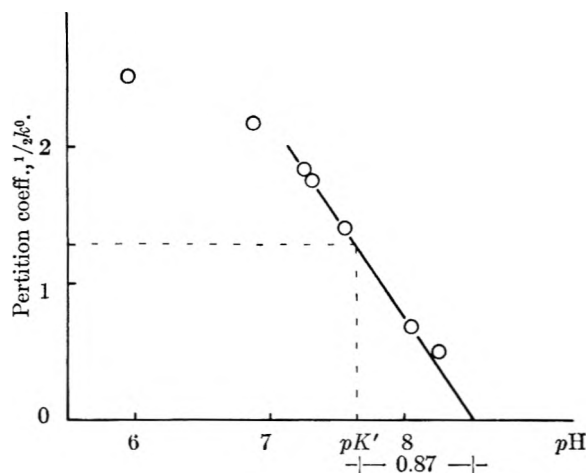


Fig. 2.—Graphical method of determining pK' and k^0 for *m*-nitrophenol in chloroform-phosphate buffer; $\mu = 0.20$.

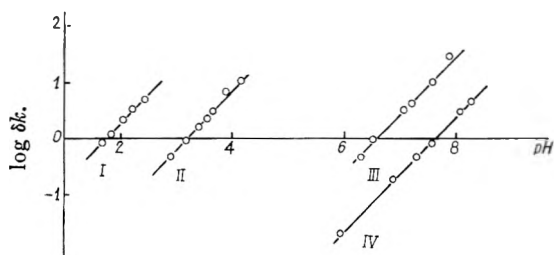


Fig. 3.—Log δk of acids as a function of pH at constant ionic strength: I, *o*-nitrobenzoic acid in benzene-sulfate buffer, $\mu = 0.16$; II, *p*-nitrobenzoic acid in benzene-acetate buffer; $\mu = 0.08$; III, *p*-nitrophenol and IV, *m*-nitrophenol in chloroform-phosphate buffer; $\mu = 0.20$.

Experimental

The partition coefficients of eight aromatic nitro compounds between organic solvents and buffered aqueous solutions were determined by measuring the concentrations in the aqueous phase before and after the mixing with the organic solvent. Partition coefficients were calculated according to formula (5), where c is the original concentration (about $10^{-3} M$), c_k the concentration after mixing with organic liquid, and ρ the ratio of the volumes of the organic and aqueous phases.

$$k = \rho \frac{c - c_k}{c_k} \quad (5)$$

The concentration of the nitro compounds was determined polarographically. The temperature of the solutions was maintained at $20 \pm 0.05^\circ$ with Höppler's ultrathermostat. The solutions were prepared and the volumes of the phases determined by weighing. Extractions were carried out at room temperature, $20 \pm 1^\circ$.

Sulfate and acetate buffers were prepared by the neutralization of 0.2 or 0.4 *M* solutions of the acid with the neces-

sary volume of NaOH solutions of the same concentration. Phosphate buffer solutions were prepared from Na_2HPO_4 and NaH_2PO_4 . The ionic strength (μ) was adjusted by the addition of NaCl.

The pH of the buffer solutions was determined by means of the pH -meter PHM3 manufactured by "Radiometer," Copenhagen. The values of H_0 of aqueous solutions of sulfuric acid were taken from Hammett and Deyrup,³ and Hammett and Paul.⁴ The results are listed in Tables I-III.

TABLE I

PARTITION COEFFICIENTS OF NITROANILINES BETWEEN TOLUENE AND AQUEOUS SOLUTIONS OF SULFURIC ACID

H_0	k_{p-}	H_0	k_{o-}	H_0	k_{m-}
7	5.5	7	44	7	15.5
1.96	5.1	0.46	35	1.96	2.5
1.23	3.5	-0.01	29	1.23	0.67
1.00	2.45	-0.14	21	0.46	.10
0.60	1.8	-.40	15.5	-0.01	.04
.46	1.10	-.60	12.0		
.27	0.61	-.12	4.1		
.05	.41	-1.20	3.4		
-.14	.21	-1.87	0.73		

TABLE II

PARTITION COEFFICIENTS OF *o*-NITROBENZOIC ACID BETWEEN BENZENE AND SULFATE BUFFERS AND *p*-NITROBENZOIC ACID BETWEEN BENZENE AND ACETATE BUFFERS

μ	pH	k_{o-}	pH	k_{p-}
0.08	1.72	0.29	2.97	1.39
	1.90	.23	3.20	1.13
	2.13	.17	3.56	0.72
	2.29	.15	3.62	.64
	2.50	.10	3.91	.40
	4.21	.22
0.16	1.68	.27	2.92	1.41
	1.85	.22	3.20	1.06
	2.07	.16	3.41	0.82
	2.24	.12	3.55	.65
	2.46	.09	3.67	.51
			3.88	.27
		4.16	.19	

TABLE III

PARTITION COEFFICIENTS OF NITROPHENOLS BETWEEN CHLOROFORM AND PHOSPHATE BUFFERS ($\mu = 0.20$)

pH	k_{m-}	pH	k_{p-}	pH	k_{o-}
5.94	2.52	6.29	0.68	7.69	83
6.87	2.17	6.53	.50	8.00	48
7.25	1.83	7.07	.25	8.39	20
7.30	1.76	7.20	.21	8.98	5.2
7.55	1.41	7.58	.09		
8.05	0.69	7.88	.04		
8.25	0.50				

p- and *m*-nitroaniline were analyzed by the chromatographic method described by Kemula⁵ and Kemula, Sybilska and Geisler.⁶ The immobile phase was rubber swelled with chloroform or a mixture of chloroform (65% by weight) and acetone (35% by weight); 4 ml. of solvent was used per gram of rubber.

Three solutions have been used as the mobile phase: (1) 0.1 *M* aqueous KCl, (2) $3 \times 10^{-3} M$ H_2SO_4 , and (3) 7% aqueous H_2SO_4 .

The mass of samples analyzed by elution method was 0.1-0.2 mg., and the initial concentration about $10^{-3} M$.

The height of the column was 12 cm.

(4) L. P. Hammett and M. A. Paul, *ibid.*, **66**, 827 (1934).

(5) W. Kemula, *Roczniki Chem.*, **26**, 281 (1952).

(6) W. Kemula, D. Sybilska and J. Geisler, *ibid.*, **29**, 643 (1955).

Discussion

We have been concerned largely with the changes of partition coefficients at acidities near to the pK or pK^a of the compounds examined. With the notation $\delta k = (k^0 - \bar{k})/k$, equation 1 and 2 may be presented in the form

$$\log \delta k = pK^a - H_0 \quad (1a)$$

or

$$\log \delta k = H_- - pK \quad (2a)$$

$\log \delta k$ should be a linear function of H_0 or H_- with the slope -1 or $+1$ and should cut the acidity axis at the point $H_0 = pK^a$ or $H_- = pK$.

In Fig. 1 the values of $\log \delta k$ for the nitroanilines in the system, toluene-water-sulfuric acid, are plotted against H_0 . The circles denote experimental points calculated from the data in Table I. The k^0 values were assumed to equal the partition coefficients found for toluene and water. This assumption is justified because the degree of ionization of nitroanilines in aqueous $10^{-3} M$ solutions is negligible. The solid lines correspond to the theoretical values of $\log \delta k$ computed from eq. 1a. The reported acidic ionization constants of nitroanilines^{4,7} have been taken as pK^a . As Fig. 1 shows, the agreement between the experimental and theoretical values is satisfactory.

Difficulties were encountered in our attempt to show in the same way that the experimental values for the nitrobenzoic acids and nitrophenols (Tables II and III) follow equation 2. pK' values at a given ionic strength (see eq. 4) are unknown, and k^0 cannot be determined by measuring partition between water and organic solvent, because (1) the degree of ionization of these compounds in water is considerable; and (2) k^0 between water and an organic phase and k^0 between a buffer and the same organic phase differ considerably due to the salting out effect. On differentiation of eq. 2 with respect to H_- we obtain

$$\frac{dk}{dH_-} = -k^0(\ln 10)(10^{H_- - pK} + 10^{pK - H_-} + 2)^{-1} \quad (6)$$

In the neighborhood of the point $H_- = pK$, the value of the derivative (6) is almost constant; therefore k is approximately a linear function of H_- near this point. Its equation is

$$k = -1/4k^0(\ln 10)(H_- - pK - 2/\ln 10) - 0.575k^0(H_- - pK - 0.87) \quad (7)$$

An analogous equation holds for pH and pK' . The deviations of the approximative values of k from the exact values, given by formula (2) depend on the difference $pH - pK'$; the deviations are smaller than 1% within the range of about one-half pH unit and slightly over 5% within one pH unit.

The straight line represented by equation 7 cuts the pH axis at $pH = pK' + 0.87$; this relation suggests a graphical method for the determination of pK' which is illustrated in Fig. 2. Since at $pH = pK'$, $k = 1/2k^0$ the value of the partition coefficient of un-ionized molecules is determined simultaneously. The values of pK' and k^0 then obtained are listed in Table IV.

(7) R. C. Farmer and F. J. Warth, *J. Chem. Soc.*, **85**, 1726 (1904).

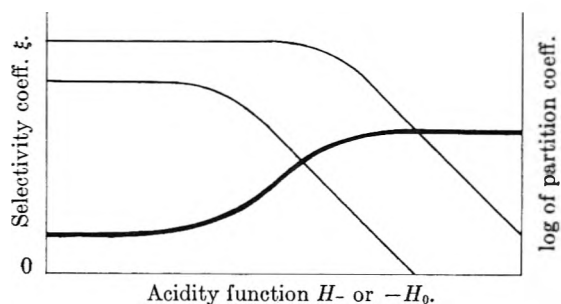


Fig. 4.—Selectivity coefficient as a function of acidity; Case A, heavy line, $\xi = |\log \beta|$; fine lines, $\log k$.

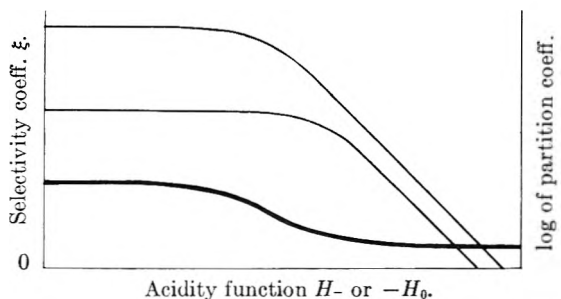


Fig. 5.—Selectivity coefficient as a function of acidity; case B1.

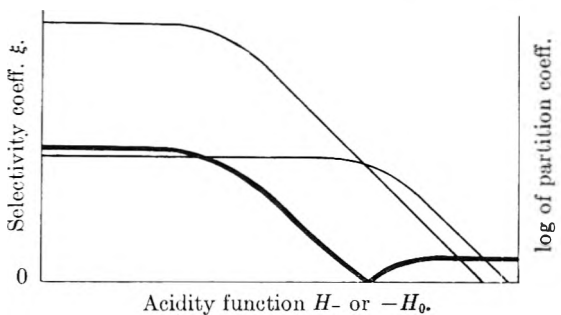


Fig. 6.—Selectivity coefficient as a function of acidity; case B2.

TABLE IV

Compound	System	μ	pK'	k^0
<i>o</i> -Nitrobenzoic acid	Benzene-sulfate buffer	0.08	1.86	0.50
<i>p</i> -Nitrobenzoic acid	Benzene-acetate buffer	.08	3.28	2.06
<i>m</i> -Nitrophenol	Chloroform-phosphate buffer	.20	7.64	2.57
<i>p</i> -Nitrophenol	Chloroform-phosphate buffer	.20	6.43	1.2

When the k^0 values are known, δk for various pH 's can be calculated. Figure 3 represents $\log \delta k$ as a function of pH . The agreement between the experimental (circles) and theoretical values (lines) is satisfactory.

The Influence of Acidity Upon Partition Coefficients of Un-ionized Molecules.—The partition coefficients of *p*-nitrobenzoic acid and *m*-nitrophenol in solutions with a pH much smaller than the pK of the compounds, are equal to k^0 ; therefore, they are constant, and independent of pH . But k^0 values in sulfate buffer differ from those in acetate buffer, so they depend on the substances used as a buffer and on the concentration of it. The influence of

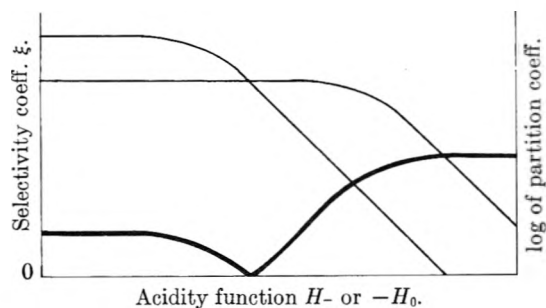


Fig. 7.—Selectivity coefficient as a function of acidity; case B3.

changes in medium on k^0 , is particularly important in the case of solutions in concentrated acids, in which the variation of H_0 with concentration is slow. The k^0 values of the nitroanilines in toluene-water-sulfuric acid are constant within the limits of experimental error, but such behavior is rather exceptional. We have observed that the k^0 values of the nitrotoluenes and chloronitrobenzenes are much affected by the increased concentration of sulfuric acid. $\log k^0$, however, is a linear function of H_0 . According to the theory of mixed solvents,⁸ if the composition of one phase is variable and that of the other is constant, the logarithm of the partition coefficient is proportional to the volume fraction of the components in the variable phase. But volume fractions are proportional to molarity, and the acidity function H_0 in water-sulfuric acid mixture is a linear function of molarity; hence $\log k^0$ is a linear function of H_0 . The behavior of azulenes in many acidic systems⁹ conforms with this relationship.

Acidity and Selectivity.—The selectivity of a liquid-liquid system with respect to a given mixture i.e., the separability of the mixture by extraction, is usually characterized by the ratio of the partition coefficients $\beta = k_2/k_1$. A system is selective if β or $1/\beta$ is high. Therefore to avoid confusion it is more convenient to use $|\log \beta| = \xi$ as a measure of selectivity. The variation of selectivity with acidity is represented in Figs. 4-7, where ξ , denoted by heavy lines, is plotted vs. H_- or pH in the case of acids and vs. $-H_0$ or $-pH$ in the case of bases, i.e., in the direction of increasing degree of ionization. With two exceptions, the selectivity of the mixtures examined increases with increasing degree of ionization, as shown in Fig. 4. The exceptions are *o*- and *m*-nitrophenol in chloroform-phosphate buffer and *p*- and *m*-nitroaniline in toluene-water-sulfuric acid. In the former case selectivity decreases with increasing pH . In the latter case the effect of acidity on selectivity, which is shown in Fig. 7, is more complicated; as the degree of ionization increases, ξ at first decreases to zero and then increases.

With the notation $\Delta \log k^0 = \log k_2^0 - \log k_1^0$ and $\Delta pK = pK_2 - pK_1$ and the assumption that $pK_2 > pK_1$, the influence of acidity on selectivity can be generalized as follows.

1. Selectivity varies appreciably for acidities

(8) W. Kemula and H. Buchowski, "Communication on XVIth International Congress of Pure and Applied Chemistry," Paris, 1957.

(9) P. A. Plattner, E. Heilbronner and S. Weber, *Helv. Chim. Acta*, **32**, 574 (1948).

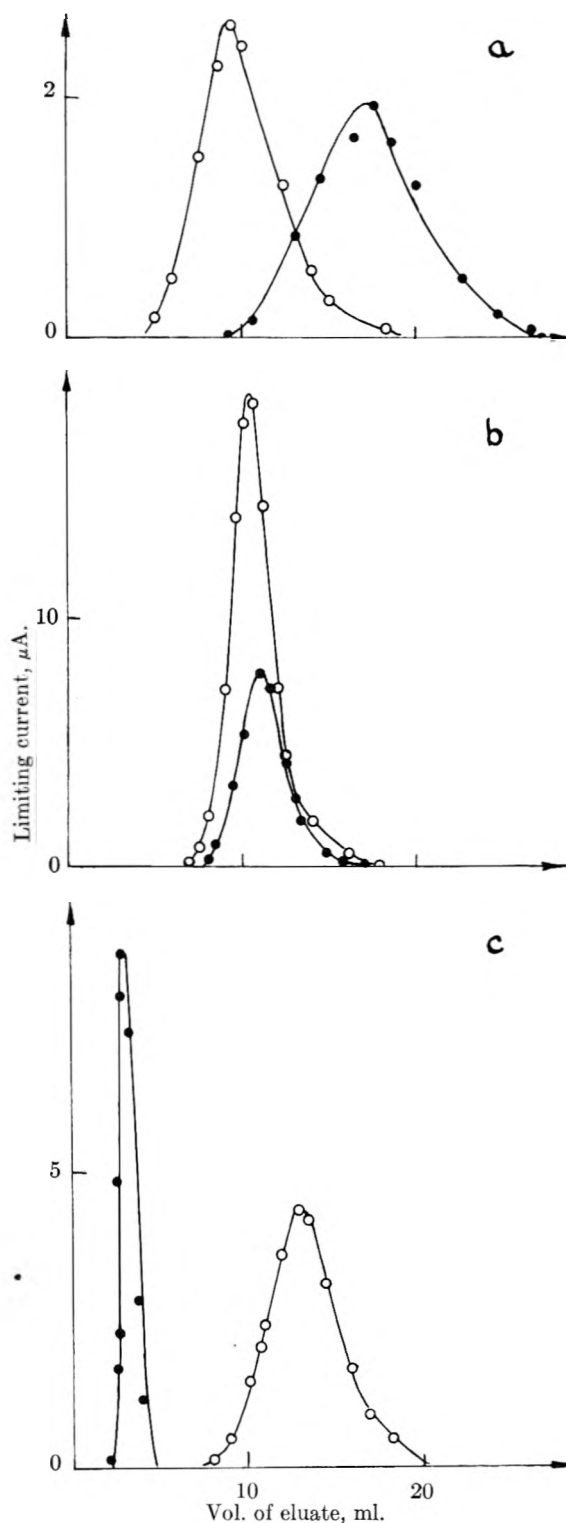


Fig. 8.—Chromato-polarographic analysis of *p*- and *m*-nitroaniline with various acidities of eluent: a, $H_0 = 7$; b, $H_0 = 2.5$; c, $H_0 = 0$; ●, *m*-nitroaniline; ○, *p*-nitroaniline.

within the range $pK_1 - 1, pK_2 + 1$. For higher or lower acidities selectivity remains constant.

2. The limiting values of ξ are $|\Delta \log k^0|$ and $|\Delta \log k^0 + \Delta pK|$ or $|\Delta \log k^0 - \Delta pK^a|$.

3. The variation of selectivity is dependent on $\Delta \log k^0$ and ΔpK . Four cases are possible.

A. If $\Delta \log k^0$ and ΔpK of acids have the same sign or if $\Delta \log k^0$ and ΔpK^a of bases have different signs (in other words if k^0 of the stronger acid or stronger base is lower than k^0 of the weaker acid or weaker base), selectivity varies as shown in Fig. 4.

B. If $\Delta \log k^0$ and ΔpK of acids have different signs or if $\Delta \log k^0$ and ΔpK^a of bases have the same sign (in other words if k^0 of the weaker acid or weaker base is lower than k^0 of the stronger acid or stronger base) there are three possibilities: (1) $|\Delta pK| < |\Delta \log k^0|$ which is shown in Fig. 5; (2) $|\Delta \log k^0| < |\Delta pK| < 2|\Delta \log k^0|$ which is shown in Fig. 6; and (3) $|\Delta pK| > 2|\Delta \log k^0|$ shown in Fig. 7.

In case A, which is the most common, and in B.3 the selectivity of a liquid-liquid system with respect to acids is highest when H_- or pH of the polar phase is greater than $pK_2 + 1$; on the contrary selectivity with respect to bases is highest when H_0 or pH is smaller than $pK_1^a - 1$. In the two other cases the most favorable acidity range is H_- (or pH) $< pK_1 - 1$ for acids and H_0 (or pH) $> pK_2^a + 1$ for bases.

Analysis of many acidic and basic substances may be improved greatly by applying above principles.¹⁰ An example is presented in Fig. 8. The effect of acidity is illustrated by the chromatopolarographic analysis of a mixture of *p*- and *m*-nitroaniline. For these compounds $pK_{meta}^a = 2.6$, $pK_{para}^a = 1.1$, $\log k_{meta}^0 = 1.2$, and $\log k_{para}^0 = 0.7$. The limiting current measured by a potential of -1.0 v. is plotted against the volume of eluate. The solid circles refer to *m*- and the open circles to *p*-nitroaniline. When H_0 of the mobile phase is 7, water as eluent, with 12 cm. long column a partial separation is obtained (Fig. 8a). With a more acidic eluent ($H_0 = 2.5$), the conditions of separation become still more unfavorable (Fig. 8b),

because the mixture belongs to type B.3 ($\Delta \log k^0 = 0.5$, $\Delta pK^a = 1.5$); the selectivity at first decreases as the degree of ionization increases. However ΔpK^a is large and selectivity reaches a maximum, $\xi_{max} = |\Delta \log k^0 - \Delta pK^a| = 1.0$, when the acidity function H_0 of the mobile phase is lower than $pK_{para}^a - 1 = 0.1$. Therefore, the use of 7% sulfuric acid ($H_0 = 0$) leads to complete separation of the mixture (Fig. 8c).

As the acidity of the aqueous phase increases, the degree of ionization of the nitroanilines increases; this results in a decrease of the partition coefficients, *i.e.*, the ratio of the concentration in the immobile to the concentration in the mobile phase falls off. This condition is unfavorable for separation, because although the selectivity is high, the mixture leaves the chromatographic column too quickly. For separation an increase of the partition coefficients is required; this was accomplished in the case discussed by the use of 65% chloroform-35% acetone as the immobile phase.

Owing to application of polarographic method very dilute solutions could be used, in which the partition coefficients of nitroanilines are independent of their concentration, *i.e.*, the partition isotherms are linear.

Our results show that optimum selectivity is not limited to a single point; a range of acidity exists in which selectivity attains a constant, maximum value. Therefore, by the choice of suitable organic solvents and proper adjustment of the acidity of the polar phase, it is always possible to obtain the most favorable conditions for the separation of a mixture, *i.e.*, maximum ξ and $\log \rho k_{1,2} = \pm 1/2\xi$. The exact values of the ionization constants and k^0 need not be known.

Acknowledgments.—The authors take the opportunity to thank Mr. and Mrs. W. Pawłowski for technical assistance.

(10) (a) H. Buchowski and Z. Olempska, *Chem. Anal.*, in press; (b) H. Buchowski and W. Pawłowski, *ibid.*, in press.

ADSORPTION OF FLUORINATED METHANES BY LINDE MOLECULAR SIEVES

BY PETER CANNON

General Electric Research Laboratory, Schenectady, New York

Received September 26, 1958

The adsorption of CHClF_2 on Linde 4A Molecular Sieve has been measured, and the effect of the gas on the Sieve has been defined by CO_2 adsorption measurements and by thermogravimetric, X-ray, mass spectrometric and classical analyses. The observed sorption of CHClF_2 is small and irreversible, and the CHClF_2 decomposes upon heating the system, leaving CO_2 in the lattice. The isotherms are type 1 (Brunauer's classification). Extended calculations have been made for some of the isotherms. CHClF_2 sorbs very strongly on Linde Sieve 5A (type 1 isotherm). On reducing the pressure of CHClF_2 over the solid, anomalous desorption results are obtained, explicable only on the basis that CHClF_2 decomposes on the Sieve at 25° , to form more volatile materials. The results are consistent with the formation of small but significant amounts of carbon dioxide. Continued evacuation of the system results in loss of adsorbent weight but no gross collapse of the solid lattice is seen by X-ray diffraction. Analytic and thermogravimetric studies of the system have also been made. CHClF_2 sorbs reversibly on an Alcoa F-1 alumina sample, in marked contrast with the behavior on Linde Sieve 5A at the same temperature and pressure. The adsorption of CCl_2F_2 by Molecular Sieve 5A is slow at pressures of the order 100 mm. No decomposition of CCl_2F_2 is seen in these experiments, in strict comparison with those results obtained from CHClF_2 systems. It was found that CCl_2F_2 is strongly bound to the sieve substrate at $25\text{--}50^\circ$, and is not removed readily by pumping. The non-equilibrium results are meaningful for an interpretation of the kinetics of CCl_2F_2 adsorption. The adsorption is thought to occur in two stages, the second of which is controlled by a pore field screening effect. Approximate energies for the adsorption process have been estimated from some of the data. The second stage adsorption gives heats in the range 6–10 kcal. per mole adsorbed, the first stage involving even higher values.

Introduction

4A Molecular Sieve is a synthetic crystalline zeolite of the general formula $\text{Na}_2\text{O}\cdot\text{Al}_2\text{O}_3\cdot 2\text{SiO}_2\cdot n\text{H}_2\text{O}$.¹ The synthetic zeolites differ from the natural zeolites (*e.g.*, chabazite) principally in their lattice geometry.

Both the natural and synthetic materials exhibit a remarkable selectivity of sorptive properties^{1,2} commonly supposed to be due to a very narrow range of physical dimensions and energetic properties of the pores. These may be altered, to a certain extent, at will, by substituting the free cations in the pores. Thus, replacement of two Na^+ ions by a Ca^{++} ion results in a net increase of the minimum cross sectional area of the pore. By such methods, 4 or 5A pores may be obtained in the zeolites.

The data issued by the Linde Company³ show the adsorption of various gases on solid materials, among the latter being Linde sieves 4A and 5A. Separations are claimed for $\text{CCl}_2\text{F}_2\text{--CCl}_3\text{F}$ and for $\text{CCl}_2\text{F}_2\text{--C}_2\text{Cl}_2\text{F}_4$ mixtures.⁴ The minimum ratio of molecular radii for which separation is claimed is 1:1.08 (CCl_2F_2 , $\text{C}_2\text{Cl}_2\text{F}_4$). However, not only the relative dimensions but also the absolute size of the diameters are of importance. Thus, the ratio of the diameters of CCl_2F_2 and CCl_2F_3 , and CCl_2F_2 and CCl_3F are 1:1.08 and 1:1.11, respectively (calculated from refraction data), and the critical dimension of CCl_3F is 4.9 Å. Here then a separation is claimed of the molecules CCl_2F_2 and CCl_3F (with diameters 4.4 and 4.9 Å.) on a 5A sieve. It is logical to suppose from this that not one but both molecular diameters influence the separation.

The diameters of the molecules of CCl_2F_2 and CHClF_2 have been calculated as 4.4 and 4.0 Å., respectively, as measured from plane projections of the molecular configurations, based on the atomic

radii cited by Neuberger.⁵ This model does not include possible polarization effects, but calculations based on the molar refraction values of the C–H, C–F and C–Cl bonds appearing in Glasstone⁶ do include these effects and give a ratio of molecular radii of 1.13:1. This relative agreement shows the smallness of permanent dipole formation. A separation might then be expected for CCl_2F_2 and CHClF_2 on a sieve material with a pore size of 4.5–4.9 Å.

Even so, the precise pore sizes of the 4A and 5A sieves cannot be used to predict the exact adsorption behavior of gases on these zeolites. It is therefore necessary to make direct measurements of adsorption to determine whether a separation of CHClF_2 and CCl_2F_2 might be obtained using sieves 4A and 5A. There are few data in the literature on this subject, except for an observation by Barrer² that CHClF_2 decomposes on natural chabazite whereas CCl_2F_2 does not sorb to a comparable extent. Breck, *et al.*,¹ have reported single points for CCl_2F_2 adsorption on Sieves 4A and 5A.

Experimental

Apparatus.—All the adsorption experiments were done on an automatic recording electromagnetic sorption balance. This instrument is operable over the pressure range 1 μ –20 atmospheres. It is to be described in full elsewhere. Its sensitivity in the configuration used in this work was 0.05 mg./g., and the experiments were planned to produce a change in weight of the specimen of the order of 1 g.

Other experiments involving storage of gases over solids were conducted in "Hoke" stainless steel flasks, equipped with "Hoke" RB231 or 2RB281 needle valves and stainless steel or prime brass pipe.

Chemicals.—Carbon dioxide gas was freeze dried and vacuum distilled.

Chlorodifluoromethane was prepared from tank grade material by low temperature distillation and stripping. The product purity was 99.3+ % molar (determined by gas chromatography).

Dichlorodifluoromethane was prepared from tank grade material by differential hydrolysis, freeze drying and vacuum distillation. The product purity was 99.8+ % molar.

(1) D. W. Breck, *et al.*, *J. Am. Chem. Soc.*, **78**, 5963 (1956).

(2) R. M. Barrer and D. W. Brook, *Trans. Faraday Soc.*, **49**, 947 (1953).

(3) Molecular Sieve Data Sheets, Linde Co., Tonawanda, N. Y.

(4) *Chemical Week*, p. 66, Nov. 20, 1954.

(5) A. Neuberger, *Z. Krist.*, **93**, 1 (1936).

(6) S. Glasstone, "Textbook of Physical Chemistry," 2nd edition, p. 538.

The Linde Molecular Sieve samples were carefully quarter-sampled from single batches.

Determination of the Surface Area of the 4A Sieve.—The isotherm (Fig. 1) of the adsorption of carbon dioxide on 4A sieve at 25° after 8 hours evacuation (10^{-2} μ) at 350° is of a simple type. No adsorption hysteresis was observed. A Langmuir plot of the sorption points was linear from 2 to 8510 mm. CO₂ pressure (Fig. 2). Below 5 mm. pressure on desorption, a branch of the Langmuir plot was obtained corresponding to a lower available specific surface area than the main line (inset, Fig. 2). The value for the principal available specific surface area (calculated on the basis that carbon dioxide is present on the surface as a liquid two-dimensional film) is 566.6 sq. m./g. This is less than the value of 810 sq. m./g. obtained by D. W. Breck, *et al.*,¹ using oxygen at low pressure and at -183°.

The observed adsorption isotherm is in agreement with the more limited data of the Linde Co.⁵ over the relevant pressure range.

Adsorption of Freon-22 (CHClF₂) on Sieve 4A.—The sample of Sieve 4A previously used for the CO₂ determination of surface area was outgassed at 350° for 15 hours. CHClF₂ gas was admitted to the system and a small type I adsorption was observed at the lowest pressures. Subsequent increases in pressure to 8000 mm. gave slight further increases in weight. The isotherm, corrected for buoyancy effects, is shown on Fig. 3 together with the Langmuir plot. A small, permanent, positive residual adsorption was observed on pumping the system at 25° for 60 hours. A "step" of constant pressure was observed at 23 μ for 10 hours during the pump down. A portion of the fouled sample, when analyzed for volatile matter, gave only carbon dioxide in a mass spectrometric run during which the sample was heated to 1000°. The amount of CO₂ corresponded with 15 mg. CO₂/g. Sieve 4A, compared with a residual adsorption of 26 mg./g. No hydrochloric or hydrofluoric acid was seen. Halogen products subsequently were found in the solid residuum where they presumably are present in a fully ionized form.

It seemed highly desirable to determine whether the carbon dioxide was formed as a result of heating the fouled sample, or was already present as such on the sieve 4A as a result of CHClF₂ sorption. A sample of Sieve 4A (4 g.) was therefore outgassed at 350° for 15 hr. in a small stainless steel (316) bomb. It was allowed to cool, and CHClF₂ was distilled in (100 g.). A separate sample of CHClF₂ also was taken in a clean, empty, stainless steel bomb. Both vessels were maintained at 25° for three weeks. Infrared spectra of the gas phase in each bomb were taken (the gas pressure was the saturation pressure of CHClF₂ in each case). The treated sample showed a band at 4.30 μ (absorbance 0.64) which was not present in the untreated sample (absorbance at 4.30 μ , 0.252). In addition, the treated sample showed a pair of less well marked bands at 14.66 and 15.08 μ which did not appear in the spectrum of the clean material. The first band is assignable to carbon dioxide; the other two have not been assigned, but they may represent some carbon-multiple chlorine grouping (-CCl₂, -CCl₃) which was not present in the original material. Quantitative analyses of the gases were obtained by gas phase chromatography. The apparatus was a Perkin-Elmer "Vapor Fractometer" ("J" column at 100°), and the sample size was 2 cc. of gas. Carbon dioxide was found to be present to the extent of less than 0.1% in the untreated sample, but was 0.4% of the treated CHClF₂ gas phase. Also found in the reacted CHClF₂ were H₂O, 0.1%, and CCl₂F₂, the content of which decreased from 0.20 to 0.15% over Sieve 4A.

The solid residue from the above experiment was once more stored with purified CHClF₂ for three weeks at 25°. No decomposition products at all were seen on this occasion. The decomposition is therefore apparently a self-limiting surface reaction. Thermogravimetric analysis of the CHClF₂-reacted sample indicated that it took up less water on exposure to the atmosphere than a clean portion used as a control. The total material volatilized between 100-400° was less for the fouled sample than for the clean material, indicating an over-all loss in surface activity.

An X-ray diffraction pattern of the fouled material showed that no gross structural change had taken place in the sample fouled with CHClF₂ at room temperature. Hence it appears likely that the oxygen in the CO₂ product was in this case not removed from Si-O-Si links but from

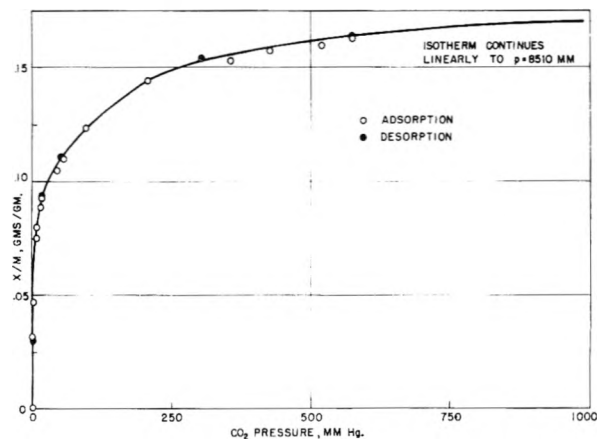


Fig. 1.—Adsorption of carbon dioxide on Sieve 4A at 25°.

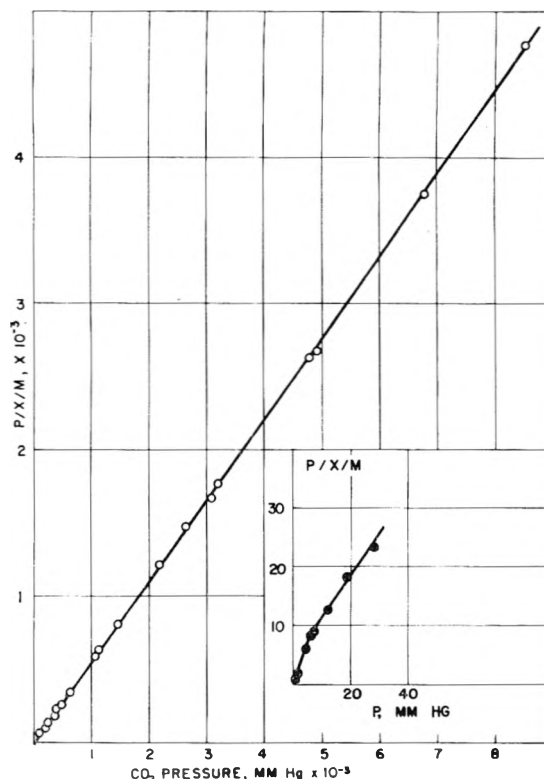


Fig. 2.—Langmuir isotherm of CO₂ on Sieve 4A at 25°.

the constitutional water of the Sieve, present as terminal silanol or aluminol groups.

CO₂ Isotherms on CHClF₂ Treated Sieve 4A.—A portion of the sample which has been in contact with CHClF₂ was restudied using carbon dioxide at 25°. The sample was pumped in the cold for more than one week to clean it as well as possible without baking it. The residual gas pressure was 0.5 μ .

Sorption was slow and the equilibrium values are less than those for CO₂ on the clean 4A sieve. The Langmuir plot is shown with the isotherm on Fig. 4. The isotherms with the reacted material showed apparent hysteresis loops when less than 8-24 hr. were allowed for each point. The extent of these apparent hysteresis loops was dependent on the previous maximum pressure of CO₂ which had been attained. This behavior suggests the presence of small traces of permanent gas formed during the earlier sorption of CHClF₂.

The surface areas corresponding with the two branches of the Langmuir plot are 220 and 290 sq. m./g., respectively, (assuming a liquid 2-dimensional model for the sorbed carbon dioxide). The thermodynamic work of compression to achieve a certain surface coverage has been calculated for

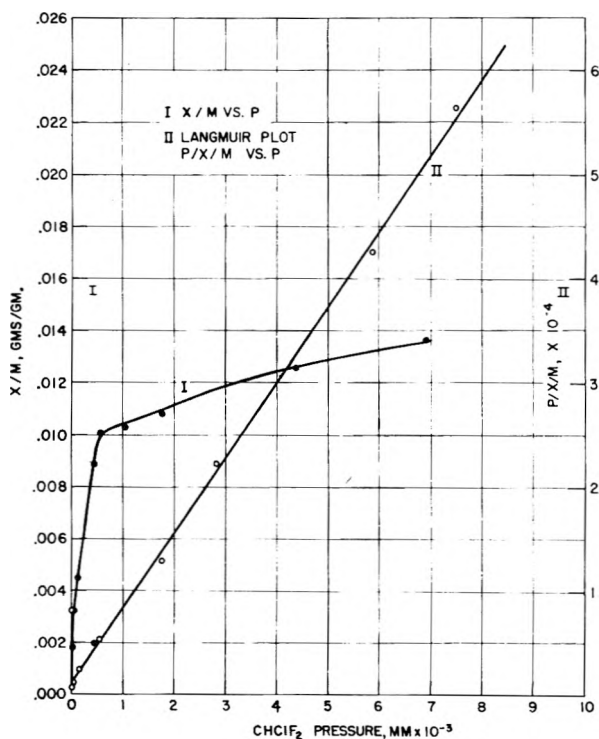


Fig. 3.—I, adsorption isotherm of CHClF_2 on Sieve 4A at 25° ; II, Langmuir plot of same.

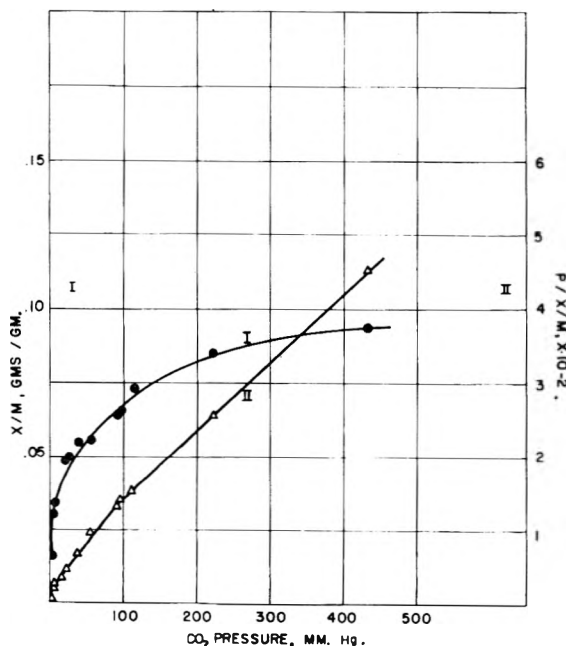


Fig. 4.—I, adsorption isotherm of CO_2 on CHClF_2 -treated Sieve 4A at 25° ; II, Langmuir plot of same.

both substrates, and is less for the CHClF_2 -treated 4A at all coverages. The available surface of Sieve 4A is apparently decreased and de-energized after contact with CHClF_2 .

Sorption of CHClF_2 on Sieve 5A.—Since the data reported above for the adsorption of carbon dioxide on clean Sieve 4A were in substantial agreement with those issued by the Linde Company,⁵ it was unnecessary to make new measurements of the adsorption of carbon dioxide on Sieve 5A, and the surface area of the 5A sieve to carbon dioxide at 25° was calculated from the published isotherm.⁵ A value of 592 sq. m./g. was obtained, using the Langmuir equation.

A sample of Sieve 5A was outgassed at 350° , as with 4A.

The sorption of CHClF_2 on Sieve 5A was measured at 25° (Fig. 5). The results are highly unusual.

The general form (Type I) of the isotherm is similar to that with Sieve 4A: however, the adsorption of CHClF_2 is much larger than with 4A. Equilibrium was attained quite rapidly: 90% of the weight increase for each dose was reached in less than one hour, and four hours only were required for experimentally steady values of weight increase to be reached. The isotherm was run up to the flat portion, and at 163.9 mm. CHClF_2 pressure a desorption cycle was commenced. Upon removing a little of the system gas, however, a large loss in weight was seen, placing the desorption curve below the adsorption plot. The divergence of the two curves became even more marked down to a pressure of approximately 20 mm. Each desorption point took more than one day to equilibrate. Below 20 mm. pressure the desorption curve approached the adsorption curve, but still lay below and to the right of it. In this pressure region, the system equilibrium pressures "bunched" together, with continuously dropping sample weights. These "steps" in the isotherm were seen at 11 and 6 mm. pressure. None of the plausible reaction products have a vapor pressure at 25° which corresponds with either of these values.

At still lower system pressures, the apparent adsorbent weight became less than the initial sample weight. On torching the cold traps between pumpings, a substantial amount of a white solid which melted well below 0° was removed; however, no etching of glass or attack on the brass lines leading in and out of the traps was seen. The absence of such degradative attack was taken to imply that water and acid fluoride products are not co-formed in the desorption. The experiment was discontinued when the sample had lost about 160 mg. of its initial weight. At this stage, the system was still very gassy, the lowest pressure reached at equilibrium after any one pumping being 23 μ .

The results have been plotted as observed (Fig. 5) and according to the Langmuir equation (Fig. 6). Using a liquid CHClF_2 model, the adsorption branch gives a value for the specific surface area of Sieve 5A to CHClF_2 of 340.4 sq. m./g. This may be compared with the value found for CHClF_2 on Sieve 4A of only 15.1 sq. m./g.

When the gas evolved from a heated sample of the reacted material was dissolved in alkali, no halide ions were found in the resultant solution. However, carbonate, and only carbonate was found: the amount corresponds with a carbon dioxide content in the pumped-out solid of 8.3 mg. CO_2 /g. Sieve.

A comparison of the X-ray diffraction patterns of the sample and a portion of clean material showed no significant differences in the over-all structure of the Sieve as a result of the CHClF_2 treatment, though an increase in amorphous background was seen. Thermogravimetric analysis curves indicated that the reacted sample evolved considerably less volatile material on heating to 400° after exposure to the atmosphere than a clean sample used as a control. It appears that the surface has been modified in such a way as to permit little water to be taken up from the atmosphere. The profiles of the TGA curves differ; that for the reacted material drops linearly from the very beginning of the heating cycle (25°) to 400° suggesting the presence on the lattice of materials volatile below 100° . The profile for the unreacted material shows no drop in weight commences until a temperature of 100° is attained.

Adsorption of CHClF_2 on Alumina.—This system was studied for comparative purposes. The adsorption isotherm (25°) of CHClF_2 on alumina (Alcoa F-1), which had been outgassed at 350° for 15 hours, is shown on Fig. 7, curve I, and the corresponding Langmuir isotherm is curve II of the same figure. The isotherm continued to rise with increasing CHClF_2 pressure and did not become flat. This suggests strongly that the isotherm would actually become concave toward the y -axis at even higher pressures (*i.e.*, of type II or IV rather than type I). The Langmuir plot is linear over a wide intermediate range of pressures, but not over all the observed pressure range, owing to this curvature. The specific surface area of the alumina sample to CHClF_2 over the intermediate range of pressure is 182 sq. m./g. The desorption curve was found to coincide with the adsorption branch. Thus this alumina does not decompose CHClF_2 at 25° .

Sorption of CCl_2F_2 on Sieve 5A.—D. W. Breck, *et al.*,¹ have published single adsorption points for the adsorption

of CCl_2F_2 on 4A and 5A sieves at room temperature. The adsorptions, expressed as x/m values in g./g. were 0.003 on 4A and 0.084 on 5A, at 700 mm. pressure and "room temperature." In the absence of any more definite information it was essential that these systems be studied further. However, the reported adsorption of CCl_2F_2 on 4A is so small that it was decided to study adsorption on 5A only, so that any peculiarities in the surface interactions in this type of system might be magnified.

The Sieve samples were degassed in the same way as before, and CCl_2F_2 was purified to better than 99.8% (mole basis) before use. When 1-2 hr. only was allowed for each point to be taken, spurious type IV isotherms were obtained (Fig. 8, 25 and 35°). Equilibration was subsequently found to be very slow between 5 and 800 mm. pressure. In each case the desorption behavior was different from that seen before. A hard vacuum ($10^{-2} \mu$) was realized in a short time, but no great decrease in sample weight was seen. In fact, the total decrease in weight that was seen was of the order 0.01 g./g. On attempting to remove the CCl_2F_2 from the 5A by heating and pumping, it was found that heat had no effect up to about 200°. Subsequently some gas began to be removed but it was still difficult to remove any large amount until 300° was reached.

Adsorption isotherms were also measured at 29.6 and 40.0° (Fig. 8). In these experiments, considerably more time was allowed at lower pressures, and the points came to equilibrium after 2 days each. As a result, these two isotherms tend more to a type I form than do the 25.0 and 35.1° measurements. The higher pressure regions of all four isotherms (p_1 more than 750 mm.) have a ready rationale, since they show the expected negative temperature coefficient of adsorption.

The saturation of the Sieve with CCl_2F_2 also was studied. A sample of Linde Sieve 5A was equilibrated with CCl_2F_2 to an x/m value of 0.193 by allowing the sample to remain seven days in contact with the vapor at more than 2000 mm. pressure at room temperature. This sample was pumped down hard at room temperature to a pressure of 0.01 μ , brought to 35° and 3138.9 mm. pressure of CCl_2F_2 admitted. After one day, a small change in weight had taken place: the change in the sorption $\Delta x/m$, between 0.01 μ and 3138.9 mm., was 0.0031, corresponding with extracrystalline sorption only. It is clear that the internal surface of the Sieve was saturated with respect to CCl_2F_2 by that quantity of gas which had been adsorbed earlier. The system was once more pumped down in the cold, for a day. The sample weight returned to its previous value, corresponding with an x/m of 0.193.

In calculating x/m values from the experimental data, buoyancy corrections were made for the volume of gas displacing by the solid higher pressures. These buoyancy and the density determinations revealed that although the sieve had been saturated with CCl_2F_2 , there was still an appreciable void space within it.

The residual gas from the 29.6° experiment was analyzed by gas phase chromatography. It was identical with the starting material: CCl_2F_2 is not decomposed by Sieve 5A (and, by inference, not by Sieve 4A).

Discussion

The Surface Chemistry of the CHClF_2 -4A System.—The results are consistent with a Langmuir type adsorption of CHClF_2 on separate, non-interacting sites. The system appears to be almost a model for this type of adsorption, except for the decomposition of CHClF_2 which sets in when the last sorbed residues are removed.

The magnitude of the observed adsorption makes it seem likely that the process occurs only on the outside of the microcrystals. Consideration of the physical size of the CHClF_2 molecule also makes this likely. However, the gradual increase in sorption at higher pressures makes slow reaction or lattice penetration also possible. The reduced adsorption of CO_2 on cold-pumped Sieve 4A after CHClF_2 contact would then be explicable in either of two ways. First, some pores may be blocked at all entrances by tightly bound CHClF_2 . In this

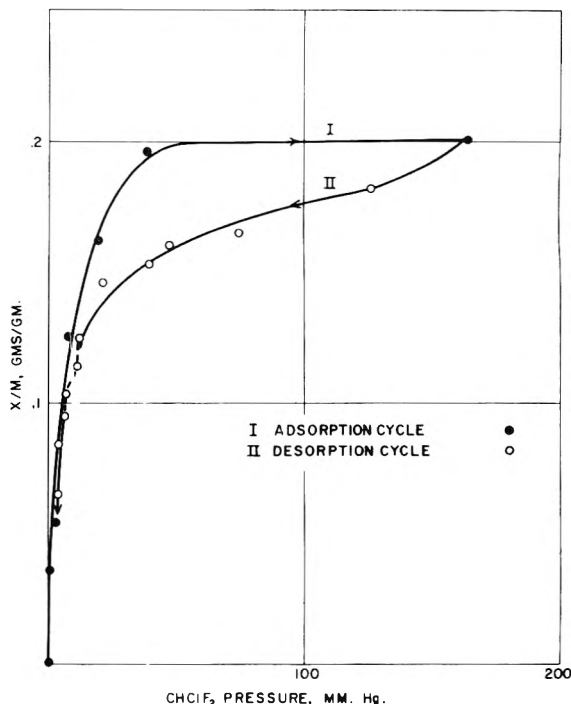


Fig. 5.—Adsorption and desorption isotherms of CHClF_2 on Sieve 5A at 25°. The anomalous desorption plot shows clearly the breakdown of CHClF_2 on the surface.

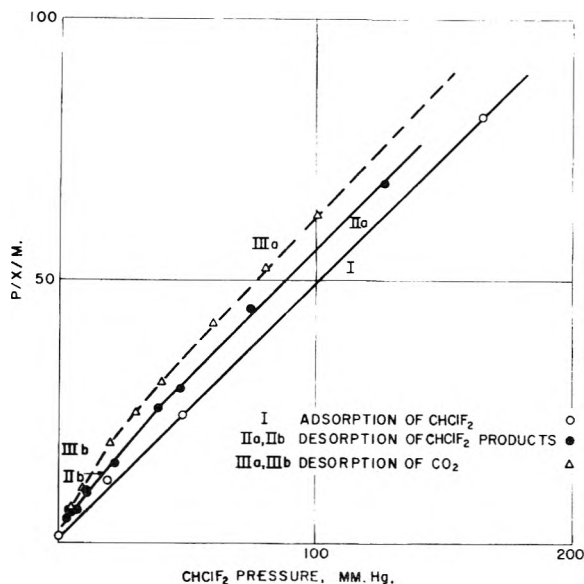


Fig. 6.—Langmuir plots for CO_2 adsorption, CHClF_2 adsorption and CHClF_2 desorption on Sieve 5A at 25°.

case, there would still be sufficient accessible pores that CO_2 adsorption at lower pressures would be the same as on the clean sieve (*i.e.*, incomplete occupation of any given set of sites). Secondly, the sorbed CHClF_2 may be coupled with the molecularly inhomogeneous ionic field of the substrate, giving strong dipole formation, or have reacted to give a reduced internal field. This would also account for the permanent weight change observed on desorption, which would be due only to those sites covered by the non-removable CHClF_2 residues and would modify not only the magnitude of the

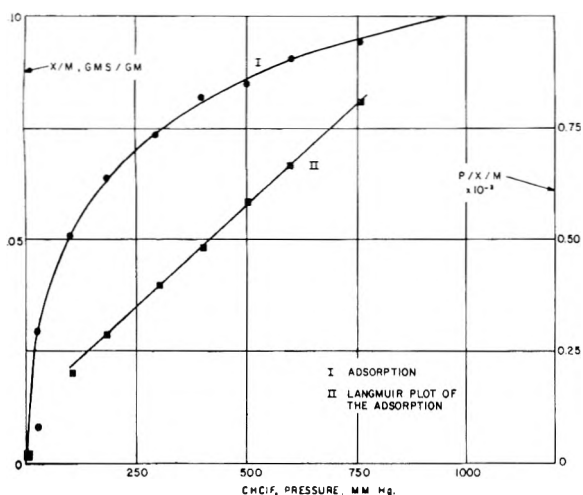


Fig. 7.—I, adsorption isotherm of CHClF_2 on Alcoa F-1 alumina; II, Langmuir plot of same.

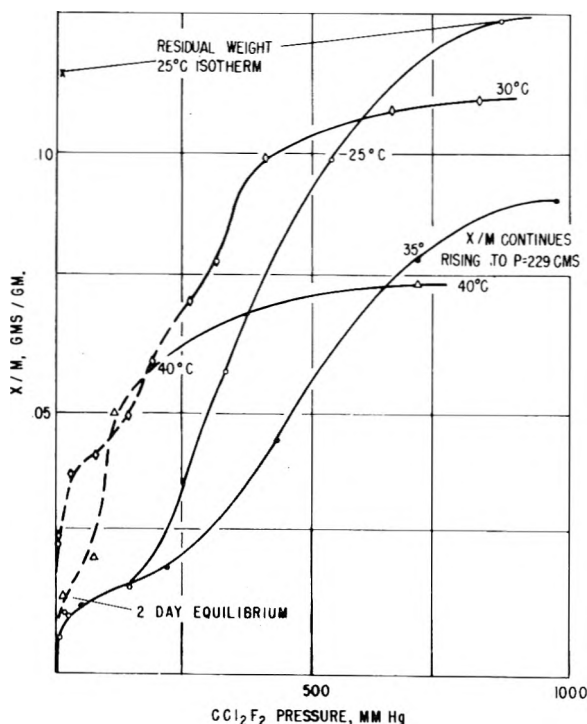


Fig. 8.—Adsorption isotherms of CCl_2F_2 on Sieve 5A at 25 and 35° (2 hour points) and at 30 and 40° (2 day points).

adsorption but also the energies involved. The second model is consistent with the results.

The Surface Chemistry of the CHClF_2 -Sieve 5A System.—The specific surface area of Sieve 5A available to CHClF_2 (340.4 sq. m./g.) and the difference between the liquid densities of CO_2 and CHClF_2 at 25° indicate that this CHClF_2 -available area should correspond with 572 sq. m./g. for CO_2 . This result differs from that calculated from the Linde Company data for CO_2 ⁵ by only 3%, the liquid volumes of the two materials adsorbed are the same, the slight difference arising presumably from packing discrepancies. In the case of Sieve 5A, the same amount of adsorption space is available to either CHClF_2 or CO_2 , in contrast with Sieve 4A, where the specific surface area to CHClF_2 is only 15 sq. m./g. compared with 544 sq. m./g. for CO_2 at

the same temperature. This contrast emphasizes the extreme selectivity of these adsorbents, and the drastic changes that may be induced in them by cation exchange.

The results of the adsorption experiment are not consistent with any type of system metastability involving only one gas component. Calculations made from the Langmuir plots of the adsorption and desorption isotherms (Fig. 7) indicate that slightly lower surface area is available on desorption if the species being removed is only CHClF_2 ; assuming it to be wholly CO_2 , then the calculation gives a higher area than with CO_2 on a clean 5A surface. The isotherms also indicate that the amount of material actually present on the surface is less on desorption than would be expected for CHClF_2 but more than for CO_2 alone.

The appearance of the desorption loop is more nearly like that for CO_2 adsorption than for CHClF_2 adsorption. The presence of CO_2 at the solid-gas interface probably controls the desorption energies, and hence the downward isotherm. Sufficient CO_2 is present in the reacted system to cause the break in the Langmuir plot at ca. 20 mm. pressure, which is also present in the isotherm of CO_2 on 4A.

The Decomposition Reaction between CHClF_2 and Molecular Sieves.—This reaction has been noted previously⁷ and would appear to be similar to that observed by Park, *et al.*,⁸ who obtained CO_2 on heating wet CHClF_2 , the water in the present case being the constitutional water of the zeolite. However, the Sieve 5A/ CHClF_2 system gives CO_2 without heating. An additional anomaly exists since CHClF_2 would normally be expected to break down *via* hydrolysis to CO *via* an orthoformic acid intermediate. Plentiful CO is indeed formed at higher temperatures in this system: by heating CHClF_2 and 5A Sieve in a bomb, but none was seen in the 25° sorption experiment. The mechanism appears not yet known since Barrer and Brook² suggest dehydrofluorination to explain the attack of CHClF_2 on natural zeolites, and Ayscough and Emeleus⁹ remark the formation of CO_2 and SiF_4 when CF_3 radicals are studied in quartz apparatus. The recent evidence of Neilson and White¹⁰ for the association of liquid CHClF_2 , and the peculiar geometry of the Molecular Sieve lattice² make it impossible to rule out an exchange mechanism based on polarization of the CHClF_2 in the present case. Adsorbed CHClF_2 behaves as a liquid on Molecular Sieves, and hence will be slightly polarized. Also, in the process of entering a pore, a CHClF_2 molecule will pass within 2 Å. of a calcium ion and considerable additional polarization will result. Even if formal charge separation is never attained in sorbed CHClF_2 , the unbalanced field of the aluminosilicate surface is sufficient to abstract a fluoride ion, because of the very small distances involved (M. J. Pryor¹¹ has shown that γ -alumina surfaces possess sufficient electrostatic inhomogeneity to dehydrate all hydrated halide ions). In

(7) P. Cannon, *J. Am. Chem. Soc.*, **80**, 1766 (1958).

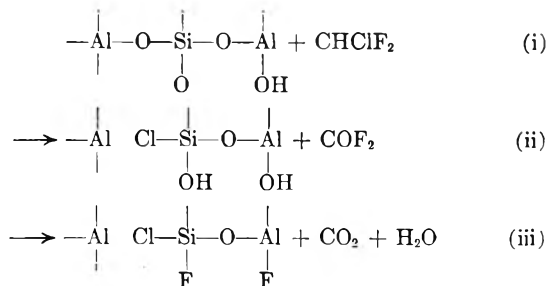
(8) J. D. Park, *et al.*, *Ind. Eng. Chem.*, **39**, 354 (1947).

(9) P. B. Ayscough and H. J. Emeleus, *J. Chem. Soc.*, 3381 (1954).

(10) E. F. Neilson and D. White, *J. Am. Chem. Soc.*, **79**, 5620 (1957).

(11) M. J. Pryor, *Z. f. Elektrochemie*, to be published.

close proximity to a Molecular Sieve substrate, CHClF_2 can be sufficiently polarized that the fluorines can undergo exchange reactions. The halogen has been found on the lattice in an ionized form by analysis. A combination of the dehydrohalogenation and polarization mechanisms enables one to arrive at the CO_2 product, thus



The decomposition is small, of the order $<1.0\%$ of the total gas phase in the observed systems. The reaction, whether exchange or hydrolysis, is restricted in the 4A case. Presumably the restriction is the amount of structural hydroxyl in the substrate, which is the origin of part of the oxygen for carbon dioxide formation. Thus, the decomposition was found to occur only on clean Sieve 4A, and not on a once-contacted sample.

Both experiments on the 4A and 5A sieve result in a substantial loss of apparent surface area of the solid material (*e.g.*, from an initial value 567 sq. m./g. to a new value of 290 sq. m./g. for CO_2 on 4A at 25.0°).

The Surface Chemistry of the CCl_2F_2 -Molecular Sieve 5A System.—The most striking observation in this series of experiments is the tenacity which sorbed CCl_2F_2 has for Sieve 5A, even when subjected to a high vacuum over a long period of time. The attainment of sorption equilibrium in the CCl_2F_2 -5A system is exceptionally slow. It appears that the penetration of the 5A lattice by CCl_2F_2 is only just possible and the peculiar geometry of the lattice gives rise to a metastable type IV isotherm which finally goes over to a type I form. This may be due to slow relaxation of the solid lattice by the adsorbate. Since the times allowed for attainment of equilibrium in many reported surface-chemical investigations are shorter than those observed here (2 days), it is possible that other works may have missed this type of metastability. Brunauer remarks that the type IV isotherm is a symptom of a non-equilibrium situation; his premise that the type IV isotherm is necessarily a special type II case is substantiated in the present system provided one also believes the type I is also a special type II case.

A calculation of the energies involved in adsorption of CCl_2F_2 on Sieve 5A in the pressure range 400–1000 mm. of mercury based on the use of the Clausius-Clapeyron equation gives a series of values which range between 10 and 6 kcal. per gram mole of CCl_2F_2 adsorbed. A common adsorption potential surface coverage plot for all experimental temperatures was realized only at the highest pressures studied. The initial portions of each pair of time-equivalent isotherms are very nearly coincident, and in this way the first low pressure points

vary from those measured at higher pressures. Since these first points are nearly coincident even at different temperatures, rather high energies must be involved. At pressures of CCl_2F_2 less than 100 mm. a linear Langmuir plot is obtained. The surface area implied by this plot for the two hour points is only 0.06 of the total area. The CCl_2F_2 molecules must initially sorb only on the windows leading into the pores (the pore is considerably wider inside than at the entrance), and the area defined in this way (of 5A to CCl_2F_2) represents only the outside area or "window sorption area" of the sieve. In Sieve 5A, the area of each window is almost exactly 0.06 of the internal area of a single pore chamber (from calculations based on the published structure of the sieve lattice).¹² The effect appears primarily one of electrostatic obstruction; Sieves 4A and 5A differ only in the number and charge of the cations which balance the negative charges in the same $\text{SiO}_2/\text{Al}_2\text{O}_3$ Sieve lattice.

The second portion of the isotherms where the adsorption rises to x/m greater than 0.1 must then follow the diffusion of the CCl_2F_2 into the pores from the windows with subsequent screening of the electrostatic field and relaxation of the lattice. Evidence for this mechanism is available from the two-day points at low pressures: the surface area calculated from that set of data is comparable to the internal surface area of the sieve. The electrostatic barrier field is presumably relaxed by the dielectric nature of the sorbed CCl_2F_2 contained inside the pore. This explanation is probably specific only to very few systems, since extremely small distances are involved in the clearance of a Molecular Sieve window by a molecule which is being adsorbed. It is only due to those small distances that the results may be discussed on this electrostatic basis. The peculiar pump-down behavior, where only a very small loss in weight was seen, is known as "lattice penetration"; on the electrostatic model this would be due to coupling of the positive Ca^{++} ion field with the electronegative CCl_2F_2 molecules. Lattice penetration has been occasionally observed in other systems. It was found by Gregg and Stock,¹³ and Barrer and MacKenzie¹⁴ in connection with the adsorption of ammonia or water on the phosphomolybdic acid pseudomorph anhydride, and the adsorption of ammonia on attapulgite, respectively. These workers found extreme "hysteresis"; a pumpdown similar to that seen here was observed in each case, though a similar explanation of the penetration was not advanced.

Acknowledgments.—I wish to thank sincerely Dr. E. L. Simons, Dr. E. H. Winslow, Dr. P. D. Zeman, Dr. F. J. Norton and Mr. C. A. Hirt of these laboratories for the various analyses, classical and instrumental, and Drs. G. L. Gaines, R. C. Burnett and L. E. St. Pierre for helpful discussions.

(12) T. B. Reed and D. W. Breck, *J. Am. Chem. Soc.*, **78**, 5972 (1956).

(13) S. J. Gregg and R. Stock, *Trans. Faraday Soc.*, **53**, 1355 (1957).

(14) R. M. Barrer and N. MacKenzie, *THIS JOURNAL*, **58**, 560 (1954).

SOLID-LIQUID AND LIQUID-LIQUID EQUILIBRIA OF THE TERNARY SYSTEM URANIUM HEXAFLUORIDE-CHLORINE TRIFLUORIDE-HYDROGEN FLUORIDE¹

BY G. P. RUTLEDGE² AND W. DAVIS, JR.

Technical Division, Oak Ridge Gaseous Diffusion Plant, Union Carbide Nuclear Company, Oak Ridge, Tennessee

Received June 16, 1958

The complete condensed phase diagram of the ternary system UF_6 - ClF_3 - HF has been determined. The measurements cover all possible compositions and temperature ranging from about -100 to $+100^\circ$. The ternary eutectic temperature is -91° at a composition of 0.0 formula % UF_6 , 19.5 formula % ClF_3 , and 80.5 formula % HF . The lowest temperature at which the miscibility gap exists for two liquids saturated with solid UF_6 is 53° at a composition of 49 formula % UF_6 , 13 formula % ClF_3 , and 38 formula % HF .

Introduction

Studies being carried out in this Laboratory of physical and chemical properties of the interhalo-

gen compounds have required the examination of a number of phase systems, one of these being the ternary system UF_6 - ClF_3 - HF . The three condensed binary systems resulting from these three components already have been published. The HF - ClF_3 systems were examined by McGill, Wendolkowski and Barber,³ the UF_6 - ClF_3 system

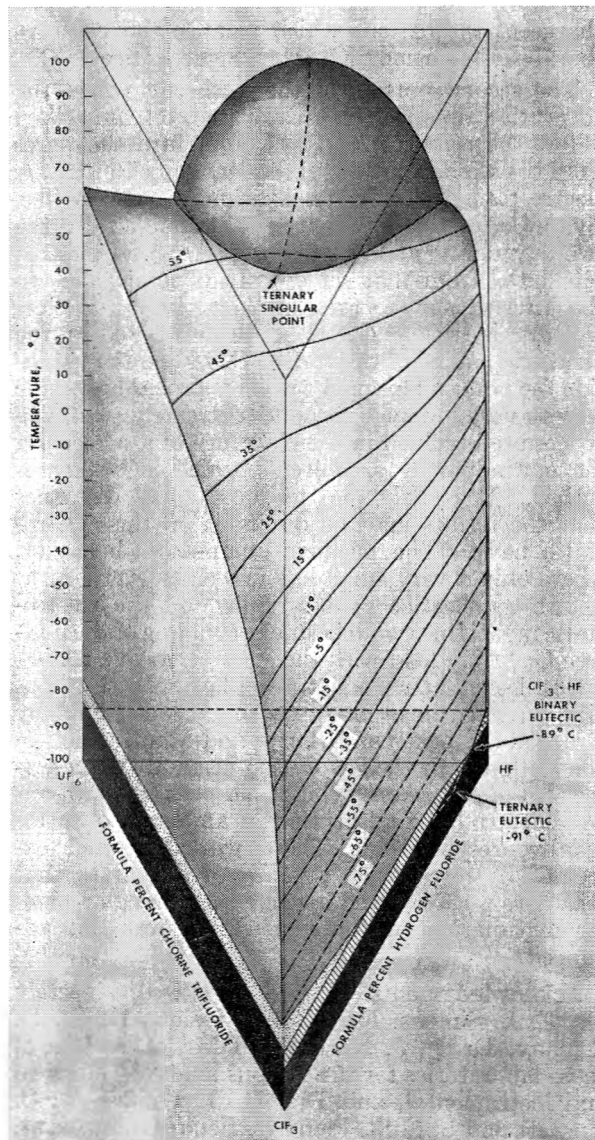


Fig. 1.—Temperature-composition prism for the condensed system UF_6 - HF - ClF_3 .

(1) This document is based on work performed at the Oak Ridge Gaseous Diffusion Plant operated by Union Carbide Corporation for the U. S. Atomic Energy Commission.

(2) Westinghouse Electric Corp., Bettis Plant, Pittsburgh, Pennsylvania.

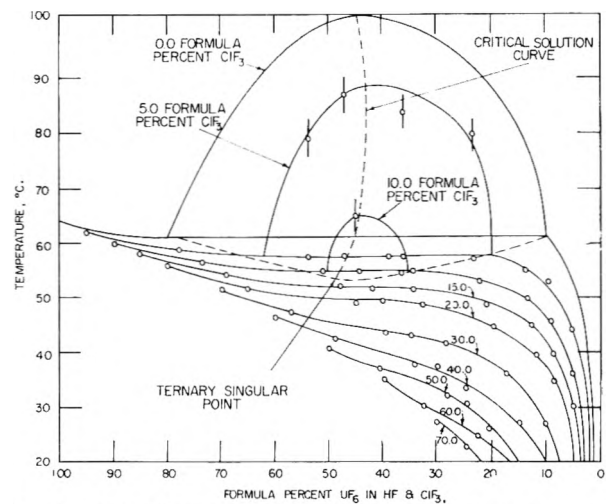


Fig. 2.—Solid-liquid and liquid-liquid equilibria in the system UF_6 - HF - ClF_3 .

by Wendolkowski and Barber⁴ and the UF_6 - HF system by Rutledge, Jarry and Davis.⁵ The purpose of the present report is to describe the solid-liquid and liquid-liquid equilibria in this ternary system in terms of these three binary systems utilizing additional experimental data on freezing points and two-liquid equilibria.

Theoretical analysis of the data in terms of solution theory has not been attempted because of the presence of HF . The existence of this material in the associated state⁶ and the variation of association with temperature, pressure and concentration have precluded further consideration of theoretical analysis other than that already published in the above mentioned binary systems.

The recovery of irradiated uranium utilizing the chlorine trifluoride process is based upon the distillation of UF_6 from mixtures containing ClF_3

(3) R. M. McGill, W. S. Wendolkowski and E. J. Barber, *This Journal*, **61**, 1101 (1957).

(4) W. S. Wendolkowski and E. J. Barber, *ibid.*, **63**, 750 (1958).

(5) G. P. Rutledge, R. L. Jarry and W. Davis, Jr., *ibid.*, **57**, 541 (1953).

(6) R. L. Jarry, F. D. Rosen, C. F. Hale and W. Davis, Jr., *ibid.*, **57**, 905 (1953).

TABLE I
CONDENSED PHASE EQUILIBRIA DATA FOR THE TERNARY SYSTEM $UF_6-HF-ClF_3$

Composition, formula %			Formula ratio,	Miscy. gap	UF_6 freezing	Composition, formula %			Formula ratio,	Miscy. gap	UF_6 freezing
UF_6	HF	ClF_3	HF/ UF_6	$t, ^\circ C.$	$t, ^\circ C.$	UF_6	HF	ClF_3	HF/ UF_6	$t, ^\circ C.$	$t, ^\circ C.$
1.09	98.91	0.00	90.7	...	12.6	34.82	56.15	9.03	1.61	58.6	54.9
1.07	97.25	1.68	90.7	...	6.1	34.63	55.84	9.13	1.61	54.8	54.8
1.01	92.13	6.86	90.7	...	-8.0	40.79	59.21	0.00	1.45	101.	61.2
0.93	84.47	14.61	90.7	...	-24.0	39.87	57.89	2.23	1.45	94.1	59.5
9.49	90.51	0.00	9.54	...	60.5	39.25	56.99	3.76	1.45	87.4	58.5
4.01	38.25	57.75	9.54	...	-13.	34.65	50.31	15.03	1.45	...	51.7
2.95	28.14	68.91	9.54	...	-23.	29.14	42.31	28.55	1.45	...	43.1
2.25	21.42	76.33	9.54	...	-35.	22.86	33.19	43.95	1.45	...	32.4
10.20	89.80	0.00	8.80	69.6	61.2	18.02	26.17	55.81	1.45	...	22.9
10.19	89.66	0.15	8.80	67.3	59.7	15.21	22.09	62.71	1.45	...	16.5
9.69	85.27	5.04	8.80	...	52.8	13.89	20.17	65.95	1.45	...	12.7
8.76	77.13	14.11	8.80	...	40.4	49.54	50.46	0.00	1.02	101.	61.2
14.54	85.46	0.00	5.88	81.0	61.2	46.82	47.68	5.50	1.02	85.4	57.6
14.00	82.43	3.57	5.88	64.6	56.9	45.06	45.89	9.05	1.02	68.7	55.3
13.56	79.83	6.61	5.88	...	54.2	44.04	44.85	11.11	1.02	58.5	54.3
12.48	73.43	14.09	5.88	...	45.8	43.50	44.30	12.21	1.02	...	53.6
11.10	65.32	23.58	5.88	...	35.5	32.60	33.20	34.21	1.02	...	40.7
24.71	75.29	0.00	3.05	92.0	61.2	24.25	24.69	51.05	1.02	...	29.9
24.26	73.90	1.84	3.05	...	59.5	56.62	43.38	0.00	0.766	97.0	61.2
23.06	70.25	6.70	3.05	64.3	55.9	54.55	41.80	3.65	.766	84.3	58.1
22.73	69.27	8.00	3.05	...	55.2	52.47	40.21	7.32	.766	66.5	56.1
19.22	58.56	22.22	3.05	...	42.9	51.46	39.43	9.11	.766	57.3	55.1
14.55	44.33	41.12	3.05	...	26.1	51.12	39.17	9.70	.766	...	54.8
38.27	61.73	0.00	1.61	101.	61.2	46.34	35.51	18.13	.766	...	50.4
36.58	59.00	4.42	1.61	85.	58.0	39.66	30.39	29.94	.766	...	43.9
35.07	56.56	8.36	1.61	65.	55.4	34.70	26.59	38.70	.766	...	38.8
28.93	22.17	48.91	0.766	...	33.0	58.23	13.00	28.77	.223	...	48.0
21.95	16.82	61.23	.766	...	23.6	47.23	10.54	42.23	.223	...	41.4
81.75	18.25	0.00	.223	...	61.3	35.98	8.03	55.99	.223	...	33.3
75.40	16.83	7.77	.223	...	57.7	28.43	6.34	65.23	.223	...	26.7
67.87	15.15	16.98	.223	...	53.4						

and HF thereby requiring a knowledge of the phase equilibria of this ternary system.⁷

Experimental

Uranium hexafluoride, anhydrous HF and ClF_3 were purified by methods previously described.³⁻⁵ A transparent Fluorothene tube was used to determine solid-liquid phase equilibrium as well as limits of the miscibility gap.⁵ The unit used in conjunction with solutions of freezing point below room temperature has been described by Davis, Conley and Rutledge.⁸ The Fluorothene tube was loaded under vacuum conditions with UF_6 and HF. Increments of the more volatile ClF_3 were added and temperatures of phase changes determined. A calibrated copper-constantan thermocouple connected to a K-2 potentiometer was used for temperature measurements. Methods and techniques used have been described in an earlier report,³ and it need only be noted that agitation of solutions was vigorous in all experiments thereby resulting in good thermal equilibrium. On each solution the temperature of a phase change was checked 2 to 5 times by repetition of the heating or cooling cycles. Temperatures reported are accurate within $\pm 0.5^\circ$.

Results and Discussion

In Tables I and II the experimental results are summarized. From these data, Figs. 1 through 4 have been constructed. It should be kept in mind that all of this work was done in the absence of foreign gases and that pressures were not atmospheric, but the normal vapor pressures of the

ternary mixtures at given temperatures. Figure 1 attempts to give three dimensions to the temperature-composition plot and every part of the diagram is drawn to scale. The general nature of the miscibility gap as a function of temperature can be seen. Rotation of the prism to show two more similar views is possible. Dashed lines at the temperatures below -55° indicate extrapolations to regions in which experimental data are difficult to obtain. The region from 101 to 53° , the ternary singular temperature, represents the miscibility gap. The shaded region below the miscibility gap (Fig. 1) represents equilibrium of liquid plus solid UF_6 . The dotted region represents equilibria involving solid ClF_3 (X-11): L + X-11 from -76.6 to -83.1° on the ClF_3-UF_6 side and to -77.4° (*i.e.*, binary eutectic for UF_6-ClF_3) on the ClF_3-UF_6 side; and solid UF_6 + X-11 from -77.4 to -83.1° . The parallel line region represents L + solid ClF_3 (X-1 form), and the cross-hatch region L + solid HF. The black region represents coexistence of solid phases and below -91° all three compounds are solid at all compositions. The dotted, crosshatch and parallel line regions appear to be only on the edge of the binary systems ClF_3-HF and ClF_3-UF_6 but they actually represent small volumes leading from their binary surfaces to the binary eutectics (ClF_3-UF_6 and $HF-UF_6$) and from there to the ternary eutectic. Experimental data connecting the three

(7) F. R. Bruce, J. M. Fletcher, H. H. Hyman and J. J. Katz, "Process Chemistry," McGraw-Hill Book Co., Inc., New York, N. Y., 1956, pp. 281-285.

(8) W. Davis, Jr., L. L. Conley and G. P. Rutledge, *Rev. Sci. Instruments*, **24**, 431 (1953).

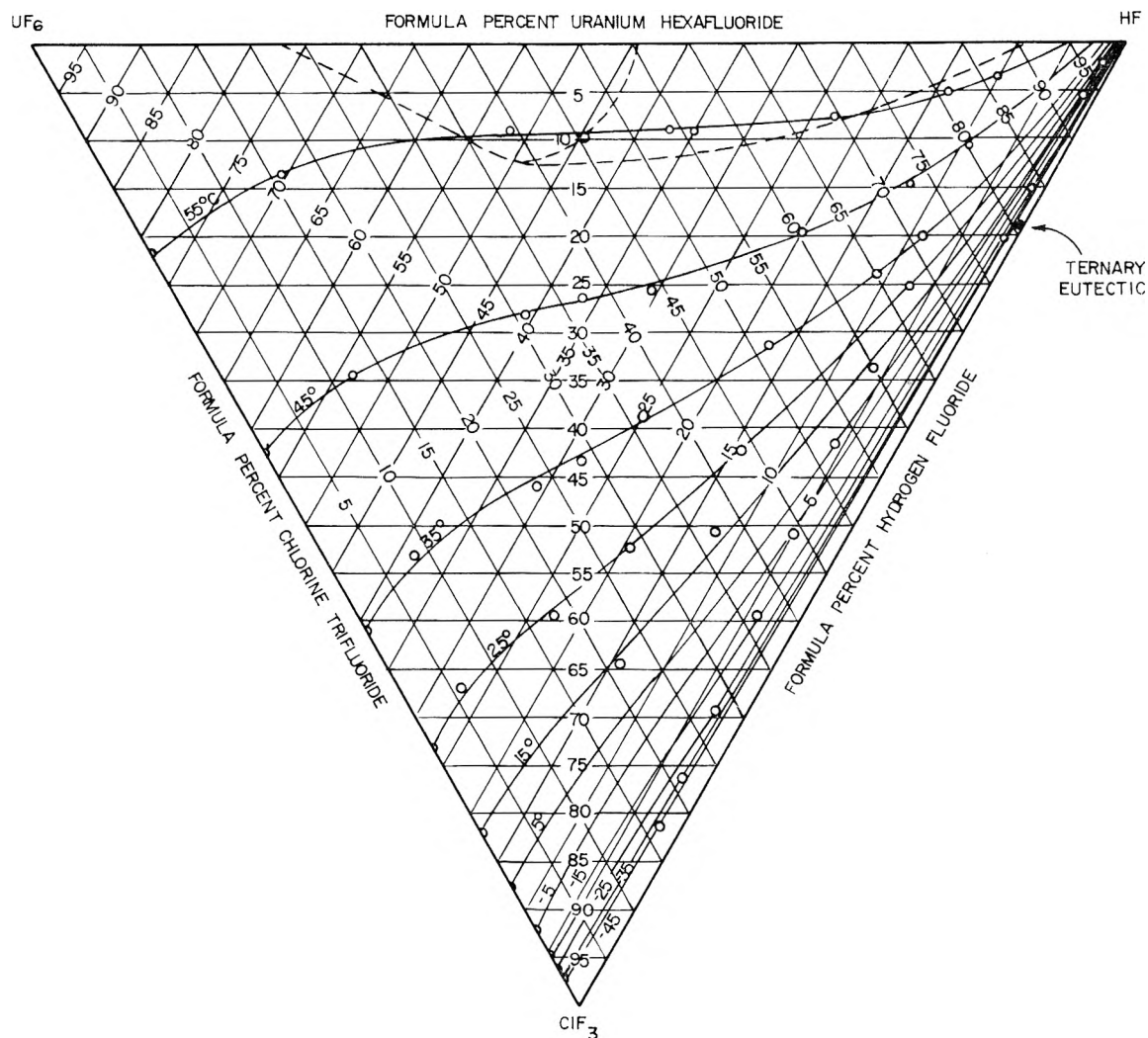


Fig. 3.—Polythermal projection of Fig. 1. showing temperature contours.

TABLE II

TERNARY EUTECTIC TEMPERATURE AND COMPOSITION^a

Gross composition, formula %			Soln. composition, ^b formula % HF	Freezing ^c t., °C.
UF ₆	HF	CIF ₃		
1.09	98.91	0.00	...	-84.5 ^d
1.07	97.25	1.68	98.3	-86.0
1.01	92.13	6.86	93.1	-88.2
0.93	84.47	14.61	85.3	-90.3
2.64	0.00	97.36	...	-78.1 ^d
0.89	66.40	32.72	67.0	-86.6
0.00	91.22	8.78	...	-88.8 ^d
1.26	90.07	8.67	91.2	-87.9
1.10	78.75	20.15	79.6	-90.4

^a Using a graphical plot of the data in this table the ternary eutectic temperature is estimated to be -91° at a composition of 19.5 formula % CIF₃ and 80.5 formula % HF assuming 0.0 to 0.2 formula % UF₆. ^b Assuming concentration of uranium hexafluoride is essentially zero (less than 0.2 formula %) at temperatures below -75° . ^c Temperature at which second thermal break begins. ^d Binary eutectic temperature.

binary eutectics to the ternary eutectic were difficult to obtain because of the extreme steepness of the UF₆ crystallization surface and the very small

amount of UF₆ in the two binary systems as well as the ternary system.

The system is simple in that the only solids are the pure solid components; the freezing point diagram therefore consists essentially of three crystallization or solubility surfaces, one for each solid component, three curves of liquid + two solids, leading from each of the three binary eutectics, and a ternary eutectic temperature of -91° at a composition of 0.0 to 0.2 formula % UF₆, 19.5 formula % CIF₃ and 80.5 formula % HF. The only complication is that there is a liquid miscibility gap in the binary UF₆-HF system, impinging on the solubility curve of UF₆, with a binary invariant, UF₆ + two liquids, at 61.2° , and a binary upper critical solution point at 101° . As shown in Fig. 2 the addition of CIF₃ lowers both the 3-phase equilibrium temperature (UF₆ + 2 liquids) and the critical solution temperature. The intersection of the 3-dimensional miscibility gap and the UF₆ crystallization surface is seen clearly in Fig. 1, and the polythermal projection of this intersection curve is shown in Fig. 3. The point of minimum temperature of this intersection curve (the curve representing equilibrium

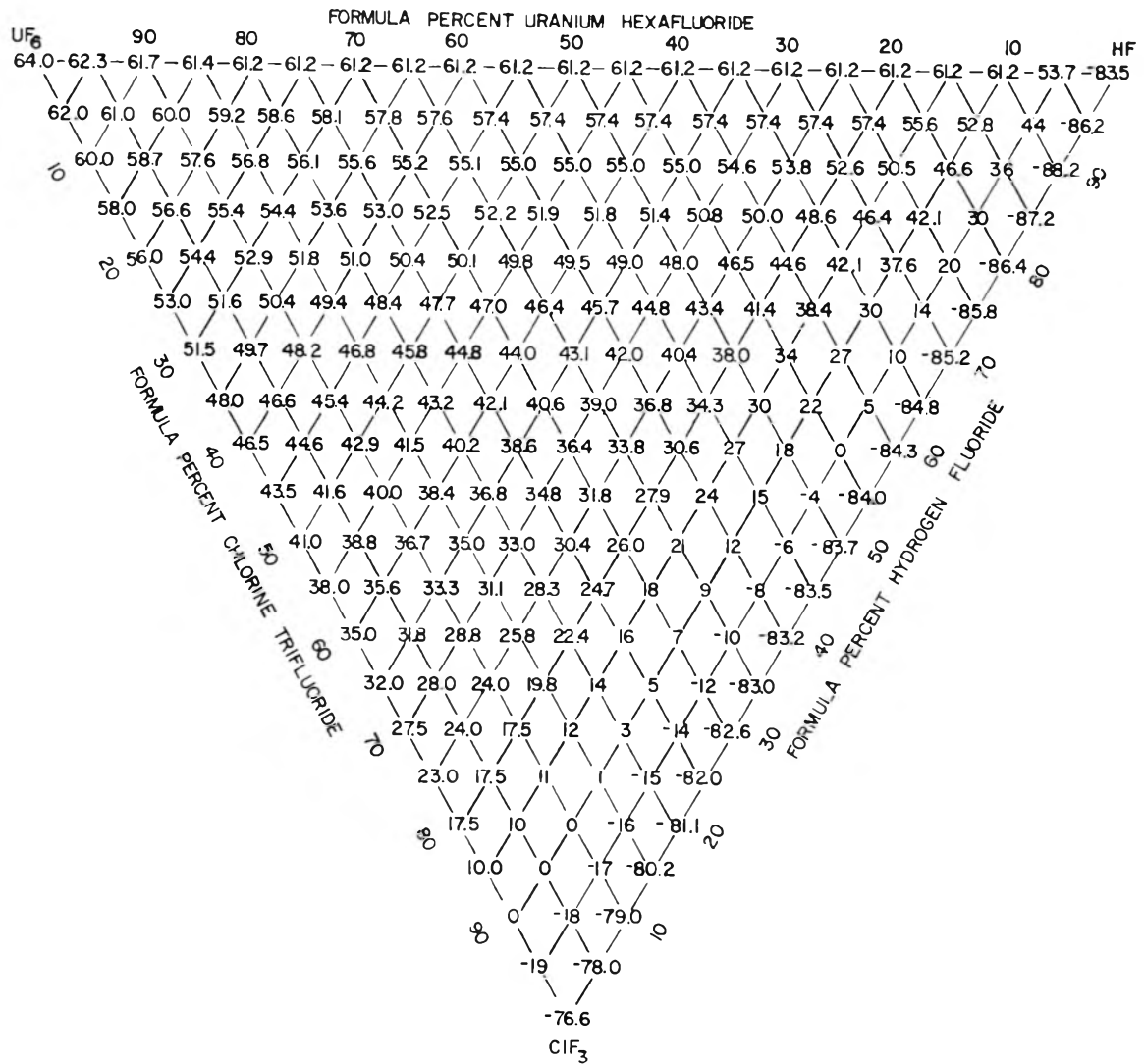


Fig. 4.—Freezing point of the UF_6 - HF - ClF_3 system as a function of composition.

of solid UF_6 + 2 liquids) is also the end of the ternary critical solution curve. It is the point (53° , composition of 49% UF_6 , 13% ClF_3 and 38% HF) at which the two conjugate liquids become consolute while saturated with UF_6 . This is a ternary singular point, involving four phases (L_1 , L_2 , UF_6 , vapor), with critical identity of L_1 and L_2 .⁹ The composition of the liquid is known simply to be on the right of the tangent from the UF_6 corner to the intersection curve, in Fig. 3, and it is not necessarily the point of the maximum ClF_3 concentration.

The temperature contours approach the ternary eutectic temperature of -91° as shown in Fig. 3. Due to the steepness of the UF_6 crystallization surface and considering the positions of the two binary eutectics involving UF_6 , the UF_6 concentration at the ternary eutectic will be very small, less than

0.2%. The quantities of ClF_3 and HF at the ternary point were obtained by determining the phase diagram of the ClF_3 - HF system with small amounts of UF_6 present. Experimental results are given in Table II. The second thermal break (uranium hexafluoride precipitation is the first break) is so near the third thermal break that it is experimentally possible to get only the beginning of the second break which is in a trough approaching the ternary eutectic. The values so obtained for the ternary eutectic composition are 19.5 formula % ClF_3 and 80.5% HF with an estimated 0.0 to 0.2 formula % uranium hexafluoride.

The temperature of solid precipitation as a function of composition is shown in Fig. 4. Except for the binary system ClF_3 - HF , UF_6 is the first compound to precipitate.

Acknowledgments.—The authors wish to acknowledge timely suggestions from Drs. E. J. Barber and J. E. Ricci and to thank Mr. L. I. Conley for his help in making some of the measurements.

(9) J. E. Ricci, "The Phase Rule and Heterogeneous Equilibrium," D. Van Nostrand Co., New York, N. Y., 1951, pp. 26, 61, 62, 208-213, 317, 353-357.

SOLUTION PROPERTIES OF DESOXYRIBONUCLEIC ACID (DNA). I. HYDRODYNAMIC BEHAVIOR

BY J. HERMANS, JR., AND J. J. HERMANS¹

Laboratorium voor Anorganische en Fysische Chemie, Universiteit, Leiden

Received June 19, 1958

The intrinsic viscosities $[\eta]$ of about 40 DNA preparations and the intrinsic sedimentation constants $[S]$ of 7 out of these 40 samples are discussed in the light of existing theories. The DNA was prepared from three different sources. No correlation between the hydrodynamic properties and either the source or the method of preparation was found. The radii of gyration ρ and the molecular weight M were derived from light-scattering data as will be described in a second article. No correlation was found between $[\eta]$ and M or between ρ^2 and M . Flory's equivalent sphere model is not applicable as is shown by the poor correlation of $[\eta]$ with ρ^2/M . A good correlation is found between $[\eta]M/\rho^3$ and M/ρ , which is suggested by the theories of Brinkman, Debye and Bueche, Kirkwood and Riseman. The best agreement is with the Brinkman-Debye-Bueche theory, but it is qualitative rather than quantitative. It is believed that the discrepancies are due to chain stiffness (worm-like character of the molecular chain). The frictional factor per unit chain length estimated from $[\eta]$ or $[S]$ suggests that the persistence length in the Kratky-Porod sense is about 400 Å., in agreement with the light-scattering results to be discussed in part II.

Introduction

The properties of DNA in solution to be considered here are intrinsic viscosity $[\eta]$ and intrinsic sedimentation constant $[S]$. These are to be compared with the values of the molecular weight M and the radius of gyration ρ obtained by light scattering. A number of measurements of this kind have been published (Doty and Bunce,² Sadron,³ Brown, McEwen and Pratt⁴), and it was found that $[\eta]$, M and ρ vary considerably from sample to sample. Attempts to correlate $[\eta]$ and ρ with M have failed; it may be mentioned, however, that Doty⁵ finds much less variation of these quantities over a number of samples, and is thus in a position to average over-all measurements.

As we were in the possession of the data for a number of DNA samples which do show an appreciable variation, we have tried to fit these data with existing theories on the hydrodynamic behavior of macromolecules in solution: Flory, Kirkwood and Riseman, Debye, Brinkman, Debye and Bueche. In a second article, we shall do the same with the light-scattering curves and the theory of Peterlin for worm-like chains and of ourselves for zig-zag chains (chains consisting of straight rods connected by hinges).

In both comparisons we must, at a certain point, make assumptions regarding the structure of DNA: the diameter of the chain and its molecular weight per unit length. These are given by the model described by Watson and Crick,⁶ which we will assume to represent the DNA structure correctly. The diameter of the chain is about 30 Å. This is rather a rough estimate, but none of our conclusions would be impaired seriously if one took 25 or 20 Å. instead. The molecular weight per Å. is 200. This is correct as long as the ratio purines: pyrimidines is close to one and the distance from one base-pair to the next along the chain equals 3.4 Å.

Preparations Used.—All the samples studied were prepared using methods adequately described in the literature. To facilitate comparison, the way the DNA was prepared, the preparator and the source have been indicated by a code number in column three of Table I. The explanation is as follows: The DNA was prepared by treating the nucleoprotein with

- (1) concentrated NaCl, Signer and Schwander⁷
- (2) chloroform-octanol, Mirsky and Pollister⁸
- (3) detergent, Marko and Butler⁹; Kay, Simmons and Dounce¹⁰
- (4) chymotrypsin, Butler, James and Conway¹⁰
- (5) phenol *p*-aminosalicylate, Kirby¹¹
- (6) dialysis against 1 molar NaCl, possible only in the case of fish sperm, owing to the low molecular weight of the protamine.

The preparation was performed at

- S. Bern, in Prof. Signer's laboratory
- V. Strasbourg, Centre de Recherches sur les Macromolécules, by R. Vendrely
- P. Strasbourg, Centre de Recherches sur les Macromolécules, by J. Pouyet and the junior author
- L. London, Chester Beatty Institute
- B. Leiden, Laboratory of Biochemistry
- F. Leiden, Laboratory of Physical Chemistry

The source was

- (a) calf thymus
- (b) fish sperm
- (c) bird erythrocytes

Remarks: Sample 31 has a green color, which is presumably caused by the presence of appreciable amounts of polyvalent cations. Samples with N/P ratio larger than 1.8 contain an amount of protein that may be of influence on the measurements.

Technique.—A. **Couette Viscometer.**—The viscosity measurements of samples 1 through 21 were performed in the Couette viscometer described by Vallet.¹² The practically uniform gradient equals 0.25 sec.⁻¹ This gradient is so low that the viscosities of DNA solutions are equal within experimental error to those at zero gradient.

B.—The measurements on the other samples were performed in a viscometer of the type described by van Duin and Hermans.¹³ It is of the Ubbelohde type, and is so constructed that the pressure p forcing the liquid through the

(1) Cellulose Research Institute, State University College of Forestry at Syracuse University, Syracuse, New York.

(2) P. Doty and B. H. Bunce, *J. Am. Chem. Soc.*, **74**, 5029 (1952).

(3) C. Sadron, "3rd Intern. Congress Biochem.," Brussels, 1955, p. 210.

(4) G. L. Brown, M. B. McEwen and M. I. Pratt, *Nature*, **176**, 161 (1955).

(5) P. Doty, "Symposium on Biocolloids," Gatlinburg, 1956, p. 27.

(6) J. D. Watson and F. H. C. Crick, *Nature*, **171**, 737 (1953).

(7) R. Signer and N. Schwander, *Helv. Chim. Acta*, **32**, 853 (1949).

(8) A. E. Mirsky and A. W. Pollister, *J. Gen. Physiol.*, **30**, 451 (1946).

(9) A. M. Marko and J. A. V. Butler, *J. Biol. Chem.*, **190**, 165 (1951).

(9a) E. R. M. Kay, N. S. Simmons and A. L. Dounce, *J. Am. Chem. Soc.*, **74**, 1724 (1952).

(10) J. A. V. Butler, D. W. F. James and B. E. Conway, *Trans. Faraday Soc.*, **50**, 1612 (1955).

(11) K. S. Kirby, *Biochem. J.*, **66**, 495 (1957).

(12) G. Vallet, Thesis, Strasbourg, 1952.

(13) P. Van Duin and J. J. Hermans, *J. Polymer Sci.*, in press (1958).

capillary decreases linearly with increasing amount of liquid passed through it.¹⁴ The measurement is performed by reading the height h of a meniscus with respect to its rest position as a function of time t ; $dt/d \log h$ is now proportional within experimental error to the viscosity of the liquid at a shear-stress σ equal to that at the wall of the capillary at that moment: $\sigma = pR/2L$, p being the pressure, R the radius and L the length of the capillary (see also ref. 14). Our instrument permitted measurements accurate to within 1% at shear-stresses as low as 0.2 dyne/cm.², which made it possible to determine the viscosity η at zero shear-stress to within 1%.

C.—Sedimentation constants were determined in a Spinco Model E analytical ultracentrifuge, using the ultraviolet absorption optics (cf. Shooter and Butler¹⁵). The quantity listed in Table I is the so-called intrinsic sedimentation constant

$$[S] = S\eta_0/(1 - \bar{v}d_0) = M\eta_0/Nf \quad (1)$$

where S is the sedimentation constant, η_0 the viscosity of the solvent, \bar{v} the partial specific volume of DNA, which we have taken to be 0.55 in all cases (Cecil and Ogston¹⁶), d_0 the density of the solvent, M molecular weight, N Avogadro's number and f the frictional constant of the DNA molecules. The value of S tabulated is $S_{1/2}$. This means that 50% by weight of the DNA has a sedimentation constant smaller than this value and 50% a larger one. The values for samples 5 and 7 were taken from Shooter and Butler.¹⁵

D.—As the light scattering will be discussed in more detail in a second article, we shall postpone the description of its measurement.

E.—The results have been collected in Table I. It may be mentioned that almost all measurements were carried out in 1 molar NaCl to suppress polyelectrolyte effects. The data for sample 30 are quoted from Doty and Zubay¹⁷; these values are averages over a large number of preparations.

The measurements of samples 1 to 8 have been performed by J. Pouyet at Strasbourg (Centre de Recherches sur les Macromolécules).

Discussion

The fact that the DNA molecule is in all probability a long chain suggests application of the macromolecular coil. First attempts in this direction were made by Sadron,³ Pouyet and Weill^{18a} Pouyet, Hermans and Vendrely.^{18b} No relation between M and $[\eta]$ or M and ρ is found. Figures 1 and 2 give these two diagrams for the samples of Table I.

Equivalent Sphere.—Sadron¹⁹ assumed that the particle could be replaced by an ellipsoid of revolution. Here we will only consider the limiting case of a sphere. Flory assumes that all polymer coils are so closely packed that one can use the limiting formulas of the Kirkwood-Riseman theory (see below). This leads to a conception of an equivalent particle, the dimensions of which can be obtained by light scattering. The theory has been quite successful in explaining measurements on a number of synthetic polymers.

It requires proportionality of $[\eta]$ to ρ^3/M , provided that the hydrodynamic radius of Flory's equivalent sphere is proportional to the radius of gyration ρ . Figure 3 shows, however, that this

(14) J. Hermans and J. J. Hermans, *Proc. Koninkl. Nederland. Akad. Wetenschap.*, in press.

(15) K. V. Shooter and J. A. V. Butler, *Trans. Faraday Soc.*, **52**, 734 (1956).

(16) R. Cecil and A. G. Ogston, *J. Chem. Soc.*, 1382 (1948).

(17) P. Doty and G. Zubay, *J. Am. Chem. Soc.*, **78**, 6207 (1956).

(18) (a) J. Pouyet and G. Weill, *J. Polymer Sci.*, **23**, 739 (1957); (b) J. Pouyet, J. Hermans and R. Vendrely, *Trans. Faraday Soc.*, **53**, 247 (1957).

(19) C. Sadron, *J. chim. phys.*, **44**, 22 (1947); *J. Polymer Sci.*, **3**, 812 (1948).

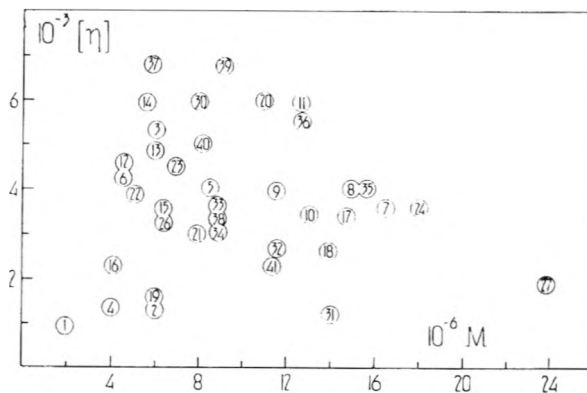


Fig. 1.—Intrinsic viscosities versus molecular weights for the samples of Table I.

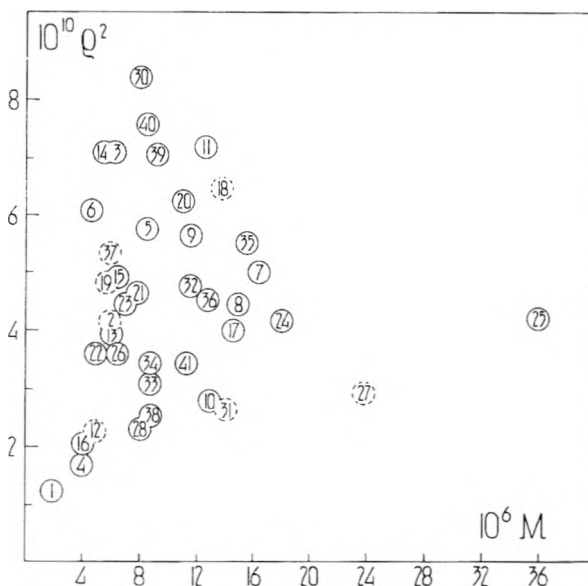


Fig. 2.—Attempt to correlate the square of the radius of gyration with the molecular weight.

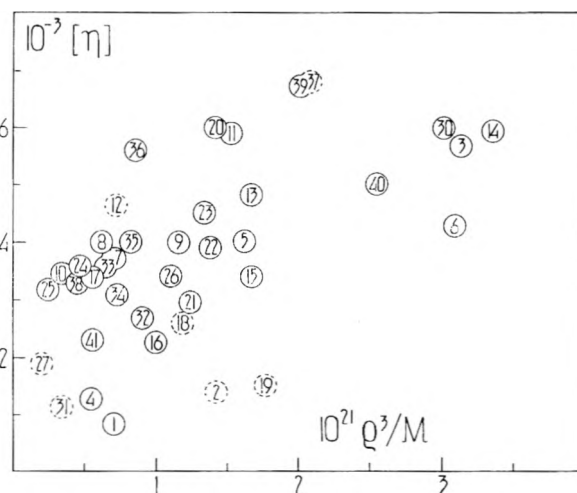


Fig. 3.—Intrinsic viscosities against ρ^3/M (test of Flory's equivalent sphere model).

correlation is extremely poor for the DNA samples of Table I. A possible solution is to drop the assumption that the hydrodynamic radius is proportional to ρ , but this assumption is reasonable. Moreover, we have nothing to replace it.

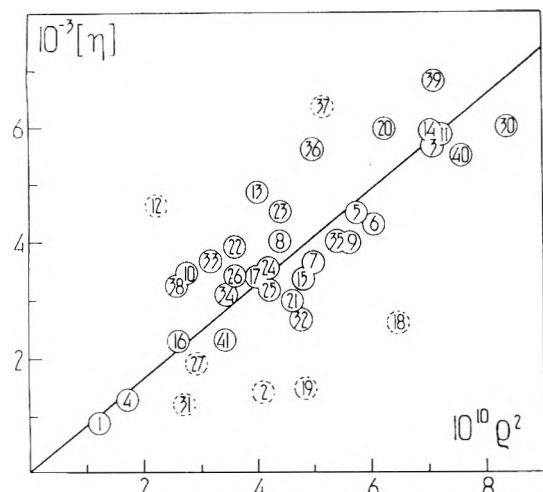


Fig. 4.—Intrinsic viscosities versus the square of the radius of gyration (free-draining particle).

I. TABLE OF SAMPLES

Column 3, code describing preparation of sample; column 4, molecular weight; column 5, radius of gyration in cm.; column 6, dissymmetry of the scattered light; column 7, intrinsic viscosity in cm.³/g.; column 8, intrinsic sedimentation constant in g./cm.; column 9, ratio of nitrogen/phosphorus content, in gram N/gram P; column 10, phosphorus content, %—age of dry weight.

No.	Name	Code	M × 10 ⁻⁶	ρ × 10 ⁸	z ₄₄	[η] × 10 ⁻³	[S] × 10 ⁻¹⁶	N/P	P, %
1	CV3	V ² a	1.9	1.10	3.6	0.85	1.74
2	SV	S1a	6.0	2.04	3.85	1.40
3	SVIII	S1a	6.0	2.66	3.7	5.70	1.65	8.72	..
4	CV42	V1a	4.0	1.30	..	1.36	1.62
5	TNA7	L4a	8.5	2.40	..	4.00	56
6	CV49	V1a	4.6	2.46	3.4	4.30	1.67	8.19	..
7	CV5a	V3a	16.5	2.24	4.3	3.65	51	..	8.42
8	CV9	V2a	15	2.10	4.6	4.00	1.70	8.75	..
9	CV51	V1c	11.5	2.38	4.5	4.00	1.62	8.17	..
10	CV62	V1a	13	1.66	4.8	3.45	47	1.79	8.40
11	CV64	V1a	12.5	2.68	4.65	5.90	73	1.61	8.96
12	CV69	V1a	4.6	1.49	2.1	4.62	1.64	9.27	..
13	CV71	V1a	6.0	2.00	2.9	4.87	1.63	9.43	..
14	CV74b	V6b	5.6	2.66	3.3	5.93	1.65	9.07	..
15	CV74a	V6b	6.4	2.20	4.2	3.40	1.69	8.81	..
16	CV72	V6b	4.1	1.60	3.9	2.27	49	1.80	8.80
17	CV78	V1c	14.5	2.00	5.1	3.40	1.65	8.86	..
18	I62	V1*a	14	2.54	4.6	2.60	1.74	8.48	..
19	I69	V1*a	6.0	2.20	3.4	1.50	1.74	8.67	..
20	JJA	P1a	11	2.50	5.2	6.00	73	1.60	9.0
21	CV91b	V1a	7.9	2.15	5.8	2.98
22	RH	F1a	5.0	1.90	3.4	3.90	1.67	8.15	..
23	HB1	B4a	7.0	2.10	4.3	4.49	1.71	8.37	..
24	AH1a	B4a	18	2.04	4.6	3.60	1.75	7.63	..
25	AH1b	B4a	36	2.05	4.9	3.17	1.84	7.43	..
26	B1	B4a	6.3	1.90	3.95	3.42	1.74	8.34	..
27	DH1	F3a	24	1.71	3.7	1.90	1.83	7.32	..
28	DH2	F3a	8.0	1.52	3.6	..	1.66	8.26	..
30	Doty	3 ² a	8.0	2.90	..	6.00	54
31	DH3	F2a	14	1.64	4.4	1.20
32	JC1	B4a	11.6	2.18	4.2	2.70	1.77	7.20	..
33	JC2	B4a	8.8	1.78	3.8	3.65	1.62	8.08	..
34	JC3	B4a	8.8	1.86	4.0	3.09	1.76	7.46	..
35	JCK1	B5a	16	2.34	4.55	4.00	1.87	7.85	..
36	JCK2	B5a	13	2.12	4.9	5.60	1.83	7.78	..
37	J40	L3a	5.9	2.30	4.4	6.80	1.62
38	J35	L3a	8.8	1.59	4.1	3.30	1.77
39	T1	L3a	9.2	2.66	4.2	6.80	1.67
40	J31	L2a	8.2	2.76	4.8	5.00
41	BB	L3a	11.5	1.85	3.93	2.30

Another relationship predicted by Flory's theory is the proportionality of $[S]$ to M/ρ . We dispose of only very few data, which seem to fall in two groups: samples JJA and CV 64 with $[S] =$

73×10^{-15} and five samples with $[S] \sim 50 \times 10^{-15}$, which show very little variation over a threefold change in M/ρ . So Flory's theory does not describe the behavior of DNA.

The Free Drained Molecules.²⁰—The free drained particle has one feature in common with DNA as is at once clear from the table of samples: the apparent constancy of $[S]$. We have the two equations

$$[\eta] = \zeta P N \rho^2 / 6M \eta_0 \quad (2)$$

and

$$[S] = M \eta_0 / NP \zeta \quad (3)$$

To derive these, the particle is divided into a number P of beads each having a frictional constant ζ . The assumption is made that none of the beads influence the flow of liquid around any of the others.

From eq. 3 it follows that $[S]$ is independent of M , M/P being a constant for the substance concerned. Furthermore, eq. 2 predicts proportionality of $[\eta]$ to ρ^2 . Now this also holds for DNA samples, within reasonable limits, as is seen from Fig. 4. The correlation is much better than the ones considered before.

We can now become more specific and try to find numerical agreement between $[\eta]$, $[S]$ and ρ , by calculating $\gamma = [\eta][S]/\rho^2$ and comparing this quantity to the value predicted by eq. 2 and 3, $\gamma = 0.17$. Table II shows this for the same samples that were used to verify Flory's theory. The values found for γ fall into two groups, identical to those we could make on the basis of sedimentation constants alone. This is not surprising, since we have seen that $[\eta]$ is proportional to ρ^2 . Neither of these two groups, however, shows a value of γ close enough to 0.17 to justify complete contentment with the free drained model.

TABLE II

VALUES OF $[\eta]$ $[S]/\rho^2$ FOR THE SEVEN SAMPLES OF WHICH $[S]$ IS KNOWN

Sample	JJA	CV	CV	CV	TNA	CV	Doty
Number	20	11	10	16	5	7	30
$\gamma = [\eta]$		64	62	72	7	5	
$[S]/\rho^2$	0.65	0.61	0.32	0.43	0.39	0.37	0.38

Brinkman,²¹ Debye-Bueche²² (BDB) and Kirkwood-Riseman²³ (KR) Models.—The assumption that the movement of one bead does not affect the movement of another bead is very questionable. Admitting interaction, the problem becomes much more difficult, and in the BDB theory a new assumption is made: that the particles are distributed with uniform density over a sphere of radius R . Introducing

$$\sigma^2 = R^2 \nu \zeta / \eta_0 = 3 \zeta P / 4 \pi \eta_0 R \quad (4)$$

where σ is called shielding ratio and ν is the density of the beads, $\nu = 3P/4\pi R^3$, one finds

(20) M. L. Huggins, *THIS JOURNAL*, **43**, 439 (1939); P. Debye, *J. Chem. Phys.*, **14**, 636 (1946); H. A. Kramers, *ibid.*, **14**, 415 (1946).

(21) H. C. Brinkman, *Proc. Koninkl. Nederland. Akad. Wetenschap.*, **50**, 618 (1947); *Physica*, **13**, 447 (1947); *Appl. Sci. Res.*, **A1**, 27 (1947).

(22) P. Debye and A. M. Bueche, *J. Chem. Phys.*, **16**, 573 (1948).

(23) J. G. Kirkwood and J. Riseman, *ibid.*, **16**, 565 (1948).

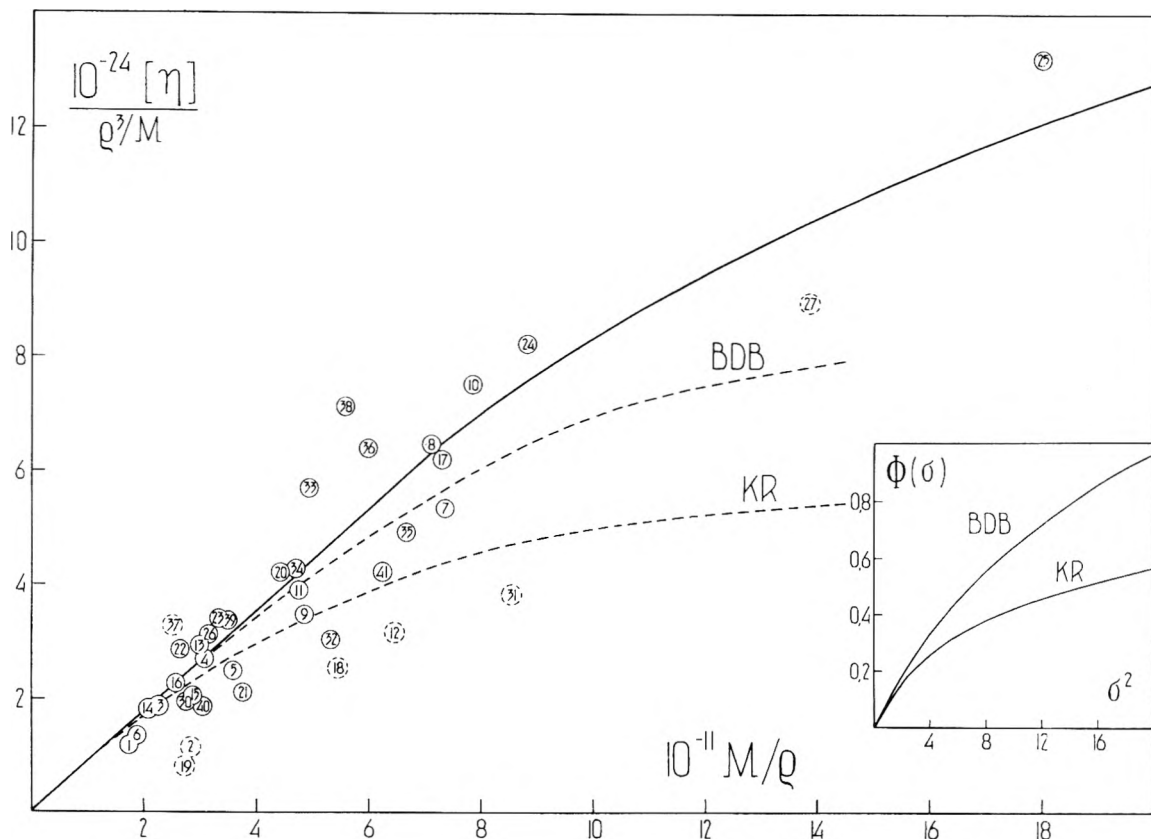


Fig. 5.—Test of the Brinkman-Debye-Bueche and Kirkwood-Riseman models. The dotted curves are theoretical and have been derived from $\Phi(\sigma)$, as a function of σ^2 , which is shown in the inset.

$$[\eta] = (4\pi/3)NR^3\Phi(\sigma)/M \quad (5)$$

$$[S] = M/6\pi NR\Psi(\sigma) \quad (6)$$

The functions Φ and Ψ are known, and their value at the limit of very small σ determines the ratio of R to the radius of gyration ρ . In this limit the formulas must become those for free drained molecules (eq. 2, 3), and as

$$\lim_{\sigma \rightarrow 0} \Phi(\sigma) = \sigma^2/m_0 \quad (7a)$$

$$\lim_{\sigma \rightarrow 0} \Psi(\sigma) = 2\sigma^2/9 \quad (7b)$$

we find

$$R^2 = 5\rho^2/3 \quad (8)$$

We may therefore write eq. 5, 6

$$[\eta] = (\zeta PN\rho^2/6M\eta_0) (10 \Phi(\sigma)/\sigma^2) \quad (9a)$$

$$[S] = M\eta_0(N\zeta P/9\Psi(\sigma)/2\sigma^2)^{-1} \quad (9b)$$

Kirkwood and Riseman have given a more detailed analysis of the forces acting between the beads and the liquid and the hydrodynamic flow caused by these forces. They come to conclusions similar to those reached in the BDB theory.

With the assumption $r = bP^{1/2} = \rho\sqrt{6}$, where r is the root mean square end to end distance and b the effective bond length, the KR formulas for the hydrodynamics of coiled molecules can be written

$$[\eta] = (\zeta PN\rho^2/6M\eta_0) \times G(\sigma^2/6.2) \quad (10a)$$

$$[S] = M\eta_0(N\zeta P)^{-1} (1 + 1.35 \sigma^2) \quad (10b)$$

in which σ is defined by eq. 4 and G is a function which has not yet been published in completely correct form, but for which data are available

(Kirkwood, Zwanzig, Plock²⁴) that are nearly exact. It has the property $G(0) = 1$, which gives us the formulas for the free drained model, eq. 2, 3, when we substitute $\sigma = 0$ in eq. 10. The similarity between eq. 9 and 10 is obvious. For comparison we write

$$\Phi_1(\sigma) = \sigma^2 G(\sigma^2/6.2)/10 \quad (11a)$$

$$\Psi_1(\sigma) = 2\sigma^2/9 (1 + 1.35 \sigma^2) \quad (11b)$$

The treatment of the experimental data for DNA in terms of the two theories will therefore be combined. To this end we have made plots of $[\eta]M/\rho^3$ and $M/\rho[S]$ against M/ρ (Figs. 5 and 6). Samples giving points, lying very far from the curve in Fig. 5 that gives the best fit, are indicated by dotted circles in Figs. 2, 3, 4 and 6. In some cases we have definite reason to do so (impurities, for instance, such as samples 27 and 31); in other cases an erroneous measurement may be the cause for the outward position. Furthermore, in Fig. 6 the points representing JJA and CV 64 were left out.

First let us remark that the correlation appears to be slightly better than that of Fig. 4. We now wish to compare these data with the theoretical formulas. To this end we have to fit a $\Phi(\sigma)$ -, a $\Psi(\sigma)$ - and a σ^2 -axis to those of the quantities plotted. From eq. 5, 6 it follows that

$$\Phi(\sigma) = 0.185 \times 10^{-24} [\eta] M/\rho^3 \quad (12a)$$

$$\Psi(\sigma) = 6.85 \times 10^{-26} M/\rho [S] \quad (12b)$$

This fixes the first two axes, and the σ^2 -axis is fitted by remembering that $(d\Phi/d\sigma^2)_{\sigma=0} = 1/10$ and

(24) J. G. Kirkwood, R. W. Zwanzig and R. J. Plock, *ibid.*, **23**, 213 (1955).

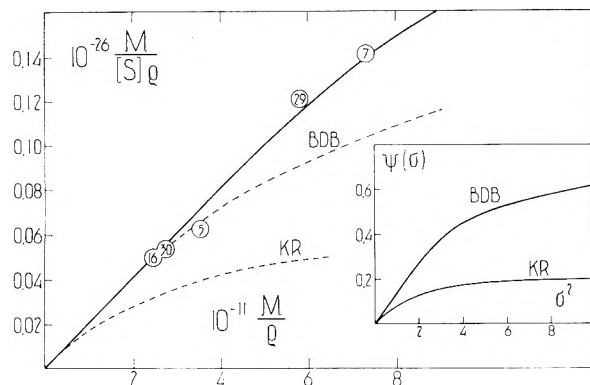


Fig. 6.—Comparison of sedimentation constants with theoretical formulas; the meaning of the various curves is explained in the caption to Fig. 5.

$(d\Psi/d\sigma^2)_{\sigma=0} = 2/9$. We equate these results with the limiting slopes of the curves which best fit the experimental points. As also $(d\Phi_1/d\sigma^2)_{\sigma=0} = 1/10$ and $(d\Psi_1/d\sigma^2)_{\sigma=0} = 2/9$ the Φ -, Ψ - and σ^2 -axes are identical for the two theories. We also see why plots of $[\eta]M/\rho^3$ and $M/\rho[S]$ against M/ρ were preferred to plots of $[\eta]/\rho^2$ and of $[S]$ against M/ρ . The fitting of the axes would in that case have been less straightforward.

The fit to the theoretical curves does not appear to be better than the fit to the straight line through the origin best fitting the points. A slight downward curvature is present, but for both the viscosity and the sedimentation data it is less than predicted by either of the two theories. It must, however, be kept in mind that in Fig. 5 the curve drawn from $10^{-11}M/\rho = 10$ onwards is rather arbitrary, since it is based on a single point, namely, sample 25, whose exceptionally large molecular weight is subject to experimental errors like all the others.

The BDB theory definitely fits the experimental data somewhat better than the KR theory. The rest of the discussion will therefore be in terms of this first theory.

A further discrepancy is found by comparing the ratios $\sigma^2[M/\rho]^{-1}$ needed to transform the M/ρ -axes into the σ^2 -axis. For the viscosity data we have used

$$\sigma_1^2 = 1.58 \times 10^{-11} M/\rho \quad (13a)$$

and for the sedimentation data

$$\sigma_2^2 = 0.68 \times 10^{-11} M/\rho \quad (13b)$$

Next we may look at the value of γ . It is easily seen that γ is to be compared with $10(\Phi)(\sigma)/27\Psi(\sigma)$. For $\gamma = 0.35$, the average of the five lowest values of Table II, one has $\sigma = 2.75$, which is found by graphical interpolation of Φ/Ψ . If we also take the average value of M/ρ for these five samples, which is 4.8×10^{11} , we find with eq. 13 $\sigma_1 = 1.8$ and $\sigma_2 = 2.75$, which is roughly in agreement with the value calculated from γ . However, M/ρ of these five samples varies from 2.5 to 7.8, without any appreciable change in γ , though the BDB theory predicts a variation of γ which is roughly proportional to σ^2 , *i.e.*, to M/ρ .

Lastly we shall derive an estimate of the quantity ζ/m , the frictional coefficient per unit of molecular weight of the monomer beads which the particle

is thought composed of, and compare this with the molecular dimensions. If we write $M = mP$ it follows from eq. 4 and 8 that

$$\zeta_1/m\eta_0 = (4\pi/3)1.29 \sigma^2/[M/\rho] \quad (14)$$

With eq. 13a and 13b, respectively, we arrive at

$$\zeta/m\eta_0 = 8.45 \times 10^{-11}$$

and

$$\zeta_2/m\eta_0 = 3.65 \times 10^{-11}$$

It would be interesting if we could compare these values with the dimensions of the DNA-chain as given by the model of Watson and Crick. This model is roughly a flexible tube of diameter about 30 Å., which has a molecular weight of 200 per Å. With synthetic polymers it has been customary to replace each monomer unit by a bead and to calculate the radius of the bead from $\zeta/m\eta_0$ with the aid of Stokes' law. This generally leads to radii far too small compared with those one finds when calculating the dimensions of these monomer units with the aid of atomic radii and distances. This often has been explained by denying the applicability of Stokes' law when we are concerned with beads as small as a few closely packed carbon atoms. One can also do this for DNA by considering a section of 30 Å. taken out of the DNA-chain as a bead of radius 15 Å. One calculates $\zeta/m\eta_0 = 6\pi 15 \times 10^{-8}/15.200 = 10^{-9}$, which is at least a factor 10 larger than the values found with the aid of the BDB and KR theories. Now this to us seems only natural. Whereas for a synthetic macromolecule the choice of the bead still appears to be logical, there is no doubt that it is quite arbitrary for the DNA-chain. As we must expect $\zeta/m\eta_0$ for two such beads to be much smaller when the two beads are close together, agreement can be expected by taking longer sections of the polymer chain.

We will therefore try to find the length of the DNA-chain, which gives the correct $\zeta/m\eta_0$ when stretched. This particle is a cylinder with radius $b = 15$ Å. and length $2a = 2p \times b$. It has a molecular weight $\mu = 400a$. The frictional constant f of this particle is given by (Burgers,²⁵ Sadron²⁶)

$$f = 6\pi\eta_0 b p^{1/2} t(p) = 6\pi\eta_0 a t(p)p^{-2/3}$$

so that

$$f/\mu\eta_0 = 0.015 \times 10^{-8} \pi t(p)p^{-2/3}$$

Here t is a known function of p . With eq. 15 the two values of $t(p)p^{-2/3}$ of this particle therefore become $t(p_1)p_1^{-2/3} = 0.18$ and $t(p_2)p_2^{-2/3} = 0.075$. From a graph of $t(p)p^{-2/3}$ against p , easily made with the help of the values of $t(p)$ given by Sadron, we find $p_1 \cong 8$ and $p_2 \cong 17$, giving $2a_1 = 240$ Å. and $2a_2 = 510$ Å. These values compare favorably with the persistence length which will be calculated in part II by considering the DNA-molecule as a coiled worm-like particle; we find values ranging from 300 to 800 Å.

Conclusions

In this first part we have discussed several attempts to correlate measurements on DNA with

(25) J. M. Burgers, "Second Report on Viscosity," North Holland Publ. Co., Amsterdam, 1938.

(26) C. Sadron, *Progr. Biophys.*, **3**, 237 (1953).

theoretical formulas, which have been derived on the basis of a number of different assumptions concerning the behavior of macromolecules. The best fit, by far, is obtained with the Brinkman-Debye-Bueche theory. The agreement, however, is only qualitative. We know of two reasons that can explain this discrepancy.

1. In our second article arguments will be produced that support the Watson and Crick model. The light-scattering data are compatible with a worm-like chain. Now the BDB theory supposes that a coiled molecule may be represented by a sphere homogeneously filled with beads. The proof of this will have to be found by comparing theory with experiment, which is what we have tried to do. On the other hand, the viscosity contribution of worm-like chains has not yet been calculated, so that a final check cannot be made.

2. In all our considerations we have supposed that the samples contain only particles of identical size and shape. This supposition is not supported by any experimental fact, but neither can we replace it by another one. It is known, however, that DNA samples are inhomogeneous as regards their chemical composition (compare for instance

Lipshitz and Chargaff,²⁷ Lucy and Butler,²⁸ Frick²⁹), so there may be any amount of dispersion in the molecular weights, radii of gyration, etc., of the particles. The influence of this polydispersity on the way the quantities measured are to be compared with theory may be appreciable.

Another point that may need some discussion is the way the points are scattered around the curves in Figs. 5 and 6. In the first place, the measurements are subject to experimental errors of the order of 10 to 20%. Secondly, the material is of biological origin and undergoes a number of delicate treatments before being investigated as DNA, which may cause variations in structure and properties, sometimes even in composition.

Although our results do not determine the shape of DNA-molecules, they at least do not contradict the points which will be developed in part II on the basis of light-scattering alone. New theoretical developments and more experimental work will be necessary.

(27) R. Lipshitz and E. Chargaff, *Biochim. Biophys. Acta*, **19**, 256 (1956).

(28) J. A. Lucy and J. A. V. Butler, *Bull. soc. chim. Belg.*, **65**, 133 (1956).

(29) G. Frick, *Biochim. Biophys. Acta*, **19**, 352 (1956).

SOLUTION PROPERTIES OF DEOXYRIBONUCLEIC ACID (DNA). II. LIGHT SCATTERING

By J. HERMANS, JR.¹

Laboratorium voor Anorganische en Fysische Chemie, Universiteit, Leiden

Received June 19, 1958

The light scattering of the samples whose hydrodynamic properties were discussed in part I is described. The dissymmetry z_{45} is appreciably less than for Gaussian chains. This result is discussed in terms of two models: zig-zag chains and worm-like chains. Fair agreement between theory and experiment is found. The effect of polydispersity is discussed.

Introduction

In our first article² we have tried to connect the hydrodynamics of DNA-solutions with the dimensions obtained by light scattering. In this article we will consider the variations that occur in the form of the scattering curves. Both the possible influence of polydispersity and of chain stiffness will be discussed. The samples studied are those given in Table I of part I, which will be referred to as Table I-I.

Technique. Apparatus.—The light scattering of samples I to 21 of Table I-I was measured with the aid of the light-scattering apparatus described by Wippler and Scheibling.³ The other measurements were done with an apparatus described by Cantow,⁴ which was however modified by us to the extent that a simple cylindrical cell was used which was placed in a bath of benzene and that the light beam had a rectangular cross-section.

Standard.—Analytical reagent grade benzene which had been centrifuged for one hour at 20,000 g was used as a standard for all the measurements. Its Rayleigh constant was taken to be $R_{90} = (16.4 \pm 0.8) \times 10^{-6} \text{ cm.}^{-1}$ for $\lambda = 5460 \text{ \AA.}$, as an average over the determinations of a num-

ber of authors. An unpolarized primary beam was used in all cases.

dn/dc was taken to be $0.170 \pm 0.002 \text{ ml./g.}$ for all samples. This value is an average over ten DNA-samples.⁵

Dust was removed by centrifuging for one hour in a Pywe-“Pirouette” centrifuge at 20,000 g .

Pipets and cells were made dust-free by a jet of freshly distilled acetone, or by heating for some time at 130° after rinsing with distilled water.

Treatment of Data.— R_{θ} -values were obtained from the experimental data by multiplication with $n_s^2 \sin^2 \theta / 16.4 \times 10^{-6} / n_s^2 (1 + \cos^2 \theta) t$, where θ is the angle of scattering, t the reading for benzene at 90° and n_s and n_b the refractive indices of the solution and benzene. From these data Kc/R_{θ} where c is the concentration in g./ml. and $K = 2\pi^2 n^2 (dn/dc)^2 / N \lambda^4$, n = refractive index of the solution and N Avogadro's number, was calculated for each measurement. Now these values were plotted against $\sin^2(\theta/2) + kc$, where k is an arbitrary constant, to give a Zimm plot. The extrapolation to $c = 0$ and $\theta = 0$ directly gives us $1/M$, and the slope of the tangent to the curve $[Kc/R_{\theta}]_{c=0} = f(\sin^2 \theta/2)$ at $\theta = 0$ is equal to $(1/M) 16\pi^2 \rho^2 / \lambda_1^2$, where λ_1 is the wave length in the solution, so that ρ can also be obtained. Finally the extrapolated dissymmetry $z_{45} = R_{45}/R_{135}$ is calculated and used as a measure of the higher order terms in the angular distribution of scattering.

Results.—The values of M , ρ and z have been collected in our first article,¹ Table I-I.

(1) Chemistry Dept., Cornell University, Ithaca, N. Y.

(2) J. Hermans and J. J. Hermans, *THIS JOURNAL*, **63**, 170 (1959).

(3) C. Wippler and G. Scheibling, *J. chim. phys.*, **51**, 201 (1954).

(4) H. J. Cantow, *Dechema Monographien*, **27**, 124 (1956).

(5) J. Pouyet and G. Weill, *J. Polymer Sci.*, **23**, 739 (1957).

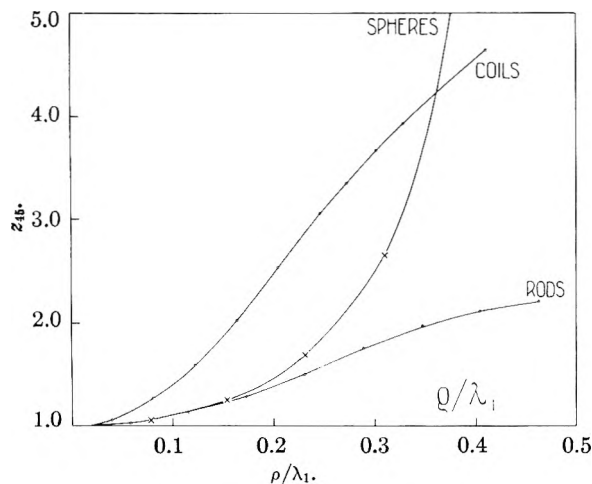


Fig. 1.—Dissymmetry versus the ratio of the radius of gyration and the wave length in the solution for three different models.

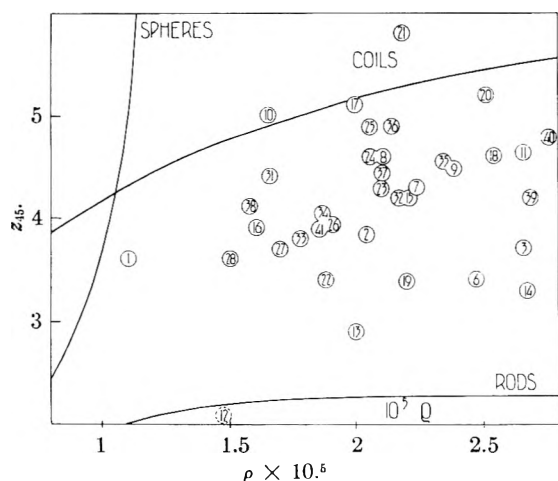


Fig. 2.—Comparison of the experimental data for DNA preparations with the theoretical curves for three models.

Discussion

By comparing the radius of gyration and the dissymmetry z_{45} of the scattered light, one can in principle distinguish between several possible models for the preparation in hand.

Figure 1 shows graphs of z_{45} against the ratio ρ/λ_1 , where λ_1 is the wave length in the solution, for three models⁶: spheres, rods and Gaussian coils, all monodisperse. By marking in Fig. 1 the point representing the substance studied, one obtains an indication regarding a possible model.

In Fig. 2 the points representing the DNA-samples studied have been marked. The numbers correspond to those in Table I-I. We remark the absence of order in this first attempt, and also that the values of z_{45} sometimes reach that for Gaussian chains of the same ρ , but are never as low as those for rods. That the particles are homogeneously filled spheres is clearly excluded. Two ways are now open: we can either assume the correctness of the Gaussian chain approximation and try to explain lower values of z in terms of heterogeneity or else we can consider a different model that has

characteristics of both the Gaussian chain and the rod and again try to fit the data to calculated curves.

A. Polydispersity.—The influence of polydispersity on the light scattering formulas of Gaussian chains has been calculated by Benoit.⁷ When the mean square of the end to end distance of these chains is proportional to M , polydispersity results in a lower value of z_{45} than is calculated for monodisperse Gaussian chains of the same radius of gyration as the mean value determined experimentally.

It can hardly be said, however, that the case of DNA is such a simple one. From sample to sample there is no simple relationship² between M and ρ , nor need we expect the existence of such a relation for particles within a single sample. The following examples illustrate this. If Benoit's theory is applicable to the case of DNA we should expect samples 10 and 20 to be practically monodisperse but samples 7, 11 and 16 to be markedly polydisperse. This is seen by comparing in Fig. 2 the value of z_{45} which was measured with that predicted by theory for monodisperse Gaussian coils of the same radius of gyration.

Now let us consider the sedimentation constant distribution curves of these samples. Shooter and Butler⁸ describe that of sample 7; of the other samples we determined the sedimentation distribution curves ourselves, following the same procedure as Shooter and Butler. We will not reproduce these curves, but wish to point out that for these curves the value $S_{1/2}$ may vary a little from sample to sample, but that the width of the distribution is in all five cases practically the same. Samples 10 and 20 are not therefore monodisperse, nor is there an indication that they are less polydisperse than the others.

We have no indication whatsoever of the distribution of the particles over the two variables M and ρ . Whereas in the case of synthetic polymers, either crude or fractionated, assumptions regarding the distribution as a function of M often can be made, no information of this kind exists in the case of our DNA samples.

A comparison of different averages of M , which generally gives a good indication of polydispersity has never been made for DNA. By light scattering one determines $(\sum M^2 N)/(\sum MN) = M_w$, the so called weight average molecular weight (N is the number of particles of a given M). If the value of M of all the particles is not the same, the number average molecular weight $M_n = (\sum MN)/\sum N$ is smaller than M_w . In general different averaging procedures produce different values of M . We must therefore look for an experimental technique which gives us another average than the weight average, and then compare this value with M_w . This never has been done, and the reason for this is that some of the common methods for obtaining these other averages are inapplicable to DNA. For one, the osmotic pressure of DNA solutions cannot be measured with sufficient precision at

(7) H. Benoit, *J. Polymer Sci.*, **11**, 507 (1953).

(8) K. V. Shooter and J. A. V. Butler, *Trans. Faraday Soc.*, **52**, 734 (1956).

(6) P. Debye, *J. Applied Phys.*, **15**, 338 (1944); B. H. Zimm, R. S. Stein and P. Doty, *Polymer Bulletin*, **1**, 90 (1945).

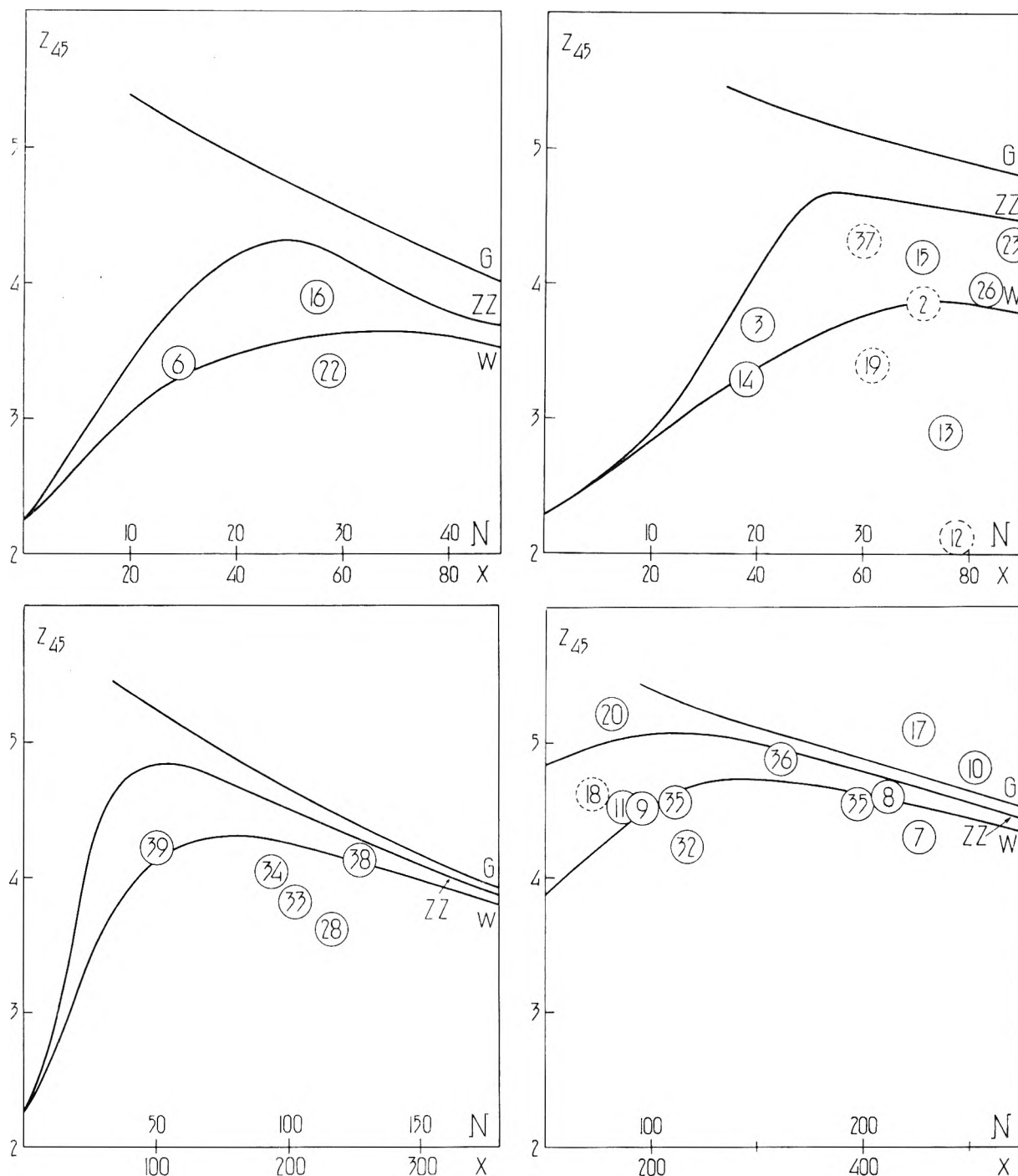


Fig. 3.—Comparison of the dissymmetry with theoretical values: G, Gaussian chains; W, worm-like chains; ZZ, zig-zag chains. This is done for molecular weights of 4.4×10^6 (a), 6×10^6 (b), 8.4×10^6 (c) and 13.5×10^6 (d). See also text.

the concentrations of practical interest, since the molecular weight is too high. Another method is the determination of the sedimentation equilibrium. A short calculation shows that if the exponent occurring in the equation describing the concentration as a function of height h is $hgM(1 - \bar{v}d)/NkT$ where $g = 10^3$ is the acceleration of gravity, $\bar{v} = 0.55$ the partial specific volume of DNA, $d = 1$ the density of water, $N = 6.10^{23}$ and $kT = 4 \times 10^{-14}$, then gravity alone is sufficient to cause a measurable difference in concentration at heights only a few cm. apart. In practice, however, this

concentration difference never sets in. For, if the sedimentation equilibrium is to be produced by sedimentation under the influence of gravity, it is clear that it will take 8×10^4 times as long as it takes in a field of 8×10^4 g., where it takes about one hour. As 8×10^4 hours is about 10 years, the method clearly is not applicable.

We do not mean to say that a method giving an average other than M_w cannot be applied. Up to now, however, this has not been done, and we remain in the dark as regards the polydispersity. We will therefore try another procedure, that of

finding a new model, assuming that DNA preparations contain only identical molecules.

B. Stiffness of the Chains.—In our first article the structural model of Watson and Crick was mentioned, which is based on X-ray data. This structure establishes the molecular weight per unit length. Taking for instance a particle with $M = 6 \times 10^6$ we find $L = 3.10^4 \text{ \AA.}$ for the total extended length. Comparing this length and the end to end distance r , which is, say, 6000 \AA. (from $\rho = 2500 \text{ \AA.}$, assuming $r^2 = 6\rho^2$) when Gaussian statistics apply, with a sample of polystyrene $M = 5 \times 10^5$, $r = 475 \text{ \AA.}$, for which the total length is of the order of $2 \times 10^4 \text{ \AA.}$, we see that the molecule possesses a degree of coiling or folding much lower than generally encountered in synthetic products. One may expect that there is a certain level below which the coiling or folding cannot descend without having an influence on the light scattering as compared with that by Gaussian chains.

To investigate this let us consider the statistics of zig-zag chains and worm-like chains. A zig-zag chain is defined as an unbranched chain consisting of straight rods connected by hinges which permit complete freedom of orientation of the rods with respect to each other. If there are N rods of length A , the average square of the end to end distance $\langle r^2 \rangle$ and the extended length L of such a chain will be given, respectively, by

$$\langle r^2 \rangle = NA^2 \text{ and } L = NA \quad (1)$$

A first treatment of the statistics of worm-like chains was given by Kratky and Porod.⁹ They consider a chain consisting of n rods of length σ . The total length of the chain is $L = n\sigma$. The angle α between successive rods can assume all values between 0 and π , but small values of α predominate. The quantity k , which is defined as the average of $\cos \alpha$, is therefore close to unity. By now letting approach σ to zero, n to infinity and k to unity in such a way that both $a = -\sigma/\ln k$ and L remain finite, limiting formulas are obtained which describe the statistics of worm-like chains.

It can be shown that a is the shortest length for which the direction of the chain at the beginning does not influence the direction of the chain at the end, and a is therefore called the persistence length. It was shown by Kratky and Porod that the average square of the end to end distance is

$$\langle r^2 \rangle = \frac{2a^2(x - 1 + e^{-x})}{x = L/a} \quad (2)$$

When $x > 40$ a good approximation is given by

$$\langle r^2 \rangle = 2a^2x \quad (3)$$

The light scattering of both zig-zag and worm-like chains has been calculated.¹⁰ We shall not reproduce the formulas, but merely mention that it is permissible to use the equation $\langle r^2 \rangle = 6\rho^2$ as long as $N > 20$ or $x > 40$. We see therefore that if a sample is described by the parameters A and N (zig-zag) or a and x (worm), that fit the radius of gyration and the length of the chain according to eq. 1, 2, 3, we have approximately

(9) O. Kratky and G. Porod, Proc. Internat. Colloq. Macrom. Amsterdam, 1949, p. 502; also *Rec. trav. chim.*, **68**, 1106 (1949).

(10) J. Hermans, Jr., and J. J. Hermans, *THIS JOURNAL*, **62**, 1543 (1958).

$$x = 2N \text{ and } A = 2a \quad (4)$$

We can then compare the experimental value of the dissymmetry with that calculated for the zig-zag and worm models with the aid of theoretical formulas.

In Fig. 3, a, b, c and d this comparison is carried out. They show z_{45} for varying values of x at constant values of L for the worm (curves W), for varying values of N but at constant L for the zig-zag chains (curves ZZ). It is seen (eq. 4) that the x - and N -axes are so fitted that the radius of gyration of the two particles is identical. We have therefore included curves G representing the value of z_{45} for Gaussian chains having values of ρ equal to those of the zig-zag and worm at the same value of the abscissa. The four values of M chosen were 4.4×10^6 , 6×10^6 , 8.4×10^6 and 13.5×10^6 , corresponding to values of L equal to 2.2×10^4 , 3×10^4 , 4.2×10^4 and $6.75 \times 10^4 \text{ \AA.}$ Of all the samples investigated x was now calculated and z_{45} carried against x in these four graphs. The choice of the graphs was made in such a way that the difference between the measured value of M and the value for which the graph was made, was as small as possible. The few samples showing rather large deviations in the graphs of our first article² were again indicated by dotted circles.

We first of all remark that only when $M < 10 \times 10^6$ is there a sufficiently large difference between the curves to enable us to distinguish between the models. What is more important, though, is that the experimental points fit the curves for worms although there is a large amount of scatter of the points. The approach seems a successful one and confirms the earlier effort of this kind made by Peterlin.¹¹

We may now again consider the possibility of polydispersity. We can hardly expect a number of preparations of varying molecular weight, which contain worm-like molecules, all to be monodisperse. As we still know nothing of the character and extent of the polydispersity, the question remains an open one. Two possibilities seem to us worth mentioning. In the first place the molecules with $M \sim 13 \times 10^6$ may be different from the (supposedly worm-like) ones with $M \sim 6 \times 10^6$. The samples with intermediary molecular weights may then be mixtures of these two species. In the second place the high molecular weights may be caused by relatively small amounts of very high molecular weight material. In both cases it would then be rather accidental that for the samples with $M > 7 \times 10^6$ the light-scattering behavior is that of worm-like chains.

Acknowledgments.—Part of the research described in Parts I and II was carried out while the author was enjoying the hospitality of Professor Ch. Sadron at the Centre de Recherches sur les Macromolécules at Strasbourg, France. He especially wants to thank Jean Pouyet and Professor Sadron for the help and advice they have at all times been ready to give. Furthermore his thanks are due to Professor A. J. Staverman of Leiden University who was so kind as to supervise the rounding off of the work.

(11) A. Peterlin, *Makromol. Chem.*, **9**, 244 (1953).

AN INFRARED STUDY OF THE WATER-SILICA GEL SYSTEM

BY H. A. BENESI AND A. C. JONES

*Shell Development Company, Emeryville, California**Received June 19, 1958*

An infrared study of bound and adsorbed water in silica gel has been made. It was found that hydrogen in silica gel could be completely replaced by deuterium upon treatment with D_2O at room temperature. Deuteration of silica gel allowed unambiguous differentiation between absorption bands arising from silica itself and those arising from atomic groupings that contain hydrogen. It was found that "bound water" in silica gel consists entirely of SiOH groups located on the surface. The infrared spectrum of physically adsorbed water closely resembles that of liquid water. Dehydration of silica gel at high temperatures removes surface SiOH groups; these can be reconstructed by reaction with adsorbed water at room temperature.

The present study was undertaken with the expectation, since fulfilled, that the use of infrared spectroscopy would lead to a better understanding of the state of bound and adsorbed water in the water-silica gel system. As the first step, we made absorption band assignments which, in turn, enabled us to make an unambiguous interpretation of the nature and location of hydroxyl groups in silica gel. At this stage of the investigation, the information derived through observation of the spectral changes that accompanied silica gel deuteration was indispensable. We then investigated the physical adsorption and chemisorption of water on silica gel, the present study being more nearly complete than that reported by Pimentel, *et al.*¹ The results obtained are presented and discussed below.

Experimental Details

Sample Preparation.—Silica gel samples consisting of particles having diameters less than one micron were obtained from Monsanto (Aerogel), Philadelphia Quartz (QUSO), Godfrey Cabot (Cab-O-Sil), Davison Chemical (Syloid 244) and Dow Corning Companies. Such silica gel powders could be used, as received, for the preparation of sample films. Samples of Grade 35, Grade 70 and Grade 950 silica gel from Davison Chemical Company were ground and sedimented from isopropyl alcohol suspension using techniques very similar to those developed by Hunt² and by Keller and Pickett.³ However, the material used in most of the present study was a sample of Davison's Grade 950 silica gel that had been air-milled⁴ by use of a Sturtevant Micronizer. The above sample of Grade 950 silica gel, as it was received from Davison Chemical Company, contained only 0.002% aluminum, had a surface area of 745 m.²/g. and a pore volume of 0.37 cc./g. The latter values dropped to 581 m.²/g. and 0.31 cc./g., respectively, through the air-milling process.

Most sample films were mounted on sodium chloride or barium fluoride windows by placing a quantity of silica gel of fine particle size on the window, adding enough isopropyl alcohol to make a slurry, wiping a microscope slide across the window, and allowing the alcohol to evaporate.

During the course of our studies we developed a technique similar to that recently described by Yang and Garland⁵ to prepare films that were much more uniform than those prepared as described above. The technique consisted of spraying a suspension of fine particle size silica gel in isopropyl alcohol (0.1 g. per 100 ml. of suspension) onto a salt window that was heated by contact with an aluminum block kept at 60 to 90°. The sprayer used was of the type suitable for the development of paper chromatograms. It was obtained from Microchemical Specialties, Inc., Berkeley, California.

(1) G. C. Pimentel, C. W. Garland and G. Jura, *J. Am. Chem. Soc.*, **76**, 803 (1953).

(2) J. M. Hunt, API Project 49, Rept. No. 8, p. 105 (1950).

(3) W. D. Keller and E. E. Pickett, ref. 2, p. 123.

(4) Kindly furnished by Dr. K. Marple, Shell Development Company, Modesto, California.

(5) A. C. Yang and C. W. Garland, *THIS JOURNAL*, **61**, 1504 (1957).

Films prepared by the spray technique appear, by visible examination, to be highly uniform in thickness. Evidence for the uniformity of thickness may be deduced from Fig. 1 in which the absorbance at each of two frequencies is plotted against thickness for a series of films. The linearity of the data attests to the fact that a good measure of film thickness was obtained from the weight of silica gel and the area (4.9 cm.²) of the salt window. Because only about 20% of the area of the film is in the light beam, it is unlikely that the average thickness would be a good measure of the thickness in the light beam if the films were not uniform.

Apparatus.—Infrared spectra were recorded by means of a Perkin-Elmer, Model 21 spectrophotometer with sodium chloride optics. The cell employed for most measurements is shown in Fig. 2. Its path length was made as short as conveniently possible in order to reduce infrared absorption by the vapor phase. A matched pair of cells was used, a reference cell and a sample cell. Both cells were attached to a high vacuum system. They could be evacuated or exposed to vapors *in situ* at room temperature while a spectrum was being recorded. The partial pressure of H_2O (or D_2O) was controlled by appropriate adjustment of the temperature of a water reservoir attached to the vacuum system.

It was found that the desorption or adsorption of water vapor on films of silica gel reached equilibrium very rapidly; *e.g.*, the spectrum of a silica gel film that was being evacuated at room temperature was unchanged upon increasing the time of evacuation from 0.5 to 16 hours. In the case of the samples whose spectra and properties are described in the present study, the time allowed for equilibration was 0.5 hour.

Sample films were mounted on the inside surface of the salt window nearest the entrance slit of the spectrophotometer. We found that films as thick as 4 mg./cm.² could be mounted in a *vertical* position. A 5 mm. wide strip of film was removed from the edge of the salt window to make way for the Apiezon W seal between the window and the lip of the glass cell.

In one case in which the silica gel film was evacuated at 400° and then cooled to room temperature, a "high temperature" cell similar to that described by Eischens, *et al.*⁶ was used. Since it is still undergoing modification, the final design will appear at a later date.

Results and Discussion

Absorption Bands Arising from Silicon-Oxygen Bonds.—Crystalline forms of silica (*i.e.*, quartz and cristobalite) have sharp, strong absorption bands at *ca.* 1200, 1100 and 800 cm.⁻¹ which presumably arise from silicon-oxygen fundamentals.^{7,8} The above bands, though broadened, easily can be discerned in the spectra of diatomaceous earth, fused silica and silica gel as shown, for example, in Fig. 6. In these amorphous forms of silica the 1200 cm.⁻¹ band appears as a shoulder on the broad 1100 cm.⁻¹ band.

The spectra of thick films of all silica samples studied (see Fig. 3, for example) show, in addition,

(6) R. P. Eischens, S. A. Francis and W. A. Plisken, *ibid.*, **60**, 194 (1956).

(7) E. K. Plyler, *Phys. Rev.*, **35**, 48 (1929).

(8) H. H. Adler, API Project No. 49, Rept. No. 8, p. 18 (1950).

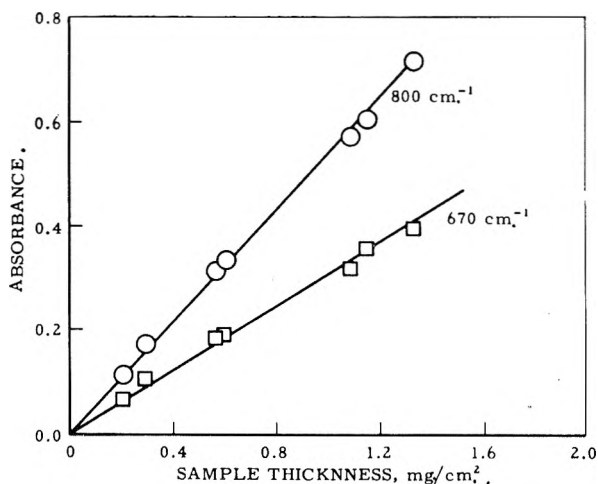


Fig. 1.—Applicability of Beer's law to silica gel films.

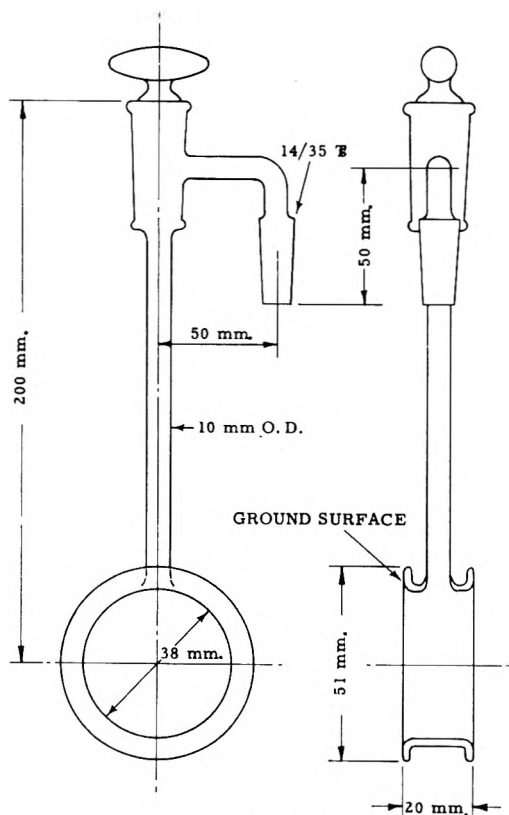


Fig. 2.—Pyrex infrared cell.

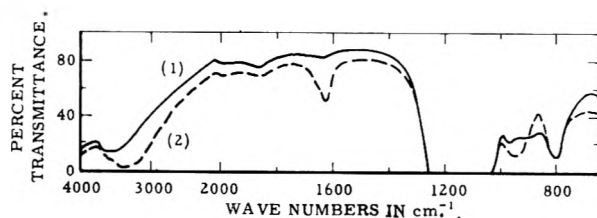


Fig. 3.—Spectra of silica gel before (curve 1) and after (curve 2) exposure to water vapor.

weak bands at 2000, 1875 and 1640 cm^{-1} . When such films are exposed to water vapor, the 1640 cm^{-1} band is obscured by the band arising from physically adsorbed water. The fact that the positions of the above three bands are unchanged

upon silica gel deuteration, as described below, is a strong indication that they are combinations or overtones of the silicon-oxygen fundamentals.

Absorption Bands Arising from Bound and Adsorbed Water.—The spectrum of an evacuated silica gel film (1 mg/cm^2) before and after it was exposed to water vapor is shown in Fig. 3. The absorption band between 3800 and 2500 cm^{-1} can arise only from OH stretching vibrations. The extreme breadth of this band indicates the existence of a wide spectrum of hydrogen bonding interactions between hydroxyl groups. It is evident that the background absorption in this spectral region increases with increasing frequency. The frequency-dependent energy loss is caused by scattering which seems to be unavoidable in the case of thick films of Grade 950 silica gel.

The appearance of a strong absorption band at 1635 cm^{-1} when silica gel is exposed to water vapor shows that this band must arise from the ν_2 fundamental for water.⁹ This spectral change is, of course, accompanied by a large increase in the intensity of the absorption band arising from OH stretching vibrations. The increased broadening indicates increased hydrogen bonding.

The spectral curves shown in Fig. 3 represent reversible states. Thus, the spectrum obtained upon re-evacuating the "wet" silica gel is identical with curve 1. Since the weak residual band whose position is virtually identical with that for adsorbed water arises from a silicon-oxygen overtone, adsorbed water is removed completely by evacuation at room temperature within the limits of our means of detection.¹⁰

Silica Gel Deuteration.—As shown in Fig. 4 the adsorption of D_2O on evacuated silica gel produced spectacular spectral changes. First, the strong band at 2500 cm^{-1} in curve 2 signaled the presence of OD groups (from SiOD , HDO and D_2O). Second, the immediate appearance of the HOD bending band (at 1430 cm^{-1})¹¹ together with the fact that its height did not change with time showed not only that hydrogen-deuterium exchange had occurred but that it had occurred at a rate too rapid to be measured. The latter finding apparently differs from that obtained by Pimentel, *et al.*, who reported, on the basis of mass spectrometric analyses, that only 5% exchange had occurred in D_2O vapor that had been in contact with a sample of highly dehydrated silica gel for four hours at room temperature. Although their observation can be interpreted as indicative of a slow rate of exchange, it also can be explained as the result of incomplete equilibration between the silica gel sample and the *entire* vapor phase which could have occurred if the vapor phase had not been stirred or circulated during the exchange experiment.

As a consequence of the above finding, we found it easy to prepare completely deuterated silica gel. We simply exposed the sample film to D_2O vapor, evacuated the resulting film, and repeated this

(9) E. K. Plyler and W. W. Sleator, *Phys. Rev.*, **37**, 1493 (1931).

(10) We estimate that we can detect the presence of 0.1 wt. % physically adsorbed water in a silica gel film having a thickness of 1 mg/cm^2 .

(11) E. F. Barker and W. W. Sleator, *J. Chem. Phys.*, **3**, 660 (1935).

process six to eight times over a period of 30 minutes. The spectrum of deuterated silica gel is compared with that of the original silica gel in Fig. 5. The absence of the OH stretching band in curve 1 shows that all of the hydrogen has been replaced by deuterium.¹² Since the weak absorption bands at 1640, 1875 and 2000 cm^{-1} are unchanged upon deuteration, it is now evident that they must arise from silicon-oxygen combinations or overtones.

At this point we emphasize the importance of our finding that the above-mentioned 1640 cm^{-1} band does *not* arise from residual adsorbed water. We can now—and only now—conclude on the basis of infrared studies that bound “water” in silica gel consists entirely of SiOH groups. Furthermore, since it is obvious that the SiOH groups are readily accessible to D_2O vapor, they must be located on the silica gel surface. The above conclusions are in good agreement with those reached by Shapiro and Weiss¹³ who, on the basis of hydrolysis measurements of diborane, were the first to establish firmly the nature of bound water in silica gel.

Absorption Arising from Silanol Groups.—The absorption of silica gel films at 870 cm^{-1} drops markedly when such films are deuterated (Fig. 5) or when they adsorb water (Fig. 3). This absorption decrease signifies the presence of a strong absorption band. From the literature¹⁴ it is found that silanols have a strong absorption band in the 830–880 cm^{-1} region which is absent from the spectrum of siloxanes. We thus feel reasonably certain that the 870 cm^{-1} band arises from the bending vibration of SiOH groups. The shift of this band upon adsorption of water must reflect the attendant increase in hydrogen-bonding of the SiOH groups.

The positions of the absorption bands in the spectra of water-silica gel systems are collected in Table I together with our assignment of them.

Physically Adsorbed Water.—The spectral curves for varying amounts of water adsorbed on a silica gel film (0.1 mg./cm^2) appear in Fig. 6. The apparent surface coverages listed in Fig. 6 were calculated from the relative pressures employed using the results obtained by Sing and Madeley¹⁵ together with a value of 10.6 \AA^2 for the area covered by an adsorbed water molecule. These investigators measured water adsorption isotherms using a sample of silica gel whose surface area and pore volume are virtually identical with those of the sample used in the present study.

Although “surface coverages” have been calculated, it is likely that the water is not adsorbed on silica gel in distinct steps or layers. The water adsorption isotherm¹⁵ has no “knee” at the point

(12) This result seems to preclude the possibility suggested by Pimentel, *et al.*,¹ namely, that D_2O adsorbed on silica gel slowly exchanges with residual unexchanged “water” in silica gel. Since the silica gel sample used by them had been outgassed at 475°, we subjected a silica gel sample that had been similarly outgassed to D_2O treatment as already described and again found that all the hydrogen was replaced by deuterium.

(13) I. Shapiro and H. G. Weiss, *THIS JOURNAL*, **67**, 219 (1953).

(14) R. E. Richards and H. W. Thompson, *J. Chem. Soc.*, 124 (1949).

(15) K. S. Sing and J. D. Madeley, *J. Appl. Chem.*, **4**, 365 (1954).

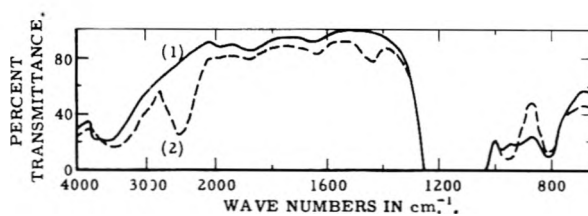


Fig. 4.—Spectra of silica gel before (curve 1) and after (curve 2) exposure to D_2O at 4 mm. at room temperature.

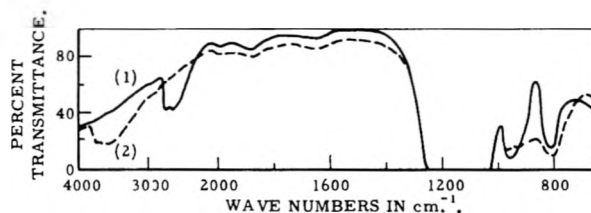


Fig. 5.—Spectra of evacuated silica gel before (curve 2) and after (curve 1) complete deuteration.

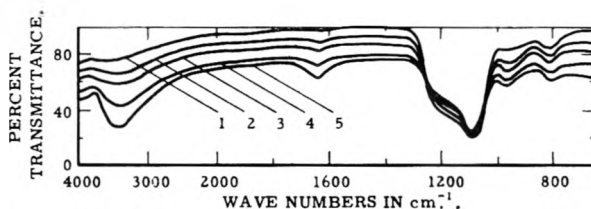


Fig. 6.—Spectra of water adsorbed on silica gel. Apparent surface coverage is 0, 0.4, 0.6, 1.3, and 1.6, respectively, for curves numbered from 1 to 5.

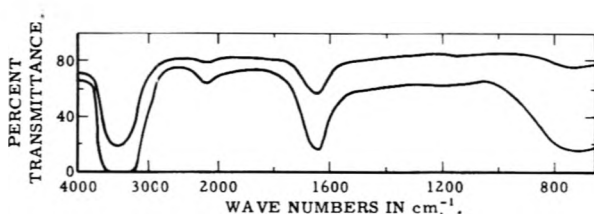


Fig. 7.—Spectra of thin films of water (pressed between silver chloride plates).

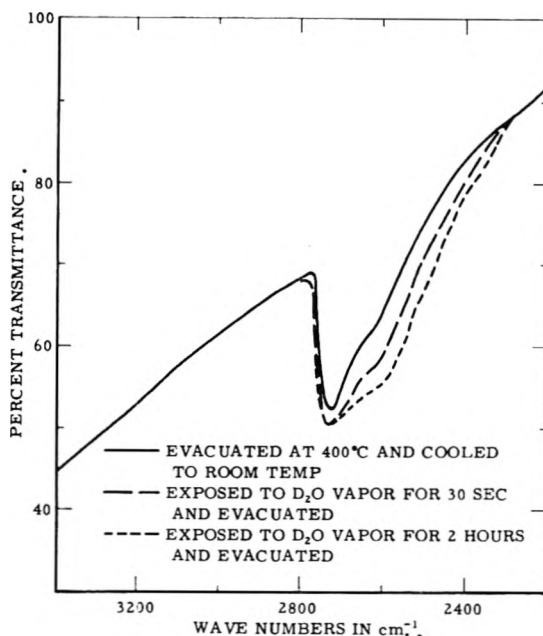


Fig. 8.—Deuterated silica gel.

TABLE I

ABSORPTION BANDS OF THE WATER-SILICA GEL SYSTEM^a

Absorption max., cm. ⁻¹	Assignment	Remarks
3730(m)	OH stretching	
3580(m)	OH stretching	Hydrogen bonded, very broad
2760(m)	OD stretching	
2620(m)	OD stretching	Deuterium bonded very broad
2000(w)	SiO combination	
1875(w)	SiO combination	
1640(w)	SiO overtone	
1635(m)	HOH bending	
1430(m)	HOD bending	
1200(sh)	SiO stretching	
1095(vs)		
870(m)	SiOH bending	
810(s)	SiO stretching	

^a vs = very strong, s = strong, m = medium, w = weak, sh = shoulder.

corresponding to a completed monolayer. It is also evident from the spectra in Fig. 6 that there is no appreciable shift in the position of the HOH bending band between 0.6 and 1.3 "monolayers" as might be expected if a close-packed monolayer actually had been completed. Thus, in the case of a fine-pore silica gel of the kind used in the present study it is likely that capillary condensation begins before completion of the first monolayer. As a result the two processes are indistinguishable.

The spectrum of water adsorbed on silica gel closely resembles that of water in its liquid state (see Fig. 7), a result that agrees with the observations made by Pimentel, *et al.*¹ The positions of the absorption band arising from the ν_2 (bending) fundamental for water in various states are listed in Table II. The difference in values for liquid and adsorbed water is barely outside experimental error.

Chemisorption of Water on Silica Gel.—The removal of hydroxyl groups from the surface of silica gel upon outgassing a sample film at successively higher temperatures up to 400° can be conveniently followed by means of infrared spectroscopy using an *in situ* cell of the general type described by Eischens, *et al.*⁶ We found that the broad OH stretching band narrows in an unsymmetrical manner upon removal of SiOH groups, *i.e.*, absorption decreases in the low frequency region (3000 to 3600 cm.⁻¹) while little change occurs in 3600 to

TABLE II

 ν_2 FUNDAMENTAL FOR WATER IN VARIOUS STATES

State	Absorption max., cm. ⁻¹
Vapor	1595 ⁹
Liquid	1645
Water adsorbed on silica gel, 0.4 "monolayers"	1635
Water adsorbed on silica gel, 1.6 "monolayers"	1640

3800 cm.⁻¹ region. This result is a direct indication of a marked decrease in hydrogen bonding between neighboring OH groups brought about, no doubt, because of an increase in the average distance¹⁶ between OH groups in the dehydroxylated silica gel.

When a film of silica gel that has been dehydroxylated as described above is exposed to water vapor, the reverse reaction occurs. That is, water is "chemisorbed" to form SiOH groups as evidenced by a marked broadening of the OH stretching band in the spectrum of the resulting silica gel film (after physically adsorbed water is removed by evacuation at room temperature).

In order to study the chemisorption of water in a lower frequency region (where there was less energy loss through scattering), we repeated the above type of experiment using the D₂O-silica gel system. A film of completely deuterated silica gel was evacuated at 400° and then was exposed to D₂O vapor at 4 mm. at room temperature for varying periods of time. The film was evacuated after each D₂O exposure, infrared spectra being recorded at each stage of the above operations. The growth of the absorption band that arises from SiOD stretching vibrations is shown in Fig. 8. It can be seen that the height of the absorption band shows little change with increasing exposure time but that the width of the band increases steadily, its integrated absorbance after 72 minutes being twice that in its initial stage.

The above findings are in complete agreement with the results obtained by Young¹⁷ whose work was published after the present measurements were made. Young found that the rehydration of silica gel was reversible up to 400°.

Acknowledgment.—The authors wish to express their gratitude to Mr. M. O. Babcock for his help with the experimental work.

(16) See the frequency shift vs. O-H...O distance correlation published by G. C. Pimentel and C. H. Sederholm, *J. Chem. Phys.*, **24**, 639 (1956).

(17) G. J. Young, *J. Colloid Sci.*, **13**, 67 (1958).

INFRARED STUDIES OF PHYSICALLY ADSORBED POLAR MOLECULES AND OF THE SURFACE OF A SILICA ADSORBENT CONTAINING HYDROXYL GROUPS

BY M. FOLMAN AND D. J. C. YATES¹

Ernest Oppenheimer Laboratory, Department of Colloid Science, University of Cambridge, England

Received June 20, 1967

Further quantitative results of infrared studies of physically adsorbed and hydrogen bonded adsorbate molecules are presented in this paper. The shift in frequency ($\Delta\nu$) of the OH absorption band due to this hydrogen bonding has been measured over a range of temperatures for ammonia and acetone. $\Delta\nu$ decreases with increasing temperature. Values are given for the half width ($\nu_{1/2}$) of the absorption bands of the perturbed OH groups; $\nu_{1/2}$ increases with increasing temperature of adsorption. The peak optical density of the perturbed OH band increases in a linear fashion with coverage. On desorption hysteresis in these optical density values occurs, this being related to changes in the distribution of adsorbed molecules between different sites of adsorption. Optical densities have been calculated for some of the CH and NH vibrations of the adsorbed molecules. As the coverage is changed the peak optical density of these bands does not vary linearly. This is due to variation in the apparent extinction coefficient (E_a) with coverage. With ammonia the E_a values decrease with increasing coverage, but for methyl chloride and acetone an increase in E_a takes place. A possible interpretation of these variations is suggested.

Introduction

In previous work on the hydrogen bonds formed between the OH groups of porous glass and ammonia, acetone, methyl chloride and sulfur dioxide it has been shown² that these hydrogen bonds are related to the anomalous effects found in the study of adsorption expansion.³ Further quantitative spectral data from new as well as from existing results on these systems now have been obtained; in particular optical densities both of the perturbed surface OH groups and of the N-H and C-H vibrations of the adsorbed molecules have been calculated from a wide range of spectra and related to the changes in concentration of the adsorbate. As the concentration of the adsorbed molecules is increased, the peak optical density of the adsorption band due to the perturbed OH groups increases linearly and thus Lambert-Beer's law is obeyed. Hysteresis in these optical density values occurs on desorption; this is related to the fact that two sites of adsorption exist on the surface of porous glass.² Where possible the effects due to varying the temperature of adsorption were studied and it was found that the shift $\Delta\nu = 3730 - \nu_{OH}$ (cm.⁻¹) of the perturbed OH band was temperature dependent; $\Delta\nu$ decreasing with increasing temperature. In contrast, the half-width of the perturbed OH band $\nu_{1/2}$, increases with the increasing temperature. Within the experimental error, no change in $\Delta\nu$ or of $\nu_{1/2}$ was found on changing the coverage. The N-H stretching frequencies of the adsorbed ammonia and the C-H stretching frequencies of the adsorbed acetone and methyl chloride have been measured and compared with known values in the gaseous and liquid states. As the amounts of gas adsorbed were measured simultaneously with the spectra, it has been possible to measure the apparent extinction coefficients of some of these stretching frequencies. It has been found that they are dependent on the coverage.

Experimental

Materials and Apparatus.—As an adsorbent porous silica "Vycor" glass was used, the surface area of the 0.4 mm.

thickness porous glass plate was found to be 238 m.²/g. by the B.E.T. method using argon as the adsorbate, with a monolayer value v_m of 60.5 cm.³/g. Data have not been obtained with the other gases as the B.E.T. method could not be used easily at temperatures at which spectra were taken. Approximate v_m values have been calculated from cross-sectional areas of the gases obtained using liquid densities. The values in cm.³/g. are: ammonia 69, acetone 33 and methyl chloride 47. The pretreatment of the sample and purification of the adsorbates have been given previously,² together with the description of the adsorption system and cell for the spectroscopic measurements.

For recording the spectra a Perkin-Elmer model 21 spectrometer was used; as this model has no readily accessible main focus, a mirror system was used to provide one. To compensate for losses in the mirrors and cell the slits were widened slightly from those used in normal operation. With the sodium chloride prism used for the ammonia experiments at 3300 cm.⁻¹ the calculated slit width was 25 cm.⁻¹ and for the calcium fluoride prism in the other experiments it was 11 cm.⁻¹ at 3000 cm.⁻¹.

Results

The spectrum of the evacuated glass sample has been given and discussed previously.²

From the spectra of the adsorbed gases, the apparent optical densities both of the perturbed OH groups and of the adsorbed molecules themselves were calculated. The densities (d) were obtained from $d = \log (T_0/T)\nu$ where T_0 and T are apparent intensities of the incident and transmitted radiation at the frequency ν . Values of d have been calculated for every gas, for each dose of gas, at all the temperatures used. The spectra were measured at intervals about 50 cm.⁻¹ apart, but near the peaks this spacing was considerably reduced; for each spectrum at least 30 points were calculated. The points are not plotted on the curves because of the overlapping which would have occurred. The figures show only selected examples, in general at least 10 doses of gas were adsorbed in a given experiment. Even at the highest pressures used the path length (approx. 1.3 cm.) of the cell used is such that no corrections were needed for any spectral effects due to the unadsorbed gas phase molecules.

Figure 1 shows as examples the apparent optical density plots for ammonia adsorbed at 20 and 150°. The lowest coverage shown is that which produced

(1) School of Mines, Columbia University, New York.

(2) M. Folman and D. J. C. Yates, *Proc. Roy. Soc. (London)* **A246**, 32 (1958).

(3) M. Folman and D. J. C. Yates, *Trans. Faraday Soc.*, **54**, 429 (1958).

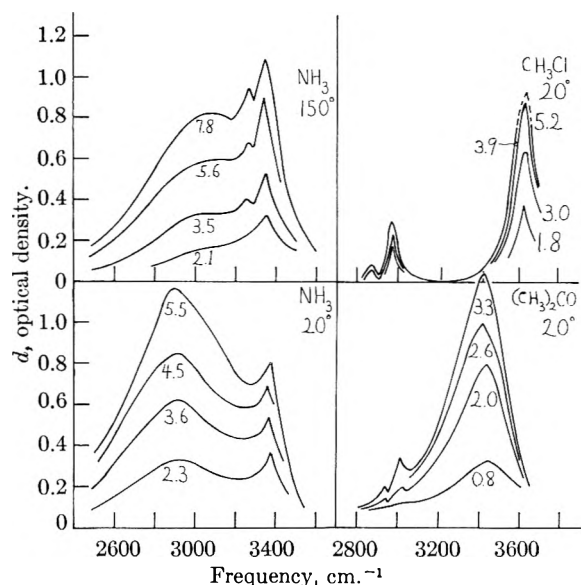


Fig. 1.—Optical density bands of the perturbed OH surface groups, and the NH and CH stretching vibrations, for ammonia adsorbed at 20 and 150° and for acetone and methyl chloride at 20°. The numbers on the curves give the volumes of gas adsorbed in cm.³/g.

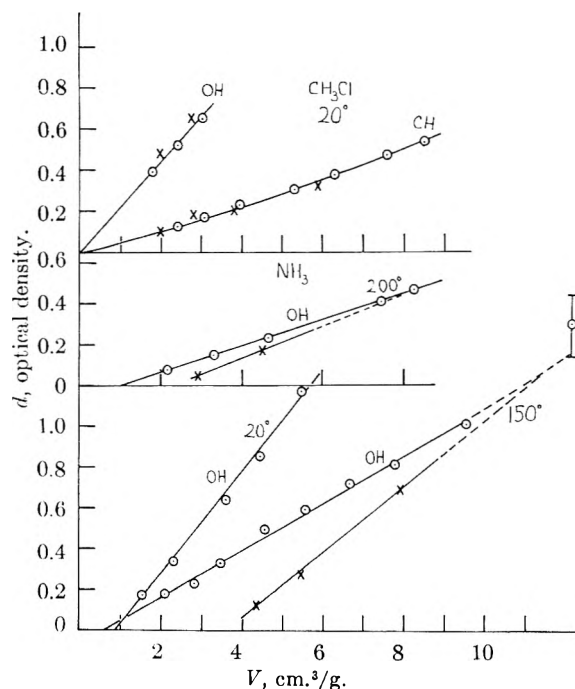


Fig. 2.—Peak optical densities of the band due to the perturbed OH groups as a function of the volume of ammonia and methyl chloride adsorbed. The dashed lines and vertical bars indicate regions of lower accuracy due to high optical densities. Points obtained by adsorption O, by desorption X.

the lowest measurable optical density curves, and the highest is the one for which the peak optical density did not exceed about 1.2. The wide bands are due to the perturbed OH groups and the narrow bands at about 3370 and 3280 cm.⁻¹ are due to the N-H stretching frequencies of the adsorbed ammonia molecules. Figure 1 also shows the optical density plots obtained with acetone and methyl chloride adsorbed at 20°. The wide band in the case of

acetone is due to the perturbed OH groups, and the weak bands near 3020 and 2930 cm.⁻¹ are due to the CH stretching frequencies of the adsorbed molecules. With methyl chloride the OH perturbed band is much weaker and is centered at 3620 cm.⁻¹. The absorption due to CH stretching frequencies at about 2970 and 2865 cm.⁻¹ is also shown. From all the data, values of the apparent peak optical densities both of the OH groups and the adsorbed molecules have been collected, both on adsorption and on desorption, and are shown in Figs. 2 and 3, as a function of volume of gas adsorbed. In the case of the N-H bands, the corrected apparent peak optical density is plotted, obtained by subtracting from the observed peak value the contribution due to the OH band. This contribution was found by assuming that the OH band was symmetrical about its peak frequency. For the OH groups for each of the molecules adsorbed the points lie on straight lines which do not, in general, intersect the abscissa at zero coverage. The slopes of the lines on desorption are different from those on adsorption; these phenomena will be discussed later. The apparent peak optical density plots for the 3370 cm.⁻¹ NH band, in contrast, (Fig. 3) are not linear but do pass through the origin; as with the OH band the desorption curve shows marked hysteresis. For methyl chloride (Fig. 2), however, the plots are very nearly linear and do pass through the origin; no hysteresis was observed. Table I gives the absorption frequencies of the adsorbed molecules themselves and comparison frequencies in the gaseous and liquid states.

TABLE I
COMPARISON OF FREQUENCIES (IN CM.⁻¹) IN THE ADSORBED,
GASEOUS AND LIQUID STATES

Molecule	Temp., °C.	Frequencies of adsorbed molecules (accuracy ± 10 cm. ⁻¹)		Frequencies of the corresponding vibration in the liquid or gas phase ^a	
		cm. ⁻¹	cm. ⁻¹	cm. ⁻¹	cm. ⁻¹
NH ₃	20	3385	3283	3443(gC)	3336.7 (gH)
	75	3365	3275
	100	3365	3275
	150	3360	3275
	200	3340	3270
(CH ₃) ₂ CO	20	3020	2935	3005(1)	2923(1)
				(accuracy ± 5 cm. ⁻¹)	
	75	3015	2930
	135	3015	2930
CH ₃ Cl	20	2970	2865	2966.2(gH)	2878.8 (gH)

^a The liquid values were measured using the CaF₂ prism, the gas values were taken from Herzberg⁴ (gH) and Cumming⁵ (gC).

The apparent extinction coefficients (E_a) of the N-H and the C-H bands have been calculated from $E_a = 1/n \log (T_0/T) \nu_{max}$ where T_0 and T have been defined previously and n is the number of adsorbed molecules per cm.² When 1 cm.³/g. of gas was adsorbed $n = 1.3 \times 10^{18}$ molecules/cm.². As it is difficult to get good optical density data, particularly at high coverages, the E_a values have been calculated from the smoothed curves shown in Figs. 2 and 3, and are given in Fig. 4. No E_a values are given for acetone as the highest appar-

(4) G. Herzberg, "Infrared and Raman Spectra," D. Van Nostrand Co. Inc., New York, N. Y., 1945.

(5) C. Cumming, *Can. J. Phys.*, **33**, 635 (1955).

ent optical density value (at 20°) obtained is about 0.21. At this amount adsorbed (12.0 cm.³/g.) for the 3020 cm.⁻¹ band $E_a = 1.4 \times 10^{-20}$ cm.²/molecule and for the 2935 cm.⁻¹ band $E_a = 0.8 \times 10^{-20}$. Both these E_a values decrease with decreasing coverage and are about 35% less at 4.4 cm.³/g. adsorbed. Liquid acetone, measured at 20° under the same spectroscopic conditions as those used for the experiments with adsorbed acetone, gave an E_a value of 2.6×10^{-20} at 3005 cm.⁻¹. The curves are thus similar in nature to those found with methyl chloride.

Discussion

The Properties of the Evacuated Adsorbent.—

A full discussion of the surface conditions of the adsorbent as obtained from the infrared spectrum is given elsewhere.² The absorption band due to the surface OH group is very strong even after 6 hours evacuation at 450°. This indicates that these OH groups are chemically bound to the surface; under such conditions of evacuation all water molecules would have been removed. This OH band has a much larger half-width than the usual absorption bands, and is also asymmetric. This indicates that it probably consists of two overlapping bands. One is probably a narrow band at about 3740 cm.⁻¹ due to isolated OH groups. The other band is much broader and probably is caused by hydrogen bonding between adjacent OH groups. This idea agrees with the work of Sidorov⁶ and McDonald⁷ who used adsorbents which had a much weaker and narrower OH band centered at 3749 cm.⁻¹.

The Absorption Bands of the Perturbed OH Groups.—It has been shown that some of the adsorbed molecules are attached to the surface OH groups giving hydrogen bonding.² The optical density curves given in Fig. 1 show the effects obtained by varying both the coverage and temperature of adsorption; it may be seen that the bands due to the perturbed OH groups are much more intense than normal absorption bands in this spectral region. This property is a general one for hydrogen bonded systems, both in the gaseous, liquid and solid phases. When the temperature is increased, at nearly the same amount of adsorbed gas, it will be seen in the case of ammonia and acetone that the intensity of the OH band is decreased. The phenomena is shown more clearly in Fig. 2 where the peak optical density of the OH bands are plotted as a function of coverage. The slope of the straight lines decreases with increasing temperature. The existence of these straight lines shows that over this region Lambert-Beer's law is obeyed. However, as these lines do not pass through the origin it follows that the first amounts of gas are not adsorbed on the OH groups (see earlier work on the length changes of porous glass due to adsorption³). It has been shown^{2,4} previously that at least two different sites of adsorption exist on this glass, one being the OH groups and the other the silica or oxygen atoms of the surface. Thus for a given temperature of adsorption the simplest interpretation of the linear optical density plots is that the

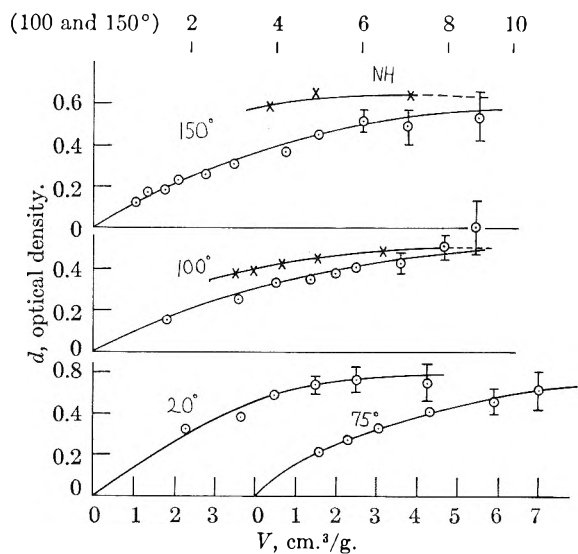


Fig. 3.—Peak optical densities of the 3370 cm.⁻¹ NH stretching vibrations of adsorbed ammonia as a function of amount adsorbed. Dashed lines and vertical bars indicate regions of lower accuracy. Adsorption points O, desorption X.

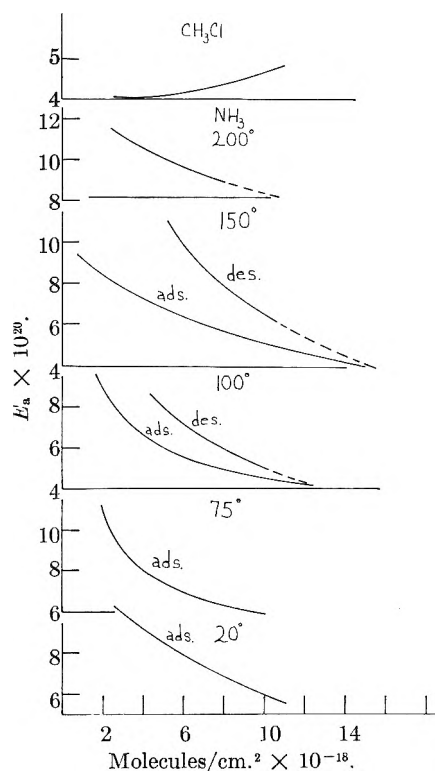


Fig. 4.—Apparent extinction coefficients for the 3370 cm.⁻¹ band of adsorbed ammonia and the 2970 cm.⁻¹ band of adsorbed methyl chloride as a function of number of adsorbed molecules per cm.² of optical path. The upper curves for ammonia at 100, 150 and 200° are obtained from desorption curves.

ratio of the number of adsorbed molecules on the two sites is constant. There may be two causes for the decrease in gradient of these lines with increasing temperature. From desorption data it is evident that the energy of adsorption on the OH sites is less than that on the other. It follows that at higher temperatures there will be relatively fewer molecules adsorbed on to the OH sites.

(6) A. N. Sidorov, *J. Phys. Chem. (Moscow)*, **30**, 995 (1956).

(7) R. S. McDonald, *J. Am. Chem. Soc.*, **79**, 850 (1957).

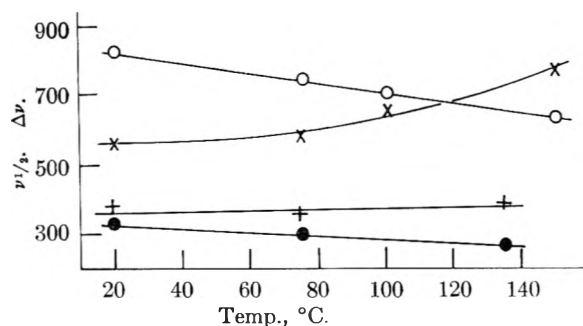


Fig. 5.—The shift ($\Delta\nu$) and half-width ($\nu_{1/2}$) in cm^{-1} of the perturbed OH groups as a function of temperature of adsorption. Shifts ($\Delta\nu$) for ammonia O, and acetone ●. Half-widths ($\nu_{1/2}$) for ammonia X and acetone +.

However, as straight lines are obtained in all cases, it is probable that a different (and constant) ratio exists for each temperature. The second cause may be that the extinction coefficients of the OH perturbed groups decrease with rise in the temperature. Recently Slowinski and Claver⁸ found a temperature dependence of intensity of infrared absorption bands in liquids. Both the integrated intensity and the peak optical density appeared to decrease with increase in temperature. For pure liquids changes of up to 30% with a 75° rise in temperature were recorded. The same phenomena also have been found by other workers⁹ in liquids where hydrogen bonding was present. Some explanations have been given¹⁰: in particular it is likely that an increase in the distance of the two atoms forming the hydrogen bond takes place.

The points for the OH perturbed bands obtained by desorbing ammonia do not lie on the lines through the corresponding adsorption points (see Fig. 2). Desorption measurements were not possible at the lower temperatures as the times of desorption were too long. The desorption points also lie on straight lines but the slopes are different. This has been interpreted in terms of the existence of two different sites of adsorption on the surface.² As the energy of adsorption on the OH sites is less, preferential desorption takes place from these sites, the peak optical density being proportional to the number of perturbed OH groups. On desorption, at a given coverage, there are fewer OH groups perturbed, consequently there is a corresponding decrease in the peak intensity. The desorption points for CH_3Cl (Fig. 3) lie on the adsorption curve. This suggests that there is little difference in the energy of adsorption of this molecule on the two sites.

The shifts in the OH bands have been related¹⁰ to the energy of the hydrogen bonds, thus the energy of the hydrogen bonds formed increases with $\Delta\nu$. As the temperature of adsorption is increased $\Delta\nu$ decreases (see Fig. 5). Few data are available in the literature on the dependence of $\Delta\nu$ on temperature^{9b} in pure liquids and solutions. This

probably is due to experimental difficulties in working with liquid systems over a wide range of temperatures. No other data are available for temperature variations in adsorbed systems. As the hydrogen bond is weak it is to be expected that $\Delta\nu$ should be temperature dependent. Calculated values^{9b} of $d/dt(\Delta\nu)$ lie within the limits 0.2 to 0.64. Experimental values^{9b} for pure liquids are between 0.3 and 0.5, and for isopropyl alcohol in ether 0.75. We found values of 1.35 for ammonia and 0.54 for acetone. Little seems to be known about the variation in half width of the perturbed OH band in hydrogen bonded systems. However, it has been reported that on increasing the temperature of pure liquids a slight increase in the half width occurs, together with the previously mentioned decrease in intensity. As even greater intensity changes have been found for other hydrogen bonded systems⁹ it is to be expected that larger changes will occur in the half width. This is the case with adsorbed ammonia (Fig. 5) but the results for acetone on the same figure are rather inconclusive.

The Spectra of the Adsorbed Molecules.— In Fig. 3 it is shown that the peak optical densities of the N-H stretching bands at 3370 cm^{-1} do not vary in a linear fashion with coverage in contrast with the OH intensities. As the coverage increases the gradient of the curve decreases, and in some cases becomes nearly zero. This effect is most marked at 20°, but is present at all temperatures other than 200°. On desorption the points lie on a curve which is above the adsorption curve. It must be remembered that the intensity of the N-H band is obtained by subtraction of the OH band on the assumption that the latter band is symmetrical. As the errors in this assumption are larger when the OH band is more intense, it is possible that the flattening is due to this effect. However, the possible errors involved decrease very markedly on desorption (due to the preferential desorption from the OH sites) and if the errors at high coverages are large it is to be expected that the desorption curve would join the adsorption curve at the point where the subtraction errors are not significant. Since the desorption curves do not show this behavior it is considered that both the flattening on adsorption and the hysteresis are real and not artifacts. It follows that the apparent extinction coefficient (E_a) changes with the amount adsorbed (Fig. 4). The ammonia molecules adsorbed on a sparsely populated surface have high coefficients; the average value of this becomes lower as more gas is adsorbed. It needs to be emphasized here that our coefficients are "apparent" ones, that is, no attempt has been made to correct for the finite slit width of the prism spectrometer.¹¹ In any case it is justifiable to use apparent E_a values for comparison purposes. Data do not seem to be available for the extinction coefficient of liquid ammonia, to enable any relevant comparisons to be made. As well as the errors involved in the use of finite slit widths,¹¹ the further difficulty exists in adsorbed systems of determining the exact number of molecules in the beam; it is obvious that this factor can be estimated with high

(8) E. J. Slowinski and G. C. Claver, *J. Opt. Sci. Am.*, **45**, 396 (1955).

(7) (a) U. Liddel and E. D. Becker, *J. Chem. Phys.*, **25**, 173 (1956); (b) J. N. Finch and E. R. Lippincott, *This Journal*, **61**, 894 (1957).

(10) (a) R. M. Badger and S. H. Bauer, *J. Chem. Phys.*, **5**, 605 (1937); (b) R. M. Badger, *ibid.*, **8**, 288 (1940).

(11) D. A. Ramsay, *J. Am. Chem. Soc.*, **74**, 72 (1952).

accuracy in liquid systems. The values used are averages over the whole sample obtained from pressure measurements, the portion of the sample in the beam may be slightly hotter as previously mentioned. If this is the case, there may be a somewhat smaller concentration of molecules in the beam than that estimated. If significant, this effect lowers the E_a values relative to the true value; the spectrometer errors¹² also act in the same direction.

Nevertheless, there is no doubt that the extinction coefficients decrease with increasing coverage of ammonia. In the most general sense it is likely that this effect is due to the heterogeneity of the surface; at low coverages sites of higher energy of adsorption are active. Coöperative effects between the adsorbed molecules themselves are not likely to be present as the largest coverage used was about 0.25. Calculations¹³ and experimental results¹⁴ show that very strong asymmetric electric fields exist at ionic surfaces. Consequently the surface field polarizes the adsorbed molecules to quite a large extent, inducing dipoles in the molecule. For any particular vibration, the intensity of absorption of radiation is proportional to $(d\mu/dq)^2$ where $d\mu/dq$ is the change in dipole moment with respect to the coördinate describing the vibration. Thus depending on the orientations of the vibration with respect to the dipole induced by the surface forces, it can be seen that $(d\mu/dq)^2$ can either increase or decrease relative to the free state of the molecule considered. On desorption, moreover, it will be seen that E_a for ammonia increases. As the results on the OH bands show, the molecules at very low coverages are adsorbed only on the sites other than the OH sites. For higher coverages, adsorption occurs also on the OH sites, and from this point on, the relative numbers of molecules adsorbed on the two different types of sites seem to remain constant (at constant temperature). The desorption experiments show from the peak optical density of the OH bands that the energy of adsorption is less on the OH sites, and thus these sites are preferentially depopulated. Consequently the distribution ratio of adsorbed

molecules changes very rapidly indeed, and as the desorption proceeds a larger percentage of the molecules are adsorbed on the most active sites—the oxygen or silicon atoms of the surface. The adsorption data at very low coverages show that the E_a value of ammonia is high in this region, thus the change in the E_a values on desorption agrees with, and supplements, the data obtained from the behavior of the OH band. The only other comparable data for adsorption systems are those reported by De Boer¹⁵ who studied the absorption of visible light by iodine on calcium fluoride. The extinction coefficient of the molecules adsorbed on the most active sites, at low coverages, was much higher (per molecule) than those at higher coverages. For methyl chloride, in contrast to ammonia, the curve of optical density of the C–H bands against coverage is slightly convex with respect to the abscissa, E_a thus increases with coverage (Fig. 4).

Consideration of the atoms by which the adsorbates become hydrogen bonded to the surface may explain the varied changes in E_a . In the case of ammonia, the molecules are most probably hydrogen bonded *via* the nitrogen atom^{2,4}; thus large changes can easily occur in all the N–H vibrations. The other molecules, in contrast, are hydrogen bonded by groups other than the C–H groups, the chlorine in methyl chloride and the CO groups in acetone. Only small changes in the E_a values of the C–H groups are thus to be expected as the C–H vibrations are not directly affected by the adsorption process; it is also possible that the change of sign of variation of E_a with coverage is related to this fact.

Acknowledgments

We are indebted to Professor J. H. Schulman, O.B.E., for his interest in the early stages of this work, and to Dr. N. Sheppard for valuable discussions and provision of spectroscopic facilities. Helpful comments on the manuscript were made by Dr. D. M. Simpson (Mrs. J. N. Agar). The design and construction of the mirror system were due to Mr. L. H. Little. The porous glass used in this work was the gift of Dr. M. E. Nordberg of the Corning Glass Works, New York. We also wish to thank the Council of the British Ceramic Research Association for personal grants.

(12) R. N. Jones and C. Sandorfy in "Chemical Applications of Spectroscopy," Interscience Publishers Inc., New York, N. Y., 1956, p. 247.

(13) J. H. De Boer "Advances in Colloid Science," **3**, 1 (1950).

(14) N. Sheppard and D. J. C. Yates, *Proc. Roy. Soc. (London)*, **A238**, 69 (1956).

(15) J. H. De Boer "Electron Emission and Adsorption Phenomena," Cambridge University Press London, 1935, p. 189.

SURFACE REACTIONS ON EVAPORATED PALLADIUM FILMS

By S. J. STEPHENS¹*Bell Telephone Laboratories, Inc., Murray Hill, New Jersey**Received June 25, 1958*

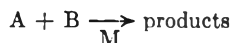
A study was made of a number of surface reactions on evaporated palladium films at 0°. The method used was to allow a monolayer of adsorbed gas to react with a second gas, added in small doses, and to follow reaction volumetrically and by analysis of the gas phase. In this way, extent of reaction, products and course of the reaction could be followed. The systems used were: Pd-O₂ + CO, Pd-CO + O₂, Pd-O₂ + H₂, Pd-H₂ + O₂, Pd-O₂ + C₂H₄, and Pd-C₂H₄ + O₂. Extensive reaction was found in each case.

Introduction

The object of this work was to study surface interactions of the type: A(ads.) + B(gas) → products. Specifically, we have determined the extent to which chemisorbed monolayers of various gases on evaporated palladium films will react with a second gas, and, where possible, the products formed. The reactions studied were Pd-O₂² + CO, Pd-CO + O₂, Pd-O₂ + H₂, Pd-H₂ + O₂, Pd-O₂ + C₂H₄, and Pd-C₂H₄ + O₂. Extensive chemical reaction between the chemisorbed gas and the gas added was found in each case. It should be recognized that the reaction



is not necessarily the same as



in which M is a catalyst.

A simple volumetric technique, combined with analysis of the gas phase, was used to follow surface reaction. The reactions Pd-O₂ + CO and Pd-CO + O₂ proved quite amenable to study by this method. For the other reactions, extent of reaction was determined in each case, but, with certain exceptions, it was not possible to recover and analyze reaction products.

This same technique has been used previously by us to study the reaction Pd-C₂H₄ + H₂,³ and also has been used by Beeck^{4a} and by Jenkins and Rideal.^{4b} Other methods which have been used to study surface interactions of the type described here include volumetric-magnetic,⁵ calorimetric,^{6,7} infrared,⁸⁻¹⁰ and field emission^{11,12} techniques.

Experimental

Materials.—Chemically pure grade palladium in the form

(1) Department of Physics-Mathematics, New Mexico Highlands University, Las Vegas, New Mexico.

(2) Chemisorbed layers are indicated by Pd-O_s, etc., without specifying whether the gas has dissociated on the surface.

(3) S. J. Stephens, *THIS JOURNAL*, **62**, 714 (1958).

(4) (a) O. Beeck, *Disc. Faraday Soc.*, **8**, 118 (1950); (b) G. I. Jenkins and E. K. Rideal, *J. Chem. Soc.*, 2490 (1955).

(5) P. W. Selwood, *J. Am. Chem. Soc.*, **79**, 4637 (1957).

(6) J. Bagg and F. C. Tompkins, *Trans. Faraday Soc.*, **51**, 1071 (1955).

(7) D. F. Klemperer and F. S. Stone, *Proc. Roy. Soc. (London)*, **A243**, 375 (1958).

(8) W. A. Pliskin and R. P. Eischens, *J. Chem. Phys.*, **24**, 482 (1956).

(9) R. P. Eischens and W. A. Pliskin, *Abstracts of Papers*, 132nd Meeting, Am. Chem. Soc., p. 7-I, Sept., 1957.

(10) A. C. Yang and C. W. Garland, *THIS JOURNAL*, **61**, 1504 (1957).

(11) J. A. Becker, "Advances in Catalysis," Vol. 7, Academic Press, Inc., New York, N. Y., 1955, pp. 135-211.

(12) R. Klein, *J. Chem. Phys.*, **21**, 1177 (1953).

of 0.2-mm. wire was obtained from Baker and Co., who reports a purity of better than 99.9%. Spectroscopic analysis done in this laboratory showed the presence of the following impurities: nickel and rhodium in amounts less than 0.001%; copper, iron and platinum, in amounts less than 0.005%; silver, boron, magnesium and silicon, in amounts less than 0.03%.

Research grade hydrogen, oxygen and carbon monoxide were obtained from Air Reduction Co., and were used as received. Mass spectrometric analysis supplied by them showed the following impurities to be present: in hydrogen, 0.013 mole % nitrogen, and possibly hydrocarbons and oxygen in quantities below the mass spectrometric threshold, estimated to be 0.005 mole %; in oxygen, possible presence of hydrogen, argon and hydrocarbons, below 0.001 mole %; chemical analysis showed carbon dioxide content to be much less than 0.05% and carbon monoxide content to be below 0.001%. Impurities in carbon monoxide were 0.06 mole % hydrogen, 0.24 mole % carbon dioxide and possibly hydrocarbons below 0.005 mole %.

Ethylene was obtained from Phillips Petroleum Co. Impurity content was reported to be 0.02% hydrocarbons and 0.03% water. The gas was purified by condensation with liquid nitrogen, then alternate melting, freezing and pumping, before distillation through a trap at -78° into the storage bulb.

Apparatus.—The apparatus consisted of: (1) a conventional pumping system including a two-stage mercury diffusion pump. The pumping system was separated from the rest of the system by a trap immersed in liquid nitrogen. (2) A dosing system, by which small known amounts of gas could be added. (3) Sample tubes, connected to the system through stopcocks. These were present only during the reactions Pd-O₂ + C₂H₄ and Pd-C₂H₄ + O₂. Samples were collected by condensing the gas phase in the sample tube with liquid nitrogen, and closing off from the system. Samples were removed later for mass spectrometric analysis. (4) A sorption system, containing the film tube, an ion gauge, a McLeod gauge and two traps. The sorption system could be isolated from the pumps by a bakeable metal valve. The film tube (10 cm. long, 2 cm. diameter) had two tungsten leads sealed in, which extended to the center of the tube. The palladium wire, coiled and bent to hairpin shape, was connected to the leads with molybdenum clips. The ion gauge was used to measure pressure before and during evaporation of a film, while the McLeod gauge was used to measure pressure (10⁻⁵ to 10⁻¹ mm.) during adsorption and reaction.

Preparation of Films.—The wire was weighed before and after an experiment to determine the weight of the film. Before being placed in the apparatus, the wire was degreased with benzene.

The entire sorption system, with the exception of the McLeod gauge, one trap and the connections to the dosing system, sample tubes and pumps, was baked at 400° for 6-8 hours before a film was prepared. The rest of the system was outgassed by flaming. During the bakeout period, the palladium wire was heated (1 amp.) and flashed (1.5 amp.) a number of times to remove dissolved gases. After this treatment, the wire released very little gas during evaporation. Wires which had been heated in hydrogen before the system was baked and outgassed as described gave the same results as were obtained with untreated wires.

The wire was protected from mercury vapor during the latter part of the bakeout and at all times subsequent to this by a trap in Dry Ice or liquid nitrogen. During evaporation of a film (1.5 amp.) the film tube was immersed in an ice-bath. After evaporation, the film was "stabilized" by

alternately cooling in liquid nitrogen and warming to 30° four times. Adsorptive capacity was found to be proportional to film weight for weights over 10 mg. The highest weight used was 60 mg. Below 10 mg., results were erratic. It is known that film structure depends on thickness of the film,¹³ and we attribute the difference in sorption characteristics between high and low weight films to this cause.

Experimental Procedure.—With the film tube immersed in an ice-bath and protected by a trap at Dry Ice or liquid nitrogen temperature, a known quantity of gas was adsorbed on the evaporated palladium film. The gas phase was then pumped out, and the second gas added in doses of known amount until no further reaction was noted. Pressure measurements were made for each dose, and the composition of the gas phase determined, if possible. For the reactions Pd-O₂ + CO and Pd-CO + O₂, this was done by separating CO₂ from CO or O₂ by immersing one of the traps in liquid nitrogen, thus condensing the CO₂. The other trap was kept at -78° at all times. The assumption was made that any non-condensable gas found was that added, and that no displacement of one gas by the other took place. Actually, no non-condensable gas was found until near the end of the reaction.

For the reactions Pd-O₂ + H₂ and Pd-H₂ + O₂, an attempt was made, after reaction was over, to measure the amount of water condensed in the trap. Very little was found. This is not proof that water was not formed, for it could either remain on the surface or be adsorbed by the glass walls of the apparatus. For the reactions Pd-O₂ + C₂H₄ and Pd-C₂H₄ + O₂, separation by condensing with liquid nitrogen showed the amount of permanent gas present. Mass spectrometric analysis of the condensable gas was made.

In some instances, after reaction was over, doses of the first adsorbed gas were added, and the reaction thus made to proceed cyclically.

Rate of Reaction.—These experiments were not designed to measure rates of adsorption or reaction, although some observations were made. Pressure measurements were made with a McLeod gauge, and the first reading was generally taken two minutes after a dose of gas was added. Any fast reaction would have been complete when this reading was made. However, in almost every case, fast reaction ($t < 2$ min.) was followed by reaction so slow that it could be followed with the McLeod gauge. In the text, we will designate as *fast* reaction or uptake that which took place in two minutes, and *slow* reaction or uptake as that which took place after the two-minute reading. This separation into *fast* and *slow* is arbitrary, and is used for convenience. It does not imply that there are actually two kinds of reaction, but merely that part of the reaction proceeds at a rate slow enough to be measured by the method used.

In the reactions Pd-O₂ + H₂ and Pd-H₂ + O₂, pressure measurements showed only the rate of disappearance of the gas added. In the other reactions, gaseous products were formed, and both rate of disappearance of the gas added and formation of reaction products were included in pressure measurements. These two processes could be separated in cases where the gas added was not condensable in liquid nitrogen by making separate runs, with and without a trap cooled in liquid nitrogen in the system.

When slow reaction was found, it generally was followed for 20 minutes before addition of another dose of gas. In some cases, reaction was allowed to continue overnight, to determine the extent of reaction over long periods of time.

Reproducibility of Data.—Adsorption data for evaporated palladium films were found to be reproducible to $\pm 10\%$ from film to film, although an occasional film showed greater deviation from the average. In the text and figures, data are given in terms of number of molecules per 100 mg. of film, assuming exact proportionality between adsorptive capacity and weight of film. This relationship was found to hold for all except low weight films. The quantity 1×10^{18} molecules/100 mg. will be designed as a *unit*, for convenience, and this term used in the text.

Results and Discussion

1. Adsorption of Gases on Palladium.¹⁴—The

(13) W. M. H. Sachtler, G. Dorgelo and W. van der Knapp, *J. chim. phys.*, **51**, 491 (1954).

(14) Detailed results for oxygen, carbon monoxide and hydrogen will be reported elsewhere.

results given here are averages of those for five or more films.

A. Oxygen.¹⁵—When doses of oxygen were added to a palladium film at 0°, some 3.0 units were taken up rapidly with low residual pressure (10^{-6} mm.), after which adsorption continued at a measurable rate which decreased exponentially with time. After 16 hours, at 10^{-2} mm. pressure (rate of adsorption is not strongly pressure dependent), the rate had become extremely slow. At this point, 3.7 units of oxygen had been adsorbed. The adsorbed oxygen was not removed by pumping for 16 hours at 0°. The heat of adsorption of oxygen on palladium has been reported to be about 75 kcal./mole,¹⁶ and to be constant during the major part of the adsorption process. We assume that oxygen is adsorbed as atoms (or ions), which are immobile.

B. Carbon Monoxide.—At 0° and 10^{-2} mm. pressure 5.7 units of CO was adsorbed. About 5% of this amount was adsorbed slowly. Part of the adsorbed CO layer could be removed by pumping. In these studies, CO was adsorbed, then the system was pumped out for a measured period of time. CO then was re-adsorbed, and pumped out for the same period of time. The amount of CO on the surface was taken to be the original amount adsorbed less that adsorbed after pumping.

C. Hydrogen.—Three kinds of sorbed hydrogen were found at 0° and 10^{-2} mm. pressure: (1) firmly held hydrogen (4.2 units), which could not be removed by pumping for two hours; (2) loosely held hydrogen (3.0 units), easily removed by pumping at 0° or by raising the temperature of the film; and (3) interstitial hydrogen (0.2 unit), sorption of which was also pressure and temperature dependent. The value for interstitial sorption was obtained by measurement of sorption of hydrogen by palladium wire. Hydrogen sorption data have been corrected for interstitial sorption, except in cases where interstitial hydrogen would be expected to take part in the reaction, such as Pd-H₂ + O₂.

D. Ethylene.²—Approximately 1.3 units of ethylene was adsorbed with low residual pressure. As more ethylene was added, self-hydrogenation took place, and ethane appeared in the gas phase. When this reaction was complete, 3.5 units of ethylene had been adsorbed, and approximately the same amount of ethane gas had been formed. The surface reaction was



The adsorbed hydrocarbon layer therefore contained only half as much hydrogen as the original ethylene.

2. Surface Reactions on Palladium. A. Pd-O₂ + CO.—Gaseous CO was found to react readily with a Pd-O₂ surface at 0°, forming CO₂ gas and adsorbed CO. Reaction continued until about 90% of the adsorbed oxygen had been removed from the surface as CO₂, after which further addi-

(15) The adsorption of oxygen and carbon monoxide by palladium at -183° has been described by Lanyon and Trapnell, *Proc. Roy. Soc. (London)*, **A227**, 387 (1955).

(16) B. M. W. Trapnell, "Advances in Catalysis," Vol. 9, Academic Press, Inc., New York, N. Y., 1957, p. 492.

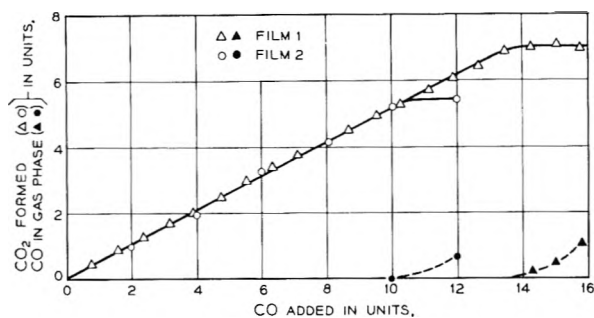


Fig. 1.—The reaction Pd-O₂ + CO at 0°; values for CO₂ formed and CO in gas phase as a function of CO added. All points represent readings at 20 min. except for last points, taken at 1000 min. to allow reaction to go to completion.

tion of CO resulted in an increase in CO pressure, but little or no adsorption or reaction. During the course of the reaction, each dose of CO was completely removed from the gas phase within 2 minutes. Most of the CO₂ produced from each dose of CO was formed rapidly, but there was some slow release of CO₂ from the surface.¹⁷ Thus, on the average, of the amount of CO₂ formed during 1000 min., 80-85% was formed in 2 min. and 90-95% in 20 min. It is probable that all CO₂ formed leaves the surface, for CO₂ is not adsorbed appreciably by palladium.¹⁸

Figure 1 shows the amounts of CO₂ and CO in the system as a function of the amount of CO added (data for films 1 and 2). The data are those taken at 20 min., except for the last dose, which was in each case allowed to react for 1000 min. Table I gives numerical data for these films, and includes two sets of data not shown in Fig. 1.

TABLE I
REACTION OF CO WITH Pd-O₂

Film	Wt., mg.	O ₂ ads. ^a	CO ads.	CO ₂ formed	Slope (Fig. 1) ^b	% O ₂ removed	CO _{ads} /O _{2ads} ^c
1	30.8	3.84	7.11	7.04	0.51	92	1.85
2	50.0	3.03	5.30	5.42	.51	89	1.75
3	53.3	3.44	run not completed		.46		
4 ¹⁹	8.9	5.23	6.97	8.99	.46	86	1.33

^a Values for amounts of gases in this and following tables are in units. ^b Slopes were determined by the method of least squares. ^c This ratio is 1.53 for clean palladium.

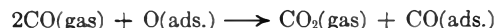
The amount of CO₂ formed (Fig. 1) was directly proportional to the amount of CO added over the entire range of reaction. There was no measurable adsorption of CO before reaction began, and no formation of CO₂ without adsorption of an approximately equivalent amount of CO (with the exception of film 4¹⁹). The average slope of the curve (CO₂ formed/CO added) for four films was 0.49. This value would be slightly higher if each

(17) Slow release of products from the surface after the reagent gas had been completely taken up was also observed in the self-hydrogenation of ethylene on palladium and in the reactions Pd-C₂H₄ + H₂ and Pd-CO + O₂.

(18) A. C. Collins and B. M. W. Trapnell, *Trans. Faraday Soc.*, **53**, 1476 (1957).

(19) Besides the high value for oxygen adsorption, attributed to a greater degree of dispersion in low weight films, this film was anomalous in other respects. The experimental points fell on a straight line of slope 0.46, but the extrapolated curve intersected the ordinate above the origin. The percentage of slow oxygen uptake was also higher than that for heavier films. Data for this film are not included in the discussion of results.

dose were allowed to react for a long period of time. We conclude that one CO molecule is adsorbed on each site²⁰ freed by removal of an adsorbed oxygen atom. The surface reaction is



This equation represents only the quantities involved, and not the mechanism of reaction.

Some 86-92% of the adsorbed oxygen was removed from the surface as CO₂ during the course of the reaction. The oxygen which did not react may be held on the surface at sites of high binding energy, or may have penetrated beneath the surface of the metal and so be inaccessible for reaction. Lanyon and Trapnell¹⁵ have suggested that the mechanism for slow oxygen uptake by metals is penetration of the metal lattice by oxygen atoms, through interchange of adsorbed oxygen with underlying metal atoms. We have found that slow oxygen uptake on palladium is 20-25% of the total oxygen uptake. The percentage of adsorbed oxygen which did not react with CO was always less than this. There would therefore seem to be no direct relationship between oxygen adsorbed slowly and non-reacting oxygen on palladium, and we prefer to regard all oxygen as being present on the surface until more definite evidence for lattice penetration is found. There is evidence of lattice penetration of certain other metals by oxygen during the slow adsorption process, and it would be interesting to see whether this "internal" oxygen can be removed by reaction with CO at low temperatures.

The amount of CO adsorbed during reaction is somewhat greater than that adsorbed by a clean palladium film under similar conditions of temperature and pressure. We base this statement on the ratio of CO adsorbed to O₂ originally adsorbed, rather than on absolute values found, since this eliminates differences in sorptive capacity of individual films. Of significance also is the fact that there is a one-to-one ratio of CO adsorbed to oxygen atoms removed by reaction. The added adsorption of CO following reaction may be due to interaction of adsorbed CO with surface oxygen, or to the circumstance that sites are formed singly during reaction, so that CO never encounters and cannot adsorb on double sites.

B. Pd-CO + O₂.—Here, surface reaction was preceded by an induction period during which no measurable CO₂ formation or O₂ adsorption took place. Once reaction had begun, however, it proceeded readily with rapid and complete uptake of O₂ (2 min.) together with formation of CO₂. Fast reaction was followed by slow release of CO₂ from the surface.

Figure 2 shows the pressure of gas in the system as a function of time and quantity of O₂ added (data for film 6). The dashed line represents the pressure of O₂ that would be found if no reaction took place. The full line and the experimental points (empty circles) represent the actual pressure measurements (CO₂ + O₂). Oxygen pressure is shown by filled circles. Except for the first dose,

(20) We will consider the number of adsorption sites to be equal to twice the number of oxygen molecules adsorbed at 0°, 10⁻² mm., after 16 hours.

for which there was an induction period (length not determined), a dose of CO was added every 20 min. For dose 1, the pressure at $t = 20$ min. was due to O_2 , while the pressure at $t = 1000$ min. was due to CO_2 only. For doses 2-8, all O_2 was removed from the gas phase within 2 min., and pressure changes were due to CO_2 formation. Beginning with dose 9, O_2 was present in the gas phase, and pressure changes were due to both CO_2 formation and O_2 adsorption. When the last point was taken, the pressure of O_2 in the system was 4.7×10^{-3} mm. and that of CO_2 5.6×10^{-2} mm. The amount of CO_2 released in the slow reaction varied with dose number, and was greatest for the first five doses.

In Fig. 3, the amounts of CO_2 and O_2 in the system are shown as functions of the amount of O_2 added (data for films 5 and 6). The values shown are those found after 20 min., except for the first and last doses, for which the time elapsed was 1000 min. Other data for these films are given in Table II, together with data for a third film, for which only a few points were taken.

TABLE II
REACTION OF O_2 WITH Pd-CO

Film	Wt., mg.	CO ads.	O_2 ads.	CO_2 formed ^a	Total O_2 re-acted	% CO re-moved	CO_{ads}/O_{2ads} ^b
5	50.3	5.48	2.95	5.09	5.50	93	1.85
6	47.2	5.94	2.66	5.50	5.41	93	2.23
7	34.8	5.38	3.48	5.37	6.15	100	1.54

^a After 1000 min. ^b This ratio is 1.53 for clean palladium.

In Fig. 3, we have drawn a separate curve through each set of points, since each film gave slightly different results. The curve is divided into two distinct portions, with a break at ~ 3.6 units of CO_2 formed. The lower portion of the curve is slightly concave to the abscissa, and has a slope changing from 1.7 to 1.5. The upper portion of the curve is a straight line with a slope of 0.7 (average for two films).

In the reaction of O_2 with a Pd-CO surface, it is necessary for the O_2 molecule to dissociate before or during reaction with adsorbed CO. We consider the induction period to be due to the inability of O_2 molecules to find sites on which dissociation can occur. Even if there were bare single sites present, the surface would be filled for O_2 adsorption if double sites were required for dissociation. These could be produced by kinetic motion in the adsorbed layer. Formation of sites suitable for O_2 dissociation would be more difficult if part of the CO layer were immobile,⁶ for this would greatly impede the movement of the less strongly bound, mobile CO. The introduction of bare sites as a result of reaction would increase mobility in the adsorbed layer. Once dissociation and reaction had begun, the presence of bare sites created by reaction would permit reaction to continue.

Over 90% of the adsorbed CO was removed by reaction. The amount of O_2 adsorbed was less than the average value for clean films, but the results are not conclusive because of variation from film to film. It is reasonable, however, that during reaction isolated single sites would be created, on which O_2 could not dissociate. Ad-

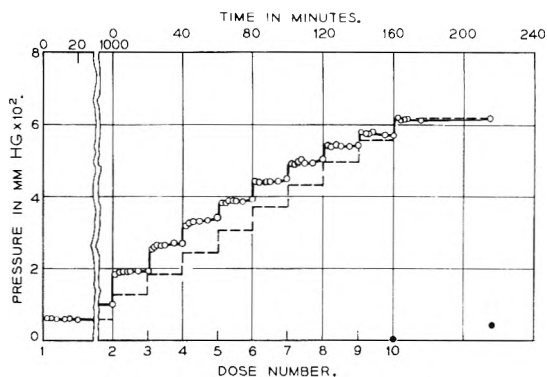


Fig. 2.—The reaction Pd-CO + O_2 at 0° ; pressure in system as a function of time and dose number. The dashed line represents the pressure of O_2 that would be found if no reaction took place, the full line the measured pressure ($CO_2 + O_2$). Oxygen pressure shown by filled points.

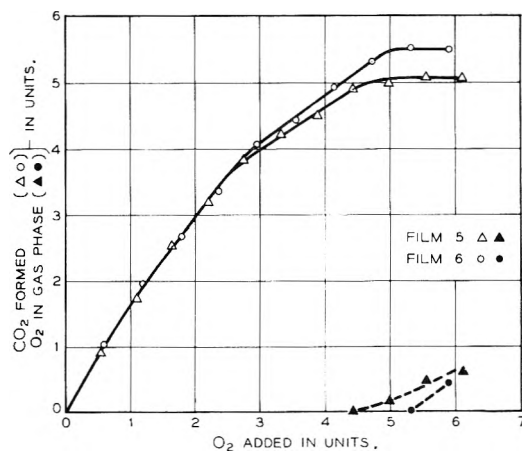
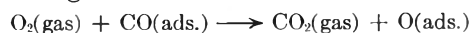


Fig. 3.—The reaction Pd-CO + O_2 at 0° ; values for CO_2 formed and O_2 in gas phase as a function of O_2 added. All points represent readings at 20 min. except for first and last points, taken at 1000 min.

sorbed oxygen, being immobile, could not migrate onto these sites, and total O_2 adsorption would be decreased.

During the first portion of the reaction of O_2 with adsorbed CO, there was considerable slow release of CO_2 from the surface after all O_2 had been removed from the gas phase (see Fig. 2). For doses 2-5, some 25% (average) of the amount of CO_2 formed in 20 min. was formed by slow desorption. If reaction were allowed to proceed for long periods of time, the amount of CO_2 formed, and so the slope of the curve (CO_2 formed/ O_2 added) in Fig. 3, would increase slightly. It is unlikely that the slope at the beginning of the curve (1.7) would be exceeded, since the first dose of O_2 was allowed to react for 1000 min. (of which part was the induction period).

The average slope for the first portion of the curve in Fig. 3 was 1.6. The reaction²¹



would give a slope of 1, and the reaction



a slope of 2. Since the experimental value for the

(21) We assume here that CO is held by one-site adsorption. If it were held by two-site adsorption, the reactions would be the same, except that bare sites would be formed in each case.

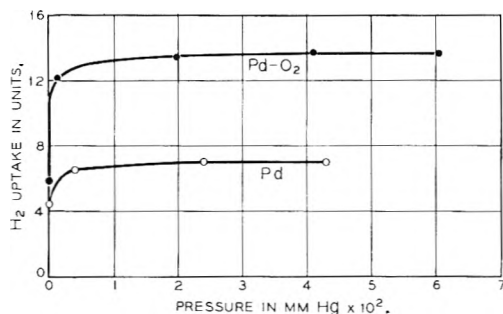
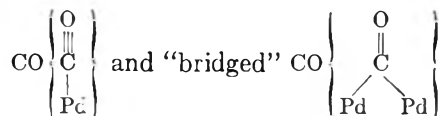


Fig. 4.—Sorption isotherms (0°) for H₂ on Pd and Pd-O₂.

slope lies between 1 and 2, both adsorbed oxygen and bare sites must appear on the surface.

The slope of the second portion of the curve is 0.7—that is, more oxygen atoms are adsorbed than CO molecules are removed by reaction. When reaction is over, virtually all CO has been removed from the surface, but less than a monolayer of O₂ has been adsorbed.

The division of the curve in Fig. 3 into two portions is interpreted as meaning that CO is adsorbed on palladium in two different forms, which react by different mechanisms, and that one of these adsorbed species reacts virtually completely before the other. There are several lines of evidence that support the idea that CO may be adsorbed in two forms on some metals: (1) Eischens, Francis and Pliskin²² have reported that there are two major bands in the infrared spectrum of CO adsorbed on palladium. These bands were attributed to the presence on the surface of two different forms of CO, "linear"



The band due to "bridged" CO appeared at lower coverage and disappeared last when CO was removed from the surface by pumping, indicating that "bridged" CO is the more strongly bound species. (2) Bagg and Tompkins⁶ found that CO was adsorbed on iron with a heat of adsorption of 32 kcal./mole up to a surface coverage equal to 0.3 of the amount adsorbed at 10⁻² mm. (32°), after which the heat of adsorption fell almost linearly with coverage. They suggested that CO exists on the surface in an immobile "bridged" form, which is adsorbed on two sites, and a mobile "linear" form, which is adsorbed on one site. The former is adsorbed first with the higher heat of adsorption. (3) The rate of adsorption of CO on nickel²³ and the sticking probability of CO on nickel²⁴ and tungsten²⁵ are high and fairly constant during the first part of the adsorption process, then fall rapidly to a much lower value. This may indicate that CO is adsorbed in two different forms, which have different heats of adsorption.

Because of uncertainty as to the actual number of adsorption sites on the surface, the fraction of

(22) R. P. Eischens, S. A. Francis and W. A. Pliskin, *THIS JOURNAL*, **60**, 194 (1956).

(23) S. Wagener, *ibid.*, **60**, 567 (1956).

(24) Z. Oda, *J. Chem. Phys.*, **25**, 592 (1956).

(25) J. Eisinger, *ibid.*, **27**, 1206 (1957).

these sites which are vacant after CO adsorption, and the amount of CO adsorbed in various forms, many assumptions must be made in interpreting the data. The following simple model is fairly successful, but is by no means the only one that can be imagined. If we assume that the 7.4 units of sites on the palladium surface are all filled with adsorbed CO, which is held by one-site ("linear" CO) and two-site ("bridged" CO) adsorption, then there will be, of the 5.7 units (average) of CO adsorbed, 4.0 units of "linear" CO and 1.7 units of "bridged" CO, the latter occupying 3.4 sites. We also make the assumption that "linear" CO reacts first, and reacts completely before "bridged" CO begins to react and, further, that there is no transition from one form to the other.

We find experimentally that approximately 3.6 units of CO₂ are formed during the first part of the reaction and about 1.7 units during the last part. There is thus fair agreement between the values predicted and found. The change in slope is taken to mean that "linear" and "bridged" CO react by different mechanisms. It is hoped that further study of this reaction will allow us to elucidate the reaction mechanism, and determine whether this model is correct.

C. Pd-O₂ + H₂.—The uptake of H₂ by a Pd-O₂ surface was found to be similar in some respects to that of H₂ by clean palladium. Hydrogen was taken up rapidly, and both strong and weak adsorption were found. However, the amount of H₂ taken up by a Pd-O₂ surface was considerably greater than that by a clean palladium surface. This is illustrated in Fig. 4, in which sorption isotherms (0°) for a palladium and a Pd-O₂ film are shown.

The amount of H₂ taken up by a Pd-O₂ film is directly related to the amount of oxygen in the monolayer. Table III gives data for the uptake of H₂ by several Pd-O₂ surfaces.

TABLE III
UPTAKE OF HYDROGEN BY Pd-O₂

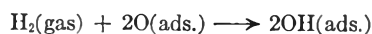
Film ^a	Wt., mg.	O ₂ ads.	H ₂ taken up	H ₂ /O ₂
9	32.9	3.08	10.40	3.4
10	36.2	3.41	13.00	3.8
11	38.9	2.81	10.02	3.6
12	20.2	3.76	13.06	3.5
13	37.8	2.81	10.02	3.6
				Av. = 3.6
Clean Pd			7.20	

^a Films 9, 11 and 13 show unusually low oxygen adsorption. Each contains a monolayer, however.

In Table III we have given values for hydrogen sorption at 10⁻² mm. Reversible sorption had already begun at this pressure.

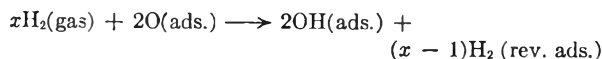
The last column of Table III gives the ratio of H₂ to O₂ uptake. This method of presenting the data eliminates variations due to differences in sorptive capacity of individual films. The H₂/O₂ ratio can be used to find the most probable surface reaction, by comparing the experimental value with values predicted for various models.

(1) If the reaction were



the amount of hydrogen taken up would be equal to the amount of oxygen on the surface, and the H_2/O_2 ratio would be 1.

(2) If reaction 1 occurred, but the film sorbed the same amount of "reversible" hydrogen as clean palladium, the reaction would be



The amount of H_2 taken up would be equal to the amount of O_2 on the surface plus the amount of reversible H_2 sorption, or $3.7 + 3.0 = 6.7$. The H_2/O_2 ratio would be 1.81.

(3) If water were the reaction product, with H_2 adsorbing in the same manner as on clean palladium, the reaction would be



If reaction of adsorbed oxygen were complete, the amount of H_2 taken up would be twice the amount of O_2 on the surface plus the amount of H_2 sorbed by clean palladium, or $2 \times 3.7 + 7.2 = 14.6$. The H_2/O_2 ratio would be 3.95.

The H_2/O_2 ratio for reaction 3 agrees most closely with the experimental result of 3.6. It was not possible to ascertain whether or not the water formed remained on the surface after reaction.

D. Pd-H₂ + O₂.—Hydrogen, whether sorbed or in the gas phase, reacted rapidly with gaseous O_2 in the presence of palladium. There was some slow uptake of O_2 , but this is believed to be due to adsorption rather than reaction, since it was of the same magnitude as that of slow adsorption of O_2 on clean palladium. Only a few data were obtained for this reaction. Table IV gives those for two films, one of which contained only firmly sorbed hydrogen (the remainder was pumped out), and the other of which was saturated with hydrogen at the pressure used, and in contact with gaseous H_2 .

TABLE IV

Film	Wt., mg.	UPTAKE OF OXYGEN BY Pd-H ₂			Conditions
		H ₂ in system	O ₂ uptake	O ₂ - 1/2H ₂	
14	31.5	(4.2)	5.59	3.49	H ₂ pumped out before O ₂ added. Value for H ₂ is av. for many films
15	13.9	10.82	8.37	2.96	Gaseous H ₂ present

The column headed (O₂ - 1/2H₂) shows the amount of O_2 taken up in excess of that required to form water, assuming that all hydrogen present undergoes this reaction. Reaction is never complete, since the value found is less than that required to form a monolayer of adsorbed oxygen (3.7 units). More O_2 was taken up than could be accounted for on the basis of -OH formation, or formation of -OH plus reaction of the remaining hydrogen to form water. The same reaction apparently occurs here as when H_2 reacts with a monolayer of adsorbed O_2 on palladium—formation of water, with sorption of the gas which is in excess.

The Pd-H₂-O₂ surface can react with more H_2 giving results comparable with those in the preceding section. Thus, film 14, after sorbing H_2 (4.2 units), then O_2 (5.59 units), will take up more H_2

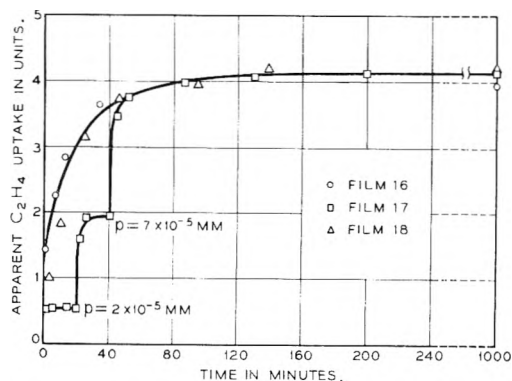


Fig. 5.—The reaction $\text{Pd-O}_2 + \text{C}_2\text{H}_4$ at 0° ; films 16 and 18, one large dose of C_2H_4 added; film 17, three doses of C_2H_4 added.

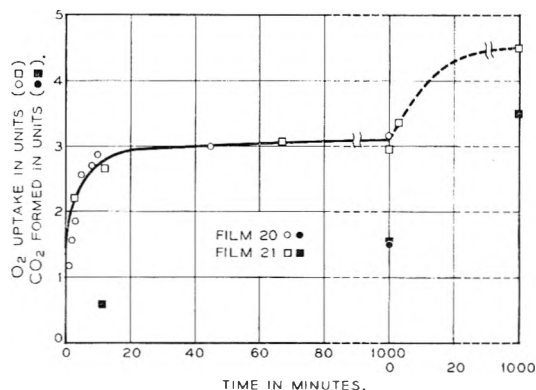


Fig. 6.—The reaction $\text{Pd-C}_2\text{H}_4 + \text{O}_2$ at 0° ; oxygen uptake and CO_2 formation as a function of time. Film 20, one dose of O_2 added; film 21, two doses.

(10.3 units), and then more O_2 (4.43 units). If all the H_2 reacted to form water, there would be 2.77 units of O_2 on the surface after the second cycle.

E. Pd-O₂ + C₂H₄.—This and the following reaction proved to be complex, with both gaseous and adsorbed products formed. The general course of the reaction was determined in each case. The results are of interest because of the prevalence of oxygen as a contaminant of metal surfaces, and the action of oxygen as a poison in catalytic reactions.

Figure 5 shows the apparent uptake of C_2H_4 by three Pd-O₂ surfaces. Other data are given in Table V. Apparent C_2H_4 uptake is that calculated from pressure measurements. This is a true measure of C_2H_4 uptake over the major part of the reaction. Of the gaseous reaction products, C_2H_6 is equivalent to C_2H_4 , being C_2H_4 which has undergone self-hydrogenation but has not adsorbed, and CO_2 appears only toward the end of the reaction, and then in small amounts only.

TABLE V

Film	Wt., mg.	REACTION OF C_2H_4 WITH Pd-O ₂		
		O ₂ ads.	Apparent C_2H_4 uptake	$\text{C}_2\text{H}_4/\text{O}_2$
16	37.6	3.26	3.94	1.21
17	37.7	3.76	4.02	1.07
18	37.5	3.08	4.22	1.37
19	44.9	2.68 ^a	3.02	1.13

^a Not a complete monolayer.

Figure 5 shows one example (film 17) of step-wise addition of C_2H_4 to a film, and two cases (films 16 and 18) in which C_2H_4 was added in one large dose. The main features of the reaction are: (1) about one unit of C_2H_4 ($\sim 1/3$ of a monolayer) is taken up rapidly (2 min.), after which uptake continues at a decreasing rate. (2) Two units or more of C_2H_4 are taken up with low residual pressure. There is no formation of gaseous reaction products during this part of the reaction, and no slow desorption from the surface. (3) A maximum uptake of C_2H_4 molecules of 1.4 times the number of O_2 molecules adsorbed was found. (4) Gaseous products were CO_2 , H_2O and C_2H_6 (mass spectrometric analysis).

The reaction products found indicate that at least two surface reactions occur—oxidation and self-hydrogenation of C_2H_4 . The self-hydrogenation reaction may take place on sites freed by the oxidation reaction. From the amounts of C_2H_6 and CO_2 found, it appears that $\sim 20\%$ of the ethylene on the surface has undergone self-hydrogenation, and 10-15% of the surface oxygen has been removed as CO_2 .

The amount of C_2H_4 taken up is much too large to be accounted for by the amount of reaction products found in the gas phase. Some C_2H_4 must be assumed to be adsorbed on the surface, either as C_2H_4 or as reaction products. Ethylene is known to be chemisorbed by some oxides.²⁶

The $Pd-O_2-C_2H_4$ surface will react with O_2 , taking up as much as 5 units with no residual pressure (only materials not condensed at -78° would be observed). Ethylene will be taken up by the $Pd-O_2-C_2H_4-O_2$ surface.

F. $Pd-C_2H_4 + O_2$.—When O_2 is added to a palladium surface covered with adsorbed ethylene residues, there is simultaneous uptake of O_2 and formation of gaseous CO_2 .

Figure 6 shows O_2 uptake as a function of time for two films, together with several values for CO_2 formation during the course of the reaction. Other data for these films are given in Table VI.

One dose of O_2 was added to film 20 and two doses to film 21. Oxygen was present in the gas

(26) B. M. W. Trapnell, "Chemisorption," Academic Press, Inc., New York, N. Y., 1955, p. 197.

TABLE VI
REACTION OF OXYGEN WITH $Pd-C_2H_4$

Film	Wt., mg.	C_2H_4 ads.	O_2 uptake	CO_2 formed	Non- condens- able gas (oxygen)
20	37.6	3.08	3.16	1.54	0.01
21	39.1	3.84	(1) 2.94 (2) 4.68	1.59 3.53	none 0.91

phase over film 21 when reaction was complete. Fairly fast uptake of O_2 by the films, with simultaneous formation of CO_2 , was observed. At the maximum O_2 uptake, about 50% of the adsorbed hydrocarbon layer had been removed as CO_2 and, presumably, H_2O . Only CO_2 , with traces of H_2O and CO , was found in the gas phase by mass spectrometric analysis.

The removal of half of the adsorbed hydrocarbon layer as CO_2 (and water) and apparent combination of at least part of the remainder with oxygen shows the high susceptibility of adsorbed hydrocarbon complexes to oxidation, and the potent action of oxygen as a poison for reactions involving chemisorbable hydrocarbons, even under mild conditions.

General Conclusions

In all the cases studied, extensive reaction between the adsorbed gas and the gas added was found. Over 85% of adsorbed O_2 and CO could be reacted off the surface under the conditions used. Other adsorbed gases (H_2 , C_2H_4) also were reactive. In only one instance ($Pd-CO + O_2$) did the adsorbed gas block the surface, and this was due apparently to the inability of O_2 to dissociate on the $Pd-CO$ surface rather than to lack of reactivity of the adsorbed CO .

In view of the present results, we may conjecture that in many cases surface contamination will not result in decrease in adsorption, but will cause an *apparent* increase in the amount of gas adsorbed, due to surface reaction. Since surface reaction may be quite rapid, contamination would not be detected by decrease in rate of gas uptake.

Acknowledgment.—The author wishes to thank E. E. Francois for making the mass spectrometric analyses.

LONG RANGE ENERGY TRANSFER AND SELF-ABSORPTION IN FLUORESCENT SOLUTIONS

BY C. W. FREEARK¹ AND R. HARDWICK

Department of Chemistry and Chemical Engineering, Stanford University, Stanford, California

Received July 10, 1958

Very long range energy transfer (~ 1 mm.) in fluorescent solutions is studied by photographic means. About 0.01% of the fluorescence is found to originate at distances of the order of 1 mm. from the source of initial excitation, depending on the system. Several systems are compared. A discussion of the relations between very long range transfer, self quenching and self absorptior is given.

Introduction

A previous paper² has discussed the long range solute-solute photon energy transfer in fluorescent

(1) Taken from a thesis submitted by C. W. F. in partial fulfillment of the requirements for the Master's Degree in Chemistry at Stanford University.

solutions and its relation to self-quenching. There it was shown that at least a third of what is usually called self-quenching in solutions of anthracene in toluene could be attributed to absorption of the

(2) E. R. Hardwick and W. G. McMillan, *J. Chem. Phys.*, **26**, 1463 (1957).

fluorescence photons by the anthracene itself (this process is hereafter referred to as self-absorption). Since some of this absorption occurs at fairly great distances from the source and since an excited molecule may re-emit as well as quench, obviously absorption re-emission in the solute is a process by which fluorescence can originate at a distance from the point of initial excitation.

There appears to be an attractive method for measuring this very small effect.³ One merely takes long time exposure pictures of a Po^{210} α -source immersed in the phosphor solution. Since the volume of initial excitation is sharply limited by the range of the α -particles, any secondary fluorescence can be detected easily as a fuzzy halo surrounding the relatively sharp, dense image of the source.

A few preliminary pictures of this type were made in the first experiment; however, these were not studied in a quantitative way. Moreover, these pictures were taken only for solutions of terphenyl in toluene, while self-quenching and self-absorption data were taken only for anthracene solutions.

Since self-absorption can lead both to long range transfer as well as to self-quenching, one could expect that some of these solutes which are highly self-quenched might also show considerable long range energy transfer. This relation would be necessary, however, only to the extent that the self-quenching is caused by self-absorption.

In an effort to make a systematic comparison of this kind, we have made further photographs, and, while these fail to reveal a relation between self-quenching and self-absorption, they do provide new information about the scintillation process. The systems chosen for study were *p*-terphenyl, anthracene, 2,5-diphenyloxazole and quaterphenyl, all in toluene solutions. Terphenyl shows little self-quenching and has been thought⁴ to have negligible self-absorption, thus we expected that terphenyl would show less long-range energy transfer than anthracene (which does self-quench and whose self-absorption is known), diphenyloxazole or quaterphenyl (both of which are very strong self-quenchers).

Experimental Method

The cell used to contain the systems studied was a thin-walled glass cylinder about 5 cm. in diameter and 1.5 cm. long. This was mounted on a movable carriage which was in turn mounted on the face of the camera used, such that the plane parallel ends of the cell were perpendicular to the axis of the camera lens. The movable carriage permitted the cell to be displaced across the field of view of the lens, thus allowing several exposures to be made on the same sheet of film. The lens was a Leitz Wetzlar, Summaron, $f = 3.5$, focal length 3.5 cm. Kodak Royal Panchromatic sheet film, used throughout the entire project, was developed in Eastman Microdol. Approximately three hundred exposures were made during the course of the research. These were developed in two large groups in order to eliminate, as far as possible, variations in the background density of the films due to variations in the developing technique.

The energy source used was approximately three milligrams of the alpha emitter, Po^{210} , plated on a platinum wire about 0.030 cm. in diameter. This needle was permanently mounted at the center of the cell, parallel to the plane of the cell faces.

(3) M. Ageo and R. Querzoli, *Nuovo Cimento*, **9**, 282 (1952).

(4) H. Kallmann and M. Furst, *Phys. Rev.*, **81**, 853 (1951).

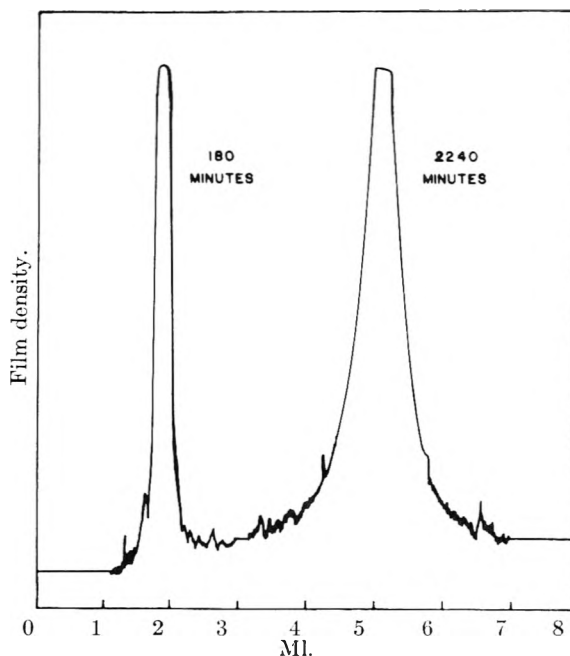


Fig. 1.—Densitometer tracings of two images produced by a source immersed in 5 g./l. terphenyl in toluene solution.

Scintillator solutions were put into the cell and film exposures were made ranging in duration from a few seconds to several days. Two standardizing exposures and one exposure for study were made on each sheet of film. One standard was common to every picture made during the entire project. This was a 5-min. exposure of a 5 g./l. solution of *p*-terphenyl in toluene which was made on each film to be used in a given sequence of pictures just prior to the actual experiment. The images resulting from these provided information necessary to correct all the picture sequences to the same scale, compensating for decay and contamination of the source. The second standard was common only to the particular solution being photographed. This exposure of 5 to 15 minutes duration was made on each film just before making the exposure for study, the time being chosen such that the degree of exposure was comparable to that of the *p*-terphenyl standard. This provided a second check on the condition of the source from beginning to end of a given sequence of pictures. Together, these standards furnished a fairly adequate set of controls from which corrections were calculated and applied to individual films.

Each exposure showed a sharp image of the needle of polonium together with varying degrees of grayness surrounding it, depending upon the time of exposure and the solution used. The images were spaced on the film about 2 cm. apart by traversing the cell carriage. The density and width of each image were measured by a microdensitometer.

Results

Figure 1 shows the densitometer tracings of two images of the source immersed in 5 g./l. terphenyl in toluene solution. The exposure times are indicated on the figure. Both of these pictures were exposed to maximum density at the center. The 2240 minute picture is actually overexposed in the center by a factor of about 200.

Since scattering within a film emulsion tends to broaden a very dense image, control experiments were made using an incandescent tungsten ribbon in place of the cell and needle. These experiments show (for our degree of image over exposure and our relative sizes of image and wire) that the image enlargement by scattering within the emulsion is not significant beyond a distance of 0.05 mm. from the wire edge (about 0.2 mm. on the

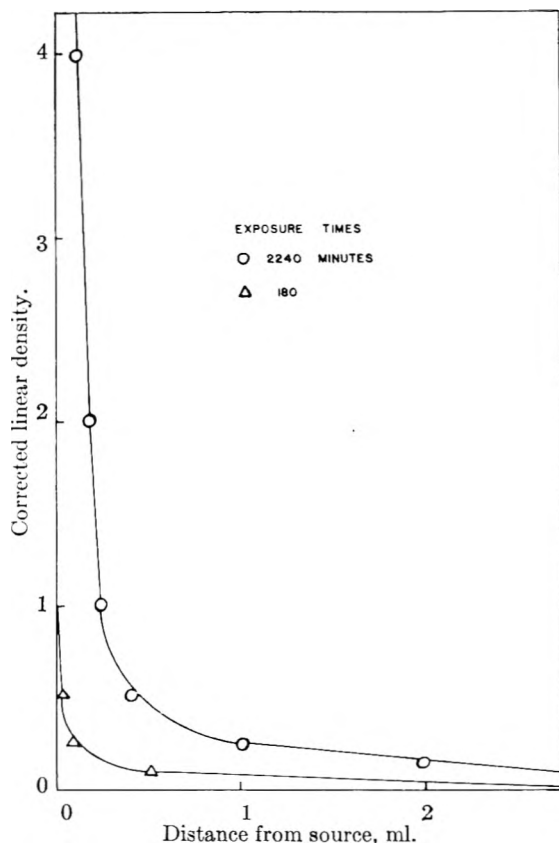


Fig. 2.—Portions of the curves of Fig. 1 as corrected for film non-linearity, source decay, etc.

image). Our results are taken for distances at least five times greater than this.

The density of a photographic image is not linear in exposure (*i.e.*, light intensity \times time) so that corrections must be made to interpret the data. We did this by first making a series of pictures at various known exposure times of the fresh alpha source in a terphenyl solution. This set then was used to prepare a calibration curve of density *vs.* exposure which was used for the determination of the exposure (in arbitrary units) of subsequent sets.

Further corrections were necessitated by the radioactive decay of the polonium, by the variable fogging of the films, and by the increasing contamination of the source by the tars, polymers, etc., created by the bombardment of the solution. This last was particularly noticeable; the source dropped to about 40% of its original strength after a few dozen photos. Corrections of this type were made by comparison of the two standard exposures on each film. The data given below are so corrected.

Figure 2 shows a portion of the curves of Fig. 1 as corrected for film non-linearity and decay and contamination of the source. Only the portions of the curve representing the fluorescence away from the needle are shown; that is, the ordinate axis represents the edge of the needle. The vertical scale of the drawing has been expanded greatly and the top portions have been removed so that only the lowermost parts of the curves are given. This may be appreciated by considering the den-

sity scale, the units of which have been arbitrarily chosen for the entire experiment to coincide with densities which would result by exposing a "linear" film with the terphenyl system for given periods. For example, a density of 4 on the arbitrary linear scale gives the density at the center of a four minute exposure with 5 g./l. of terphenyl. The greater density of 2240, which is experimentally indistinguishable from one of 180 (since both are overexposed), must be calculated from exposure time data. Fortunately, the densities in areas away from the needle itself are all measurable. These are compared with the calculated densities at the needle center.

Figure 2 demonstrates that the amount of light originating at a distance is indeed small relative to that having its origin at the surface of the needle. In the 2240 minute curve, the density at 1/2 mm. from the wire edge is only about 1/2 unit, this to be compared with the calculated 2240 units at the source.

Comparison of the times required for different phosphor solutions to produce a central image of given measurable density gives the relative (technical) fluorescence efficiencies of the solutions. Table I gives a few examples of such relative efficiencies, some of which are compared to literature values which were determined in other ways.

TABLE I
RELATIVE FLUORESCENCE EFFICIENCIES

Solute	Concn. (g./l. toluene)	Apparent fluorescence efficiency	
		This Lab.	Lit.
<i>p</i> -Terphenyl	5.0	1.0	1.0
Diphenyloxazole	1.7	5	$\sim 1.0^6$
	56	0.2	...
Anthracene	1.5	.3	0.19 ⁶
	5.0	.2	0.12 ⁶
Quaterphenyl	sat.	.3	...

The long-range energy transfer efficiency is not so easy to obtain. Relative transfer efficiencies for solutions of different phosphors are easily estimated, but finding for a single phosphor the amount of light originating at a given distance compared to the amount at the source is complicated in this experiment because the camera photographs the radiation originating throughout a cylinder of solution, the axis of which is the active wire, rather than that from a plane parallel to the film. The image at any given distance from the image of the wire edge, then, results from radiation originating at many points within the cylinder, thus at different distances from the wire. We have been unsuccessful in deriving a workable, detailed expression predicting the amount of light apparently originating at a given distance from the needle, consequently we are able to submit only a semi-quantitative comparison of the transfer efficiencies of the various solutions studied.

Table II gives the ratios of the corrected densities at the wire edge to those taken at 0.25 and 0.75 mm. away. For example, the 1/2 unit of density at 0.5-mm. distance in the 2240 minute exposure in Fig. 3 will give a transfer efficiency of 0.5/2240

(5) F. N. Hayes and co-workers, *Nucleonics*, **13**, 35 (Dec. 1955).

(6) H. Kallman and M. Furst, *Phys. Rev.*, **79**, 857 (1950).

or about 2.3×10^{-4} for that distance. Each efficiency in the table represents an average from several photos of a given system and is significant to only one figure. The values have meaning only when compared to those of another system.

TABLE II
RELATIVE LONG RANGE TRANSFER EFFICIENCIES^a

Solute	Concn. (g./l. toluene)	Transfer efficiency at 0.25 mm.	Transfer efficiency at 0.50 mm.
<i>p</i> -Terphenyl	5.0	1.0	0.5
Diphenyloxazole	1.7	1.3	0.9
	56.6	11.0	3 est.
Quaterphenyl	sat.	4.0	2 est.
Mixed system		2.0	1.5 est.
<i>p</i> -Terphenyl	2.5		
Diphenyloxazole	0.85		
Anthracene	Transfer too small for measurement		

^a Normalized to *p*-terphenyl 5 g./l. = 1.0 at 0.25 mm.

Discussion

Because of the impossibility of making direct measurements, the failure of reciprocity, and the difficulty of determining and controlling errors, the photographic method as we used it must be considered to give only qualitative results. Other methods, however, have been even less satisfactory. For instance, one attempt to detect the long range transfer by using ultraviolet excitation and variable thickness cells⁷ has been without success, presumably because of the small amount of distant fluorescence. A well-designed experiment might utilize transverse illumination of a very thin layer of solution with a carefully collimated exciting beam of ultraviolet light. One would scan the fluorescence across the beam edge with a filtered microscope, slit system and photomultiplier. In this way, the problems arising from the use of photography and from a three-dimensional solution could be largely avoided.

Although they are qualitative in nature, the present data give the first estimates of the magnitude of the long range transfer efficiency. As one might expect, this transfer efficiency differs widely from one solute to another and from one concentration to another. At 0.25 mm., for instance, 1.7 g./l. diphenyloxazole shows more transfer ability than 5 g./l. terphenyl. If the diphenyloxazole concentration is increased to 56.6 g./l., the relative amount of distant fluorescence increases by a factor of about 9.

Long range energy transfer and self-quenching do not necessarily accompany each other. (Witness the case of terphenyl, which seems to show very little self-quenching but demonstrates considerable transfer.) On the other hand, the transfer efficiency of anthracene, which is markedly self-quenched, is too small to be measurable. Diphenyloxazole demonstrates both appreciable self-quenching and long range energy transfer.

The situation with the terphenyl may be fairly easily explained. Since terphenyl shows little self-absorption but very high emission efficiency,⁸

it could easily display a high transfer efficiency and still not appear to be greatly self-quenched (*i.e.*, the transferred energy would eventually be emitted as fluorescence and the main loss would be due to the isotropic nature of the re-emission). The opposite reasoning, however, would seem to apply to anthracene. This compound is known to have appreciable self-absorption, so that relatively many distant molecules are excited; however, if the probability of re-emission were very small (*i.e.* if the internal quenching were high), then most of the molecules excited at a distance would fail to emit. Of course, it would also be true that most of the excited molecules of this system would internally quench, whatever their location, so that very little fluorescence would be seen even at the source. Anthracene seems to fit this requirement of low emission efficiency, since it has been shown to be only 15–20% as efficient a phosphor as terphenyl. An alternate explanation of self-quenching not accompanied by appreciable long range energy transfer is that the self-quenching might be accomplished by processes other than self absorption (*e.g.*, non-radiative transfer followed by internal quenching). Indeed, about 2/3 of the self-quenching of anthracene has been shown to be due to non-absorbent processes.² It is very likely that both mechanisms contribute in anthracene.

Since there is no obvious relation between self-quenching and long-distance transfer, further information regarding the roles of the various processes in the over-all scintillation event must come from the separate investigation of each process. The measurements involved are: (1) self-quenching; many data of this kind already exist but they are for various solvents under different conditions of excitation, detection, etc., (2) self-absorption; although many spectral data exist⁶ and some attention has been given to overlap between absorption and emission wave lengths, very little information is available for self-absorption *per se*, (3) quantitative long-range transfer efficiencies; no results of this kind have been published.

To complete the study, data are needed for internal quenching and relative scintillation efficiency.⁹ Fortunately, much of the existing information of this kind is readily usable.

Summary

Although its results are quantitatively unreliable this experiment furnishes the first estimate of the magnitude of very long range energy transfer. The fluorescence which originates at appreciable fractions of a millimeter from the source of excitation is very small ($\sim 0.01\%$) compared to that originating at the source. Some systems transfer more efficiently than others.

No relation has been found between self-quenching and transfer efficiency although it is quite possible that a connection exists, at least in some cases.

Acknowledgment.—We wish to thank Dr. Elton Johnston, Mr. R. L. Gunther and Mr. Robert Magill, all of the University of California,

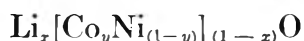
(7) S. G. Cohen and A. Weinreb, *Phys. Rev.*, **93**, 1117 (1954).

(8) G. T. Reynolds, *Nucleonics*, **10**, 46 (1952).

(9) R. C. Sangster and J. W. Irvine, *J. Chem. Phys.*, **24**, 670 (1956).

for their kindness in supplying the source and some gratefully acknowledges also the F. P. Whitaker of the fluorescent materials. One of us (C. F.) Fellowship of 1956-1957.

A STUDY OF SEVERAL SYSTEMS OF THE TYPE



BY W. D. JOHNSTON, R. C. MILLER AND R. MAZELSKY

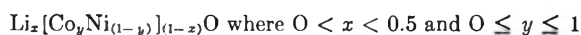
Westinghouse Research Laboratories, Pittsburgh 35, Pa.

Received July 11, 1968

Compositions in the systems $\text{Li}_x[\text{Co}_y\text{Ni}_{(1-y)}]_{(1-x)}\text{O}$, $\text{Li}_x[\text{Mn}_y\text{Co}_{(1-y)}]_{(1-x)}\text{O}$ and $\text{Li}_x[\text{Ni}_y\text{Zn}_{(1-y)}]_{(1-x)}\text{O}$ have been prepared by reaction of Li_2O_2 and the appropriate transition metal monoxide solid solution. In general the products have been shown to be single phase materials of rock salt symmetry with the lattice parameter decreasing with increasing lithium content. In the case of $\text{Li}_x[\text{Co}_y\text{Ni}_{(1-y)}]_{(1-x)}\text{O}$, the lattice parameter data have been interpreted in terms of a preferential oxidation of cobalt to the trivalent state. Where $x = 0.08$ in this system, the lattice parameter has been measured as a function of temperature. From the data the energy required for the oxidation of divalent to trivalent nickel in the crystal was shown to be 3 kcal./mole greater than that for the corresponding cobalt oxidation.

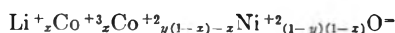
The electrical and magnetic properties of a number of lithium substituted transition metal oxides have been reported recently.¹⁻³ In particular, the electrical conductivities of the systems $\text{Li}_x\text{Mn}_{(1-x)}\text{O}$, $\text{Li}_x\text{Co}_{(1-x)}\text{O}$, $\text{Li}_x\text{Ni}_{(1-x)}\text{O}$ and $\text{Li}_x\text{Cu}_{(1-x)}\text{O}$ have been found to increase with increasing atomic number of the transition metal. This increase in electrical conductivity comes about through a corresponding decrease in the activation energy required for conduction.

In order to provide materials which might yield additional information about the conduction process, a study was made to determine whether solid solutions of some of the above systems could be prepared. An example of such a solid solution would be

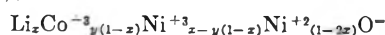


In systems of this type the substitution of a given number of lithium ions into the crystal lattice causes the oxidation of an equal number of divalent transition metal ions to the trivalent state. In the case where two different divalent transition metal ions are present in the lattice, a question arises as to whether one or both of the ions are oxidized. A consideration of the experimental evidence based on electrical conductivity studies in perovskite systems containing two different transition metal ions such as $[\text{La}_x\text{Sr}_{(1-x)}][\text{Mn}_y\text{Fe}_{(1-y)}]\text{O}_3$ suggests that only one ion will be oxidized.⁴

If we accept this assumption and further assume that Co^{+2} is more easily oxidized than Ni^{+2} , we may write



where the lithium content is smaller than the cobalt content ($x < y(1-x)$). When the lithium content is higher than the cobalt content ($x > y(1-x)$), the chemical formula becomes



(1) W. D. Johnston and R. R. Heikes, *J. Am. Chem. Soc.*, **78**, 3255 (1956).

(2) R. R. Heikes and W. D. Johnston, *J. Chem. Phys.*, **26**, 582 (1954).

(3) W. D. Johnston and R. R. Heikes and E. Sestrich, *J. Phys. Chem. Solids*, **7**, No. 1, 1 (1958).

(4) G. H. Jonker, *Physica*, **20**, 1118 (1954).

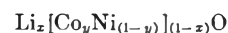
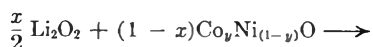
Similar formulas can be written if Ni^{+2} is expected to be preferentially ionized. On the other hand, if the ionization is assumed to be random, the formula should be written



Solid solutions of lithium substituted transition metal oxides have not been studied before, so suitable preparational methods had to be developed. In addition, it was not at all clear that such a solid solution would form, particularly if one transition metal ion was preferentially oxidized. In such a case a two phase mixture might develop, *e.g.*, $\text{Li}_x\text{Co}_{(1-x)}\text{O}$ and NiO . Other possibilities would involve the ordering of the transition metal ions, or, in the extreme case, the formation of new crystal structures. Such possibilities would, of course, preclude the electrical study planned for these materials. This paper deals with the preparation and the evaluation of the structures of a number of these systems. In addition, the distribution of charges of the transition metal ions was investigated in one of these systems.

Discussion

The method used for the preparation of compounds of this type involved, first, forming the required solid solution of the transition metal oxides, *e.g.*, $\text{Co}_y\text{Ni}_{(1-y)}\text{O}$, and then treating this material with lithium peroxide. The second step of the procedure is given in the reaction

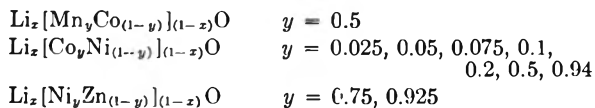


It is essentially the same procedure that has been used previously in the preparation of lithium substituted transition metal oxides and can be used essentially independently of the mixtures of transition metals involved.

The lattice parameters of the oxide systems $\text{Co}_y\text{Ni}_{(1-y)}\text{O}$, $\text{Mn}_y\text{Co}_{(1-y)}\text{O}$ and $\text{Ni}_y\text{Zn}_{(1-y)}\text{O}$ are shown graphically in Fig. 1. In all cases the graphs show that the lattice parameter is linear with composition within experimental error. The CoO-NiO and the CoO-MnO systems are single phase rock salt structures in their entirety. The NiO-

ZnO phase is a single phase material with rock salt symmetry when the Zn content is between 0 to 28 atom %. Beyond this point the hexagonal ZnO phase appears.

These lithium substituted systems have been prepared in this work



The lattice parameters obtained from the X-ray examination of many of these materials are given in Fig. 2, with the data previously obtained for $\text{Li}_x\text{Mn}_{(1-x)}\text{O}$, $\text{Li}_x\text{Co}_{(1-x)}\text{O}$ and $\text{Li}_x\text{Ni}_{(1-x)}\text{O}$ included for comparison. In all cases the curves show a smoothly decreasing lattice parameter with increasing lithium content. In many cases these curves were terminated arbitrarily at $x = 0.15$. This should not be interpreted as necessarily reflecting any chemical instability or multiple phase behavior. In none of the cases where $x < 0.15$ was there any indication of impurity phases or ordering.

The data for $\text{Li}_x[\text{Co}_y\text{Ni}_{(1-y)}]_{(1-x)}\text{O}$ may be plotted in a more informative manner. In Fig. 3 are plotted lattice parameters as a function of y at constant x (i.e., $x = 0.08$). The figure shows that the data obtained at 25° can be represented approximately as two straight lines intersecting at the cobalt content (where in this case $y = 0.087$) which is equal to the lithium content ($x = 0.08$). Similar behavior is also found for other values of x with the intersection of the straight lines always occurring roughly at the equivalence point of Co and Li. This behavior immediately suggested that cobalt was preferentially oxidized to the +3 state. In order to test this idea, the lattice parameter was calculated as a function of the cobalt composition, assuming preferential cobalt ionization and using Vegard's law. Vegard's law states that the lattice parameter is a function of the sum of the radii of the individual ions multiplied by their mole fractions. This calculation gives the results that where $y(1-x) \geq x$

$$a/2 = y[(1-x)(R_{\text{Co}^{+2}} - R_{\text{Ni}^{+2}})] + x[R_{\text{Li}^+} + R_{\text{Co}^{+3}} - R_{\text{Co}^{+2}} - R_{\text{Ni}^{+2}}] + R_{\text{Ni}^{+2}} + R_{\text{O}^-}$$

and where $y(1-x) \leq x$

$$a/2 = y[(1-x)(R_{\text{Co}^{+2}} - R_{\text{Ni}^{+2}})] + x[R_{\text{Li}^+} + R_{\text{Ni}^{+2}} - 2R_{\text{Ni}^{+2}}] + R_{\text{Ni}^{+2}} + R_{\text{O}^-}$$

These equations show that the dependence of the lattice parameter upon y at constant x consists of two straight lines intersecting at the equivalence point $x = y(1-x)$.

The lithium and oxygen radii used in this calculation are those of Wyckoff.⁵ The radii for Ni^{+2} , Ni^{+3} , Co^{+2} and Co^{+3} were obtained using the linear portions ($x > 0.05$) of the lattice parameter vs. composition curves of $\text{Li}_x\text{Ni}_{(1-x)}\text{O}$ and $\text{Li}_x\text{Co}_{(1-x)}\text{O}$.³ These radii are listed in Table I. As can be seen from the table, the radii of Ni^{+2} , Co^{+2} and Co^{+3} are in good agreement with the Wyckoff radii. The radius of Ni^{+3} is within 0.01

(5) R. W. G. Wyckoff, "Crystal Structures," Vol. I, Interscience Publishers, Inc., New York, N. Y., 1945.

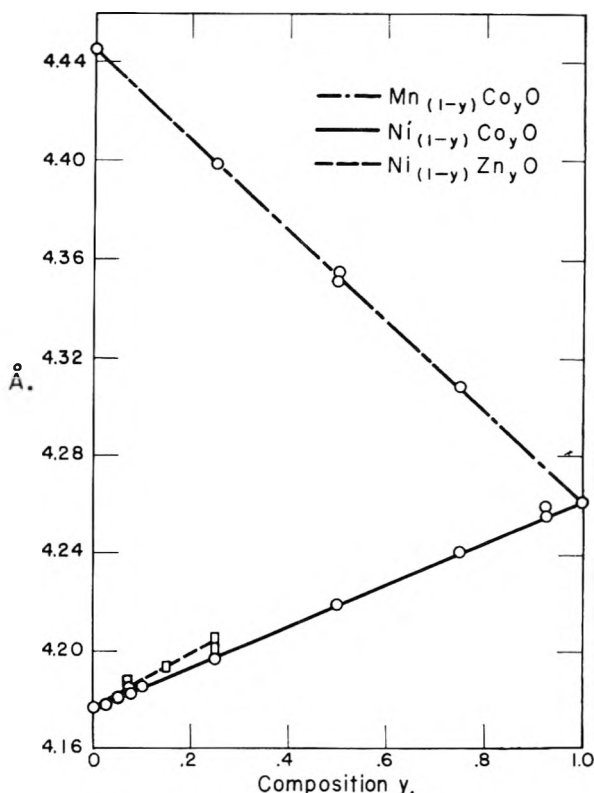


Fig. 1.—Lattice parameter vs. composition.

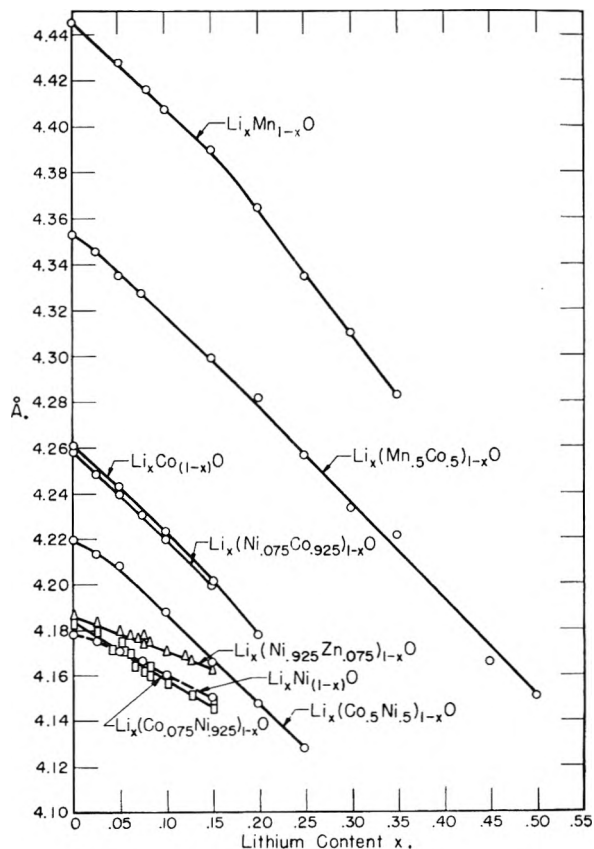


Fig. 2.—Lattice parameter vs. lithium content.

Å. of the radius calculated from LiNiO_2 .⁶ Only

(6) L. D. Dyer, B. S. Borie, Jr., and G. P. Smith, *J. Am. Chem. Soc.*, **76**, 1499 (1954).

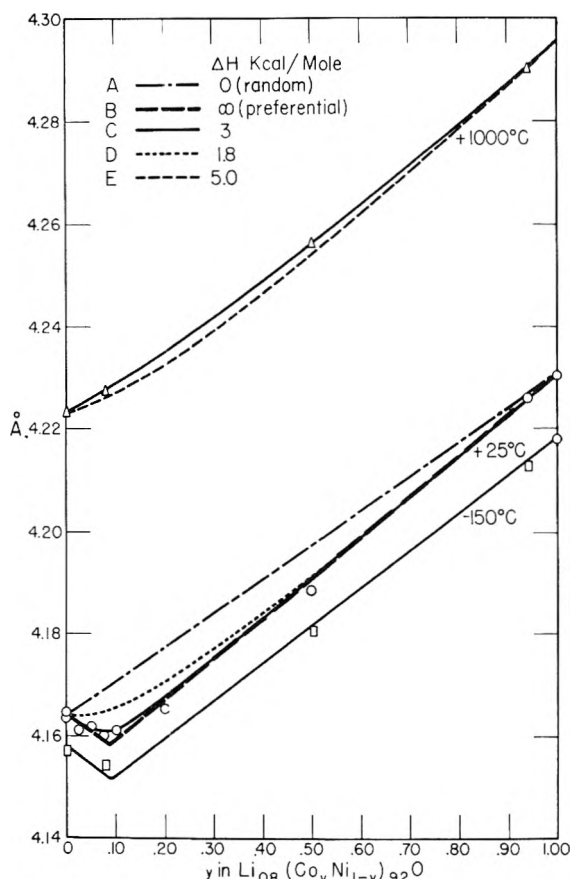
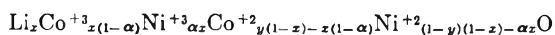


Fig. 3.—Lattice parameter as a function of composition and temperature.

the linear portions of the lattice parameter vs. composition curves were used in deriving the ionic radii, since at low lithium contents the lattice parameter is believed to be influenced strongly by lattice vacancies.⁷

By substituting the tabulated radii in the equations, a good fit with the experimental data is obtained as shown by the dashed lines indicated as B in Fig. 3. The minimum in Fig. 3 comes about through the fortunate combination of conditions $R_{Co^{+3}} > R_{Ni^{+3}}$, and $R_{Co^{+2}} < R_{Ni^{+2}}$. A minimum or a maximum should not be expected as a general occurrence when preferential ionization occurs, although a change in slope at the equivalence point might be expected.

The ionization in this case is, of course, not completely preferential. A more accurate way of writing the chemical formula for this system is



where α is defined as the fraction of the total number of plus three ions that are nickel ions. The formula for the lattice constant which results is

$$a/2 = \alpha x [R_{Ni^{+3}} - R_{Co^{+3}} + R_{Co^{+2}} - R_{Ni^{+2}}] + y(1-x) [R_{Co^{+2}} - R_{Ni^{+2}}] + x [R_{Li^{+}} + R_{Co^{+2}} - R_{Co^{+3}} - R_{Ni^{+2}}] + R_{Ni^{+2}} + R_{O^{2-}}$$

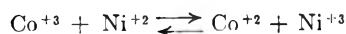
Thus, if α is known, the lattice parameter may be calculated as a function of composition. This quantity may be related to the difference in ioniza-

(7) L. D. Brownlee and E. W. I. Mitchell, *Proc. Phys. Soc.*, **65**, 710 (1952).

TABLE I
IONIC RADII FOR FIGURE 3

	Derived radii, Å.	Wyckoff radii, Å.
Li ⁺		0.7
O ²⁻		1.35
Co ⁺²	0.783	0.78
Co ⁺³	.644	.65
Ni ⁺²	.740	.74
Ni ⁺³	.680	...

tion energies of Co and Ni from a consideration of the equilibrium



The equilibrium constant for this reaction may be written

$$K = \frac{Co^{+2} \cdot Ni^{+3}}{Co^{+3} \cdot Ni^{+2}} = \frac{y(1-x) - x(1-\alpha)}{(1-y)(1-x) - x\alpha} \times \frac{\alpha}{1-\alpha}$$

where the concentration has been expressed in terms of x , y and α from the chemical formula above and the activity coefficients are assumed to be unity. Because of the limitations of the data, it will be necessary to assume that the standard free energy change ΔF^0 is independent of temperature and thus equal to the change in heat content ΔH for the reaction.

From the familiar relation $\Delta F^0 = -RT \ln K$, we obtain the desired expression for α

$$e^{-\Delta H/RT} = \frac{y(1-x) - x(1-x)}{(1-y)(1-x) - x\alpha} \times \frac{\alpha}{1-\alpha}$$

If $\Delta H = 0$, corresponding to random ionization, this equation reduces to $\alpha = 1 - y$. By introducing this expression into the equation for the lattice parameter, it can be demonstrated that the dependence of a upon y is linear from $y = 0$ to $y = 1$ and that at $y = 0$ and $y = 1$ the lattice parameters derived are that of $Li_x Ni_{(1-x)} O$ and $Li_x Co_{(1-y)} O$. This is shown as curve A in Fig. 3. If we assume that ΔH is large compared to kT and positive, corresponding to preferential ionization of the cobalt, two solutions are obtained.

$$\alpha = 0 \text{ where } y(1-x) \geq x$$

and

$$\alpha = \frac{x + xy - y}{x} \text{ where } y(1-x) \leq x$$

By substituting these last two values of α in the equation for the lattice parameter, it reduces to the two equations presented earlier for completely preferential ionization.

From the foregoing it can be seen that the distribution of plus three ions is expected to be a function of temperature. In order to determine ΔH , which may be considered the difference in ionization energies of Ni^{+2} and Co^{+2} in the solid oxides, X-ray diffraction measurements were made at -150° and 1000° . These data are shown in Fig. 3. The solid lines indicated as C are drawn assuming a value of 3 kcal./mole for ΔH . The calculation was made by evaluating the difference, Δa , between the perfectly random and partially ordered lattice parameter, as a function of y according to the equation

$$\Delta a = 2[R_{Ni^{+2}} - R_{Co^{+2}} + R_{Co^{+2}} - R_{Ni^{+2}}]_{(1-y-\alpha)x}$$

The value of α in this equation is calculated by assuming a value for ΔH . By drawing a straight line through the end-points which corresponds to a random ionization plot and using Δa obtained above, a calculated curve may be obtained which most nearly fits the experimental data. This process assumes that the term in the brackets is independent of temperature. In addition to the plots given for $\Delta H = 3$ kcal./mole, dotted lines in Fig. 3 are drawn for $\Delta H = 1.8$ and 5 kcal./mole, lines D and E, respectively. These values give noticeably poorer agreement.

Some indication of the degree of preferential ionization may be gained from the values of α at the equivalence point where the deviation from random is greatest. At this point $\alpha = 0.02$ at -150° , $\alpha = 0.37$ at 25° , and $\alpha = 0.79$ at 1000° , which may be compared with $\alpha = 0.92$ for random ionization at any temperature. The effect of this preferential ionization at low temperatures and its partial disappearance at high temperature has been noted in the electrical properties of these compounds. This work will be reported separately. For the purposes of this paper it will be sufficient to point out that in the composition range where the cobalt ions occur in two valence states, the activation energy for electrical conductivity is close to that of $\text{Li}_x\text{Co}_{(1-x)}\text{O}$ while in the composition range where the nickel ions occur in two valence states the activation energy is closer to that of $\text{Li}_x\text{Ni}_{(1-x)}\text{O}$. There is a rapid change in the activation energy term at the equivalence point as the conduction process changes from one transition ion to the other.

For the $\text{Li}_x[\text{Mn}_y\text{Co}_{(1-y)}]_{(1-x)}\text{O}$ system plots of unit cell dimensions vs. y at constant x yield almost straight lines, although only a few experimental points have been obtained. A Vegard's law calculation indicates that a noticeable change in slope should be observed for preferential ionization. Thus these data suggest that the ionization is largely random and that ΔH is less than kT or 600 cal./mole. This estimate must be considered as relatively uncertain since temperature dependence measurements have not been made.

A similar approach in the $\text{Li}_x[\text{Ni}_{(1-y)}\text{Zn}_y]_{(1-x)}\text{O}$ system has not yielded significant results. At high lithium concentrations the deviation of the observed lattice parameter from the calculated value, assuming preferential nickel oxidation and a Zn^{2+} radius derived from Fig. 1, is 3-5 times the expected experimental error. The assumption that random oxidation or preferential zinc oxidation occurs does not yield reasonable zinc radii ($\text{Zn}^{+3} > \text{Zn}^{+2}$). Roughly half of this discrepancy may be due to the loss of lithium during reaction.

Experimental

Preparations.—Samples in the $\text{Co}_y\text{Ni}_{(1-y)}\text{O}$ system were prepared by blending and then grinding with a ball mill or a mechanical mortar and pestle a mixture of reagent grade CoCO_3 and NiO . The material then was pressed into pellets and fired in air by slowly increasing the temperature to 900° and holding at this temperature for 36 hours. Where $y > 0.5$, the reactants were first treated according to the above schedule and finally heated *in vacuo* at 850° for 9 hours in order to prevent the formation of higher oxides of cobalt. The grinding, pressing, and firing frequently had to be repeated to obtain a homogeneous prod-

uct. A phase diagram for this system has been reported by Robin.⁸

The $\text{Mn}_y\text{Co}_{(1-y)}\text{O}$ system was prepared by blending, grinding and pelleting a mixture of MnCO_3 and CoCO_3 . The mixture then was heated in a continuously pumped vacuum from room temperature to 900° and maintained at this temperature for 24 hours. This system has been studied recently by Bacon, *et al.*⁹

The $\text{Ni}_y\text{Zn}_{(1-y)}\text{O}$ system was prepared by firing a mixture of NiO and ZnO in air for 36 hours at 900° . The kinetics of formation of this system have been examined by Kedesdy and Drukalsky.¹⁰

All the lithium substituted materials may be prepared by firing pressed pellets of an intimate mixture of Li_2O_2 and the proper transition metal oxide solid solution at 900° for 24 hours in a sealed Vycor container and then quenching as previously described.¹ In the case of the $\text{Li}_x[\text{Co}_y\text{Ni}_{(1-y)}]_{(1-x)}\text{O}$ and $\text{Li}_x[\text{Ni}_y\text{Zn}_{(1-y)}]_{(1-x)}\text{O}$ systems, it is possible to prepare compositions by firing the reactants in air at 1200° for 2 hours. The products fired in air are indistinguishable from those fired in sealed tubes. Firing in air would not be suitable for the $\text{Li}_x[\text{Mn}_y\text{Co}_{(1-y)}]_{(1-x)}\text{O}$ system. Typical analytical data are given in Table II.

X-Ray Studies.—Iron ($\lambda K_{\alpha 1} = 1.93597$, $\lambda K_{\alpha 2} = 1.93991$) or copper ($\lambda K_{\alpha 1} = 1.54051$, $\lambda K_{\alpha 2} = 1.54433$) radiation was used throughout. For the room temperature X-ray studies, an 11.54 cm. diameter powder camera was used. The samples were ground under mineral oil and the resulting slurries drawn into X-ray capillaries in order to prevent oxidation or hydrolysis.

The high temperature X-ray study was made by using a Unicam 19 cm. diameter high temperature X-ray camera at $1/2$ atm. oxygen pressure. A sintered fiber of the material was mounted on an Alundum pedestal because of the reactivity of the material at high temperatures. The low temperature study was made with a 19 cm. diameter camera designed and built by Dr. A. Taylor. The cooling mechanism and X-ray source have been described previously.³

In the case of $\text{Li}_{0.98}(\text{Co}_{0.5}\text{Ni}_{0.5})_{0.92}\text{O}$ and $\text{Li}_{0.98}(\text{Co}_{0.94}\text{Ni}_{0.06})_{0.92}\text{O}$ the X-ray pattern showed line splitting indicative of tetragonal symmetry which may be correlated with the onset of antiferromagnetism, such as has been previously reported for $\text{Li}_x\text{Co}_{(1-x)}\text{O}$.³ For these cases the cube root of the volume was plotted in Fig. 3, since it has been shown previously that this parameter varies uniformly with temperature regardless of changes in symmetry.³ At these temperatures $\text{Li}_{0.98}\text{Ni}_{0.92}\text{O}$ and $\text{Li}_{0.98}(\text{Co}_{0.94}\text{Ni}_{0.06})_{0.92}\text{O}$ appear to be cubic although a small deformation to rhombohedral symmetry such as has been observed in NiO cannot be completely ruled out.⁷ It might be mentioned in passing that the tetragonal deformation at -150° decreases uniformly with increasing nickel concentration. The lattice parameters of the tetragonal phases are $a = 4.222$, $c = 4.199$, $c/a = 0.9946$, and $3\sqrt{V} = 4.212 \text{ \AA}$. for $\text{Li}_{0.98}(\text{Co}_{0.925}\text{Ni}_{0.075})_{0.92}\text{O}$ and $a = 4.184$, $c = 4.175$, $c/a = 0.9978$ and $3\sqrt{V} = 4.181 \text{ \AA}$. for $\text{Li}_{0.98}(\text{Co}_{0.8}\text{Ni}_{0.2})_{0.92}\text{O}$. These data may be compared with $a = 4.228$, $c = 4.201$, $c/a = 0.9936$, and $3\sqrt{V} = 4.218 \text{ \AA}$. which are derived for $\text{Li}_{0.98}\text{Co}_{0.92}\text{O}$ from previously published data.³

In several cases attempts were made to prepare compositions where $x = 0.5$. One of these cases was the compound $\text{Li}_{0.5}(\text{Co}_{0.5}\text{Ni}_{0.5})_{0.5}\text{O}$. This might be considered a solid solution of equimolar amounts of $\text{Li}_{0.5}\text{Ni}_{0.5}\text{O}$ and $\text{Li}_{0.5}\text{Co}_{0.5}\text{O}$, both of which have been shown to have the rhombohedral CsCl_2I structure.^{3,6} A preparation of this composition gave partially a CsCl_2I structure with the lattice parameters between those of the end members. These data are given in Table III. In addition to the CsCl_2I structure, a comparable quantity of material having a rock salt structure was also observed in the X-ray pattern of the product. The lattice parameter of the phase with rock salt structure is 4.1012 \AA . The formation of two phases in this material is believed to be a result of lithium and oxygen being lost by volatilization during sintering. This loss would move the gross composition of the product into a two phase region, consisting of phases with NaCl and CsCl_2I symmetry, such

(8) J. Robin, *Compt. rend.*, **235**, 1301 (1952).

(9) G. E. Bacon, R. Street and R. H. Tredgold, *Proc. Roy. Soc. (London)*, **A217**, 252 (1953).

(10) H. Kedesdy and A. Drukalsky, *J. Am. Chem. Soc.*, **76**, 5941 (1954).

TABLE II
 ANALYTICAL DATA

Theoretical formula	Li, %		Ni, %		Co, %		Zn, %		<i>y</i> Found e.g., moles Co moles (Co + Ni)	<i>z</i> Found e.g., moles Li moles (Li + Co + Ni)
	Calcd.	Found	Calcd.	Found	Calcd.	Found	Calcd.	Found		
Li _{0.08} Ni _{0.92} O	0.79	0.66	76.5	77.6	0				0	0.067
Li _{0.08} (Co _{0.025} Ni _{0.975}) _{0.92} O	.79	.71	74.6	75.0	1.9	1.9			.023	.072
Li _{0.08} (Co _{0.05} Ni _{0.95}) _{0.92} O	.79	.76	72.7	73.5	3.8	3.8			.049	.077
Li _{0.08} (Co _{0.10} Ni _{0.90}) _{0.92} O	.79	.75	68.9	69.4	8.0	7.7			.100	.076
Li _{0.08} (Co _{0.2} Ni _{0.8}) _{0.92} O	.79	.75	61.2	61.5	15.4	15.5			.200	.076
Li _{0.08} (Co _{0.5} Ni _{0.5}) _{0.92} O	.78	.76	38.2	38.5	38.4	38.0			.496	.078
Li _{0.08} (Co _{0.94} Ni _{0.06}) _{0.92} O	.78	.78	4.6	4.8	72.0	70.8			.938	.080
Li _{0.08} Co _{0.92} O	.78	.74	0		76.6	76.5			1.00	.082
Li _{0.08} (Ni _{0.75} Zn _{0.25}) _{0.92} O	.77	.67	56.2	56.6			20.9	20.9	.751	.070
Li _{0.08} (Ni _{0.925} Zn _{0.075}) _{0.92} O	.78	.75	70.3	71.3			6.4	6.5	.925	.076
Li _{0.12} (Ni _{0.925} Zn _{0.075}) _{0.88} O	1.21	1.07	69.3	70.6			6.3	6.5	.923	.106
Li _{0.15} (Ni _{0.925} Zn _{0.075}) _{0.85} O	1.54	1.26	68.5	70.7			6.2	6.4	.925	.123
Co _{0.075} Ni _{0.925} O			72.7	73.1	5.9	6.6			.082	
Co _{0.25} Ni _{0.75} O			58.9	59.0	19.7	20.2			.253	
Co _{0.6} Ni _{0.4} O			39.2	40.1	39.4	38.4			.488	
Co _{0.75} Ni _{0.25} O			19.6	20.1	59.0	57.8			.741	
Li _{0.01} (Co _{0.5} Ni _{0.5}) _{0.99} O	.09	.08								.009
Li _{0.025} (Co _{0.5} Ni _{0.5}) _{0.975} O	.23	.20								.022
Li _{0.075} (Co _{0.5} Ni _{0.5}) _{0.925} O	.69	.68								.074
Li _{0.15} (Co _{0.5} Ni _{0.5}) _{0.85} O	1.55	1.43								.138

as was observed for Li₂Co_(1-x)O.³ Additional experiments have indicated that this region is not at all simple, and that cobalt and nickel partition to a certain extent between the two phases.

A sample of Li_{0.5}(Co_{0.5}Mn_{0.5})_{0.5}O was also made in order to determine the crystal structure. In this case the material may be considered as a solid solution of orthorhombic

Li_{0.5}Mn_{0.5}O¹ and rhombohedral Li_{0.5}Co_{0.5}O.³ Surprisingly, the product was predominantly a rock salt structure. As can be seen from Fig. 2, the lattice parameter for this phase is a reasonable one. An impurity phase having a CsCl₂I structure also was present in the amount of 10–20%. The lattice parameters on the CsCl₂I phase are larger than that of pure Li_{0.5}Co_{0.5}O, as would be expected on the basis of ionic radii. The relationship between the two phases in the Li_{0.5}(Mn_{0.5}Co_{0.5})_{0.5}O preparation is not clear at this time.

Acknowledgment.—The authors take pleasure in acknowledging the work of Mr. D. E. Sestrich, who assisted in the preparation of these materials, Mr. E. W. Beiter, who performed the chemical analyses, and Mr. R. M. Jones and Mr. N. J. Doyle, who assisted in the X-ray work. The authors also wish to express their appreciation to Dr. R. R. Heikes for many valuable discussions.

TABLE III

	<i>c</i>	<i>a</i>	<i>c/a</i>
Li _{0.5} Ni _{0.5} O	14.19	2.878	4.93
Li _{0.5} (Co _{0.5} Ni _{0.5}) _{0.5} O ^a	14.06	2.840	4.95
Li _{0.5} Co _{0.5} O	14.05	2.817	4.99
Li _{0.5} (Co _{0.5} Mn _{0.5}) _{0.5} O ^a	14.27	2.857	4.99

^a Data from two phase products. The actual chemical formulas probably do not consist of equal amounts of the transition metal ions.

LAMINAR FLOW DEGRADATION OF POLYISOBUTENE*

BY ROGER S. PORTER AND JULIAN F. JOHNSON

California Research Corporation, Richmond, California

Received July 25, 1958

A concentric cylinder viscometer has been used to measure the degradation of polyisobutene in cetane at high shear rates under laminar flow conditions. Results were obtained for 10% solutions at 25, 40, and 80° and at several rates of shear up to 3×10^6 seconds⁻¹. Temperatures and rates of shear were closely defined and measured. The degradation process is rapid and terminates at an equilibrium polymer molecular weight which is characteristic for a particular shear stress and decreases linearly with increasing shear stress. Polyisobutene degradation may be clearly attributed to the extending forces in laminar flow.

Shear rates reach at least 10^6 reciprocal seconds in conventional machine elements. Viscosities measured at known rates of shear generally have been limited experimentally to shear rates below 10^4 seconds⁻¹. Recently, however, design of an excellent rotational viscometer has been re-

ported which overcomes the major limitations of previous variable shear viscometers. Full details of this concentric cylinder viscometer and its operation have been described.¹ This instrument with minor modifications has been used in this work.

* Presented before the Petroleum Division of the 134th National Meeting of the American Chemical Society, Chicago, Sept., 1958.

(1) E. M. Barber, J. R. Muenger and F. J. Villforth, Jr., *Anal. Chem.*, **27**, 425 (1955).

Two phenomena are encountered in polymer solutions at high shear rates. A temporary and reversible decrease in viscosity occurs with increasing shear rate due to polymer deformation and orientation. A second effect is an irreversible decrease in viscosity caused by the breaking of bonds in polymer molecules which reduces the molecular weight.

Many studies of mechanical degradation of polymers in solution have been made by such means as ultrasonic irradiation, passage through gear pumps and orifices, and milling.² Most of these methods produce turbulent flow, cavitation and/or the possibility of local thermal or oxidative degradation. This work was performed to see whether the same degradation occurs at high shear rates under strictly laminar flow conditions with a negligible possibility of local effects. These are the existing conditions in many bearings. Degradation studies have been made on polyisobutene at shear rates higher than those previously reported. The degradation may be clearly attributed to the extending forces present in laminar flow.

Experimental

The concentric cylinder viscometer was constructed from working plans which graciously were made available by Mr. E. M. Barber of the Texas Company. The sensitivity of this viscometric procedure has been improved by using strain gages and bridge circuits to record electronically torques and r.p.m.'s from which viscosities and shear rates are calculated.

The test fluid is contained between the concentric cylinders. The inner cylinder is rotated, and the torque necessary to restrain rotation of the outer cylinder is measured. The cylinders are approximately one inch in diameter and have an effective length of $1\frac{7}{8}$ inches. The thickness of the test film between the cylinders, 3.05×10^{-4} inch, was calculated from data obtained on API oils of known viscosity. Both cylinders are thermostated and temperatures measured by four thermocouples placed symmetrically within the outer cylinder at $\frac{1}{16}$ -inch from the fluid film.

Shear rate is equal to the linear velocity of the film divided by the film thickness. Since the inner and outer radii of the film differ by only 3.05×10^{-4} inch, the shear rate is essentially constant across the film. Small film thicknesses minimize temperature gradients produced in the film by shearing. Temperature gradients in the test fluid increase as the square of the film thickness.¹ Calculations indicate that the maximum temperature buildup in the film in this work was about 1°. No correction has been entered for this effect.

Small film thicknesses result in streamline or laminar flow of fluid between the cylinders. Reynolds numbers did not exceed one. It is generally accepted that laminar flow exists at Reynolds numbers below 2000. Taylor has developed an equation for calculating the region of turbulent flow for rotational viscometers.³ The maximum speed of rotation used in the viscometer was much lower than the speed calculated from Taylor's equation for the onset of turbulence.

The polyisobutenes used were taken from the Vistanex series which were kindly contributed by the Enjay Company, Inc. Vistanexes 100 and 120 are solids at room temperature. The polymers used for making up cetane and carbon tetrachloride solutions were taken from the center of large blocks of Vistanexes 100 and 120 which had been freshly cut. Vistanexes MS and MH are viscous fluids at room temperature. Aliquots were dipped from clear samples of these two lower molecular weight polymers.

The cetane used was a du Pont Petroleum Chemical. The Vistanexes were dissolved in cetane by agitation and heating below 80°. One week was required for the solutions to become homogeneous. All solutions were made up to

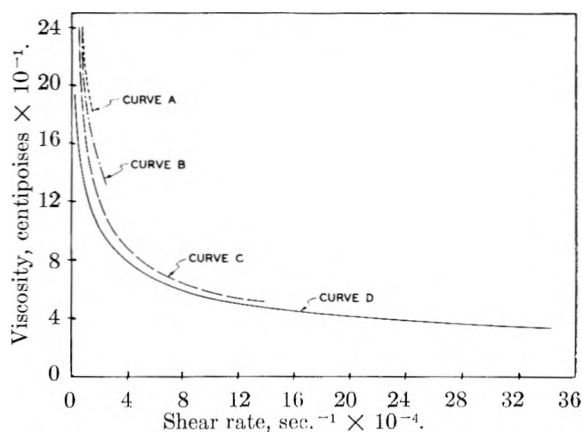


Fig. 1.—10% Vistanex 100 in cetane, 40°.

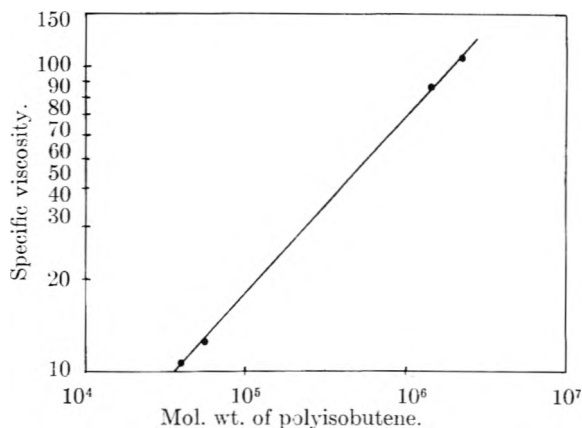


Fig. 2.—10% polyisobutene solutions in cetane at 40°.

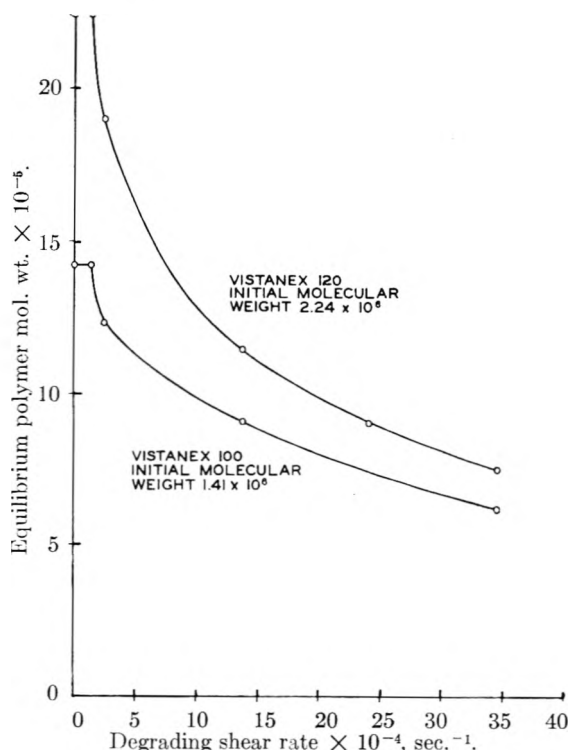


Fig. 3.—Degradation of 10% solutions of polyisobutene in cetane at 40°.

(2) H. H. G. Jellinek, "Degradation of Vinyl Polymers," Academic Press, Inc., New York, N. Y., 1955.

(3) G. I. Taylor, *Phil. Trans.*, **A223**, 289 (1922).

10.08 \pm 0.01 g. per 100 ml. of cetane at room temperature. The accuracy of viscosity measurements obtained from the high shear rate viscometer has been checked with *n*-dodec-

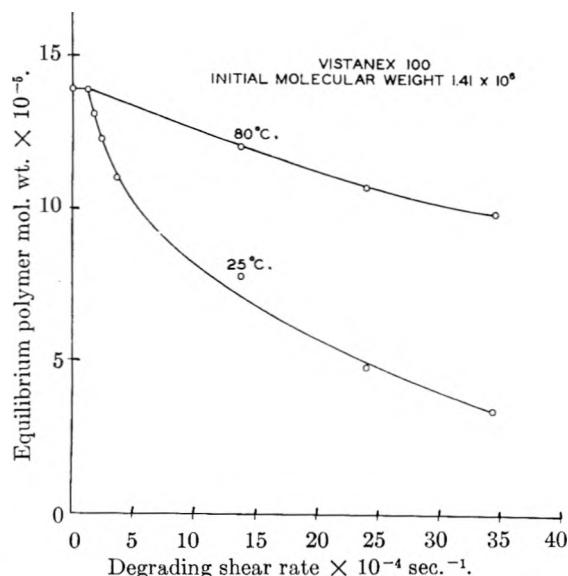


Fig. 4.—Degradation of a 10% solution of polyisobutene in cetane.

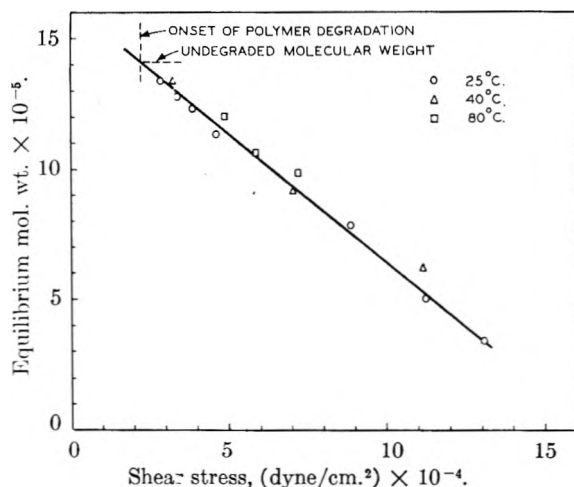


Fig. 5.—Degradation of 10% Vistanex 100 in cetane.

ane, *n*-hexadecane and *n*-eicosane as well as a number of petroleum base stocks whose viscosities are well established. Shear rate factors have been checked on a fluid measured by several workers using different methods over the range of shear rates reported in this work.¹ Results obtained here are in excellent agreement with the consistent data obtained by others. On the basis of all accuracy, calibration and precision studies, it is felt the viscosities and rates of shear are measured in the high shear rate viscometer to better than $\pm 2\%$ of the true values.

The intrinsic viscosity determinations are believed to be better than $\pm 5\%$. Determinations were made in duplicate at four levels of concentration and extrapolated to zero concentration. Capillary viscosities were not corrected to zero rate of shear.

Results

Polyisobutene solutions, 10% weight to volume, in cetane were tested in a high shear rate viscometer at 25, 40 and 80° over the shear rate range from 5000 to 34,000 seconds⁻¹. Intrinsic viscosities were used to derive viscosity average molecular weights for the four grades of polyisobutene which were tested. Table I shows the Vistanex specification and the molecular weight calculated from the Staudinger equation for polyisobutene in CCl₄ at 30°.⁴

TABLE I
VISCOSITY AVERAGE MOLECULAR WEIGHTS OF POLYISOBUTENE

Vistanex specification	Intrinsic viscosity	Mol. wt.
MS	0.39	4.00×10^4
MH	0.53	6.18×10^4
100	4.4	1.41×10^6
120	5.9	2.24×10^6

Figure 1 shows the effect of shearing on a 10% solution of Vistanex 100 at 40°. The solution was placed in the viscometer and measurements were started at low rates of shear. No permanent degradation was observed after prolonged shearing at shear rates up to 1.72×10^4 seconds⁻¹. The viscosity as a function of shear rate is shown as curve A in Fig. 1. The shear rate then was increased to 2.41×10^4 seconds⁻¹. After about 10 minutes the shear rate was lowered, and the viscosity again was measured at 10^4 seconds⁻¹. This cycle was repeated until no further change was observed. At this point equilibrium had been reached. The viscosity as a function of shear rate was determined for shear rates below 2.41×10^4 seconds⁻¹. These results are shown as curve B in Fig. 1. The shear rate then was increased to 1.38×10^5 seconds⁻¹ and curve C determined. Curve D was obtained in a similar manner. It is interesting to observe that the viscosity decreases from much greater than 5000 centipoises at low shear to 35 centipoises at 340,000 seconds⁻¹. Measurements showed the viscosity of cetane to be effectively independent of shear rate over the entire temperature and shear rate range investigated.

The molecular weight of polymers in the several degradation curves in Fig. 1 was estimated by measuring the viscosities of four undegraded polyisobutenes listed in Table I in 10% solution at 10^4 seconds⁻¹. Permanent viscosity reductions were measured at 10^4 reciprocal seconds because the effect of molecular weight on viscosity will be greatest at the lowest conveniently measured shear rate. A scale for calculating molecular weight was established by plotting the logarithm of molecular weight versus the logarithm of specific viscosity which was obtained in 10% solutions at 40° and 10^4 seconds⁻¹. Using this plot, shown in Fig. 2, a correlation has been obtained between degrading shear rate and the resultant polymer molecular weight. The specific viscosity-molecular weight correlation is empirical but serves to compare degraded molecular weights.

Figure 3 shows this change in molecular weight with rate of shear for 10% solutions of Vistanex 100 and 120. It may be seen that the molecular weights of the two polyisobutenes approach one another at high rates of shear. It is expected that at even higher rates of shear the curves would superimpose. The shapes of the curves are due at least in part to a reasonably large spread in molecular weights for the Vistanex starting materials. In a theoretical estimation of degradation in laminar flow, Frenkel concludes that the square root of

(4) T. G. Fox, Jr., and P. J. Flory, *THIS JOURNAL*, **53**, 197 (1949).

the molecular weight of degraded polymer should vary inversely with rate of shear.⁵

Degradation studies also were made on a 10% solution of Vistanex 100 at 25 and 80°. By using similar log-log plots at 25 and 80° molecular weights have been calculated for polyisobutene solutions degraded at a series of shear rates. These results are compared in Fig. 4. It is of interest to interpret this degradation in terms of applied shear stress. Figure 5 shows data for Vistanex 100 at 25, 40 and 80°. All points fit a linear correlation for decrease of polymer molecular weight with applied shear stress. The equilibrium molecular weight for degraded polymer will also depend linearly on rate of energy application.

Table II summarizes viscosities measured at 10⁴ seconds⁻¹ on solutions of Vistanex 100 and 120 at several temperatures after degradation at a series of shear rates.

TABLE II
VISCOSITY REDUCTIONS DUE TO POLYMER DEGRADATION
Viscosity, centipoise at 10⁴ sec.⁻¹
at indicated temp.

Degradation shear rate, sec. ⁻¹	Viscosity, centipoise at 10 ⁴ sec. ⁻¹ at indicated temp.			
	25°	Vistanex 100 40°	80°	Vistanex 120 40°
No degradn.	262	202	156	250
1.20 × 10 ⁴	257			
1.72 × 10 ⁴	252			
2.41 × 10 ⁴	243	183		235
3.44 × 10 ⁴	231			
1.38 × 10 ⁵	195	154	131	174
2.40 × 10 ⁵	179		121	151
3.44 × 10 ⁵	145	127	115	138

Discussion

The geometry of the viscometer ensures conditions of laminar flow.^{3,6} The results of Bestul⁷ and the low volatility of the solutions make the presence of cavitation unlikely. Polyisobutene

begins to decompose at 300°.² Therefore the thermal contribution to degradation should be negligible at 80°, the highest test temperature. Although thixotropy has been reported^{7,8} for a similar system, it was not observed in this work. On the basis of these facts, it is concluded that mechanical degradation takes place under laminar flow conditions.

Degradation is envisioned as a mechanically induced chemical reaction. The mechanically supplied activation energy is certainly in excess of the 80 kcal. bond energy of an aliphatic carbon-carbon bond. This is equivalent to 5.5×10^{-12} ergs per broken bond.⁹

The extending forces on polymer molecules increase as the square of molecular length.⁵ Under stress the longer molecules will therefore be ruptured preferentially. The viscosity average molecular weights reported for degraded polymer must represent highly skewed averages which are weighted in favor of lower molecular weight species.

Capillary shearing experiments on Vistanex 100 have been performed by Bestul and Goodman.⁸⁻¹⁰ At 40° and a nominal shear rate of 66,000 seconds⁻¹, polyisobutene was degraded from an initial molecular weight of 1.75×10^6 to 1.13×10^6 . The two sets of data plus others obtained by capillary shearing^{7,11} cannot be compared directly. In a capillary viscometer the shear rate is not uniform, and degradation is dependent on the geometry of the capillary.¹² However, qualitatively, the results by the two different methods are the same and show the same temperature and molecular weight dependence.¹³

(5) J. Frenkel, *Acta Physicochem. URSS*, **19**, No. 1, 52 (1944).

(6) C. Gazley, Jr., *Trans. Am. Soc. Mech. Engrs.*, **80**, 79 (1958).

(7) A. B. Bestul, *THIS JOURNAL*, **61**, 418 (1957).

(8) A. B. Bestul, *J. Appl. Phys.*, **25**, 1069 (1954).

(9) P. Goodman and A. B. Bestul, *J. Polymer Sci.*, **18**, 235 (1955).

(10) A. P. Bestul, *J. Chem. Phys.*, **24**, 1196 (1956).

(11) A. B. Bestul and H. V. Belcher, *J. Appl. Phys.*, **24**, 1011 (1953).

(12) H. S. White and H. V. Belcher, *J. Research Natl. Bur. Standards*, **60**, 215 (1958).

(13) P. Goodman, *J. Polymer Sci.*, **25**, 322 (1957).

METAL-POLYELECTROLYTE COMPLEXES. VI. PREPARATION AND PROPERTIES OF A NEW POLYCHELATE— POLYVINYL METHYLGLYOXIME

BY JULIAN B. ANDELMAN,¹ GUENTHER K. HOESCHELE AND HARRY P. GREGOR

Contribution from the Department of Chemistry of the Polytechnic Institute of Brooklyn, New York, N. Y.

Received July 30, 1958

Polyvinylmethylglyoxime was prepared by treating polyvinyl ethyl ketone with ethyl nitrite and converting the α keto-monoxime to the glyoxime with hydroxylamine hydrochloride. The acid dissociation constants and some metallic ion binding constants were determined in 4/1 dioxane-water solutions for the polymer and its monomeric analog, dimethylglyoxime. Using a modified Bjerrum technique, formation constants were calculated for the displacement of a proton from the chelate acid by the metallic cation. On this basis it was found that both the polymer and its monomeric analog bound $\text{UO}_2(\text{II})$ to approximately the same extent; weaker binding was observed with both $\text{Nd}(\text{III})$ and $\text{Pr}(\text{III})$ for the polymer. Binding to $\text{Ni}(\text{II})$ was weak relative to UO_2^{++} , but stronger than with the rare earth cations.

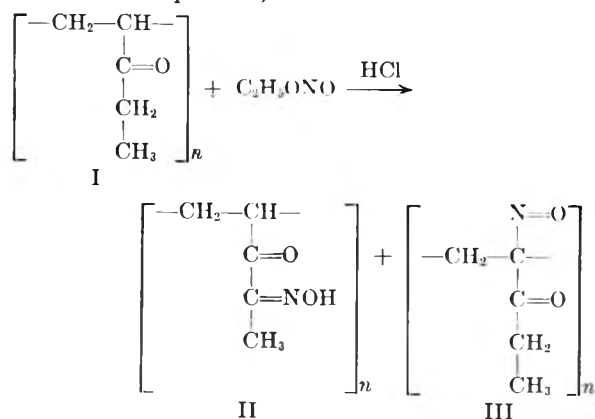
Previous papers^{2,3} in this series discussed the chelating properties of polymers. This contribution concerns itself with the synthesis and properties of a new polychelate, polyvinylmethylglyoxime (PMG), the polymeric analog of dimethylglyoxime.

Experimental

Preparation of Polymer.—The polymer was prepared by treating polyvinyl ethyl ketone with ethyl nitrite so as to add an α -oxime group to the carbonyl, followed by the addition of hydroxylamine hydrochloride to convert the carbonyl to an oxime. First, polyvinyl ethyl ketone was obtained by free radical polymerization of vinyl ethyl ketone at 90° using 0.5% benzoyl peroxide as a catalyst. Ethyl nitrite was prepared by slowly adding a mixture of an aqueous ethanol solution (8.5% by volume; 125 ml.) and 22 g. of concentrated sulfuric acid to 32 g. of sodium nitrite dissolved in 125 ml. of 8.5% ethanol in water. The gaseous ethyl nitrite was passed for a period of one hour into a solution of 35 g. of polyvinyl ethyl ketone in 120 ml. of ethanol containing 2% (by volume) concentrated hydrochloric acid.

The reaction temperature was maintained at $40\text{--}50^\circ$. The resulting reaction mixture was agitated for an additional hour, and then added slowly with constant stirring to 700 ml. of water. After suction filtering and drying the resulting precipitate, a yellow-brown powder was obtained.

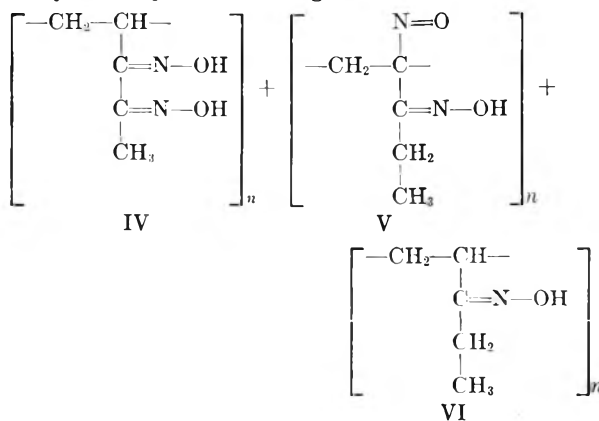
As a chemical analysis indicated that only half of the theoretical nitrogen content was introduced, the nitrosation procedure was repeated and the polymer then was found to contain 9.11% nitrogen. A calculation indicated that 67.4% of the monomeric units were converted to two probable nitrosation products, II and III



This reaction is analogous to the nitrosation of ethyl isopropyl ketone reported by Aston, *et al.*⁴ They found that nitrosation occurred in both positions α to the carbonyl, the relative amounts of the two products depending on the reaction conditions.

A mixture of 5 g. of the composite polymer (I, II and III), 5 g. of hydroxylamine hydrochloride and 10.8 g. of anhydrous sodium acetate was refluxed for 5 hours in 100 ml. of absolute ethanol. In the course of the reaction the deep red solution became yellow and precipitation occurred. The cooled reaction mixture was poured into water with stirring and then centrifuged. The brown precipitate (forms IV, V and VI) was washed with water and dried under vacuum. The 5 g. yield contained 14.99% nitrogen. A calculation indicates that at this stage of the reaction, oxime formation took place with a yield of 84.7% of the theoretically possible conversion. This polymeric product was soluble in dioxane, dioxane-water mixtures containing less than 50% water by volume, alcohol, dimethylformamide, pyridine, acetone and tetrahydrofuran. It was slightly soluble in ethyl acetate and insoluble in ether, carbon disulfide, carbon tetrachloride, chloroform and water.

Forms I, II and III all could have reacted with the hydroxylamine hydrochloride to give



all of which may exist on the same polymer chain along with unreacted forms I, II and III. The combination of the small conversion (67.4%) of the ethyl nitrite reaction and the larger conversion (84.7%) of the hydroxylamine reaction suggests that forms IV, V and VI will predominate over I, II and III.

The synthesis of polyvinylmethylglyoxime by the polymerization from vinylmethylglyoxime was not attempted because Harries and Gley⁵ showed that an oxime with an α -vinyl group (vinylmethylglyoxime) is unstable.

Titration.—Polyvinylmethylglyoxime is insoluble in dioxane-water solutions containing less than 50% dioxane by volume. Further, the addition of a metallic cation which

(1) A portion of this work is abstracted from the Dissertation of Julian B. Andelman to be submitted in partial fulfillment of the requirements for the degree of Doctor of Philosophy in Chemistry, Polytechnic Institute of Brooklyn.

(2) H. P. Gregor, with L. B. Luttinger and E. M. Loebel, *THIS JOURNAL*, **59**, 34, 366, 559, 990 (1955).

(3) G. K. Hoeschele, J. B. Andelman and H. P. Gregor, *ibid.*, **62**, 1239 (1958).

(4) J. G. Aston, D. F. Menard and M. G. Mayberry, *J. Am. Chem. Soc.*, **54**, 1530 (1932); J. G. Aston and M. G. Mayberry, *ibid.*, **57**, 1888 (1935).

(5) C. Harries and R. Gley, *Ber.*, **31**, 1808 (1898).

formed a metal chelate usually resulted in precipitation in all mixtures of this solvent pair. Gregor, Luttinger and Loebel² showed that binding phenomena are essentially the same when the polymer precipitates as for soluble polychelates. However, the precipitate formed on mixing PMG and Ni(II) in aqueous solution was such that pH equilibrium was not attained for approximately 30 days, precluding the use of water as a solvent for practical titrations. At high dioxane-water ratios the nature of the precipitate was such that constant pH readings were attained within 48 hours. As in the previous study,³ all titrations were performed at room temperature with 4/1 (v.v.) dioxane-water as the solvent and 0.1 M sodium nitrate as the "swamping" electrolyte.

The purification of dioxane as well as the "step-wise" titration technique of equilibrating the solutions between increments of base have been described.³ This titration technique was required for both PMG and its monomeric analog dimethylglyoxime (DMG), as they each form a precipitate with metal ions that can be chelated. No data were used above the pH of precipitation of the metal hydroxides.

In order to determine the base equivalent weight of the polymer, a conductimetric titration was performed. A fiber tip saturated calomel electrode and a Beckman 1190-80 glass electrode were used with a Beckman model G pH meter to determine hydrogen ion activity.

Theoretical and Results

Titration Curves.—The titration curves of polyvinylmethylglyoxime in the presence and absence of metal ions cannot be interpreted in terms of the reactions of a single monomeric species on the polymer chain. Forms II, III, IV and V all have acidic and chelating properties to varying degrees. Form IV, the analog of dimethylglyoxime, would be expected to bind metal ions and act as a weak acid. Forms II and possibly III in their enol states are analogous to the α -hydroxy-nitroso grouping in the nitroso-naphthols whose acid dissociation constants have been reported (pK_a 11 to 12), as have been their chelation properties.⁶

The lack of a defined end-point in either the potentiometric or conductimetric titrations of PMG in Fig. 1 precludes the assignment of a definite base mole equivalent weight. Arbitrarily, this equivalent weight has been based on the complete conversion of polyvinyl ethyl ketone to form IV which would act as a monobasic acid with a base equivalent weight of 128.1. The effect of this choice upon the calculation of the chelation constants will be discussed below. Accordingly, the parameter α in the titration curves was defined as the number of equivalents of added base per total number of base equivalents of chelating acid. Figure 1 shows the potentiometric titrations of PMG and dimethylglyoxime and the conductimetric titrations of the former. Figures 2 and 3 represent the titrations of these two chelating agents with typical concentrations of metal salts.

Interpretation of pH Meter Readings.—As was shown previously,³ pH_a , the negative logarithm of the hydrogen ion activity, is related to pH_M , the reading of the pH meter with a saturated calomel reference electrode, by $pH_a - pH_M = 1.65$. One can calculate the hydrogen ion activity and concentration in 4/1 dioxane-water by a pH meter measurement and known values of mean activity coefficients.

Calculation of Chelation Constants.—The modi-

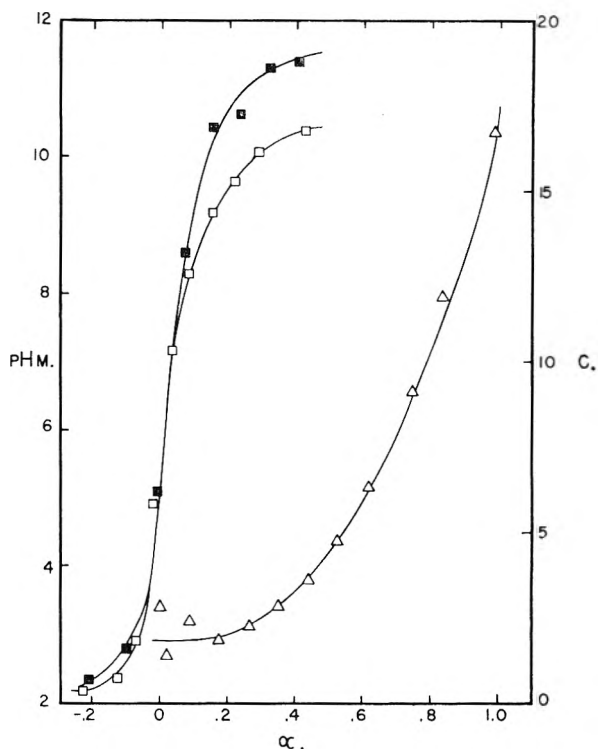


Fig. 1.—Titrations of 0.01 M solutions of chelate acids with sodium hydroxide in 4/1 dioxane-water mixtures 0.1 M in sodium nitrate (except for conductimetric titration): potentiometrically for polyvinylmethylglyoxime (□) and dimethylglyoxime (■); conductimetrically for polyvinylmethylglyoxime (Δ).

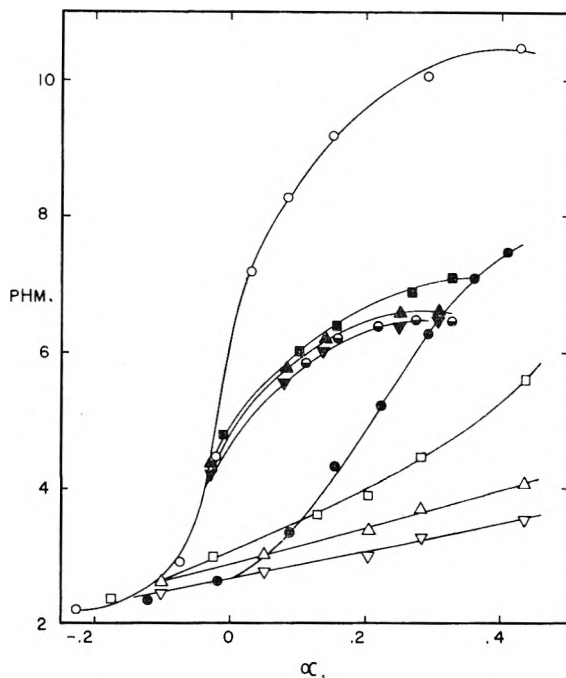


Fig. 2.—Titrations of 0.01 M solutions of polyvinylmethylglyoxime with sodium hydroxide in the absence of metal ions (○); with 0.0023 M (□), 0.0057 M (Δ) and 0.011 M (▽) uranyl nitrate; with 0.0013 M (■), 0.0026 M (▲) and 0.0040 M (▼) neodymium(III) nitrate; with 0.0039 M (●) praseodymium(III) nitrate; and with 0.0057 M (●) nickel(II) sulfate. All solutions were 4/1 dioxane-water with 0.1 M sodium nitrate.

(6) C. M. Callahan, W. C. Fernelius and B. P. Block, *Anal. Chim. Acta*, **16**, 101 (1957).

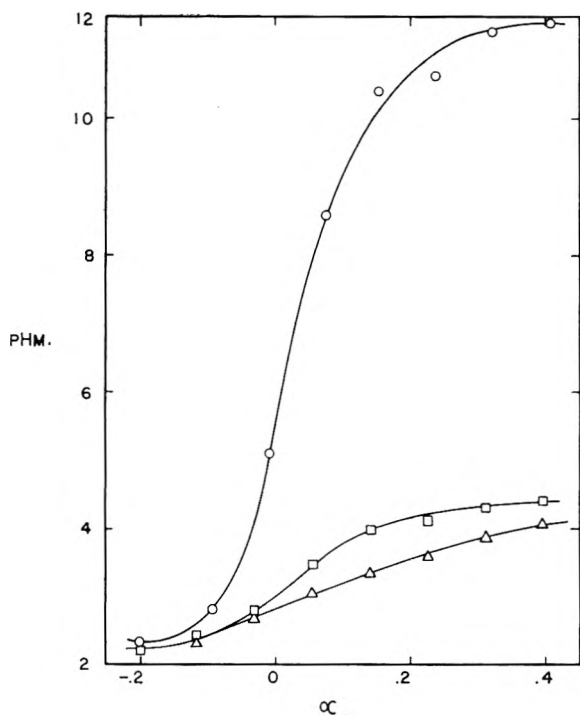


Fig. 3.—Titrations of 0.01 *M* dimethylglyoxime with sodium hydroxide in the absence of metal ions (O) and with 0.0023 *M* (□) and 0.0057 *M* (Δ) uranyl nitrate, all in 4/1 dioxane-water with 0.1 *M* sodium nitrate.

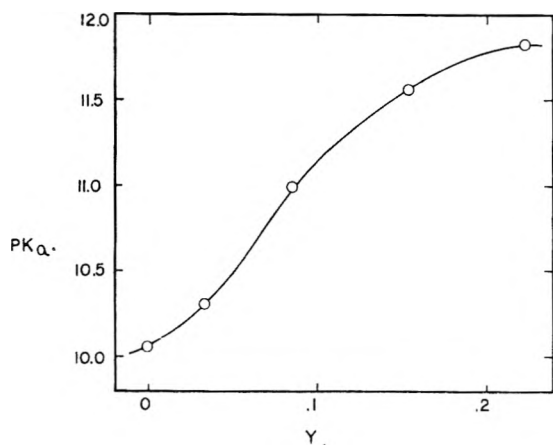
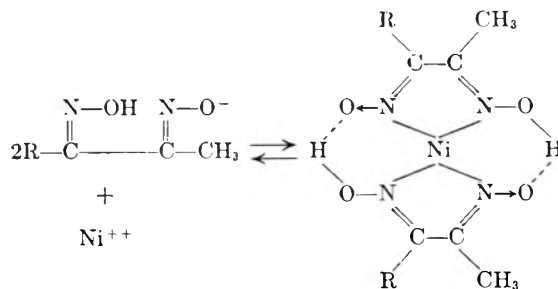


Fig. 4.— pK_a as a function of negative charge (Y) per monomeric unit for polyvinylmethylglyoxime.

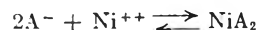
fied Bjerrum method² was used to calculate chelation constants. For a chelation system of maximum coordination number two, one which binds a divalent metal ion M^{++} , there are two successive chelation constants, K_1 and K_2 , such that

$$K_1 = \frac{[MA^+]}{[M^{++}][A^-]}, \quad K_2 = \frac{[MA_2]}{[MA^+][A^-]} \quad \text{and} \\ \beta_2 = K_1 K_2 = \frac{[MA_2]}{[M^{++}][A^-]^2}$$

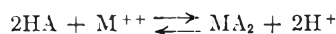
where A^- is the dissociated acid ligand while MA^+ and MA_2 are the two possible metal chelate species. All bracketed terms will refer to concentration except for hydrogen ion where the reference is to activity. An example of such a reaction is



where "R" is methyl for dimethylglyoxime, while for form IV of PMG it is the backbone of the polymer chain. This reaction may be written



The displacement constant B is defined by a reaction in which the polymer charge does not change

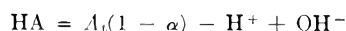


For such a reaction $B_2 = K_1 K_2 K_a^2$ where K_a is the acid dissociation constant of the weak chelate acid. For a polymeric acid, K_a is a function of Y , the negative charge per monomeric unit. In an acid-base titration in the absence of a metal ion that can be chelated, Y is equal to α , the degree of neutralization. From the titration curve of PMG in Fig. 1, one can calculate K_a as a function of Y ; this plot appears in Fig. 4. Defining \bar{n} as the concentration of bound ligands divided by the total metal concentration, M_t , one can make a Bjerrum plot of \bar{n} vs. $p[A^-]$, the negative logarithm of the unbound dissociated ligand, such that at $\bar{n} = 1$, $\log \beta_2 = 2p[A^-]$. From the modified Bjerrum plot of \bar{n} vs. $p([HA]/[H^+])$, $\log B_2 = 2p([HA]/[H^+])$ at $\bar{n} = 1$.

For HIA binding a trivalent metal M^{+++} with a maximum coordination number $N = 3$, the analogous calculations indicate that in a modified Bjerrum plot at $\bar{n} = 3/2$, $\log B_3 = 3p([HA]/[H^+])$ provided that $b_2^2 = b_1 b_3$. Here $B_3 = \beta_3 K_a^3$. For binding of neodymium(III) by FMG it was assumed that $N = 3$. A determination of the chelation constants of lanthanum(III) with dimethylglyoxime supports this assumption which is discussed in detail for that case.⁷

For PMG these calculations are complicated by the presence of different forms of chelating acids on the same polymer chain. As this cannot be resolved, the calculations will be made as though there were only one species present. The additional problem of the lack of precise knowledge of the base equivalent weight of chelating species can, however, be resolved. All the subsequent primed symbols will refer to the correct values of species in solution and their chelation constants, although these values are unknown here. The unprimed values are based upon the arbitrary base equivalent weight of 128.1 mentioned earlier. The ratio between the correct equivalent weight and 128.1 is defined as R , with $R \geq 1$.

Using the previously described equations³ and



$K_n = ([H^+][A^-])/[HA]$, as well as the analogous

(7) R. G. Charles and H. Freiser, *Anal. Chim. Acta.*, **11**, 101 (1954).

equations for the primed species, it is found that

$$\bar{n} = \frac{A_t' \left(1 - \frac{K_a'}{[H^+]} + \frac{K_a'}{[H^+]R} \right) - HA' - \frac{[A^-]'}{R}}{M_t}$$

If the polymer is a very weak acid as is PMG, the terms $K_a'/[H^+]$ and $K_a'/[H^+]R$ are very small. In that case

$$\bar{n} \cong \frac{A_t' - HA' - \frac{[A^-]'}{R}}{M_t}$$

Because of the small acid dissociation constant of the polymer and the relatively high hydrogen ion concentration, $[A^-]'$ is much smaller than A_t' or HA' , making the $[A^-]'/R$ term negligible. Thus

$$\bar{n} \cong \frac{A_t' - HA'}{M_t}$$

But since

$$\bar{n} \cong \frac{A_t' - HA' - [A^-]'}{M_t} \cong \frac{A_t' - HA'}{M_t}, \text{ then } \bar{n} \cong \bar{n}'$$

There is then a negligible error in the calculation of this parameter using the arbitrary equivalent weight. One can also show that

$$\frac{K_a}{K_a'} = \frac{1 - Y'}{R - Y'}$$

Again, because of the relatively small amount of A^- in solution, the Y' is very small and $K_a/K_a' \cong 1/R$. Using this equality it follows that

$$[A^-]/[A^-]' = \frac{1}{R} + \frac{[A_t]'}{[HA]'} (1 - 1/R)$$

The greater the excess of total ligand present over M_t , the closer that $[A_t]'/[HA]'$ approaches unity. This is true because again the unchelated ligand is almost completely in the form HA . In this case $[A^-]/[A^-]' \cong 1$. Thus one can see that, since $\bar{n} \cong \bar{n}'$, the Bjerrum plot of \bar{n} vs. pA^- should yield almost the same value of the formation constant for both the correct and the arbitrary choice of the equivalent weight.

Considering the B_2 constant, we see, assuming that $\beta_2' = \beta_2$, that

$$B_2 = \beta_2 K_a^2 \cong \beta_2' K_a^2 \cong \beta_2' (K_a')^2 / R^2$$

Therefore

$$B_2 \cong B_2' / R^2 \text{ or } \log B_2 \cong \log B_2' - 2 \log R$$

Thus although the formation constants β_2 and β_2' are almost identical, the displacement constants for the correct and the arbitrary equivalent weights will be different. In comparing the binding of the different divalent metal ions by the polyelectrolyte, the pB_2' value will always exceed the calculated pB_2 value by the same constant factor $2 \log R$. For B_2' to be an order of magnitude greater than B_2 , R would have to be greater than three.

The validity of these equations may be tested by calculations of binding constants of a polychelate for which the correct base equivalent weight is known. In the previous paper³ of this series, B_2 and β_2 were calculated for polyvinyl acetyl ketone binding $Cu(II)$, the correct base equivalent weight of 291 having been determined by a conductimetric titration. The same calculations were made for the equivalent weight of 112.1, R being 2.60. For this case $\log \beta_2' = 7.0$ and $\log \beta_2 =$

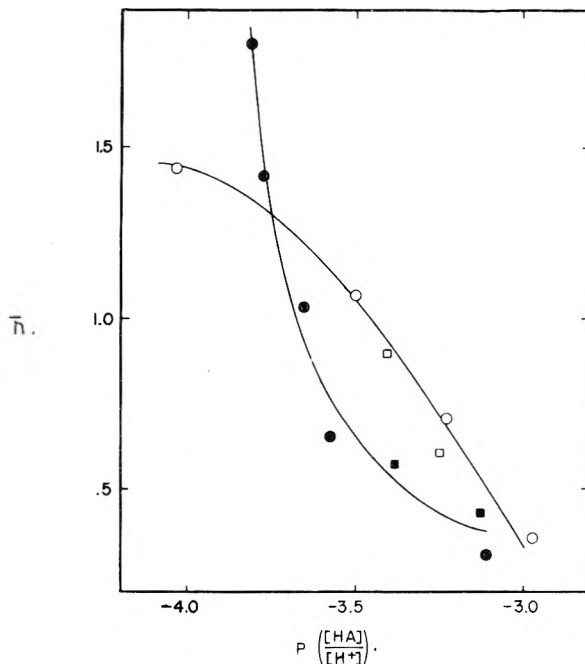


Fig. 5.—Modified Bjerrum plot for 0.01 M polyvinylmethylglyoxime with 0.0023 M (\circ) and 0.0057 M (\square) uranyl nitrate and for 0.01 M dimethylglyoxime with 0.0023 M (\bullet) and 0.0057 M (\blacksquare) uranyl nitrate.

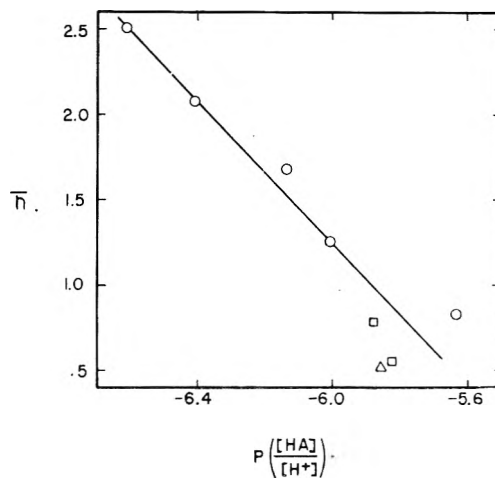


Fig. 6.—Modified Bjerrum plot for 0.01 M polyvinylmethylglyoxime with 0.0013 M (\circ), 0.0026 M (\square) and 0.0040 M (\triangle) neodymium(III) nitrate.

6.8, while $\log B_2' - \log B_2 = 1.0$. This is in good agreement with the above treatment which predicts that β_2 and β_2' are approximately equal and that $\log B_2' - \log B_2 = 2 \log R = 0.83$.

Figures 5 and 6 are modified Bjerrum plots for UO_2^{++} and $Nd(III)$, respectively. The formation and displacement constants for these systems are summarized in Table I. Although β_2 values for UO_2^{++} seem to indicate that the binding with the monomer is greater than that with the polymer, the B_2 parameters show a negligible difference. This latter parameter is the more significant one as it takes into account the two competing reactions. Due to the approximations involved in the calculations, the small differences in these binding constants do not warrant further discussion.

TABLE I
DISPLACEMENT AND BINDING CONSTANTS

Acid	Metal ion	<i>N</i>	log <i>B</i>	log β	<i>pK_a</i>
DMG	UO ₂ ⁺⁺	2	-7.4	15.3	11.3
PMG	UO ₂ ⁺⁺	2	-6.9	13.2	10.1
PMG	Nd(III)	3	-18.4	12.0	10.1

The binding of Nd(III) by dimethylglyoxime and Ni(II) by the polymer were not determined due to the lack of sufficient data in the critical range. On a qualitative basis Ni(II) binding by

PMG is weaker than that of UO₂⁺⁺ because, as seen in Fig. 2, at a given value of α the Ni(II) titration curve falls at a higher *pH_M*, indicating that fewer hydrogen ions are displaced from the polymer by metal ions.

The fact that the PMG titration curves in Fig. 2 coincide for Pr(III) and Nd(III) at similar concentrations shows that the binding of these metals is almost identical, the relatively small *B₃* value for Nd(III) in Table I indicating weak binding.

Acknowledgment.—This investigation was supported in part by the National Science Foundation.

EFFECT OF BINDING OF IONS AND OTHER SMALL MOLECULES ON PROTEIN STRUCTURE. V. ON THE INTERPRETATION OF THE ELECTROPHORETIC PATTERNS OF PROTEINS IN ACIDIC MEDIA¹

BY JOHN R. CANN

Contribution No. 76 from the Department of Biophysics, Florence R. Sabin Laboratories, University of Colorado Medical Center, Denver, Colorado

Received July 31, 1958

The moving boundaries shown by the electrophoretic patterns of bovine serum albumin and ovalbumin in acetate buffers at *pH* 4 correspond neither to single stable protein components nor to single components involved in a slowly adjusted equilibrium. Resolution of the patterns into multiple moving boundaries is intimately related to the production of conductance and *pH* gradients during electrophoresis. However, it should not be inferred from this that serum albumin and ovalbumin do not undergo some reaction during electrophoresis. Rather, it would appear that resolution of the patterns results from a coupling of such reactions with electrophoretic transport of the ions of the supporting medium.

Introduction

A new effect of carboxylic acids on the electrophoretic behavior of bovine serum albumin (BSA), ovalbumin and γ -pseudoglobulin in acidic media has been described in previous papers of this series.²⁻⁵ The progressive changes in the electrophoretic patterns of these proteins in supporting media containing varying quantities of acetate or other carboxylic acid buffers, were interpreted in terms of reversible complexing of the protein with undissociated buffer acid. The extremely non-enantio-graphic nature of the patterns was likewise attributed to interaction of the protein with the supporting medium. Although quantitative interpretation of the electrophoretic patterns does not seem possible at this time, the experiments presented in the present report define more clearly the nature of the problem and suggest in very qualitative terms a possible approach to its solution.

Experimental

Materials.—The BSA was Armour crystallized plasma albumin. BSA was esterified in acidic methanol according to the method of Fraenkel-Conrat and Olcott.⁶ Crystalline ovalbumin was prepared by the method of Sorensen and Høyrup.⁷

(1) Supported in part by research grant No. E-1482 from the National Institute of Allergy and Infectious Diseases of the National Institutes of Health, Public Health Service, and in part by the Damon Runyon Fund and the American Cancer Society.

(2) R. A. Phelps and J. R. Cann, *J. Am. Chem. Soc.*, **78**, 3539 (1956).

(3) J. R. Cann and R. A. Phelps, *ibid.*, **79**, 4672 (1957).

(4) R. A. Phelps and J. R. Cann, *ibid.*, **79**, 4677 (1957).

(5) J. R. Cann, *ibid.*, **80**, 4263 (1958).

(6) H. A. Fraenkel-Conrat and H. S. Olcott, *J. Biol. Chem.*, **161**, 259 (1945).

Methods.—Most of the methods used are described in the second paper of this series.³ Glass needles were used for all manipulations in order to avoid contaminating protein solutions and buffers with the acid-corrosion products of the metal hypodermic needles usually used to fill the electrophoresis cell. The durations of the on-and-off cycles in most of the intermittent-electrophoresis experiments were controlled mechanically, using synchronous-motor-driven cams, a microswitch and mechanical relay. The total on-cycle time was recorded on an electric clock inserted into the relay circuit. The author is indebted to Dr. Leonard Tolmach for his kindness in permitting the use of this equipment. In all the schlieren patterns shown in the figures the apparent mobilities, *v*, were positive. The values of $10^5 \times v$ cm.² sec.⁻¹ volt⁻¹, are given in the figures. In general, these values cannot be placed in correspondence with mobilities, since it will be shown that very large changes in conductance and *pH* occur in the electrophoresis cell during passage of the current.

Results

Most of the electrophoretic experiments reported herein were carried out on BSA in acetate buffer of ionic strength 0.01 and *pH* 4.0 (0.01 *M* NaAc-0.05 *M* HAc). The rising electrophoretic pattern of BSA in this buffer shows a very sharp, rapidly moving boundary (actually composed of two poorly resolved peaks) and a diffuse, slow moving one, Fig. 6—Continuous Electrophoresis. In contrast, the descending pattern shows two diffuse and very poorly resolved boundaries. It previously has been shown³ and is confirmed by the present study, that these boundaries do not correspond to single, stable protein components. Rather, they appeared to correspond to single components involved in a slowly adjusted equilibrium of the type $A \rightleftharpoons B$, where A and B represent interconvertible states in

(7) S. P. L. Sorensen and M. Høyrup, *Compt. rend. trav. lab. Carlsberg*, **12**, 12 (1916).

which the protein molecule differs in electrophoretic mobility but not molecular weight. The theory of isomerization equilibrium and electrophoresis⁸ indicates that for an equilibrium of this type, resolution of the electrophoretic patterns into two boundaries will occur for times of electrophoresis less than, or of the order of, the half-time of reaction, but that for longer times a single moving boundary will be observed. Since our experiments are of the order of one hour, it should be possible to determine the rate of conversion in at least one direction. Actually, experiments designed to make such measurements and the other experiments described below, show that the various boundaries correspond neither to stable protein components nor to single components involved in a slowly adjusted equilibrium. A possible interpretation of the electrophoretic patterns in terms of interaction of BSA with buffer constituents, in particular with the un-ionized buffer acid, will be discussed in light of these new findings. (All of the critical experiments described below for BSA also were carried out on ovalbumin in either 0.01 M NaAc-0.05 M HAC or 0.01 M NaAc-0.05 M HAC-0.03 M NaCl. The results were essentially the same for both proteins and, therefore, any conclusions concerning the electrophoretic patterns of BSA are equally applicable to ovalbumin.)

Two types of experiments originally designed to measure rates of interconversion, will be described. In the first type of experiment the two rising boundaries shown by a 1% solution of BSA in 0.01 ionic strength acetate buffer, pH 4.0, were separated a distance of about 1.4 cm. by electrophoresis to give the pattern shown in Fig. 1A. The electric current was then turned off and the boundaries allowed to sit in the cell for varying lengths of time before the current was turned on again. The only changes in the patterns which occurred during this time were simply those expected of diffusion. When the electric field was reapplied, the resultant electrophoretic pattern now showed three or four peaks. The patterns obtained after 1, 2, 4 and 18 hours are shown in Fig. 1B, C, D and E, respectively, where the new boundaries are indicated by vertical arrows. For example, when the original two boundaries were allowed to sit for either 2 or 4 hours before reapplication of the electric field, two new boundaries appeared. One of the new boundaries seemed to separate from the original, slow-moving boundary, while the other was left behind by the original, fast-moving boundary. When the boundaries were allowed to sit 18 hours before reapplication of the field, a single, new boundary was observed. The growth of these new boundaries is relatively slow, having a half-time greater than 4-5 hours. (A plot of the area under the new boundaries vs. the length of time the original boundaries were allowed to sit in the cell before reapplication of the electric field, showed that the new boundaries grow at a constantly decreasing rate as though approaching a limit.) It would thus seem that during the time between stopping the first electrophoresis and reapplication of the field, some of the material disappear-

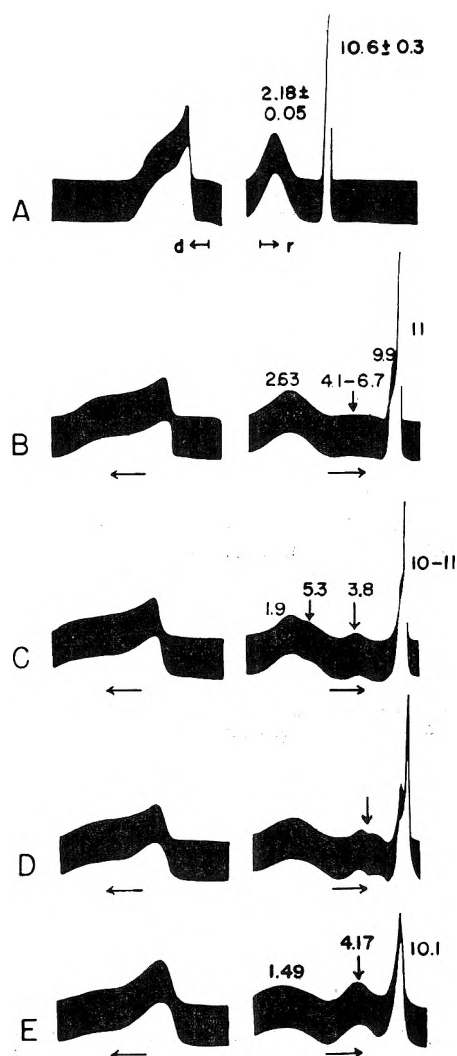


Fig. 1.—Electrophoretic patterns of 1% BSA in ionic strength 0.01 acetate buffer, pH 4.0. The experiments giving rise to these patterns are described in the text. In computing the apparent mobilities of the slowest and fastest peaks of B-E, the initial positions were taken as the positions of the original slow and fast boundaries, respectively, in pattern A which was obtained on the first application of the electric field. The apparent mobilities of the new rising peaks were referred to the original fast boundary except for the slower of the two new peaks in C which was referred to the original slow-moving boundary. The significance of the resolution of the leading rising boundary into two peaks in some of the patterns shown in this and other figures, is discussed in ref. 5.

ing across the leading boundary was slowly converted to a new electrophoretic component of lower mobility. The electrophoretic patterns in Fig. 1 also show concomitant changes in the descending limb of the cell, the slower boundary growing at the expense of the faster one. These experiments were repeated with the modification that the original rising boundaries were separated only 0.5 cm. by the first application of the field. In this series of experiments, the new rising boundary grew more rapidly than in the first series, the half-time being about 2 hours. (The new boundary also migrated somewhat slower than in the first series.) Nevertheless, both half-times are considerably greater than the time of electrophoresis. These results are there-

(8) J. R. Cann, J. G. Kirkwood and R. A. Brown, *Arch. Biochem. Biophys.*, **72**, 37 (1957).

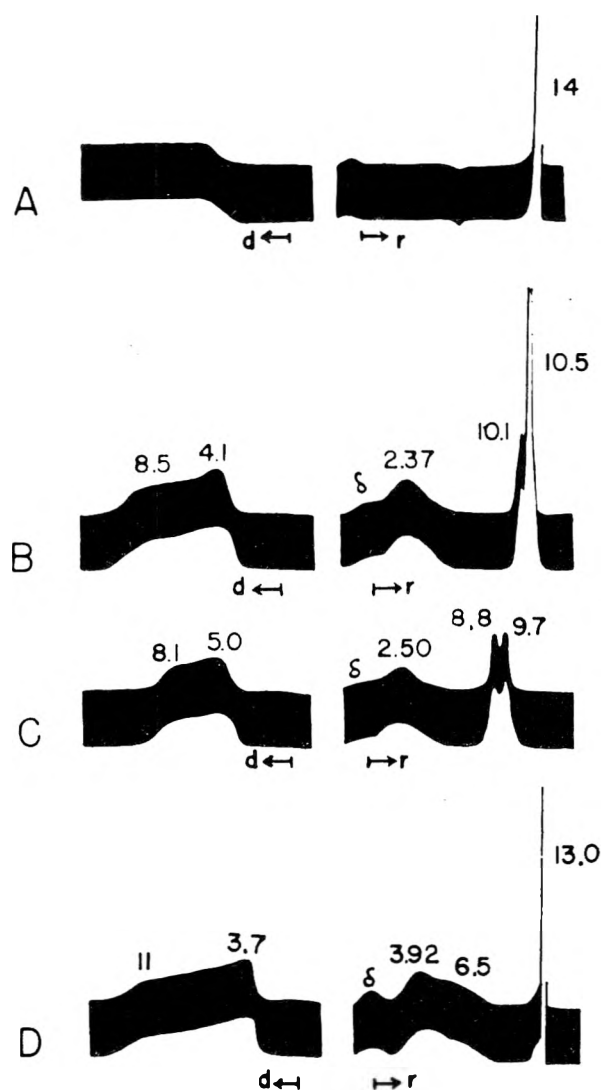


Fig. 2.—Electrophoretic patterns of a fraction of BSA (see text for details): A, unadjusted and undialyzed analyzed against 0.01 *M* acetate buffer, pH 4.0; B, dialyzed fraction analyzed against 0.01 *M* acetate buffer, pH 4.0; C, adjusted fraction analyzed against 0.01 *M* acetate buffer, pH 4.0; D, unadjusted and undialyzed fraction analyzed against 0.0064 *M* acetate buffer, pH 3.87.

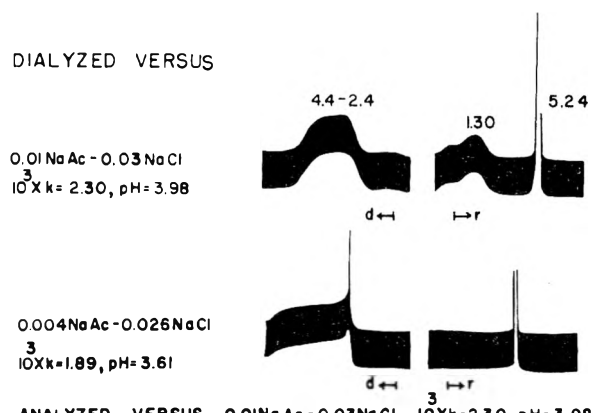


Fig. 3.—Electrophoretic patterns of 1.3% ovalbumin.

fore consistent with the theory of isomerization equilibrium and electrophoresis. It might thus be concluded from this experiment alone that the two

rising boundaries correspond to single components involved in a slowly adjusted equilibrium.

In order to confirm this conclusion, the second type of kinetic experiment was performed. In this experiment a 3% solution of BSA, equilibrated against the 0.01 acetate buffer, was fractionated in the electrophoresis cell by withdrawing the material disappearing across the fast-moving boundary (30–50% of the protein). Preliminary experiments showed that when such a fraction is redialyzed against buffer for 18 hours before electrophoretic analysis, the resultant patterns, Fig. 2B, are the same as those shown by the same concentration of unfractionated protein. In the kinetic experiments the conductance and pH of the fraction were readjusted to the original values by addition of buffer of the appropriate concentration and pH rather than by dialysis, and the fraction aged for varying lengths of time at 0° before electrophoretic analysis. The initial boundary was formed between the adjusted and aged fraction and the same buffer used in the fractionation. The unexpected result of this experiment is that within 27 min. after removal from the cell and adjustment of conductance and pH, the fraction showed the same electrophoretic pattern, Fig. 2C, as the control experiment with unfractionated BSA. The same result was obtained when the unadjusted fraction was analyzed using buffer of the same conductance and pH as the fraction to form the initial boundary, Fig. 2D. (The control experiment was likewise carried out using buffer of about the same conductance and pH as the fraction.) Thus, in contrast to the first type of kinetic experiment which suggests a slow conversion of BSA from one state to another, the second type of experiment indicates a rapid conversion with a half-time much less than the time of electrophoresis; which is, of course, inconsistent with theoretical predictions. It must be concluded, therefore, that the theory of isomerization equilibrium and electrophoresis is not applicable and that the two moving boundaries correspond neither to single stable components nor to single components involved in a slowly adjusted equilibrium.

It is clear that resolution of the paradox raised by these experiments would be a major step toward an understanding of the electrophoretic patterns shown by proteins in acidic media. An important observation in this direction was made when a fraction of BSA obtained as described above, was analyzed electrophoretically without prior reequilibration against buffer or adjustment of its conductance and pH by addition of a concentrated buffer. When the initial boundary was formed between the unadjusted fraction and the buffer used for fractionation, the rising pattern now showed only a single rapidly-moving boundary and the descending pattern, a very broad boundary, Fig. 2A, even after the fraction had been aged 18 hours at either room temperature or 0°. This suggested that if unfractionated

(9) Similar results have been obtained by H. M. Dintzis, S. N. Timasheff and S. J. Singer (personal communication from Dr. Serge N. Timasheff) who fractionated BSA in 0.1 ionic strength glycine-HCl buffer of pH 2.35. BSA also shows two rising boundaries in this buffer. The fraction obtained by withdrawing the protein disappearing across the leading boundary was analyzed electrophoretically before and after re-equilibration against the buffer used for fractionation.

tionated protein is dialyzed against a buffer of the same conductance and pH as the fraction prior to electrophoretic analysis against the usual buffer, then only a single rising boundary should be observed. Indeed, this was realized with ovalbumin, Fig. 3, and nearly so with BSA, although it was necessary to dialyze the proteins against buffers whose conductances and pH 's deviated somewhat more markedly from the usual buffers than did the fractions. These experiments indicate that the normal resolution of the rising patterns into two moving boundaries is related to changes in conductance and pH in the electrophoresis cell during passage of current.

This latter conclusion is supported by measurements of conductance and pH on portions of solution removed from various positions in the rising limb of the Tiselius cell following electrophoresis. These measurements are summarized in Fig. 4 and Table I, where k is the conductance in ohms^{-1}

TABLE I
CHANGE IN CONDUCTANCE AND pH ACROSS THE LEADING RISING BOUNDARY

System	$\Delta k, \%$		ΔpH	
	Measured	Calcd.	Measured	Calcd.
(A)				
1% BSA, 0.01 M NaAc, pH 4.02 ^a	19.7	16.1	0.08	0.05
3% BSA, 0.01 M NaAc, pH 4.01 ^a	25.6	38.1	.14	.12
(B)				
1% Ovalbumin, 0.01 M NaAc, pH 4.01 ^a	14.8	14.6	.11	.05
1.3% Ovalbumin, 0.01 M NaAc-0.03 M NaCl, pH 4.00 ^a	12.3	8.0	.11	.03
1.3% Ovalbumin, 0.01 M NaAc-0.09 M NaCl, pH 3.92 ^a	9.8	5.0	.07	.02
(C)				
1.3% Ovalbumin, 0.002 M Na formate-0.038 M NaCl, pH 3.96 ^b	20.3	18.5	.11	.08
1.3% Ovalbumin, 0.04 M Na formate, pH 3.90 ^a	12.4	7.3	.10	.03
(D)				
1.3% Ovalbumin, 0.01 M NaAc, pH 5.26 ^{c,d}	22.9	26.8	.09	.16
1.3% Ovalbumin, 0.01 M NaAc-0.03 M NaCl, pH 5.20 ^c	13.7	17.1	.03	.08

^a Calculations made assuming two stable components with mobilities equal to the velocities of the poorly resolved descending boundaries. ^b Patterns showed a single boundary, Fig. 2 of ref. 3. ^c A_1 and A_2 lumped into single component for calculations. ^d A small boundary moved with low velocity toward the cathode.

cm.^{-1} ; Δk , the per cent. change in conductance across the leading boundary; and ΔpH , the change in pH across the leading boundary. On consideration of these data, several things became immediately apparent. First, the changes in conductance

and pH across the leading boundary are large even at ionic strengths as high as 0.1. However, as shown in Table I, the Dole theory of electrophoresis of strong electrolytes¹⁰ predicts changes in conductance during electrophoresis of mixtures of stable proteins which are in good agreement with those observed in the present system. While the predicted changes in pH are rather smaller than the observed changes at pH 4 (and in one case is actually opposite in direction), this is most probably a reflection of the unrealistic assumption made in the present application of the Dole theory. The second observation relates the resolution of electrophoretic patterns to the production of conductance and pH gradients. Thus, electrophoresis of 3% BSA equilibrated against 0.01 ionic strength acetate buffer of pH 4.01, results in two rising boundaries and also in large changes in conductance and pH , Fig. 4A. However, when the unadjusted and undialyzed fraction is analyzed against the same buffer used for fractionation, only a single boundary is observed and there is no further change in conductance and pH across this boundary during passage of the current, Fig. 4B. On the other hand, electrophoresis of the unadjusted and undialyzed

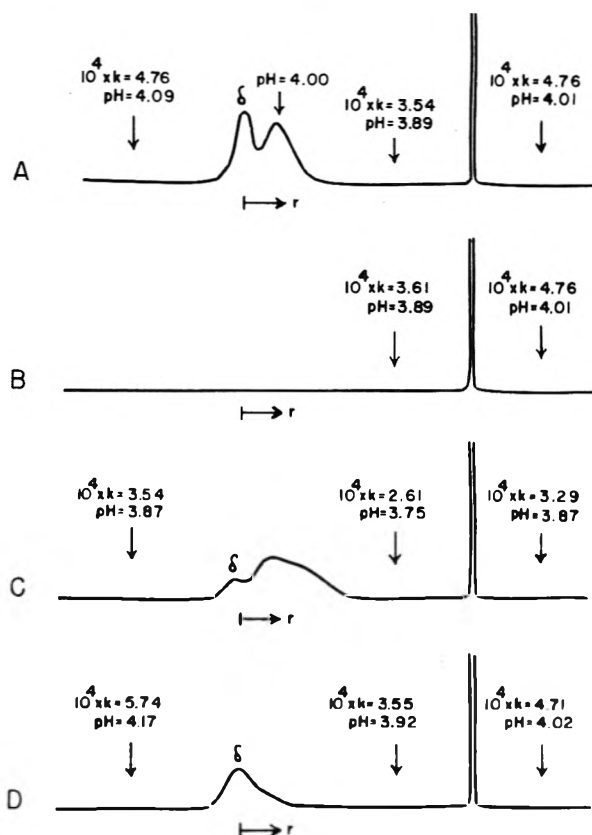


Fig. 4.—Conductance and pH of the protein and buffer solutions at various positions in the rising limb of the electrophoresis cell: A, 3% BSA equilibrated against 0.01 acetate buffer, pH 4.01; B, unadjusted and undialyzed BSA analyzed against 0.01 acetate buffer, pH 4.01, protein concentrations between 1 and 1.5%; C, unadjusted and undialyzed fraction analyzed against 0.0064 acetate buffer, pH 3.87, protein concentration between 1 and 1.5%; D, 1% esterified-BSA equilibrated against 0.01 acetate buffer, pH 4.02. The mean deviations of the conductances are 1-2%.

and pH across the leading boundary are large even at ionic strengths as high as 0.1. However, as shown in Table I, the Dole theory of electrophoresis of strong electrolytes¹⁰ predicts changes in conductance during electrophoresis of mixtures of stable proteins which are in good agreement with those observed in the present system. While the predicted changes in pH are rather smaller than the observed changes at pH 4 (and in one case is actually opposite in direction), this is most probably a reflection of the unrealistic assumption made in the present application of the Dole theory. The second observation relates the resolution of electrophoretic patterns to the production of conductance and pH gradients. Thus, electrophoresis of 3% BSA equilibrated against 0.01 ionic strength acetate buffer of pH 4.01, results in two rising boundaries and also in large changes in conductance and pH , Fig. 4A. However, when the unadjusted and undialyzed fraction is analyzed against the same buffer used for fractionation, only a single boundary is observed and there is no further change in conductance and pH across this boundary during passage of the current, Fig. 4B. On the other hand, electrophoresis of the unadjusted and undialyzed

fraction against a buffer of about the same conductance and pH results in two rising boundaries and resolution is once again accompanied by large changes in conductance and pH , Fig. 4C. Finally, while resolution of the rising pattern of BSA into two boundaries is clearly related to changes in conductance and pH , such changes are not a sufficient condition for resolution. This is well illustrated by experiments on esterified BSA. The electrophoretic behavior of this protein derivative is quite different from that of BSA. At pH 4, its rising patterns shows essentially a single, rapidly moving boundary over a wide range of concentrations of acetate buffer.¹¹ Yet, as shown in Fig. 4D, electrophoresis of esterified-BSA is accompanied by large changes in both conductance and pH . The failure of the rising pattern to show two moving boundaries could conceivably be related to the pronounced conductance and pH gradients across the initial boundary. (The large change in conductance and pH of the esterified BSA solution during dialysis is due to the large net positive charge on this macromolecule.) This possibility would seem to be eliminated by a control experiment in which BSA was equilibrated against ionic strength 0.01 acetate buffer, pH 4.02, but analyzed against ionic strength 0.0064 buffer of pH 3.82. Except for apparent mobilities, the resultant patterns were essentially the same as those obtained in a normal analysis of BSA in the ionic strength 0.0064 buffer, despite the fact that both the conductance and the pH of the dialyzed protein were considerably greater than those of the buffer used to form the initial boundary.

The relationship between resolution of the rising pattern into two moving boundaries and the production of conductance and pH gradients during electrophoresis suggests an explanation for the dependence of electrophoretic patterns on interruption of the electric field, Fig. 1. Conductance and pH measurements have shown that during the initial separation of the boundaries, the Donnan equilibrium is badly disturbed by the electrophoretic process. When the field is interrupted, diffusion of the buffer ions tends to restore the disturbed Donnan equilibrium. Subsequent reapplication of the field once again disturbs the distribution of buffer ions in the cell and new moving boundaries appear. The rate of growth of these new boundaries should now be interpreted in terms of the rate of diffusion of the buffer ions rather than the rate of an isomerization reaction. This interpretation is consistent with the observed dependence of the rate of growth of the new boundaries upon the distance of separation of the original two boundaries. It is not implied, however, that BSA does not undergo some electrophoretically demonstrable interaction with acid media but, rather, it would appear that resolution into multiple boundaries is a result of the coupling of such interactions with changes in conductance and pH during the electrophoretic process. Two different types of experiments lend support to these ideas. In the first experiment the rising boundaries shown by 3% BSA equilibrated

(11) J. R. Cann, unpublished experiments. Saroff and his co-workers¹² first showed that esterified-BSA shows only a single moving boundary in 0.1 M acetate buffer, pH 4-6.

against 0.01 M acetate buffer, pH 4.01, were separated a distance of 1.4 cm. by electrophoresis, the current then was turned off and the boundaries allowed to sit in the cell for 13 hours at which time the solution between the boundaries was withdrawn for pH measurement. It was found that during the time the boundaries sat undisturbed in the cell, the pH of the solution between the boundaries had increased 0.12 pH unit. Other experiments showed that the rate of increase in pH depends upon the distance of separation of the boundaries, the greater the distance of separation, the slower the rate. When a similar experiment was carried out on a 1.3% ovalbumin solution equilibrated against 0.01 M NaAc-0.03 M NaCl, pH 3.99, the pH between the boundaries increased 0.04 pH unit and the conductance increased 6% in 18 hours. The second type of experiment was carried out using 3% BSA equilibrated against 0.01 M acetate buffer, pH 4.02, and two initial rising boundaries were formed as follows—dialyzed protein: 0.01 M NaAc, pH 4.02; 0.0064 M NaAc, pH 3.84. During the early stage of electrophoresis of this system the usual two moving boundaries should resolve. However, since the 0.0064 M acetate buffer has about the same conductance and pH as the protein solution behind the leading boundary, it would be expected that when the leading boundary migrates into the region of the cell containing this buffer, a new, slow moving boundary should resolve rapidly from the original leading peak. Indeed, as shown in Fig. 5-2, this was found to be the case. This experiment demonstrates once again that the various rising boundaries correspond neither to stable protein components nor to single components involved in a slowly adjusted equilibrium.

The above findings suggest that under proper conditions, intermittent application of the electric field, *i.e.*, alternate on-and-off cycles of electrophoresis, should give patterns showing single rising and descending boundaries. Indeed, it has been possible to realize approximately this prediction by appropriate choice of time intervals and field strength. Whereas intermittent electrophoresis with on-and-off cycles of equal duration, 0.065 second-1 minute, gave the usual type of patterns, markedly altered patterns were obtained when the off-cycle was 13-30 times as long as the on-cycle which was varied from 0.44 second to 2 minutes. The results of an experiment in which the on-cycle was 2 minutes and the off-cycle 1 hour, are presented in Fig. 6. It will be noted that the slow-moving rising boundary and the fast-moving descending boundary in the patterns obtained by intermittent electrophoresis are very small in area but that the apparent mobilities of the major rising and descending boundaries are still greatly different. In another set of two experiments with an on-cycle of 0.44 second and an off-cycle of 5.6 seconds, striking changes in the patterns were observed when the field strength was lowered from 27 to 7 volts cm^{-1} (over-all times of 205 and 794 minutes, respectively), the areas under the slow-moving rising boundary and fast-moving descending boundary decreasing markedly with the field strength. The results of the intermittent-electrophoresis experi-

ments as well as those of a previously described continuous-electrophoresis experiment demonstrating a strong effect of field strength on the patterns of ovalbumin (Fig. 7 of ref. 3), are best interpreted in terms of the time available for diffusion of buffer ions to restore the Donnan equilibrium as it is disturbed by the electrophoretic process.

While most of the measurements described above have been concerned with the rising pattern of BSA, the descending pattern has not been completely neglected. Since the descending boundaries shown in 0.01 acetate buffer, *pH* 4.0, are very poorly resolved, it is difficult to carry out fractionation experiments and to measure changes in conductance and *pH* in the descending limb of the cell during electrophoresis under these conditions. However, well resolved descending patterns can be obtained in supporting media containing much lower concentrations of acetate buffer. Thus, as shown in Fig. 7A, the descending pattern obtained in 0.0008 *M* NaAc-0.004 *M* HAc-0.0092 *M* NaCl, *pH* 4.1, shows a diffuse fast-moving boundary and a very sharp slow-moving one. A 3% solution of BSA was fractionated under these conditions by withdrawing from the descending limb of the cell, the protein disappearing across the slow-moving boundary. Chemical analysis of the fraction showed that approximately 80% of the total protein disappears across this boundary. The fraction was also analyzed electrophoretically. After re-equilibration by dialysis against the buffer, the fraction gave the same electrophoretic patterns as shown by unfractionated BSA. (Relatively small differences between some of the boundary velocities of the fraction and the unfractionated material are attributable to difference in concentration.) However, this was not the case when the fraction was analyzed without prior adjustment of its conductance and *pH* by dialysis against the buffer. The descending pattern of the unadjusted fraction showed the very sharp slow-moving boundary but only a very small fast-moving boundary. The area under the fast peak was less than 20% of the expected value even though the unadjusted fraction had been aged for 18 hours at 2°. These results are similar to those obtained in the fractionation experiments carried out on the rising pattern in 0.01 acetate buffer.

The conductance and *pH* of the protein and buffer solutions at various positions in the descending limb of the cell after electrophoresis of a 3% solution of BSA in the acetate-poor medium, are presented in Fig. 7B. It will be noted that a 29% change in conductance and 0.14 unit change in *pH* occurred across the fast-moving boundary during electrophoresis. The Dole theory was used to calculate the changes in conductance and *pH* which one would expect to find in the descending limb after electrophoresis of a solution containing the proper proportion of two stable components equilibrated against the appropriate buffer. While the model is unrealistic, the calculated change in conductance (27%) is in excellent agreement with the measured change, but the calculated change in *pH* (0.07 unit) is only one-half of the measured change.

Finally, it should be noted that the changes in conductance and *pH* which occur in the two limbs of

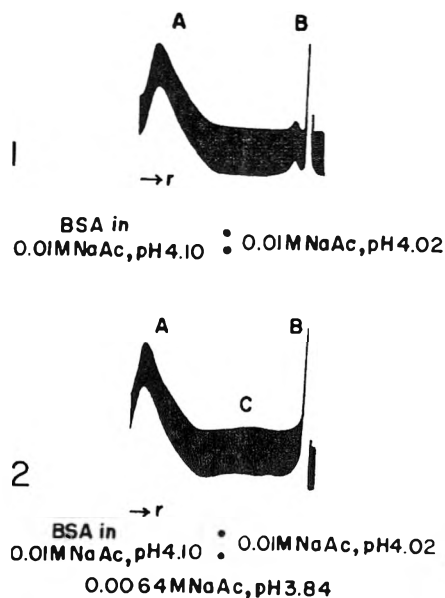


Fig. 5.—Electrophoretic patterns of 3% BSA: 1, control; 2, experiment described in text.

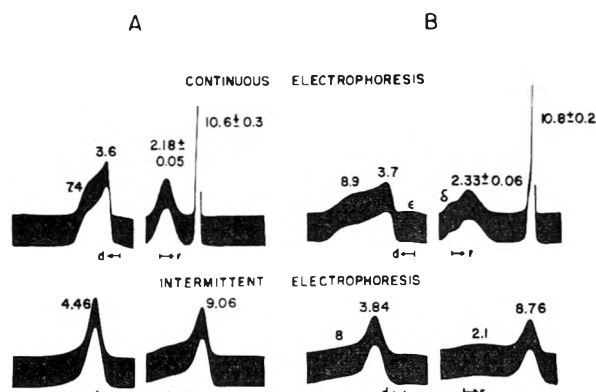


Fig. 6.—Electrophoretic patterns of 1% BSA equilibrated against 0.01 acetate buffer, *pH* 4.01; A, field applied for a total time of 0.5 hour; B, field applied for 1 hour. Over-all time of intermittent-electrophoresis experiments (on-cycle of 2 minutes and off-cycle of 1 hour): A, 14.5 hours; B, 30 hours.

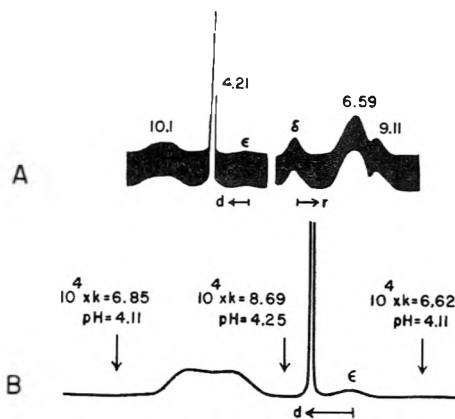


Fig. 7.—Electrophoretic behavior of BSA equilibrated against 0.0008 *M* NaAc-0.004 *M* HAc-0.0092 *M* NaCl, *pH* 4.1: A, electrophoretic patterns of 1% protein; B, conductance and *pH* of the protein and buffer solutions at various positions in the descending limb of the electrophoresis cell, 3% protein.

the Tiselius cell during electrophoresis, correlate nicely with the shapes of the various moving boundaries.

Discussion

The present experiments once again emphasize the great complexity of the electrophoretic behavior of proteins in acidic media and caution against a literal interpretation of the velocities and proportions of the various moving boundaries shown by the electrophoretic patterns. While the protein concentration changes across these boundaries, they must be considered as false boundaries in the sense that they correspond neither to single, stable protein components nor to single components involved in a slowly adjusted equilibrium. Furthermore, resolution of these boundaries is intimately related to the changes in conductance and pH produced by the electrophoretic process. However, this should not be interpreted to mean that BSA and other proteins do not undergo some interaction with acidic media; rather, it would appear that resolution of their electrophoretic patterns is the result of coupling of such interactions with electrophoretic transport of the ions of the supporting medium. That serum albumin does, indeed, undergo some reaction in acetate and other carboxylic acid buffer-containing media is indicated by several observations. For example, not all serum albumin preparations show the electrophoretic behavior under consideration. Thus, Keltz and Mehl¹³ have isolated a rat plasma albumin which shows normal electrophoretic patterns, *i.e.*, a single moving boundary at low as well as high pH 's. More recently, Schmid¹⁴ prepared a human plasma albumin which also gave normal patterns in ionic strength 0.1 acetate buffer, pH 4.0. However, after treatment with cysteine and an ion exchanger, his albumin now showed the same complex patterns as the human plasma albumin of fraction V. This suggests that cysteine removed a blocking agent from the protein, thereby permitting the protein to interact with acetate buffer. In previous papers of this series²⁻⁵ evidence was presented to show that this interaction involves complexing of the protein with un-ionized carboxylic acid of the buffer medium and that the extremely non-enantiographic nature of the patterns is a reflection of this interaction and is not due to the high protein concentration *per se*. The dependence of the electrophoretic patterns on the concentration of carboxylic acid-containing buffer in the supporting medium, suggested that the protein-acid complexes have more positive electrophoretic mobilities than the uncomplexed molecules. Sedimentation experiments indicated that complexing of the protein molecule with undissociated buffer acid produces rather subtle changes in structure which change the net charge on the protein but not its molecular weight and frictional coefficient. While quantitative interpretation of the electrophoretic patterns must await a more complete development of the moving-boundary theory for weak electrolytes,¹⁵ an ideal-

ized qualitative explanation of the patterns appears possible at this time. This explanation was arrived at jointly with Dr. Serge N. Timasheff of the United States Department of Agriculture, Eastern Utilization Research and Development Division, Philadelphia. It is assumed that the fast moving protein-acid complexes exist in instantaneous equilibrium with the undissociated buffer acid as well as other constituents of the supporting medium. Let us consider those processes which could conceivably occur during electrophoresis under hypothetical conditions such that the production of conductance gradients can be ignored. (Actually the non-enantiography typical of the electrophoretic patterns of BSA and ovalbumin in acetate-containing media at pH 4, have been observed at ionic strengths as high as 0.3). When the electric field is applied the faster-migrating, protein-acid complexes in the rising limb of the cell will migrate out of the equilibrium mixture and into fresh buffer. However, a fraction of these complexes will dissociate instantaneously to re-establish equilibrium with the supporting medium. Re-equilibration will result in liberation of acid which lowers the pH behind the leading edge of the boundary. As a result, the protein molecules in this region will migrate faster than those moving into fresh buffer, and the front of the boundary will sharpen as, for example, in Fig. 2B of ref. 5. In the descending limb of the electrophoresis cell the situation is different in that the postulated complexes move into an equilibrium mixture, and a fraction of the protein left behind will associate with buffer acid. As a result, the pH below the trailing edge of the boundary will increase and the back of the boundary will sharpen as in Fig. 2B of ref. 5, since the rear portion of the boundary migrates in the original, lower pH buffer. Indeed, resolution into two boundaries may actually occur despite rapid equilibration. Gilbert and Jenkins¹⁶ have considered the system $A + B \rightleftharpoons C$, assuming instantaneous establishment of equilibrium, and have shown that such a three-component equilibrium system will give two moving boundaries provided that the mobilities of the components are different.

It is significant that the type of non-enantiography induced by the postulated interactions is typical of that observed under a variety of conditions of buffer composition (see, for example, Fig. 2 of ref. 2 and Figs. 1 and 2 of ref. 3). At very low concentrations of buffer, interactions of the protein with the undissociated acid may be negligible in which case single, symmetrical boundaries should be observed, Fig. 2 of ref. 3. As the concentration of buffer is increased the interactions will become more pronounced and will be reflected in the electrophoretic patterns as described above. At a sufficiently high concentration of buffer acid, essentially all of the protein should exist as complexes and the electrophoretic patterns should once again show single, symmetrical boundaries. This has also been realized approximately (Fig. 2 of ref. 1). The proposed explanation also is consistent with the fact that while the Dole theory accounts adequately

(12) H. A. Saroff, N. R. Rosenthal, E. R. Adamik, N. Hages and H. A. Scheraga, *J. Biol. Chem.*, **206**, 255 (1953).

(13) A. Keltz and F. W. Mehl, *J. Am. Chem. Soc.*, **77**, 5764 (1955).

(14) K. Schmid, *ibid.*, **79**, 4679 (1957).

(15) J. C. Nichol, E. B. Dismukes and R. A. Alberty, *ibid.*, **80**, 2610 (1958).

(16) G. A. Gilbert and R. C. Ll. Jenkins, *Nature* **177**, 853 (1956).

for the changes in conductance which occur in the Tiselius cell during electrophoresis of BSA and ovalbumin at pH 4, it fails to account for the large changes in pH. Furthermore, the deviations of the observed from the theoretical changes in pH are

in the direction expected on the basis of the model.

Acknowledgments.—The author wishes to thank Drs. John G. Kirkwood, Lewis G. Longworth and Serge N. Timasheff for their helpful discussions of this work.

AN IMPROVED APPARATUS FOR OSCILLOGRAPHIC OBSERVATION OF POLAROGRAPHIC PHENOMENA. OXIDATION-REDUCTION PATTERN OF Cd(II): EFFECTS OF OXYGEN AND GELATIN¹

BY DONALD C. KAUFMAN, J. WEST LOVELAND AND PHILIP J. ELVING

Contribution from The Pennsylvania State University, University Park, Pa., Sun Oil Company, Marcus Hook, Pa., and University of Michigan, Ann Arbor, Michigan

Received August 5, 1958

An improved triangular wave sweep generator apparatus is described, which is satisfactory for the investigation of phenomena at polarizable electrodes. It has been used to investigate the oxidation-reduction pattern of cadmium, and the effects of oxygen and of gelatin upon the pattern. The relationships between current, sweep frequency and concentration for Cd(II) in a solution containing oxygen approach those theoretically expected at low frequencies and low Cd(II) concentrations where the oscillographically observed oxygen maximum following the Cd(II) wave does not interfere. The data indicate the oxygen maximum to be a combined capacitive and faradaic current peak, the result of the high dielectric nature of the cadmium hydroxide layer formed around the mercury drop and of the reduction of this film. The oxygen maximum does not occur in iodide solution, probably because of the formation of the more stable cadmium-iodide complex.

Oscillographic polarography, which has been applied to analysis, investigation of electrode phenomena, reaction rate measurement, determination of the differential capacity of the electrical double layer, complex formation, etc.,² consists essentially of the presentation on a cathode ray oscillograph (CRO) screen of the current-potential record or derived function obtained when an alternating potential of amplitude equal to the potential range to be studied, *e.g.*, 0.5 to 2 v., and of frequency ranging from one to hundreds of c.p.s., is applied to a polarographic cell-electrode arrangement.

In practice, the alternating potential is applied both to the polarographic cell and to the horizontal deflection plates of a CRO tube; the current passing through the cell also passes through a resistor in series with it. The resulting potential drop is amplified and applied to the vertical deflection plates; the latter potential may be electronically differentiated or integrated before being applied to the CRO. One particular advantage of oscillographic polarography is in the instantaneous recording of phenomena at electrode interfaces.

The present paper describes a multi-sweep apparatus which combines many of the better features of previously described instruments,² *e.g.*, it produces both the cathodic and anodic traces, and requires no compensation, and its application to the study of the oxidation-reduction pattern of cadmium, which was chosen because its oxidation-reduction is almost completely reversible, and of the effects of dissolved oxygen and of a typical maximum suppressor, gelatin, on that pattern. The purpose of the present investigation was three-

fold: to evaluate the apparatus developed, to determine the effects of initial potential, sweep frequency, Cd(II) concentration and oxygen on the oscillographically recorded oxidation-reduction pattern of cadmium, and to study the process or processes by which gelatin acts as a maximum suppressor.

Data and Discussion

The experimental data were obtained by measurement and analysis of photographs of the CRO traces, which were enlarged to original size, *e.g.*, Fig. 1. The vertical axis is current; the horizontal is potential. From left to right, the first peak on the top or cathodic part of the trace is the cadmium reduction peak; the second is the oxygen maximum. (It has been observed in oscillographic polarography that the presence of oxygen results in maxima appearing on the polarographic curve of many reducible ions; much work has been done in attempts to find the reason for these effects.) On the bottom portion of the trace the potential is sweeping from right to left and the cadmium oxidation peak is observed. The dots at either end of the trace are the potential calibration points.

Potentials cited are referred to the mercury pool which was in contact with 1 *M* potassium chloride or iodide solution.

Evaluation of the Apparatus.—The apparatus described (see Experimental) has the following advantages for the investigation of phenomena at polarizable electrodes: (a) the unit is completely line-operated when output circuit 1 is used, and requires only one battery when output circuit 2 is used. (b) It is very stable; this is important since even a small amount of drift can severely limit the reproducibility of results. (c) The frequency is variable from 1 to 200 c.p.s., the potential span from 0 to 3 v., and the initial potential from 0 to -0.3 v. with output circuit 1, and 0 to

(1) Correspondence concerning this paper should be directed to P. J. Elving, Department of Chemistry, University of Michigan, Ann Arbor, Michigan.

(2) P. Delahay, "New Instrumental Methods in Electrochemistry," Interscience Publishers, Inc., New York, N. Y., 1954; J. W. Loveland and P. J. Elving, *Chem. Revs.*, **51**, 67 (1952).

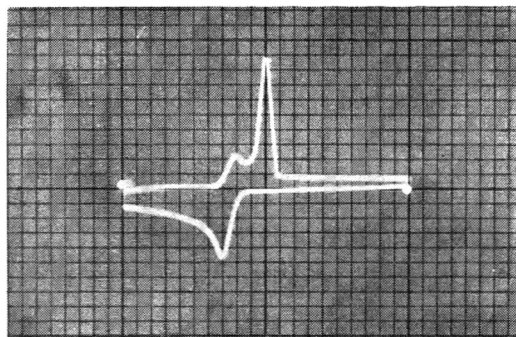


Fig. 1.—Trace of i - E curve for solution 0.3 mM in CdCl_2 , 1 M in KCl , and saturated with air. Frequency, 5 c.p.s.; R , 15 ohms; sensitivity, 2 mv./in. Left dot, -0.308 v.; right dot, -1.334 v. Initial potential, -0.308 v.; span, 1.026 v.

-1 v. with output circuit 2; this flexibility permits investigation under a wide range of conditions. (d) The triangular voltage wave form produced is perfectly symmetrical, allowing simultaneous investigation of both cathodic and anodic processes. (e) The resistance introduced into the cell circuit is kept to a minimum, thus eliminating distortion of the CRO trace.

A limitation of the apparatus is the lack of provision for automatically operating the camera used to record the CRO trace. When a dropping mercury electrode is used, this must be done manually using a stopwatch to time the growth of the mercury drop.

Current Relationships.—In conventional polarography, where the electrode potential is increased slowly, the diffusion current of a reducible species attains a constant value, which is generally defined by the familiar Ilkovic equation. In multisweep oscillographic polarography, where the rate of potential variation is generally greater than 2 v./sec., the current rises to a maximum value (peak current, i_p) and immediately declines. The relation

$$i_p = KC_M V^{1/2} \quad (1)$$

where C_M is the concentration and V the potential variation (dE/dt), holds well at low sweep rates, but not so well at higher rates³⁻⁶; the ideal value for V is between 0.1 and 1 v./sec.^{6b} Delahay³ attributed the curvature of the i vs. $v^{1/2}$ plots at higher sweep rates to the greater iR drops at high frequencies and to the slowness of the reaction rates for the species involved. Subsequently, he⁵ stated that the curvature may be due to capacity current effects and showed that the diffusion current of Cd(II) decreases with increasing resistance in the cell circuit.

Capacity effects must be considered in oscillographic polarography. The large differential capacity of the electrical double layer and the rapid rate of potential variation may produce a relatively large capacity current, i_c . At constant V , i_c is proportional to the differential capacity, C , of the electrical double layer

(3) (a) P. Delahay, *J. Am. Chem. Soc.*, **75**, 1190 (1953); (b) *THIS JOURNAL*, **53**, 1279 (1949); (c) **54**, 402, 630 (1950).

(4) P. Delahay and T. J. Adams, *J. Am. Chem. Soc.*, **74**, 5740 (1952).

(5) P. Delahay and G. L. Stiehl, *THIS JOURNAL*, **55**, 570 (1951).

(6) (a) J. E. B. Randles, *Analyst*, **72**, 301 (1947); (b) *Trans. Faraday Soc.*, **44**, 322 (1948); (c) A. Sevcik, *Collection Czechoslov. Chem. Commun.*, **13**, 349 (1948); (d) G. S. Smith, *Nature*, **163**, 290 (1949).

$$i_c = kCV \quad (2)$$

Equation 2 was verified by measurement of the capacity of mercury in chloride solutions⁷; the results agree well with those of Grahame⁸ obtained using a Wheatstone bridge.

To obtain a straight-line plot of i_p vs. $V^{1/2}$, correction must be made for i_c and the ohmic drop.⁴

In all of the investigations cited, solutions were used from which oxygen had been removed or to which maxima suppressors had been added. This was done to avoid the maximum mentioned.

Test of Peak Current Relation.—The validity of equation 1 was tested for solutions saturated with air for various Cd(II) concentrations at three different initial potentials (-0.1 , -0.3 and -0.5 v.), since the heights of the oxygen maximum and cadmium reduction wave were quite dependent on this factor. K values obtained for the Cd(II) reduction at an initial potential of -0.5 v. and a frequency range of $V^{1/2}$ (Table I) indicate that a linear relationship exists at the lower sweep frequencies, but a deviation at the higher frequencies; K for the anodic waves are fairly constant except at the extreme low and high frequencies. Data obtained at starting potentials of -0.1 and -0.3 v. show similar trends, although the best agreement with equation 1 was obtained at a starting potential of -0.5 v. This is due primarily to the much larger maximum occurring at starting potentials of -0.1 and -0.3 v. than at -0.5 v. Distortion of a wave may occur when successive waves are close together,⁵ as was observed in the present case.

TABLE I

CALCULATED K VALUES FOR THE RELATION: $i_p = KC_M V^{1/2}$
(Initial potential of -0.5 v. vs. mercury pool)

Cd(II) concn., mM	$V^{1/2}$ or $(dE/dt)^{1/2}$ (v./sec.) ^{1/2}	Cathodic branch		Anodic branch	
		i_p , $\mu\text{a.}$	K	i_p , $\mu\text{a.}$	K
1	2.20	0.090	41	0.135	61
	3.12	.129	41	.154	49
	4.43	.167	38	.205	46
	6.34	.265	42	.298	47
	8.75	.325	37	.318	36
0.3	2.25	.029	43	.031	46
	3.20	.039	41	.052	54
	4.48	.068	45	.073	54
	6.38	.097	50	.112	58
	8.93	.140	52	.160	60
0.1	2.25	.012	53	.013	58
	3.20	.016	50	.022	67
	4.45	.023	51	.030	67
	6.30	.034	54	.040	64
	9.00	.053	59	.067	74

Table II gives average K values for the five different sweep frequencies used at each starting potential and each Cd(II) concentration. In the presence of oxygen K for the Cd(II) reduction is dependent on the starting potential and on the Cd(II) concentration; the anodic K values appear to be less dependent on these factors.

The lower cathodic K values at starting potentials of -0.1 and -0.3 v. and at higher Cd(II) concen-

(7) J. W. Loveland and P. J. Elving, *THIS JOURNAL*, **56**, 250 (1952).

(8) D. C. Grahame, *Rec. Chem. Prog.*, **11**, 93 (1950).

TABLE II

AVERAGE K VALUES FOR THE RELATION $i_p = KC_M V^{1/2}$, AT DIFFERENT INITIAL POTENTIALS

Cd(II) concn., mM	Initial potential, v.	K Values		Ratio of $K_{cath} : K_{anod}$
		Cathodic	Anodic	
1	-0.1	30	58	0.52
	-0.3	30	48	.62
	-0.5	40	48	.84
0.3	-0.3	33	58	.57
	-0.5	46	54	.85
0.1	-0.3	48	66	.73
	-0.5	54	66	.82

trations are influenced by the larger maxima observed at these conditions, as discussed in the next section.

The K value of 30 to 54 for the Cd(II) reduction compares favorably with those of Randles,^{6b} where a K of 49 for 0.25 mM Cd(II) in degassed 1 M KCl solution can be calculated. K , of course, is dependent on electrode characteristics, but if one assumes that there is not too much difference between the present conditions and those of Randles, this is fair agreement, particularly if one considers only data at a starting potential of -0.5 v., where the effect of the oxygen maximum is minimized. The average K value at -0.5 v. starting potential is 47.

Oxygen Maximum.—A primary reason for undertaking the present study was to investigate the cause of the oxygen maximum. If the solution is purged with nitrogen or sufficient gelatin is added, the maximum disappears.

Investigation⁹ of the effect of oxygen on the Cd(II) reduction by conventional polarography indicated that i_d for Cd(II) was suppressed to a greater or less extent in neutral or alkaline solution, presumably due to a cadmium hydroxide film formed around the mercury surface with the hydroxide ion concentration necessary being furnished by the OH^- produced in the first and second reduction stages of oxygen.¹⁰ There was no effect in acidic solution.

The variation of i_{max} for the CRO observed oxygen maximum with sweep frequency at various starting potentials is shown in Fig. 2. The variation of i_{max} with starting potential for various Cd(II) concentrations is shown in Fig. 3A; the dependency of i_{max} on Cd(II) concentration for various potential sweep rates is shown in Fig. 3B.

The height of the oxygen maximum varies linearly with V in a 1 mM Cd(II) solution (Fig. 2). Similar plots for 0.3 and 0.1 mM Cd(II) solutions are less linear; i_{max} actually decreases with increasing

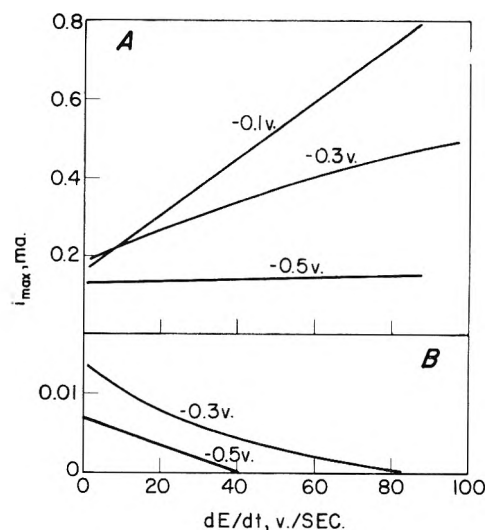


Fig. 2.—Oxygen maximum current vs. rate of potential variation for (A) 1 mM CdCl₂ and (B) 0.1 mM CdCl₂.

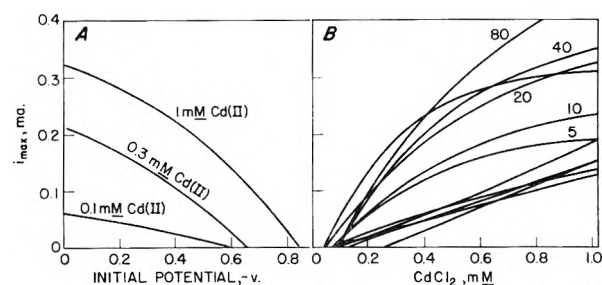


Fig. 3.—(A) Oxygen maximum current vs. initial potential at 10 c.p.s. or 20 v./sec. (B) Oxygen maximum current vs. CdCl₂ concentration. The top (numbered) family of curves has an initial potential of -0.3 v.; the bottom family one of -0.5 v.; the numbers refer to V , v./sec., for a 2-v. potential span; the bottom family of curves has the same V values.

frequency for 0.1 mM Cd(II). If i_{max} were proportional to V , one could conclude that the maximum phenomenon is due to adsorption (capacitive change). If i_{max} were proportional to $V^{1/2}$, the reduction of oxygen would be indicated. Plots of i_{max} vs. V gave more nearly straight lines than did plots of $i - V^{1/2}$, although in neither case was an ideal plot realized; consequently, the phenomenon is due, at least in part, to adsorption effects.

Since i_{max} is dependent upon starting potential (Fig. 3A), a process occurring at the electrode surface prior to the cadmium reduction is suggested. In addition, the dependence of i_{max} on cadmium concentration (Fig. 3B) indicates that cadmium is involved in the process. When KI is used as a background electrolyte, no oxygen maximum appears at any initial potential (Fig. 4A), indicating either that chloride ion contributes to formation of the maximum or that iodide ion prevents it from appearing.

Origins of the Current Variations.—If, in oxygen-containing solutions, i_p is assumed to be proportional to concentration of the oxidized or reduced species, the data can be interpreted to cast additional light on the reduction process. At any particular concentration of Cd(II) there is an increase in the amount of Cd(II) reduced as the starting potential increases from -0.1 to -0.5 v., as

(9) I. M. Kolthoff and C. S. Miller, *J. Am. Chem. Soc.*, **63**, 1013 (1941); W. Kemula and Z. R. Grabowski, *Collection Czechoslov. Chem. Commun.*, **15**, 1085 (1950).

(10) When oxygen is polarographically reduced in neutral solution, the hydroxide ions formed in the first and/or second reduction stages can react with any heavy metal ions present to produce a precipitate near the mercury drop. In addition, in a cell with an internal pool anode and a solution containing a large chloride ion concentration, an appreciable reduction of the dissolved oxygen to H_2O_2 and OH^- can occur, e.g., I. M. Kolthoff and J. J. Lingane, "Polarography," Interscience Publishers, New York, N. Y., 1952, pp. 396 and 553-554, and B. Behr and J. Chodkowski, *Roczniki Chem.*, **26**, 650 (1952); *C. A.*, **48**, 3816i (1954).

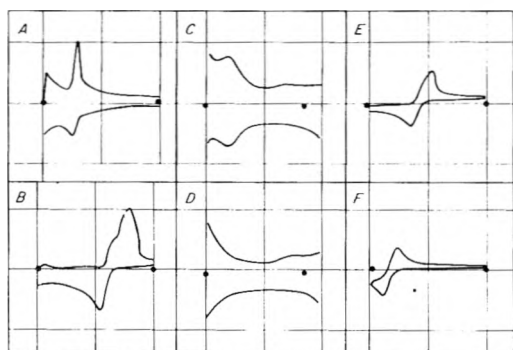


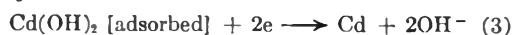
Fig. 4.—(A) Trace of i - E curve for solution, 0.1 mM in $CdCl_2$, 1 M in KI , and saturated with air. (B) Trace of i - E curve for solution, 1.0 mM in $CdCl_2$, 1 M in KCl , and saturated with air. (C) Effect of gelatin on oxygen maximum in 1 M KCl solution. (D) Effect of gelatin on oxygen maximum in 1 M KCl solution, containing 0.005% gelatin and saturated with air. (E) and (F) Effect of initial potential; solution, 1 mM $CdCl_2$, 1 M KCl , 0.005% gelatin, saturated with air. (The heavier lines of the CRO grid (every tenth line) have been shown to indicate the actual trace magnitude.)

Fig.	Frequency c. p. s.	R , ohms	Sensi- tivity, mv./in.	Left dot, v.	Right dot, v.
A	10	20	2	-0.118	-1.103
B	40	5	5	-0.080	-1.091
C	10	60	2	-0.165	-1.558
D	10	60	2	-0.214	-1.597
E	10	12	5	-0.254	-1.270
F	10	12	5	-0.537	-1.510

Fig.	Initial potential, v.	Span, v.	$i_{Cd(red)}$, ma.	$i_{Cd(ox)}$, ma.	i_{max} , ma.
A	-0.118	1.000	0.080	0.029	
B	-0.080	1.011	0.47	0.69	0.75

shown by the average K values. Secondly, in going from 1 to 0.1 mM $Cd(II)$, there is an increase in the proportion of Cd reduced at starting potentials of -0.3 v. and -0.5 v. This indicates that a thick cadmium hydroxide barrier exists at 1 mM $Cd(II)$, and a thin barrier at 0.1 mM $Cd(II)$, as one might expect.

If the anodic peak height (coulometric integration beneath the curve is better) is assumed to indicate the amount of cadmium ion reduced, the following can be deduced: Where K anodic values are the same, the same proportion of $Cd(II)$ was reduced. In such cases, equal K values should be seen for the reduction of cadmium, but they are not. Therefore, some cadmium probably is reduced during the maximum peak. For example, in Table II at 1 mM $Cd(II)$, the anodic K values at -0.3 and -0.5 v. are both 48; the cathodic values are 30 and 40, respectively. The 30 value at -0.3 v. should be at least 40 to give enough cadmium for the anodic K value of 48. One might then postulate, that in addition to the $Cd(II)$ reduced to give the K value of 30, there is an irreversible adsorption of a $Cd(OH)_2$ film, together with a reduction of the film, e.g.



The reduction of the film gives the additional current flow required to meet the anodic K value of 48.

This appears to tie in with the higher i_{max} peaks observed at -0.1 than at -0.3 v., both of which are greater than those at -0.5 v. The sums of i_p

(cathodic) plus i_{max} are greater than i_p (anodic), but one may surmise that the integrated areas may be close to equal. Calculation of areas on several cathodic and anodic peaks indicates that where maxima occur the cadmium reduction area is less than anodic area, but the total cadmium reduction area plus the maximum area is always equal to or generally greater than the anodic area. Thus, the maximum is both faradaic and capacitive in nature.

The peak for the usually observed irreversible reduction of oxygen can be observed at about -0.1 v. (far left of the cathodic trace, Fig. 4B) as expected for the first oxygen wave. It is the authors' belief that the more negative oxygen maximum observed in the present and other CRO studies is due to both the capacity current and the reduction current arising from the formation of a film of cadmium hydroxide or cadmium hydroxy chloride around the mercury drop.¹⁰ The magnitude of the capacity current should be proportional to the thickness and extent of the adsorbed film and its dielectric properties. At low negative potentials there are more Cl^- and OH^- ions at the surface, i.e., in the inner Helmholtz layer. As the negative potential is increased, the anions are repulsed and cations come in closer. At a starting potential of -0.1 v. there is a greater OH^- concentration than at one of -0.5 v. Consequently, a $Cd(OH)_2$ film is formed more easily at -0.1 v. than at -0.5 v.

At 0.1 mM cadmium ion concentration, no oxygen maximum is evident at rates above 40 v./sec. at an initial potential of -0.5 v. (Fig. 2B). A small maximum is present at all frequencies at a starting potential of -0.1 v. Apparently, there are insufficient $Cd(II)$ ions present near the electrode to form a film even though the oxygen concentration is the same at all $Cd(II)$ concentrations. The oxygen concentration in pure water in equilibrium with air at 25° and 760 mm. is 0.25 mM and somewhat less in electrolyte solution. Since the two-wave oxygen reduction yields 4 hydroxide ions, the solution in the vicinity of the electrode may be as high as 1 mM OH^- , equivalent to 0.5 mM cadmium in formation of the hydroxide. At higher $Cd(II)$ concentration, there would be an excess of cadmium ions, and, if the hydroxide film is the cause of the maximum, a leveling off of the height of the maxima would be expected above 0.5 mM cadmium. This is actually the case, e.g., Fig. 3B.

Failure of a maximum to appear in 1 M KI solution (Fig. 4A) can be explained by the greater stability of the iodocadmium complex as compared to the chloro.¹¹

Influence of Gelatin on the Cadmium-Oxygen Maximum.—Maximum suppressors have long been used in polarography, yet the mechanisms by which they achieve their effects are still uncertain. Gelatin has been the most thoroughly investigated suppressor; the two main theories of the mechanism of gelatin action are based on adsorption and complexation.^{12,13} The adsorption theories are further

(11) I. M. Kolthoff and J. J. Lingane, "Polarography," Interscience Publishers, New York, N. Y., 1952, pp. 509 and 554.

(12) B. Keilin, *J. Am. Chem. Soc.*, **70**, 1984 (1948); J. Heyrovsky and M. Matyas, *Collection Czechoslov. Chem. Commun.*, **16/17**, 455 (1951/1952); J. E. Strassner and P. Delahay, *J. Am. Chem. Soc.*, **74**,

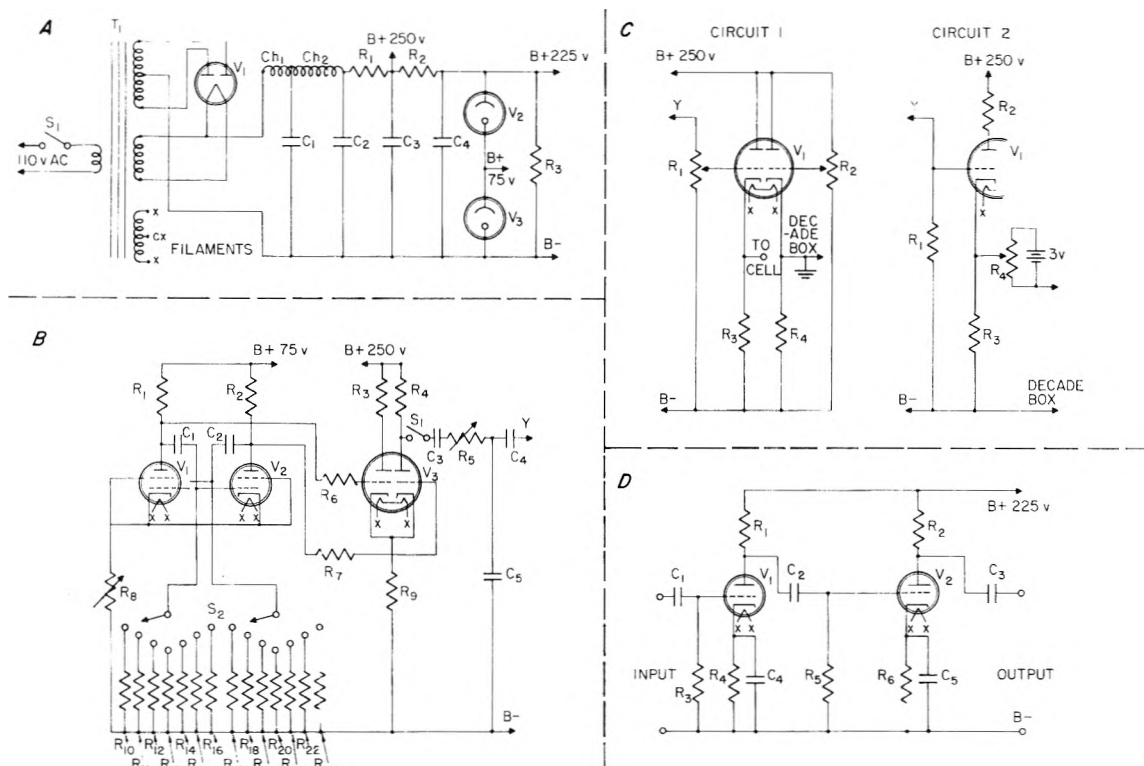


Fig. 5.—Circuit diagrams of the electronic apparatus.

(A) Power supply

S_1	SPST switch	Ch_2	choke, 8 hys.
T_1	transformer, Thordarson No. T 22R06	C_1, C_2, C_3	20-mfd., 450-wv. electrolytic
V_1	full-wave rectifier tube, 5Y3	C_4	4-mfd., 350-wv. electrolytic
V_2	voltage regulator tube, OD3	R_1, R_2	600-ohm, 10-watt wire-wound
V_3	voltage regulator tube, OA3	R_3	30 K-ohm, 5-watt wire-wound
Ch_1	choke, 5-10 hys., swinging		

(B) Triangular wave generator (R_{10} to R_{23} are 0.5-watt precision resistors, $\pm 1\%$ of rated value)

S_1	SPST switch	R_6, R_7	470K-ohm, 0.5 watt
S_2	2-gang, 8-position rotary switch	R_8	400-ohm, 0.5-watt
V_1, V_2	gas-filled tubes, 2050	R_9	12K-ohm, 1-watt
V_3	vacuum tube, 69N7	R_{10}, R_{17}	100K-ohm
C_1, C_2	0.005-mfd, 450-wv.	R_{11}, R_{18}	250K-ohm
C_3, C_4	1-mfd. 450-wv.	R_{12}, R_{19}	500K-ohm
C_5	0.5-mfd, 450-wv.	R_{13}, R_{20}	1-megohm
R_1, R_2	20K-ohm, 0.5-watt	R_{14}, R_{21}	2-megohm
R_3, R_4	50K-ohm, 0.5-watt	R_{15}, R_{22}	3.5-megohm
R_5	5-megohm, 0.5-watt	R_{16}, R_{23}	5.6-megohm

(C) Output circuits

Circuit 1

V_1	Vacuum tube, 6SN7
R_1, R_2	500K-ohm, 0.5-watt variable
R_3	620-ohm, 1-watt
R_4	630-ohm, 1-watt

Circuit 2

V_1	Vacuum tube, $1/2(6SN7)$
R_1	500K-ohm, 0.5-watt
R_2	1000-ohm, 1-watt
R_3	124-ohm, 1-watt
R_4	30-ohm, 2-watt wirewound

(D) Preamplifier circuit

V_1, V_2	vacuum tube, 6SF5	R_1, R_2	0.22-megohm, 0.5-watt
C_1, C_2, C_3	0.5-mfd., 450-wv.	R_3, R_5	0.15-megohm, 0.5-watt
C_4, C_5	25-mfd., 50-v. electrolytic	R_4, R_6	4K-ohm, 0.5-watt

divided on the basis that the adsorption of gelatin around the mercury drop results in (a) the prevention of ionic diffusion to the drop, (b) disruption of the capacity of the electrical double layer, or (c) retardation of the rate of reaction at the electrode interface.

The present study indicates that gelatin acts as a maximum suppressor because it is adsorbed on the electrode interface, thereby changing the capacitance of the dielectric layer.

6232 (1952); R. H. Coe and L. B. Rogers, *ibid.*, **70**, 3276 (1948).
(13) L. Meites and T. Meites, *ibid.*, **73**, 177 (1951).

Typical results are shown in Fig. 4. The capacity current bumps are evident on the left (Fig. 4C). After the addition of 0.005% gelatin, the oxygen wave is still evident but the capacity pattern has been almost completely removed (Fig. 4D). At 0.01% gelatin both the capacity and oxygen waves are completely removed.

The critical gelatin concentration necessary to disrupt completely the capacity pattern was determined by plotting i_c vs. concentration for 1 M KCl solutions saturated with air and with nitrogen. The results were the same in both cases,

i.e., 0.006%, in good agreement with the value of 0.005%, above which the capillary drop-time is affected.¹³

In 1 *M* KI solution, 0.01% gelatin was sufficient to disrupt completely the capacity pattern.

In another similar series of experiments on solutions of Cd(II) in 1 *M* KCl, 0.005% gelatin almost completely suppressed the oxygen maximum while 0.01% completely suppressed it and at the same time somewhat shifted $E_{1/2}$ for the Cd(II) reduction.

Interesting phenomena were observed which are significant in showing that the gelatin effect is related to the rate of growth of the surface area of the mercury drop as well as to the surface area itself, thus adding weight to the adsorption theory of maximum suppression. As drop formation begins in a solution of 1 mM Cd(II) in 1 *M* KCl, saturated with air and containing 0.005% gelatin, both the cadmium reduction peak and the oxygen maximum are slightly evident. As the drop grows, the two peaks blend into one wide peak. At the starting potential used in Fig 4E, the cadmium reduction peak is suppressed and combined with the oxygen maximum. As the potential span is shifted to more negative values, the contribution of the oxygen maximum to the combined peak is reduced while that of the cadmium peak is emphasized. Thus, as the initial potential is made more negative, $E_{1/2}$ approaches that of the cadmium reduction peak in oxygen-free solution (Fig. 4F). When the gelatin concentration exceeds 0.005%, only one wide reduction peak is observed regardless of the drop formation stage and the potential span setting.

A similar effect was observed with 0.005% gelatin in 1 *M* KCl. The capacity current peaks are slightly evident at the time drop-formation begins, but disappear as the drop grows. With 0.01% gelatin the peaks are not evident at any time during the growth of the mercury drop.

It seems likely that the bulky gelatin molecule adsorbed is capable of withholding any Cd(OH)₂ from being adsorbed on the surface of the electrode. From the capacity oscillograms it is observed that gelatin is adsorbed at lower negative potentials than that at which Cd(II) is reduced. Cd(II) ions slip through and are reduced. Oxygen also slips through and the OH⁻ ions produced form Cd(OH)₂. However, the precipitate has less space to be adsorbed because of the prior adsorption of gelatin. Hence, there is less capacity current change and less chance of reduction of Cd(OH)₂. At concentrations of gelatin greater than 0.006% the surface of the mercury is completely covered with gelatin. Only the mobile Cd(II) ions and O₂ are able to slip through to the Hg surface, but with reduced speed. The more immobile Cd(OH)₂, although formed quite close to the surface, cannot be adsorbed. Actually, if transfer of electrons *via* a chloride bridge is postulated, reduction may take place a few atomic distances away from the electrode which allows room for gelatin between the Hg surface and the precipitate.

The following definite conclusions can be stated:

(a) Gelatin disrupts the capacity current of the

potassium chloride and potassium iodide solutions, the critical gelatin concentration necessary to disrupt completely the capacity current being 0.006%. (b) Gelatin suppresses the oxygen maximum associated with the CRO Cd(II) reduction wave. (c) This maximum is due to both the capacity and reduction currents arising from a cadmium hydroxide film formed around the electrode. (d) The effects of gelatin are related to the area and rate of growth of the mercury drop. (e) Gelatin disrupts the capacity current and suppresses the oxygen maximum by interfering with the film formation through an adsorption mechanism.

Experimental

Apparatus.—The block diagram of the apparatus is the same as Fig. 1 of reference 7. However, all of the electrical components other than the oscilloscope have been combined into a single instrument, *i.e.*, items A, B, C and E, and the power supply are combined on one chassis, and D and F are the amplifiers in the oscilloscope used. Thus, the experimental arrangement consists of two instruments connected to a polarographic cell.

Figure 5 is a circuit diagram of the electronic apparatus (omitting the CRO), which was assembled in accordance with accepted procedure in electronic device construction: connections were soldered, leads kept as short as possible, and wiring insulated or shielded as necessary. Components were of the highest quality and within the required tolerances. No attempt will be made to show mathematically the interrelation between the various tubes, resistors and capacitors; instead, it will be indicated how the various portions of the circuit work together to form a complete instrument.

The d.c. power supply (Fig. 5A) furnishes a steady a.c.-free voltage to the various tubes in the instrument. After rectification (V_1), the current passes through an LC-RC filtering network which removes at least 99.99% of the a.c. component. Voltage regulator tubes V_2 and V_3 maintain a steady voltage.

The triangular wave generator (Fig. 5B) consists of items A and B of Fig. 1 of reference 7. V_1 and V_2 (gas-filled tetrodes wired in a multi-vibrator circuit) produce a very good square wave, whose frequency is controlled by switch 2 and variable resistor R_8 . This square wave is amplified and corrected by V_3 , and at switch 1 has a peak to peak amplitude of 110 v. and is almost perfectly symmetrical. The square wave is then electrically integrated by a simple RC circuit (R_5 - C_5) to produce a triangular wave form; R_5 is varied to produce the best integration at the frequency being used. The triangular wave at the generator output has a peak to peak voltage of about 6 v.

To avoid distortion of the polarographic trace, the triangular wave must be applied to the cell through a low resistance circuit. The cathode follower output circuits of Fig. 5C fit the requirement. At the same time provision must be made to control the d.c. component of the triangular wave. Circuit 1 is a depressed B-cathode follower circuit. R_1 controls the amplitude of the triangular wave and thus the potential span of the applied voltage. R_2 controls the d.c. component and thus regulates the starting potential of the triangular sweep. The effective resistance introduced into the cell circuit by R_3 and R_4 can mathematically be shown to be less than 200 ohms. When this circuit is used, the apparatus is completely line-operated. Circuit 2 is a conventional cathode follower output; when this circuit is used, the potential span is controlled by R_5 of Fig. 5B and the initial potential by R_4 of Circuit 2.

Use of the voltage preamplifier (Fig. 5D) in conjunction with the CRO amplifier allows the use of a small resistance at R in Fig. 1 of reference 7. In practice, R was a Leeds Northrup No. 4748 decade box. The capacitors used in the preamplifier have a large enough time constant and sufficient current leakage to enable it to act as a d.c. amplifier for small input voltages.

Testing and Calibration.—The assembled apparatus was tested by the following procedures: (a) The symmetry of the triangular wave form was checked by CRO presentation at various frequencies. (b) The d.c. component of the output voltage was checked with a vacuum-tube voltmeter.

(c) The amplitude of the triangular wave was measured with a DuMont voltage calibrator in conjunction with the CRO. The maximum amplitude was 3 v. peak to peak; 2 v. is sufficient for most work in oscillographic polarography. (d) The a.c. component of the d.c. power supply was found to be less than 0.01%. (e) The frequency range of the triangular sweep, determined using a DuMont signal generator and the CRO, was 1 to 200 c.p.s. The fine and coarse frequency controls were calibrated at this time. (f) As a final check, the instrument was used to obtain an oscillographic trace for a solution 1 m.M. in cadmium chloride and 1 M in potassium chloride; a d.m.e. was used with a mercury pool reference electrode. The result was visually compared with those obtained by previous investigators.

The strong 60-cycle interference originally present was largely eliminated by using shielded leads for all external connections; further reductions were achieved by wrapping the mercury reservoir and hose with aluminum foil connected to ground and placing the entire apparatus on a grounded copper sheet. The slight amount of interference remaining did not hinder observation of the trace.

Chemicals.—Oil-free air and oxygen-free nitrogen were obtained using customary gas purifying trains. Mallinckrodt A.R. grade potassium chloride, potassium iodide and cadmium chloride were used.

Procedure.—Since the depressed B-cathode for lower output circuit (Fig. 5C) would not develop the sufficiently negative starting potentials (-0.5 v.) desired for the present experiments, the conventional cathode follower output circuit was used. A mercury pool in the polarographic cell bottom served as reference electrode. The resistance of the dropping mercury electrode (d.m.e.) was considerably lowered by sealing a platinum wire into the capillary tube about 0.5 inch from the tip; the resistance was then about 10 ohms. At the mercury column height of 84 cm. used throughout, the drop-time was 12.6 sec. and the rate of flow of mercury was 0.344 mg./sec. The total cell resistance with 1 M KCl solution and the capillary was repeatedly measured, using 1000 c.p.s. and a Wheatstone bridge; a value of 50 ohms was consistently obtained.

In an experiment, the cell, maintained at $25 \pm 1^\circ$ and containing the mercury pool, was filled with the test solution. In the oxygen runs, air was then bubbled through the solution for 5 min. to saturate it; in the oxygen-free

runs, nitrogen was bubbled through for 20 min. In the meantime, the apparatus was allowed to warm up.

The triangular wave generator was set to the desired frequency, initial potential and potential span. The vertical and horizontal centering and horizontal amplifier controls of the CRO were then adjusted to produce a 2-in. wide pattern in the center of the screen. With the vertical CRO amplification control advanced to a previously calibrated sensitivity of 2 to 5 mv./in., the pattern was adjusted to a height of about 2 in. using R. In this manner, the resistance, R, was kept to a minimum, and the trace was large enough for accurate measurement, yet not so large as to be distorted by the screen curvature.

The trace was photographically recorded by multiexposure on 35-mm. Eastman Kodak Plus X film, using a DuMont No. 271-A oscillographic record camera and 0.5-sec. exposure at f5.6. The photograph of the trace itself was always taken 10 sec. after the drop began to form, timed to ± 0.1 sec. using a stopwatch. To obtain details of the trace against the plastic grid of the screen, the procedure described was followed. After photographing the trace, the triangular wave was temporarily shut off, using switch 1 (Fig. 5B), resulting in cessation of the voltage sweep to the cell; a spot then appeared on the screen, whose horizontal position was indicative of the applied potential relative to the mercury pool. The latter potential was measured to ± 1 mv. on a potentiometer connected across the cell and an exposure of the spot taken. The applied potential then was changed by means of the initial potential regulator control (R, circuit 2, Fig. 5C), another reading made on the potentiometer, and the new spot photographed. Two points thus were obtained, from which the potential span and the initial potential of the triangular sweep could be calculated. Next, the spot was deflected off the screen, the brightness turned up to give a slight glow and the final exposure made, recording the calibration lines on the grid.

Acknowledgments.—The authors wish to thank the Atomic Energy Commission and the Office of Naval Research for helping to support this investigation. Thanks are also due to Professor Charles Marsh, who helped design the electronic equipment used, and to Professor John R. Hayes.

DIFFUSION OF SILVER IN SILVER SULFIDE¹

BY ROY L. ALLEN AND WALTER J. MOORE

Chemical Laboratory, Indiana University, Bloomington, Indiana

Received August 6, 1958

Diffusion of radioactive Ag-110 in silver sulfide has been measured in polycrystalline specimens of the low temperature (monoclinic) and high temperature (cubic) form. The diffusion coefficients are: cubic Ag_2S , $D'_{\text{Ag}} = 2.8 \times 10^{-4} \exp(-3450 \text{ cal./RT}) \text{ cm.}^2 \text{ sec.}^{-1}$ and monoclinic Ag_2S , $D_{\text{Ag}} = 1.4 \times 10^{-2} \exp(-11,100 \text{ cal./RT})$ to $2.7 \times 10^{-3} \exp(-9800 \text{ cal./RT}) \text{ cm.}^2 \text{ sec.}^{-1}$. The D_{Ag} is sensitive to conditions of preparation but D'_{Ag} is not. Neither D_{Ag} nor D'_{Ag} appears to depend on the effective vapor pressure of sulfur during preannealing, and thus the diffusion is probably not caused by defects due to departure from stoichiometry in the Ag_2S structure.

Silver sulfide crystallizes in a low temperature monoclinic form, the crystal structure of which has recently been determined,² and in a cubic form above the transition temperature of 177° . The structure of the high temperature form appears to consist of a body-centered-cubic array of sulfur atoms with silver atoms randomly distributed among the interstitial sites.³ Diffusion of silver and sulfur in the low temperature form was measured by Mme. Pechanski⁴ by means of the ex-

change between radioactive silver nitrate and sodium sulfide solutions and finely divided crystallites of silver sulfide in suspension. This method is satisfactory, but has a limited accuracy owing to the size distribution of the crystallites and the necessity of approximating their geometric form by spheres. She found $D_{\text{S}} = 0.24 \exp(-26.3 \text{ kcal./RT}) \text{ cm.}^2 \text{ sec.}^{-1}$ and $D_{\text{Ag}} = 9.3 \times 10^{-1} \exp(-9.1 \text{ kcal./RT})$. The diffusion of S-35 in cubic Ag_2S was reported⁵ to be $D'_{\text{S}} = 2.4 \times 10^{-4} \exp(-24.0 \text{ kcal./RT})$. It is not easy to reconcile this result with that for D_{S} . No measurements of diffusion of silver in cubic silver sulfide have been

(1) This work was supported by the U. S. Atomic Energy Commission, Contract No. AT-(11-1)-250. Contribution No. 829 from the Chemistry Department of Indiana University.

(2) A. H. Fruch, *Z. Krist.*, **110**, 2 (1958).

(3) P. Rahlfs, *Z. physik Chem.*, **B31**, 157 (1936).

(4) D. Pechanski, *J. chim. phys.*, **47**, 157 (1936).

(5) M. Ishiguro, F. Oda and T. Fujino, *Mem. Inst. Sci. Indus. Res., Osaka University*, **10**, 1 (1953).

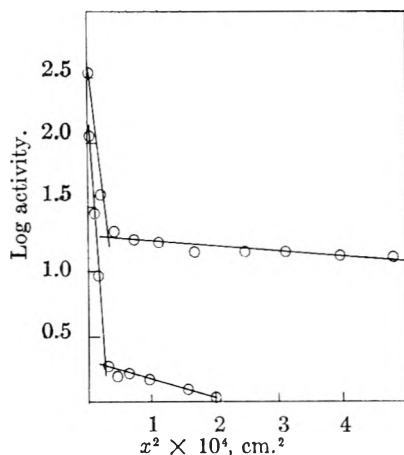


Fig. 1.—Two runs at 204° showing the anomalous penetration curves from a sulfided layer of evaporated Ag-110 on Ag₂S.

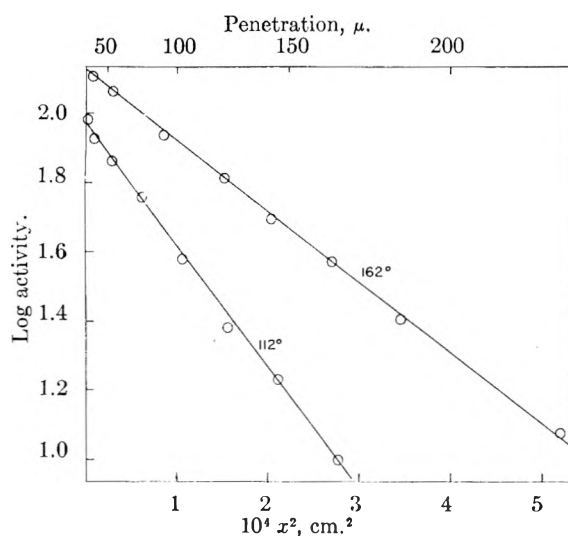


Fig. 2.—Typical penetration curves in monoclinic Ag₂S in accord with eq. 1 after exchange of Ag-110 with surface.

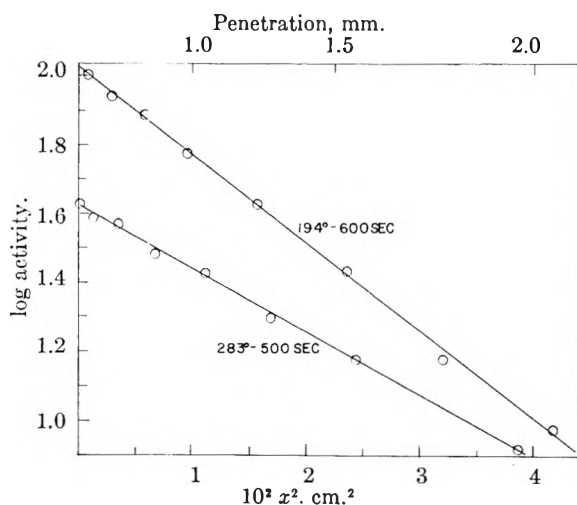


Fig. 3.—Typical penetration curves in cubic Ag₂S in accord with eq. 1 after exchange of Ag-110 with surface.

reported, although estimates of the diffusion coefficient have been made.⁶

In the present work, diffusion of silver in poly-

crystalline specimens has been followed both above and below the transition temperature by means of penetration of the radioactive silver-110 into silver sulfide.

Experimental Procedures

Silver sulfide was prepared by the reaction between sulfur vapor and silver. A current of pure dry nitrogen was passed over sulfur at 200° and thence over silver grain at 300°. The silver was a "Specpure" product from Johnson Matthey and Co. and the sulfur was a U.S.P. product recrystallized from carbon bisulfide. After the supply of sulfur was exhausted, the silver sulfide was heated in pure nitrogen for an additional hour at 300° in order to remove excess sulfur. The composition of the silver sulfide, determined by weight gain, was always stoichiometric within the limits of error, $\pm 0.01\%$.

The product was broken into small pieces and melted under vacuum in a sealed quartz tube. The tube was lowered slowly through a furnace maintained 100° above the melting point (825°), but attempts to prepare single crystals by this method were not successful because of the transition at 177°. Possibly single crystals of the cubic form could have been prepared if a method had been available for handling them at elevated temperatures. The grain size of the final product was about 0.01 mm. The surface of the rod of silver sulfide contained numerous small bubble holes. The rod was therefore machined until the diameter was reduced from 8.0 to about 6.5 mm., the surface then being free from imperfections. The rod was then cut into disks from 1 to 2 mm. in thickness for the studies on monoclinic Ag₂S, or 7 to 8 mm. for those on cubic Ag₂S. The disks usually were annealed for 140 to 150 hours at 300° in sulfur vapor at a pressure of 2.1 mm. In a few experiments the annealing was carried out at 400°, but no difference in the subsequent diffusion behavior was noted.

The radioactive tracer, Ag-110, was applied as an extremely thin layer to the ground surface of the disk. In the first experiments the silver was evaporated from a tantalum ribbon *in vacuo* and the active layer sulfided by means of hydrogen sulfide or sulfur vapor. In later experiments, a drop of active silver nitrate solution and a drop of nitric acid were placed on the surface of the disk and left for 30 minutes. Partial exchange took place with the result that some Ag-110 was transferred to the silver sulfide. The excess solution then was removed and the surface washed and treated briefly with water saturated with hydrogen sulfide, washed again and dried at room temperature. Autoradiographs of this surface revealed a uniform distribution of tracer.

Preliminary experiments were carried out on the high temperature form at 200 to 400°, with the specimens prepared by the evaporation method. The length of the diffusion anneal varied from 0.3 to 10 hours in helium, vacuum and sulfur vapor. In later experiments the pellets were pre-annealed at the diffusion temperature and a diffusion anneal initiated by evaporation of the radioactive silver onto the pellet held at the annealing temperature thus avoiding a heating and cooling cycle. The results of this first series of experiments were unusual. In all cases there was a high concentration *c* of Ag-110 on the surface, which decreased steeply until at approximately 50 μ depth the rate of decrease became considerably less steep. A typical curve of $\log c$ vs. x^2 is shown in Fig. 1. Two lines can be drawn through the points, corresponding to a slow diffusion followed by some more rapid process.

The cause of this anomaly is believed to be imperfect adherence of the active layer of silver sulfide. A microscopic examination of the evaporated layer of silver after sulfidation showed that in some cases it was formed of a mass of tiny crystals, which would make poor contact with the bulk of the disk. In two cases, whiskers of pure silver sulfide were observed growing outward from the surface. It appeared therefore that the standard method of applying the tracer by evaporation was not suitable in the present case because the silver sulfide formed from the active silver did not form a coherent thin layer. Probably the outward migration of the silver during the sulfidation process was too rapid. Therefore the second method of preparing the tracer layer was used in subsequent experiments, and no further difficulties due to anomalous penetration curves were encountered.

(6) C. Wagner *J. Chem. Phys.*, **21**, 1824 (1953).

The diffusion coefficients in both forms of silver sulfide are high, so that a special apparatus was constructed, adapted for short diffusion times and the use of thin specimens. The vessel holding the specimen was made of 0.010" stainless steel, flanged at the open end and provided with a stainless steel lid. The vacuum seal was an aluminum gasket. A 1/4 inch Kovar-Pyrex seal was brazed to the lid so that the vessel could be attached to a glass vacuum system. Two leads of a calibrated copper-constantan thermocouple were sealed through the glass. The specimen was placed in the diffusion vessel between two sheets of platinum foil and pressed tightly against the bottom by a steel spring. The thermocouple junction was soldered to another piece of platinum foil pressed tightly against the upper platinum covering of the disk, which was therefore sandwiched between the thin bottom of the diffusion vessel and the thermocouple junction. The vessel was evacuated to less than 10^{-6} mm. and in most cases filled with pure helium, but in some cases an atmosphere of sulfur vapor or a vacuum was used in the diffusion anneal. A cylindrical bored aluminum block was mounted in a furnace controlled with a platinum resistance thermometer to $\pm 0.1^\circ$. The block was filled with Wood's metal to accelerate heat transfer to the diffusion vessel. At the beginning of the anneal the diffusion vessel was plunged into the Wood's metal. The thermocouple showed that the specimen was heated to the desired temperature in approximately 40 sec., and after 15 sec. was only 3° below final temperature. Annealing times were usually 2000 sec. Following the anneal the vessel was cooled rapidly to room temperature by immersion in cold running water.

The specimens were sectioned on a precision grinder.⁷ This instrument also was used for the preliminary polishing of the circular disks to a standard size of 6.5 mm. by 1.5 mm. with parallel plane faces. The disk was attached to an aluminum mount by means of uncured Araldite 6060. Before sectioning, the outer edge of the disk was removed on a lathe to a depth of 1 mm., in order to eliminate possible effects of surface diffusion. Silicon-carbide paper of grades 2/0 to 4/0 was used for the sectioning and the surface so produced was planar to better than 0.1μ . After each section was removed the abrasive paper was folded into a tube and counted in a well-type scintillation counter with a γ -ray spectrometer. The counting was done on the peak at 0.9 mev. The mass of each section was determined by weighing the mounted disk on a Mettler single-pan microbalance, which afforded accuracy of ± 0.002 mg. The thickness of the section was calculated from the experimentally measured density of the silver sulfide. From 10 to 30μ was removed in each section.

Results of Diffusion Experiments

The solution of the diffusion equation for the case of a plane source on a semi-infinite solid is given by

$$c = c_0(\pi Dt)^{1/2} \exp(-x^2/4Dt) \quad (1)$$

where c is the activity of the tracer at time t and depth x , c_0 is the initial activity and D is the diffusion coefficient. Thus D can be calculated from the slope of a plot of $\log c$ vs. x^2 .

Typical experimental curves are shown in Fig. 2 for the low temperature silver sulfide and in Fig. 3 for the high temperature material. The excellent linearity of these plots indicates that there is good agreement with the diffusion model assumed. It also tends to indicate that grain boundary diffusion does not play a major role in the processes studied.

In Fig. 4 we have plotted the diffusion coefficients in the form of $\log D$ against T^{-1} . It will be noted that the coefficients for cubic silver sulfide fall on a single straight line and evidently minor changes in the preparative procedure and the annealing have little effect on this coefficient. In the case of the monoclinic silver sulfide, runs with any given preparation fall on a straight line, but there

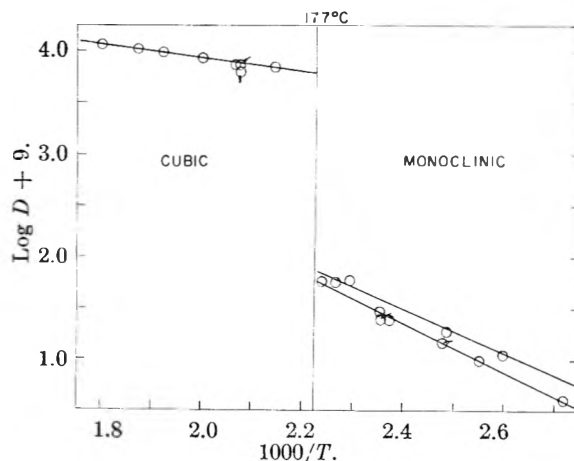


Fig. 4.—Diffusion coefficients of Ag-110 in Ag_2S above and below transition temperature: O, preannealed in S (2.1 mm.) for about 150 hr. at 300 to 400° . Run in He; \square , preannealed in He for 150 hr. at 375° . Run in He; \circ , preannealed in S (48 mm.) for 150 hr. at 375° . Run in S.

are different lines for different preparations. Only two extreme lines are shown; there were two other lines falling between them. In neither case, however, does there appear to be an appreciable dependence of the diffusion coefficient on the pre-annealing treatment of the silver sulfide. This independence is shown by the sets of experiments in which the specimens annealed in sulfur vapor are compared with the specimens annealed in helium. We may conclude that the diffusion coefficients do not depend on any non-stoichiometric defects in the structure of silver sulfide, in contrast with the usual situation in metallic oxides.

The least-squares values for the Arrhenius plots are represented by

Monoclinic Ag_2S

$$D_{\text{Ag}} = 1.4 \times 10^{-2} \exp(-11000 \text{ cal./RT}) \text{ to } 2.7 \times 10^{-3} \exp(-9800 \text{ cal./RT})$$

Cubic Ag_2S

$$D'_{\text{Ag}} = 0.28 \times 10^{-3} \exp(-3450 \text{ cal./RT})$$

The diffusion coefficient of silver in cubic silver sulfide is extraordinarily high, being about the same as that calculated for a gas of silver atoms at the same temperature and density. The transition temperature of 177° therefore represents a point at which the silver atoms in the structure lose the rigidity characteristic of the solid state, while the sulfur atoms retain a rigid structure.

The activation entropies for the diffusion processes can be calculated from the equation⁸

$$D = (kT/h)d^2 \exp(\Delta S^*/R) \exp(-\Delta H^*/RT) \quad (2)$$

if we assume a model for the jump distance d . Typical results at the transition temperature, 177° , are

$$\begin{aligned} \text{Monoclinic } d &= 1.52 \text{ \AA. } \Delta S^* = -1.5 \text{ to } +1.7 \text{ cal. deg.}^{-1} \\ \text{Cubic } d &= 1.22 \text{ \AA. } \Delta S^* = -0.7 \text{ cal. deg.}^{-1} \end{aligned}$$

These values of ΔS^\ddagger close to zero are consistent with models in which the silver is able to move without creating any additional disorder in the structures.

Our general conclusion is that diffusion of silver

(7) H. Letaw, L. M. Slifkin and W. M. Portnoy, *Rev. Sci. Instr.*, **25**, 865 (1954).

(8) H. Eyring and W. Wynne-Jones, *J. Chem. Phys.*, **3**, 492 (1935).

in silver sulfide is not determined by defects due to deviations from stoichiometry. All the silver atoms may be mobile in cubic Ag_2S whereas mobility in monoclinic Ag_2S may require displacement of a normal lattice silver into an interstitial position (Frenkel defect).

ADSORPTION OF RADIOSTEARIC ACID AND RADIOSTEARYL ALCOHOL FROM *n*-HEXADECANE ONTO SOLID SURFACES¹

BY HURLEY D. COOK AND HERMAN E. RIES, JR.

Research Department, Standard Oil Company (Indiana), Whiting, Indiana

Received August 11, 1958

The rate, extent and strength of adsorption of radiolabeled polar compounds from a hydrocarbon solution were measured directly on the window of a specially designed Geiger tube. Radiostearic acid and radiostearyl alcohol were adsorbed from dilute *n*-hexadecane solutions to form mixed films with the solvent on mica, and on iron and gold deposited on mica by thermal evaporation. Within a few minutes after contact between window and solution, 0.2 to 0.3 of a monolayer of polar compound was adsorbed; the ratio of polar compound to *n*-hexadecane in the first layer is, therefore, about 1:2. With the more inert surfaces of mica and gold, this ratio remained nearly constant for as long as one week of continuous contact. In the same length of time, iron surfaces adsorbed the equivalent of almost two monolayers of stearic acid but only one of radiostearyl alcohol. Strength of adsorption was studied by rinsing with solvents a thicker film that had been deposited from the vapor phase. Exhaustive treatment with benzene reduced such a stearic acid film to about 0.2 of a monolayer. Furthermore, mixed monolayers of stearic acid and *n*-hexadecane exert surface pressures on the film balance when only one-third of the area is occupied by stearic acid. This fraction is similar both to that observed initially in monolayers formed by adsorption from solution and to that remaining after extensive desorption. Possible structures of stable monolayers of stearic acid and *n*-hexadecane are schematically presented. Suggested distributions of vertically oriented molecules in a hexagonal close-packed configuration are consistent with both kinetic and equilibrium data.

Introduction

In studies of the adsorption of polar organic molecules from hydrocarbon solvents onto solid surfaces, the rate, extent and strength of adsorption are of primary interest. The monolayer, or first layer of adsorbed molecules, deserves special study; it is the only layer that can react chemically with the surface. Succeeding layers are held by much weaker physical forces. Little is known about how adsorbed films on solid surfaces compare with those formed under controlled conditions on the water surface of the film balance. Three techniques in the present study give information on rate, extent and strength of adsorption and provide information on the structure of monolayers.

Because radiolabeled polar molecules are uniquely suited to studies of adsorption, this area of research is growing rapidly.²⁻¹⁵ In the present study, a specially constructed Geiger tube with a metal-coated window was brought into direct contact with a hydrocarbon solution of radiolabeled polar mole-

cules. The rate and extent of adsorption could thus be measured continuously.¹⁰ Strength of adsorption is related to resistance of the adsorbed material on the window surface to various solvent treatments.

Information on the structure of the adsorbed films was obtained by spreading the same solutions used in the adsorption studies on the water surface of a film balance. The packing of polar and solvent molecules produced a mixed film in which the relative ratio of polar molecules to solvent molecules could be calculated. Monolayers consisting of two or more different kinds of molecules have been studied previously, but most investigations have been concerned primarily with mixtures of polar molecules, rather than of polar and non-polar molecules.¹⁶⁻²⁰

The present study was focussed on the adsorption of a long-chain fatty acid and the corresponding alcohol onto solid surfaces of widely different reactivity. Stearic acid and stearyl alcohol were chosen because they have the same hydrocarbon chain attached to a relatively strong and a relatively weak polar group. Stearic acid is a classical compound in monolayer studies and is representative of many types of lubricant additives. The solid surfaces, iron and gold, represent the reactive and non-reactive metals. The reactivity of iron is reflected in the many corrosion and wear problems found in industry; gold exhibits very low reactivity—it is unique in that it does not chemisorb oxygen.²¹

(1) Presented in part at the ACS Meeting, Miami, Florida, April 7-12, 1957.

(2) F. P. Bowden and D. Tabor, "The Friction and Lubrication of Solids," Oxford University Press, Oxford, England, 1950.

(3) D. E. Beischer, *THIS JOURNAL*, **57**, 134 (1953).

(4) J. E. Willard, *ibid.*, **57**, 129 (1953).

(5) N. Hackerman and R. A. Powers, *ibid.*, **57**, 139 (1953).

(6) H. A. Smith and K. A. Allen, *ibid.*, **58**, 449 (1954).

(7) E. Rideal and J. Tadayon, *Proc. Roy. Soc. (London)*, **A225**, 346 (1954).

(8) J. E. Young, *Austr. J. Chem.*, **8**, 173 (1955).

(9) J. W. Shepard and J. P. Ryan, *THIS JOURNAL*, **60**, 127 (1956).

(10) H. D. Cook, *Rev. Sci. Instr.*, **27**, 1081 (1956).

(11) H. D. Cook and H. E. Ries, Jr., *THIS JOURNAL*, **60**, 1533 (1956).

(12) H. E. Ries, Jr., H. D. Cook and C. M. Loane, in "Symposium on Steam Turbine Oils," ASTM Special Technical Publication No. 211, Philadelphia, Pa., 1957, p. 55.

(13) O. Levine and W. A. Zisman, presented before the Division of Colloid Chemistry, A.C.S. meeting, New York, N. Y., September 8, 1957 (preprint).

(14) H. A. Smith and T. Fort, ref. 13.

(15) H. Sobotka, ref. 13.

(16) N. K. Adam, "The Physics and Chemistry of Surfaces," 3rd Ed., Oxford University Press, Oxford, 1941.

(17) W. D. Harkins, "The Physical Chemistry of Surface Films," Reinhold Publ. Corp., New York, N. Y., 1952.

(18) G. H. A. Clowes, "Surface Chemistry," Ed. by F. R. Moulton, American Association for the Advancement of Science, Washington, D. C., 1943.

(19) E. D. Goddard and J. H. Schulman, *J. Colloid Sci.*, **8**, 309 (1953).

(20) H. E. Ries, Jr., and H. D. Cook, *ibid.*, **9**, 535 (1954).

Mica, used as a support for the metal films, ensured smooth and flat surfaces; it is itself representative of a relatively non-reactive and non-conducting surface.

Experimental

Solutions of radiostearic acid and radiostearyl alcohol in *n*-hexadecane were brought into contact with the mica or metal-coated mica window of a specially designed Geiger tube. The rate and extent of adsorption of the acid and alcohol onto the window were thus measured directly and continuously. The vapor-phase adsorption of radiostearic acid onto the Geiger-tube window and subsequent desorption by means of solvents were similarly investigated. Pressure-area isotherms also were obtained on related mixed films of stearic acid and *n*-hexadecane.

Materials.—The radiostearic acid (m.p. 69.6°), from the Nuclear Instrument and Chemical Corporation, was of the highest purity available. It was labeled with C-14 and had a specific activity of 0.97 millicurie per millimole. The radiostearyl alcohol, from the same source, was labeled with C-14 and had a specific activity of 0.93 millicurie per millimole.

Stearic acid (m.p. 69.61°) used in the film-balance experiments was a special preparation obtained from the Research Division of Armour and Company. The volatile spreading solvent was C.P. benzene that had been distilled twice to remove non-volatile impurities. Ion-exchange water used in the film balance was in equilibrium with atmospheric CO₂; it had a pH of 5.8 and a specific conductivity of less than 1 micromho. The *n*-hexadecane, from Humphrey-Wilkinson, was passed through a 14-foot silica gel column; this treatment reduced polar impurities to a negligible level, as shown by measurements of interfacial tension.

Apparatus.—A model D-47 gas-flow Geiger tube, obtained from the Nuclear Instrument and Chemical Corporation, was fitted into an open-ended stainless-steel cylinder with the counting chamber flush with the lower end of the cylinder. A sheet of cleaved Indian Ruby mica, obtained from Wakefield Industries, was cut into a circular disk 6.6 cm. in diameter and was mounted over the end of the outer cylinder in a friction-fitted steel cap. Threaded fittings and Teflon gaskets held the window firmly and prevented leakage of the solution into the window holder. The "Micro-mil" window supplied with the D-47 unit also covered the counting chamber; the mica windows could be changed between experiments without extensive flushing of the chamber.

The mica ranged from 1.5 to 2.0 mg. per sq. cm. and was used as received or was coated with iron or gold on both sides by thermal evaporation. Electron micrographs of both the mica and the metal-coated mica revealed extremely flat surfaces; less than 1% of the area examined showed "stair-step" roughness due to imperfect cleavage. The metal coatings were estimated to be 1000 to 2000 Å. thick and were electrically grounded to the Geiger tube. Each window was used for only one adsorption experiment.

The film balance and associated equipment have been described.^{11,20} The modified D-47 Geiger tube was used in place of the TGC-1 for obtaining the counting rate of radioactive monolayers on the water surface of the film balance.

Procedure.—About 10 ml. of a 0.05% solution (by weight) of the radioactive polar material in *n*-hexadecane was sufficient to fill a shallow cup placed directly under the Geiger-tube window. The cup had a diameter slightly larger than the tube window and was filled until the surface of the liquid was slightly above the edge of the cup. The entire tube assembly was lowered slowly to a position as close as possible to the liquid surface without making contact, and the counting rate of the solution surface was noted. The tube was then lowered into contact so that all of the window was wetted by the solution. Adsorption of the radioactive compound, evidenced by the increase in counting rate, was recorded for each two-minute interval after contact. After the initial rapid adsorption had slowed, intervals of 10 and then 30 minutes were used. All experiments were at room temperature, which varied from 21 to 24°.

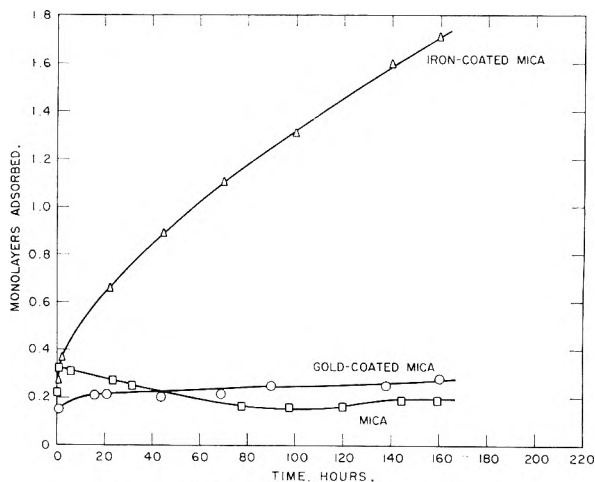


Fig. 1.—Adsorption of radiostearic acid.

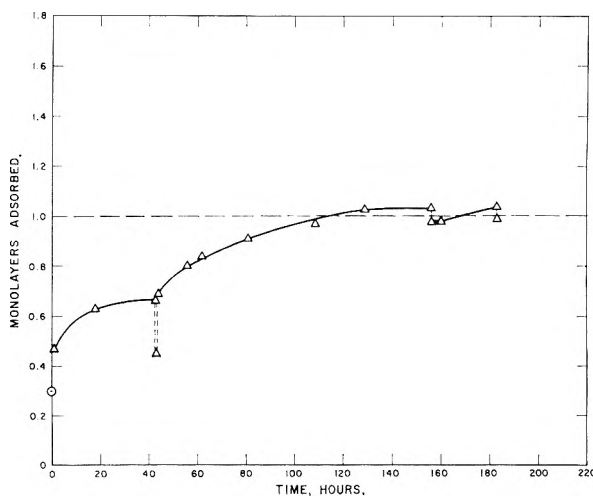


Fig. 2.—Adsorption of radiostearyl alcohol on iron.

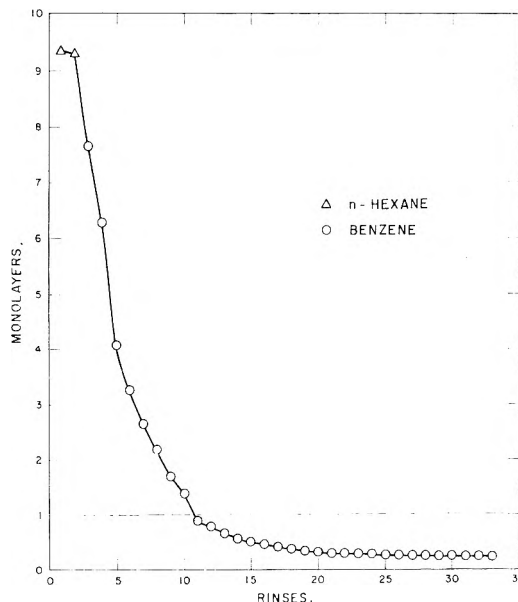


Fig. 3.—Desorption of radiostearic acid from mica.

To interpret the increase in counting rate in terms of monolayers adsorbed, the counting rate of a monolayer of the same radioactive compound was determined by bringing the Geiger-tube window as close as possible to the mono-

(21) B. M. W. Trapnell, *Proc. Roy. Soc. (London)*, **A218**, 566 (1953).

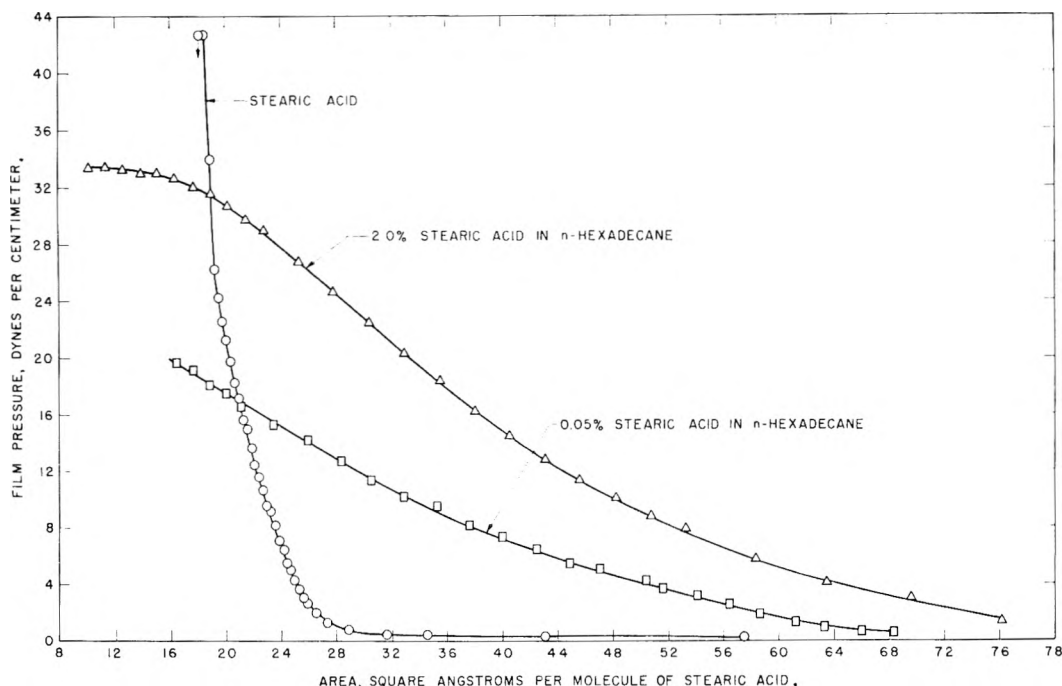


Fig. 4.—Pressure-area isotherms for stearic acid and *n*-hexadecane-stearic acid mixtures.

layer compressed to 30 dynes per cm. on the film balance.¹¹ The counting rate remained unchanged when the window was brought in contact with the monolayer on the water surface. The backscattering effect of the water was assumed to be about the same as that of *n*-hexadecane. The counting rate of a C-14 standard source was then determined with the same window assembly so that, with the standard source, subsequent windows could be corrected for variations in radiation absorption.

For the study of desorption by means of solvents, a plain mica window on the Geiger tube was brought within a few millimeters of the surface of a heated solution of radiostearic acid in *n*-hexadecane, and the vaporized stearic acid was allowed to condense on the tube window. Care was taken to keep the window far enough from the solution surface to allow multilayer film formation; when the window was placed about 0.5 mm. from the solution surface, it apparently became heated, and adsorption ceased at one monolayer or less.

To reveal how strongly the stearic acid was held, rinses of *n*-hexane and benzene were employed. The window, still held in the holder, was removed from the Geiger tube and mounted with the adsorbing surface up. Solvent was fed from a pipet onto the window near one edge, and was removed continuously by suction into a second pipet placed near the opposite edge. For each rinse, the pipets were adjusted to deliver and remove 50 ml. of solvent in one minute. The shallow cup formed by the edges of the window holder was kept full during this process; the depth of the flowing solvent was about 2 mm. At the end of the rinse the second pipet was lowered and all solvent was removed. After each rinse, the window was counted to determine the amount of radioactive material remaining.

Adsorption from Solution.—Figure 1 shows the adsorption of radiostearic acid onto mica, gold and iron surfaces from a 0.05% solution in *n*-hexadecane. In the first few minutes of contact, all of the surfaces were covered with 0.15 to 0.33 of a monolayer. The more-inert surfaces—mica and gold—showed little or no increase in coverage after the initial fast adsorption. The more reactive surface—iron—continued to adsorb after 160 hours of contact with the solution, although the rate diminished. Adsorption beyond the monolayer level may be due to the increased surface roughness that accompanies the formation of oxides of iron. This condition

may also account for the slightly higher initial adsorption observed in some of the experiments with iron. Stearic acid also may react chemically with iron or iron oxide surfaces, and the reaction products may remain on or near the metal surface.²²

The results of an experiment with radiostearyl alcohol on iron are shown in Fig. 2. In this and duplicate experiments, no adsorption beyond a monolayer was observed. The vertical dashed lines show the points at which a *n*-hexane rinse was applied after removing the radioactive solution from the window. When the rinse was used early in the experiment, about 0.2 of a monolayer could be removed, all of which apparently reabsorbed immediately when the window was again placed in contact with the solution. Rinsing the window at the end of the experiment removed only 0.05 of a monolayer. After about 20 hours and before the first rinse, the adsorption rate apparently decreased markedly.

A possible explanation is that the first molecules adsorbed are held by weaker physical forces and may require time to become activated individually to the chemisorbed state. Alternatively, the contact angle between the *n*-hexane solvent and the iron surface may undergo a great change when the adsorbed monolayer is about half completed.²³ The *n*-hexane may have to wet the iron surface for efficient solvent action.

Two additional experiments with radiostearyl alcohol and iron revealed the adsorbate to be in an unstable state. In one instance, a sudden increase in the adsorption rate after 24 hours resulted in about 0.9 of a monolayer at 70 hours. In another instance, adsorption remained at about 0.6 of a monolayer from 40 to 160 hours, but after rinsing with *n*-hexane and recontacting the solution, ad-

(22) E. B. Greenhill, *Trans. Faraday Soc.*, **45**, 625 (1949).

(23) L. S. Bartell and R. J. Ruch, *This Journal*, **60**, 1231 (1956).

sorption increased rapidly to one monolayer. The *n*-hexane rinse may result in a skeletonization process in which the more weakly adsorbed material—possibly *n*-hexadecane molecules—is leached away from the film. New adsorption sites thus produced may be more accessible to the polar molecules when the surface is again wetted by the solution.

Solvent Desorption.—Data for solvent desorption of radiostearic acid are plotted in Fig. 3. To form the adsorbed layers, a solution of 0.05% radiostearic acid in *n*-hexadecane was placed about 2 mm. under the mica window of the Geiger tube and heated to about 70°. Within 30 minutes, the counting rate indicated that the equivalent of 9.5 monolayers of stearic acid had deposited on the mica surface. After the solution was removed, the surface of the mica window had a fogged appearance due to small droplets of condensate. Rinsing with *n*-hexane removed the condensate and gave an apparently dry window, but the counting rate was still equivalent to more than 9 monolayers. A second *n*-hexane rinse removed only 0.05 of a monolayer. The first three benzene rinses that followed removed a total of 5 monolayers. Succeeding benzene rinses each removed less than one monolayer, the amount removed with each rinse diminishing steadily until only the last equivalent monolayer remained. Further benzene rinses removed smaller fractions. When the remaining adsorbed stearic acid approached 0.2 of a monolayer, the rinses became ineffective. The greater solubility of thicker physically held films than of layers adjacent to the surface clearly revealed the gradient of forces between adsorbed layers and between the first layer and the surface.

Pressure-Area Isotherms.—Pressure-area isotherms for stearic acid and for typical mixed films of stearic acid and *n*-hexadecane are shown in Fig. 4. In the mixed-film isotherms, surface pressure is observed at a much greater area per molecule than with stearic acid alone. Compressibility is much greater for the mixtures, and the steep curve at small areas is completely missing.

Surface pressures at large areas per molecule for the dilute solutions suggest interaction between the stearic acid and the *n*-hexadecane molecules. A thin film of *n*-hexadecane exhibits negligible film pressure; yet pressures are obtained when apparently about three out of four molecules in the mixed film are *n*-hexadecane. The general shape of the isotherms for the mixtures suggests that the films are liquid. The absence of the steep portion below 30 Å.² per molecule and the gradual slope below 20 Å.² indicate that during compression some of the stearic acid molecules move from the water surface, where they are normally held by strong polar attraction, into the upper layers of *n*-hexadecane molecules.

The area per molecule at which pressure first develops in the mixed films varies from about 75 to 100 Å.². If the area covered by one uncompressed stearic acid molecule is 25 Å.², then 75 and 100 Å.² per molecule are, respectively, equivalent to 0.33 and 0.25 monolayer of stearic acid.

Nature of Mixed-Film Adsorption.—The combined evidence from three different techniques sug-

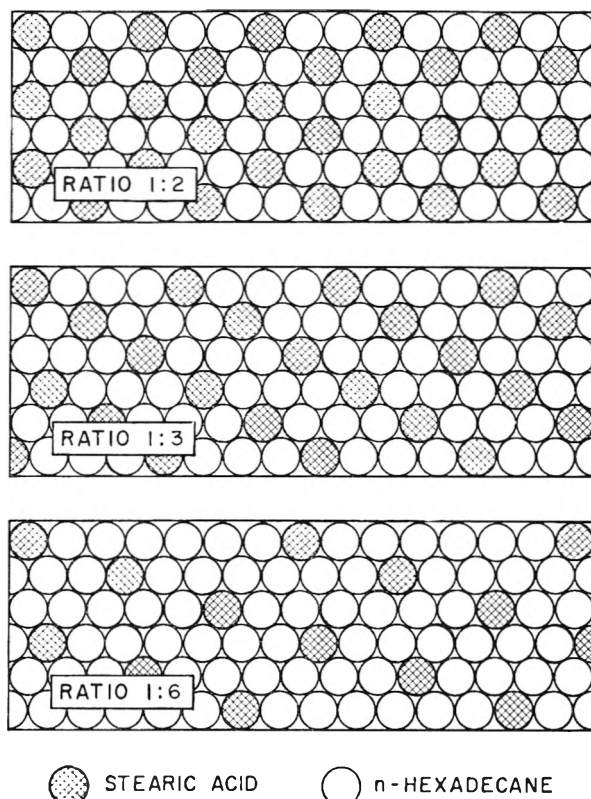


Fig. 5.—Schematic molecular packing of mixed monolayers of stearic acid and *n*-hexadecane.

gests that, when stearic acid adsorbs on water, metal or mica in the presence of a large excess of *n*-hexadecane, a surprisingly stable mixed film is rapidly formed that contains fewer stearic acid than *n*-hexadecane molecules. The ratio of stearic acid to *n*-hexadecane molecules appears to range from 1:2 to 1:4.

Figure 5 shows schematically, as circular cross-sections, hexagonal close-packed and vertically oriented stearic acid and *n*-hexadecane molecules. When the ratio is 1:2, each stearic acid is in contact with six *n*-hexadecanes, and each of the *n*-hexadecanes is in contact with three stearic acids and three *n*-hexadecanes. The ratio 1:3 is similarly diagrammed; here, each *n*-hexadecane contacts two stearic acids. The structure for the 1:6 ratio shows each *n*-hexadecane contacting only one stearic acid. For the ratios 1:4 and 1:5, some of the *n*-hexadecanes would be in contact with one and some with two molecules of stearic acid.

It seems reasonable that stearic acid molecules should not initially be contiguous, and that each *n*-hexadecane molecule at the surface should be in contact with at least one stearic acid molecule. The monolayer-fraction limits of 0.33 (1:2 ratio) to 0.14 (1:6 ratio) for adsorbed stearic acid in the presence of excess *n*-hexadecane are thus derived from the schematic structures of Fig. 5. The average monolayer fraction of either stearic acid or stearyl alcohol adsorbed in the first ten minutes of contact with mica, iron or gold surfaces for nine experiments was 0.26. The average value for three experiments with octadecyl alcohol on iron was 0.3,

as shown by the initial circled point on the curve in Fig. 2.

These considerations suggest a mechanism for the adsorption process. The first stearic acid molecules adsorb individually in a widely scattered fashion and either bring with them, or are immediately surrounded by, six of the more-plentiful *n*-hexadecane molecules. The remainder of the surface is covered by *n*-hexadecane molecules that are weakly held by the solid surface only. As more stearic acid molecules diffuse to the surface, the *n*-hexadecane molecules not already in contact with a stearic acid molecule are quickly displaced, but those in contact with one or more stearic acid molecules are less easily dislodged. Those in contact with three stearic acid molecules can be dislodged only with difficulty at room temperature. The extent to which replacement occurs determines the limiting monolayer fraction of stearic acid adsorbed.

Levine and Zisman¹³ suggest the existence of mixed films of solute and solvent molecules, but only where insufficient time is allowed for equilibrium to be attained. They interpret such mixed films as representing either a transient or metastable state. They also feel that such mixed films form only when both solvent and solute molecules

are paraffinic, so that chain adlineation can exist. These concepts agree in part with the conclusions drawn from the present study.

Stearic acid molecules may adsorb onto solid surfaces from benzene solution with the same degree of coverage as obtained with nitrogen in the BET technique for measuring surface area.²⁴ The more-nearly complete coverage may have resulted from the absence of mixed-monolayer formation because of the non-linear structure of the benzene molecules.

Many variables remain to be investigated before the data from this study can be fully interpreted. Concentration of the solutions, temperature during adsorption, preparation of the mica surface, and choice of solvent may all affect the mechanism of adsorption.

Acknowledgment.—The authors thank W. A. Kimball for preparing the metal-coated mica windows and examining the mica surfaces under the electron microscope, and Joseph Gabor, Bernard Girman and Norman Isaacs for assistance in the experimental work.

(24) H. E. Ries, Jr., M. F. L. Johnson and J. S. Melik, *THIS JOURNAL*, **63**, 638 (1949).

THE BISMUTH-BISMUTH TRICHLORIDE SYSTEM¹

BY S. J. YOSIM, A. J. DARNELL, W. G. GEHMAN AND S. W. MAYER

Atomics International, A Division of North American Aviation, Inc., Canoga Park, California

Received August 12, 1958

A phase equilibrium study of the bismuth-bismuth trichloride system has been carried out. The experimental techniques included sampling at temperature, thermal analysis and visual observations. The miscibility gap was found to be closed at a consolute temperature of 780° and 51 mole % Bi. In the two liquid phase region, the solubility of the salt in the metal increased with increasing temperature while the solubility of bismuth in bismuth trichloride decreased from 45% at 320° to 28% at about 550°. Results in the liquid-solid region are reported and compared with those of earlier workers.

Introduction

The results of solubility studies have indicated that in many cases metals and their salts are mutually soluble to a surprising degree.² In fact, it has been shown that the alkali metals and their halides^{3,4} are soluble in all proportions as is also the case for barium and BaCl₂.⁵ The purpose of this work was to determine whether the phenomenon of complete miscibility also occurs in the bismuth-bismuth trichloride system since the mutual solubilities near the melting points of the components are relatively high.⁶ Because the results of previous studies in the lower temperature liquid-solid region⁶⁻¹⁰ are in disagreement, this region

also was investigated in an effort to resolve the discrepancies.

Experimental

Materials.—Reagent grade bismuth trichloride was dried under a current of HCl gas and distilled under HCl and then under argon. The first and last eighths of the distillate were discarded. The salt had a melting point of 232.2°. Chemical analysis of the salt showed a 66.2 ± 0.1 wt. % bismuth as compared to 66.27% theoretical. Because of the hygroscopic nature of bismuth trichloride, it was handled at all times in a glove box flushed with argon. Reagent grade bismuth was melted under an inert atmosphere and filtered through Pyrex glass wool to yield a bright ingot with a melting point of 271.0°.

Experimental Methods and Procedures.—A decantation method, similar to that of Bredig,^{3,4} was used to sample the salt rich phase at temperature. A quartz tube, equipped with a side arm and containing the sample, was mounted in a Marshall furnace. The entire sample was held in a uniform temperature zone for a minimum period of 20 hours during which time the solution was continuously mixed by rocking the furnace assembly. The system was then tilted to permit decantation of a portion of the salt-rich layer into the side arm. The weighed decantate was dissolved in 25% HNO₃ at room temperature and analyzed for total bismuth and

(1) This work was supported by the Atomic Energy Commission. This paper has been presented in part before the Division of Inorganic Chemistry at the National Meeting of the A.C.S. in September, 1957.

(2) D. Cubicciotti, "High Temperature Equilibria in Metal-Metal Halide Systems," MDDC-1058.

(3) M. A. Bredig, J. W. Johnson and W. T. Smith, *J. Am. Chem. Soc.*, **77**, 307 (1955).

(4) M. A. Bredig, H. R. Bronstein and W. T. Smith, *ibid.*, **77**, 1454 (1955).

(5) H. Schafer and A. Niklas, *Angew. Chem.*, **64**, 611 (1952).

(6) B. G. Eggink, *Z. physik. Chem.*, **64**, 449 (1908).

(7) M. A. Sokolova, G. G. Urazov and V. G. Kuznetsov, *Akad. Nauk. S.S.S.R. Inst. Gen. Inorg. Chem.*, **1**, 102 (1954).

(8) A. Aten, *Z. physik. Chem.*, **66**, 641 (1909).

(9) W. Herz and A. Guttman, *Z. anorg. Chem.*, **56**, 422 (1908).

(10) L. Marino and R. Becarelli, *Atti Accad. Lincei*, **24**, 625 (1915); **25**, 221, 328 (1916).

total chlorine. Bismuth was determined by EDTA titration at pH 2.0 using thiourea as indicator,¹¹ while chlorine was determined by the Volhard method.

To determine the metal-rich side of the miscibility gap, a visual method was used. Mixtures of bismuth and bismuth trichloride were sealed in evacuated heavy walled (1.5 mm.) quartz bombs, 1 cm. o.d. by 7 cm. long. The loaded tubes were mounted in a Marshall furnace equipped with two sight-holes and a light source in the rear of the furnace. The sample, which was agitated frequently, was heated until the interface disappeared. However, with samples containing 40–60 mole % bismuth, the similarity in appearance of the two phases at the higher temperatures necessitated the use of a quartz rod to direct an intense beam of light on the interface. This permitted the detection of very faint differences between the two phases.

For thermal analysis experiments, the Bi–BiCl₃ mixture was contained in a sealed Pyrex tube provided with a thermocouple well in the bottom. A chromel–alumel thermocouple was inserted in the well, and the e.m.f. was automatically recorded on a Brown Elektronik potentiometer after amplification by a Leeds and Northrup microvolt amplifier. Cooling and heating curves were obtained while the mixture was continuously mixed in a rocking Marshall furnace. Cooling curves were taken in the regions between the pure components and the eutectics. To avoid difficulties due to supercooling, arrests on heating were used to determine the syntectic temperature. However, the results of thermal analysis experiments in the regions between the eutectic and syntectic compositions were not always reproducible. Therefore, decantation experiments were used in these regions.

Results and Discussion

The phase diagram of the Bi–BiCl₃ system under its own pressure is shown in Fig. 1. A consolute temperature of 780° was found, *i.e.*, above this temperature the metal and the salt are mutually soluble in all proportions. The solubility of the metal in the salt decreased with increasing temperature from 45 mole % at 320° to 28 mole % at about 550°, and then increased. On the other hand, the solubility of the salt in the metal continued to increase with temperature from the metal-rich eutectic.

The internal consistency of the results outlining the miscibility gap was checked by plotting the mean values of the bismuth metal compositions of the two conjugate solutions *versus* temperature (a variation of the law of rectilinear diameters). The resulting curve was linear and the composition, corresponding to the consolute temperature, 780°, was 51 ± 1%.

Visual observations of two-phase metal-rich mixtures showed the following: above 320° the mixture consisted of a silvery metallic phase on the bottom and a black, opaque, salt-rich phase on the top. In the case of mixtures containing 70–95 mole % Bi, the black salt-rich phase continued to decrease in volume as the sample was heated until a single phase, which was not as shiny as pure molten bismuth but which had a metallic luster, remained. In the case of mixtures containing 50–60 mole % Bi, the position of the interface remained relatively constant during the heating. However, as the temperature was increased, the interface became fainter as a result of the increasingly similar appearance of the two phases. Above the miscibility gap, the resulting solution was still metallic-looking but somewhat less shiny.

The results of the liquid–solid portion of the system are included in Fig. 1 and are compared to

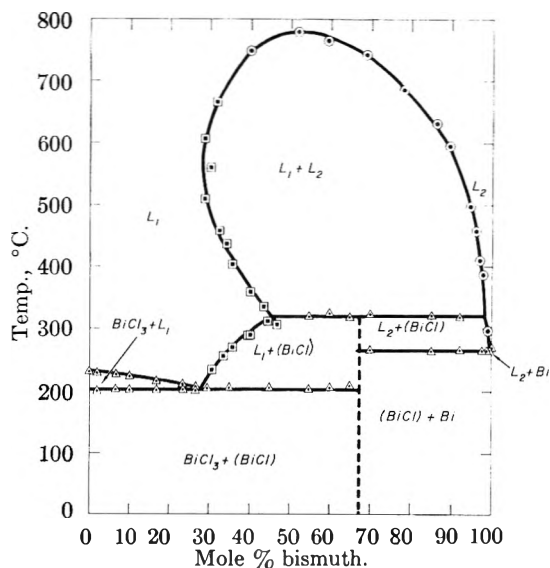


Fig. 1.—The bismuth–bismuth trichloride system: ○, visual; □, decantation; △, thermal analysis.

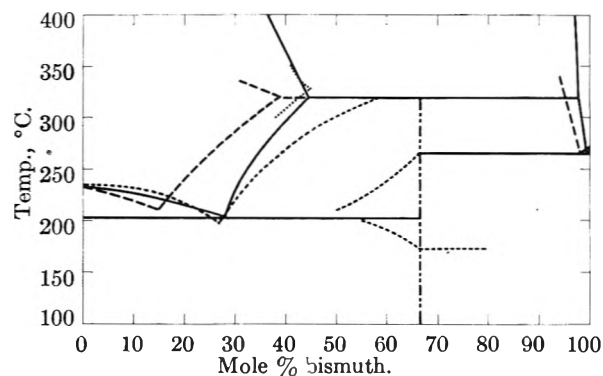


Fig. 2.—Comparison of results: —, present work; ---, Eggink; ·····, Sokolova; - · - · - ·, Aten.

the results reported by Eggink,⁶ Sokolova *et al.*,⁷ and Aten⁸ in Fig. 2. Three horizontal lines were found, in agreement with Eggink and Sokolova; these correspond to the salt-rich eutectic at 202°, the metal-rich eutectic at 267°, and the syntectic at 320°. Because the two eutectic temperatures are not identical, it is necessary to postulate, as did Eggink and Sokolova, an intermediate compound. Since the phase diagrams of Herz and Guttman⁹ and Marino and Becarelli¹⁰ did not include the intermediate compound, their results were not included in Fig. 2. It is probable that this intermediate compound has a composition corresponding to a mole ratio of Cl/Bi of 1/1. However, the isolation of pure BiCl has not been confirmed, and therefore the formula BiCl in Fig. 1 is enclosed in parentheses and the vertical line representing the BiCl compound is drawn as a broken line in both Figs. 1 and 2.¹²

The liquidus curve from 0–29 mole % bismuth, as determined by thermal analysis, is in good agreement with that of Sokolova but disagrees with

(12) Work on the preparation, structure and thermodynamics of this compound is currently in progress, both at Iowa State College by Professor J. D. Corbett and in this Laboratory. ADDED IN PROOF: Since this article was written, J. D. Corbett (*J. Am. Chem. Soc.*, **80**, 4757 (1958)) has described some chemical and physical properties of bismuth subchloride.

(11) J. S. Fritz, *Anal. Chem.*, **26**, 1978 (1954).

that of Eggink. In the liquid–solid region between the salt-rich eutectic and the base of the miscibility gap (29–45 mole % Bi) the liquidus curve lies between those of Eggink and Sokolova, and agrees reasonably well with Aten.

The majority of the discrepancies between the results reported in this work and those of earlier workers in the lower temperature salt-rich region of the Bi–BiCl₃ system can be explained, if one assumes that the system is slow to reach equilibrium. Eggink's results would be expected to be low because of insufficient contact time (30 min.) and ineffective mixing. Many of the thermal arrests found by Sokolova also were observed in the present work unless precautions were taken to ensure equilibrium conditions.

Both the species and the nature of the chemical bonding in solutions of bismuth dissolved in BiCl₃ are still unknown. Several suggestions have been offered by earlier workers as to the form of bismuth in solution and these are: (1) colloidal dispersion,¹³ a mechanism which is no longer taken seriously, (2) a bismuth subhalide¹⁴ and (3) bismuth atoms, dimers, higher polymers or their ions. In evaluating proposed mechanisms and species, these experimental results must be considered.

1. Above 780° bismuth and BiCl₃ are completely miscible.

2. From results to date the solution of bismuth in pure salts is specific,¹⁵ *i.e.*, solution of bismuth is restricted to its own halides if one disregards solution due to oxidation of bismuth by the non-bismuth salt.

3. The equivalent conductance of salt-rich solutions decreases as bismuth is added to BiCl₃ from 250 to 350°.⁸

4. Results of vapor pressure measurements of salt-rich Bi–BiCl₃ solutions indicate positive deviation of BiCl₃ from Raoult's law.¹⁶

5. Salt-rich solutions are diamagnetic.¹⁷ Therefore, the mechanisms leading to the species described above will be discussed with these points in mind.

The chemical reaction of a metal with its normal halide to produce a lower valent halide, *i.e.*, a subhalide, which is soluble in the normal salt, has often been suggested as a mechanism for solution of metals in their normal halides.^{17,18} In the bismuth case, this mechanism appears attractive in view of the existence of the solid subhalide. However, the existence of bismuth subchloride in the solid state does not assure its existence in the liquid. Further, it is important to note that such a mechanism cannot explain the entire phase diagram (Fig. 1). Based solely on the formation of

the subhalide, one would not expect the complete miscibility which exists above 780°. For example, if solution occurred due to formation of BiCl only, the solubility could not exceed 66 2/3%.

Therefore, a process other than, or at least in addition to, oxidation–reduction to yield a subhalide, must be considered. The explanation or mechanism of such a process is unknown but may be similar to that in the case of the alkali systems. In these systems, solid subhalides such as Na₂Cl are unknown, and, in fact, the term subhalide is not often associated with alkali systems probably because the cation would have an effective charge of less than unity.¹⁹ Bronstein and Bredig,²⁰ on the basis of the results of electrical conductivity experiments on these systems suggest that at least in the case of sodium–sodium halide systems, the metal dissolves as neutral dimers, although the formation of dimer ions was not ruled out.

Thus, the possibility of bismuth existing as dimers when dissolved in BiCl₃ must be considered. The existence of such species would be consistent with the electrical conductivity, vapor pressure and magnetic susceptibility results. It would also be consistent with, but by no means proven by, the facts that Bi₂ exists in the vapor phase²¹ and that bismuth dissolves in lead as a dimer.²² It is possible that the dimer may be ionized. The existence of the dimer ion, Bi₂⁺ or Bi₂⁺⁺⁺, is not likely since such ions are expected to be paramagnetic; however, Bi₂⁺⁺ is possible since such species could be diamagnetic. Any mechanism for solution of bismuth as a dimer or dimer ion must take into account the apparent specificity of bismuth halides as solvents for bismuth.

Solution of bismuth as atoms or as ions plus electrons is also a possibility. If the latter occurs, the electrons are not considered to be free in view of the electrical conductivity results. Keneshea and Cubicciotti²³ suggest that the added bismuth atom or ions enter into the octahedral holes in the chloride quasi-lattice. However, again this picture, like that of the subhalide, can explain only a portion of the phase diagram, *i.e.*, up to a concentration of 66 2/3 mole % bismuth. Further, no account is taken for the specificity of solution of Bi in BiCl₃. From the information available to date it is therefore impossible to select the actual mechanisms or species.

The observed retrograde solubility, *i.e.*, the decrease in solubility of bismuth in BiCl₃ as the temperature is increased from 320 to 550°, followed by the increase in solubility as the tempera-

(13) R. Lorenz, "Die Electrolyse Geschmolzener Salze," W. Knapp, Halle A-S, 1906.

(14) The term subhalide is defined in this paper as a lower valent salt (M_aX_b) formed by an oxidation–reduction reaction of a metal with its normal halide. Further, *a* and *b* are small integers.

(15) F. Cleary and D. Cubicciotti, *J. Am. Chem. Soc.*, **74**, 557 (1952).

(16) D. Cubicciotti, F. J. Keneshea, Jr., and C. M. Kelley, *THIS JOURNAL*, **62**, 463 (1958).

(17) J. D. Corbett, S. Winbush and F. C. Albers, *J. Am. Chem. Soc.*, **79**, 3020 (1957).

(18) K. Grjotheim, F. Gronvold and J. Krogh-Moe, *ibid.*, **77**, 5824 (1955).

(19) However, Grjotheim, *et al.*,¹⁸ have suggested that one might look upon the alkali metal–metal halide solution as consisting of halide ions and dimerized metal ions (*e.g.*, Na₂⁺), the latter formed by reduction of the normal chloride by the metal and stabilized by the metal–metal one electron bond. Nevertheless, as admitted by Grjotheim, this subhalide formation could not explain the complete miscibility at elevated temperatures.

(20) H. R. Bronstein and M. A. Bredig, *J. Am. Chem. Soc.*, **80**, 2077 (1958).

(21) E. Brackett and L. Brewer, "The Heat of Dissociation of Bi₂," UCRL-3712 (1957).

(22) K. K. Kelley, "Contributions to the Data on Theoretical Metallurgy," U. S. Bureau of Mines Bulletin 393, 1936.

(23) F. J. Keneshea, Jr., and D. Cubicciotti, *THIS JOURNAL*, **62**, 843 (1958).

ture is increased to the consolute temperature can be interpreted as the resultant of two processes, one predominant at lower temperatures and the other predominant at higher temperatures. However, as is shown below, many combinations of processes can account for the retrograde solubility and can also be consistent with the observed positive deviations of BiCl_3 from Raoult's law. Three examples of these are:

(a) Solution of bismuth, predominantly as dimers or higher polymers at the lower temperatures with partial or complete dissociation taking place at the higher temperatures.

(b) Solution of bismuth predominantly as a polymeric subhalide followed by dissociation at higher temperatures.

(c) Solution of bismuth both by formation of atoms, polymers or their ions and by formation of subchlorides, the latter being predominant at the lower temperatures.

Very little is known regarding the species existing in solutions of BiCl_3 dissolved in bismuth. If a subhalide is formed, its solubility in the metal must still be explained. It is apparent, therefore, that considerable work is required to understand the nature of these solutions.

Acknowledgment.—The authors are grateful to Dr. D. E. McKenzie for enlightening discussions, to Dr. A. L. Landis for suggestions on experimental techniques and to Mr. G. W. Dollman who carried out the chemical analyses.

THE LITHIUM BOROHYDRIDE-AMMONIA SYSTEM: PRESSURE-COMPOSITION-TEMPERATURE RELATIONSHIPS AND DENSITIES

BY EDWARD A. SULLIVAN AND SIDNEY JOHNSON

Contribution from the Research and Development Laboratories, Metal Hydrides, Inc., Beverly, Mass.

Received August 14, 1958

Pressure-composition-temperature relationships have been determined for the lithium borohydride-ammonia system between 0 and 80°. The data, obtained from isothermal studies, are presented for ready interpolation of pressures as a function of the other two variables. The phase diagram for the system has been constructed from the experimental data. Lithium borohydride and ammonia form four stable compounds: the mono-, di-, tri- and tetraammoniates. All but the triammoniate show congruent melting points. The densities of liquid lithium borohydride ammoniates have been determined hydrometrically as a function of temperature at several compositions.

Introduction

The discovery of the borohydrides, by Schlesinger^{1,2} and co-workers, has produced a new class of reducing agents having their own particular chemical properties. Among the compounds resulting from this discovery is lithium borohydride, an ionic compound with a characteristically high melting point, 275–280°.³ In recent years, many of the properties of lithium borohydride have been determined.^{4–9}

The coordination compounds formed between lithium borohydride and ammonia at 20° have been described briefly by Hunt and Cowie,¹⁰ who determined the vapor pressure above a lithium borohydride-ammonia mixture as a function of the sample's composition. The purpose of the present investigation was to extend the knowledge of this system's properties.

(1) H. I. Schlesinger, R. T. Sanderson and A. B. Burg, *J. Am. Chem. Soc.*, **61**, 536 (1939).

(2) H. C. Brown, *Chem. Eng. News*, **29**, 5231 (1951).

(3) H. I. Schlesinger and H. C. Brown, *J. Am. Chem. Soc.*, **62**, 3429 (1940).

(4) P. M. Harris and E. P. Meibohm, *ibid.*, **69**, 1231 (1947).

(5) W. D. Davis, L. S. Mason and G. Segeman, *ibid.*, **71**, 2775 (1949).

(6) W. C. Price, H. C. Longuet-Higgins, E. Rice and T. F. Young, *J. Chem. Phys.*, **17**, 217 (1949).

(7) W. G. Brown, L. Kaplan and K. E. Wilzbach, *J. Am. Chem. Soc.*, **74**, 1343 (1952).

(8) N. C. Hallett and H. L. Johnston, *ibid.*, **75**, 1496 (1953).

(9) A. P. Altschuller, *ibid.*, **77**, 5455 (1955).

(10) D. J. Hunt and P. A. Cowie, Summary Report XXXI, Subcontract No. M-3181-14, St. Louis U., March 31, 1955.

Experimental

Apparatus.—The experimental work described here was carried out in all-glass high vacuum apparatus of a general type described adequately by Sanderson.¹¹ Isolation of various sections of the vacuum apparatus was accomplished by means of mercury float valves, so as to avoid contamination from stopcock grease.

The oil-baths used to maintain constant sample temperatures were heated by 750 watt (115 volt) Cal-rod immersion heaters and controlled by Philadelphia Roto-stats through Fisher-Serfass electronic relays to within $\pm 0.2^\circ$. Temperatures were measured by mercury-filled thermometers, the calibrations of which were checked at the freezing and boiling points of pure water; these thermometers had ranges from -1 to $+101^\circ$, with 0.1° subdivisions.

Pressure levels in the mercury manometer, which was immersed in the oil-bath, were read with the aid of a Gaertner cathetometer having 1 mm. subdivisions and a vernier permitting readings to 0.05 mm.

Materials.—Lithium borohydride: Metal Hydrides Incorporated, purified by recrystallization from ethyl ether inside a dry-box and subsequent drying by vacuum evaporation at 100° for several hours. Analyses of lithium borohydride samples used in this study are given in Table I, together with that used by Hunt and Cowie. It must be remembered that with compounds of such a low molecular weight, impurities will lower the calculated purity by weight disproportionately, because of their much higher molecular weights. For example, lithium borohydride containing 5.0 weight % ether is 98.5 mole % pure; one containing 5 weight % lithium borate is 97.8 mole % pure. Molar purities eliminate the influence of molecular weights, but are not used conventionally. Agreement of data from samples of different purity indicates the impurity content to be inert to ammonia, so that the sample weight can be corrected for actual lithium

(11) R. T. Sanderson, "Vacuum Manipulation of Volatile Compounds," John Wiley and Sons, Inc., New York, N. Y., 1948.

TABLE I
 LITHIUM BOROHYDRIDE ANALYSES

	Theor.	Sample A	Sample B	Sample C	Sample D	Sample H	Sample Z (ref. 10)
Weight %							
Li	31.85	28.5	29.7	29.0	29.3	30.5	27.9
B	49.65	47.4	47.1	48.6	47.8	48.2	43.9
H ⁻	18.50	17.2	17.0	17.7	17.4	16.7	16.2
OCH ₃		3.74	0.48	2.5	5.4	2.75	
Cl		1.39	0.17	0.42	0.40	0.19	
	100.0	98.2	94.5	98.2	100.3	98.3	88.0
Mole Ratios							
Li/B	1.000	0.940	0.983	0.930	0.955	0.987	0.99
H ⁻ /B	4.000	3.895	3.874	3.909	3.900	3.719	3.96
OCH ₃ /B		0.027	0.004	0.018	0.039	0.020	
Cl/B		0.009	0.001	0.003	0.002	0.001	
Purity, %							
$\frac{100 \text{ H}^-}{18.50}$	100.0	93.0	91.9	95.8	93.9	90.5	88.0

borohydride content without affecting the validity of the results.

Ammonia: the Matheson Co., Inc., purified by passage over sodium and stored in a bulb connected to the vacuum line.

Ethyl ether: Mallinckrodt Chemical Works, purified by distillation from lithium aluminum hydride.

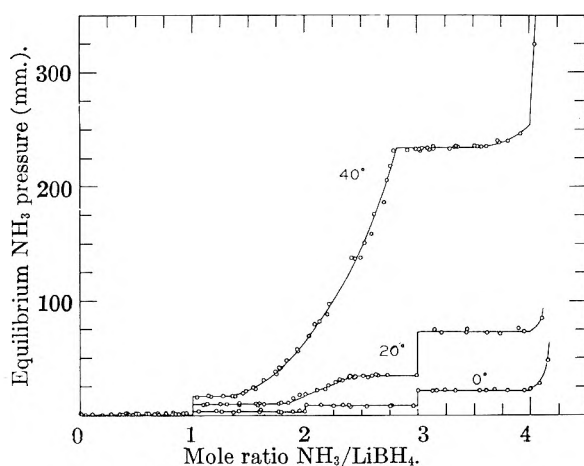


Fig. 1.—LiBH₄-NH₃ isotherms.

Procedures.—The major portion of experimental data was obtained by means of isotherms, in which the equilibrium pressure of ammonia was determined as a function of the sample's composition at constant temperature. In most cases, data were duplicated by desorption as well as absorption isotherms. Some of the information necessary for construction of the temperature-composition phase diagram could not be obtained from the isotherms; these data, *e.g.*, melting and transition points, were determined by visual observation and by analysis of the behavior of pressure as a function of temperature, for the specific compositions involved.

The isothermal studies were conducted utilizing essentially standard techniques for the investigation of binary systems with one volatile component.¹²

A carefully measured increment of gaseous ammonia was condensed onto a 0.1-g. sample of lithium borohydride at -196° . The system was isolated and the sample allowed to warm to room temperature. Rough equilibration was established at room temperature, after which a constant temperature bath was applied to the sample until the pressure remained constant. This required from less than one hour to several days, depending on the temperature and composition of the sample. The ammonia pressure and the cor-

rected over-all composition of the condensed phase(s) were recorded and the procedure repeated until addition of another increment of ammonia would give a pressure greater than one atmosphere.

As a check of the validity of the absorption data, desorption isotherms were carried out at several temperatures by making measured removals of ammonia from a lithium borohydride tetrammoniate sample and determining the equilibrium pressure by the previously described method. Successive removals were made until essentially pure lithium borohydride remained. In this way, good agreement between absorption and desorption data was obtained, giving assurance that true chemical equilibrium had been attained throughout this series of experiments. The data were also checked by duplication of absorption isotherms with separate lithium borohydride samples.

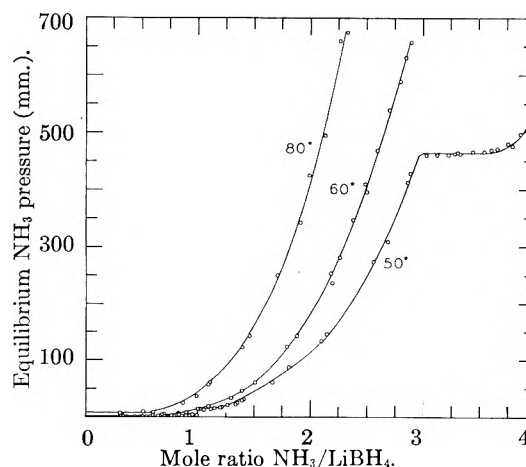


Fig. 2.—LiBH₄-NH₃ isotherms.

Correction of Isotherm Data.—In calculating the composition of a lithium borohydride-ammonia sample at equilibrium, corrections were applied for the amount of ammonia in the gas phase and for thermal expansion of mercury in the differential manometer.

In addition, it was found that small amounts of a non-condensable gas were generated in the sample tubes. This effect was observed even with samples maintained at 0° , but became more pronounced at higher temperatures. At and above 40° , it was necessary to correct the isotherm data for this gas evolution. In view of the components of the system, and of the fact that the gas could not be condensed with liquid nitrogen (-196°), it was deduced that the gas was hydrogen and must have been produced by an ammonolysis reaction. While the gas was not analyzed, the reaction

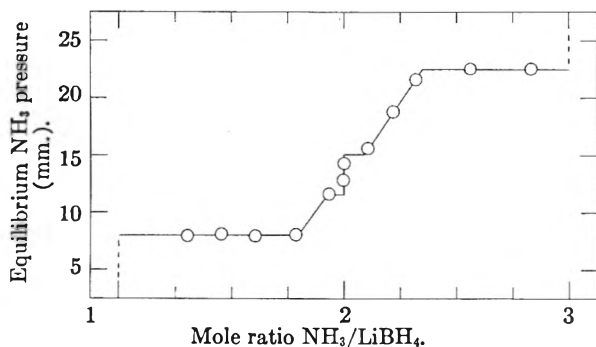
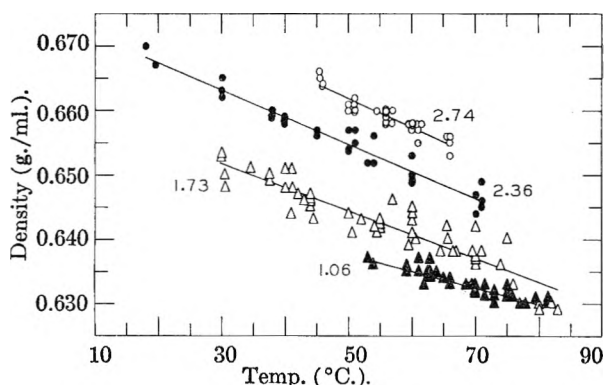
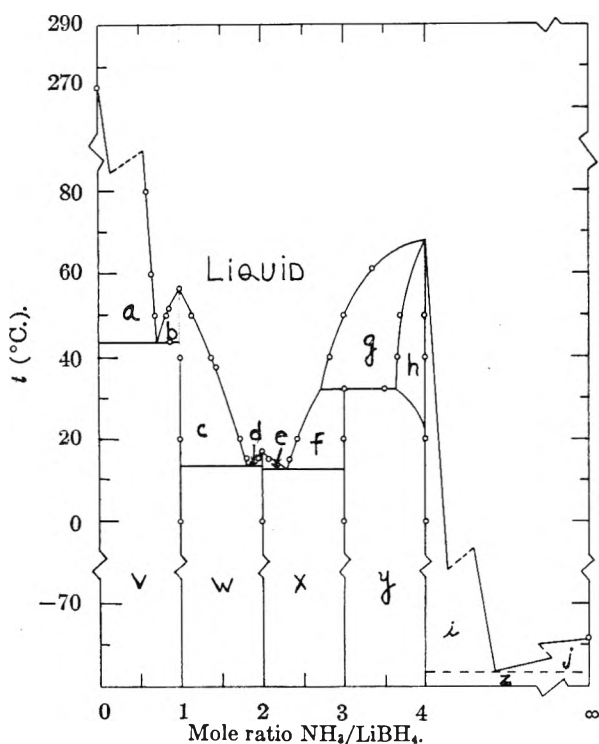
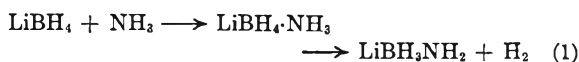
(12) D. H. Howard, Jr., F. Friedrichs and A. W. Browne, *J. Am. Chem. Soc.*, **56**, 2332 (1934).

TABLE II

LiBH₄-NH₃ ISOTHERM DATA

0°		15°		20°		40°		50°		60°		80°	
Mole ratio NH ₃ LiBH ₄	Equil. NH ₃ press. (mm.)	Mole ratio NH ₃ LiBH ₄	Equil. NH ₃ press. (mm.)	Mole ratio NH ₃ LiBH ₄	Equil. NH ₃ press. (mm.)	Mole ratio NH ₃ LiBH ₄	Equil. NH ₃ press. (mm.)	Mole ratio NH ₃ LiBH ₄	Equil. NH ₃ press. (mm.)	Mole ratio NH ₃ LiBH ₄	Equil. NH ₃ press. (mm.)	Mole ratio NH ₃ LiBH ₄	Equil. NH ₃ press. (mm.)
0.192	0.1	1.30	8.0	0.001	0.1 ^a	0.112	0.0 ^a	0.371	1.5	0.319	2.0	0.307	8.5
.347	.2	1.46	8.2	.045	.1 ^a	.402	1.4	.439	1.5	.333	3.4	.516	10.8
.438	.0	1.61	8.0	.273	.6 ^a	.427	1.5	.481	1.3	.505	2.6	.597	9.3
.692	.2	1.78	8.0	.376	.8	.491	1.0 ^a	.508	2.2	.507	3.1	.866	26.1
.825	.6	1.93	11.6	.470	.3 ^a	.515	1.5	.540	1.2	.681	4.3	.980	38.5
.855	.2 ^a	1.99	12.8	.588	1.0	.607	1.5	.574	1.6	.698	5.7	1.09	59.4
1.05	3.0	2.00	14.2 ^a	.657	0.3 ^a	.687	1.8	.595	2.8 ^a	.836	8.5	1.11	62.8
1.21	3.6	2.11	15.5	.824	1.0 ^a	.765	1.6	.598	1.8	.895	9.5	1.40	123
1.26	2.8 ^a	2.22	18.7	.876	0.2 ^a	.825	2.7	.639	2.3	1.00	17.6	1.47	143
1.37	2.1 ^a	2.32	21.5	.877	0.7	.845	1.2	.657	1.8	1.02	17.4	1.71	252
1.42	3.0	2.57	22.3	.914	1.0	.854	1.4	.701	2.6	1.09	19.7	1.92	343
1.58	2.8 ^a	2.83	22.5	1.02	0.0 ^a	.944	1.3	.704	4.5	1.30	36.5	1.99	426
1.60	3.2	3.07	56.6	1.10	8.7	1.03	15.7	.706	2.5	1.39	49.3	2.13	495
1.76	3.1			1.11	8.4 ^a	1.05	2.0 ^a	.769	4.2	1.51	62.4	2.27	659
1.78	2.8 ^a			1.12	9.8	1.14	17.0	.773	4.5	1.79	125	2.34	675
1.88	3.0			1.25	9.6 ^a	1.16	16.7	.778	3.0	1.88	144		
1.95	3.4			1.30	9.4 ^a	1.27	16.8	.830	4.9	2.18	255		
2.00	8.0 ^a			1.42	10.0	1.35	16.8	.854	3.9	2.20	237 ^a		
2.01	7.7 ^a			1.42	9.1 ^a	1.37	17.0 ^a	.893	4.7	2.27	282		
2.13	7.9			1.56	9.7 ^a	1.45	19.2	.919	5.1	2.38	348		
2.24	7.6			1.57	9.1	1.47	21.3	.950	5.9	2.49	411		
2.33	8.0 ^a			1.65	9.5 ^a	1.53	24.7	.950	8.8 ^a	2.51	394 ^a		
2.38	8.3			1.64	10.0	1.57	22.4 ^a	.984	4.9	2.60	469		
2.39	7.5			1.68	9.9	1.63	30.6	1.02	16.2	2.71	539		
2.54	7.5			1.76	10.2 ^a	1.73	38.4	1.05	14.0	2.81	591		
2.75	7.4			1.78	11.3	1.74	34.8 ^a	1.12	16.5	2.85	631		
2.77	7.7 ^a			1.85	11.2 ^a	1.77	41.7	1.15	17.3	2.90	657 ^a		
2.77	8.9			1.89	14.8	1.83	47.8	1.20	17.8	3.00	740		
2.96	7.6			1.95	17.7	1.93	57.9	1.20	19.4 ^a				
3.00	21.7 ^a			2.00	18.0 ^a	1.94	55.7 ^a	1.21	18.8				
3.13	21.1			2.00	18.1	2.03	69.1	1.27	22.0				
3.17	22.3			2.01	16.4 ^a	2.09	79.4	1.27	22.5				
3.24	22.1 ^a			2.11	21.7	2.13	82.3	1.33	23.3				
3.34	21.4			2.12	21.6	2.21	87.9 ^a	1.35	27.6				
3.55	21.2			2.18	22.9 ^a	2.22	96.5	1.39	30.8 ^a				
3.61	22.1 ^a			2.21	25.9	2.42	139	1.41	34.0				
3.68	22.7			2.27	28.9 ^a	2.45	138	1.67	61.1 ^a				
3.80	22.1			2.31	31.1	2.50	137 ^a	1.81	89.4 ^a				
3.95	20.9			2.33	29.6 ^a	2.53	151 ^a	2.11	133 ^a				
4.00	23.2 ^a			2.41	33.8	2.60	159	2.15	148 ^a				
4.08	27.8			2.44	33.6	2.62	176	2.57	275 ^a				
4.16	48.0			2.52	35.8	2.71	187	2.69	309				
4.22	454			2.57	32.2 ^a	2.73	206	2.87	413 ^a				
				2.60	34.6 ^a	2.76	218	2.89	428 ^a				
				2.63	35.7	2.79	232 ^a	3.03	460				
				2.65	36.1	2.80	233	3.13	461				
				2.73	35.4	2.82	216	3.24	462				
				2.77	31.5 ^a	2.92	233	3.29	462 ^a				
				2.97	77.7	2.92	234 ^a	3.30	461				
				3.00	33.3 ^a	2.99	234	3.32	467 ^a				
				3.16	74.7	3.02	233	3.34	463				
				3.22	71.6 ^a	3.03	232	3.45	467				
				3.43	72.0 ^a	3.04	234	3.46	461				
				3.44	75.4	3.09	254	3.55	467				
				3.62	71.9	3.11	233 ^a	3.62	470				
				3.74	71.2 ^a	3.15	233	3.66	471 ^a				
				3.90	75.9	3.15	236	3.66	472				
				3.95	72.1 ^a	3.28	233	3.76	481				
				4.11	84.9	3.33	235	3.80	476 ^a				
				4.32	413 ^a	3.34	236	3.87	498				
				4.33	547	3.36	236 ^a	3.93	503				
				4.34	692	3.51	237	3.97	537				
						3.54	235						
						3.57	235 ^a						
						3.62	235						
						3.72	241						
						3.73	238 ^a						
						3.81	240						
						3.92	246						
						4.05	326						
						4.06	553						

^a Denotes desorption.

Fig. 3.—LiBH₄-NH₃ isotherm at 15°.Fig. 4.—Densities of liquid LiBH₄-ammoniates.Fig. 5.—LiBH₄-NH₃ phase diagram.

was assumed.

On the basis of the stoichiometry of equation 1, a correction was applied to both the amounts of lithium borohydride and of ammonia present to account for the hydrogen formed. The maximum total ammonolysis never exceeded 0.6% during a run. This correction, while necessary at higher tem-

peratures, was still so small that solvation of ammonolysis products could be neglected.

Density Determinations.—The techniques applicable to determining the densities of liquid lithium borohydride ammoniates were severely limited by the properties of the system. Ultimately densities were determined hydrometrically in essentially the same apparatus as used for isothermal pressure measurements, except that much larger samples were used (15–20 g. LiBH₄ vs. 0.1 g.). Ammonia measurements were made in the liquid state at –35° with the aid of a buret sealed to the vacuum line.

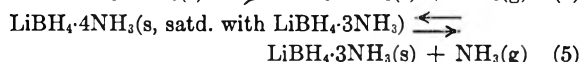
The temperature range in which measurements could be made for a given sample was limited by the liquidus temperature for the specified composition and by the ammonia vapor pressure above the sample.

Results

The experimental pressure data obtained by the isotherm method are given in Table II and are plotted in Figs. 1, 2 and 3. The density data are found in Fig. 4.

Discussion

At 0°, where four horizontal plateaus are found to be bounded by whole number mole ratios of ammonia to lithium borohydride from zero to four, the equilibria are



On the basis of the 0° isotherm alone, equation 5 could be replaced by



but the existence of a solid solution between the triammoniate and the tetraammoniate is proved by data at higher temperatures. The equilibrium constants for equations 2 through 5 can be represented by their respective equilibrium ammonia pressures

$$K_n = P_{\text{NH}_3} \quad (7)$$

assuming the activities of all solid phases to be unity.

The equilibrium pressures are independent of the sample's over-all composition (between consecutive whole number mole ratios), since only the relative amounts of the two condensed phases are changing in each of the four regions of composition.

At temperatures above 15°, the isotherms become more complex because one or more parts of the isotherm represent an all-liquid condensed phase. In these areas where only one condensed phase is found, the ammonia vapor pressure above the sample depends on its composition and increases as more ammonia is added.

At and above 17°, the lithium borohydride-diammoniate solid phase disappears completely, as is shown in the isotherms by the fact that no discontinuity is found at a mole ratio of 2 to 1, as had been the case at lower temperatures. Instead, a continuous curve is found at 20°, extending between mole ratios of 1.73 and 2.43. This region has but one condensed phase (a liquid) and in it, as mentioned above, the equilibrium pressure is composition dependent. In higher temperature isotherms, this curve extends over wider compo-

sition ranges, representing increased solubility of adjacent solid phases in the liquid ammoniate. Above 56.5°, the monoammoniate phase also disappears and the continuous curve of the all-liquid region covers a composition range of from less than one to more than three moles of ammonia per mole of lithium borohydride.

Although the pressures involved made it impossible to work in glass apparatus at temperatures above 50° at a composition of four to one, sufficient data have been obtained in nearby regions to predict by extrapolation that the melting point of the tetraammoniate phase would be about 68°.

Lithium borohydride-triammoniate displayed an incongruent melting point.

The tri- and tetraammoniates of lithium borohydride form a solid solution; this was first detected in the isotherms determined above 20°. As the over-all composition of the sample approached four moles of ammonia per lithium borohydride, the equilibrium pressure once more became composition-dependent, indicative of a single homogeneous condensed phase. Since the over-all composition had not yet reached four to one and the sample was obviously solid, this single phase must be a solid solution of triammoniate in tetraammoniate.

At 15° (Fig. 3), the system was investigated only between mole ratios of one and three; this temperature was studied to elucidate the behavior of compositions adjacent to the diammoniate just below its melting point.

At 40°, the all-liquid region centering on a mole ratio of two has been extended in both directions due to the increased solubility of adjacent solid phases in the liquid, now showing limiting ratios of 1.40 and 2.83. In addition, a new inflection point was found at a ratio of 3.65. Between this point and a ratio of 4.0, the ammonia pressure above the sample increased as more ammonia was added, showing that only one condensed phase was present, a solid solution of the triammoniate in the tetraammoniate. The results obtained at 50° were as expected from trends indicated in the work at lower temperatures. The inflection indicating transition to the solid solution occurred at a mole ratio of 3.70 (3.65 at 40°), showing a more limited solid solution range as the temperature was increased above the incongruent melting point of the triammoniate. The isotherm studies were completed with determinations made at 60 and 80°. These determinations were limited, as explained previously, by the pressure which could be contained in the glass apparatus and were terminated when the ammonia pressure at equilibrium was one atmosphere.

When compared to the results of the present study, Hunt and Cowie's data¹⁰ at 20° are found to be displaced to the left of the curve shown in Fig. 1. This effect is more pronounced at higher mole ratios of ammonia to lithium borohydride, indicating a systematic error, possibly due to an impurity not accounted for in their calculations.¹³

(13) Since the preparation of this paper, D. J. Hunt has presented more recent and more extensive isotherm data for this system in his

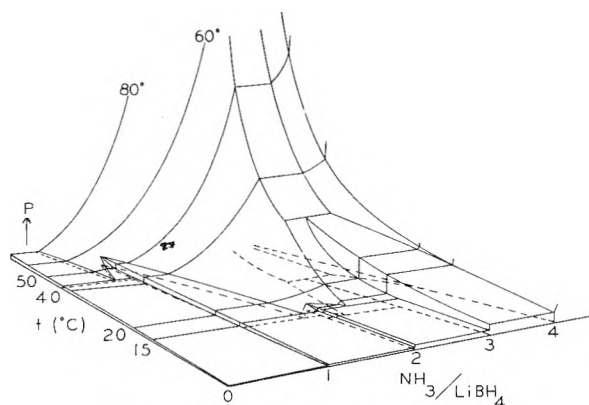
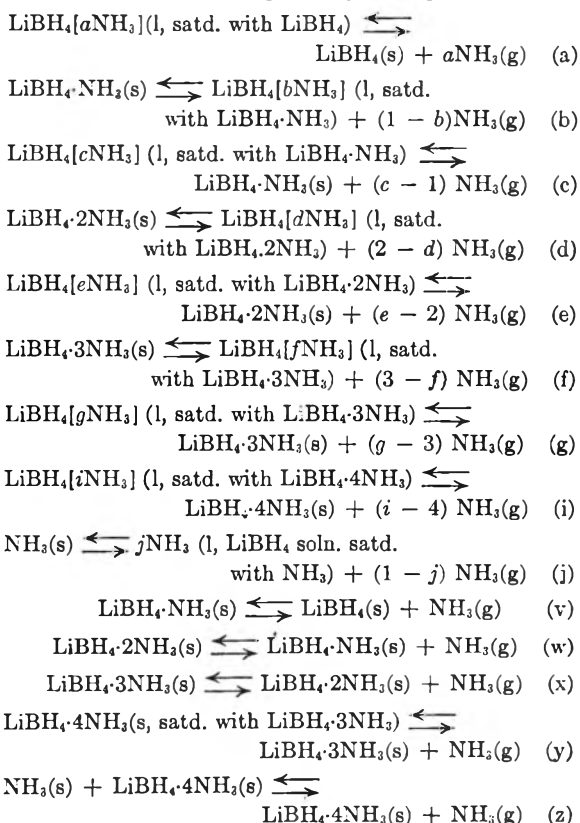


Fig. 6.—LiBH₄-NH₃ P-C-T diagram.

By combining the isotherm data between 0 and 80° with special attention to the compositions at which phase changes occurred, a temperature-composition phase diagram was constructed (see Fig. 5); this diagram shows the temperature and composition limits within which each of the phases can exist. The general natures of the various phase regions are considered to be conclusive and the equilibria involved in each of the two-phase regions indicated in Fig. 5 may be expressed as



The area designated as "h" is the one phase, solid solution region of lithium borohydride triammoniate in lithium borohydride tetraammoniate. Similar one-phase, solid solution regions may exist to some extent in the cases of the lower ammoniates, but the isotherms indicate that these areas must be very small, if they exist at all.

doctoral thesis at St. Louis Univ. The newer data are in substantial agreement with the results presented here.

All of the data for the lithium borohydride-ammonia system have been combined to form a three-dimensional P - C - T diagram, Fig. 6. This diagram defines the behavior of the system at equilibrium between mole ratios of zero and four, between 0 and 80°, and between pressures of 0 and 760 mm. The base plane of this figure is the temperature-composition phase diagram, Fig. 5.

In addition, the data have been treated as $\log P$ vs. $1/T$ for mole ratios from 0.8 to 3.8 between 0 and 80°. The experimental points were least-squared where possible to obtain the equation for the best straight line through them. Where only two points were available, the equation was

TABLE III
EQUILIBRIUM EQUATIONS FOR $\text{LiBH}_4\text{-NH}_3$

Composition mole ratio $\frac{\text{NH}_3}{\text{LiBH}_4}$		$\log P_{(\text{mm})} = -A/T + B$			$\frac{\Delta H}{\text{mole}}$ (kcal.)
Temp. range of applicability, °C.	A	B			
Liquid					
0.8	Above 48	2491	8.389	11.3	
1.0	Above 57	2339	8.263	10.7	
1.2	Above 53	2415	8.709	11.1	
1.4	Above 40	2276	8.528	10.4	
1.6	Above 30	2308	8.818	10.6	
1.8	Above 16	2391	9.259	10.9	
2.0	Above 17	2368	9.356	10.8	
2.2	Above 16	2344	9.429	10.7	
2.4	Above 17	2512	10.100	11.5	
2.6	Above 26	2345	9.709	10.7	
2.8	Above 40	2127	9.145	9.7	
Liquid + solid					
1 + 1(s)	Varies with compn. (cf. phase diagram)	1161	4.934	5.3	
1 + ss(s)	Varies with compn. (cf. phase diagram)	2970	11.852	13.6	
Solid					
3 \rightleftharpoons 2	Below 32	2141	9.177	9.8	
3 \rightleftharpoons 1	Below 15	2697	10.735	12.3	
2 \rightleftharpoons 1	Below 15	2253	8.722	10.3	

obtained using the two-point form. Mole ratios below 0.8 were omitted because the extremely small pressures involved were subject to large relative errors and a subsequent graph was unreliable. The empirical constants for the equation, $\log P_{\text{mm}} = -A/T + B$, determined as described above are found in Table III, together with the values of heat of vaporization per mole of ammonia, which was calculated from the slope of each line *via* the Clausius-Clapeyron equation.

When the density data obtained in this study had been plotted, it was found that they fell on a straight line for each of the compositions investigated. Application of the method of least squares gave equations for the best straight line through each set of data, the constants for which are listed in Table IV, together with the standard deviation of experimental densities from each line. The constant b is physically equivalent to the coefficient of expansion of the liquid having the corresponding composition. Figure 4 shows all four equations plotted together to demonstrate the regularity with which the density increases with composition.

TABLE IV
DENSITY EQUATIONS FOR $\text{LiBH}_4 \cdot x\text{NH}_3(\text{liq.})$

Composition Mole fraction ammonia (NH_3)		Mole ratio $\text{NH}_3/\text{LiBH}_4$ (x)	No. of exptl. detns.	Stand. dev. of exptl. values (σ)	a	b
0.515	1.06	38	0.001	0.651	2.54	
.634	1.73	52	.002	.663	3.68	
.702	2.36	33	.001	.676	4.20	
.733	2.74	31	.001	.684	4.43	

Acknowledgment.—The authors wish to acknowledge the many helpful suggestions of Dr. M. D. Banus and the assistance of Mr. M. B. Giusto.

The experimental work reported here was carried out under a contract with the Union Carbide Nuclear Company, Oak Ridge, Tennessee.

A PROTON MAGNETIC RESONANCE COMPARISON OF SILICOCHLOROFORM AND CHLOROFORM IN BASIC SOLVENTS

BY C. M. HUGGINS AND D. R. CARPENTER

General Electric Research Laboratory, Schenectady, New York

Received August 16, 1958

As part of a study of the physical properties of silicon-containing materials, the hydrogen-bonding behavior of silicochloroform (trichlorosilane) was investigated by the proton magnetic resonance technique. The resonance frequency of silicochloroform was measured over a concentration range in four solvents: cyclohexane, acetone, benzene and chloroform. From these measurements and comparison to previous data on chloroform, it was concluded that silicochloroform is a considerably weaker base and a slightly weaker acid than chloroform. These observations lend some evidence to the existence of $d\pi$ - $p\pi$ multiple bonding between silicon and chlorine.

Introduction

The proton magnetic resonance (p.m.r.) properties of chloroform (CHCl_3) dissolved in various solvents have been the subject of a reasonable amount of study.^{1,2} The single chloroform peak

has been shown to shift consistently to low field in such basic solvents as acetone, triethylamine and

(1) C. M. Huggins, G. C. Pimentel and J. N. Shoolery, *J. Chem. Phys.*, **23**, 1244 (1955).

(2) L. W. Reeves and W. G. Schneider, *Can. J. Chem.*, **35**, 251 (1957).

cyclohexene. These shifts have been attributed to molecular polarization effects associated with the formation of hydrogen bonds between chloroform and the basic solvent. To the contrary, however, the chloroform peak shifts to high field in the presence of such basic solvents as benzene, toluene and mesitylene.² It was argued that these shifts to high field are the result of the chloroform molecule assuming a preferential orientation with respect to the aromatic ring in which the proton is located along the ring axis. Diamagnetic currents induced in the ring set up dipole fields which are negative with respect to the applied field along the ring axis; hence, the resonance is shifted to higher applied fields. In addition, other p.m.r. investigations in previously-characterized, hydrogen-bonding systems have demonstrated that the technique can be used successfully to study the properties of systems for which other data are unavailable.³⁻⁷

As part of a continuing program for the study of the physical properties of silicon-containing compounds, the p.m.r. spectra of several systems are being studied. It would be expected that the silicon-containing compound should behave rather like the corresponding carbon compound with differences attributable to the changes in chemical bonding associated with replacing carbon by silicon. In particular, it is hoped to shed some light on the question of the existence of multiple bonding between silicon and certain electronegative elements.⁸⁻¹⁰

The hydrogen-bonding properties of silicochloroform (SiHCl_3) have been investigated by p.m.r. techniques as a part of this study. This compound affords an opportunity to study the effect of silicon substitution on the proton-donor properties of chloroform. Silicochloroform is particularly interesting because of the extent of previous work on the corresponding carbon compound and for its relative chemical stability compared to some other systems involving the silicon-hydrogen bond.

Experimental

All spectra were obtained on a Varian Associates V-4300B High Resolution NMR spectrometer operating at a field strength of approximately 9400 gauss and frequency of 40 megacycles. Chemical shifts were measured by the usual technique of superimposing an audiofrequency side band of a reference band onto the principal peak of the sample. The smaller total effects observed with silicochloroform made it necessary to measure chemical shifts to a precision of ± 0.2 c.p.s., so that each recorded measurement is the average of at least three determinations. For all measurements, except at the extreme dilutions, the individual measurements differed by not more than ± 0.4 c.p.s. The audiofrequency signal was furnished by a Hewlett-Packard 200CD Audio Oscillator and measured with a Hewlett-Packard 524B Frequency Counter from which the frequency could be read to ± 0.1 c.p.s.

The reference field was furnished by the absorption peak of cyclohexane which was added to the extent of 5% by

- (3) U. Liddel and N. F. Ramsey, *J. Chem. Phys.*, **19**, 1608 (1951).
- (4) C. M. Huggins, G. C. Pimentel and J. N. Shoolery, *THIS JOURNAL*, **60**, 1311 (1956).
- (5) B. N. Bhar and G. Lindström, *J. Chem. Phys.*, **23**, 1958 (1955).
- (6) A. D. Cohen and C. Reid, *ibid.*, **25**, 790 (1956).
- (7) E. D. Becker, U. Liddel and J. N. Shoolery, *J. Mol. Spect.*, **2**, 1 (1958).
- (8) K. S. Pitzer, *J. Am. Chem. Soc.*, **70**, 2140 (1948).
- (9) H. Gilman and G. E. Dunn, *Chem. Revs.*, **52**, 77 (1953).
- (10) A. G. MacDiarmid, *Quart. Rev.*, **10**, 208 (1956).

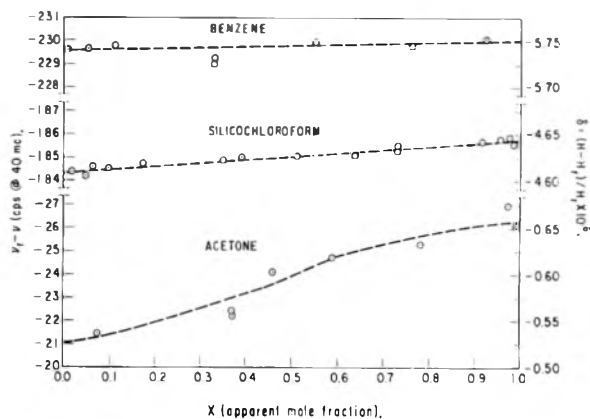


Fig. 1.—P.m.r. frequencies of benzene, silicochloroform and acetone dissolved in cyclohexane; $H_r = \text{C}_6\text{H}_{12}$.

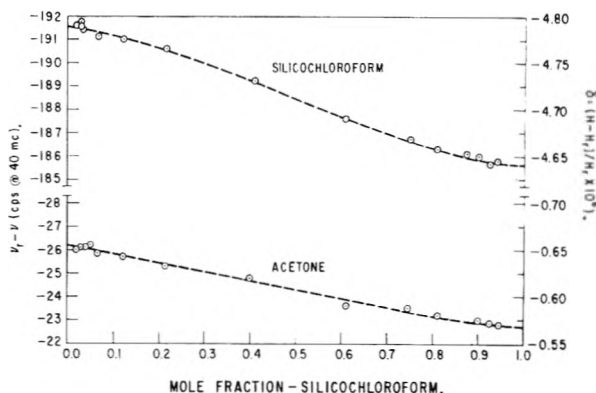


Fig. 2.—Concentration dependence of p.m.r. for silicochloroform in acetone solution; $H_r = \text{C}_6\text{H}_{12}$.

volume to all solutions not already including cyclohexane. The difficulty of making accurate corrections for volume susceptibilities of the several solutions precluded the use of an external reference. The concentration data, in every case, were corrected for the dilution effect of the cyclohexane; however, no attempt was made to correct the observed chemical shifts for the dilution effect of the added cyclohexane. This dilution effect, although finite, is quite small, as shown by the data for the silicochloroform-cyclohexane concentration dependence. It is, of course, assumed that the cyclohexane is chemically inert in these systems and that the only effect on the chemical shift is due to the small dilution.

All the solvents were commercial, analytical grade reagents which were used without further purification except for drying over Linde Molecular Sieve. The silicochloroform had been prepared locally and was redistilled in a packed column (b.p. 29.5°) to give a clear, colorless liquid, which was stored at 5° in an air-tight bottle until used. All glassware was baked overnight at 120° and rinsed in the solvent to be used. The final solutions were scanned at maximum gain for any spurious p.m.r. absorptions with particular attention to the region in which water would be expected; none were found.

Results and Discussion

The concentration dependence of the silicochloroform and solvent chemical shifts was studied in four solvents: cyclohexane, acetone, benzene and chloroform. The observations are plotted in Figs. 1-4. The concentrations are apparent mole fractions (moles SiHCl_3 /total moles solution) and the chemical shifts are shown both in c.p.s. (at 40 mc.) and in the dimensionless unit, $\delta = (H - H_r)/H_r$. The chemical shifts for the solvents (acetone, benzene and chloroform) are included on Figs. 2, 3 and 4.

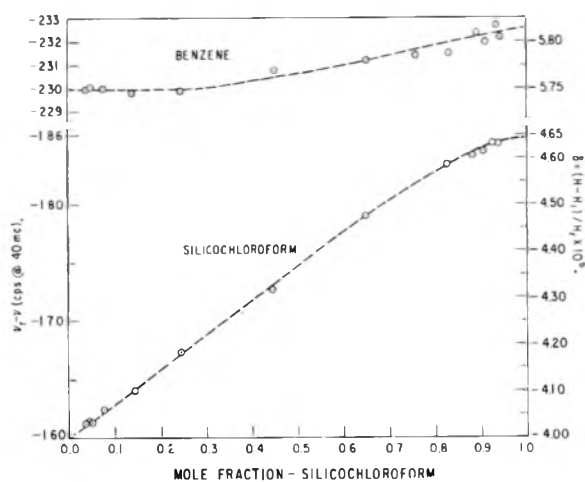


Fig. 3.—Concentration dependence of p.m.r. for silicochloroform in benzene solution; $H_r = C_6H_{12}$.

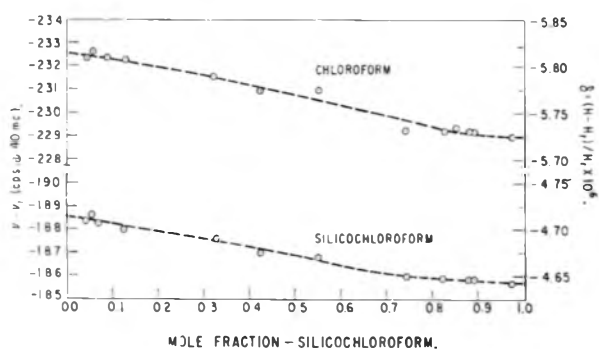


Fig. 4.—Concentration dependence of p.m.r. for silicochloroform and chloroform in mutual solutions; $H_r = C_6H_{12}$.

The data for the silicochloroform-cyclohexane system shows a dilution shift of +1.4 c.p.s. to high field as silicochloroform is dissolved in the inert solvent. This should be compared with the value of +11 c.p.s. for chloroform reported by Reeves and Schneider² (see note). This shift is considered to be a measure of a limited degree of self-association of chloroform. The smaller interaction could be attributed to a lowering of the acidity, basicity or a combination of both effected by the substitution of silicon in chloroform.

The dilution shifts of silicochloroform in acetone and benzene show definite interactions with these materials. For acetone, it is assumed that a weak hydrogen bond is formed between the silicochloroform proton and the lone-pair electrons of acetone. The resulting polarization of the silicochloroform shifts the resonance by about -5.8 c.p.s. to low field. The dilution shift of silicochloroform itself requires a correction of -1.4 c.p.s., so that the total observed shift of silicochloroform in acetone becomes -7.2 c.p.s. Due to the equilibrium between silicochloroform and the complex with acetone not proceeding to completion, the actual shift due to the formation of the hydrogen bond is considerably larger. (See Appendix for a quantitative discussion.)

The concentration dependence of silicochloroform in benzene shows the behavior to be expected with a π -donor material. Here, a larger shift of +24.3 c.p.s. (corrected for self-association) to high

field is observed for the silicochloroform protons to be compared with the previously-reported value of +54 c.p.s.² for chloroform in benzene.

NOTE Added on September 17, 1958.—Since submission of this report, E. D. Becker has informed us that he and J. N. Shoolery (unpublished work) determined the association shift of chloroform in cyclohexane to be 7 c.p.s. measured both with respect to cyclohexane as an internal standard and with respect to dioxane as an external reference. We remeasured the association shift by the techniques used in this paper and found 6.8 ± 0.2 c.p.s. for chloroform in cyclohexane. This revised datum required certain revisions in the text which have been incorporated where applicable.

These observations lend some evidence to the interpretation that while the chloroform interaction with n -donor systems is properly called hydrogen bonding, the interaction with π -donor systems is, in some ways, considerably different. First, the direction of the shift is opposite in the two systems and is determined by different factors: the induced polarization decreases the shielding upon interaction with n -donors by an amount roughly proportional to the strength of the hydrogen bond,⁴ but the shift to high fields observed with aromatic bases is undoubtedly due to increased shielding due to the "ring" diamagnetism of the aromatic. Second, the behavior of these shifts with respect to silicon substitution in chloroform indicates some difference in the kind of interaction: the observed shift is reduced sixfold in acetone, but is only reduced twofold in benzene solution.

Both of the solvents, acetone and benzene, behave as would be expected in the hydrogen-bonding environment. The observed shift of the acetone protons is -1.8 c.p.s. (including the dilution correction shown on Fig. 1) and for benzene the corresponding shift is -2.9 c.p.s. Each of these indicates mild polarization of the solvent molecule in which electrons are drawn away from the protons and toward the reactive center. It should be noticed that the measured shifts are with respect to an internal reference, cyclohexane. The apparent concentration independence of the relative shift may well reflect a net cancellation of two larger shifts. This effect is assumed not to be important here since only the differences are interpreted.

An interesting observation is shown in Fig. 4, in which the concentration dependence of both the chloroform and silicochloroform chemical shifts in mutual solutions are shown. As was shown earlier, the self-association shift for chloroform in cyclohexane of -6.8 c.p.s. is reduced to -1.4 c.p.s. for silicochloroform—a reduction of 80%. The data for silicochloroform-chloroform solutions make it possible to assign qualitatively portions of the lowered shifts to the Si-Cl and Si-H bonds individually. The extrapolated values of the various shifts are shown in Table I. It is seen that with a common base Cl_3CH the shift is reduced from 6.8 c.p.s. for $CHCl_3$ to 4.2 c.p.s. for $SiHCl_3$ and with the other common base, Cl_3SiH , the association shift is reduced from 2.5

c.p.s. for CHCl_3 to 1.4 c.p.s. for SiHCl_3 —reductions of about one-third in each case. A similar rearrangement of the data shows reductions of about two-thirds in the association shift due to the influence on the C-Cl bond. Consequently, subject to the naive assumption that the bonds can be treated independently, the lowered self-association due to the substitution of silicon for carbon in chloroform can be ascribed to a two-thirds decrease in basicity and a one-third decrease in acidity of chloroform.

TABLE I

COMPILATION OF PMR DATA FOR CHCl_3 AND SiHCl_3 AT INFINITE DILUTION

Data in parentheses estimated from refs. 1 and 2.

System	$(\nu - \nu_r)^a$	$\Delta\nu^b$
Cl_3CH in C_6H_{12}	-226.5	
Cl_3CH in $\text{O}=\text{C}(\text{CH}_3)_2$	(-264)	(-34)
Cl_3CH in C_6H_6	(-172)	(+54)
Cl_3CH in Cl_3CH	-233.3	-6.8
Cl_3CH in Cl_3SiH	-229.0	-2.5
Cl_3SiH in C_6H_{12}	-184.3	
Cl_3SiH in $\text{O}=\text{C}(\text{CH}_3)_2$	-191.5	-7.2
Cl_3SiH in C_6H_6	-160.0	+24.3
Cl_3SiH in Cl_3CH	-188.5	-4.2
Cl_3SiH in Cl_3SiH	-185.7	-1.4

^a ν_r : C_6H_{12} at 40 mc. ^b $\Delta\nu$ indicates shift from dilute solution in C_6H_{12} .

The p.m.r. behavior of silicochloroform with respect to intermolecular association has been shown to be quite similar to that of chloroform with suitable allowances for the differences in chemical bonding to silicon. In dilute solution in an inert solvent, the p.m.r. peak of the silicochloroform hydrogen is located 42 c.p.s. to higher field from chloroform—indicative of greater electron shielding as would be expected from the smaller electronegativity of silicon compared with carbon. This increased electron density at the silicochloroform proton is confirmed by the series of intermolecular association experiments in which it is shown that silicochloroform is a considerably weaker acid than chloroform.

The simple electronegativity argument would lead one to expect a corresponding increase in the basicity of silicochloroform due to the increased ionic character of the Si-Cl bonds. However, it was shown that actually the silicon compound is a weaker base, indicative of a smaller Si-Cl bond moment. This observation is consistent with other studies on the basicity of certain silicon compounds.^{9,10} The present interpretation of the anomaly lends evidence to the hypothesis of multiple bonding between silicon and highly electronegative elements such as chlorine. The electronegativity difference (Huggins: carbon, 2.6; silicon, 1.9; and chlorine, 3.15)¹¹ would tend to make the Si-Cl bond more ionic with a greater electron density on the chlorine atoms; however, it is argued that the electron-withdrawal power of the unfilled d-orbitals on the silicon more than compensates resulting in a decreased effective ionicity. This multiple $d_{\pi}-p_{\pi}$ bonding to silicon also has been invoked by West¹² to correlate observations on intermolecular association in silanols.

(11) M. L. Huggins, *J. Am. Chem. Soc.*, **76**, 4123, 4126 (1953).

Appendix

In this work, as well as many others,^{1,2,4,13} an attempt is made to measure the total effect on some spectrographic variable caused by the formation of a hydrogen bond to a particular material. The usual experiment involves the measurement of this quantity as a function of concentration and extrapolating to infinite dilution in the solvent of interest. For example, the p.m.r. shift of SiHCl_3 from the free molecule (actually measured at infinite dilution in inert solvent) to infinite dilution in acetone is 7.2 c.p.s. It is then often implied that this number represents the actual magnitude of the shift incurred in the formation of that particular hydrogen bond in the complex. It has been shown, but probably needs emphasizing, that this observed number is only a lower limit and may be an order of magnitude too low.

By making the usual assumptions,² the observed p.m.r. frequency (ν') is the arithmetic average of the monomer frequency, ν_A , and the complex frequency, ν_X

$$\nu' = \frac{A}{A+X} \nu_A + \frac{C}{A+X} \nu_X \quad (1)$$

In the particular example of chloroform-acetone, a 1-1 complex was assumed

$$A + B = X \quad (2)$$

where A is the total moles of monomer, B the total moles of base, and X the total moles of complex formed. If, then, A_0 and B_0 are the original numbers of moles added to the solution, the equilibrium constant in mole fraction units is

$$K = \frac{(X)(A+B+X)}{(A)(B)} = \frac{(X)(A_0+B_0-X)}{(A_0-X)(B_0-X)} \quad (3)$$

At infinite dilution, the fraction of A_0 in the complexed state is given by

$$\frac{(X)}{(A_0)} = \frac{K}{K+1} \quad (4)$$

Hence, it is obvious that A_0 is not completely complexed, except in the limit of large K . Substituting in equation 1, the measured p.m.r. frequency becomes

$$\nu' = \frac{1}{1+K} (K\nu_X + \nu_A) \quad (5)$$

In the chloroform-acetone system, $K = 1.8$. Hence, the total hydrogen-bonded shift would be 59 c.p.s. at 40 mc. compared to the observed dilution shift of 38 c.p.s.

In such systems as chloroform-benzene and silicochloroform-acetone, the smaller interaction indicates an even lower value of K and a corresponding increase in the deviation between the observed infinite-dilution value and the desired value for the pure complex.

It is obvious that this difficulty exists only when the measured quantity is a colligative property and, hence, is averaged over several states. At higher spectrographic frequencies (*i.e.*, infrared or ultraviolet), it is often possible to resolve the separate states, in which case no problem occurs.

(12) R. West, private communication, 1958.

(13) R. C. Lord, B. Nolin and H. D. Stidham, *J. Am. Chem. Soc.* **77**, 1365 (1955).

RESTRICTED DIFFUSION IN THREE-COMPONENT SYSTEMS WITH INTERACTING FLOWS

BY HIROSHI FUJITA¹

Department of Chemistry, University of Wisconsin, Madison, Wisconsin

Received August 15, 1968

The exact solutions are derived for one-dimensional restricted diffusion in a three-component system with interacting flows, under assumptions similar to those employed previously for the corresponding study of free diffusion for such a system. It is also assumed that the system contains two ionized solutes and that the specific conductance of the solution can be represented as a linear function of both solute concentrations. Combining this assumption with our exact solutions of the basic diffusion equations, two procedures are described which permit evaluation of the main and cross-term diffusion coefficients of the system. For the electrolyte solutes the measurement selected is the specific conductance of the solution as a function of time at some fixed positions along the cell. The equations presented may be applied to ternary solutions of non-electrolyte solutes, provided some quantity which depends linearly on solute concentrations can be accurately measured.

In a recent article Fujita and Gosting² presented procedures for the computation of the four diffusion coefficients of three-component systems from appropriate sets of experimental data obtained with the Gouy diffusimeter. These methods were based on the exact solution² of a modified form³ of Onsager's phenomenological flow equations, subject to the boundary conditions of *free* diffusion.⁴ Gosting and co-workers⁵⁻⁷ have applied them to several systems, electrolytes and non-electrolytes, with the ultimate aim to obtain data which may be used to verify Onsager's reciprocal relationships⁸ in the thermodynamics of irreversible processes.

In view of the increasing interest in experimental studies of the interaction of flows in multi-component systems, it seems worthwhile to develop additional approaches to the accurate evaluation of both the main and cross-term diffusion coefficients in such systems. In this connection it is to be noted that the current optical methods for the observations of free diffusion are inapplicable to solutions at very low concentrations. Harned and co-workers^{9,10} have developed a precise conductometric method for measuring the diffusion coefficient of a solution containing an electrolyte; they achieved remarkable success in studies at the very low concentrations. Their method is based on an approximate (series) relation for conductance *vs.* time when the redistribution of components takes place under the conditions of restricted diffusion.

The purpose of this report is to develop equa-

tions for the evaluation of studies of *restricted* diffusion as applied to three-component systems with interacting flows, and to present two procedures which may be used to determine the four diffusion coefficients of such systems with a reasonably high accuracy. The equations are applicable in the case of any experimental method which can provide the concentrations of the solution (or linearly related quantities) at two fixed levels in the diffusion cell as functions of time. For the present we shall restrict our discussion to systems which contain ionized solutes, as in the experiments of Harned and co-workers for binary solutions.

Solutions to the Diffusion Equations

Basic Equations.—We shall consider one-dimensional diffusion of two solutes in a liquid medium contained in a cylindrical cell of length $2l$, mounted vertically. The general equations for describing this diffusion process are³

$$\frac{\partial C_1}{\partial t} = D_{11} \frac{\partial^2 C_1}{\partial x^2} + D_{12} \frac{\partial^2 C_2}{\partial x^2} \quad (1)$$

$$\frac{\partial C_2}{\partial t} = D_{21} \frac{\partial^2 C_1}{\partial x^2} + D_{22} \frac{\partial^2 C_2}{\partial x^2} \quad (2)$$

where C_1 and C_2 are solute concentrations for components 1 and 2 (solvent is conveniently defined as component 0), expressed in moles per unit volume of solution; D_{11} and D_{22} are the main diffusion coefficients; and D_{12} and D_{21} are the cross-term diffusion coefficients. The positive direction of coordinate x is taken downward along the cell, with its origin at the mid-point between the top and bottom of the cell, and t is the time variable. It is noted that equations 1 and 2 have been derived on the same assumptions as those used previously for the earlier similar study on free diffusion² (see footnote 4).

Because neither solute can flow through the top and bottom of the cell, solutions $C_1(x,t)$ and $C_2(x,t)$ to equations 1 and 2 must satisfy the boundary conditions

$$\frac{\partial C_i}{\partial x} = 0 \quad (x = \pm l, t > 0) \quad (3)$$

where $i = 1$ and 2. The initial condition chosen here is that a sharp boundary is formed at $t = 0$ between the solutions A and B which are placed above and below the position $x = 0$, respectively. Thus for the two solutes ($i = 1, 2$)

(1) On leave from the Physical Chemistry Laboratory, Department of Fisheries, University of Kyoto, Maizuru, Japan.

(2) H. Fujita and L. J. Gosting, *J. Am. Chem. Soc.*, **78**, 1099 (1956).

(3) R. L. Baldwin, P. J. Dunlop and L. J. Gosting, *ibid.*, **77**, 5235 (1955); P. J. Dunlop and L. J. Gosting, *ibid.*, **77**, 5238 (1955).

(4) It was further assumed that the diffusion coefficients are all independent of solute concentrations and that no volume change occurs on mixing. These conditions are satisfied if the concentration differences across the diffusing boundary are taken sufficiently small; cf. L. J. Gosting and H. Fujita, *J. Am. Chem. Soc.*, **79**, 1359 (1957); H. Fujita, *THIS JOURNAL*, in preparation.

(5) P. J. Dunlop, *ibid.*, **61**, 994 (1957).

(6) P. J. Dunlop, *ibid.*, **61**, 1619 (1957).

(7) I. J. O'Donnell and L. J. Gosting, a paper in a Symposium at the 1957 meeting of the Electrochemical Society in Washington, D. C., John Wiley and Sons, N. Y., 1959.

(8) L. Onsager, *Phys. Rev.*, **37**, 405; **38**, 2265 (1931); S. R. de Groot, "Thermodynamics of Irreversible Processes," North-Holland Publishing Co., Amsterdam, 1952.

(9) H. S. Harned and D. M. French, *Ann. N. Y. Acad. Sci.*, **46**, 267 (1945).

(10) H. S. Harned and R. L. Nuttall, *J. Am. Chem. Soc.*, **69**, 736 (1947).

$$C_i(x,0) = \bar{C}_i + (\Delta C_i/2) \quad (0 < x < l, t = 0) \quad (4)$$

$$C_i(x,0) = \bar{C}_i - (\Delta C_i/2) \quad (-l < x < 0, t = 0) \quad (5)$$

where \bar{C}_i is the mean concentration of solute i between solutions A and B, *i.e.*

$$\bar{C}_i = [(C_i)_A + (C_i)_B]/2 \quad (6)$$

and ΔC_i is the concentration difference of solute i across the initial sharp boundary, *i.e.*

$$\Delta C_i = (C_i)_B - (C_i)_A \quad (7)$$

Solute Distributions.—The solutions of equations 1 and 2 subject to the initial and boundary conditions given above may be obtained using the technique of Laplace transform (*cf.* Appendix I). The final results are

$$C_1(x,t) = \bar{C}_1 + K_1^+ \Psi_1(x,t) + K_1^- \Psi_2(x,t) \quad (8)$$

$$C_2(x,t) = \bar{C}_2 + K_2^+ \Psi_1(x,t) + K_2^- \Psi_2(x,t) \quad (9)$$

in which

$$\Psi_1(x,t) = \frac{4}{\pi} \sum_{n=0}^{\infty} \frac{\sin [(2n+1)\pi x/2l]}{2n+1} \exp[-(2n+1)^2 \pi^2 t / 4l^2 \sigma_+] \quad (10)$$

$$\Psi_2(x,t) = \frac{4}{\pi} \sum_{n=0}^{\infty} \frac{\sin [(2n+1)\pi x/2l]}{2n+1} \exp[-(2n+1)^2 \pi^2 t / 4l^2 \sigma_-] \quad (11)$$

and

$$K_1^+ = \frac{(\sigma_+ - E) \Delta C_1 - F \Delta C_2}{2(\sigma_+ - \sigma_-)} \quad (12)$$

$$K_2^+ = \frac{(\sigma_+ - H) \Delta C_2 - G \Delta C_1}{2(\sigma_+ - \sigma_-)} \quad (13)$$

$$K_1^- = -\frac{(\sigma_- - E) \Delta C_1 - F \Delta C_2}{2(\sigma_+ - \sigma_-)} \quad (14)$$

$$K_2^- = -\frac{(\sigma_- - H) \Delta C_2 - G \Delta C_1}{2(\sigma_+ - \sigma_-)} \quad (15)$$

Here σ_+ , σ_- , E , F , G and H are constants which are related to the four diffusion coefficients D_{ij} ($i, j = 1, 2$) by the equations

$$\sigma_+ = \frac{1}{2} \{ D_{11} + D_{22} + [(D_{11} - D_{22})^2 + 4D_{12}D_{21}]^{1/2} \} / |D_{ij}| \quad (16)$$

$$\sigma_- = \frac{1}{2} \{ D_{11} + D_{22} - [(D_{11} - D_{22})^2 + 4D_{12}D_{21}]^{1/2} \} / |D_{ij}| \quad (17)$$

$$E = D_{11} / |D_{ij}| \quad (18)$$

$$F = D_{12} / |D_{ij}| \quad (19)$$

$$G = D_{21} / |D_{ij}| \quad (20)$$

$$H = D_{22} / |D_{ij}| \quad (21)$$

where

$$|D_{ij}| = D_{11}D_{22} - D_{12}D_{21} \quad (22)$$

In the limit $l \rightarrow \infty$, equations 10 and 11 reduce to (*cf.* Appendix II)

$$\Psi_1(x,t) = \Phi(\sqrt{\sigma_+} y) \quad (23)$$

$$\Psi_2(x,t) = \Phi(\sqrt{\sigma_-} y) \quad (24)$$

where $\Phi(q)$ is the error function defined by

$$\Phi(q) = \frac{2}{\sqrt{\pi}} \int_0^q \exp(-q^2) dq \quad (25)$$

and

$$y = x / (2\sqrt{t}) \quad (26)$$

Thus it is found that for a sufficiently long column equations 8 and 9 agree with the equations for sol-

ute distributions which were obtained previously² for the one-dimensional free diffusion in three-component systems with interacting flows.

Methods for Evaluation of the Four Diffusion Coefficients

An Equation for the Specific Conductance *vs.* Time.—As mentioned in the Introduction, it is assumed that the three-component system considered here contains ionized solutes. As in the treatment of Harned and co-workers^{9,10} for binary solutions of an electrolyte it is further assumed that the specific conductance L in such a three-component system is a linear function of solute concentrations C_1 and C_2 .

$$L = L\bar{C} + S_1(C_1 - \bar{C}_1) + S_2(C_2 - \bar{C}_2) \quad (27)$$

Here $L\bar{C}$ is the value of L for a solution in which the concentrations of solutes 1 and 2 are \bar{C}_1 and \bar{C}_2 , respectively, and S_1 and S_2 are defined by

$$S_1 = (\partial L / \partial C_1)_{C_2 = \bar{C}_2}, \quad S_2 = (\partial L / \partial C_2)_{C_1 = \bar{C}_1} \quad (28)$$

In general, $L\bar{C}$, S_1 and S_2 are all functions of \bar{C}_1 and \bar{C}_2 for a given three-component system and can be measured experimentally. Solute fractions β_1 and β_2 are defined on the basis of specific conductance as

$$\beta_1 = S_1 \Delta C_1 / \Delta L(0) \quad (29)$$

$$\beta_2 = S_2 \Delta C_2 / \Delta L(0) \quad (30)$$

where $\Delta L(0)$ is the difference in specific conductance between the given initial solutions A and B. It follows from equations 4, 5, 7 and 27 that

$$\Delta L(0) = S_1 \Delta C_1 + S_2 \Delta C_2 \quad (31)$$

Let us consider that two pairs of electrodes are placed at the positions $x = \pm 2l/3$ (Fig. 1) and that

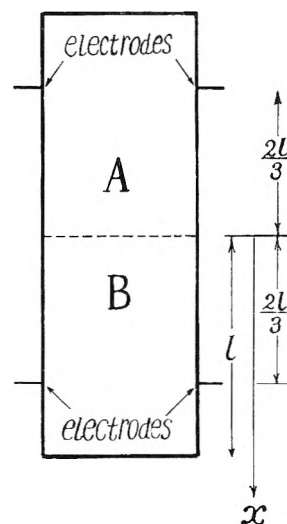


Fig. 1.—Diagram of the diffusion cell with two pairs of electrodes.

the specific conductance of the solution between each pair of electrodes is measured as a function of time. The two pairs of electrodes might be placed at other values of x so far as the first calculation method presented below is concerned. The only important condition here is that both pairs of electrodes are symmetric with each other about the position $x = 0$. In the second calculation method given below the particular positions of the elec-

trodes, $x = \pm 2l/3$, become essential to obtain a working equation for the development of the method.

The difference in specific conductance between the lower and upper pairs of electrodes at any time t will be denoted by using a notation $\Delta L(t)$, because in the limit $t \rightarrow 0$ it agrees with $\Delta L(0)$ defined above under the initial condition considered here. By definition we may write

$$\Delta L(t) = L(2l/3, t) - L(-2l/3, t) \quad (32)$$

Then, with equation 27, we have

$$\Delta L(t) = S_1[C_1(2l/3, t) - C_1(-2l/3, t)] + S_2[C_2(2l/3, t) - C_2(-2l/3, t)] \quad (33)$$

Introduction of the solute distributions, equations 8 and 9, into equation 33 and consideration of equations 29 and 30 leads to the desired expression for the difference in specific conductance at the electrodes as a function of time.

$$\Delta L(t) = 2\Delta L(0) \left[\left(\frac{\beta_1 K_1^+}{\Delta C_1} + \frac{\beta_2 K_2^+}{\Delta C_2} \right) \Psi_1(2l/3, t) + \left(\frac{\beta_1 K_1^-}{\Delta C_1} + \frac{\beta_2 K_2^-}{\Delta C_2} \right) \Psi_2(2l/3, t) \right] \quad (34)$$

Here use has been made of the property that $\Psi_i(x, t)$ ($i = 1, 2$) are odd functions of x . In the discussion which follows, the relation between $\Delta L(t)$ and t is simply called the curve of specific conductance *vs.* time. This curve may be obtained experimentally with very high accuracy if we use an apparatus such as that constructed and used by Harned and co-workers^{9,10} for the study of diffusion in binary solutions of an electrolyte. In what follows, two methods for calculating the values of the four diffusion coefficients are given under the assumption that curves of $\Delta L(t)$ *vs.* t are measured for at least two different values of β_1 with the same solute concentrations (\bar{C}_1 and \bar{C}_2) in each case. From the fact that $\Psi_i(x, t)$ ($i = 1, 2$) converge to zero as t goes to infinity it is seen that $\Delta L(t)$ approaches zero in the corresponding limit. In actual cases, the measurement of specific conductance cannot be continued for an infinitely long time but must be stopped when values of $\Delta L(t)$ become close to zero. Therefore, the experimental data for $\Delta L(t)$ may not be sufficient for evaluating accurately the zeroth and first moments of the $\Delta L(t)$ curve about $t = 0$ which appear in the methods presented below. Appropriate extrapolations of the measured $\Delta L(t)$ data beyond the time of actual measurement may then be required to compute the desired moments.

First Procedure. Evaluation of D_{ij} Using the Zeroth and First Moments from Curves of Specific Conductance *vs.* Time.—Integration of both sides of equation 34 with respect to t over the range $0 < t < \infty$ and use of the relation¹¹

$$\sum_{n=0}^{\infty} \frac{1}{(2n+1)} \sin \frac{(2n+1)\pi x}{2l} = \frac{\pi^3}{16l^2} \left(lx - \frac{x^2}{2} \right) \quad (0 < x < 2l) \quad (35)$$

yields

(11) See, for example, S. Moriguchi, *et al.*, "Mathematical Formulas," Vol. II, Iwanami Book Co., Tokyo, 1957, p. 74.

$$\int_0^{\infty} \Delta L(t) dt = \frac{8l^2 \Delta L(0)}{9} \left[\sigma_+ \left(\frac{\beta_1 K_1^+}{\Delta C_1} + \frac{\beta_2 K_2^+}{\Delta C_2} \right) + \sigma_- \left(\frac{\beta_1 K_1^-}{\Delta C_1} + \frac{\beta_2 K_2^-}{\Delta C_2} \right) \right] \quad (36)$$

Substitution for K_1^+ , K_1^- , K_2^+ and K_2^- from equations 12 to 15 and simplification of the resulting equations using the relations¹²

$$\beta_1 + \beta_2 = 1 \quad (37)$$

$$\beta_2(\Delta C_1/\Delta C_2) = (S_2/S_1)\beta_1 \quad (38)$$

$$\sigma_+ + \sigma_- = E + H \quad (39)$$

leads to the result

$$\frac{9}{4l^2} \int_0^{\infty} \frac{\Delta L(t)}{\Delta L(0)} dt = E - F(S_1/S_2) + \beta_1[H - E + F(S_1/S_2) - G(S_2/S_1)] \quad (40)$$

The definite integral appearing here represents the zeroth moment of the "reduced" $\Delta L(t)$ curve (*i.e.*, $\Delta L(t)/\Delta L(0)$) about the axis $t = 0$. It may be evaluated by numerical integration if the values of $\Delta L(t)$ are given over the complete range of t (> 0). In practice, where experimental data are used to evaluate this integral, some adequate extrapolation may be needed to find the values of $\Delta L(t)$ for t beyond the interval of actual measurement, as noted previously. It is obvious from their definitions that both $\Delta L(t)$ and $\Delta L(0)$ are functions of ΔC_1 and ΔC_2 . However, according to equation 40, a graph of the quantity in the left side of this equation is a straight line when plotted against β_1 ; and if its intercepts at $\beta_1 = 0$ and $\beta_1 = 1$ are denoted, respectively, by I_A and M_A , we have

$$I_A = E - F(S_1/S_2) \quad (41)$$

$$M_A = H - G(S_2/S_1) \quad (42)$$

In order that these two quantities, I_A and M_A , may be evaluated, it is apparent that the measurements of $\Delta L(t)$ have to be carried out for at least two different values of β_1 , while keeping the mean solute concentrations \bar{C}_1 and \bar{C}_2 fixed.¹³ Of course, more than two measurements are desirable to increase the accuracy of the intercepts in question.

Next, let us consider the integral

$$\int_0^{\infty} \Delta L(t)t dt$$

which represents the first moment of the $\Delta L(t)$ curve (for $t > 0$) about the axis $t = 0$. Following a procedure similar to that which we used to derive equation 40, it is shown that

$$\frac{243}{44l^4} \int_0^{\infty} \frac{\Delta L(t)}{\Delta L(0)} t dt = (E + H) [E - F(S_1/S_2)] - \sigma_+ \sigma_- + \beta_1(E + H) [H - E + F(S_1/S_2) - G(S_2/S_1)] \quad (43)$$

Combination of equations 16 to 22 gives

$$\sigma_+ \sigma_- = EH - FG \quad (44)$$

Then equations 41, 42 and 44 are substituted into equation 43, giving

$$\frac{243}{44l^4} \int_0^{\infty} \frac{\Delta L(t)}{\Delta L(0)} t dt = (E + H)I_A - EH + FG + \beta_1(E + H)(M_A - I_A) \quad (45)$$

(12) Equations 37 and 38 immediately follow from equations 29, 30 and 31, while equation 39 is obtained by adding equations 16 and 17 and then using equations 18 and 21.

(13) In general, all the diffusion coefficients, and hence E , F , G and H , are functions of C_1 and C_2 . Therefore, if the values of \bar{C}_1 and \bar{C}_2 are changed for different β_1 chosen, the linear relation in β_1 indicated by equation 40 may not be obtained.

This indicates that the quantity in the left side varies linearly with β_1 and gives I_B and M_B as the intercepts at $\beta_1 = 0$ and $\beta_1 = 1$.

$$I_B = (E + H)I_A - EH + FG \quad (46)$$

$$M_B = (E + H)M_A - EH + FG \quad (47)$$

In general, the value of the integral in equation 45 depends more importantly on the details of the asymptotic behavior of the $\Delta L(t)$ curve for large t than does the value of the integral in equation 40. Therefore, in order to obtain high accuracy for the intercepts I_B and M_B extreme caution is required for the extrapolations of experimental $\Delta L(t)$ curves to the region beyond the interval of the measurement. In any event, it is recommended that the conductance measurements be continued until $\Delta L(t)$ is as close as possible to zero. In practice, however, this may require that the experimental measurements be made over an exceedingly long period of time.

Equations 41, 42, 46 and 47 may be solved for E , F , G and H . Substitution of the results into equations 18 through 22 then yields the equations of D_{ij} in terms of I_A , M_A , I_B , M_B and (S_1/S_2) . They are

$$D_{11} = \frac{a(c - b) - d}{d(a - b)} \quad (48)$$

$$D_{12} = \left(\frac{S_2}{S_1}\right) \frac{a(c - a) - d}{d(a - b)} \quad (49)$$

$$D_{21} = \left(\frac{S_1}{S_2}\right) \frac{b(b - c) + d}{d(a - b)} \quad (50)$$

$$D_{22} = \frac{b(a - c) + d}{d(a - b)} \quad (51)$$

in which

$$a = I_A, b = M_A, c = \frac{M_B - I_B}{M_A - I_A}, d = \frac{M_B I_A - M_A I_B}{M_A - I_A} \quad (52)$$

Thus if the values of I_A , M_A , I_B and M_B are determined from $\Delta L(t)$ curves for more than one value of β_1 using the procedure described above and moreover if the ratio S_1/S_2 is measured, all the diffusion coefficients are evaluated readily by simple algebraic calculations. It is interesting to note that the evaluation of the main diffusion coefficients needs no experimental value of S_1/S_2 .

Second Procedure. Evaluation of D_{ij} Using Curves of Specific Conductance vs. Time and their Zeroth Moments.—The procedure described above involves no mathematical approximation and may be useful for practical purposes. However, it should be noted that experimental values of the first moment of the $\Delta L(t)$ curve usually are less accurate than those of zeroth moment because of their stronger dependence on the asymptotic behavior of $\Delta L(t)$ for large t . In this section, another method of calculation is developed which is based on directly measured $\Delta L(t)$ curves and their zeroth moments about the axis $t = 0$.

It is seen from equations 10 and 11 that if the electrodes are placed at $x = \pm 2l/3$, the second terms in the series $\Psi_1(x, t)$ and $\Psi_2(x, t)$ vanish, and we have

$$\Psi_1(2l/3, t) = \frac{2\sqrt{3}}{\pi} \left[e^{-(\tau/\sigma_+)} - \frac{1}{5} e^{-(25\tau/\sigma_+)} + O(e^{-(49\tau/\sigma_+)}) \right] \quad (53)$$

$$\Psi_2(2l/3, t) = \frac{2\sqrt{3}}{\pi} \left[e^{-(\tau/\sigma_-)} - \frac{1}{5} e^{-(25\tau/\sigma_-)} + O(e^{-(49\tau/\sigma_-)}) \right] \quad (54)$$

Here for simplicity of notation we have put

$$\tau = \pi^2 t / 4l^2 \quad (55)$$

Because the second and higher terms in the brackets in equations 53 and 54 approach zero much faster than do the first terms as τ increases, very good approximations to $\Psi_1(2l/3, t)$ and $\Psi_2(2l/3, t)$ would be¹⁴

$$\Psi_1(2l/3, t) = \frac{2\sqrt{3}}{\pi} e^{-(\tau/\sigma_+)} \quad (56)$$

$$\Psi_2(2l/3, t) = \frac{2\sqrt{3}}{\pi} e^{-(\tau/\sigma_-)} \quad (57)$$

if τ is not too small. The reason that we have chosen the positions $x = \pm 2l/3$ for the electrodes is to obtain these approximations for Ψ_1 and Ψ_2 . This is, of course, not a new idea but was originally used by Harned^{9,10} in accordance with the suggestion of Onsager.

Introduction of approximations 56 and 57 into equation 34, and rearrangement of the resulting equation after substituting for K_1^+ , K_2^+ , K_1^- and K_2^- from equations 12 through 15 yields

$$\frac{\pi}{2\sqrt{3}} \frac{\Delta L(t)}{\Delta L(0)} = \frac{e^{-(\tau/\sigma_+)}}{\sigma_+ - \sigma_-} \{ \sigma_+ - H - F(S_1/S_2) + \beta_1 [H - E + F(S_1/S_2) - G(S_2/S_1)] - \frac{e^{-(\tau/\sigma_-)}}{\sigma_+ - \sigma_-} \{ \sigma_- - H - F(S_1/S_2) + \beta_1 [H - E + F(S_1/S_2) - G(S_2/S_1)] \} \} \quad (58)$$

Here use has been made of equations 37 and 38 to rearrange the terms. By making use of equations 39, 41 and 42 this equation is simplified to

$$\frac{\pi}{2\sqrt{3}} \frac{\Delta L(t)}{\Delta L(0)} = e^{-(\tau/\sigma_-)} + \frac{1}{\sigma_+ - \sigma_-} [I_A - \sigma_- + \beta_1 (M_A - I_A)] [e^{-(\tau/\sigma_+)} - e^{-(\tau/\sigma_-)}] \quad (59)$$

As mentioned before, $\Delta L(t)$ curves have to be obtained experimentally for more than one value of β_1 (at the same mean solute concentrations) in order that the values of I_A and M_A may be determined. Let us take two of such experimental $\Delta L(t)$ curves and denote them by $\Delta L(t, \beta_1')$ and $\Delta L(t, \beta_1'')$. Here β_1' and β_1'' are the values of β_1 for which the $\Delta L(t)$ curves chosen have been measured. Because $\Delta L(0)$ is also a function of β_1 we have to write $\Delta L(0, \beta_1')$ and $\Delta L(0, \beta_1'')$ for $\Delta L(0)$ for $\beta_1 = \beta_1'$ and β_1'' , respectively.

By combining the above equations written for $\beta_1 = \beta_1'$ and β_2'' it can be shown that

$$f(t) - \sigma_+ g(t) = e^{-(\tau/\sigma_+)} \quad (60)$$

$$f(t) - \sigma_- g(t) = e^{-(\tau/\sigma_-)} \quad (61)$$

where

$$f(t) = \frac{\pi}{2\sqrt{3} (M_A - I_A) (\beta_1'' - \beta_1')} \{ [I_A + \beta_1'' (M_A - I_A)] \times [\Delta L(t, \beta_1') / \Delta L(0, \beta_1')] - [I_A + \beta_1' (M_A - I_A)] \times [\Delta L(t, \beta_1'') / \Delta L(0, \beta_1'')] \} \quad (62)$$

(14) Since, as noted previously, $\Psi_1(x, t)$ and $\Psi_2(x, t)$ are odd functions of x , the corresponding equations for $x = -2l/3$ are

$$\Psi_1(-2l/3, t) = -\frac{2\sqrt{3}}{\pi} e^{-(\tau/\sigma_+)}$$

$$\Psi_2(-2l/3, t) = -\frac{2\sqrt{3}}{\pi} e^{-(\tau/\sigma_-)}$$

$$g(t) = \frac{\pi}{2\sqrt{3}(M_A - I_A)(\beta_1'' - \beta_1')} \{[\Delta L(t, \beta_1') / \Delta L(0, \beta_1')] - [\Delta L(t, \beta_1'') / \Delta L(0, \beta_1'')]\} \quad (63)$$

From equations 60 and 61 we may derive the relations

$$[g(t)]^2 (\sigma_+)^2 + [g(2t) - 2g(t)f(t)] (\sigma_+) + [f(t)]^2 - f(2t) = 0 \quad (64)$$

$$[g(t)]^2 (\sigma_-)^2 + [g(2t) - 2g(t)f(t)] (\sigma_-) + [f(t)]^2 - f(2t) = 0 \quad (65)$$

Then it follows that

$$2g(t)f(t) - g(2t) = (\sigma_+ + \sigma_-) [g(t)]^2 \quad (66)$$

and

$$[f(t)]^2 - f(2t) = (\sigma_+ \sigma_-) [g(t)]^2 \quad (67)$$

These equations indicate that graphs of $2g(t)f(t) - g(2t)$ vs. $[g(t)]^2$ and $[f(t)]^2 - f(2t)$ vs. $[g(t)]^2$ are both straight lines passing through the coordinate origin and provide the values of $\sigma_+ + \sigma_-$ and $\sigma_+ \sigma_-$ as their slopes. It is important to note that these equations are based on the approximations for $\Psi_1(2l/3, t)$ and $\Psi_2(2l/3, t)$, i.e., equations 56 and 57, so that the expected linear plots may not be obtained with $f(t)$ and $g(t)$ for very small values of t .

With the values of $\sigma_+ + \sigma_-$ and $\sigma_+ \sigma_-$ known in this way I_B and M_B may be evaluated from the equations

$$I_B = (\sigma_+ + \sigma_-)I_A - \sigma_+ \sigma_- \quad (68)$$

$$M_B = (\sigma_+ + \sigma_-)M_A - \sigma_+ \sigma_- \quad (69)$$

which are derived by substituting equations 39 and 44 into equations 46 and 47. Of course, we assume here that the values of I_A and M_A have been determined from the zeroth moments of the given $\Delta L(t)$ curves. In fact, these values were already necessary to compute $f(t)$ and $g(t)$ from equations 62 and 63. When the numerical values for I_A , M_A , I_B and M_B are known in this way, the required four diffusion coefficients can be computed by substituting them into equations 48 through 52.

Discussion

No experimental data are as yet available in the literature on which the methods presented above may be tested. It is hoped that the availability of these methods will stimulate measurements of flow interactions in three-component systems. In the present study we have assumed that the system contains only ionized solutes. However, it is apparent that the theory developed can be applied to ternary solutions of non-electrolytes, provided some quantity which depends linearly on solute concentrations can be accurately measured (corresponding to the conductivity for electrolyte solutions). It may be possible to design an appropriate optical apparatus for measuring such quantities. In principle, the conductometric method may be used even if one solute of the given three-component system is a non-electrolyte (such as the system KCl-*raffinose*- H_2O^5). In general, the specific conductance L of such a solution will depend not only on the concentration of the electrolyte solute but also on the concentration of the coexisting non-electrolyte component. Then to a first approximation L may be represented as a linear function of both solute concentrations, as in equation 27.

Acknowledgments.—It is a pleasure to thank Professor L. J. Gosting for his interest and help given in the course of this investigation. Thanks are also due to Professor J. W. Williams who made it possible for the author to participate in the research program of his Laboratory. This work was supported in part by the National Institutes of Health (RG4912) and by the National Science Foundation (G2365).

Appendix I

The problem is to obtain the solutions of equations 1 and 2 subject to conditions 3, 4 and 5 by using the method of Laplace transform.

The subsidiary equations to equations 1 and 2 are

$$D_{11} \frac{d^2 u_1}{dx^2} + D_{12} \frac{d^2 u_2}{dx^2} = p u_1 - C_1(x, 0) \quad (1')$$

$$D_{21} \frac{d^2 u_1}{dx^2} + D_{22} \frac{d^2 u_2}{dx^2} = p u_2 - C_2(x, 0) \quad (2')$$

where u_1 and u_2 are the Laplace transforms of $C_1(x, t)$ and $C_2(x, t)$, respectively, i.e.

$$u_1 = \int_0^\infty e^{-pt} C_1 dt, \quad u_2 = \int_0^\infty e^{-pt} C_2 dt \quad (3')$$

Elimination of u_2 from equations 1' and 2' gives

$$(D_{12}D_{21} - D_{11}D_{22}) \frac{d^4 u_1}{dx^4} + p(D_{11} + D_{22}) \frac{d^2 u_1}{dx^2} - p^2 u_1 = -p C_1(x, 0) \quad (4')$$

Similarly we obtain for u_2

$$(D_{12}D_{21} - D_{11}D_{22}) \frac{d^4 u_2}{dx^4} + p(D_{11} + D_{22}) \frac{d^2 u_2}{dx^2} - p^2 u_2 = -p C_2(x, 0) \quad (5')$$

Here use has been made of the fact that $d^2 C_1(x, 0)/dx^2 = 0$ and $d^2 C_2(x, 0)/dx^2 = 0$; these are obvious from equations 4 and 5.

It is shown that the solutions of equations 4' and 5' satisfying the initial condition 4 and 5 are given by

$$u_1 = (1/p) [\bar{C}_1 + (\Delta C_1/2)] + P_1 e^{\alpha_1 x} + P_2 e^{-\alpha_1 x} + P_3 e^{\alpha_2 x} + P_4 e^{-\alpha_2 x} \quad (6')$$

$$u_2 = (1/p) [\bar{C}_2 + (\Delta C_2/2)] + A(P_1 e^{\alpha_1 x} + P_2 e^{-\alpha_1 x}) + B(P_3 e^{\alpha_2 x} + P_4 e^{-\alpha_2 x}) \quad (7')$$

for $0 < x < l$

and

$$u_1 = (1/p) [\bar{C}_1 - (\Delta C_1/2)] + P_1' e^{\alpha_1 x} + P_2' e^{-\alpha_1 x} + P_3' e^{\alpha_2 x} + P_4' e^{-\alpha_2 x} \quad (8')$$

$$u_2 = (1/p) [\bar{C}_2 - (\Delta C_2/2)] + A(P_1' e^{\alpha_1 x} + P_2' e^{-\alpha_1 x}) + B(P_3' e^{\alpha_2 x} + P_4' e^{-\alpha_2 x}) \quad (9')$$

for $-l < x < 0$

Here P_i and P_i' ($i = 1, 2, 3, 4$) are arbitrary constants; α_1 and α_2 are

$$\alpha_1^2 = (p/2|D_{ij}|) \{D_{11} + D_{22} + [(D_{11} + D_{22})^2 - 4|D_{ij}|]^{1/2}\} \quad (10')$$

$$\alpha_2^2 = (p/2|D_{ij}|) \{D_{11} + D_{22} - [(D_{11} + D_{22})^2 - 4|D_{ij}|]^{1/2}\} \quad (11')$$

with $|D_{ij}| = D_{11}D_{22} - D_{12}D_{21}$; and A and B are

$$A = (p - D_{11}\alpha_1^2)/(\alpha_1^2 D_{12}) \quad (12')$$

$$B = (p - D_{11}\alpha_2^2)/(\alpha_2^2 D_{12}) \quad (13')$$

The Laplace transforms of the boundary conditions for C_i ($i = 1, 2$), equation 3, are

$$\frac{du_i}{dx} = 0 \quad (x = \pm l) \quad (14')$$

The constants P_i and P'_i ($i = 1,2,3,4$) in equations 8' and 9' can be determined using these conditions and the requirement that both u_i and du_i/dx ($i = 1,2$) must be continuous at $x = 0$. Substitution of the results into equations 6' to 9' completes the solutions to equations 1' and 2'.

$$u_1 = (1/p) [\bar{C}_1 + (\Delta C_1/2)] + 1/[2(B - A)p] \times \left[(\Delta C_2 - B\Delta C_1) \frac{\cosh \alpha_1(x-l)}{\cosh \alpha_1 l} - (\Delta C_2 - A\Delta C_1) \frac{\cosh \alpha_2(x-l)}{\cosh \alpha_2 l} \right] \quad (15')$$

$$u_2 = (1/p) [\bar{C}_2 + (\Delta C_2/2)] + 1/[2(B - A)p] \times \left[A(\Delta C_2 - B\Delta C_1) \frac{\cosh \alpha_1(x-l)}{\cosh \alpha_1 l} - B(\Delta C_2 - A\Delta C_1) \frac{\cosh \alpha_2(x-l)}{\cosh \alpha_2 l} \right] \quad (16')$$

for $0 < x < l$

and

$$u_1 = (1/p) [\bar{C}_1 - (\Delta C_1/2)] - 1/[2(B - A)p] \times \left[(\Delta C_2 - B\Delta C_1) \frac{\cosh \alpha_1(x+l)}{\cosh \alpha_1 l} - (\Delta C_2 - A\Delta C_1) \frac{\cosh \alpha_2(x+l)}{\cosh \alpha_2 l} \right] \quad (17')$$

$$u_2 = (1/p) [\bar{C}_2 - (\Delta C_2/2)] - 1/[2(B - A)p] \times \left[A(\Delta C_2 - B\Delta C_1) \frac{\cosh \alpha_1(x+l)}{\cosh \alpha_1 l} - B(\Delta C_2 - A\Delta C_1) \frac{\cosh \alpha_2(x+l)}{\cosh \alpha_2 l} \right] \quad (18')$$

for $-l < x < 0$

The required solutions to equations 1 and 2 can then be obtained by inverting these equations for u_i to $C_i(x,t)$ using the Bromwich inversion theorem. Thus we have for $C_1(x,t)$ in $0 < x < l$

$$C_1(x,t) = \bar{C}_1 - \frac{2(\Delta C_2 - B\Delta C_1)}{\pi(B - A)} \sum_{n=0}^{\infty} \frac{\sin [(2n + 1) \pi x/2l]}{2n + 1} \times \exp [-(2n + 1)^2 \pi^2 t/4l^2 \sigma_+] + \frac{2(\Delta C_2 - A\Delta C_1)}{\pi(B - A)} \sum_{n=0}^{\infty} \frac{\sin [(2n + 1) \pi x/2l]}{2n + 1} \exp [-(2n + 1)^2 \pi^2 t/4l^2 \sigma_-] \quad (19')$$

where σ_+ and σ_- are the quantities given by equations 16 and 17 in the text.

Equations 12' and 13' are combined with equations 10' and 11' to give

$$A = \frac{2|D_{ij}| - D_{11} \{D_{11} + D_{22} + [(D_{11} + D_{22})^2 - 4|D_{ij}|]^{1/2}\}}{D_{12} \{D_{11} + D_{22} + [(D_{11} + D_{22})^2 - 4|D_{ij}|]^{1/2}\}} \quad (20')$$

$$B = \frac{2|D_{ij}| - D_{11} \{D_{11} + D_{22} - [(D_{11} + D_{22})^2 - 4|D_{ij}|]^{1/2}\}}{D_{12} \{D_{11} + D_{22} - [(D_{11} + D_{22})^2 - 4|D_{ij}|]^{1/2}\}} \quad (21')$$

These may be written in terms of σ_+ and σ_- as

$$A = \frac{1 - D_{11} \sigma_+}{D_{12} \sigma_+} \quad (22')$$

$$B = \frac{1 - D_{11} \sigma_-}{D_{12} \sigma_-} \quad (23')$$

Therefore we have

$$\frac{\Delta C_2 - B\Delta C_1}{2(B - A)} = \frac{\sigma_+ \sigma_- D_{12} \Delta C_2 - (\sigma_+ - \sigma_+ \sigma_- D_{11}) \Delta C_1}{2(\sigma_+ - \sigma_-)} \quad (24')$$

$$\frac{\Delta C_2 - A\Delta C_1}{2(B - A)} = \frac{\sigma_+ \sigma_- D_{12} \Delta C_2 - (\sigma_- - \sigma_+ \sigma_- D_{11}) \Delta C_1}{2(\sigma_+ - \sigma_-)} \quad (25')$$

Using equations 18, 19, 20, 21, 22 and 44 in the text these are rewritten

$$-\frac{\Delta C_2 - B\Delta C_1}{2(B - A)} = \frac{(\sigma_+ - E)\Delta C_1 - F\Delta C_2}{2(\sigma_+ - \sigma_-)} \quad (26')$$

$$\frac{\Delta C_2 - A\Delta C_1}{2(B - A)} = -\frac{(\sigma_- - E)\Delta C_1 - F\Delta C_2}{2(\sigma_+ - \sigma_-)} \quad (27')$$

which are in agreement with K_1^+ and K_1^- defined by equations 12 and 14. Thus equation 19' is written

$$C_1(x,t) = \bar{C}_1 + K_1^+ \Psi_1(x,t) + K_1^- \Psi_2(x,t) \quad (28')$$

with $\Psi_1(x,t)$ and $\Psi_2(x,t)$ given by equations 10 and 11. In a similar way we can derive from equation 17' an expression for $C_1(x,t)$ which is exactly of the same form as equation 28'. Also equations 16' and 18' can be inverted to give an equation for $C_2(x,t)$ which is in agreement with equation 9 in the text.

Appendix II

The problem is to derive the limiting forms of equations 8 and 9 in the case when l is indefinitely large. Because $\Psi_1(x,t)$ and $\Psi_2(x,t)$ are mathematically of the same form, it is sufficient if we can calculate the limiting form of J for $l \rightarrow \infty$, where

$$J = \frac{4}{\pi} \sum_{n=0}^{\infty} \frac{\sin [(2n + 1)\pi x/2l]}{2n + 1} \exp \left[- \left(n + \frac{1}{2} \right)^2 \pi^2 T/l^2 \right] \quad (1'')$$

Here T is t/σ_+ for $\Psi_1(x,t)$ and t/σ_- for $\Psi_2(x,t)$. It is readily shown that J can be written in the form

$$J = \frac{2}{\pi} \int_0^z \left[2 \sum_{n=0}^{\infty} q^{(n+(1/2))^2} \cos (2n + 1)z \right] dz \quad (2'')$$

where z and q are defined as

$$z = \pi x/2l \quad (3'')$$

$$q = e^{-\pi^2 T/l^2} \quad (4'')$$

The series in the brackets in equation 2'' may be expressed in terms of the theta function $\vartheta_2(v|\tau)$,¹⁵ giving

$$J = 2 \int_0^z \vartheta_2(z|\tau) dz \quad (5'')$$

Here τ is a pure imaginary quantity defined by

$$\tau = i\pi T/l^2 \quad (i = \sqrt{-1}) \quad (6'')$$

The Jacobi imaginary transformation¹⁶ in the theory of the ϑ functions gives for $\vartheta_2(z|\tau)$

$$\vartheta_2(z|\tau) = (-i\tau)^{-1/2} \exp \left(\frac{z^2}{\pi i \tau} \right) \vartheta_4 \left(-\frac{z}{\tau} \middle| -\frac{1}{\tau} \right) \quad (7'')$$

In the limit $l \rightarrow \infty$, we have from equations 3'' and 6''

$$1/\tau = O(-il^2) \rightarrow -i\infty \quad (8'')$$

$$z/\tau = O(-il) \rightarrow -i\infty \quad (9'')$$

$$z^2/\pi i \tau \rightarrow -x^2/4T \quad (10'')$$

It can be shown from the definition¹⁵ of $\vartheta_4(v|\tau)$ that under the limiting conditions 8'' and 9''

$$\lim_{l \rightarrow \infty} \vartheta_4 \left(-\frac{z}{\tau} \middle| -\frac{1}{\tau} \right) = 1$$

It is therefore seen that

(15) E. T. Whittaker and G. N. Watson, "A Course of Modern Analysis," 4th Ed., Cambridge Univ. Press, Cambridge, 1952, p. 464.

(16) E. T. Whittaker and G. N. Watson, ref. 15, pp. 474-6.

$$\lim_{l \rightarrow \infty} \vartheta_2(z|\tau) = \lim_{l \rightarrow \infty} l(\pi T)^{-1/2} \exp(-x^2/4T) \quad (11'')$$

Substitution of this into equation 5'' and consideration of equation 3'' leads to

$$\lim_{l \rightarrow \infty} J = (\pi T)^{-1/2} \int_0^x \exp(-x^2/4T) dx \quad (12'')$$

This integral may be expressed in terms of the error function Φ (see equation 25 in the text), and we have finally

$$\lim_{l \rightarrow \infty} J = \Phi(x/2\sqrt{T}) \quad (13'')$$

Thus

$$\lim_{l \rightarrow \infty} \Psi_1(x, l) = \Phi(\sqrt{\sigma_+} y) \quad (14'')$$

$$\lim_{l \rightarrow \infty} \Psi_2(x, l) = \Phi(\sqrt{\sigma_-} y) \quad (15'')$$

where

$$y = x/(2\sqrt{l}) \quad (16'')$$

THE STABLE CRYSTAL STRUCTURES OF PURE *n*-PARAFFINS CONTAINING AN EVEN NUMBER OF CARBON ATOMS IN THE RANGE C₂₀ TO C₃₆

BY STANLEY M. OHLBERG¹

Mellon Institute, Pittsburgh 13, Pa.

Received August 16, 1958

The long spacings of six pure *n*-paraffins containing an even number of carbon atoms were measured with an X-ray diffractometer. Application of a three-year incubation period at 37.5° permitted the unequivocal characterization of the stable crystalline modification for each compound and substantiated the purity of the samples as well. In the stable structures of eicosane, tetracosane and hexacosane the chains form a 63° 35' angle of tilt with the basal plane; this same angle is 60° 41' for octacosane, dotriacontane and hexatriacontane.

I. Introduction

A variety of polymorphic forms is reported in the literature² for *n*-paraffins containing an even number of carbon atoms despite the fact that only one solid phase is possible for a one-component system at equilibrium if the temperature is not invariant. The reasons for this apparent contradiction of the phase rule are the following: measurements were made on impure samples; the X-ray techniques were not sufficiently sensitive; the samples were not at equilibrium. The three phases most commonly reported can be designated as types A, B and C following the nomenclature of Müller³ and Piper, *et al.*,⁴ and correspond to orthorhombic, triclinic and monoclinic crystal systems, respectively.⁵

The purpose of the present work was to establish unequivocally the stable crystalline modification of pure even-numbered *n*-paraffins in the range C₂₀ to C₃₆.

II. Experimental

The samples were prepared at the Pennsylvania State University by Research Project 42 of the American Petroleum Institute.⁶ No solvent or other contaminants were used in preparing the X-ray diffraction samples. Five to ten mg. of the material was melted on a frosted glass slide and allowed to cool slowly. Van Nordstrand⁷ has found that the use of a frosted glass slide promotes good orientation of the crystallites as well as a layer of uniform thickness.

(1) Pittsburgh Plate Glass Research Center, P. O. Box 11472, Pittsburgh 38, Pa.

(2) W. C. McCrone, WADC Technical Report 54-349, 1954.

(3) A. Müller, *Proc. Roy. Soc. (London)*, **A127**, 417 (1930).

(4) S. H. Piper, A. C. Chibnall, S. J. Hopkins, A. Pollard, J. A. B. Smith and E. F. Williams, *Biochem. J.*, **25**, 2072 (1931).

(5) A. A. Schaefer, C. J. Busso, A. E. Smith and L. B. Skinner, *J. Am. Chem. Soc.*, **77**, 2017 (1955).

(6) R. W. Schiessler, C. H. Herr, A. W. Rytina, C. A. Weisel, F. Fischl, R. L. McLaughlin and H. H. Kuehner, *Proc. Am. Petroleum Inst.*, **26**, III, 254 (1946).

(7) Private communication from R. L. Van Nordstrand of the Sinclair Refining Company, Harvey, Illinois.

Measurements were made with a North American Philips X-ray diffractometer using nickel filtered Cu K radiation. The instrument was calibrated with micronized quartz as a primary standard and pure *n*-octacosane as a secondary standard. The 10-0 quartz peak occurring at 20.88° 2 θ for Cu K α radiation was carefully measured from a trace and the indicated instrumental correction was applied to the measured value of the 008 reflection for *n*-octacosane (see Fig. 1d) which occurs within 0.5° 2 θ of the value observed for the quartz peak. The Bragg angles for the 14 remaining 00 *l* reflections observed in the *n*-octacosane pattern were calculated from the corrected 008 reflection and these were compared with the measured values. It was found that the value of 2 θ could be read directly from the trace with an accuracy better than ± 0.02 over the range 2.7° to 40.6°.

III. Results

The effect of impurities and the nature of these phases is elucidated by an examination of some actual diffraction patterns. The diffraction pattern for recrystallized Eastman Kodak *n*-octacosane is shown in Fig. 1(a). This sample was of moderate purity and the crystalline phase is of the A type, *viz.*, the molecules are perpendicular to the basal plane. The basal reflections are labeled 001, 002, etc., and the long spacing is calculated readily from the Bragg equation. The reflections labeled 110 and 200 are side spacings characteristic of this orthorhombic structure.

The pattern for a distillation fraction of this material is shown in Fig. 1b. Two sets of basal spacings are observed, indicating the existence of two crystalline phases. The basal spacing for that phase characterized by the solid lines is nearly the same as that found for the undistilled material (37.5 Å.; see Fig. 1a) demonstrating that the phase is of the A type. That phase indicated by the dashed lines has a long spacing characteristic of the high purity C structure.⁵ Since the A phase reflections are more

(8) A. J. C. Wilson and H. Lipson, *Proc. Phys. Soc.*, **53**, 245 (1941).

intense than those observed for the C phase, the former is the major species present.

In Fig. 1c the diffraction pattern for another distillation fraction is shown. Here, the major phase is the high-purity, or C-type structure. By comparison with data obtained from binary mixtures of hexacosane and octacosane, the purity of this fraction is estimated to be better than 95% octacosane. It is to be noted that these two distillation fractions could not be differentiated by measurements of refractive index, distilling temperature or freezing point.

Finally, the pattern for pure *n*-octacosane (PSC 176-A.P.I. 42) is shown in Fig. 1d. Only the C phase characteristic of a high-purity material is found. A new pair of side spacings around the 008 reflection is also observed.

The initial measurements made on samples of hexacosane, dotriacontane and hexatriacontane show the existence of 2 phases in the case of the former compound and 3 phases for the latter two (see columns 2 and 3, Table I). Therefore, it follows that these samples were not at equilibrium and/or not pure. It was observed that when these samples were remelted, cooled and re-examined on the diffractometer, the relative concentrations of the phases changed. Hence, it was immediately obvious that the samples were not at equilibrium. Consequently the three samples were stored at 37.5° and examined intermittently with the X-ray diffractometer.

TABLE I

Compound	Long spacing (± 0.02 Å.)	Phase initially obsd. (relative concn.)	Equi- librium phase after 3 yr.	Angle of tilt which paraffin chain makes with basal plane
<i>n</i> -C ₂₀ H ₄₂	25.83	B	B	63°35'
<i>n</i> -C ₂₄ H ₅₀	30.42	B	B	63°35'
<i>n</i> -C ₂₆ H ₅₄	32.68	B (major)	B	63°35'
	31.08	C (minor)		60°41'
<i>n</i> -C ₂₈ H ₅₈	33.32	C	C	60°41'
	42.47	A (major)		90°0'
<i>n</i> -C ₃₂ H ₆₆	37.68	C (medial)	C	60°41'
	34.88	D (minor)		55°34' (?)
	47.60	A (major)		90°0'
<i>n</i> -C ₃₆ H ₇₄	42.22	C (minor)	C	60°41'
	39.08	D (medial)		55°34' (?)

At the end of six months the existence of more than one phase could still be detected in each sample; however, there was a very obvious trend toward an increase in the relative concentration of one particular phase. At the end of three years each sample exhibited the diffraction pattern of a single phase characteristic of a high-purity material. The measurements made on all six compounds are summarized in Table I.

The angle of tilt which an *n*-paraffin chain makes with the basal plane may be calculated from the long spacings provided the existence of a homologous series of crystals⁹ is established. The homologous nature of phases A, B and C, respectively, is demonstrated by a plot of the number of carbon atoms versus long spacing in Fig. 2.

(9) V. Vand, A. Aitken and R. K. Campbell, *Acta Cryst.*, 2, 398 (1949).

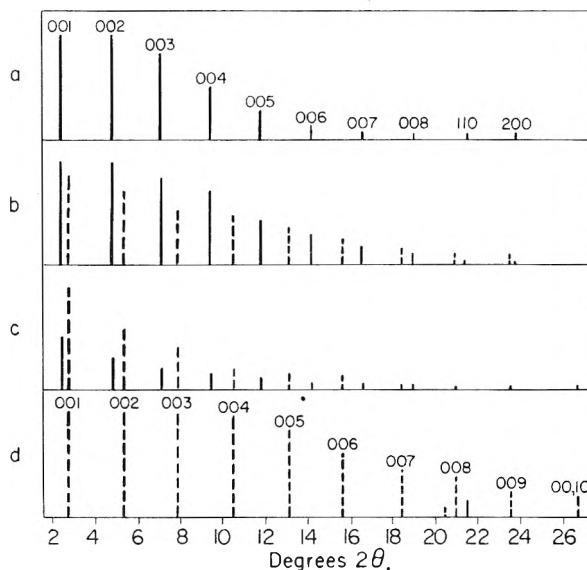


Fig. 1.—(a) X-Ray diffraction pattern of moderately pure *n*-octacosane; the single phase evidenced is orthorhombic. (b) X-Ray diffraction of a distillation fraction of moderately pure *n*-octacosane. The major phase (solid lines) corresponds to the same orthorhombic structure shown in (a). The minor phase (dashed lines) corresponds to a monoclinic structure. (c) X-Ray diffraction pattern of a distillation fraction of moderately pure *n*-octacosane. The major phase (dashed lines) corresponds to a monoclinic structure. The minor phase (solid lines) corresponds to the same orthorhombic structure shown in (a). (d) X-Ray diffraction pattern of a high purity sample of *n*-octacosane (PSC 176-A.P.I. 42). The single phase evidenced corresponds to the same monoclinic structure shown in (b) and (c).

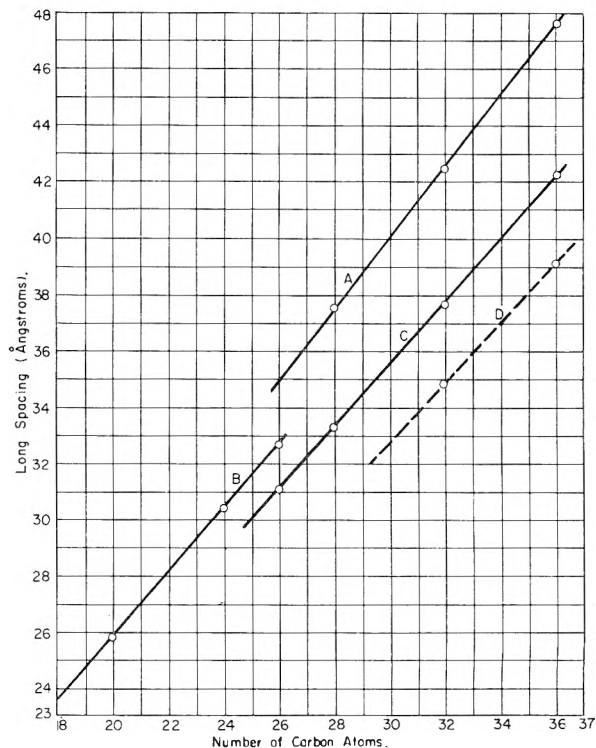


Fig. 2.—Long spacings initially observed for high purity *n*-paraffins except for the octacosane value on curve A, which was taken from a sample of only moderate purity.

The orthorhombic phase A is characteristic of normal alkanes having an odd number of carbon

atoms and either impure or metastable forms of those having an even number of carbon atoms. The chains are perpendicular to the basal plane and from the difference in basal spacing between the metastable A phases of dotriacontane and hexatriacontane (Table I), the length of one zig-zag of the chain is found to be 2.565 Å. If one then takes this value together with the value 1.534 Å. for C-C bond length determined by Shearer and Vand¹⁰ on a single crystal of hexatriacontane, the angle of the zig-zag can be calculated. The value found is 113° 28', in fairly good agreement with the value 112° 1' found by Shearer and Vand, and again demonstrates the discrepancy with the tetrahedral angle predicted by Ingold.¹¹

The average length of one zig-zag of a chain (2.546 Å.) taken from the single crystal work on hexatriacontane¹⁰ and the average increment per zig-zag in the long spacings of phase B (2.28 Å.) and phase C (2.22 Å.) were used to calculate the angle of tilt of the chains with respect to the basal plane (Table I).

It is to be noted that the C phase initially observed in hexacosane was metastable and a precursor of a stable phase for compounds containing a higher number of carbon atoms. In like manner, the metastable D phase initially observed in dotriacontane and hexatriacontane may be the precursor of a stable phase for *n*-paraffins containing more than 36 carbon atoms. If one assumes that the two metastable phases tentatively called D in Table I belong to the same homologous series of crystals, the average increment per zig-zag for the D phase would be 2.10 Å. and the molecular angle of tilt would be 55° 34'. Thus, the chains might be inclined to the basal plane at this angle in equilibrated samples of pure *n*-C₃₈H₇₈ or *n*-C₄₆H₉₂.

(10) H. M. M. Shearer and V. Vand, *ibid.*, **9**, 379 (1956).

(11) C. K. Ingold, *J. Chem. Soc.*, 305 (1921).

IV. Discussion

The *n*-paraffin crystal is held together by what is probably coordinate type bonding due to the end methyl groups¹² and the van der Waals forces between -CH₂- groups. Since the change in molecular angle of tilt is accompanied by a change in the number of -CH₂- groups in the chain, it must be a change in van der Waals forces which is responsible for the variation of the aforementioned angle. The additivity of van der Waals forces between -CH₂- groups on neighboring chains has been described by Vand and de Boer¹³ for *n*-paraffins having an odd number of carbon atoms. For these compounds, the additivity results in a decrease in the cross-sectional area of the chain with an increase in chain length. The results here show that the additivity of van der Waals forces in *n*-paraffins containing an even number of carbon atoms results in a decrease in the angle which the chain makes with the basal plane. At the same time, this angle does not change continuously with chain length. Thus, there is a suggestion of energy barriers which can be correlated with angles of tilt. It is hoped that when theoretical chemists are furnished with more detailed structural information, these phenomena can be explained quantitatively.

Acknowledgment.—The author wishes to express his appreciation to the Advisory Committee of the American Petroleum Institute Research Project 42 for the loan of the pure hydrocarbons and to the Petrolatum Fellowship at Mellon Institute for financing part of this research. Discussions with W. S. McClenahan and R. L. McLaughlin, formerly of the Petrolatum Fellowship, and H. P. Klug and L. E. Alexander of the Department of Research in Chemical Physics at Mellon Institute were very helpful in this work.

(12) E. W. Gorin, J. Walter and H. Eyring, *J. Am. Chem. Soc.*, **61**, 1876 (1939).

(13) V. Vand and J. H. de Boer, *Proc. Koninkl. Ned. Akad. Wet.*, **50**, 991 (1947).

A NEW APPROACH TO THE COMPARISON OF METAL CHELATE STABILITY CONSTANTS

BY HENRY FREISER, QUINTUS FERNANDO AND GRAEME E. CHENEY

Department of Chemistry, University of Arizona, Tucson 25, Arizona, and the

Department of Chemistry, University of Pittsburgh, Pittsburgh 13, Pennsylvania

Received August 18, 1968

The stability constants of metal chelates involving a wide variety of ligands have been correlated by plotting the log β_2 values (log K_1 for terdentates and polydentates) for nickel(II) against those for zinc(II). A similar plot using manganese(II) and zinc(II) has enabled the crystal field stabilization energy for nickel(II) to be calculated. The observed correlations have been discussed on the basis of crystal field theory.

In recent years a number of attempts have been made to correlate the stability constants of metal chelates with various properties of either the metal ion or ligand in order to evaluate the many factors affecting metal chelate stability.

The rationales for some of the correlations of properties of the metals with chelate stability such as that involving the number of d-electrons¹ or the

ionization potentials of the gaseous metal atoms² are based on the valence bond concept of bonding in metal chelates. Others, utilizing the electrostatic approach, include relations of stability to z/r the ionic potential,³ or z^2/r the coefficient of the Born

(1) H. Irving and R. J. P. Williams, *Nature*, **162**, 746 (1948).

(2) M. Calvin and N. C. Melchior, *J. Am. Chem. Soc.*, **70**, 3270 (1948).

equation.⁴ A third approach utilizing no particular structural model but rather the thermodynamic properties of the reactants also has been applied.⁵

Chelate stability has been found to increase linearly with variation of ligand basicity (proton affinity) in closely related compounds, as might be expected from the Lewis acid-base theory.^{6,7} Other qualitative correlations reveal the importance of such ligand properties as electronegativity of bonding atoms, resonance interactions, ring size and other steric factors.⁸

The correlation of stability with ligand basicity, although useful, has two major shortcomings with which this paper is concerned in eliminating. First, since the ligand molecule has at least two basic functionalities it is difficult to justify the use of but one pK value or attempt to use a proper combination of all. This difficulty is inherent in any comparison of the properties of a monobasic acid H^+ , with those of a polybasic acid M^{n+} . By replacing the pK of the ligand in the above relation with the logarithm of the stability of a metal capable of having the same coordination number as that of the metal already used, a comparison of ligands with two equally polybasic acids is achieved.⁹

Second, the relation has the shortcoming of implicitly involving all the complex-forming properties of the metal without permitting the specific evaluation of any of these. The proposed correlation will minimize the effect of all of those properties which the metal pair will have in common and will, by emphasizing those properties in which they differ, permit an assessment of these differences.

Largely because of these shortcomings, the pK -stability relationship is greatly restricted and only applies within a closely related series of ligands; the relationship that obtains for the β -diketones would not be applicable to the amino acids, etc. The proposed correlation will be seen to be much more general in scope.

Tables I and II give the stabilities of nickel and zinc chelates of seventy-nine chelating agents. The data for this correlation are from a recent comprehensive compilation of stability constants.¹⁰

TABLE I

No.	Ligand (-N-C-C-O)	Ni ⁺⁺	log β_2 Zn ⁺⁺	Mn ⁺⁺
1	Aminoacetic acid	11.15	9.72	6.63
2	α -Aminopropionic acid	10.66	9.56	6.05
3	Proline	11.3	10.2	5.5
4	Glutamic acid	10.34	9.46	
5	α -n-Propylaminoacetic acid	10.10	9.19	
6	α -S-Aminovaleric acid	8.74	7.30	
7	2-Aminohexanoic acid	11.1	10.4	5
8	2,6-Diaminohexanoic acid	8.8	7.6	

(3) A. E. Martell and M. Calvin, "Chemistry of the Metal Chelate Compounds," Prentice-Hall Inc., New York, N. Y., 1953, p. 191.

(4) G. Schwarzenbach, H. Ackermann and P. Ruckstuhl, *Helv. Chim. Acta*, **32**, 1175 (1949).

(5) H. Irving and H. Rossotti, *J. Chem. Soc.*, 2904, 2910 (1954).

(6) R. J. Bruehlman and F. H. Verboek, *J. Am. Chem. Soc.*, **70**, 1401 (1948).

(7) M. Calvin and K. W. Wilson, *ibid.*, **67**, 2003 (1945).

(8) Ref. 3, 1955, p. 134.

(9) L. G. Van Uitert and W. C. Fernelius, *J. Am. Chem. Soc.*, **76**, 193 (1954).

(10) "Stability Constants Parts I and II," The Chemical Society, London, 1957.

9	Arginine	9.2	7.8	
10	8-Hydroxycinnoline	14.9	12.73	
11	8-Hydroxyquinoline	20.40	17.56	15.45
12	8-Hydroxy-4-methylcinnoline	16.70	13.69	
13	Tyrosine	10.1	9.1	
14	8-Hydroxyquinoline-5-sulfonic acid	18.5	16.2	11.5
15	Quinoline-2-carboxylic acid	10.40	9.7	
16	8-Hydroxy-2-methylquinoline	17.76	18.72	13.99
17	8-Hydroxy-4-methylquinoline	22.29	20.24	15.55
18	8-Hydroxy-2,4-dimethylquinazoline	14.88	14.78	
19	Pteroylglutamic acid	9.0	7.5	
20	α -Isopropylaminoacetic acid		14.36	11.6
21	2-Amino-4-methylpentanoic acid		8.93	5.45

Ligand (-N-C-C-N)

22	1,2-Diaminopropane	13.71	10.87	
23	Dimethylglyoxime	21.7	13.9	
24	Dimethylglyoxime O-monomethyl ether	12.07	14.36	11.6
25	α - β -Diaminopropionic acid	15.2	11.5	
26	Ethylenediamine	13.34	10.43	4.79

Ligand (-O-C-C-O)

27	Tropolone	17.8	17.5	
28	Kojic acid	12.6	13.2	
29	α -Bromotropolone	12.1	12.7	
30	α -Methyltropolone	15.1	15.7	
31	β -Methyltropolone	15.0	15.2	
32	α -Isopropyltropolone	15.5	16.2	
33	β -Isopropyltropolone	19.0	19.3	
34	O,O-Dimethylpurpurogallin	11.8	12.5	
35	Oxalic acid	6.51	7.36	5.25

Ligand (-S-C-C-N-)

36	2-Mercaptoethylamine	19.81	18.90	
37	α -Amino- β -mercaptopropionic acid	19.3	18.2	

Ligand (-N-C-C-C-O-)

38	Quinoline-8-carboxylic acid	11.40	9.0	
----	-----------------------------	-------	-----	--

Ligand (-O-C-C-C-O)

39	Dibenzoylmethane	20.72	19.65	17.79
40	Acetylacetone	10.38	8.81	
41	Salicylaldehyde	9.19	8.10	6.79
42	Salicylaldehyde-5-sulfonic acid	6.56	5.4	

Ligand (-N-C-C-C-N)

43	1,3-Diaminopropan-2-ol	10.02	9.02	
44	Histamine	11.80	10.50	
45	1,3-Diamino-2,2-dimethylpropane	11.50	10.41	
46	2-O-Hydroxyphenylbenzothiazole	10.43	13.66	

Although not all the data were obtained under the same conditions of temperature, ionic strength or solvent medium, care was taken to select individual pairs of values for nickel and zinc which were obtained under the same experimental conditions. It may be noted further that whereas for most of the ligands log β_2 values have been employed, for ter-

TABLE II

No.	Polydentates	Ni ⁺⁺	$\log K_1$ Zn ⁺⁺	Mn ⁺⁺
47	Iminodiacetic acid	8.26	7.03	
48	Aminosuccinic acid	7.12	5.84	4
49	β -Carboxymethylaminopropionic acid	7.35	6.17	
50	Methyliminodiacetic acid	8.73	7.66	5.40
51	Cyanomethyliminodiacetic acid	6.2	5.8	3.50
52	N-(Carbamoylmethyl)-iminodiacetic acid	8.02	7.03	4.93
53	Glycylglycylglycine	3.99	3.33	1.41
54	N-2-Hydroxyethyliminodiacetic acid	9.28	8.33	5.55
55	Di-(2-hydroxyethyl)-aminoacetic acid	6.38	5.36	3.15
56	3-Hydroxypropyliminodiacetic acid	9.1	7.7	
57	Glycylglycine	4.49	3.80	2.15
58	2-Methoxyethyliminodiacetic acid	9.39	8.43	5.53
59	2-Methylthioethyliminodiacetic acid	10.00	8.28	5.10
60	2-Ethoxycarbonylaminoethyliminodiacetic acid	7.94	6.86	4.60
61	2-Di-(carboxymethyl)-aminoethyltrimethylammonium cation	6.0	5.34	2.87
62	3,3-Dimethylbutyliminodiacetic acid	8.70	7.92	5.55
63	Ethylenediamine-N,N-diacetic acid	13.73	11.93	7.71
64	2-Carboxyethyliminodiacetic acid	11.1	9.8	
65	Carboxymethyliminodipropionic acid	9.0	7.9	
66	2-Hydroxyethyliminodipropionic acid	5.7	4.6	
67	Ethylenediamine-N,N'-dipropionic acid	9.3	7.6	3.4
68	Nitrilotripropionic acid	5.8	5.3	
69	Phenyliminodiacetic acid	3.53	3.22	1.58
70	Ethylenediaminetetraacetic acid	18.56	16.26	13.58
71	N'-2-(Hydroxyethyl)-ethylenediamine-N,N,N'-triacetic acid	17.0	14.5	10.7
72	Ethylenediamine-N,N'-diacetic-N,N'-dipropionic acid	15.5	14.5	
73	2,2'-Bis-[di-(carboxymethyl)-amino-]-diethyl sulfide	14.95	13.17	9.64
74	Ethylenediamine-N,N,N',N'-tetrapropionic acid	9.7	7.8	4.7
75	N,N,N',N'-Tetrakis-(2-aminoethyl)-ethylenediamine	19.30	16.24	9.37
76	Nitrilotriacetic acid	11.26	10.45	7.44
77	2,2'-Diaminodiethylamine	10.7	8.9	3.99
78	2,2'-Diaminodiethyl sulfide	7.27	5.31	
79	2,2',2''-Triaminotriethylamine	14.8	14.65	5.8
80	N,N'-Di-(2-aminoethyl)-ethylenediamine	14.0	12.1	4.9
81	2-Mercaptoethyliminodiacetic acid	13.75	15.92	9.32

dentate and polydentate ligands only $\log K_1$ values have been used.

Previous workers have attempted a correlation using copper and nickel.¹¹ Nickel and zinc were chosen as the pair of metals from the same period, best suited for this correlation, for the following reasons.

(1) They both have the same charge and can assume the same coordination number. Both metals have the same octahedral configuration in their 6-coordinated compounds and contrast in their 4-coordinated complexes by having square coplanar and tetrahedral configurations for nickel and zinc, respectively. It is of course understood that the use of $\log \beta_2$ does not imply the assumption of a 4-coordinate nickel, or zinc since water molecules may occupy those positions not involved with the ligand. Indeed one of the advantages inherent in this correlation is the greater stability difference that would appear in the event that both metals assumed 4-coordination because of the resulting difference in steric requirements of the ligands.

(2) Although choice of a pair of metals from the same period balances most of their properties, the difference in the radii of these metals is sufficiently great to emphasize steric factors in chelate formation.

(3) Inasmuch as nickel has an incompleting subshell whereas zinc does not, a greater stability difference should be observed in chelates of ligands having the ability to π -bond.

(4) The difference in crystal field stabilization energy is almost at a maximum for zinc and nickel¹² so that an ordering of ligands with respect to their field strengths would be expected to be revealed in this correlation.

The most interesting feature of the correlation is its applicability to many types of chelating agents. For about forty-two compounds including bi- and polydentate aminoacids, 8-quinolinols, salicylaldehydes and β -diketones, the data may be represented to within 0.5 $\log K$ units by the line

$$\log \beta_{Ni} = 1.13 \log \beta_{Zn} \quad (1)$$

It is of further interest that those ligands for which marked deviations from this line are observed fall into well defined groups. For example, the behavior of the 5-membered ring-forming ligands involving two oxygen atoms may be described by a line parallel to the first but having an intercept of $-2.0 \log K$ units. Similarly the 5-membered ring-forming ligands involving two nitrogen atoms are described by a line displaced by almost $2.0 \log K$ units above the original line. These findings are consistent with trends in maximum stabilization energy as discussed by George.¹³ It is tempting to discover further family relationships among the remaining data. For instance the two examples of 5-membered ring-forming ligands involving sulfur and nitrogen fall on a line displaced by $-1.5 \log K$ units from the original line. It might be expected that ligands involving sulfur and oxygen would give rise to a line having a still more negative intercept.

(11) H. Irving and H. Rossotti, *Acta Chem. Scand.*, **10**, 72 (1955).

(12) O. G. Holmes and D. S. McClure, *J. Chem. Phys.*, **26**, 1686 (1957).

(13) P. George, *Rev. trav. chim. Pays-Bas*, **75**, 671 (1956).

Somewhat unexpected in the light of the behavior of the 5-membered ring-forming ligands is the independence of the position of the 6-membered ring formers upon the nature of the bonding atoms.

It may be noted that for most ligands below the line of equation 1, the metal stability sequence for the pair used is not in agreement with the Mellor-Maley order.¹⁴

The families of lines corresponding to the behavior of various ligands give strong indication that as electron donor capacity increases ($O > S, N$), nickel, the metal of greater π -bonding tendency, is favored over zinc.

The observed correlation is somewhat different from what might have been anticipated on the basis of crystal field theory. Since in nickel complexes as contrasted with those of zinc, there is a considerable contribution to stability from crystal field stabilization, one might have expected the slope of equation 1 to be significantly higher than unity. Instead, the slope of the line corresponding to equation 1 is so close to unity that the crystal field stabilization energy would have to be almost independent of the over-all stability. As a matter of fact, an alternative line of unit slope, reminiscent of the relation postulated by Irving and Rossotti,¹¹ may be drawn corresponding to the equation

$$\log \beta_{Ni} = \log \beta_{Zn} + 1.7 \quad (2)$$

which will adequately describe the behavior of almost forty of the compounds covered by equation 1. With equation 2, crystal field stabilization energy is independent of the stability and would seem to be dependent almost entirely on the nature of the bonding atoms. That the charge type of the ligand does not influence significantly the crystal field stabilization energy, may be seen from the adherence of both the simple and polydentate aminoacids to the same line.

As a means of further isolating the influence of crystal field and possibly also π -bond interactions, a second plot was carried out in the manner mentioned above using manganese(II) and zinc(II) as the metal pair. With the thirty-nine points available, a high degree of correlation was observed. Equation 3, $\log \beta_{Mn} = \log \beta_{Zn} - 3.0$, describes the behavior of about twenty-two ligands including many ligands which correspond to those obeying equation 1 in the nickel-zinc correlation. Unfortunately, insufficient data prevented our learning whether other ligands fell on the same line or whether a family of parallel lines would be necessary as with the nickel and zinc correlation.

(14) D. P. Mellor and L. Maley, *Nature*, **161**, 436 (1958).

With the help of equation 3 and the assumption of linear variation of stability with atomic number, it is possible to calculate a hypothetical nickel stability in which no crystal field stabilization effects are present. Subtracting this from the observed nickel stability, one obtains thereby an evaluation of the crystal field stabilization energy for manganese or zinc. This value is given by the expression

$$\text{C.F.S.E. for Ni} = 0.13 \log \beta_{Zn} + 1.2 \quad (4a)$$

or

$$= 2.9 \quad (4b)$$

depending on whether equation 1 or 2 is used in its derivation. In either case the crystal field stabilization for nickel is seen to vary between 2 and 3 log K units (2–3.5 kcal./mole) for five-membered ring formers involving nitrogen and oxygen as well as for a variety of 6-membered ring formers. The analysis of the spectra of nickel chelates of these types of ligands would make an interesting test of our findings.

The nickel-zinc correlation is a useful frame of reference against which to measure special ligand effects such as steric factors and resonance interaction. For example, both 2-methyl-8-quinolinol (16) and 8-hydroxy-2,4-dimethylquinazoline (18) in which steric hindrance to chelate formation has been recognized¹⁵ have nickel values that are low by some 2 to 3 log K units. Similarly the nickel value for 2,2',2''-triaminotriethylamine (79), a compound which conforms more easily to a tetrahedral than planar configuration,¹⁶ is low by about 2 log K .

The behavior of the tropolones¹⁷ which had been heretofore considered as somewhat anomalous are here shown to conform to a logical pattern, fitting with oxalic acid into the O-C-C-O family. This example underscores the greater utility of the correlation presented here over the conventional ligand basicity-chelate stability plot.

The positions of the chelates of both dimethylglyoxime (23) and its monomethyl ether (24) both seem unusual. Possibly in the former case the zinc complex may have a tetrahedral configuration so that the strong hydrogen bonds stabilizing the nickel chelate do not contribute to the zinc stability.

Acknowledgment.—The authors gratefully acknowledge the financial assistance of the U. S. Atomic Energy Commission.

(15) H. Irving, Butler and Ring, *J. Chem. Soc.*, 1489 (1949).

(16) H. Ackermann, J. E. Prue and G. Schwarzenbach, *Nature*, **163**, 723 (1949).

(17) B. E. Bryant and W. C. Fernelius, *J. Am. Chem. Soc.*, **76**, 4864 (1954).

SONICALLY INDUCED HETEROLYTIC CLEAVAGE OF POLYMETHYLSILOXANE

BY J. R. THOMAS AND L. DEVRIES

California Research Corporation, Richmond, California

Received August 19, 1968

The degradation of high polymers in solution by sonic radiation is known to be due to mechanical forces arising from cavitation of the fluid. The products of such degradation are known to be free radicals in the case of polymethyl methacrylate as shown by reaction of the products with 2,2-diphenyl-1-picrylhydrazyl (DPPH). Similar behavior is reported here for other vinyl polymers such as polystyrene and polyisobutene. In contrast polymethylsiloxane does not give products which react with DPPH when degraded. The products do react with methanol, an excellent nucleophile, however, indicating a heterolytic rather than a homolytic cleavage of the Si-O bond. It is suggested that the methanol reacts with an ion pair formed by mechanical stressing of the Si-O backbone bonds.

It has been shown that the degradation of high polymers in solution by ultrasonic radiation is due to hydrodynamic forces arising from cavitation of the fluid.¹

Henglein² has reported the use of 2,2-diphenyl-1-picrylhydrazyl (DPPH) to detect free radical fragment products of degradation of polymeric materials in solutions by ultrasonics. His work, which has been confirmed in this Laboratory, shows that polymethyl methacrylate yields free radicals when degraded by sonic or ultrasonic irradiation. We have observed similar behavior with other vinyl polymers such as polystyrene and polyisobutylenes and will report in detail upon this work at a later date. In the course of this study, the degradation of polymethylsiloxane was also examined. In contrast to the vinyl polymers, this material does not yield radicals when degraded. The purpose of this paper is to report the results of experiments showing that polymethylsiloxane, stressed by mechanical forces arising from cavitation of the fluid, degrades by a mechanism involving an ionic intermediate.

Experimental

Degradation of the polymer solutions was carried out in a Raytheon DF101 sonic oscillator operating at 10 kc. The machine was equipped with Teflon gaskets to avoid reaction of DPPH with the rubber commonly used. In all cases standard runs were included in each series of experiments so that daily variations in the power output of the oscillator would not affect the results. Samples were degassed and run under dry nitrogen.

The solvents were all of C.P. reagent grade, dried by distillation over calcium hydride. Care was used to exclude water during the transfer of solution to the sonic oscillator cell, although solutions were in contact with room air during the transfer. The polyisobutene (Paratone N) and polymethylsiloxane (DC 200-1,850,000 cs) were commercial polymers cleaned up by repeated precipitations with methanol. Molecular weights were determined by ultracentrifugation. The polystyrene was a laboratory sample prepared by bulk polymerization using dibenzoyl peroxide as catalyst.

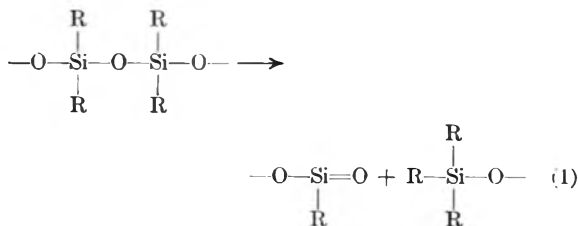
The radioactive methanol and benzene were purchased. Counting was done using a scintillation counter. In the tracer experiments the polymer was recovered for counting by repeated precipitations with methanol. The count did not change with additional precipitation.

Results

When polyisobutene is degraded by sonic irradiation in the presence of DPPH, free radical production is observed and measured by conversion of the highly colored radical state of DPPH to a

colorless form resulting from reaction with reactive radicals. In our experiments 3% (by weight) of polyisobutene in either isoöctane or benzene produced enough radicals to decolorize the order of 10 mg. DPPH/100 cc. in 15 minutes. The rate of radical production as measured by DPPH decolorization was independent of DPPH concentration down to concentrations of the order of 5 mg./100 cc. With 3% dimethylsiloxane in these solvents, as well as in *n*-heptane, however, the loss in DPPH in 15 minutes was no greater than the loss with pure solvent under similar conditions. This amounted to about 0.3 mg./100 cc. in 15 minutes which was about the uncertainty in the measurements. Degradation of the polysiloxane was taking place, however, as shown by the loss in viscosity of the solution. Under conditions where the reduced specific viscosity (η_{sp}/C) of polyisobutene at 1% in isoöctane dropped 18% that of the polysiloxane decreased 24%. The average degree of polymerization of the polyisobutene was 2110, while that of the polysiloxane was 2570 as determined by ultracentrifuge sedimentation measurements. The similar reduction in η_{sp}/C for polymers of nearly the same degree of polymerization is good evidence that about the same number of bonds are being broken in both polymers.

Failure to detect free radicals during the degradation of the polysiloxane could be explained in several ways. It is possible that the radicals formed by rupture of the Si-O bond do not react with DPPH. This seems very unlikely, however, since there is not a prior reason to expect such behavior. A second possibility is that the polysiloxane degrades by an intramolecular disproportionation reaction to give two stable molecular fragments as shown in 1



A third possibility is that the bond cleavage is heterolytic yielding ions rather than radicals. The highly polar nature of the Si-O bond suggests this as a likely possibility.

(1) H. H. G. Jellinek, "Degradation of Vinyl Polymers," Academic Press, Inc., New York, N. Y., 1955.

(2) Von Arnim Henglein, *Makromol. Chem.*, **15**, 188 (1955).

To test the possibility of heterolytic cleavage, the degradation of the polysiloxane was studied in the presence of C^{14} tagged methanol. Methanol, an excellent nucleophile, is known to react very rapidly with carbenium ions and would be expected to react similarly with siliconium ions. Recovery of the polymer following degradation showed that the tagged methanol was incorporated in the polymer fragments. Figure 1 shows the amount of methanol incorporated in the degraded polysiloxane as a function of concentration of methanol during 20 minutes of irradiation. These data show that at a concentration of about 1%, the methanol is scavenging all of the reactive intermediates with which it will react. In these experiments 20 mg. DPPH/100 cc. was present to ensure against reaction of any free radicals produced with the methanol. Separate experiments showed the DPPH to have no effect upon methanol incorporation. Similar experiments with polyisobutene and polystyrene both in the presence and absence of DPPH showed zero incorporation of methanol. In order to show that thermal reaction between silicone and methanol cannot be responsible for the observed behavior, a solution of polysiloxane in benzene was refluxed for four hours with 1% tagged methanol and the polymer recovered. No activity was incorporated in the polymer. A similar result was obtained when a polysiloxane solution was degraded for 20 minutes and the tagged methanol added to the solution immediately thereafter.

Calculation of the number of broken bonds in the polysiloxane from the methanol incorporation (assuming one methanol capture per break) gives 19×10^{-7} mole of broken bonds per gram of polymer. Under similar conditions (assuming the destruction of two DPPH's per break), DPPH experiments show 8×10^{-7} mole of broken bonds per gram of polymer for the polyisobutene. This is satisfactory agreement to support our previous contention that about the same number of bonds were broken in the two polymers. The polymer samples under study were not fractionated samples. Since the change in η_{sp}/C is a complex function of the molecular weight distribution, it is not surprising the number of broken bonds of the two samples differ somewhat.

The change in η_{sp}/C was determined for the polysiloxane in benzene, isoöctane and in benzene plus 1% methanol. These data are plotted in Fig. 2. The data obtained in dry benzene and benzene plus methanol are the results of triplicate runs. Methanol has a measurable but very slight effect upon the rate of degradation as shown.

Experiments also were run in which C^{14} and H^3 tagged benzene were used as solvents. In neither case was radioactivity present in the recovered polymer.

Discussion

The pronounced efficiency of methanol, a strongly nucleophilic reagent, in reacting with the fragments of polymethylsiloxane suggests strongly that the degradation process involves heterolytic cleavage of the Si-O bonds. It is unlikely, however, that the ionic fragments are separated by an ap-

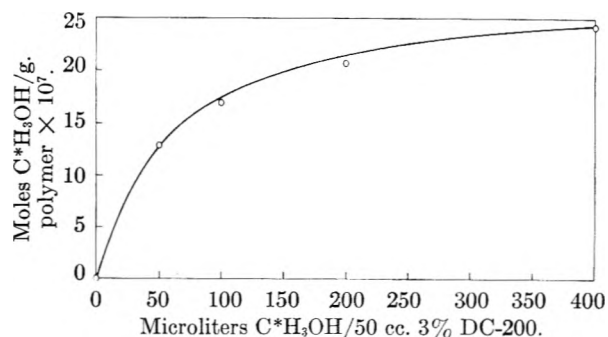


Fig. 1.—Moles of C^{14} tagged methanol incorporated per gram of polymethylsiloxane versus methanol concentration.

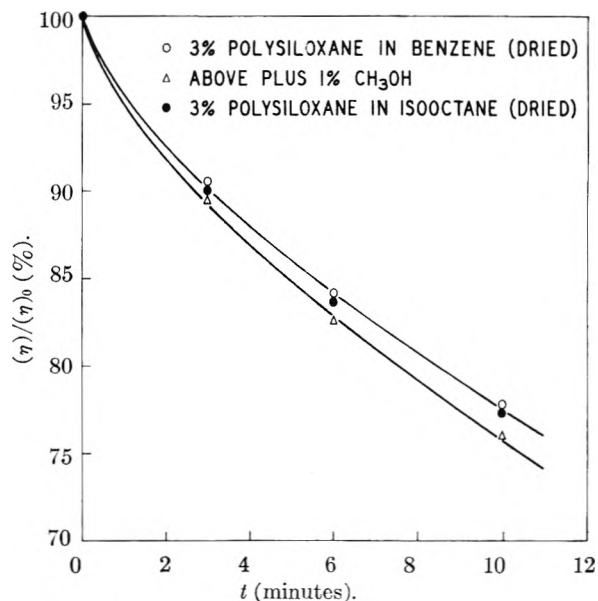
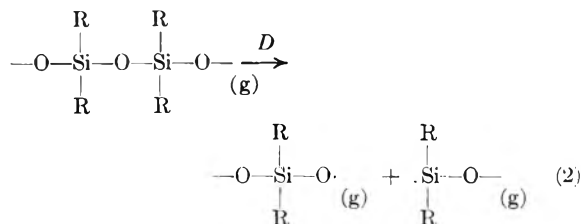


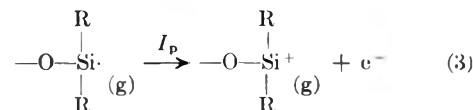
Fig. 2.—Loss in reduced specific viscosity versus time.

preciable distance. Energetically such a process would probably be unfavorable in comparison to separation into radicals.

Reaction 2 shows the cleavage of an Si-O bond to give radical fragments with the dissociation energy D . The ionization of $-OSiR_2\cdot$ radical as in

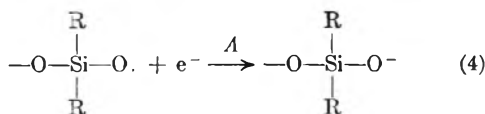


(3) would require 187 kcal./mole



assuming that the radical has the same ionization potential as silicon.³ The energy of the reaction of $-OSiR_2O\cdot$ to give the counter ion as in (4) is calculated to be 50.6 kcal./mole assuming the radical to have the same electron affinity as oxygen.³

(3) W. M. Latimer, "Oxidation Potentials," Prentice-Hall Inc., New York, N. Y., 1938



Since the heat of solution of polysiloxane is relatively very small it is apparent that degradation into ions can be less energetic than cleavage into radicals only if $I - A - 2H_{\pm} < 0$ (5) where H_{\pm} is the average heat of solution of the ions in the solvent. Using the above values of I and A , H_{\pm} would have to be greater than 68 kcal./mole for (5) to be satisfied. The heat of solution of Na^+ in water is given by Latimer³ as 96.8 kcal./mole. By comparison it seems unlikely that the heats of solution of the ions under consideration in low dielectric media such as benzene could be as large as 68 kcal. Calculation of the polarization energy of the ions in a non-polar medium cannot be made with any accuracy because not enough is known about ionic sizes, dielectric saturation and specific orientation effects of the solvent molecules about the ion. Estimation of the heat of solution of Si^+ ($r = 0.65 \text{ \AA.}$) in benzene by Born's equation⁴ gives 145 kcal./mole which is obviously much too high.

While the above argument is not rigorous in excluding the formation of ions separated to large distances, it suggests that an ion pair is more likely to be the reactive intermediate formed in degradation of the polysiloxane and that it then reacts rapidly with the methanol in cases where methanol is present.

In the absence of methanol a competing reaction must be in effect. Solvent does not appear to be involved since there is no evidence for participation of benzene, the most nucleophilic solvent used, as shown by the tagged benzene results. It is possible that disproportionation of the ion pair to give the products shown in equation 1 may be in-

(4) M. Born, *Z. Physik*, **1**, 45 (1920).

involved. It is also possible that trace impurities of highly nucleophilic materials such as water may be involved in the experiments devoid of methanol. Although care was taken to exclude water, experimental considerations necessitated contact of the samples with room air for a brief period. Furthermore, it should be noted that the total reaction involved only about 2×10^{-6} mole of broken bonds, and small quantities of impurity might suffice.

At first sight it is surprising that methanol has so little effect upon the rate of degradation as measured by changes in η_{sp}/C and that the rates in different solvents are essentially identical. In conventional thermally activated reactions, the alternative degradation reactions proposed would be expected to have different activation energies and the ratio of the rates would be proportional to the Boltzmann factor, $e^{\Delta E/RT}$. Reactions induced by mechanical forces, such as arise from cavitation, are quite different, however. Since the activation energy is not supplied thermally, the number of molecules having sufficient energy to react is not given by the Boltzmann factor. Instead it will be determined by the number of molecules occupying sites where the mechanical forces are sufficiently high. The number of effective sites will be determined by the required activation energy for a particular process. For polymer degradation by cavitation, it will be shown in a subsequent publication that the rate of degradation is approximately proportional to the inverse of the activation energy. Consequently, a difference of several kcal./mole in activation energy in processes requiring the order of 80 kcal./mole, $D(\text{C}-\text{C})$ will cause a difference in rate of only a few per cent.

Acknowledgment.—The authors wish to thank Dr. B. A. Fries for making the radioactive analyses and Prof. S. Winstein for a helpful discussion.

SEPARATION OF METAL IONS BY MEANS OF ION EXCHANGE MEMBRANES. I. SEPARATION OF RARE EARTH MIXTURES, AND OF THORIUM-RARE EARTH MIXTURES USING ETHYLENEDIAMINETETRAACETIC ACID

BY K. BRIL, S. BRIL AND P. KRUMHOLZ

Contribution from the Research Laboratory of Orquima S.A., São Paulo, Brazil

Received August 22, 1968

A method of separation of metal ions by electromigration in partially complexed solutions is described. The method makes use of ion-exchange membranes. Ethylenediaminetetraacetic acid is used as the complexing agent. Good separations are obtained in mixtures of lanthanum, praseodymium and neodymium as well as of thorium and neodymium. The separation is affected by the nature of the accompanying anions. The influence of perchlorate, chloride, nitrate and acetate is studied.

Complexing agents are widely used for the separation of metal ions of otherwise very similar properties, as for instance rare earth ions. If a solution containing two metal ions Me_1 and Me_2 is partially complexed with a complexing agent Y , the relative composition of the complexed part of the mixture,

$(\text{Me}_1\text{Y})/(\text{Me}_2\text{Y})$, will be different from that of the uncomplexed one, $(\text{Me}_1)/(\text{Me}_2)$, and also from the original composition, $(\text{Me}_1^0)/(\text{Me}_2^0)$, provided that the complexes formed are of different stability. In order to achieve a practical separation a method has to be applied which permits the separation of

the complexed and uncomplexed part of the mixture. Ion-exchange resins, precipitating agents, solvents, etc., are commonly used for this purpose. We thought that a rather clean separation should be possible by means of electromigration, with the use of ion-exchange membranes, provided that the complexes formed be either charge free or anionic. In the following some results are reported concerning the separation of lanthanum-neodymium, lanthanum-praseodymium-neodymium, and thorium-neodymium, partially complexed with ethylenediaminetetraacetic acid (Edta = Y).

$$K_1^2 = \frac{(Me_1)(Me_2Y)}{(Me_2)(Me_1Y)} F = \frac{K_2}{K_1} \quad (1)$$

where K_1 and K_2 represent stability constants of Me_1Y and Me_2Y , respectively, and F is the activity coefficient factor¹; ionic charges are omitted. It is convenient to define the "decontamination factors" α_2^1 and β_2^1

$$\alpha_2^1 = \frac{(Me_1Y)/(Me_2Y)}{(Me_1^0)/(Me_2^0)} \quad (2)$$

$$\beta_2^1 = \frac{(Me_1)(Me_2)}{(Me_1^0)(Me_2^0)} \quad (3)$$

Both α_2^1 and β_2^1 depend upon the equilibrium constant K_1^2 , upon the relation of the initial concentrations and upon the degree of complexation x

$$x = \frac{(Y^0)}{(Me_1^0) + (Me_2^0)} \quad (4)$$

Figure 1 shows the dependence of the decontamination factors on the degree of complexation for different values of K_1^2 and for a particular mixture with $(Me_1^0) = (Me_2^0)$. Figure 1 shows clearly that for a given K_1^2 the better the separation factor α_2^1 , the poorer the separation factor β_2^1 . For this particular mixture $\alpha_2^1 = 1/\beta_2^1$ for $x = 0.5$.

If such a partially complexed mixture of rare earths is placed between a cationic and an anionic ion-exchange membrane, and if a potential difference is applied, as shown in Fig. 1, the free Me ions should migrate toward the cathode, while the complexes MeY should migrate toward the anode compartment. If the ions Me_1 and Me_2 on the one side, and the ions Me_1Y and Me_2Y on the other, are transported at the same rate, which should be approximately true for the chosen system,² and if the membranes are perfectly semipermeable, separations thus obtained should follow equation 1 even if the complexed and uncomplexed ions are removed from the original solution at a quite different rate. Some complications may arise due to ion pair formation, which affects the exchange equilibrium.³ However, the separation will still follow equation 1 if those ion pairs do not pass through the

(1) If the metal ions have the same charges and similar chemical properties, the activity coefficient factor F should be in the first approximation independent of the ionic strength and close to unity at least at moderate ionic concentrations. See K. Bril and P. Krumholz, *THIS JOURNAL*, **57**, 874 (1953).

(2) This is supported by the transference numbers and conductivity data reported for the rare earth salts by F. H. Spedding and J. L. Dye, *J. Am. Chem. Soc.*, **76**, 879 (1954).

(3) The effect of ion pair formation was discussed previously; see ref. 1, equations 3-10.

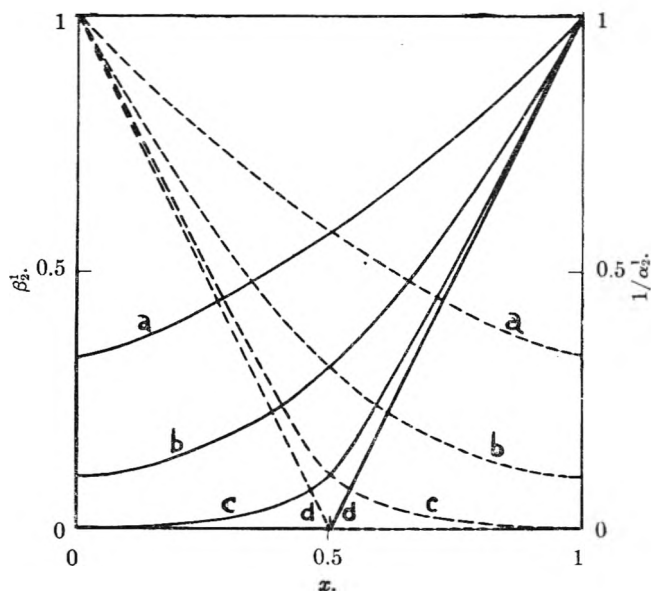


Fig. 1.—Decontamination factors $1/\alpha_2^1$ and β_2^1 as a function of the complexation degree x for an equimolar mixture of Me_1 and Me_2 and for different values of K_1^2 : ——— gives the variation of $1/\alpha_2^1$; ——— gives the variation of β_2^1 . K_1^2 is equal 3, 10, 100 and infinite for curves a, b, c and d, respectively.

ion-exchange membranes, or if the stability factors³ of the ion pairs formed, cancel each other out. The latter should be approximately true for the ion pairs of rare earths.

It will be shown in the following that practical separations may be achieved by the method proposed. The decontamination factors in the case of the rare earths studied here, are close to those predicted by equation 1.⁴ The separation method proposed may thus serve for the determination of the relative stability constants K_1^2 .

Experimental

Materials and Analytical Methods.—Reagent grade Edta was used in the acid form. It was analyzed by titration with pure thorium nitrate solution.⁵ The rare earth (purity 99.9%) and thorium (purity 99.9%) solutions were analyzed for their oxide content by the usual oxalate gravimetric method. Nd and Pr were determined spectrophotometrically with a precision of about 2%. La was determined by difference. Th in the presence of rare earths was determined by photometric titration with Edta using Alizarin Red S as indicator⁶; 0.1% of Th in the rare earths could be thus determined. Edta in the rare earth solution was determined by addition of a known excess of thorium nitrate and complexometric titration of excess Th.⁵ Nitrate^{6a} and chloride^{6b} ions were determined polarographically. Perchlorate was estimated colorimetrically with methylene blue.⁷

Partially complexed solutions of the rare earths were prepared by mixing an analyzed solution of the complexes, $MeYNH_4$, with aliquots of solutions of rare earth perchlorates, chlorides, nitrates or acetates in a proportion corre-

(4) Using stability constants of rare earth-Edta complexes as determined by E. J. Wheelwright, F. H. Spedding and G. Schwarzenbach, *J. Am. Chem. Soc.*, **75**, 4196 (1953).

(5) K. Bril, S. Holzer and B. Rethy, to be published.

(6) (a) M. Kolthoff and J. J. Lingane, "Polarography," 2nd ed., Interscience Publishers, Inc., New York, N. Y., 1952, p. 537; (b) p. 577; chloride was determined from solutions acidified with perchloric acid in order to prevent the interference of Edta.

(7) G. Charlot and D. Bézier, "Analyse Quantitative Minérale," 2nd ed., Masson and Co., 1955, p. 486. By comparison with freshly prepared standards 0.5-3 mg. of $HClO_4$ in 10 ml. could be thus estimated with a precision of ± 0.5 mg.

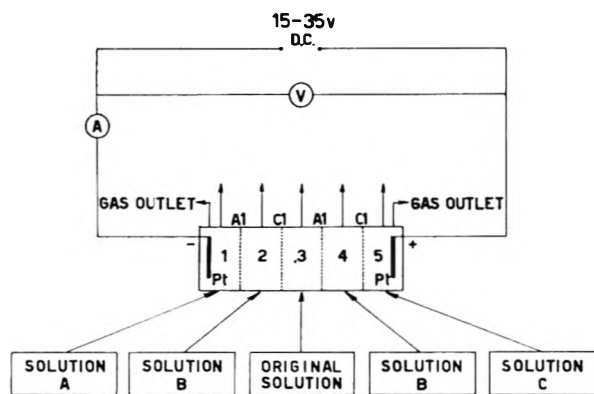


Fig. 2.—Experimental arrangement: solution A, 0.2 M $\text{CH}_3\text{COOH} + 0.05 M$ CH_3COONa ; solution B, 0.001 M $\text{CH}_3\text{COOH} + 0.01 M$ CH_3COONa ; solution C, 0.2 M CH_3COONa . Al and Cl stand for the anionic, respectively, cationic ion-exchange membranes.

sponding to the desired degree of complexation. The MeYNH_4 solution was prepared by absorbing a rare earth chloride solution on a Dowex 50, X4, 100–200 mesh cationic resin in the ammonium form, washing the resin with distilled water, and batch elution with the stoichiometric amount of the tetraammonium salt of Edta. Some measurements were performed with solutions having the stoichiometric composition: $(\text{MeY})_3\text{Me}$,⁸ which corresponds to 75% complexation. Such solutions free from foreign anions, were prepared by dissolving rare earth hydroxides in the calculated amount of Edta acid. To obtain complete dissolution it is necessary to prepare rare earth hydroxides free from basic salts.

Apparatus.—The electrolyzer used is shown schematically in Fig. 2. The cylindrical cells were made from Lucite, allowing visual observation of the interior. Each compartment had an inside diameter of 75 mm., and a thickness of 10 mm., corresponding to a volume of about 40 ml. Rubber gaskets were used to make the system tight. The ion-exchange membranes were pressed between the gaskets and supported by a star-like support placed into each compartment. Amberplex membranes Al and Cl were used. According to the data of the manufacturer, and under our experimental conditions, the total working capacities of the membranes Al and Cl, were, respectively, 2.18 and 5.36 meq. All experiments were performed with the same set of membranes. The partially complexed solution of the rare earths was flowing through the central compartment 3. The anionic and cationic constituents of the mixture migrated into compartments 4 and 2 through Al and Cl, respectively. The electrode compartments 1 and 5 were separated by ion-exchange membranes from compartments 2 and 4, respectively. In order to prevent pH changes within the compartments 2, 3 and 4 due to the diffusion of hydrogen and/or hydroxyl ions formed in the electrode reactions, the cathode compartment 1 was flushed continuously with a solution 0.2 M in acetic acid and 0.05 M in sodium acetate, whereas a 0.2 M solution of sodium acetate was flowing through the anodic compartment 5 (solutions A and C, respectively, see Fig. 2). Excessive current density may also produce pH changes.⁹

In each experiment the current was raised slowly and finally maintained at such a value that the pH of the solutions flowing out of compartments 2, 3 and 4 did not differ from the pH of the original solutions by more than 0.5 pH unit. Excessive pH changes within the electrolyzer would produce in our particular system rare earth hydroxide or even Edta acid precipitations (which actually occurred in our preliminary experiments). As a further precaution the solution flowing into compartments 2 and 4 (solution B, see Fig. 2) was slightly buffered by addition of 0.001 M acetic acid and 0.01 M sodium acetate.

Platinum electrodes were used. Continuous current was drawn from a selenium rectifier, and the voltage applied to

the cell regulated by means of a constant voltage transformer. Current was maintained constant during each experiment by means of the voltage regulator device within about 2%. The flow of the liquids (upwards through each compartment) was maintained at 100 ± 10 ml. per hour. The whole system was immersed in a water thermostat and the temperature maintained at $30 \pm 0.5^\circ$.

Experimental Results.—Each experiment was preceded by an equilibration period. Measurements were started as soon as the stationary state was reached (after about 3 hours). Fractions of 100 to 500 ml. were collected, according to the expected concentrations of the effluent solutions.

The semipermeability of the membranes used was tested under our experimental conditions. A solution containing 10 g./l. of rare earth oxides as perchlorates, chlorides or nitrates was flowing through compartment 3. A current of 0.15 amp. was maintained. The semipermeability of both membranes Al and Cl was found better in perchlorate or chloride, than in nitrate solutions. In perchlorate and chloride solutions the amount of the rare earths transported into compartment 4 was found to be 0.2–0.3% of the amount transported into compartment 2. In nitrate solutions this relation was around 1%. Using nitrate solutions about 0.01 mole of nitrate per mole of rare earths was found in the solution flowing out of compartment 2, whereas only 0.002 mole of chloride was found when chloride solutions were used. Perchlorate concentration was below our detection limit. An experiment was made in which a 100% complexed solution of La, Nd and Pr was flowing into compartment 3. No rare earths could be detected in compartment 2. It is impossible to decide whether the small amounts of foreign ions found in compartments 2 and 4, respectively, are due to the Donnan effect or/and to the migration of ion pairs.

In experiments where the degree of complexation was either 100% or zero no separation of the rare earths was observed within the limits of our experimental error.¹⁰

In Tables I and II results are given of attempted separations of La and Nd, and La, Pr and Nd. The total oxide concentration, the degree of complexation and the concentration of foreign anions were varied. In each experiment five to ten fractions were collected in the stationary state. The rare earths were recovered as oxalates and analyzed spectrophotometrically. From the composition of the original solution and from the composition of the solutions flowing out from compartment 2 and 4, experimental decomplexation factors were calculated, and as a first approximation identified with α_2^1 and β_2^1 as defined by equations 2 and 3. The values of α_2^1 and β_2^1 thus obtained were averaged. The maximum deviation from the mean value of β_2^1/α_2^1 was 5%.

In some experiments Edta was analyzed in the solutions flowing out from compartment 2. The concentration of Edta was found to be only 0.015, 0.013, 0.025, 0.013, 0.007 and 0.002 of the metal concentration in experiments 2, 3, 4, 5, 7 and 9, respectively.

Outflow concentrations of the rare earths depend upon the current and upon the total composition of the solution flowing into compartment 3. The concentration of the rare earths in the solutions flowing out of compartment 2 varied in our experiments between 0.5 g./l. oxides (experiment 2) and 5.5 g./l. oxides (experiment 9). The concentration of the Edta complexes flowing out of compartment 4 varied between 0.04 g./l. oxides (experiment 10) and 1.5 g./l. oxides (experiment 3).

Current efficiency calculated assuming that the transported species are the rare earth trivalent cations and the monovalent rare earth–Edta anions, is given in Table III, for experiments in which solutions free from foreign ions were used.

We also attempted the separation of Th and Nd. ThY is a much more stable complex¹¹ than NdY^- . If to an equimolar mixture of Th and Nd, Edta is added in an amount such that $x = 0.5$, practically the whole Th will be present as ThY , while most of the Nd will remain uncomplexed. As ThY is charge free, it should not migrate out from compartment 3. The experiment confirms this conclusion.

(10) Rare earth separations by electromigration have been reported in the literature: K. Clusius and E. R. Ramirez, *Helv. Chim. Acta*, **36**, 1160 (1953), M. Lederer, F. P., 1.068.504 (1954).

(11) $\log K_{\text{Nd}} = 16.06$ (see ref. 4); $\log K_{\text{Th}} = 23.2$, see G. Schwarzenbach, R. Gut and G. Anderegg, *Helv. Chim. Acta*, **37**, 957 (1954).

(8) See Th. Moeller, F. A. M. Moss and R. H. Marshall, *J. Am. Chem. Soc.*, **77**, 3182 (1955).

(9) See N. W. Rosenberg and G. E. Tirrell, *Ind. Eng. Chem.*, **49**, 780 (1957).

TABLE I
SEPARATION OF LANTHANUM FROM NEODYMIUM BY ELECTROMIGRATION

The original mixture was composed of equal wt. % of neodymium and lanthanum oxides. (Me^o) stands for the total molar concentration of the rare earths; all concentrations are expressed in 10⁻² M.

Expt. no.	i (amp.)	z	pH	Compn. of original soln.					α_{Nd}^{La}	β_{Nd}^{La}	$\frac{\beta_{Nd}^{La}}{\alpha_{Nd}^{La}}$
				(Me ^o)	(ClO ₄ ⁻)	(Cl ⁻)	(NO ₃ ⁻)	(AcO ⁻)			
1	0.05	0.760	4.5	6.22	0.108	1.60	14.8
2	.05	.780	5.6	6.13127	1.76	13.9
3	.13	.735	4.5	15.1136	1.66	12.2
4	.50	.736	5.2	6.24	20130	1.76	13.5
5	.50	.728	4.9	6.24	..	20136	1.49	11.0
6	.60	.740	4.5	6.30	20	..	.132	1.45	11.0
7	.50	.742	5.0	6.24	20	..	.137	1.52	11.1
8	.40	.738	5.5	6.06	20	.171	1.66	9.7
9	.36	.246	4.2	6.10	12	2.6	.56	7.40	13.3
10	.15	.246	4.2	6.10	12	2.6	.535	7.33	13.7

TABLE II

SEPARATION OF LANTHANUM, PRASEODYMIUM AND NEODYMIUM BY ELECTROMIGRATION

The original mixture had the composition: 42.2 wt. % Nd₂O₃, 17.3 wt. % Pr₂O₃ and 40.5 wt. % La₂O₃. (Me^o) stands for the total molar concentration of the rare earths. All concentrations are expressed in 10⁻² M.

Expt. no.	i (amp.)	z	pH	Compn. of original soln.			α_{Nd}^{La}	α_{Nd}^{Pr}	β_{Nd}^{La}	β_{Nd}^{Pr}	$\frac{\beta_{Nd}^{La}}{\alpha_{Nd}^{La}}$	$\frac{\beta_{Nd}^{Pr}}{\alpha_{Nd}^{Pr}}$
				(Me ^o)	(NO ₃ ⁻)	(AcO ⁻)						
11	0.05	0.750	4.3	6.00	0.577	0.123	1.07	1.86	15.0	1.86
12	.15	.750	3.9	5.00	4.2598	.140	1.11	1.89	13.5	1.36
13	.05	.760	5.3	6.00	4.2598	.135	1.11	1.64	12.1	1.87
14	.15	.765	5.8	6.00	..	4.2	.655	.188	1.13	1.81	9.65	1.72
15	.15	.800	5.1	6.06	1.8	1.8	.675	.149	1.06	1.73	11.6	1.72
16	0.15	.720	5.7	6.07	3.3	1.8	.615	.194	1.09	2.29	11.4	1.77
17	.15	.490	5.0	6.19	7.3	1.8	.696	.314	1.23	3.62	11.5	1.77

TABLE III

Expt. n°.	Current efficiency for MeY ⁻	
	Me ²⁺	MeY ⁻
11	0.80-0.90	0.40-0.45
1	.80-.90	.40-.45
3	.60-.70	.20-.25
2	.45-.50	.15-.20

An equimolar mixture of Th(NO₃)₄ and NdYNH₄ (1.78 × 10⁻²M), pH 4.4, was electrolyzed, using a current of 0.15 amp. From the solution flowing out of compartment 2 neodymium oxide was recovered containing less than 1% of thorium oxide. The yield of Nd was 28%. The solution flowing out of compartment 4, contained less than 0.1% of the oxides entering compartment 3.

Discussion

As can be seen from Tables I and II, the values of $\beta_{Nd}^{Pr}/\alpha_{Nd}^{Pr}$ are, within the experimental error of 5%, constant and independent of the degree of complexation and of the composition of the solution. The observed variations of the values of $\beta_{Nd}^{La}/\alpha_{Nd}^{La}$, exceed the experimental error. The effect is however too small to be interpreted in a quantitative way. The value of $\beta_{Nd}^{La}/\alpha_{Nd}^{La}$ is smaller in the presence of acetates, than in the presence of equal concentrations of nitrates, chlorides, or perchlorates.

Values of β_2^1/α_2^1 obtained in solutions free from foreign ions should be rather near to the true value of the relative stability constant K_1^2 , (see equations 1, 2 and 3) although, ion pair formation between MeY and Me may be still here of some importance.³ We find thus at 30° for K_{La}^{Nd} the value of about 14 and for K_{Pr}^{Nd} the value of about 1.9 (see Tables I and II). Both values are in a good agreement with those calculated from the stability constants of the Edta complexes reported by Schwarzenbach *et al.*,⁴ which are $K_{La}^{Nd} = 22 \pm 6$ and $K_{Pr}^{Nd} = 2.05 \pm 0.6$.¹²

The method described should be useful for practical separations. In analogy with water desalting systems a multi-cell arrangement should be used in order to decrease power consumption and undesirable pH changes.¹³ The separation efficiency of the method could be probably increased by cascading the whole process.

(12) Stability constants reported by Schwarzenbach *et al.*, are valid at the ionic strength of 0.1, chloride medium, 20° and rare earth concentration 0.001 M. $\log K_{Nd} = 16.06 \pm 0.06$; $\log K_{Pr} = 15.75 \pm 0.06$; $\log K_{La} = 16.06 \pm 0.06$.

(13) See "Electrochemical Separations" by K. S. Spiegel in "Ion Exchange Technology," Edited by F. C. Nachod and J. Schubert, Academic Press, Inc., New York, N. Y., 1956.

THE CALORIMETRIC DETERMINATION OF THE HEATS OF COÖRDINATION REACTIONS

BY DAVID FLEISCHER AND HENRY FREISER

Department of Chemistry, University of Pittsburgh, Pittsburgh 13, Pennsylvania

Received August 25, 1958

Two methods for calorimetrically determining the heats of stepwise coördination reactions with metal ions are described. One of these methods enables the calculation of the stability constant from the calorimetric data. The calorimetrically determined heats of reaction of the divalent ions of copper, nickel and cobalt with 8-quinolinol, 2-methyl- and 4-methyl-8-quinolinol are compared with the heats of reaction obtained from the temperature dependence of the stability constant. The solvent system employed is 50 volume % dioxane-water.

In spite of the great value of detailed thermodynamic data for interpreting chelation effects on a molecular basis, very few heat and entropy data have been determined. Almost without exception, these quantities have been found from the temperature dependence of the equilibrium constant (stability method). The data on diamines collected by McIntyre¹ shows that the heats of chelation for the same systems, reported by different investigators, are often in disagreement.

A very few investigators have determined the heats of coördination reactions by direct calorimetric measurement. Fyfe² found the heats of coördination for some metal ions with ammonia calorimetrically. His results are in good agreement with those found from the stability method. The heats of reaction of ethylenediamine and N-methylethylenediamine with copper(II) and nickel(II) have been determined calorimetrically by Basolo and Murmann³ and by Davies, *et al.*⁴ While the calorimetric results agree with each other and with the stability method results of some investigators,^{1,5} they are in conflict with the stability method heats of others.^{6,7} Charles⁸ found the heats of reaction of a series of divalent cations with ethylenediaminetetraacetic acid by calorimetric measurement and compared his results with those derived from the stability method by Carini and Martell.⁹ The agreement is poor.

The move toward calorimetric determinations has, despite the inadequacies of the stability method, been very slow. The systems investigated have all been amenable to experimental simplifications that are not generally applicable to chelate reactions. None of the examples presented above involves solubility problems, since all of these chelates are charged species, but this is not generally true. Only in the case of the ethylenediamine reactions was more than one product formed, necessitating the use of the stability constants in analyzing the data. The presence of more than one chelate species, however, is the rule

rather than the exception. Also, the organic species is usually in the acidic form, and chelation is accompanied by large pH changes and attendant side reactions.

Two calorimetric methods have been developed in this study which are applicable to chelation reactions in general. Both of these methods are dependent upon some means of determining the concentrations of the various species present after the calorimetric reaction. One method (K-method) necessitates a knowledge of the acid dissociation constants and of the stepwise formation constants. The other method (extrapolation method) requires a knowledge of only the acid dissociation constants of the organic reagent.

Experimental

The reagents 8-quinolinol and 2-methyl-8-quinolinol, were purified by vacuum distillation followed by crystallization from ethanol-water. The 4-methyl-8-quinolinol was synthesized from O-aminophenol and methyl vinyl ketone by the method of Phillips, Elbenger and Merritt,¹⁰ and purified as above. The uncorrected and literature (in parentheses) melting points are: 8-quinolinol, 72.5–73.5° (72–74°); 2-methyl-8-quinolinol, 72.8–74.0° (74°); 4-methyl-8-quinolinol, 138.3–139.9° (141°).

The metal solutions were prepared from G. F. Smith reagent grade perchlorates. The nickel solution was standardized gravimetrically with dimethylglyoxime. The copper and cobalt solutions were standardized by electrodeposition.

The dioxane was refluxed over sodium for 24 hours and distilled. It was tested for peroxides before each experimental determination.

Baker and Adamson perchloric acid and Fisher carbonate-free sodium hydroxide were used.

The calorimeter consisted of a 600-ml. Dewar flask with a tight-fitting wooden top 5 cm. thick. Through the top was mounted a glass motor-driven stirrer fitted with ball bearings, a Beckmann thermometer, a glass-enclosed electrical heater, and alternately a glass sample bulb or a chemical heater.¹¹ A beeswax seal at the bottom of the sample bulb could be punctured by a glass rod which extended through the top of the calorimeter, and the contents of the bulb were ejected by squeezing a rubber bulb.

The pH measurements were made with a Beckman model G meter and a glass-saturated calomel electrode pair.

The 50 v./v. % dioxane-water solution was chilled below room temperature and 412.3 g. (400 ml.) was weighed into the Dewar flask. To this was added a weighed amount of organic reagent. Into the sample bulb were pipetted 5 ml. each of the inorganic reagent and dioxane, which were then thoroughly mixed. The inorganic reagent was either perchloric acid, sodium hydroxide or metal perchlorate solution according to whether the heats of neutralization of the tertiary nitrogen or the phenolic oxygen, or the heat of chelation, respectively, was being determined. After stirring was started the temperature was raised to 24° with the electrical heater, which then was turned off. When the

(1) G. H. McIntyre, Jr., Ph.D. Thesis, The Pennsylvania State College, 1953.

(2) W. S. Fyfe, *J. Chem. Soc.*, 2018, 2023 (1952).

(3) F. Basolo and R. K. Murmann, *J. Am. Chem. Soc.*, **76**, 211 (1954).

(4) T. Davies, S. S. Singer and L. Stavelly, *J. Chem. Soc.*, 2304 (1954).

(5) M. Calvin and R. Bailes, *J. Am. Chem. Soc.*, **68**, 953 (1946).

(6) F. Basolo and R. K. Murmann, *ibid.*, **74**, 5343 (1952).

(7) H. Irving, Report No. BRL/146, May 1951. Presented at Discussion on Coördination Chemistry, held by Imperial Chemical Industries, Ltd., at Welwyn, Herts, September, 1950.

(8) R. Charles, *J. Am. Chem. Soc.*, **76**, 5854 (1954).

(9) F. F. Carini and A. E. Martell, *ibid.*, **76**, 2163 (1954).

(10) J. P. Phillips, R. L. Elbenger and L. L. Merritt, *ibid.*, **71**, 3986 (1949).

(11) R. G. Charles, *J. Chem. Ed.*, **31**, 577 (1954).

heat of stirring had brought the temperature to 24.5°, readings were taken at five-minute intervals to establish the fore-period rate. The reaction was initiated at 25°. A reaction period of one minute was found to be ample and gave the same results as when longer reaction periods were used. The temperature rise was corrected for the heat of mixing of the inorganic solution. When heat capacities were determined with the chemical heater a reaction period of ten minutes was necessary and the Regnault-Pfaundler equation was used to calculate the temperature rise.¹²

The chemical heater employed 5 ml. each of 2 *N* sodium hydroxide and 2 *N* sulfuric acid. The same quantities and concentrations of these reagents were used to find the heat equivalent of the calorimeter with the sample bulb installed. In this case the acid was pipetted into a weighed amount of water in the Dewar and the base was contained in the bulb. The heats of both neutralization reactions were calculated.¹³

The stability constants for the metal(II)-8-quinolinol systems were obtained by the Calvin-Bjerrum technique, as previously described.¹⁴

TABLE I

REAGENT ACID DISSOCIATION CONSTANTS			
Reagent	pK_{NH} (± 0.03)	pK_{OH} (± 0.03)	t (°C.)
8-Quinolinol	4.20 (2) ^a	11.61 (2)	15
	4.07 (3)	11.46	25
	3.98	11.35	32
	3.89 (2)	11.25 (2)	40
2-Methyl-8-quinolinol	4.65 (4)	11.80 (2)	25

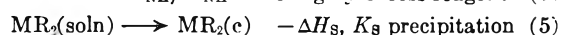
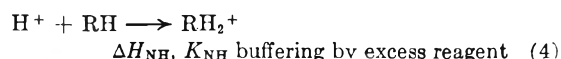
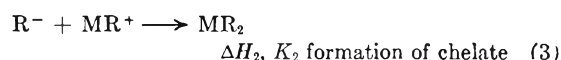
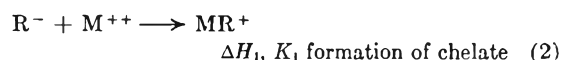
Calculations

The following reactions, each characterized by a molar heat and an equilibrium constant occur during a calorimetric determination



TABLE II CHELATE STABILITY CONSTANTS			
System	$\log K_{12}$	t (°C.)	
8-Quinolinol- Cu(II)	25.94 \pm 0.24 (2) ^a	15	
	25.35 \pm .03 (2)	25	
	24.79 \pm .23 (2)	40	
Ni(II)	22.04 \pm .20 (2)	15	
	21.54	25	
	20.68 \pm .04 (2)	40	
Co(II)	19.84 \pm .16 (4)	15	
	19.50	25	
	19.17 \pm .01 (2)	40	

^a No. of determinations.



Examination of the temperature *vs.* time data showed that within certain ranges of concentration the rate of temperature rise during the first part of the after period was the same as that during the fore period. The rate then gradually increased to a maximum and finally returned to a constant value. Visual examination of the reaction under identical conditions confirmed that precipitation was preceded by a short induction period. Accordingly, the equality of the fore- and after-period rates was used as the criterion for using data.

TABLE III

FREE ENERGIES, ENTHALPIES AND ENTROPIES OF NEUTRALIZATION AT 25°
Stability method (S.M.); calorimetric method (C.M.)

Reagent	$-\Delta H_{NH}$ (kcal.)		$-\Delta H_{OH}$ (kcal.)		$-\Delta F_{NH}$ (kcal.)	$-\Delta F_{OH}$ (kcal.)	ΔS_{NH}^a (e.u.)	ΔS_{OH}^a (e.u.)
	S.M.	C.M.	S.M.	C.M.				
8-Quinolinol	5.2	5.7	6.0	6.0	5.6, 5.6 ^b	15.7, 15.9 ^b	-0.3	32
2-Methyl-8-quinolinol	6.9 ^b	6.9	7.5 ^b	6.4	6.4, 6.3 ^b	16.2, 16.1 ^b	-1.7	33
4-Methyl-8-quinolinol	7.1 ^b	6.3	9.1 ^b	6.2	6.4 ^b	15.9 ^b	-0.3	32

^a Calculated from calorimetric heats. ^b Reference 15.

TABLE IV

FREE ENERGIES, ENTHALPIES AND ENTROPIES OF CHELATION AT 25°

Metal	Reagent	$-\Delta H_{1,2}$ (kcal.)				$-\Delta F_{1,2}$ (kcal.)	$\Delta S_{1,2}^a$ (e.u.)	$\Delta S_{1,2}^b$ (e.u.)
		Stability method	<i>K</i> -Method	Extrapolation method				
Cu	8-Quinolinol	19.2	20.6	20.8	35.2	48	53	
Ni	8-Quinolinol	19.0	21.3	20.8	29.4	29	35	
Co	8-Quinolinol	11.1	21.6	20.4	26.8	21	52	
Cu	2-Methyl-8-quinolinol	17.3 ^c	15.5	17.0	32.5 ^c	52	51	
Ni	2-Methyl-8-quinolinol	10.7 ^c	10.3	10.6	24.3 ^c	47	45	
Co	2-Methyl-8-quinolinol	10.3 ^c	11.6		25.2 ^c	45	50	
Cu	4-Methyl-8-quinolinol	34.0 ^c	24.4		37.6 ^c	44	12	
Ni	4-Methyl-8-quinolinol	26.0 ^c	25.8		30.4 ^c	15	15	
Co	4-Methyl-8-quinolinol	20.3 ^c	25.0		27.3 ^c	8	23	

^a Derived from calorimetric method heats. ^b Derived from stability method heats. ^c Reference 15.

(12) W. P. White, "The Modern Calorimeter," Chemical Catalogue Co., New York, N. Y., 1928.

(13) F. D. Rossini, "Selected Values of Chemical Thermodynamic Properties," National Bureau of Standards Circular 500, 1952.

(14) H. Freiser, R. G. Charles and W. D. Johnston, *J. Am. Chem. Soc.*, **74**, 1383 (1952).

(15) W. D. Johnston and H. Freiser, *Anal. Chim. Acta*, **11**, 201 (1954).

A comparison of pK_{OH} for the three reagents with pK_W (in 50 v./v. % dioxane-water)¹⁶ showed that conversion of the reagents to the anionic form was quantitative under the experimental conditions used and ΔH_{OH} was calculated from the expression:

(16) H. S. Harned and B. B. Owen, "The Physical Chemistry of Electrolytic Solutions," Reinhold Publ. Corp., New York, N. Y., 1950.

TABLE V
CALORIMETRIC VALUES OF THE STEPWISE HEATS OF CHELATE
FORMATION

System	-ΔH ₁ (kcal.)	
	K-Method	Extrapolation method
8-Quinolinol-		
Cu(II)	10.5	
Ni(II)	6.6	8.5
Co(II)	4.9	6.4
2-Methyl-8-quinolinol-		
Cu(II)	8.7	6.5
Ni(II)	6.5	5.2
Co(II)	4.6	
4-Methyl-8-quinolinol-		
Cu(II)	-9	
Ni(II)	6.8	
Co(II)	7.1	

TABLE VI
SUMMARY OF CALCULATED ERRORS

Quantity	Stability method	Extrapolation method
log K ₁₂	0.21	
ΔH ₁₂ , kcal.	4.5	1.1
ΔH _{NH} , kcal.	0.7	0.4
ΔH _{OH} , kcal.	.7	0.04
ΔF ₁₂ , kcal.	.4	
ΔF _{NH} , kcal.	.04	
ΔS ₁₂ , e.u.	15	4
ΔS _{NH} , e.u.	2	1

$\Delta H_{OH} = h/T_R - \Delta H_N$, where h is the measured heat, T_R is the total reagent and ΔH_N is the heat of neutralization of water.

The equilibrium between the neutral and cationic species of the reagent was considered when ΔH_{NH} was determined, and ΔH_{NH} is expressed as

$$\Delta H_{NH} = \frac{h}{T_R} (1 + K_{NH}/[H^+])$$

(a) **K-Method.**—The heat change resulting from reactions 1–4 is given by the expression

$$h = MR\Delta H_1 + MR_2\Delta H_{12} + RH_2\Delta H_{NH} - (MR + 2MR_2)\Delta H_{OH} \quad (6)$$

where $\Delta H_{12} = \Delta H_1 + \Delta H_2$, $K_{12} = K_1K_2$ and the coefficients of the ΔH terms represent the equilibrium quantities of the various species present. To solve for the values of these coefficients Bjerrum's \bar{n} function¹⁴ was used. This function may be expressed in two forms

$$\bar{n}_H = \frac{T_R}{T_M} - \frac{T_R - H^+}{T_M} \times \frac{K_{NH} + H^+}{K_{NH} + 2H^+} \quad (7)$$

$$\bar{n}_R = \frac{K_1R + 2K_{12}R^2}{1 + K_1R + K_{12}R^2} \quad (8)$$

where T_M is the total metal and R is the anionic form of the organic reagent, given by the expression¹⁴

$$R^- = \frac{(T_R - H^+)K_{NH}K_{OH}}{H^+(K_{NH} + 2H^+)} \quad (9)$$

At equilibrium $\bar{n}_H = \bar{n}_R$ and $H^+ = f(T_M, T_R, K_{NH}, K_{OH}, K_1, K_{12})$. This equation was solved by a linear approximation method using H^+ as the independent variable. The values of K_1 and K_{12} were found by using smoothed data from the titration \bar{n} vs. pR^- curve in the equation

$$\frac{\bar{n}}{R(1 - \bar{n})} = K_{12}R \times \frac{2 - \bar{n}}{1 - \bar{n}} + K_1$$

derived from (8). The data of Johnston¹⁷ were used for the 2-methyl- and 4-methyl-8-quinolinol systems.

The equilibrium value of H^+ can be used to solve for the coefficients of (6)

$$MR^+ = K_1M^{++}R$$

$$MR_2 = K_{12}M^{++}R^2$$

where

$$M^{++} = \frac{T_M}{1 + K_1R + K_{12}R^2}$$

$$RH_2^+ = \frac{T_R - T_M\bar{n}}{1 + RH/RH_2^+}$$

where

$$p \frac{RH}{RH_2^+} = pK_{NH} - pH$$

The difference between pK_{NH} and pK_{OH} was such that the second ionization of the reagent did not influence RH/RH_2^+ , justifying this simplified expression. The equation for the heat change resulting from chelation alone can now be written

$$h' = MR\Delta H_1 + MR_2\Delta H_{12}$$

and solved simultaneously. The coefficients were varied by adjusting the ratio T_R/T_M .

(b) **Extrapolation Method.**—Only K_{NH} and K_{OH} must be known to apply this technique. The final pH was measured immediately following the reaction period. This value was used to evaluate \bar{n}_H and RH_2^+ . The heat change, ΔH , resulting from chelation alone, under the condition that two moles of organic reagent are chelated is

$$\frac{\Delta H}{2} = \frac{h}{T_M\bar{n}} + \Delta H_{OH} - \frac{RH_2^+}{T_M\bar{n}} \Delta H_{NH}$$

This equation was used to calculate ΔH . By use of the condition $MR + 2MR_2 = 2$ and the equations $\bar{n} = (MR^+ + 2MR_2)/T_M$, $T_M = (M^{++} + MR^+ + MR_2)$ ΔH can be represented in terms of ΔH_1 and ΔH_{12}

$$\Delta H = 2\Delta H_1 + \left[\frac{2(\bar{n} - 1)}{\bar{n}} + M^{++} \right] (\Delta H_{12} - 2\Delta H_1)$$

As $\bar{n} \rightarrow 2$, $M \rightarrow 0$ and ΔH vs. $2(\bar{n} - 1)/\bar{n}$ will approach linearity, permitting extrapolation to ΔH_{12} . In practice it was found that $\bar{n} \sim 1.45$ was the minimum coordinate of a point for it to fall on the extrapolated line.

The constant K_{12} can be calculated from the deviation of a low valued \bar{n} point from the limiting line. The internal agreement of these calculations for several points provides a measure of the goodness of the limiting line. This calculation is illustrated in Fig. 1. The value intersected on the abscissa by the perpendicular dotted line is the quantity of MR_2 that would have been formed for the $\bar{n} = 1.24$ point for the condition $MR^+ + 2MR_2 = 2$. The length of the horizontal dotted line, in units of $2(\bar{n} - 1)/\bar{n}$, equals the free metal, M^{++} , under the same condition as stated above. The concentration of R^- is calculated readily from (9) where the experimental value for T_R is used.

(17) W. D. Johnston, Ph.D. Thesis, University of Pittsburgh, 1953.

(c) **Errors.**—A formal error analysis was made. The error in pH was taken as 0.02, the error in h , 0.3 cal., was taken from a series of heat capacity measurements, and errors in weighing and volume measurement were ignored. All quantities used to evaluate the partial derivatives were taken from typical experimental data. The results are given in Table V. The expression used to calculate ΔH_{12} by the K-method is so complex that a formal analysis could not be made. The K-method heat for cobalt(II)-8-quinolinol was recalculated with values of K_{12} and K_1 so altered that their average deviation from their former values corresponded to the calculated error in K_{12} . This recalculated heat differed by one kcal. from the value previously obtained.

Discussion

The discrepancies between the calorimetric and stability method heats (Tables III and IV) are immediately apparent. Only for one system, the 2-methyl-8-quinolinol chelates, is good agreement found. The most unusual feature, in comparisons of the stability and calorimetric heats, is that while the former vary in all cases the latter are constant for the reactions involving 8-quinolinol and its 4-methyl homolog. The very small amount of heat data that has appeared in the literature is not adequate for estimating how the heats of chelation of a particular ligand with a series of metals should vary, but this data does indicate that heats of chelation do not necessarily conform to a series analogous to that discovered by Mellor and Maley^{18,19} for free energy changes of chelation.

In an attempt to resolve the anomalous discrepancies between the stability and calorimetric methods the reaction heats for the metal(II)-8-quinolinolates were determined by converting an excess of reagent to the anionic form with sodium hydroxide before the chelation reaction was initiated. Thus complete chelation resulted, and no method for determining the concentration of various species was necessary. This method, while overcoming the necessity of calculating or measuring the pH , introduces an error of a different kind. It is known that metal(II)-8-quinolinol precipitates partially redissolve at higher values of pH in the presence of excess reagent.²⁰ It has also been shown that it is possible to form species of the type $M(II)R_3^-$ with 8-quinolinol.²¹ As a result, it was not certain what species was formed. The results of these determinations, in kilocalories, are: Cu(II), -26; Ni(II) -26; Co(II), -24. It is significant, although these heats are more exothermic than those found with the K- and extrapolation methods, that cobalt(II) differs from copper(II) and nickel(II) by only 2 kcal. Confidence in the K- and extrapolation methods is

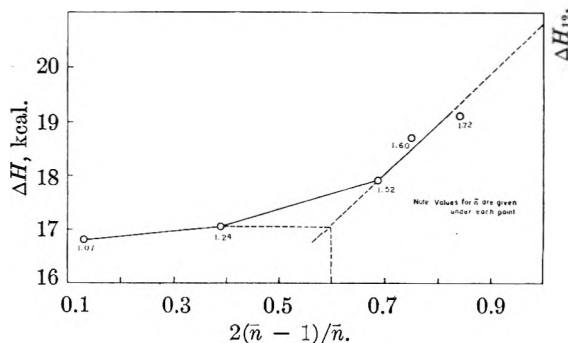


Fig. 1.—Extrapolation method for the Co(II)-8-quinolinol system.

also increased by the fact that $\bar{n} = 2$ values were achieved for copper(II) and nickel(II) with 8-quinolinol in the extrapolation method determinations. The ΔH_{12} values calculated from these $\bar{n} = 2$ data agreed within 0.8 kcal. with the results derived from the K-method.

Both calorimetric procedures can be used to evaluate the stepwise heats ΔH_1 and ΔH_2 . It is seen (Table V), although ΔH_{12} values are in agreement by the two calorimetric methods, that the average discrepancy in ΔH_1 is ± 2 kcal. In addition, in view of the uniformly exothermic behavior of these reactions, the value $\Delta H_1 = +9$ kcal. for copper(II)-4-methyl-8-quinolinol is very unusual. The low solubility of the 4-methyl substituted chelates prevented the determination of ΔH_1 by the extrapolation method.

The trend in the thermodynamic quantities of neutralization (Table III) is what would be expected from a knowledge of the electron-releasing tendency of the methyl group. The entropies of neutralization of the tertiary nitrogens and of the phenolic oxygens are constant, within experimental error, indicating that basicity changes in these compounds are effected by changes in bond strength alone. Phillips²² found precisely the same increments in ΔF_{NH} and ΔF_{OH} for this series of reagents, although, since his photometric measurements were made at a higher ionic strength than that employed herein, the absolute values of his quantities are quite different.

The calculated errors (Table VI) indicate the higher accuracy of the calorimetric methods. An additional attraction is found in the extrapolation method, since not only does it not require previous knowledge of the stability constant, but permits calculation of this quantity from the calorimetric data. The $\log K_{12}$ values calculated by this method for cobalt(II)-8-quinolinol, are 19.14 and 19.25. These values show better agreement than $\log K_{12}$ values found by the Bjerrum technique (Table II).

Acknowledgment.—The authors gratefully acknowledge the financial assistance of the Atomic Energy Commission in carrying out this work.

(18) D. P. Mellor and L. Maley, *Nature*, **159**, 370 (1947).

(19) D. P. Mellor and L. Maley, *ibid.*, **161**, 436 (1948).

(20) R. G. W. Hollingshead, "Oxine and Its Derivatives," Butterworths Scientific Publications, London, 1954.

(21) S. Jankowski, University of Pittsburgh, private communication.

(22) J. P. Phillips, *J. Am. Chem. Soc.*, **74**, 552 (1952).

DECOMPOSITION KINETICS OF NITROUS OXIDE ON α -MANGANESE SESQUIOXIDE¹BY L. RHEAUME AND G. PARRAVANO²*Frick Chemical Laboratory, Princeton University, Princeton, New Jersey**Received August 25, 1958*

The detailed kinetics of the catalytic decomposition of nitrous oxide on α -Mn₂O₃ has been determined in the temperature range 286 to 346°. The experimental results are consistent with a reaction mechanism in which the slow, rate determining step is the decomposition of adsorbed N₂O molecules. The derived rate equation is eq. 11, where k_2 is the rate constant for the rate-determining step, $[S]_0$ is the total concentration of sites suitable for reaction, and b_1 and b_3 , the equilibrium functions for the adsorption of N₂O and O₂, respectively. This rate equation is capable of expressing the experimental results: (a) the reaction rate is less than 1st order with respect to N₂O, (b) the reaction rate is not affected by N₂, (c) the reaction rate is retarded by oxygen. The rate equation derived only from initial rate data (2-6% reaction) also expresses the "course of reaction" rate. From the temperature dependence of k_2 , an activation energy of 35.0 kcal./mole is obtained. The temperature dependence of b_1 yields, for N₂O, an adsorption enthalpy of -16.9 kcal./mole and an entropy of adsorption of -36.4 cal./mole °C. The temperature dependence of b_3 yields, for O₂, an adsorption enthalpy of -43.2 kcal./mole and an entropy of adsorption of -66.0 cal./mole °C. An idea of the mobility of the adsorbed molecules is given by comparing the experimental with calculated entropy changes, the calculated changes being based on the assumption that the adsorbed molecules have lost certain degrees of freedom. Rate equations derived from kinetic mechanisms involving other rate-determining steps are shown to be inconsistent with experimental results.

The catalytic decomposition of nitrous oxide has been used repeatedly as a test reaction for a number of concepts which are now prevailing in the field of heterogeneous catalysis. The conclusions reached in these studies are largely based on the validity of a reaction scheme deduced from kinetic investigations of the decomposition reaction. It is, then, fitting to assess critically the soundness of the proposed reaction mechanism with more detailed studies of the rate of the reaction.

With this aim in view, and as a continuation of previous work on the catalytic activity of semi-conducting materials,³ we have endeavored to gather information on α -manganese sesquioxide, since there are no quantitative recorded data on the catalytic activity of this metal oxide for the decomposition of nitrous oxide. The results of this investigation are collected in the present communication, together with a discussion on the reaction mechanism which can be deduced from a kinetic analysis of the experimental data.

Experimental

Materials.— α -Manganese sesquioxide was prepared by thermal decomposition of reagent grade manganous carbonate (Baker and Adamson). A paste of manganous carbonate and acetic acid (1:1) was heated slowly in a porcelain crucible up to 400°, and kept at that temperature for three hours. The resulting oxide was thoroughly ground, mixed in an agate mortar and fired in a stream of air in a porcelain crucible at 800° for four additional hours. The oxide was then cooled overnight, mixed again and fired under the same conditions previously. This procedure was repeated six times, giving a total ignition period of 27 hours at 800 ± 10°.

An X-ray pattern of the resulting black powder produced values of interplanar spacings and line intensities in good agreement with previous work.⁴ Surface area determinations by means of the B.E.T. method, using nitrogen as

adsorbate, gave a value of 4.5 m.²/g. In most of the temperature range studied, the oxide showed a semi-conducting p -type behavior. This result was obtained by means of measurements of thermoelectric power, which, in the temperature range investigated, was found to decrease with increasing temperature. Nitrous oxide, from a commercial cylinder (Matheson), was purified by passing it through a column of phosphorus pentoxide and solidified by freezing it with liquid nitrogen. The solid was evacuated for a half hour to remove non-condensable gases, the temperature then was raised to -80°, and one-third of the nitrous oxide was allowed to distil off. The middle third fraction was collected by distillation into an evacuated container. This fraction was again solidified, pumped off for a half hour, and finally collected into a storage bulb. Oxygen from a commercial tank (Matheson) was purified by passing it through calcium chloride, palladized asbestos, calcium chloride, Ascarite, magnesium perchlorate and, finally, phosphorus pentoxide. Pre-purified nitrogen (Matheson) was purified by passing it through calcium chloride, hot activated copper, calcium chloride, Ascarite and phosphorus pentoxide.

Experimental Procedure.—Experimental data were obtained in an all-glass closed system, the gases being circulated by means of a motor driven bellows-type gas pump. Catalytic activity was tested at several circulating speeds in order to make sure that mass transfer effects would not control the rate of the chemical reaction. The catalyst was placed in a Pyrex reactor ($\pm 0.3^\circ$), supplied with a pre-heater. Gold foils were inserted in the gas lines to protect the catalyst from mercury vapor. The pressure increase due to the decomposition reaction was followed on a mercury manometer and manometric readings were taken as an indication of the course of the reaction.

A standard pretreatment of the catalyst was used throughout this study. The system was evacuated a half hour at room temperature; the reactor then was heated at 200° during a one hour period and maintained at that temperature for two hours. Nitrous oxide subsequently was introduced and the circulating pump turned on. This completed the pretreatment of the catalyst. For a typical run, the catalyst was heated to the desired reaction temperature, the circulation pump turned off and the system evacuated for six minutes. The reactant or reactant-products mixture was introduced, the circulation pump turned on and pressure readings were taken with a cathetometer (± 0.005 cm.). At the end of the run, the circulation pump was turned off, the system evacuated, and a fresh reactant or reactant-products mixture introduced. Following this procedure, a good reproducibility of the reaction rate and catalytic activity constant with time was obtained. Gas mixtures of the desired compositions were prepared with the use of a Toepler pump, connected with the reaction system.

Results

Preliminary data showed that the rate of the reaction was retarded by oxygen. Therefore, the

(1) This communication is based on a dissertation submitted by L. Rheume in partial fulfillment of the requirements for the degree of Doctor of Philosophy at Princeton University.

(2) Department of Chemical and Metallurgical Engineering, University of Michigan, Ann Arbor, Mich.

(3) G. Parravano, *J. Am. Chem. Soc.*, **74**, 1194 (1952); **75**, 1448, 1452, 5233 (1953); G. Parravano, M. Boudart, "Advances in Catalysis," Vol. VII, Academic Press, Inc., New York, N. Y., 1955; P. P. Clapp and G. Parravano, *THIS JOURNAL*, **62**, 1055 (1958).

(4) T. E. Moore, M. Ellis and P. W. Selwood, *J. Am. Chem. Soc.*, **72**, 856 (1950). For detailed X-ray data on the present preparation see: L. Rheume Thesis, Princeton, 1955.

kinetics of the reaction was determined by measurements of initial rates. For this purpose, a sufficient number of pressure readings were taken at short intervals of time and plotted *versus* time. The best straight lines were drawn through the points. The prevailing partial pressures at the midpoint of these lines were those recorded for the given rate. The effect of the partial pressure of nitrous oxide on the rate of the reaction was determined by measuring initial rates at different initial pressures of nitrous oxide, $p^0_{N_2O}$. These results are presented in Table I.

TABLE I

DECOMPOSITION OF N_2O ON α - Mn_2O_3 . EFFECT OF $p^0_{N_2O}$ AND $p^0_{N_2}$

$T = 333^\circ, p^0_{O_2} = 0.22 \text{ cm.}, Mn_2O_3 = 1 \text{ g.}$		
$p^0_{N_2O}$ (cm.)	$p^0_{N_2}$ (cm.)	Initial rate (cm./min.)
4.88	...	0.0233
9.680450
13.930558
18.710632
26.150858
32.43100
32.54	14.69	.104
33.12	15.02	.102
33.38	15.27	.0999
33.59106
33.65103
33.68107
33.94102
34.13105
34.41106
35.27108
44.25106
47.57142
56.41158

The order of the reaction with respect to nitrous oxide was determined by means of data obtained at constant $p^0_{O_2}$, $p^0_{N_2}$, and temperature. The order was found equal to 0.75. This result was obtained with $p^0_{O_2} = 0.13$ to 0.33 cm. The effect of p_{N_2} on the rate was determined by making initial rate measurements on premixed nitrous oxide-nitrogen mixtures. Some typical results of these measurements are collected in Table I. An inspection of Table I shows that nitrogen has no effect on the rate of the decomposition reaction. In a similar fashion, the effect of p_{O_2} on the rate of reaction was studied by making rate measurements on premixed nitrous oxide-oxygen mixtures. As the data reported in Fig. 1 show, oxygen has a strong inhibiting action on the rate of the reaction. Typical reaction velocity data obtained at different temperatures are collected in Table II. These data represent the average values of three to four runs for each set of experimental conditions.

Discussion

The catalytic decomposition of nitrous oxide may be visualized to occur according to the reaction sequence

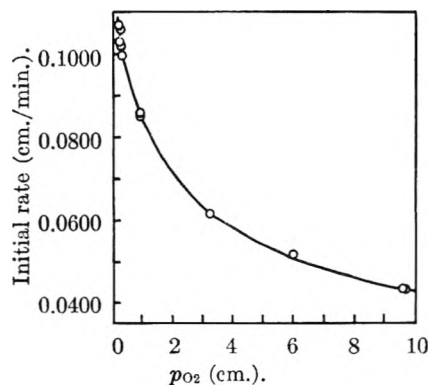
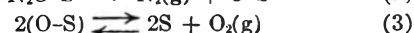
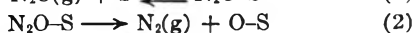
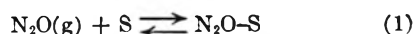


Fig. 1.—Effect of oxygen on the decomposition of nitrous oxide on α - Mn_2O_3 , temp. = 333° , α - $Mn_2O_3 = 1 \text{ g.}, p^0_{N_2O} = 33.5 \text{ cm.}$

TABLE II

EFFECT OF TEMPERATURE ON THE DECOMPOSITION OF N_2O ON α - Mn_2O_3

Temp. ($^\circ\text{C.}$)	$p^0_{N_2O}$ (cm.)	$p^0_{O_2}$ (cm.)	Initial rate (cm./min.)
286	33.80	0.16	0.0131
286	49.84	.18	.0166
286	33.74	.81	.00808
286	34.63	3.34	.00478
300	33.47	0.15	.0333
300	45.35	.13	.0411
300	33.47	.86	.0225
300	35.74	3.40	.0151
317	32.96	0.20	.0544
317	49.24	.30	.0676
317	33.56	.89	.0406
346	19.37	.18	.127
346	32.82	.93	.156
346	34.57	3.43	.120

where S is a surface site at which reaction occurs, and N_2O-S and $O-S$ are an adsorbed nitrous oxide molecule and an adsorbed oxygen atom, respectively. The reaction sites S are assumed to be energetically all of the same kind, or belonging to a narrow energy range. Reaction 1 represents the chemisorption of nitrous oxide, reaction 2 the decomposition of adsorbed nitrous oxide, and reaction 3 the desorption of oxygen. If it is assumed that reaction 2 is the slowest of the sequence, the rate of the over-all decomposition reaction can be expressed as

$$-\frac{dp_{N_2O}}{dt} = k_2[N_2O-S] \quad (4)$$

where k_2 is the rate constant for reaction 2 and $[N_2O-S]$ is the concentration of adsorbed nitrous oxide molecules. Furthermore, assuming that equilibrium is established rapidly in processes 1 and 3, then

$$b_1 = \frac{[N_2O-S]}{p_{N_2O}[S]} \quad (5)$$

$$b_3 = \frac{[O-S]^2}{p_{O_2}[S]^2} \quad (6)$$

where [S] and [O-S] are the concentrations of bare surface sites and surface sites occupied by chemisorbed oxygen, respectively. Moreover

$$[S] = [S]_0 - [N_2O-S] - [O-S] \quad (7)$$

where $[S]_0$ is the total concentration of available

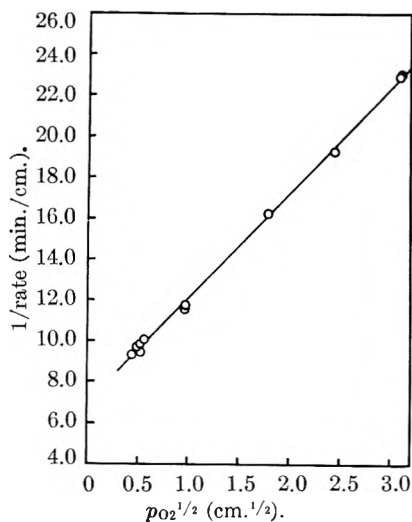


Fig. 2.—Plot 1/rate vs. $p_{O_2}^{1/2}$ for nitrous oxide decomposition on α - Mn_2O_3 , temp. = 333° , α - Mn_2O_3 = 1 g., $p_{N_2O}^0$ = 33.5 cm.

surface sites for the reaction. Substitution of (7) into (5)

$$b_1 p_{N_2O} = \frac{[N_2O-S]}{[S]_0 - [N_2O-S] - [O-S]} \quad (8)$$

and (7) into (6) gives

$$b_3^{1/2} p_{O_2}^{1/2} = \frac{[O-S]}{[S]_0 - [N_2O-S] - [O-S]} \quad (9)$$

Solving (8) for $[O-S]$, substituting into (9), one obtains

$$[N_2O-S] = \frac{[S]_0 b_1 p_{N_2O}}{1 + b_1 p_{N_2O} + b_3^{1/2} p_{O_2}^{1/2}} \quad (10)$$

and combining (10) and (4)

$$-\frac{dp_{N_2O}}{dt} = \frac{k_2 [S]_0 b_1 p_{N_2O}}{1 + b_1 p_{N_2O} + b_3^{1/2} p_{O_2}^{1/2}} \quad (11)$$

Let us now check the rate expression (11) with the experimental data. The data have shown that (a) the reaction rate is less than 1st order with respect to N_2O ; (b) the reaction rate is not affected by N_2 ; (c) the reaction rate is retarded by O_2 . Equation 11 may be rewritten as

$$\frac{1}{\text{Rate}} = \frac{1 + b_1 p_{N_2O} + b_3^{1/2} p_{O_2}^{1/2}}{k_2 [S]_0 b_1 p_{N_2O}} = \left(\frac{1}{k_2 [S]_0 b_1 p_{N_2O}} + \frac{1}{k_2 [S]_0} \right) + \frac{b_3^{1/2} p_{O_2}^{1/2}}{k_2 [S]_0 b_1 p_{N_2O}}$$

According to this equation, a plot of 1/rate versus $p_{O_2}^{1/2}$ should result in a straight line, when using experimental rate data taken at constant temperature and p_{N_2O} . One such plot is presented in Fig. 2. A straight line can be drawn fairly well through the experimental points. Oxygen is considered to be adsorbed with dissociation, and as a result p_{O_2} shows at half power in the rate equation 11. If, however, oxygen is assumed to be adsorbed without dissociation, one oxygen molecule per site S, it can be shown easily that p_{O_2} will appear in the rate equation 11 as an additive term to the first power, and the points of a log 1/rate versus p_{O_2} plot should be fitted into a straight line. When this is done, the experimental data deviate considerably from a straight line.

A further test of the derived rate equation may

be obtained by computing "course of reaction" data. To this end, the constants in equation 11 were determined with the method of least squares.⁵ The results of such computation are collected in Table III.

TABLE III
VALUES FOR THE CONSTANTS OF EQUATION 11

Temp. ($^\circ C.$)	$k_2 [S]_0 b_1$ (1/min.)	b_1 (1/cm.)	$b_3^{1/2}$ (1/cm.) ^{1/2}	$k_2 [S]_0$ (cm./min.)
286	0.00192	0.043	6.21	0.044
300	.00309	.031	2.80	.10
317	.00482	.023	2.14	.21
333	.00616	.011	1.07	.55
346	.0107	.011	0.91	.93

In order to integrate equation 11, let a , $a - x$, x and $x/2$, be the initial concentration of nitrous oxide, the concentration of nitrous oxide remaining at time t , the concentration of nitrogen formed at time t , and the concentration of oxygen at time t , respectively. Introducing these symbols into the rate equation 11, we obtain

$$-\frac{d(a-x)}{dt} = \frac{dx}{dt} = \frac{k_2 [S]_0 b_1 (a-x)}{1 + b_1 (a-x) + b_3^{1/2} (x/2)^{1/2}}$$

and, upon integration

$$\frac{1}{k_2 [S]_0 b_1} \ln \frac{a}{(a-x)} + \frac{x}{k_2 [S]_0} + \frac{(2b_3)^{1/2}}{k_2 [S]_0 b_1} \left[\frac{a^{1/2}}{2} \ln \left(\frac{a^{1/2} + x^{1/2}}{a^{1/2} - x^{1/2}} \right) - x^{1/2} \right] = t \quad (12)$$

A run on the decomposition of N_2O was performed up to 53.7% completion at 333° . Using the values of the constants obtained from initial rate data at 333° (Table III), pressure-time points were calculated by means of the integrated rate equation 12. The calculated and observed data for this run are recorded in Fig. 3, which shows good agreement between calculated and experimental values.

From a knowledge of values of k_2 at different temperatures (Table III), the value of the activation energy for reaction 2 was computed by means of the Arrhenius equation and found to be equal to 35.0 kcal./mole, and the value for the pre-exponential factor, $A [S]_0 = 2.09 \times 10^{12}$.

Furthermore, let ΔF^0 , ΔH^0 and ΔS^0 be the standard Gibbs free energy, enthalpy and entropy changes associated with reactions 1 and 3, the standard states being one cm. of pressure for the gas and one site per cm.² for the adsorbed and bare sites. In the present case, due to the form of the equilibrium functions, ΔS^0 is independent of the standard state for the adsorbed and bare sites. Since the pressures used in the present work are not too high, the equilibrium functions b_1 and b_3 may be used to compute ΔS and ΔH under the experimental conditions. By application of the method of least squares to values of b_1 and b_3 at different temperatures, the values of ΔH and ΔS in Table IV were obtained.

Utilizing a value of -19.4 for the enthalpy change for the over-all decomposition reaction,⁶ the energy

(5) J. B. Scarborough, "Numerical Mathematical Analysis," The Johns Hopkins Press, Baltimore, Md., 1930.

(6) F. D. Rossini, D. D. Wagman, W. H. Evans, S. Levine and I. Jaffe, "Selected Values of Chemical Thermodynamic Properties," Circular National Bureau of Standards 500, U. S. Government Printing Office, Washington, D. C., 1952.

TABLE IV
ENTHALPY ΔH AND ENTROPY, ΔS , CHANGES FOR REACTIONS
1 AND 3

Temperature range 286 to 346°

Reaction	ΔH (kcal./mole)	ΔS (cal./mole °C.)
1	-16.9	-36.4
3	-43.2	-66.0

changes derived for the catalytic reaction on α -manganese sesquioxide are schematically summarized in Fig. 4.

The values for ΔS reported in Table IV can be compared with computed values for the entropy change following adsorption for oxygen and nitrous oxide. Assuming immobile adsorption for the former one, with the loss of two vibrational and three translational degrees of freedom of the oxygen upon adsorption, the equilibrium function, b_3 , in terms of the partition functions is

$$b_3 = \frac{\left(\frac{Q}{N}\right)_{\text{O-S}}}{\left(\frac{Q}{N}\right)_{\text{O}_2} \times \left(\frac{Q}{N}\right)_{\text{S}}} e^{-E_0/RT}$$

If the partition functions of reaction sites and adsorbed species, together with the vibrational contribution of the gaseous oxygen molecule, are assumed to cancel each other, the equilibrium constant becomes

$$b_3 = \frac{1}{\left(\frac{2mkT}{h^2}\right)^{3/2} \times \frac{kT}{P} \times \frac{8\pi^2IkT}{\sigma h^2}} e^{-E_0/RT}$$

and since

$$\Delta F = -RT \ln b_3 \text{ and } \Delta S = -\left[\frac{\Delta F}{T}\right]_P$$

then

$$\Delta S = -\left[R \ln \left(\frac{2mkT}{h^2}\right)^{3/2} \times \frac{kT}{P} + \frac{5}{2} R\right] - \left[R \ln \left(\frac{8\pi^2IkT}{\sigma h^2}\right) + R\right] \quad (13)$$

where the first term corresponds to the entropy change due to the loss of three translational degrees of freedom and the second term to the loss of two rotational degrees of freedom. With the standard state for oxygen being one cm. of pressure, and using a moment of inertia of 19.3×10^{-40} g. cm.², it is possible to calculate from equation 13 a value of $\Delta S = -60$ cal./mole °C. in close agreement with the experimental value of -66.0 cal./mole °C. This agreement is taken as supporting evidence for the postulated dissociative adsorption of oxygen. Following a similar procedure for nitrous oxide and assuming that the partition function of reaction sites and of adsorbed species, together with the vibrational and rotational contributions of the gaseous nitrous oxide molecule, cancel each other, one obtains an expression of ΔS identical with the first term of the second member of equation 13. This treatment is tantamount to assuming the loss of three translational degrees of freedom of the nitrous oxide molecule upon adsorption. A calculated value of $\Delta S = -49.3$ cal./mole °C. results. If, however, we assume the loss of only two translational degrees of freedom upon adsorption, $\Delta S = -(2/3) 49.3 = -32.9$ cal./mole °C., the

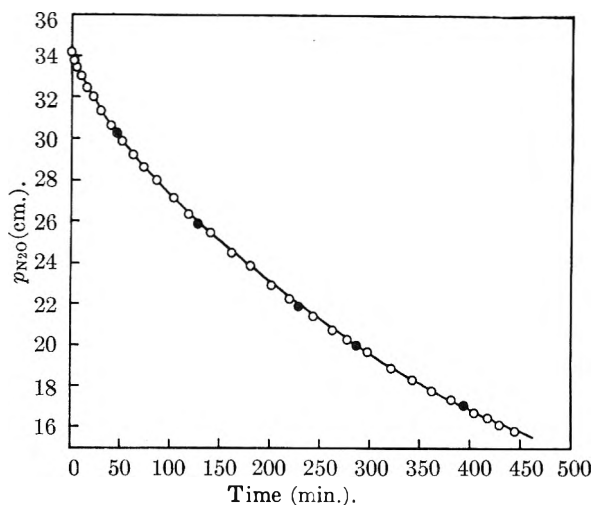


Fig. 3.—Experimental (O) and calculated (●) $p_{\text{N}_2\text{O}}$ from initial rate data for the decomposition of nitrous oxide on α - Mn_2O_3 , temp. = 333°, α - Mn_2O_3 = 1 g.

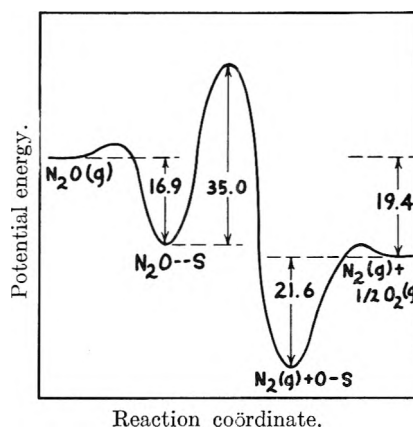


Fig. 4.—Energy diagram for the decomposition of nitrous oxide on α - Mn_2O_3 .

experimental value is -36.4 cal./mole °C. These comparisons indicate that the adsorbed nitrous oxide molecule has a considerable amount of freedom, and it is probably accommodated on the surface by means of the oxygen end of the molecule only. The decomposition of the N_2O molecule by rupture of the N-O bond is similar to the primary step postulated for the homogeneous decomposition of N_2O^7 and more recently for the mercury photosensitized decomposition of N_2O^8 .

Previous values of the adsorption enthalpy of O_2 determined calorimetrically on Mn_2O_3 , treated in high vacuum and 450°, are of the order of 24 kcal./mole at 17° and $p_{\text{O}_2} = 5 \times 10^{-3}$ cm.,⁹ and 12.2 kcal./mole for the differential enthalpy obtained from adsorption isotherms between 180 and 320°.¹⁰ The value of 43.2 kcal./mole obtained in the present work, although differing from the two reported values, should be compared with the calorimetric adsorption enthalpies of 55 kcal./mole for O_2 on Cu_2O^{11} and 37 kcal./mole on Cr_2O_3 .¹²

(7) H. S. Johnston, *J. Chem. Phys.*, **19**, 663 (1951); L. Friedman and J. Bigeleisen, *J. Am. Chem. Soc.*, **75**, 2215 (1953).

(8) R. J. Cvetanovic, *J. Chem. Phys.*, **23**, 1203 (1953).

(9) W. E. Garner and T. Ward, *J. Chem. Soc.*, 837 (1939).

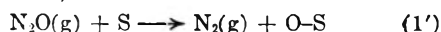
(10) H. Saito, *J. Chem. Soc., Japan, Pure Chem. Sect.*, **72**, 262 (1951).

The value of the enthalpy of adsorption obtained for N_2O supports the mechanism of a reversible adsorption-desorption of N_2O molecules followed by a slower decomposition of adsorbed nitrous oxide molecules. The concept of adsorbed N_2O molecules is further substantiated by photoelectric investigations of a Pt surface in a N_2O atmosphere.¹³ These studies showed that a strong interaction exists between adsorbed N_2O molecules and the metal surface, under conditions such as to minimize the decomposition of the adsorbed N_2O molecules.

Discussion of Other Reaction Mechanisms.— Since the decomposition of nitrous oxide has been investigated on several oxide catalysts by different authors, it is fruitful to examine the rate equations which are obtained, if a kinetically slow step differing from (2) is considered. Let us discuss first the case resulting from assuming reaction 1 as the slow step of the over-all reaction. By means of a treatment similar to that outlined previously, rate expression (14) is obtained in this case

$$-\frac{dp_{N_2O}}{dt} = \frac{k_1[S]_0 p_{N_2O}}{1 + b_2^{1/2} p_{O_2}^{1/2} + (b_2^{1/2}/b_1) p_{N_2} p_{O_2}^{1/2}} \quad (14)$$

According to equation 14 the reaction rate should be retarded by oxygen or nitrogen and show a first-order dependence on nitrous oxide. Only the first condition is brought out by the experimental data. Therefore the assumption that step 1 is slow compared to (2) and (3) cannot be justified in the present case. If steps 1 and 2 are combined into one reaction, that is



and it is further supposed that reaction 1' is slow compared to reaction 3, the rate equation (15) obtains

$$-\frac{dp_{N_2O}}{dt} = \frac{k_1[S]_0 p_{N_2O}}{1 + b_2^{1/2} p_{O_2}^{1/2}} \quad (15)$$

Equation 15 can be derived from (14) when $[N_2O-S]$ is very small compared to $[O-S]$, and the term containing b_2 in the denominator of the rate law may be neglected. According to equation 15 the rate of reaction should be retarded by oxygen, unaffected by nitrogen, and show a first-order dependence on nitrous oxide pressure. This last condition cannot be confirmed experimentally.

Let us now consider the case in which reaction 3 is assumed to be the slow step of the reaction sequence 1, 2 and 3. In this instance the rate of the over-all reaction becomes

$$-\frac{dp_{N_2O}}{dt} = \frac{k_{3f}([S]_0 b_1 b_2 p_{N_2O})^2 - k_{3b}([S]_0 p_{N_2O})^2 p_{O_2}}{(p_{N_2} + b_1 p_{N_2} p_{N_2O} + b_1 b_2 p_{N_2O})^2} \quad (16)$$

where k_{3f}, k_{3b} refer to the forward and reverse reaction rate constant of step 3 and $b_2 = p_{N_2} [O-S]/[N_2O-S]$. According to equation 16 the reaction rate should be 2nd order with respect to nitrous oxide, and retarded by oxygen and nitrogen. This latter condition is, again, not fulfilled experimentally.

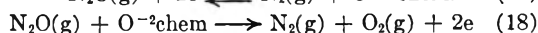
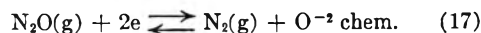
In previous studies and discussions of the N_2O

(11) W. E. Garner, F. S. Stone and P. F. Tiley, *Proc. Roy. Soc. (London)*, **A211**, 472 (1952).

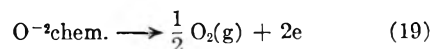
(12) D. A. Dowden and W. E. Garner, *J. Chem. Soc.*, 893 (1939).

(13) R. Suhrmann and W. Sachtler, *Z. Naturforsch.*, **A14**, (1954).

decomposition on metal oxides, it has been suggested often that p -type semi-conductors are the best catalysts for this reaction and that the rate-determining step of the reaction sequence on these materials is not the chemisorption of N_2O , but the desorption of O_2 from the catalytic surface,¹⁴ that is



or



These conclusions were based on measurements of electrical conductivity of metal oxides, mainly NiO, in N_2O-O_2 mixtures.¹⁵ It is possible that the discrepancy between the decomposition mechanism presently suggested for $\alpha-Mn_2O_3$ and that previously deduced for NiO is due to an inherent difference in surface behavior between two chemically dissimilar surfaces. There is also the possibility, however, that measurements on changes of electrical conductivity of NiO during the decomposition reaction are influenced by adsorbed nitrous oxide molecules. They will, in fact, affect the electrical conductivity of the oxide in the same manner as adsorbed oxygen. Deriving a rate equation from steps 17, 18 and considering step 18 rate determining, the expression (20) is obtained

$$-\frac{dp_{N_2O}}{dt} = \frac{k_{18}[S]_0^2 p_{N_2O}}{p_{N_2} + b_{17} p_{N_2O}} \quad (20)$$

and from steps 17 and 19, considering 19 to be rate determining

$$-\frac{dp_{H_2O}}{dt} = k_{19} \left(\frac{[S]_0 b_{17} p_{N_2O}}{p_{N_2} + b_{17} p_{N_2O}} \right)^2 \quad (21)$$

Equations 20 and 21 require that N_2 should influence the rate of reaction, while O_2 should not. Previously, a retardation effect of O_2 on the rate of decomposition of N_2O on NiO and Cu_2O was reported.¹⁶ A similar conclusion also was recently reached in a more general study of the electrical and catalytic effects of adsorption of gases on semi-conducting materials.¹⁷ A final comment is appropriate on the effect of O_2 on the rate of reaction. In the present work it was shown that the rate equation, derived from initial rate data only (2-6% conversion), is capable of expressing the kinetics of the reaction up to about 53% conversion at least. This result throws some doubt on the suggestion that O_2 formed during the decomposition of N_2O has a different effect than added O_2 .¹⁸

(14) (a) K. Hauße, R. Glang and H. J. Engel, *Z. physik. Chem.*, **201**, 22 (1952); (b) H. J. Engell and K. Hauße, *Z. Elektrochem.*, **57**, 762 (1953); (c) R. M. Dell, F. S. Stone and P. F. Tiley, *Trans. Faraday Soc.*, **49**, 201 (1953); (d) W. E. Garner (Editor), "Chemistry of the Solid State," Academic Press, Inc., New York, N. Y., 1955, Article by F. S. Stone; (e) K. Hauße, *Advances in Catalysis*, **7**, 213 (1955); **9**, 187 (1957).

(15) C. Wagner and K. Hauße, *Z. Elektrochem.*, **44**, 172 (1938).

(16) G. M. Schwab and R. Staeger, *Z. physik. Chem.*, **B25**, 418 (1934).

(17) T. Takaishi, *Z. Naturforsch.*, **11a**, 297 (1956).

(18) H. Cassell and E. Glückauf, *Z. physik. Chem.*, **B17**, 380 (1932); **B9**, 427 (1930); G. M. Schwab and B. Eberle, *ibid.*, **B19**, 102 (1932); E. W. R. Steacie and J. W. McCubbin, *J. Chem. Phys.*, **2**, 585 (1934); "Catalysis," Vol. 1, P. H. Emmett, Editor, Reinhold Publ. Corp., New York, N. Y., 1954, p. 146, article by K. J. Laidler.

TRACER DIFFUSION COEFFICIENTS OF STRONTIUM ION IN AQUEOUS POLYSTYRENE SULFONIC ACID SOLUTIONS¹

By J. P. DUX AND J. STEIGMAN²

Department of Chemistry, Polytechnic Institute of Brooklyn, Brooklyn, New York

Received August 26, 1958

Tracer diffusion coefficients of strontium-90 in dilute solution of polystyrenesulfonic acid were measured at 25°. The coefficients were low and decreased markedly with increasing time of diffusion. This was explained on the basis of irreversible binding of strontium ions to the polyions. Theory showed that the number average diffusion coefficient of the polyions could be calculated from the strontium coefficients. It was found experimentally that the tracer diffusion coefficients of sodium and cesium ions were practically unaffected by the polyacid, in contrast to strontium. Preparation of polystyrene sulfonic acid with radioactive sulfur permitted the simultaneous measurement of the self-diffusion coefficient of the polymer and the tracer diffusion of strontium-90. In the limit the two diffusion coefficients approached the same value, showing that the strontium moved with the polyion.

I. Introduction

Among the outstanding achievements of radiochemical techniques is the measurement of self-diffusion coefficients and tracer diffusion coefficients. A previous communication by the authors³ described a series of experiments in which the self-diffusion coefficient of strontium as counterion to polystyrenesulfonate ions in acid solution was studied. This paper is concerned with the measurement of tracer diffusion coefficients of strontium in solutions of polystyrenesulfonic acid. The tracer diffusion coefficient of an ion is one which is measured for a solution in which the concentration of the diffusing ion is negligibly small compared to the concentrations of the other electrolytes which are present. For this situation Onsager⁴ has shown that both the diffusion potential and the electrophoretic effect may be neglected. The activity coefficient of the diffusing ion is essentially constant over the diffusion path, in spite of the fact that its concentration varies from zero to a finite (but extremely small) value. Because of the very low concentration of the ion in question, these diffusion coefficients are most accurately measured by radiochemical methods. Other electrolytes must be present in more conventional concentrations in order for the activity coefficient of the tracer to remain constant as well as for the purpose of minimizing side effects like adsorption on container walls and interaction with impurities which are found even in the most carefully purified water. In this research the polyelectrolyte polystyrenesulfonic acid was present in concentrations of approximately 10^{-4} molar in sulfonate ions, while the strontium-ion concentration (as the radioactive isotope strontium-90) was of the order of 10^{-8} molar or less.

Under these conditions of concentration it was found that the value of the tracer diffusion coefficient was unexpectedly low and decreased with increasing time of diffusion, contrary to the behavior of such solutions at higher strontium concentrations.³ The effect can be interpreted as an irreversible binding of strontium to the polyelectrolyte, or else an exchange between bound and free strontium which is slower than the diffusion proc-

ess. In either case, with a polydisperse polymeric system, free strontium ions will diffuse out first, followed by strontium bound to lower molecular weight polymers, and finally by strontium bound to the larger, more slowly moving polyanions. Hence the diffusion coefficient will decrease as the diffusion time is increased.

II. Theory

It has been shown⁵ that it is convenient to divide small counterions in the vicinity of large polyions into two groups: those which are bound to a polyion, and hence move with it, and those which are free, and move independently of it. There will be some finite rate of exchange between bound and free counterions. It also has been demonstrated³ that if the exchange is rapid compared to the diffusion, the measured diffusion coefficient of the counterion will be independent of the time of diffusion, and will be equal to the mean diffusion coefficient of the counterion. Thus, if D is the observed diffusion coefficient, then

$$D = f_A D_A + f_p \bar{D}_p \quad (1)$$

where f_A is the fraction of counterions which are free, moving with coefficient D_A , f_p is the fraction of counterions which are bound and \bar{D}_p is the weighted diffusion coefficient of the bound counterions. That is

$$\bar{D}_p = \sum_n g_n D_n \quad (2)$$

where D_n is the diffusion coefficient of the n th polyion, and g_n is the fraction of the total of the bound counterions which are bound to the n th polyion. One consequence of this rapid exchange is that D is independent of time.

However, if the exchange rate between bound and free counterions is slow, the situation is markedly different. The limiting case will be examined, in which all counterions are bound, and there is no exchange of these ions between the polyions and the solution, or among the polyions. Hence the counterion moves with the mobility of the polyion to which it is bound, and, if radioactive, will trace the diffusion of the polyelectrolyte. The assumption is made that the polyelectrolyte solution is dilute so that the polyions diffuse independently of each other. We may then write Fick's law separately for each polyion. If there are n of the latter (*i.e.*,

(1) From a thesis submitted by James P. Dux to the Graduate School of The Polytechnic Institute of Brooklyn in partial fulfillment of the requirements for the degree of Doctor of Philosophy.

(2) To whom inquiries should be addressed.

(3) J. P. Dux and J. Steigman, *THIS JOURNAL*, **62**, 288 (1958).

(4) L. Onsager, *Ann. N. Y. Acad. Sci.*, **46**, 278 (1945).

(5) J. Huiizenga, P. Grieger and F. Wall, *J. Am. Chem. Soc.*, **72**, 2636 (1950).

if we have a degree of polymerization n) we may describe linear diffusion in this manner

$$\frac{\partial C_n}{\partial t} = D_n \frac{\partial^2 C_n}{\partial x^2} \quad (3)$$

in which C_n is the concentration of the n th polyion (tagged), x represents distance along the diffusion path, t is time and D_n is the diffusion coefficient of the radioactive bound tracer, and hence that of the polyion to which it is attached. Since it is assumed that there is no exchange between polyions,³ we must solve each equation 3 separately according to the boundary conditions of the experiment in which D_n is measured.

The technique used to measure diffusion coefficients in this research was the open-ended capillary method originated by Anderson and Saddington.⁶ The rigorous solution of Fick's law for these particular conditions yields

$$\gamma_n = \frac{C_n}{C_n^0} \frac{8}{\pi^2} \sum_{m=0}^{m=\infty} \frac{1}{(2m+1)^2} \exp\left(-\frac{(2m+1)^2 \pi^2 D_n t}{4l^2}\right) \quad (4)$$

in which γ_n is the fraction of the initial concentration of n -polyion remaining in the capillary at time t , C_n is the average concentration of n polyion remaining in the capillary at time t , C_n^0 is the initial concentration in the capillary of the same polyion, and l is the capillary length. If $D_n t / \pi^2 \geq 0.2$, all terms in the sum except the first may be neglected, so that

$$\gamma_n = \frac{8}{\pi^2} e^{-D_n t \theta} \quad (5)$$

where θ is a constant of the system, and is equal to $\pi^2/4l^2$. The total concentration of tagged polyion (symbol C_T) which remains in the capillary at time t is the sum of the concentrations of the individual polyions, C_n , so that

$$C_T = \sum_n C_n = \frac{8}{\pi^2} \sum_n C_n^0 e^{-\theta D_n t} \quad (6)$$

Dividing by the total initial concentration $C_T^0 = \sum C_n^0$, we obtain

$$\gamma_T = \frac{8}{\pi^2} \sum_n f_n^0 e^{-\theta D_n t} \quad (7)$$

in which f_n^0 is the fraction of the initial polyion concentration which is present as the n -mer; that is $f_n^0 = C_n^0 / C_T^0$. If we now define a diffusion coefficient D_T by the equation

$$\gamma_T = \frac{8}{\pi^2} e^{-\theta D_T t} \quad (8)$$

after substitution in equation 7, we obtain

$$D_T = -\frac{1}{\theta l} \ln \sum f_n^0 e^{-\theta D_n t} \quad (9)$$

This equation shows that D_T will be a function of time, to the extent that the logarithm of the sum is not equal to the sum of the logarithms of the individual terms. It is to be expected, then, that D_T will decrease with time as the smaller, faster-moving polyions diffuse out of the capillary first, followed by the larger particles.

The sum represented in equation 7 is the average value of the function $e^{-\theta D_n t}$ for the particular molecular-weight distribution of the polyions present

in the solution. If the exponential in this equation is expanded as a power series, we obtain

$$\gamma_T = \frac{8}{\pi^2} \left(1 - \theta l \sum f_n^0 D_n + \frac{(\theta l)^2 \sum f_n^0 D_n^2}{2!} - \frac{(\theta l)^3 \sum f_n^0 D_n^3}{3} + \dots \right) \quad (10)$$

or

$$\gamma_T = \frac{8}{\pi^2} \left((1 - \theta l \bar{D}_n + \frac{(\theta l)^2 \overline{D_n^2}}{2} - \frac{(\theta l)^3 \overline{D_n^3}}{3} + \dots) \right) \quad (11)$$

in which \bar{D}_n is the mean diffusion coefficient (defined as $\sum_n f_n D_n$), $\overline{D_n^2}$ is the mean square diffusion coefficient, etc. Thus, if we were to plot γ against θl and fit a power series in θl to the resulting curve, it should be possible theoretically to calculate not only \bar{D}_n but also the various moments of the distribution curve for D over n from the successive coefficients. However, there are two restrictions on this procedure. First, in order for equation 5 to hold, it is necessary that $D_n t / \pi^2 > 0.2$. Secondly, the power series in equation 10 must be convergent, and this requires that the argument $D_n \theta l$ must be less than one for all values of D_n .

The work which is reported here includes the measurement of the tracer diffusion coefficient of strontium ions for different times of diffusion in solutions of polystyrenesulfonic acid derived from different polymers, the measurement of the tracer diffusion coefficients of sodium and cesium in one of these solutions, and the simultaneous measurement of the self-diffusion coefficient of a sulfonated polystyrene and the tracer diffusion coefficient of strontium in the same solution.

III. Experimental

Materials.—Unless otherwise noted, reagent grade materials were used.

Polystyrene Sulfonic Acids.—Three different samples of polystyrene were sulfonated. Product A was prepared from a polymer of weight average molecular weight 1230. Products C-1 and C-2 were made from commercial polystyrene of weight average molecular weight 32,500. A and C-1 were described in a previous paper.³ Products B-1 and B-2, like Product A, were made from polystyrene prepared by chain transfer in carbon tetrachloride. However, it was subsequently fractionated by precipitation from dioxane-water solution. Its number average molecular weight was 953. It represented a much more sharply defined polymer than the polystyrene of Product A.

Products A and C-1 were made by sulfonation with hot, concentrated sulfuric acid.³ Products C-2, B-1 and B-2 were prepared by sulfonation with anhydrous sulfur trioxide according to the method of Baer.⁷ Redistilled dichlorodimethyl ether (25.5 ml.) in 80 ml. of chloroform was mixed with 4 ml. of Sulfan B (anhydrous sulfur trioxide, General Chemical Company). The temperature during addition was kept between -10 and 0° . Ten ml. of a 10% solution of polystyrene in chloroform was added rapidly to 15.6 ml. of the sulfonating solution, previously chilled to -20° . The sulfonated polymer separated out immediately, the temperature rising to 2° . The slurry stood for a half-hour, was then diluted with chloroform, filtered and washed with more solvent. The polymer was dissolved in water (100 ml.) and steam-distilled under reduced pressure to remove traces of organic solvents. It then was subjected to freeze-drying, yielding one gram of almost white powder with a degree of sulfonation of 1.11, determined by titration with standard NaOH to a phenolphthalein end-point.

Products B-1 and B-2 were sulfonated with sulfur trioxide which had been tagged with sulfur-35. A solution con-

(6) J. S. Anderson and K. Saddington, *J. Chem. Soc.*, S381 (1949).

(7) M. Baer, U. S. Patent No. 2,533,210 and 2,533,211 (December 12, 1950).

taining 25 millicuries of carrier-free S-35 as sulfate in hydrochloric acid was treated with one ml. of 10% sulfuric acid. The bulk of the water was removed at 105°. Anhydrous sulfur trioxide was added and polymerized immediately because of the water. It dissolved with shaking in a Dry Ice-chilled solution of dichlorodiethyl ether in ethylene dichloride. A similar solution was prepared using non-radioactive sulfur trioxide. Both solutions were stored in Dry Ice before use.

Sulfonation of Product B-1 was carried out by chilling 5 ml. of each of the sulfonating solutions (radioactive and inactive) until a frozen mush developed, and adding to each with rapid swirling two ml. of a 10% solution of the appropriate polystyrene in ethylene dichloride. The sulfonated polymer precipitated in ten minutes, and was allowed to stand overnight at Dry Ice temperature. The precipitates were then centrifuged, and washed with ethylene dichloride several times. They were finally vacuum-dried. Titration with standard NaOH showed a degree of sulfonation of 0.948 for the radioactive polymer and 0.937 for the inactive sample.

Product B-2 was prepared by sulfonating the polystyrene in the same manner, but changing the method of recovery in an attempt to reduce the presence of free sulfuric acid in the final product. After sulfonation, the mixture was frozen in Dry Ice, and ice was added to hydrolyze unreacted SO₃. Volatile organic compounds were removed by vacuum evaporation, 10 ml. of water was added, and the solution was extracted with four 25-ml. portions of benzene. The aqueous solution was then freeze-dried. The residue was diluted with water to 100 ml., 5 g. of Dowex 2 anion-exchange resin in the hydroxyl state was added, and the solution was shaken until the titer (determined by analyzing 5-ml. aliquots with NaOH) remained constant. The solution was filtered to remove the resin and diluted to 100 ml. The normality of the radioactive solution was 0.00393, and that of the inactive solution was 0.00687.

Diffusion Measurements.—The apparatus and the general procedure were the same as those described previously.³

Liter quantities of solutions of products A, C-1 and C-2 were prepared by dilution of stock solutions. The final concentration of product A was $8.43 \times 10^{-5} M$ in sulfonate; that of product C-1 was $1.67 \times 10^{-4} M$, and that of C-2 was $1.73 \times 10^{-4} M$. Each solution was filtered just before use. A 10-ml. aliquot then was centrifuged for a half-hour, and the supernatant liquid was transferred to a clean, dry volumetric flask. A small drop (about 0.01 ml.) of carrier-free radioactive Sr⁹⁰-Y⁹⁰ solution was transferred to the 10-ml. aliquot by means of a small wire loop. This was the radioactive solution with which the capillary diffusion cells were filled. Four cells were used for each run. The results reported in this paper represent averages of at least three, and usually all four, of the capillaries. Each capillary contained enough activity to yield a counting rate of approximately 2000 counts per minute.

Solutions which were used in sulfur-35 diffusion measurements were prepared in similar fashion, with the difference that the radioactive and non-radioactive samples were separately diluted to the same final concentration. This concentration was determined by two requirements: that at least half a liter of non-radioactive solution be available for a single run, and that a reasonable specific activity of sulfur-35 be present in the capillaries in order to avoid extended counting times. The final concentration inside and outside the capillaries for product B-1 was $8.63 \times 10^{-4} M$ in sulfonate, and for product B-2 was $6.37 \times 10^{-4} M$. After these final concentrations were achieved, strontium-90 was added to each radioactive solution in the manner described for products A and C. The resulting solutions contained both radioactive sulfur (in the polymer) and radioactive strontium, so that a comparison of strontium tracer diffusion and polymer self-diffusion could be made. It was possible, by means of an aluminum absorber, to count both radioisotopes in the same sample because of the great difference in maximum energies of the emitted betas (2.18 Mev. for the yttrium product of strontium decay, and 0.167 Mev. for the sulfur). It was found that an aluminum absorber with a thickness of 21.60 mg./cm.² (approximately 0.08 mm.) reduces the sulfur activity to 0.5% of its initial value, whereas the strontium activity is reduced by only 23.8%. Hence the activity observed with such an absorber in place would yield the strontium activity after division by the appropriate factor. The sulfur activity then was calculated by

difference from the initial mixed activity measured without the absorber. In this fashion it was possible to determine the tracer diffusion coefficient of the strontium and the self-diffusion of the sulfur-tagged polyion in the same solution.

Adsorption of strontium on the capillary walls was found in these solutions, and was taken into account in the calculations of diffusion coefficients. In general, as before,³ the magnitude of this correction was not large. No adsorption of the sulfur activity was observed.

Tracer diffusion measurements of carrier-free cesium-137 and high specific activity sodium-24 were made in solutions of product A in the same manner as the tracer diffusion measurements of strontium. No adsorption of sodium was found, but there was rather extensive adsorption of cesium, for which a correction was applied.

IV. Experimental Results and Conclusions

A. Tracer Diffusion Coefficients of Strontium in Polystyrene Sulfonic Acid Solutions.—Table I shows the tracer diffusion coefficients of Sr⁹⁰ in solutions of polystyrenesulfonic acid for different times of diffusion. *D* represents the experimentally determined coefficient; it corresponds to *D_T* in equation 8. The symbol γ_0 at the head of the fourth column stands for the value of γ (the fraction of the original activity remaining in a capillary after time *t*) normalized to an idealized capillary and permitted direct comparison of γ for polymers sulfonated by different procedures.

TABLE I
TRACER DIFFUSION COEFFICIENTS OF SR⁺⁺ IN POLYSTYRENE SULFONIC ACID SOLUTIONS

Product	Monomer concn., $\times 10^4$, mole/l.	Time of diffusion, hr.	γ_0	$D \times 10^4$, cm. ² /sec.
A	8.43	67.0	0.492	0.528 ± 0.032
		91.0	.422	$.504 \pm .007$
		115.0	.373	$.472 \pm .011$
		163.0	.313	$.411 \pm .013$
C-1	16.7	42.0	.540	$.682 \pm 0.039$
		68.0	.393	$.767 \pm .055$
		90.3	.337	$.684 \pm .014$
		117.0	.338	$.534 \pm .026$
		139.0	.315	$.471 \pm .024$
		162.5	.265	$.482 \pm .016$
C-2	17.3	42.0	.514	$.795 \pm 0.025$
		68.0	.455	$.606 \pm .040$
		90.0	.422	$.523 \pm .032$
		120.0	.373	$.458 \pm .035$

It appears that the tracer diffusion coefficient of the carrier-free strontium is decreasing in time, pointing either to an irreversible adsorption on the dissolved polyelectrolyte, or else a slow exchange. The initial measured values are all rather high, not far from the Nernst limiting diffusion coefficient for strontium ion at 25° (0.796×10^{-5} cm.²/sec.). It is possible that this represents free tracer ions not yet adsorbed, or else ions which are bound to low molecular weight fragments arising from cracking of the chain during sulfonation.

If the values of γ_0 from Table I are plotted against θt (where *t* is time, θ is $\pi^2/4l^2$, and *l*² has the value 6.25 cm.²—i.e., the square of the idealized capillary length of 2.500 cm.), and if it is assumed that the tracer strontium is completely bound to the polyions and does not exchange, then it is possible to calculate \bar{D}_n for the polyions, using equation 11. This has been applied to the data for products A-1

and C-2 (low and high molecular weight materials), treating the curves as approximate straight lines. For a straight line, the power series in equation 11 degenerates to

$$\gamma\tau = (8/\pi^2)(1 - \theta\bar{D}_n) \quad (12)$$

The slopes of the curves when multiplied by $\pi^2/8$ yield the values 0.135×10^{-5} and 0.130×10^{-5} cm.²/sec. These values are somewhat low, but point up what can be seen in Table I, that the diffusion coefficients do not seem to vary much with molecular weight. Product C-2 is derived from a polymer which has approximately 32 times the molecular weight of the parent material of product A. This apparent anomaly may be due to several factors. First, not all of the strontium may be bound. In this case, the diffusion of free ions may be entering into the measurement. Secondly, if the true average polymer diffusion coefficient is being measured, the low molecular weight material may be more fully extended—i.e., less coiled in random fashion—than the higher molecular weight substance. To the extent that the diffusion coefficient of a molecule is inversely proportional to its linear extension, the coefficient for the smaller particle may not be very far off from that of the larger particle. In this connection, it has been reported elsewhere that the diffusion of salt-free sodium polymethacrylate solutions at high degrees of ionization is independent of the molecular weight of the polyacid.⁸ Thirdly, cracking of the polymer chain probably occurs during sulfonation, and it would be relatively more severe for a high molecular weight material. This is borne out by the curve for product C-1, which was made by sulfonating high molecular weight polystyrene with hot concentrated sulfuric acid. The initial values of γ decrease with time, then remain approximately constant, and finally decrease again. This indicates that the distribution of molecular weights is bimodal. Thus, the initial decrease may correspond to degraded low molecular weight material diffusing out, the plateau represents a lack of diffusing material, and the final decrease points to the emergence of higher molecular weight fractions.

B. Tracer Diffusion Coefficients of Other Ions in Polystyrene Sulfonic Acid Solutions. Table II shows the tracer diffusion coefficients of sodium and cesium in solutions of product A. A suitable value for strontium is included for comparison. The measurements were limited to a single time of diffusion (67 hours). This was necessary because the alkali ion diffusion coefficients were so high that it was not feasible to study the process for diffusion times comparable to those employed with the strontium. In the table the symbol D_0 represents the limiting ionic diffusion coefficients at 25° calculated from the Nernst equation.

It is clear that the alkali ions are behaving as if they are essentially free, in contrast to the strontium. It should be pointed out that the time of diffusion employed here was associated with values of γ of approximately 0.1 to 0.2 for the alkali ions, compared to a value of γ for strontium of about 0.5. That is, 80 to 90% of the alkali ions had diffused out

TABLE II

TRACER DIFFUSION COEFFICIENTS OF Na²⁴, Cs¹³⁷ AND Sr⁹⁰ IN POLYACID SOLUTION

Concn. of product A = 8.43×10^{-5} M (in monomer)

Ion	Time of diffusion, hr.	$D \times 10^6$, cm. ² /sec.	$D_0 \times 10^6$, cm. ² /sec.
Na	67	1.43 ± 0.03	1.33
Cs	67	$1.89 \pm .26$	2.08
Sr	67	$0.53 \pm .03$	0.796

of the capillary with no indication of a serious decrease in diffusion coefficient, indicating very little if any binding to the polyion. The difference in behavior between the alkali ions and strontium ions may reflect simply a difference in the effect of ionic charge in counterion-binding,⁹ or may be based on a rather specific strontium-sulfonate interaction. There is at present no sufficient basis for deciding between these alternatives.

C. Comparison of Diffusion Coefficients of Polyions and Strontium Ions.—The self-diffusion coefficients of products B-1 and B-2 were determined at the same time as the tracer diffusion coefficient of strontium, in the manner described in the Experimental section. Table III gives the results of these experiments.

TABLE III

SELF-DIFFUSION OF S³⁵-TAGGED POLYIONS AND TRACER DIFFUSION OF Sr⁹⁰

Product	Concn. $\times 10^5$ mole/l. monomer)	Time of diffusion, hr.	$D \times 10^6$, cm. ² /sec.	
			Sr ⁹⁰	S ³⁵
B-1	86.3	67.2	0.373 ± 0.014	0.684 ± 0.009
		91.0	$.375 \pm .007$	$.505 \pm .026$
		112.0	$.386 \pm .030$	$.422 \pm .036$
B-2	68.7	67.0	0.464 ± 0.007	0.573 ± 0.023
		93.4	0.412 ± 0.012	0.446 ± 0.030

It can be seen that for product B-1 the coefficient for strontium is essentially independent of time, whereas that of the sulfur decreases with time, ultimately approaching the value of the strontium. For product B-2 the strontium coefficient is higher than that for B-1, decreases slightly with time and is lower than the corresponding sulfur diffusion coefficient. The constancy with time of the strontium diffusion coefficient in solutions of product B-1 (in contrast to its behavior with products A and C) is explained by the fact that this polymer represented a rather narrow molecular weight fraction, rather than the polydisperse systems of products A and C. The higher value for the strontium coefficient in product B-2, and its slight decrease in time, compared to the other product, are explained by the difference in method of purification of the two materials. Product B-2 was evaporated to dryness in the presence of free sulfuric acid. This would lead to some degradation of the polymer, and perhaps some chain scission, producing lower molecular weight fragments and broadening the molecular weight distribution. In turn this would result in an initially higher diffusion coefficient of strontium (assuming that it was bound to the chain), and to a

(8) O. Kedem and A. Katchalsky, *J. Polymer Sci.*, **16**, 321 (1955).

(9) F. Osawa, M. Imai and I. Kagawa, *J. Polymer Sci.*, **13**, 93 (1954).

decrease in that coefficient with time of diffusion. The fact that the sulfur diffusion coefficient is higher than that of the strontium is explained on the two assumptions: (a) that the strontium is all bound to the polyions, and (b) that there is some free sulfuric acid left in the sulfonated polymer. Such free sulfuric acid, which is, of course, tagged with sulfur-35, would diffuse out more rapidly than the polymer, giving rise to a rather high diffusion coefficient which would then decrease with increasing time of diffusion. That this is very likely the cause of the effect is shown by the fact that product B-2 was treated with anion exchange resin, whereas product B-1 was not. The initial S^{35} coefficient is much lower than that of B-1, which is to be expected if the residual sulfate has been decreased.

If it is assumed that the strontium diffusion coefficient is the same as the diffusion coefficient of the polyions, then it is possible to calculate both the fraction of sulfur-35 present in the solution as sulfate, and the diffusion coefficient of the sulfate. By way of definition, let

$$\begin{aligned} \gamma &= \text{ratio of final to initial activities for } S^{35} \\ \gamma' &= \text{ratio of final to initial activities for } Sr^{90} \\ C_s &= \text{concn. of sulfur present as } SO_4^{2-} \\ C_n &= \text{concn. of the } n\text{th polyion} \\ C_p &= \sum_n C_n, \text{ i.e., the total concn. of polyion} \\ D_s &= \text{diffusion coefficient of } SO_4^{2-} \\ D_n &= \text{diffusion coefficient of the } n\text{th polyion} \end{aligned}$$

Assuming $Dt/l^2 > 0.2$ for all species of ions, we may write from equation 7

$$\gamma = \frac{8}{\pi^2} f_s e^{-\theta D_s t} + \frac{8}{\pi^2} \sum_n f_n e^{-\theta D_n t} \quad (13)$$

and

$$\gamma' = \frac{8}{\pi^2} \sum_n f'_n e^{-\theta D_n t}$$

where

$$f_s = \frac{C_s}{C_s + C_p}, f_n = \frac{C_n}{C_s + C_p}, f'_n = \frac{C_n}{C_p}$$

and hence

$$f_n = (1 - f_s) f'_n$$

By substitution in equation 13, we get

$$\gamma = \frac{8}{\pi^2} f_s e^{-\theta D_s t} + \frac{8}{\pi^2} (1 - f_s) \sum_n f'_n e^{-\theta D_n t} \quad (14)$$

or

$$\gamma = \frac{8}{\pi^2} f_s e^{-\theta D_s t} + (1 - f_s) \gamma' \quad (15)$$

If we now have two observations of γ and γ' at time t_1 and t_2 , we may write

$$\gamma_1 - \gamma_1' = \frac{8}{\pi^2} f_s e^{-\theta D_s t_1} - f_s \gamma_1' \quad (16)$$

and

$$\gamma_2 - \gamma_2' = \frac{8}{\pi^2} f_s e^{-\theta D_s t_2} - f_s \gamma_2' \quad (17)$$

These two expressions may be solved simultaneously for f_s and D_s .

When this analysis is applied to the data of Table III, the following values are obtained: (a) for product B-1, the fraction of sulfur-35 present as SO_4^{2-} is 0.298, and the diffusion coefficient of SO_4^{2-} is 0.98×10^{-5} cm.²/sec.; (b) for Product B-2, the fraction of sulfur-35 present as SO_4^{2-} is 0.111, and the diffusion coefficient of SO_4^{2-} is 0.95×10^{-5} cm.²/sec. The limiting diffusion coefficient from the Nernst equation for sulfate ion at 25° is 1.08×10^{-5} cm.²/sec. The agreement is much better than expected, in view of the experimental errors involved.

It will be noted that although treatment of product B-2 with a small quantity of ion-exchange resin removed a very large fraction of the sulfate ion, the latter was by no means reduced to a negligible value. Possibly percolation of the radioactive solution through a column of resin would have been a more efficient procedure for removal of sulfuric acid than the shake-out batch technique which was actually used. The batch technique was adopted because of the small quantities of material involved in the sulfonation, and the possibility of greater loss of radioactive polymer by adsorption in a column.

It is concluded that strontium ion, present in very low levels of concentration, is adsorbed on the polystyrene sulfonate ions and diffuses with the coefficient of the polyion to which it is attached. This suggests the possibility of measurement of the diffusion coefficients of strongly dissociated poly-electrolytes by adding traces of suitable radioactive counterions.

Acknowledgment.—This research was supported by the U. S. Army Signal Corps under contract number DA36-039, Sc5596. We are grateful to Dr. L. Arond, who performed the sulfonations with sulfur trioxide reported in this paper. We thank Professor F. C. Collins for many helpful discussions.

THE INFLUENCE OF THE NET PROTEIN CHARGE ON THE RATE OF FORMATION OF ENZYME-SUBSTRATE COMPLEXES¹

BY GORDON G. HAMMES² AND ROBERT A. ALBERTY

Contribution from the Department of Chemistry, University of Wisconsin, Madison, Wisconsin

Received August 29, 1968

A theory is presented which allows the calculation of the dependence of the rate of formation of enzyme-substrate complexes on electrolyte concentration when this reaction is diffusion controlled. The influence of the net protein charge on this reaction is considered, although an exact theoretical treatment has not been achieved. An approximate solution is obtained by considering an "average" diffusion process which is spherically symmetric. The electrostatic interactions of the net protein charge and the enzymatic site charge with the substrate charge are taken into account. The dependence of the second-order rate constant upon net protein charge is computed for proteins of radii 25 and 43 Å. This theory is tested experimentally for the fumarase reaction by utilizing an indirect measurement of the effect of ionic strength on this rate constant. The effect of ionic strength on the net charge of fumarase was studied through electrophoresis experiments. Qualitative agreement between theory and experiment was obtained, and the results indicate a net charge of +2 on the enzymatic site of fumarase.

Introduction

The general theory of diffusion controlled reactions in solution has been formulated by several investigators.³⁻⁷ In a previous publication,⁸ this theory was specialized to allow the calculation of the rate of formation of enzyme-substrate complexes if this reaction is diffusion controlled. This was done by considering spherically symmetric diffusion into a hemispherical active site located on a plane on the surface of an enzyme molecule (Fig. 1a). For this case, the second-order rate constant in $M^{-1} \text{ sec.}^{-1}$ was found to be given by

$$k = \frac{2\pi N}{1000} R_{12} D_{12} f \quad (1)$$

where N is Avogadro's number, R_{12} is the reaction radius, D_{12} is the sum of the diffusion coefficients of enzyme and substrate, and f is a factor taking into account electrostatic interactions which is given by

$$f = \frac{1}{R_{12} \int_{R_{12}}^{\infty} e^{V/kt} \frac{1}{r^2} dr} \quad (2)$$

In this equation, V is the electrical potential energy which is a function of r . The electrostatic factor was calculated at infinite dilution and in the limiting law region assuming that the effect of the net protein charge is negligible compared with that of the net charge of the active site. The potential energy used for these cases was⁴

$$V = \frac{1}{2} \left\{ \frac{e\kappa R_1}{1 + \kappa R_1} + \frac{e\kappa R_2}{1 + \kappa R_2} \right\} \frac{z_1 z_2 e^2}{\epsilon r} (1 - \kappa r) \quad (3)$$

Here R_1 and R_2 are the radii of the spherical substrate and the hemispherical active site, respectively, z_1 and z_2 are the net charges of the substrate

and active site, e is the charge on the electron, ϵ is the dielectric constant of the medium and κ is the usual Debye-Hückel parameter. The above equations are for one active site per protein molecule; if there is more than one site, the rate constant given in equation 1 is multiplied by the number of active sites per protein molecule to obtain the theoretical rate constant for the reaction between protein and substrate molecules. This assumes that the rates of reaction at different enzymatic sites on the same protein molecule are independent of each other.

The above results were found to be in reasonable agreement with available experimental data. The purpose of the present paper is to extend the theory to take into account the effect of the net protein charge on the rate of formation of the enzyme-substrate complex. If the net protein charge is of the same sign as the charge on the substrate, this rate should be reduced as the magnitude of the net protein charge increases, while if the net protein charge and the substrate charge are of opposite sign, this rate should be increased as the net protein charge increases. A qualitative agreement with experimental data for the enzyme fumarase has been found.

Theoretical

A model for the calculation of the rate of formation of enzyme-substrate complexes, assuming the rate of formation is diffusion controlled, is illustrated in Fig. 1b. The net charge of the protein is considered to be located at the center of the protein molecule. This, of course, is equivalent to assuming a uniform distribution of charges on the surface of an impenetrable sphere. A rigorous calculation of the flux into the hemispherical sink would involve solving the differential equation (4) with appropriate boundary conditions.^{3,9}

$$\nabla \cdot [D\nabla c + (Dc/kT)\nabla V] = 0 \quad (4)$$

The charge at the center of the protein molecule destroys the spherical symmetry of the model, and both V and c , the concentration, are functions of r' and θ (or r and θ). The exact solution of equation 4 for $c(r, \theta)$ would be extremely complex, but a solution of interest can be obtained if the approximation is made that the potential energy is independent of

(1) This research was supported by grants from the National Science Foundation and from the Research Committee of the Graduate School of the University of Wisconsin from funds supplied by the Wisconsin Alumni Research Foundation.

(2) W. A. R. F. Fellow, 1956-1958.

(3) M. V. Smolichowski, *Z. physik. Chem.*, **92**, 129 (1917).

(4) P. Debye, *Trans. Electrochem. Soc.*, **82**, 265 (1942).

(5) E. J. Verwey and J. Th. G. Overbeek, "Theory of the Stability of Lyophobic Colloids," Elsevier Publ. Co., Inc., Amsterdam, 1948, p. 165.

(6) R. M. Noyes, *J. Chem. Phys.*, **22**, 1349 (1954); *J. Am. Chem. Soc.*, **78**, 5486 (1956).

(7) T. R. Waite, *Phys. Rev.*, **107**, 463 (1957); *J. Chem. Phys.*, **29**, 103 (1958).

(8) R. A. Alberty and G. G. Hammes, *THIS JOURNAL*, **62**, 154 (1958).

(9) J. Umberger and V. LaMer, *J. Am. Chem. Soc.*, **67**, 1099 (1945).

angle but depends on R , the radius of the protein molecule, and r , the radial distance from the center of the active site to the center of the substrate ion. Consequently c itself is assumed independent of angle but dependent on R (through the potential) and r . This is reasonable if one considers the symmetry involved in the model, namely, that the average value of the angle θ is equal to zero. What we will consider, therefore, is an "average" potential energy or, to put it another way, the asymmetry of the model is eliminated by considering only an "average" of the angular variable.

For the simplified model proposed above, the problem is identical to that previously solved for the case of spherical symmetry, except that V is somewhat altered. Therefore, the previous results, as expressed in equations 1 and 2, can be used directly. Assuming linear superposition of potentials, the potential energy is now the sum of two separate potential energies, one involving the electrostatic interaction between the substrate and the active site, and the other involving the electrostatic interaction between the substrate and the remainder of the protein molecule. The potential energy at infinite dilution and in the limiting law region can be expressed by an equation similar to equation 3.

$$V = \frac{1}{2} \left\{ \frac{e^{\kappa R_1}}{1 + \kappa R_1} + \frac{e^{\kappa R_2}}{1 + \kappa R_2} \right\} \frac{z_1 z_2 e^2}{\epsilon r} e^{-\kappa r} + \frac{1}{2} \left\{ \frac{e^{\kappa R}}{1 + \kappa R} + \frac{e^{\kappa R_1}}{1 + \kappa R_1} \right\} \frac{z_3 z_1 e^2}{\epsilon(r + R)} e^{-\kappa(r + R)} \quad (5)$$

The form of the above equation differs from equation 3 in that $(1 - \kappa r)$ has been replaced by the more exact $e^{-\kappa r}$. However, in dealing with proteins, equation (6) for the potential energy frequently is used¹⁰

$$V = \left(\frac{e^{\kappa R_{12}}}{1 + \kappa R_{12}} \right) \frac{z_1 z_2 e^2}{\epsilon r} e^{-\kappa r} + \left(\frac{e^{\kappa R_{13}}}{1 + \kappa R_{13}} \right) \frac{z_1 z_3 e^2}{\epsilon(r + R)} e^{-\kappa(r + R)} \quad (6)$$

Here R_{13} is the sum of the radii of protein and substrate. Equations 5 and 6 give identical results in the limit of low ionic strength and small molecules (*i.e.*, molecules 2-3 Å. in radius); however equation 6 is probably slightly better for the larger molecules being considered here.

The integral in equation 2 cannot be evaluated explicitly for the potentials given by equation 5 or 6, but must be evaluated numerically for each special case. This numerical integration has been carried out for many cases by the Numerical Analysis Laboratory using an IBM 704 computer. An occasional check of these results was made by carrying out graphical integrations manually. The maximum error of the computer values is less than $\pm 1\%$. The results for various ionic strengths are shown in Figs. 2-4 where $\log f$ is given as a function of $z_1 z_3$. The expression used for the potential energy was that given in equation 6. The results obtained using the potential energy as given by equation 5 were very similar to those shown here except that the ionic strength dependence is slightly greater ($\sim 15\%$ at maximum deviation). It is of interest

(10) G. Scatchard in E. J. Cohn and J. T. Edsall, "Proteins, Amino Acids and Peptides," Reinhold Publ. Corp., New York, N. Y., 1943, p. 64.

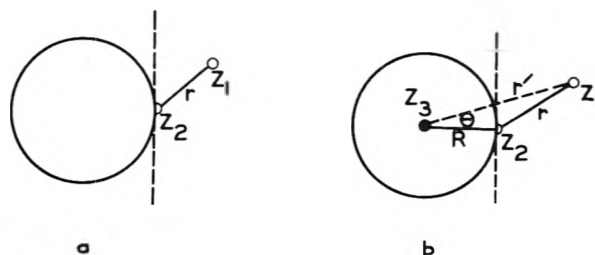


Fig. 1.—Model for the diffusion of substrate into the enzymatic site: (a) neglecting the net protein charge; (b) including the net protein charge.

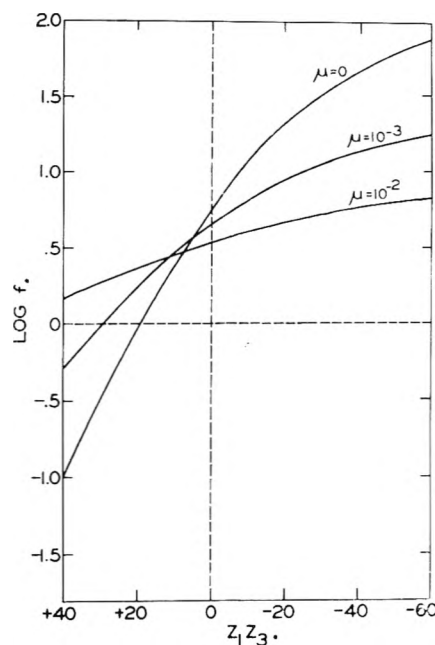


Fig. 2.—Plot of $\log f$ vs. $z_1 z_3$ at various ionic strength values from equations 2 and 6. Here $z_1 z_2 = -4$, $R_{12} = 5$ Å., $R_{13} = 46$ Å. and $R = 43$ Å.

to note that when the net protein charge is zero, the ionic strength dependence of f is slightly different from that published previously.⁸ The slope of a plot of $\log f$ vs. $\mu^{1/2}$ is about 0.6 of that for a similar plot of the older results. The present values are probably more accurate because $e^{-\kappa r}$ is used in evaluating the integral rather than the approximation $(1 - \kappa r)$. The present results indicate that the Brønsted-Debye-Hückel equation¹¹

$$\log k = \log k_0 + z_1 z_2 \mu^{1/2} \quad (7)$$

will not be followed for this particular type of reaction. However, the expected dependence of the rate constant on ionic strength can be found by utilizing numerical integrations of equation 2. The effect on f of changing $z_1 z_2$ and the protein radius can be seen by comparison of Fig. 2 with Figs. 3 and 4, respectively. As expected when $z_1 z_2$ becomes larger, the effect of the net protein charge becomes less important in determining f . On the other hand the net protein charge becomes increasingly important in determining f as the protein radius decreases.

To summarize a simple treatment has been presented which will allow the calculation of the diffusion controlled rate of formation of enzyme-sub-

(11) J. N. Brønsted, *Z. physik. Chem.*, **102**, 169 (1922); **115**, 337 (1925).

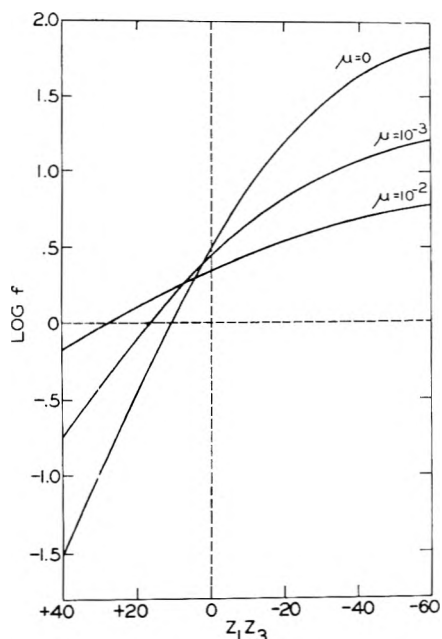


Fig. 3.—Plot of $\log f$ vs z_1z_3 at various ionic strength values from equations 2 and 6. Here $z_1z_2 = -2$, $R_{12} = 5 \text{ \AA}$, $R_{13} = 46 \text{ \AA}$, and $R = 45 \text{ \AA}$.

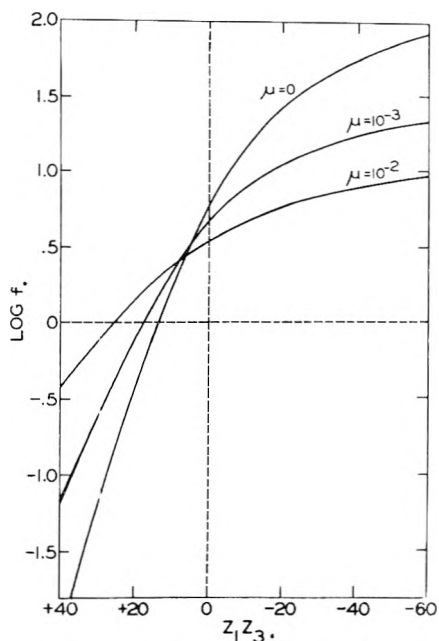


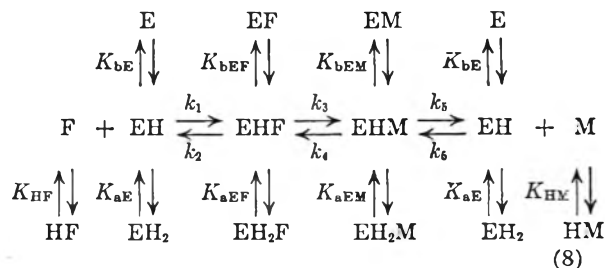
Fig. 4.—Plot of $\log f$ vs z_1z_3 at various ionic strength values from equations 2 and 6. Here $z_1z_2 = -4$, $R_{12} = 5 \text{ \AA}$, $R_{13} = 28 \text{ \AA}$, and $R = 25 \text{ \AA}$.

strate complexes and which may be used to predict the dependence of this rate on ionic strength. Both the net protein charge and the net charge on the active site are taken into consideration. In order to obtain usable results, a numerical integration must be carried out for each case of interest. The application of this theory to a particular enzyme reaction will now be considered.

Application to the Fumarase Reaction

The reaction catalyzed by the enzyme fumarase is fumarate⁻ + H₂O = L-malate⁻. The simplest

possible mechanism has been shown to be¹²



The rate constants for the combination of enzyme and substrate are k_1 and k_6 . There are three possible methods of measuring such rate constants. Assuming that the mechanism is $E + S \rightleftharpoons X \rightleftharpoons E + P$, the two second-order rate constants can be calculated from the Michaelis constants and maximum initial velocities of the forward and reverse reactions. For the more complicated mechanism represented by $E + S \rightleftharpoons X_1 \rightleftharpoons X_2 \rightleftharpoons E + P$ or mechanism 8, the *minimum* values of the second-order rate constants can be calculated from the Michaelis constants and maximum velocities of the forward and reverse reactions.¹³ For the fumarase reaction, the minimum values of k_1 and k_6 , obtained from the *pH* independent kinetic constants (which are assumed to be independent of the net protein charge), are in reasonable agreement with the values calculated using equation 1 with $z_3 = 0$.⁸ A second method of determining rate constants such as k_1 and k_6 is direct measurement by mixing solutions of enzyme and substrate and following the rise in concentration of the enzyme-substrate complex. In the case of fumarase, experimental means of detecting EHF or EHM are not known, but even if this were not the case the *minimum* values obtained as described above indicate that the rate constants are too large to be measured in this way. A third method would involve perturbing a solution of enzyme and substrates at equilibrium and following the return to equilibrium; three relaxation times could be measured for mechanism 3.¹⁴ These relaxation times depend upon all of the rate constants in the mechanism, but there is the *possibility* of determining the values of the second-order rate constants from the shorter relaxation times. An experimental investigation of this method has not been made yet, but in principle rate constants of the order of magnitude of the minimum values found for the fumarase reaction could be measured.

Since neither of the latter two methods can be used at present to determine the effect of the net protein charge on the rate of formation of enzyme-substrate complexes, it is necessary to find some indirect measure of k_1 and k_6 . In particular it would be desirable to study the effect of electrolyte concentration on these rates since this could be compared directly with the results of the theory. The net protein charge can be changed by varying the *pH*. In the following we will consider only k_6 since the reverse reaction is much easier to study experimentally than the forward reaction.

(12) C. Frieden and R. A. Alberty, *J. Biol. Chem.*, **212**, 859 (1955).

(13) R. A. Alberty and W. H. Peirce, *J. Am. Chem. Soc.*, **79**, 1529 (1957).

(14) Dr. M. Eigen, personal communication. See *Disc. Faraday Soc.*, **17**, 194 (1954).

For mechanism 8, the Michaelis constants and maximum velocities for the reverse reaction can be represented by the equations

$$K_M = K_M' \frac{[1 + (H^+)/K_{aE} + K_{bE}/(H^+)] [1 + (H^+)/K_{HM}]}{[1 + (H^+)/K_{aEM} + K_{bEM}/(H^+)]} = K_M' F(K) \quad (9)$$

$$K_M' = \frac{(k_2k_5 + k_2k_4 + k_3k_5)}{k_6(k_2 + k_3 + k_4)} \quad (10)$$

$$V_M = V_M' \frac{1}{[1 + (H^+)/K_{aEM} + K_{bEM}/(H^+)]} \quad (11)$$

$$V_M' = \frac{k_2k_1(E)_0}{(k_2 + k_3 + k_4)} \quad (12)$$

$$\frac{V_M}{K_M} = \frac{V_M'}{K_M'} \frac{1}{[1 + (H^+)/K_{aE} + K_{bE}/(H^+)] [1 + (H^+)/K_{HM}]} = \frac{V_M'}{K_M'} F'(K) \quad (13)$$

All of the rate constants other than k_6 appear to characterize *intramolecular* reactions; therefore it is reasonable to assume that all rate constants other than k_6 are relatively independent of ionic strength. This hypothesis is supported by the calculated values of the various rate constants¹³ and the fact that V_M' and V_F' are essentially independent of ionic strength in the pH range 5.5–8.5.¹⁵

The ionization constants in the above equations are independent of pH and ionic strength. This dependence is given by¹⁶

$$K = K_0 e^{z_1 w} \quad (14)$$

where K_0 is the value of the ionization constant at the isoelectric point of the protein and

$$w = \frac{e^2}{2 \epsilon kT} \left[\frac{1}{R} - \frac{1}{1 + \kappa a} \right] \quad (15)$$

Here a is the radius of exclusion and other symbols are as previously defined. Equations 14 and 15 are derived for an impenetrable sphere with charges distributed uniformly and continuously on the surface. Recently Tanford and Kirkwood^{17,18} have treated the case of discrete charge distributions; they found that for 8 or more ionizable groups per protein molecule the effect of ionic strength on the ionization constants is very close to that indicated in equation 15. If the net protein charge is close to zero, the ionization constants will be essentially independent of ionic strength.

Assuming that all unimolecular rate constants in the enzymatic mechanism are independent of ionic strength and that the net protein charge is close to zero, equations 9 and 13 can be written in the form

$$\log(1/K_M) = C + \log k_6 = C + \log f \quad (16)$$

$$\log(V_M/K_M) = C + \log k_6 = C + \log f \quad (17)$$

In these equations, the C 's denote various constants. These equations are valid near the isoelectric point and for pH independent parameters. The top three lines in Fig. 5 are consistent with equations 16 and 17. The ordinate has been arbitrarily adjusted for the sake of convenience. The net pro-

(15) C. Frieden, R. G. Wolfe, Jr., and R. A. Alberty, *J. Am. Chem. Soc.*, **79**, 1523 (1957).

(16) C. Tanford in T. Shedlovsky, ed., "Electrochemistry in Biology and Medicine," John Wiley and Sons, Inc., New York, N. Y., 1955.

(17) C. F. Tanford and J. G. Kirkwood, *J. Am. Chem. Soc.*, **79**, 1533 (1957).

(18) C. F. Tanford, *ibid.*, **79**, 5340 (1957).

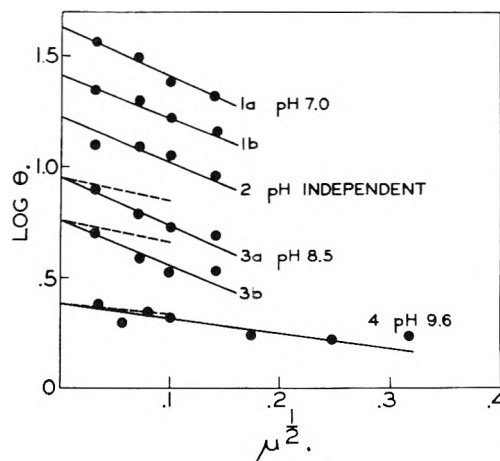


Fig. 5.—Plot of $\log \theta$ vs. $\mu^{1/2}$ at various pH values. The buffer for lines 1–3 was tris acetate; for line 4 the buffer was 0.001 *N* NaOH-glycine + NaCl. The ordinate is arbitrarily adjusted for the sake of convenience. For lines 1a and 3a, $\theta = 1/K_M$; for 1b and 3b, $\theta = V_M/K_M$; for 2, $\theta = 1/K_M'$; for 4, $\theta = v$.

tein charge at pH 7 is about -1 at an ionic strength of 0.01,¹⁹ so the slope obtained at this pH should be essentially the same as the slope for the pH independent values obtained by assuming that z_3 is equal to zero. The pH -independent parameters are calculated from data obtained over a range of pH 5.5–8.5. The slope of all three lines is about -2 . By looking at Figs. 2 and 3 for $z_1 z_3 = 0$, one can see that a slope of about -2 is predicted when $\log f$ is plotted versus $\mu^{1/2}$ if $z_1 z_2 = -4$. Since $z_1 = -2$, the net charge on the active site is about $+2$.

Effect of Net Protein Charge.—As soon as the net protein charge differs appreciably from zero ($|z_3| \geq 1$), the situation becomes quite complicated. Equations 16 and 17 now must be written as

$$\log(1/K_M) = C + \log f + \log F(K) \quad (18)$$

$$\log(V_M/K_M) = C + \log f + \log F'(K) \quad (19)$$

Here $F(K)$ and $F'(K)$ are appropriate functions of the ionization constants as given in equations 9 and 13. The ionization constants are in turn dependent on ionic strength in a manner given by equations 14 and 15. Substituting equation 14 in $F(K)$ and $F'(K)$, the slope of plots of $\log(1/K_M)$ or $\log(V_M/K_M)$ vs. $\mu^{1/2}$ can be calculated using equations 18 and 19 if K_0 , z_1 , z_2 and z_3 are known. However, the net protein charge itself may be a function of ionic strength, and before proceeding further, this dependence will be considered.

The net protein charge can be determined approximately through electrophoresis experiments. The electrophoretic mobility is related to the net protein charge for spherical molecules through the following equation^{20,21}

$$z_3 = \frac{6\pi\eta R(1 - \kappa R + \kappa r_i)}{f(\kappa R)(1 + \kappa r_i)} \frac{300u}{e} \quad (20)$$

where η is the coefficient of viscosity, R is the protein radius, r_i is the "average" radius of the ions in the ion atmosphere, u is the mobility in $\text{cm}^2 \text{ volt}^{-1}$

(19) N. Shavit, R. G. Wolfe, Jr., and R. A. Alberty, *J. Biol. Chem.*, in press.

(20) D. C. Henry, *Proc. Roy. Soc. (London)*, **A133**, 106 (1931).

(21) H. A. Abramson, L. S. Moyer and M. H. Gorin, "Electrophoresis of Proteins," Reinhold Publ. Corp., New York, N. Y., 1942, p. 121 and 152.

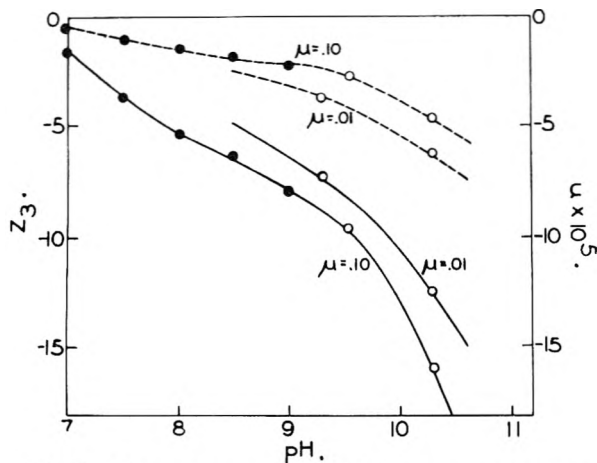


Fig. 6.—Plot of z_3 vs. pH (solid lines) and mobility u in $\text{cm}^2 \text{ volt}^{-1} \text{ sec}^{-1}$ vs. pH (dashed lines): ● designates previously published data¹⁹ in 0.01 *N* tris acetate and 0.09 *N* NaCl buffer; ○ designates values obtained in 0.001 *N* NaOH-glycine + NaCl buffers.

sec^{-1} and $f(\kappa R)$ is a function calculated by Henry²⁰ which is available in tabular form.²¹ The net charge on the protein varies with ionic strength because of changes in ion binding and changes in ionization constants of dissociable groups. Figure 6 summarizes the data which have been obtained for fumarase in the region of interest. It can be seen readily that the net protein charge is actually somewhat dependent on ionic strength. In principle the dependence of the net protein charge on ionic strength should be included in equations 18 and 19, but in practice this cannot be done because electrophoresis experiments cannot be made in the limiting law region ($\mu < 0.01$). For the region between pH 6.5 and 9.6, an "average" net protein charge at any pH value can be estimated from electrophoretic data. A cautionary note should be added, namely, that the net protein charge is also strongly dependent on the nature of the buffer itself because of preferential ion binding by the protein.

Figure 5 shows plots of $\log(1/K_M)$ and $\log(V_M/K_M)$ vs. $\mu^{1/2}$ at pH 8.5; the solid lines indicate experimental results (slope = -2), while the dashed lines are calculated using equations 18 and 19 with $z_3 = -5$ and $z_1 z_2 = -4$ (slope = -1). All the kinetic data shown on Fig. 5 for pH ≤ 8.5 , including the pH independent data, are from references 15 and 22. A qualitative agreement between the theoretical and experimental lines at pH 8.5 is apparent although the slopes differ by almost a factor of two. Considering the approximations made in both the theory and the interpretation of experimental data, this agreement is satisfactory.

At pH values greater than about 8.5, K_M becomes so large that it is not possible to determine it experimentally at low ionic strength values; however one can take advantage of this large Michaelis constant in the following manner. The initial steady state velocity v is represented by

$$v = \frac{V_M}{1 + K_M/(M)} \quad (21)$$

If experimental conditions are adjusted so that $(M) \ll K_M$

$$\log v = \log(V_M/K_M)(M) = C + \log f + \log F'(K) \quad (22)$$

Thus a plot of $\log v$ vs. $\mu^{1/2}$ can be calculated from the theory outlined above. It was estimated from preliminary experiments that at pH 9.6, $K_M \geq 2 \text{ mM}$. In order to test the assumption $(M) \ll K_M$, initial velocity measurements were made at two malate concentrations (80 and 120 μM). The apparent first-order rate constants obtained in several experiments at the two malate concentrations were essentially the same. A typical set of data is shown in Fig. 5. Once again the solid line designates the experimental result (slope = -0.7), while the dashed line is estimated from equation 22 assuming $z_3 = -8$ and $z_1 z_2 = -4$ (slope = -0.5). The two lines are in satisfactory agreement.

Critique of Theory.—In the preceding discussion careful note has been made of the various assumptions involved. The model itself is certainly a vast simplification of the actual situation, but even if this were not the case, a severe limitation is placed on the theory because the expression for the potential energy is valid only in the limiting law region. Furthermore this potential is assumed to be correct for all spherical molecules from 5 to 43 Å. in radius and for $|z_1 z_3|$ up to 16. The Debye-Hückel theory is derived considering the ionic atmosphere to be at equilibrium, but in actuality the diffusing substrate disturbs the ionic atmosphere from equilibrium. An exact treatment of such a non-equilibrium situation would be extremely complex. Even assuming the theory used is correct does not eliminate all difficulties since experimental results could only be obtained at the borderline of the limiting law region. Moreover, many approximations had to be made in treating the experimental data. Estimation of the net protein charge involves the implicit assumption that z_3 is the same at 0 and 25°. In addition, at high pH values, protein configurational changes and the resulting alteration of the ionization constants of protein groups should be considered.

Previously published data¹² indicate that the Michaelis constant becomes larger than indicated by equation 9 at pH values greater than about 8. The present results indicate that this is not only due to the expected decrease in k_6 as the net protein charge becomes increasingly negative, but also probably involves ionizations in addition to those shown in mechanism 8. There seems to be no clear out experimental method of distinguishing between these two possibilities.

To conclude, in spite of all the forementioned difficulties, a general theory for the diffusional controlled formation of enzyme-substrate complexes has been presented which appears to be in qualitative agreement with experimental results—which is all that can be expected when considering a system as complicated as this.

Experimental

All solutions were made from freshly boiled distilled water in order to eliminate CO_2 . Reagent grade chemicals were used throughout for preparation of buffers. Measurements of the initial velocity of the dehydration of L-malate

(22) C. Frieden, Doctoral Thesis, University of Wisconsin, 1955.

by fumarase were made as described earlier²³ using a Beckman DUR spectrophotometer with an expanded scale of 80 to 100% transmission. Additional measurements were made on a Cary 14 recording spectrophotometer with a 0-0.1, 0.1-0.2 absorbancy scale. Fumarase was isolated and crystallized by methods developed in this Laboratory.²⁴ All kinetic data were obtained at $25 \pm 0.2^\circ$. Experiments were done at pH 9.45-9.65 (± 0.05) in 0.001 ionic strength NaOH-glycine buffer and 80 and 120 μM malate. The ionic strength was varied by adding NaCl. The averaged initial velocities presented here are uncertain by approximately $\pm 10\%$. Rough determinations of the Michaelis constant K_M in 0.01 in ionic strength NaOH-glycine-NaCl buffer were made at pH 9.6-10.0 by use of Lineweaver-Burk plots.

Electrophoresis experiments were made following pre-

(23) R. M. Bock and R. A. Alberty, *J. Am. Chem. Soc.*, **75**, 1921 (1953).

(24) C. Frieden, R. M. Bock and R. A. Alberty, *ibid.*, **76**, 2482 (1954).

viously described procedures¹⁹ in 0.001 ionic strength NaOH-glycine buffer plus NaCl. Nitrogen was bubbled through the buffer solution during dialysis to prevent CO₂ absorption. In all cases, the conductivity of the buffer rather than that of the protein solution was measured. The fumarase concentration was about 0.3 to 0.4 g./100 ml. The pH was measured at 0° using a line operated Leeds and Northrup pH meter. At $\mu = 0.01$, the field strength was about 2.1 volt cm.⁻¹ and at $\mu = 0.1$ about 2.9 volt cm.⁻¹. The heat dissipation was 0.0028 and 0.050 watt cm.⁻³, respectively.

Acknowledgments.—The authors are extremely grateful to Dr. John G. Kirkwood for several illuminating discussions concerning a rigorous solution of the problem discussed in this paper. The authors are indebted to the Numerical Analysis Laboratory for the numerical integrations required for Figs. 2, 3 and 4. Thanks are also due to Miss Selma Hayman for the isolation of crystalline fumarase.

THE CRYSTAL STRUCTURE OF PERCHLORIC ACID MONOHYDRATE¹

BY FREDERICK S. LEE AND GENE B. CARPENTER

Contribution from the Metcalf Chemical Laboratories, Brown University, Providence, R. I.

Received September 2, 1958

The crystal structure of perchloric acid monohydrate has been determined in detail by X-ray diffraction methods. The structure confirms that the solid is really hydronium perchlorate. The perchlorate ions are nearly perfect tetrahedra with an average Cl-O distance of 1.42 Å.

Introduction

Solid perchloric acid monohydrate has been regarded as a classic example of a hydronium salt on the basis of the qualitative similarity of its X-ray diffraction pattern to that of ammonium perchlorate²; however, no complete structure determination has been reported. Other lines of evidence have supported the hydronium-salt interpretation: nuclear magnetic resonance,³ infrared spectra^{4,5} and Raman spectra.^{5,6} The purpose of the present work was to determine the crystal structure accurately in order to confirm the presence of the hydronium ion and to examine its hydrogen-bonding pattern.

Determination of the Structure

Sample.—Perchloric acid monohydrate was prepared by mixing the appropriate amounts of anhydrous and 72% acid. The material was sealed in thin-walled Pyrex capillaries to prevent the absorption of moisture during the X-ray examination. Small single crystals were then grown in the capillaries by zone melting; these were used for the X-ray studies. The *b*-axis of the crystal normally grew parallel to the axis of the capillary; one crys-

tal was obtained with the *a*-axis along the capillary by growing the crystal slowly around a bend.

Unit Cell and Space Group.—The crystal was found to be orthorhombic, as reported.² Unit cell dimensions were determined from measurements on the equatorial layers of rotation photographs prepared with the crystal rotating about the *a*- and *b*-axes, respectively. These measurements were calibrated with a superimposed powder pattern from sodium chloride using 5.638 Å. as its lattice constant. The cell dimensions are *a* = 9.065 (0.008), *b* = 5.569 (0.004), and *c* = 7.339 (0.004) Å. where the quantities in parentheses are the estimated standard deviations.

The density calculated from these dimensions on the basis of four formula units per unit cell is 2.12 g./cc. A rough determination carried out by titrating a known volume of the acid against a standard base verified that the value is indeed definitely larger than the value 1.88 g./cc. estimated by Volmer.²

The centrosymmetric space group Pnma-D_{2h}¹⁶ was assigned to the crystal from the systematic absences and by analogy with ammonium perchlorate; this choice subsequently was confirmed by the successful refinement of the structure.

TABLE I

ATOMIC COORDINATES AND TEMPERATURE FACTOR PARAMETERS FOR PERCHLORIC ACID MONOHYDRATE

Atom	<i>x</i>	<i>y</i>	<i>c</i>	<i>B</i> (Å. ²)
ClA	0.4217 (0.0001)	1/4	0.1971 (0.0001)	3.8
O ₁	.3011 (.0012)	1/4	.0718 (.0012)	5.5
O ₂	.5579 (.0012)	1/4	.1038 (.0013)	5.7
O ₃	.4081 (.0008)	0.0432 (.005)	.3112 (.0009)	7.1
O ₄	.6746 (.0010)	3/4	.3268 (.0011)	4.5

(1) This research was supported by the Office of Naval Research' reproduction in whole or part is permitted for any purpose of the United States Government. This work constitutes part of the Ph.D. thesis work of F. S. L. Presented in part at the San Francisco meeting of the American Chemical Society, April, 1958.

(2) M. Volmer, *Ann.*, **440**, 200 (1924).

(3) R. E. Richards and J. A. S. Smith, *Trans. Faraday Soc.*, **47**, 1261 (1951); Y. Kakiuchi, H. Shono, H. Komatsu and K. Kigoshi, *J. Phys. Soc. Japan*, **7**, 102 (1952).

(4) D. E. Bethell and N. Sheppard, *J. Chem. Phys.*, **21**, 1421 (1953).

(5) J. T. Mullhaupt, Thesis, Brown University, 1958.

(6) R. C. Taylor and G. L. Vidale, *J. Am. Chem. Soc.*, **78**, 5999 (1956).

TABLE II

OBSERVED AND CALCULATED STRUCTURE FACTORS FOR PERCHLORIC ACID MONOHYDRATE ($\times 10$)

<i>hkl</i>	F_o	F_c	<i>hkl</i>	F_o	F_c	<i>hkl</i>	F_o	F_c	<i>hkl</i>	F_o	F_c
002	622	-655	703	116	-102	511	<30	-9	321	<30	13
004	77	-89	704	<40	17	512	<30	8	322	138	130
006	100	94	705	57	61	513	138	134	323	125	-121
008	111	-122	706	<40	-1	514	131	117	324	309	-324
			707	43	-47	515	128	-138	325	44	42
101	241	-220				516	55	-55	326	143	146
102	242	-230	800	198	-202	517	<40	32	327	<30	13
103	<30	8	801	166	-176						
104	34	42	802	63	71	610	60	64	420	<30	-4
105	<30	-0	803	32	42	611	302	301	421	136	-123
106	88	-83	804	<40	6	612	<30	-13	422	52	-49
107	81	80				613	101	-96	423	202	206
108	<30	8	901	<40	15	614	<30	19	424	<30	17
			902	59	68	615	50	-46	425	52	52
200	357	341	903	<40	-18	616	<40	8	426	40	23
201	604	591	904	33	-54	617	44	60	427	62	76
202	297	-288									
203	248	-234	1001	50	-65	711	<40	30	521	68	-70
204	<30	16	1002	<40	-17	712	135	-137	522	<40	-7
205	<30	30	1003	38	41	713	64	-78	523	227	238
206	49	33				714	75	72	524	106	-96
207	81	84				715	<40	39	525	138	-155
208	<30	25	011	638	-679	716	47	-63	526	56	69
			013	111	-95						
301	62	-65	015	49	-70	810	127	-113	620	78	67
302	223	211	017	46	-35	811	105	94	621	51	-34
303	225	223	019	59	68	812	59	57	622	73	-65
304	170	164				813	<30	0	623	<40	13
305	85	-77	111	75	-92	814	<30	-16	624	<40	31
306	119	-107	112	458	483	815	<30	13	625	<40	-19
307	<30	-13	113	98	-87						
308	<30	24	114	175	-159	911	46	42	721	109	-114
			115	<40	-24	912	55	-52	722	<40	-16
400	319	-320	116	116	103	913	38	-55	723	134	131
401	452	461	117	65	67	914	<40	35	724	<40	32
402	255	248	118	39	-42	915	40	50	725	72	78
403	373	-355									
404	37	-24	210	689	691	1010	82	-99	820	152	160
405	91	-101	211	422	-415	1011	<40	-19	821	86	82
406	64	-61	212	348	-366	1012	50	72	822	54	-57
407	107	119	213	131	125				823	<40	-17
408	30	35	214	64	61	020	687	-692	824	<40	-7
			215	82	84	022	73	61			
501	38	-33	216	88	93	024	80	63	921	<40	-5
502	84	71	217	46	-47	026	<40	-17	922	65	-82
503	130	-116	218	74	-88	028	69	74	923	<40	2
504	94	78							924	52	71
505	104	102	311	118	106	121	341	340			
506	67	-70	312	134	126	122	358	355	1020	<40	-6
507	<30	-24	313	168	-184	123	317	-313	1021	39	45
508	<30	17	314	<30	9	124	183	-179			
			315	226	-228	125	154	139	031	145	146
600	270	-280	316	<30	-17	126	113	106	033	41	65
601	<30	-23	317	65	58	127	89	-88	035	76	57
602	201	195							037	<40	12
603	<30	3									
604	<40	-38	410	85	-58	220	49	11			
605	<40	32	311	89	91	221	78	68	131	92	83
606	<40	-32	412	272	-265	222	69	72	132	371	-340
607	<40	10	413	89	-89	223	38	53	133	59	-35
608	<40	42	414	127	134	224	<30	-13	134	213	192
			415	<30	-6	225	48	-65	135	65	54
701	107	110	416	67	64	226	<30	5	136	112	-100
702	<40	-46	417	<40	24	227	<40	-32	137	55	-49

223	209	-190	431	<30	5	731	<40	-32	145	56	-54
231	172	154	432	115	118	732	88	109	146	35	-49
232	133	116	433	34	36	733	58	74			
233	70	-60	434	79	-82	734	58	-71	051	188	-169
234	55	-37	435	<30	-4				053	<30	25
235	<40	-43				830	55	54	055	<30	-14
236	<40	-57	531	<30	23	831	48	-65			
237	<40	29	532	67	59	832	31	-27	151	<30	-14
			533	107	-107	833	<30	4	152	91	92
331	40	23	534	115	-124				153	<30	-4
332	72	75	535	84	102	040	445	449	154	74	-62
333	228	-216	536	37	56	042	174	-163	155	<30	-15
334	<30	-15				044	<30	-14	156	47	42
335	189	198	630	42	-62				060	159	-149
336	<30	13	631	140	-151	141	98	-88	062	81	67
337	39	-52	632	<30	24	142	108	-104	064	<30	-0
			633	55	54	143	96	87			
430	47	66	634	<40	-12	144	76	61	163	67	-51

All X-ray photographs were prepared with copper $K\alpha$ radiation (1.5418 Å.).

Structure Factors.—The intensities of the reflections were estimated visually by the multiple film technique from a series of Weissenberg photographs prepared with crystals rotating about the a - and b -axes, respectively. A small correction was made for the absorption in the cylindrical sample and Pyrex capillary. A total of 282 reflections were of measurable intensity, out of a total of 474 which are accessible with copper radiation.

Trial Structure.—Initially, approximate atomic positions were assigned to all except the hydrogen atoms by assuming the values found in the isomorphous ammonium perchlorate.⁷ (The later work of Venkatesan⁸ was not yet known to us.) It was recognized that the atomic coordinates reported there⁷ have been inadvertently referred to several different choices of origin.

Refinement of the Structure.—Improved values of the atomic coordinates were obtained from projections of the electron density onto the a,c -plane and the b,c -plane. This calculation employed measured structure factor magnitudes with signs calculated from the trial structure.

The subsequent stages of refinement utilized the least squares method. The atomic coordinates were thereby adjusted so as to minimize $\sum w(|F|_o - |F|_c)^2$, where the sum is over all observed reflections. Here $|F|_o$ is the observed, and $|F|_c$ the calculated structure factor magnitude and w is a weight given by the expression $w = n/|F|_o$ where n is the number of independent measurements entering into the average value $|F|_o$. Each cycle of least squares adjustment of atomic coordinates was followed by a separate least squares adjustment of the parameters B in the individual isotropic temperature factors $\exp[-B(\sin^2 \theta)/\lambda^2]$, and of the scale factor.

The final atomic coordinates and temperature factor parameters are recorded in Table I. The atomic coordinates are given in fractions of a cell edge, and the quantities in parentheses are the estimated standard deviations from the normal equations of the least squares treatment. Atom O_4 , not

included in the table, is the image of O_3 across the mirror plane at $y = 1/4$.

No direct evidence for the locations of the hydrogen atoms appeared in the electron density projections and no further attempt was made to locate them directly.

The structure factors calculated from the final structure are compared with the observed magnitudes in Table II. The conventional discrepancy factor, $R = \Sigma(|F|_o - |F|_c)/\Sigma|F|_o$, amounted to only 7.7% for the observed reflections, so that the refinement appears to be quite satisfactory.

Description and Discussion of the Structure

The structure of perchloric acid monohydrate is illustrated schematically in Fig. 1. The perchlorate groups are conspicuous; the chlorine atom and

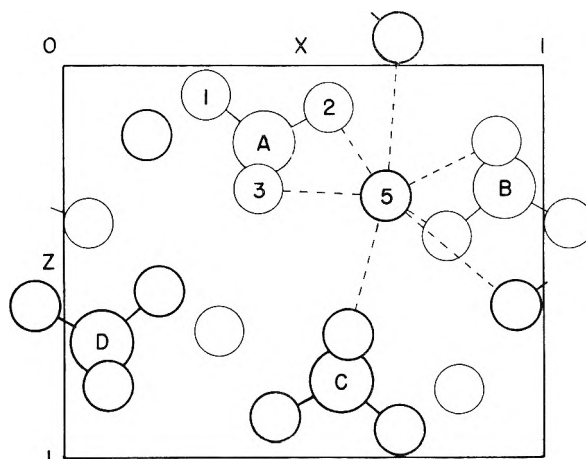


Fig. 1.—The structure of perchloric acid monohydrate viewed along the b -axis. The larger circles are chlorine atoms, the smaller are oxygen atoms. Heavily outlined atoms lie at or near $3/4$, lightly outlined ones at or near $1/4$, of the b -axis.

oxygen atoms O_1 and O_2 lie in a mirror plane while oxygen atoms O_3 and O_4 are mirror images across this plane. The bond lengths and angles in this group are recorded in Table III. From these dimensions it is seen that the perchlorate group is a nearly perfect tetrahedron (although not required by the symmetry of the crystal to be so), so that it must represent a perchlorate ion. If instead it were a perchloric acid molecule, one bond would

(7) C. Gottfried and C. Schusterius, *Z. Krist.*, **84**, 65 (1932).

(8) K. Venkatesan, *Proc. Indian Acad. Sci.*, **46A**, 134 (1957).

be expected to be noticeably longer than the other three.

TABLE III
PERCHLORATE ION DIMENSIONS IN PERCHLORIC ACID
MONOHYDRATE

Cl-O ₁	1.43 (0.01) Å.
Cl-O ₂	1.41 (.01)
Cl-O ₃ = Cl-O ₄	1.43 (.01)
O ₁ . . . O ₂	2.34 (.02)
O ₂ . . . O ₃ = O ₂ . . . O ₄	2.34 (.04)
O ₃ . . . O ₄	2.30 (.04)
O ₄ . . . O ₁ = O ₄ . . . O ₂	2.32 (.02)
O ₁ -Cl-O ₂	110.6 (0.6)°
O ₂ -Cl-O ₃ = O ₂ -Cl-O ₄	109.8 (.5)
O ₃ -Cl-O ₄	107.4 (.8)
O ₄ -O ₁ -O ₂	108.2 (.5)

Previously determined structures containing the perchlorate ions are those of ammonium perchlorate^{7,8} and potassium perchlorate.^{7,9} The average Cl-O lengths found therein are 1.49⁷ and 1.46 Å.⁸ in ammonium perchlorate and 1.44⁷ and 1.47 Å.⁹ in potassium perchlorate. Another value for potassium perchlorate is 1.43 Å.,¹⁰ communicated to us recently; this appears to be the most extensive and accurate work. The same reference¹⁰ mentions that slightly longer bonds are found in anhydrous and hydrated lithium perchlorate. More details and work on other perchlorates are required before the significance of the differences can be assessed.

From the presence of a perchlorate ion in perchloric acid monohydrate, it can be inferred that the one remaining independent oxygen atom (O₅) represents a hydronium ion. Unfortunately the diffraction pattern in this case is not sufficiently sensitive to the hydrogen atoms to give any direct indication of their positions. Nevertheless, it seems clear that the substance is really hydronium perchlorate rather than that implied by the usual name perchloric acid monohydrate.

The general arrangement of the ions is that in the well-known barium sulfate structure, so that there is no obvious crystallographic consequence of replacing the spherical barium ion by the pyramidal hydronium ion. Each hydronium ion is surrounded by a cage of twelve oxygen atoms belonging to several perchlorate ions. The distances from O₅ to these surrounding oxygen atoms are tabulated in Table IV; all have standard deviations of about 0.02 Å. Here the atoms are labelled to correspond with Fig. 1. The four perchlorate ions in one unit cell are designated A(000), etc., and those in adja-

(9) N. V. Mani, *Proc. Indian Acad. Sci.*, **46A**, 143 (1957).

(10) R. J. Prosen and K. N. Trueblood, private communication.

TABLE IV

DISTANCES FROM A HYDRONIUM OXYGEN ATOM TO NEIGHBORING OXYGEN ATOMS IN PERCHLORIC ACID MONOHYDRATE

Neighbor atom	Distance, Å.	Neighbor atom	Distance, Å.	Neighbor atom	Distance, Å.
A(000)3	2.92	C(001)1	2.93	B(010)1	3.10
A(010)3	2.92	B(000)3	2.86	D(100)2	3.16
A(000)2	3.40	B(010)3	2.86	C(000)3	2.99
A(010)2	3.40	B(000)1	3.10	C(000)4	2.99

cent units cells are designated by A(*t*, *t'*, *t''*), etc., where *t*, *t'* and *t''* give the translations along *a*, *b*, and *c* which specify a particular adjacent cell. The oxygen atoms in one ion have the additional label 1, 2, 3 or 4; those with the same number but in different ions are symmetrically equivalent. Even the shortest of the distances in Table IV, 2.86 Å., is relatively long to be a strong hydrogen bond.

Furthermore, no set of three of these neighboring oxygen atoms is disposed so as to suggest that hydrogen bonds are directed uniquely at them. It is possible, therefore, that in this crystal (the form stable at room temperature) the hydronium ions are rotating or are disordered among several orientations. Some support for this possibility is offered by the nuclear magnetic resonance spectrum: in the temperature range from about 150°K. to room temperature, the spectrum differs from that at lower temperatures and is interpreted³ as indicating that some kind of reorientation of the hydronium ions occurs at these higher temperatures. The transition at -30°⁶ was not, however, detected in these experiments. Another possible ordered arrangement of the hydronium ion has some features to recommend it: if each of the O-H bonds is assumed to be directed not toward a single oxygen atom but toward a neighboring perchlorate ion as a whole, then the expected pyramidal configuration of the hydronium ion is retained. In this arrangement each O-H bond is then directed toward the mid-point of the line joining a pair of oxygen atoms in one perchlorate ion, and the distances from the hydronium oxygen atom to the three nearest such midpoints are 2.75 to B(000), 2.75 to B(010), and 2.76 Å. to C(000). The three O-H bonds form angles with one another of 107, 102 and 102°. Some support for this model is the fact that it has been used successfully by Mullhaupt⁵ in a calculation of the vibration frequencies of the hydronium ion in perchloric acid monohydrate; this calculation takes account of the interaction with neighboring perchlorate ions.

Since large crystals of perchloric acid monohydrate are relatively easy to grow, a neutron diffraction study would appear to be a promising way to locate the hydrogen atoms more definitely.

THE SECOND VIRIAL COEFFICIENT FOR POLYELECTROLYTES. THEORY AND EXPERIMENT¹

BY T. A. OROFINO^{2,3} AND P. J. FLORY³

Department of Chemistry, Cornell University, Ithaca, N. Y.

Received September 5, 1958

The theory of the second virial coefficient A_2 for non-ionic polymers has been extended to include polyelectrolytes in salt solutions. Each polymer molecule is assumed to be described satisfactorily by a gaussian distribution of chain elements about its center of gravity; each small region of volume within the molecular domains is considered to be in Donnan equilibrium with the external (salt) solution. Summation over all volume elements and subsequent integration over the coordinates of the centers of gravity of two neighboring polyelectrolyte molecules yields an expression for A_2 identical in form with that found previously for non-ionic polymers, $A_2 = (\text{const.})[(s^2)^{3/2}/M^2]I_2(X_1, X_2)$, but with the interaction quantities X_1 and X_2 redefined as $X_1 = 10^3(3^{3/2}/2^2\pi^{3/2})(1/NV_1)(MV_u/M_u)^2(s^2)^{-3/2}(1/2 - \chi_1 + V_1i^2/4V_uS^*)$ and $X_2 = 10^6(3^{3/2}/2^2\pi^3)(1/N^2V_1)(MV_u/M_u)^3(s^2)^{-3}(1/3 - \chi_2 + V_1(z_- - z_+)i^3/12V_u^3S^{*2})$. M_u is the molecular weight of a segment, V_1 and V_u the molar volumes of solvent and segments, respectively, $(s^2)^{1/2}$ the radius of gyration of the polymer coils, i their degree of neutralization, and S^* the ionic strength of the external solution. The parameters χ_1 and χ_2 have been defined previously in the theory for non-ionic polymers. The function $I_2(X_1, X_2)$ is a definite integral which takes into account the extent of interpenetration of polymer molecular domains. Two useful approximations, suitable for stipulated ranges of X_1 and X_2 , have been previously given. Parameters calculated from the above relationships are compared with the results of light scattering measurements on the systems poly-(acrylic acid), NaCl, water and polystyrene-*p*-sulfonic acid (K-salt), KCl, water. The agreement is qualitatively good although the osmotic effects of the small ions are greatly depressed by the charges on the chain, particularly for high degrees of neutralization.

Introduction

Theories of dilute polyelectrolyte solutions heretofore have been largely concerned with the expansion of a single macromolecule. Before proceeding further, it would be well therefore to examine briefly the progress made in this connection. Several treatments have been published in which the electrostatic free energy was directly considered in arriving at expressions for the equilibrium size of the polyion in solution. Harris and Rice,⁴⁻⁶ for example, have applied this method to a random chain model of the polymer. A survey of earlier theoretical treatments is given in their publications and we shall therefore not reiterate.

An equivalent and more direct theoretical interpretation⁷ of polyelectrolyte solutions can be developed on the basis of the conditions for Donnan type osmotic equilibrium between mobile electrolyte within the domain of the coil and its external environment. Electrostatic interactions affect the equilibria, of course, but they need not be separately taken into account, provided that the net electrical charge within the polymer domain is negligible in comparison with the sum of the charged sites on the polyelectrolyte chain; this latter condition is almost universally met by high molecular weight polyelectrolytes under experimental conditions.

In accordance with the method described above, the following relationship for the equilibrium size of a high molecular weight polyelectrolyte molecule immersed in an infinite bath of salt solution was established^{7,8}

$$\alpha^5 - \alpha^3 = 10^3(3^{3/2}/2^2\pi^{3/2})(1/NV_1)(MV_u/M_u)^2 (s_0^2)^{-3/2}[1/2 - \chi_1 + V_1i^2/4V_u^3S^*] + \dots \quad (1)$$

In this equation, α is the factor by which the unperturbed linear dimensions of the molecules are expanded due to segment-solvent interactions, V_1 and V_u are the molar volumes of solvent and segments, respectively, N is Avogadro's number, M and M_u are the molecular weights of the polymer and its repeating unit, and $(s_0^2)^{1/2}$ is the radius of gyration of the unperturbed molecule; i and S^* are, respectively, the degree of ionization of the fixed charges on the chain and the ionic strength of the medium surrounding the polymer molecule. The parameter χ_1 has been defined previously.⁹ Higher terms in the series of eq. 1 are negligible in most cases of interest.

The second virial coefficient A_2 in the semi-empirical equation for the reduced osmotic pressure

$$\pi/c = RT[1/M_n + A_2c + A_3c^2 + \dots] \quad (2)$$

where c is the polymer concentration and M the molecular weight, or in the equation for the excess scattering intensity

$$Kc/R_0 = 1/\bar{M}_w + 2A_2c + 3A_3c^2 + \dots \quad (3)$$

where K is the optical constant and R_0 is Rayleigh's ratio at zero angle, bears an intimate relationship to the sizes of the dissolved polymer molecules. It is the object of the present communication to extend the foregoing treatment of the isolated polyelectrolyte molecule to the interaction of two identical polyions in salt solution. We shall employ the methods used previously^{10,11} in the treatment of the second virial coefficient for non-ionic polymers. The theory will be compared with light scattering results on the systems poly-(acrylic acid), NaCl, water and polystyrene-*p*-sulfonic acid (K-salt) KCl, water.

Theory

Consider a single polyelectrolyte molecule im-

(9) P. J. Flory, "Principles of Polymer Chemistry," Cornell University Press, Ithaca, N. Y., 1953; *J. Chem. Phys.*, **17**, 303 (1949).

(10) P. J. Flory, *ibid.*, **17**, 1347 (1949); P. J. Flory and W. R. Krigbaum, *ibid.*, **18**, 1086 (1950).

(11) T. A. Orofino and P. J. Flory, *ibid.*, **26**, 1067 (1957).

(1) Presented before the 130th American Chemical Society Meeting, Atlantic City, N. J., September, 1956.

(2) U. S. Rubber Company Fellow, 1955-1956.

(3) Mellon Institute, Pittsburgh, Pa.

(4) F. E. Harris and S. A. Rice, *THIS JOURNAL*, **58**, 725 (1954).

(5) S. A. Rice and F. E. Harris, *ibid.*, **58**, 733 (1954).

(6) See also R. A. Marcus, *ibid.*, **58**, 621 (1954).

(7) P. J. Flory, *J. Chem. Phys.*, **21**, 162 (1953).

(8) P. J. Flory and J. E. Osterheld, *THIS JOURNAL*, **58**, 653 (1954).

mersed in an infinite bath of solution of strong electrolyte (salt), $M_+^+ A_-^-$ at a concentration c_s^* moles/l. The polymer chain bears ionizable substituents which are taken to be identical with M^{z+} . The domain of the polymer is considered to be divided into a succession of spherical shells of volume δV (volume elements), each of which contains segments, ionized gegenions from the chain, and salt which has migrated into the volume element. The volume elements are assumed to be in Donnan equilibrium¹² with the external salt solution. If mean ionic activity coefficients of all mobile ion species are taken as unity, the difference in solvent chemical potential between the j th shell and the external solution in this approximation¹³ may then be written⁷

$$\mu_{1j} - \mu_1^* = -RT[1/2 - \chi_1 + V_1 i^2 / 4V_u^2 S^*] v_{2j}^2 + [1/3 - \chi_2 + V_1(z_- - z_+) i^2 / 12V_u^3 S^{*2}] v_{2j}^3 + \dots \quad (4)$$

where v_{2j} is the volume fraction of segments in the volume element and S^* is the ionic strength of the external solution. The parameters χ_1 and χ_2 also appear in the treatment¹¹ of non-ionic polymers; they retain their formal significance in the present case.

The free energy difference $\delta\Delta F_j$ between the j th volume element and the salt solution follows from integration of eq. 4

$$\delta\Delta F_j = kT(10^3/N)(V_u^2 \delta V_j / V_1) \{ [1/2 - \chi_1 + V_1 i^2 / 4V_u^2 S^*] v_{2j}^2 + (10^3/2N)V_u(1/3 - \chi_2 + V_1(z_- - z_+) i^2 / 12V_u^3 S^{*2}) v_{2j}^3 + \dots \} \quad (5)$$

In this equation the volume fraction of polymer in the volume element has been replaced by its equivalent in terms of the segment density ρ_j .

In analogy with the previous treatment for uncharged polymers, we compute the total free energy ΔF_a associated with the process of bringing two identical polymer molecules, initially well separated, within a separation of centers a . The distribution of segments of each molecule is assumed to be gaussian. The result is

$$\Delta F_a = kT \sum_{i=1} X_i \exp(-\sigma_i a^2) \quad (6)$$

where

$$X_1 = 10^3(3^{3/2}/2^2\pi^{3/2})(1/NV_1)(MV_u/M_u)^2(\bar{s}^2)^{-3/2} (1/2 - \chi_1 + V_1 i^2 / 4V_u^2 S^*) \quad (7)$$

$$X_2 = 10^6(3^{3/2}/2^3\pi^3)(1/N^2V_1)(MV_u/M_u)^3(\bar{s}^2)^{-3} (1/3 - \chi_2 + V_1(z_- - z_+) i^2 / 12V_u^3 S^{*2}) \quad (8)$$

$$\sigma_1 = 3/4\bar{s}^2$$

$$\sigma_2 = 1/\bar{s}^2$$

where \bar{s}^2 is the square of the radius of gyration for each polymer molecule.

Each of the interaction quantities X_1 and X_2 in

(12) An expression for the second virial coefficient for polyelectrolytes in salt solutions has been given previously by D. T. G. Pals and J. J. Hermans. *Rec. trav. chim.*, **71**, 458 (1952). They considered the Donnan equilibrium between two phases, one of which contained a uniform dispersion of polyelectrolyte segments (with ionizable groups) and the other a solution of simple, strong electrolyte. The model treated by them is formally identical with that employed here on a microscopic scale. Their treatment, however, neglects the discontinuous nature of the polyelectrolyte solution in the dilute region.

(13) The results of the present treatment would be unaffected however if we were to impose instead the less stringent requirement of equality of mean ionic activity coefficients in both phases.

eq. 7 consists of two additive terms: the first ones, represented by $1/2 - \chi_1$ and $1/3 - \chi_2$ in X_1 and X_2 , are identical with the corresponding X_1 and X_2 for non-ionic systems¹¹; the second represent the ionic contributions to X_1 and X_2 and will generally assume dominant importance in determining the values of these quantities, although the contribution of the non-ionic terms (e.g. $1/2 - \chi_1$) may become appreciable for a sufficiently small ratio i^2/S^* (under which conditions the ionic characteristics of the polyelectrolyte molecules are considerably suppressed).

The excluded volume is given by

$$u = 4\pi \int_0^\infty a^2 [1 - \exp(\Delta F_a/kT)] da \quad (9)$$

and in accordance with the relationship $A_2 = Nu/2M^2$ yields

$$A_2 = (16\pi N/3^{3/2}) [(\bar{s}^2)^{3/2}/M^2] \int_0^\infty t^2 [1 - \exp(-X_1 e^{-t^2} - X_2 e^{-4t^2/3})] dt = (16\pi N/3^{3/2}) [(\bar{s}^2)^{3/2}/M^2] I_2(X_1, X_2) \quad (10)$$

The above equation is identical in form with the expression developed previously for non-ionic systems.¹¹ If i were set equal to zero, or S^* equal to ∞ , the total mobile ion concentration inside and outside the polymer coils would be equal; under these conditions the system could be regarded as consisting of only two components, i.e., polymer and salt solution, and accordingly the eq. 7 would reduce to their previous definitions for uncharged polymers.

For the case of a symmetrical added electrolyte, $z_+ = z_-$, and according to the defining relation in eq. 7, the ionic contribution to X_2 vanishes. In the general case, the total contribution of X_2 to the second virial coefficient is usually small. As in the intramolecular treatment,⁸ the higher terms in the series of eq. 6 appear to be negligible in all cases of interest.

The expression for A_2 in eq. 10 may be simplified through use of the approximations to $I_2(X_1, X_2)$ given previously.¹¹ There it was shown

$$A_2 \simeq (16\pi N/3^{3/2}) [(\bar{s}^2)^{3/2}/M^2] \ln [1 + (\pi^{1/2}/4)X_1 + (\pi^{1/2}3^{3/2}/32)X_2] \quad (11)$$

$$X_1 < 100$$

or, in accordance with the limiting approximation for $I_2(X_1, X_2)$ for large X_1

$$A_2 \simeq (16\pi N/3^{3/2}) [(\bar{s}^2)^{3/2}/M^2] [\ln(X_1 + X_2^{3/4}) + \gamma]^{1/2} \quad (12)$$

$$\gamma = 0.577\dots$$

$$X_1 > 35$$

The closed form used for $I_2(X_1, X_2)$ in eq. 11 becomes increasingly accurate as the argument of I_2 approaches zero, whereas the approximation to this integral employed in eq. 12 becomes a better representation for large values of the argument. In the neighborhood of $X_1 = 35$, the two approximations are equally satisfactory. Although the limiting expression for A_2 in eq. 12 is to be preferred for *ca.* $X_1 > 35$, the approximation in eq. 11 may be used for values of X_1 as large as 100 without introducing appreciable error. The latter has the advantage that it permits representation of A_2 by a single simple expression applicable to both

non-ionic polymers and polyelectrolytes, provided only that X_1 is not excessively large.

Comparison of the defining relations for X_1 and X_2 in eq. 7 with the expression for the intramolecular expansion factor α in eq. 1 yields

$$\alpha^2 - 1 = X_1/2 + X_2/3 \quad (13)$$

With an error which is negligible, we may incorporate this result in eq. 11 to yield another expression for the second virial coefficient¹⁴

$$A_2 \approx (16\pi N/3^{3/2})[(\bar{s}^2)^{3/2}/M^2] \ln [1 + (\pi^{1/2}/2)(\alpha^2 - 1)] \quad (14)$$

The above equation succinctly combines the *inter-* and *intramolecular* theories: it is applicable to both polyelectrolytes and non-ionic polymers and, moreover, in the former case, circumvents the necessity of assigning a particular value to the degree of ionization (*cf. seq.*).

The equations 11, 12 and 14 express the second virial coefficient, in accordance with the model chosen, in approximate closed form over the entire range of segment-solvent interaction. It should be borne in mind, however, that although the mathematical representations of $I_2(X_1, X_2)$ for all values of the argument do not in any sense invalidate these equations, other limitations of theory (*e.g.*, assumption of spherical symmetry) probably place an upper limit on the range of usefulness of the theoretical expressions for A_2 .

Experimental

Polymer Samples.—The poly-(acrylic acid) fraction used in this investigation was prepared by Newman, *et al.*¹⁵ Light scattering measurements on the polysalt in NaCl solutions gave $\bar{M}_w = 7.7 \times 10^5$.

In order to ascertain the acid content, the sample was titrated with carbonate-free 0.05 *M* NaOH, using phenolphthalein as indicator, in the presence of approximately 0.1 *M* NaCl. The sample assayed about 92% purity. Similar assays were found for other fractions of the same polymer by Newman, *et al.* They ran Karl Fischer titrations on the samples and found a water content of *ca.* 5%. The remaining impurity is probably dioxane (fractionation solvent).

Light scattering measurements on a polystyrene-*p*-sulfonic acid (K-salt) fraction¹⁶ also were made and yielded a weight average molecular weight of 4.8×10^5 . The ratio of sulfonic acid to styrene groups in the sample used was believed to be unity, although no analysis was made.

Preparation of Solutions.—For each given value of i and S^* , the solutions used in these measurements were prepared as follows: a stock solution of the desired degree of neutralization and NaCl content was obtained by adding the calculated amounts of 0.05 *M* NaOH and dry NaCl to a volumetric flask containing a known weight of the polyacid. Boiled distilled water was added to make up the final volume. After filtration through a fine glass frit, measured volumes (pipet) of the stock solution were transferred into 100-cc. flasks. The dilutions were made by adding NaCl solution (previously filtered through a fine glass frit) of the same salt concentration as the stock solution. Preparatory to the light scattering measurements each solution was filtered directly into the cell through an ultrafine frit (porosity 0.9–

1.4 μ), using 5 rinses. The procedure described was found to be satisfactory when care was taken to exclude dust during the operations. Upon completion of the light scattering, the same solutions were used in the determination of the refractive index increments. At the termination of these runs the polyacid concentration and degree of neutralization were checked by dry weight analysis and titration. No significant changes from the original values were ever observed. The poly-(acrylic acid) concentrations in the sections which follow are all expressed in terms of the pure polyacid.

Light Scattering.—The light scattering apparatus and differential refractometer employed in these measurements have been described previously.^{17,18} Proper cell alignment was confirmed by measuring the light intensity from a fluorescein solution as a function of angle. Measurements of the scattered intensities, using unpolarized light ($\lambda = 4358 \text{ \AA.}$), were made at angles from 45 to 135° on each of the solutions. The temperature of the solution in the cell was 27.5 ± 0.5°. Before and after each series of readings, the galvanometer deflection was observed for scattering at 90° by one of two secondary standards, depending on the intensity of the scattered light exhibited by the solutions: a polished block of poly-(methyl methacrylate), or a sealed solution of polystyrene in toluene. The ratios of the secondary standard scattering intensities to that of the Cornell Standard Styron (0.5 g. of polystyrene in 100 cc. of toluene solution) at 90° were determined. The known absolute scattering power of the latter permits expression of Rayleigh's ratio as

$$R_\theta = (i_s/i_o - i_o/i_c)(i_c/i_{cps})R_{cps}[\sin \theta/(1 + \cos^2 \theta)]n_o^2/n_{cps}^2 \quad (15)$$

where i_s , i_o and i_c are, respectively, the galvanometer readings for the solution, the solvent and the secondary standard. R_{cps} for the Cornell Styron at 90° was taken¹⁹ as 2.08×10^{-4} . The quantity i_c/i_{cps} is the ratio of the galvanometer reading at 90° for the secondary standard to the (excess) reading for the Cornell Styron when the latter is in the same cell used for the scattering measurements, n_o is the refractive index of the solution (solvent) and n_{cps} that for the Styron (toluene).

Depolarization measurements were made at each concentration for each system studied. The ratios of the horizontal and vertical excess polarization readings were sometimes found to vary erratically with concentration, due to the unavoidably large experimental error involved in this measurement (the galvanometer readings for horizontally polarized light at 90° were often less than 0.1 the smallest division on the galvanometer scale). It was found, however, that either the lowest concentration used for each system gave no depolarization, or, when this was not the case, that the measured values for a series of concentrations extrapolated to zero. The Cabannes factor was therefore taken as unity for all the systems studied.

Results

Refractive Index Increments.—In Table I are given the experimentally observed values of the refractive index increment $\partial n/\partial c$ for each of the polyelectrolyte systems investigated. The measurements recorded were made at $30 \pm 0.1^\circ$.

The increments listed for poly-(acrylic acid) are expressed in terms of the pure polyacid. While the values observed appear to be independent of the ionic strength (NaCl) of the medium over a one hundredfold change in salt concentration, a progressive increase with increasing degree of neutralization is clearly indicated. This variation in $\partial n/\partial c$ apparently is due to corresponding changes in the optical characteristics of the polymer segments.

The value of $\partial n/\partial c$ for polystyrene-*p*-sulfonic

(14) N. S. Schneider and P. Doty, *THIS JOURNAL*, **58**, 762 (1954), have presented an expression for A_2 , applicable to polyelectrolytes, equivalent to eq. 14. Their relation appears to have been based on the assumption that for polyelectrolytes $\alpha^2 - 1 = X_1/2$. This theoretical identity had previously been established for non-ionic polymers (with neglect of X_2); its validity for ionic polymers as well is established by the results of the present treatment.

(15) S. Newman, W. R. Krigbaum, C. Laugier and P. J. Flory, *J. Polymer Sci.*, **14**, 451 (1954).

(16) Prepared by Dr. L. C. Cerny, Department of Chemistry, John Carroll University, Cleveland, Ohio.

(17) E. V. Gouinlock, Jr., P. J. Flory and H. A. Scheraga, *J. Polymer Sci.*, **16**, 383 (1955).

(18) M. L. Hunt, S. Newman, H. A. Scheraga and P. J. Flory, *THIS JOURNAL*, **60**, 1278 (1956).

(19) D. K. Carpenter and W. R. Krigbaum, *J. Chem. Phys.*, **24**, 1041 (1956).

TABLE I
REFRACTIVE INDEX INCREMENTS (30°)

i	S^* (moles/l.)	$\partial n/\partial c$ (cc./g.)
Poly-(acrylic acid)		
0.102	0.100	0.158
.105	.010	.156
.335	.100	.179
.344	.010	.186
.947	1.00	.253
.959	0.100	.253
.994	0.010	.261
Polystyrene- <i>p</i> -sulfonic acid (K salt)		
1	0.100	0.197

acid (K salt) in Table I refers to this polymer in 0.100 *M* KCl and is expressed in terms of the fully neutralized polysalt.

The application of the $\partial n/\partial c$ values in Table I to light scattering theory requires some discussion. For simple two component systems the observed (macroscopic) refractive increments determined as described above may be used directly in the calculation of the light scattering constant

$$K = (2\pi^2 n_0^2 / \lambda^4 N) (\partial n / \partial c)^2 \quad (16)$$

For multicomponent systems, however, the (microscopic) $\partial n/\partial c$ appearing in the definition of K is not in general equal to the corresponding quantity experimentally observed. Some time ago Ewart, *et al.*,²⁰ considered this problem for the case of polymer-solvent-precipitant systems and arrived at the expression for K

$$K = (2\pi^2 n^2 / \lambda^4 N) [(\partial n / \partial c) - (\partial \psi / \partial c)(\partial n / \partial \psi_0)]^2 \quad (17)$$

where ψ_0 is the volume fraction of solvent in the solvent-precipitant mixture and ψ its value in the medium surrounding the polymer domains. Their expression reduces to equation 16 when either $\partial \psi / \partial c = 0$, in which case the composition of the solvent-precipitant mixture is unaffected by the presence of solute (*i.e.*, the polymer does not selectively absorb one component from the external medium), or, $\partial n / \partial \psi_0 = 0$, in which case the solvent and precipitant have the same refractive indices.

It is possible to adapt the treatment of Ewart, *et al.*, in an approximate manner to the polyelectrolyte systems studied here and so obtain an estimate of the size of the term $(\partial \psi / \partial c)(\partial n / \partial \psi_0)$. For this purpose consider the sodium polyacrylate-NaCl systems to be made up from the three components polysalt, 1 *M* NaCl and water. A dilute polymer solution of concentration c g./cc. may be regarded as formed in the following manner: to 1 liter of aqueous NaCl solution of initial ionic strength S_0^* , made by mixing appropriate volumes of 1 *M* NaCl solution and water, are added $10^3 Nc/M$ permeable, Donnan spheres (polymer molecules) each of volume V liters. M is the molecular weight of a sphere. The spheres are initially devoid of solvent but each contains its complement of ix gegenions (Na^+), where x is the number of ioniz-

able groups per sphere. NaCl and water from the external solution now permeate the spherical boundaries and completely fill the spheres. If the equilibrium concentration of NaCl molecules within the spheres is y moles/l., the volume fraction of water ψ in the external solution (bearing in mind that this solution consists of the mixed solvents 1 *M* NaCl and water) may be expressed

$$\psi = 1 - (S_0^* - 10^3 NVyc/M) / (1 - 10^3 NVc/M) \quad (18)$$

Assuming V independent of c , we have from eq. 18

$$\lim_{c \rightarrow 0} (\partial \psi / \partial c) = -10^3 NV(S_0^* - y_0) / M \quad (19)$$

At infinite dilution the Donnan condition requires

$$(ix/NV + y_0)y_0 = S_0^{*2}, \text{ or,}$$

$$V(S_0^* - y_0) = ix y_0 / N(S_0^* + y_0)$$

which in conjunction with eq. 19 yields

$$\lim_{c \rightarrow 0} (\partial \psi / \partial c) = -10^3 ix y_0 / M(S_0^* + y_0) \quad (20)$$

The second term in brackets in eq. 17 should be most significant when i is large or S_0^* is small. The largest value of i (effective) encountered in the systems studied here is about 0.1 (*cf. seq.*); the minimum ionic strength is 0.01. Substitution of these values together with $x = 10^4$, $y \simeq S_0^*$ and $M = 10^6$ into eq. 20 yields $(\partial \psi / \partial c)_{c=0} \simeq -0.5$. For the two component system 1 *M* NaCl-water, $\partial n / \partial \psi_0 = 0.01$, and thus the second term in brackets in eq. 17 is of the order 0.005. The observed value of $\partial n / \partial c$ for the particular system considered is about 0.2. Within the limits of the development presented above therefore, the quantity $(\partial \psi / \partial c) \cdot (\partial n / \partial \psi_0)$ in eq. 17 should make only a small contribution in the systems studied here. Accordingly, the observed value of $\partial n / \partial c$ should be directly applicable, without introducing serious error, in the light scattering equations. The experimental data presented in subsequent sections appear to confirm this conclusion.

Molecular Dimensions.—In the determination of the average dimensions of the polyelectrolyte molecules the extrapolation method of Zimm²¹ was employed. The quantity c/R_θ , calculated with the aid of eq. 15, was plotted against $\sin^2(\theta/2)$ for each of the systems investigated. The data were found to obey a linear relationship in all cases except for the two lowest concentrations studied in the system poly-(acrylic acid), $i = 0.994$, $S^* = 0.01$, where upward curvature was observed at the higher angles. In this instance the low angle data were employed in the linear extrapolation to $\theta = 0$. The smoothed values of c/R_θ thus obtained were then plotted against c for various values of θ and extrapolated to zero concentration. These plots generally exhibited curvature, particularly for those systems with large dissymmetries (large values of i^2/S^*). In the latter cases, however, experimental measurements had been made at sufficiently low concentrations to permit reliable extrapolation of the c/R_θ values. The extrapolated ratios $(c/R_\theta)_{c=0}$ thus obtained were then plotted against $\sin^2(\theta/2)$ in accordance with the relationship

$$(Kc/R_\theta)_{c=0} = 1/\bar{M}_w [1 + (16\pi^2 n_0^2 / 3\lambda^2) (\bar{s}^2)_{90} \sin^2 \theta/2 + \dots] \quad (21)$$

(21) B. H. Zimm, *ibid.*, **16**, 1093 (1948).

(20) R. H. Ewart, C. P. Roe, P. Debye and J. R. McCartney, *ibid.*, **14**, 687 (1946). For detailed discussions on light scattering in multicomponent systems the reader is also referred to papers by H. C. Brinkman and J. J. Hermans, *ibid.*, **17**, 574 (1949); J. G. Kirkwood and R. J. Goldberg, *ibid.*, **18**, 54 (1950); and W. H. Stockmayer, *ibid.*, **18**, 58 (1950).

The curves for the poly-(acrylic acid) systems are shown in Fig. 1. The corresponding values of the z -average radii of gyration $(\bar{s}^2)_z^{1/2}$ follow from the slopes and intercepts and are given in Table II.

Second Virial Coefficients.—In the calculation of the second virial coefficient A_2 the quantities (c/R_0) , obtained from the intercepts of the c/R_0 versus $\sin^2(\theta/2)$ plots, were plotted against c in accordance with eq. 3. The resulting curves for the poly-(acrylic acid) systems studied are shown in Fig. 2. We were unable to ascertain any systematic trend in intercepts when the curves were drawn separately through the experimental points.

TABLE II

RESULTS OF LIGHT SCATTERING MEASUREMENTS			
i	S^* (moles/l.)	$A_2 \times 10^4$ (cc. mole/g. ²)	$(\bar{s}^2)^{1/2} \times 10^6$ (cm.)
Poly-(acrylic acid) in NaCl soln., $\bar{M}_w = 7.7 \times 10^6$			
0.102	0.10	5.95	0.56
.335	.10	22.2	0.72
.344	.01	69.5	1.08
.947	1.00	10.0	0.67
.959	0.10	43.9	0.75
.994	0.01	196	1.24
Polystyrene- <i>p</i> -sulfonic acid (K salt) in KCl soln., $\bar{M}_w = 4.8 \times 10^6$			
1	0.10	4.68	0.443

It was felt, therefore, that the curves should be drawn as shown, *i.e.*, the best curves leading to a common intercept. The dissymmetry plots were similarly constructed. Equivalently, it has been assumed that the aforementioned dependence of K on ionic strength and degree of neutralization (other than that explicitly taken into account by the experimentally observed $\partial n/\partial c$) may be ignored.

The initial linearity of the plots in Fig. 2 is somewhat surprising, since for all but the smallest virial coefficients the data are outside the range in which linearity is normally encountered.²² Apparently, the third and higher terms in the virial expansion of eq. 2 are to a large extent compensating. The theoretical justification for this observation unfortunately is not presently available.

The experimental points for the system $i = 0.102$, $S^* = 0.10$ appear to exhibit upward curvature at low concentrations. A corresponding phenomenon was observed in the intrinsic viscosity studies published previously.⁸ It was suggested there that the curvature is due to enhanced ionization of polyacid groups in very dilute solutions. In this region the total degree of ionization increases with increasing dilution and thus affects the observed values of (c/R_0) and the reduced viscosities. When the molecule is initially fully neutralized by strong base ($i = 1$) the ionization of carboxylic acid groups is of course complete. Ionization of the unneutralized COOH groups should further be of no consequence for $i = 1/3$ over the concentration range covered in these experiments.

The values of A_2 obtained from the initial slopes and intercepts of the curves in Fig. 2 are given

(22) W. R. Krigbaum and P. J. Flory, *J. Am. Chem. Soc.*, **75**, 1775, 5254 (1953).

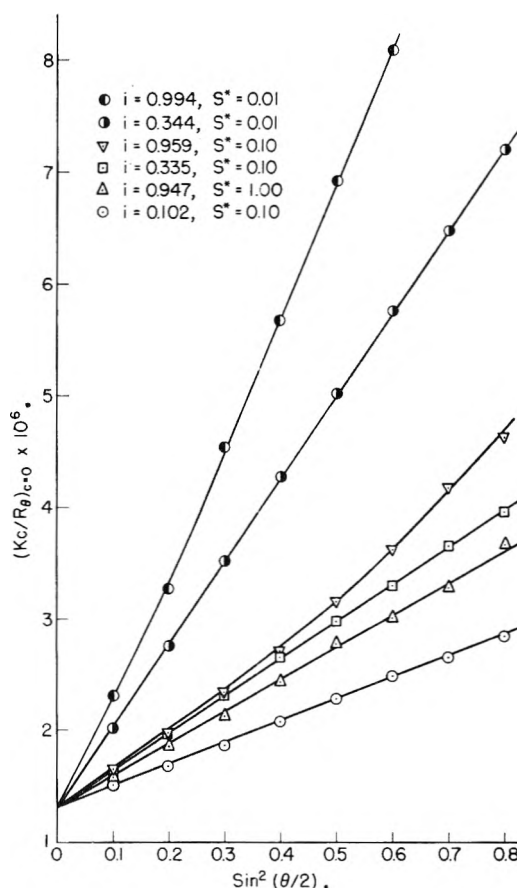


Fig. 1.—Plots of $(Kc/R_0)_{c=0}$ vs. $\sin^2(\theta/2)$ poly-(acrylic acid) in NaCl solutions.

in Table II. Included here also are the data on the polystyrene-*p*-sulfonic acid (K salt) fraction in 0.1 *M* KCl.

Comparison of Theory and Experiment

The application of eq. 7 and 10 to relevant experimental data is summarized in Table III. The quantity $X_{1(\text{theo})}$ in column 3 was calculated from eq. 7 using the known values of i , S^* and $(\bar{s}^2)_z$ (Table II). The term $1/2 - \chi_1$ was assumed much smaller than $V_1 i^2 / 4V_u^2 S^*$ and was consequently ignored in these calculations. The electrolyte contribution to the secondary interaction term X_2 is identically zero for the two systems investigated and the higher X terms can be shown to be negligible. The theoretical values of the second virial coefficients given in column 4 were calculated from eq. 11 for $X_1 < 35$ and from eq. 12 for $X_1 \geq 35$. The errors involved in the approximations to $I_2(X_1, 0)$ of eq. 10 were in all cases less than a few per cent.

The quantity $X_{1(\text{obs})}$ in column 5 was computed from the experimental values of A_2 and $(\bar{s}^2)_z^{1/2}$ by the reverse of the procedure used for calculating the quantities in preceding columns. Since the values of $I_2(X_1, 0)$ calculated in this manner were small (< 1), eq. 11 was employed in all cases.

In column 6 are given values of the parameter p defined

$$p = [X_{1(\text{obs})}/X_{1(\text{theo})}]^{1/2} = i_{(\text{obs})}/i_{(\text{theo})}$$

TABLE III
COMPARISON OF THEORY WITH EXPERIMENT

1	2	3	4	5	6	7	8
i	S^*	\bar{X}_1 (Theo)	$A_2 \times 10^4$ (Theo)	$\bar{X}_1(\text{obs})$	From A_2 data	From $[\eta]$ data	$A_2 M^2 / (\bar{s}^2)^{3/2} \times 10^{-24}$
Poly-(acrylic acid) in NaCl soln.							
0.102	0.10	6.67	23.3	0.95	0.38	0.44	2.05
.335	.10	32.6	102	1.84	.24	.30	3.47
.344	.01	105	488	1.73	.13	.30	3.31
.947	1.00	32.4	82	0.89	.17	.15	1.94
.959	0.10	240	208	4.23	.13	.15	6.1
.994	.01	580	1124	4.24	.09	...	6.2
Polystyrene- <i>p</i> -sulfonic acid (K salt) in KCl solution							
1	0.10	52	70	0.54	0.10	0.06	1.24
Sodium carboxymethylcellulose in NaCl soln. (data of Hermans, Pals and Trap)							
0.434	0.0464	1.108	118	0.381	0.59	0.45	0.91
	.0116	2.83	376	0.485	.41	.50	1.14
	.0029	6.94	1058	0.762	.33	.46	1.70
	.000725	14.85	2850	1.67	.34	.60	3.23

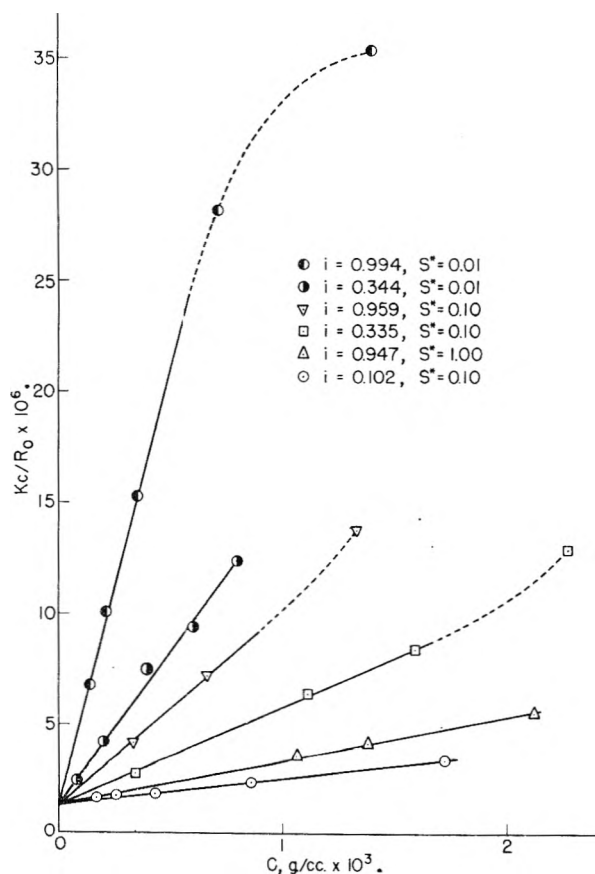


Fig. 2.—Plots of Kc/R_0 vs. c poly-(acrylic acid) in NaCl solutions.

For comparison, corresponding values of p for the same systems, as derived from intrinsic viscosity studies in accordance with the theory of intramolecular interactions³ for polyelectrolytes, are given in column 7.

In column 8 are listed values of the quantity $A_2 M^2 / (\bar{s}^2)^{3/2}$ as computed from the experimental virial coefficients and molecular dimensions (Table II).

In the last portion of Table III the theoretical

relationships of this section are applied to the system sodium carboxymethylcellulose-NaCl-water. The data are those of Trap and Hermans²³ and Pals and Hermans,²⁴ obtained from measurements using the isoionic dilution method. The values listed in columns 3-8 have been calculated as described above except for the p parameters in column 7. In arriving at the values listed there the experimentally observed intramolecular expansion factor α was assumed to be satisfactorily approximated by the ratio $[\eta]/[\eta]_\infty$, where $[\eta]_\infty$ is the intrinsic viscosity of the polymer extrapolated to infinite ionic strength. The values of $\alpha^5 - \alpha^3$ computed from this ratio were then compared with the theoretical values of $\alpha^5 - \alpha^3$ as given by the intramolecular theory. The factors p by which the degrees of ionization appearing in that theory must be multiplied in order to bring the values of α into agreement with experiment are those listed in column 7.

For polymer molecules consisting of spherically symmetric distributions of segments about their centers of gravity, the intrinsic viscosity may be related to the cube of the root-mean-square end-to-end distance in accordance with the equation $[\eta] = \Phi(r^2)^{3/2}/M$, where Φ is approximately 2.2×10^{21} . This simple relation has received ample verification^{11,25} in non-ionic polymer systems. Values of Φ for the polyelectrolytes studied here are given in Table IV. The $[\eta]$ values used in the calculations for the poly-(acrylic acid) systems are for the most part from previously published⁸ viscosity data on a fraction of approximately the same molecular weight. Those for the systems $i = 0.102$, $S^* = 0.10$ and $i = 0.994$, $S^* = 0.01$ and that for the sulfonic acid polymer were determined in the course of the present investigation. It has been assumed in these calculations that the experimentally derived (\bar{s}^2) values may be converted to the cor-

(23) H. J. L. Trap and J. J. Hermans, *THIS JOURNAL*, **58**, 757 (1954).

(24) D. T. F. Pals and J. J. Hermans, *Rec. trav. chim.*, **71**, 458 (1952).

(25) W. R. Krigbaum and D. K. Carpenter, *THIS JOURNAL*, **69**, 1166 (1955), have questioned the constancy of Φ for polymer-solvent systems exhibiting second virial coefficients very near zero.

responding (\bar{r}^2) values by the relation $(\bar{r}^2) = 6(s^2)$ (strictly applicable only to randomly coiled chain molecules).

TABLE IV
CALCULATION OF Φ VALUES FROM VISCOSITY DATA

i	S^*	$\Phi \times 10^{-21}$
Poly-(acrylic acid) in NaCl soln.		
0.102	0.10	0.65
.335	.10	.88
.344	.01	.90
.959	.10	1.09
.994	.01	0.79
		Av. 0.86
Polystyrene- <i>p</i> -sulfonic acid (K salt)		
1	0.1	0.90

Discussion and Conclusions

In attempting to assess the results of the application of the preceding relationships to experimental data, as summarized in Table III, we note first the discrepancies between the values of the theoretical X_1 in column 3 and the observed X_1 in column 5. This quantity represents the primary intermolecular interaction term, as calculated from theory and from experimental A_2 values, respectively. A similar discrepancy between theory and experiment has been observed in the application of the intramolecular theory to viscosity data.⁸ The parameter p in columns 6 and 7 is a measure of the disparity between theory and experiment, assuming that this disparity arises from ignorance of the (average) effective degree of ionization encountered within the subvolumes of the polymer domain. The values of p listed in column 6 appear to exhibit several characteristics. We note that this parameter is generally much less than unity, particularly when the theoretical degrees of neutralization are large or the ionic strength is low.²⁶ The observation that the effective degrees of ionization are less than the corresponding values obtained from titration of the polyacids is not unexpected. The charged sites on the polyelectrolyte chain must restrict the mobility of the gegenions thus depressing their activities from those which would prevail in the absence of interaction. Equivalently, this restriction of mobility gives rise to a lower effective degree of ionization of the chain. Rigorous treatment of the problem would demand introduction of activity coefficients for all the mobile ion species involved. These coefficients were taken as unity throughout the theoretical treatment given here.

We note next that the values of the parameter p , as calculated from the inter- (column 6) and intramolecular (column 7) theories, are in most cases not appreciably different, although those calculated from the former theory tend to be somewhat smaller. For the poly-(acrylic acid) systems, the values deduced from the intramolecular theory were found to be practically independent of ionic strength,

(26) Values of p for poly-(acrylic acid) considerably less than unity can also be deduced from the conductance studies of F. T. Wall, *et al.*, *J. Polymer Sci.*, **20**, 477 (1956), and the osmotic pressure data of W. Kern, *Macromol. Chem.*, **2**, 279 (1943).

and the entries for this polymer in column 7 represent the average values for each given degree of neutralization. The values derived from the intermolecular theory for these systems, however, exhibit a dependence on ionic strength at fixed degree of neutralization. It is perhaps noteworthy that if the intermolecular p values had instead been calculated in each case by substituting $[\eta]M/6^{3/2}\Phi$ for $(\bar{s}^2)^{1/2}$, with $\Phi = 2.2 \times 10^{21}$ as usually found for non-ionic polymers, then columns 6 and 7 would be in even better agreement. In particular, the dependence of the intermolecular p on S^* at fixed i would virtually disappear. The above-mentioned value of Φ , however, is not in accord with the (average) value obtained here from light scattering and viscosity measurements. In any event, it will suffice to observe that the intermolecular p values are relatively insensitive to the molecular dimensions, for all but the largest i^2/S^* values, and therefore that either method for determining them (from experimental $(\bar{s}^2)^{1/2}$ values or from intrinsic viscosities) yields reasonably satisfactory agreement between the inter- and intramolecular polyelectrolyte theories.

We should emphasize that use of eq. 15 for the second virial coefficient, in which the \bar{X} interaction quantities are replaced by their (approximate) equivalents in terms of the intramolecular expansion factor, does not require a knowledge of the value of p . It is merely necessary to assume that a single value of p characterizes the polyion size and interaction for a given system. Thus, if α can be independently determined (*e.g.*, from intrinsic viscosity measurements at the θ -point⁸), then the corresponding value of A_2 can be calculated from eq. 15.²⁷ Equivalently, α can be computed from the experimentally observed second virial coefficient.

Strauss and Wineman²⁷ point out that the value of p which must be arbitrarily assigned to a given polymer-solvent system in order to reconcile theory and experiment is not unique, but depends upon the kind of experimental measurement used to evaluate it. We do not agree, however, with their conclusion that the significance of p is therefore ambiguous. The assignment of a value ip as the "effective charge" of the polyelectrolyte coil does not commit one to acceptance of an idealized model in which, for any specified system, all of the thermodynamic properties of this system may be rigorously described in terms of a single value of the charge per molecule. In general, p takes into account deviations from ideality of a more complex nature, and while serving as a useful and convenient parameter of the system, should be expected to be reproducible only when evaluated under comparable conditions. It has been found,²⁸ for example, that values of p in good agreement with those deduced here from dilute solution theory can be derived from osmotic pressure data on the same systems at relatively high polymer concen-

(27) U. P. Strauss and P. L. Wineman, *J. Am. Chem. Soc.*, **80**, 2366 (1958), have recently employed this method in an analysis of dilute solution data on aqueous polyphosphate-salt solutions, using an alternate form of our eq. 15.

(28) T. A. Orofino, to be published.

tration, if these solutions are treated theoretically in a manner completely analogous to the methods presently described for the infinitely dilute polyelectrolyte coil.

The significance of the quantity $A_2M^2/(\bar{s}^2)^{3/2}$ given in the last column of Table III has been discussed previously in connection with the intermolecular theory for non-ionic polymers.¹¹ It was shown there that $A_2M^2/(\bar{s}^2)^{3/2}$, or the proportional quantity, $A_2M/[\eta]$, represents an experimental measure of the extent of interpenetration of molecular domains. (The former quantity has been chosen for consideration here as its use avoids the necessity of assigning a particular value to Φ in the relationship $[\eta] = \Phi 6^{3/2}(\bar{S}^2)^{3/2}/M$.) It was also observed that for high molecular weight non-ionic polymers in organic media, a value of $A_2M/[\eta]$ of ca. 150 was characteristic of a good solvent and, indeed, seemed to represent an upper limit for this quantity. The corresponding value of $A_2M^2/(\bar{s}^2)^{3/2}$ is ca. 5×10^{24} . It is of interest to note that the magnitudes of $A_2M^2/(\bar{s}^2)^{3/2}$ observed for the polyelectrolyte systems investigated here do not appreciably exceed this limit, in spite of the enormous A_2 values exhibited in some cases. Since the excluded volume of the polyelectrolyte molecule is related to the second virial coefficient by the equation $u = 2A_2M^2/N$, the attainment of the upper limit on the quantity $A_2M^2/(\bar{s}^2)^{3/2}$ is equivalent to asserting that under

these conditions $u \cong 8(4\pi/3)[(\bar{s}^2)^{1/2}/1.3]^3$, or, that the molecules behave like impenetrable spheres of radii roughly equal to $(\bar{s}^2)^{1/2}$.

Turning next to the data in Table IV we observe that the values of Φ calculated for the polyelectrolyte systems studied are a factor of two or more lower than those usually found for uncharged polymers.¹¹ Similar results may be deduced from the data of Pals and Hermans and Trap and Hermans on Na carboxymethylcellulose. The values of Φ calculated for these systems (and also the calculations in Table III), however, are subject to some doubt inasmuch as the inherent stiffness of the carboxymethylcellulose chain and the low molecular weight of the fraction studied render less satisfactory the assumption of spherical symmetry. Although the values for the poly(acrylic acid) and polysulfonic acid polymers are low, those for the former do not display any consistent trend with solvent medium or degree of ionization.

Despite the discrepancy between theory and experiment shown by the polyelectrolyte systems investigated, it is felt that the development presented here affords a practical and realistic approach to the problem of binary interactions between polyelectrolyte molecules in dilute solution. The final evaluation of the theoretical methods presented, however, must await a detailed study of the activities of small ions within the domain of a polyelectrolyte coil.

THE SPARK IGNITION OF DUST CLOUDS

BY LLOYD E. LINE, JR., HAROLD A. RHODES AND THOMAS E. GILMER, JR.¹

Combustion Laboratory, Experiment Incorporated, Richmond, Va.

Received September 5, 1958

The spark ignition of lycopodium dust clouds suspended in oxygen-nitrogen mixtures has been studied under controlled conditions. Unlike homogeneous fuel-air mixtures, the spark ignition of lycopodium cannot be characterized solely by a minimum spark ignition energy as determined in the usual way for gases. This energy appears to be strongly dependent upon the electrical characteristics of the spark circuit that affect the discharge time. As the discharge time increases, the ease of ignition (measured by the minimum oxygen concentration or minimum stored condenser energy for ignition) goes through a maximum. A tentative explanation for the increase in ease of ignition is put forward in terms of the disturbance of the dust cloud by the spark discharge prior to ignition. Data comparing the ease of igniting confined and unconfined dust clouds also are presented and discussed.

Introduction

In general the ignition of a combustible gas mixture is characterized by a minimum thermal ignition energy, which is a function of the pressure and the fuel-oxidant ratio. The manner or rate in which this energy is introduced is not specified, except that the release of thermal energy should occur in a time that is short compared to the time required to establish a self-propagating flame kernel and in a volume that is small compared to such a kernel. Normally this energy is determined by means of a capacitance discharging in an extremely short time.²

The same criteria should apply also to a non-tur-

bulent heterogeneous system. The discharge time, however, may be much longer owing to the relatively slow chemical reactions between the phases in the ignition regime. In fact, if the discharge time is too short, the spark may disturb the heterogeneous mixture before a self-propagating flame kernel can be established.

It is the purpose of this paper to present data on the spark ignition of a non-turbulent dust cloud of a monodisperse organic material (lycopodium) suspended uniformly in various oxygen-nitrogen mixtures. The effects of modifying the spark characteristics on the minimum stored condenser energy and the minimum oxygen concentration for ignition have been measured under controlled conditions and interpreted qualitatively in terms of the spark discharge rate.

(1) Virginia Polytechnic Institute, Blacksburg, Va.

(2) H. F. Calcote, C. A. Gregory, C. M. Barnett and R. B. Gilmer, *Ind. Eng. Chem.*, **44**, 2656 (1952).

Experimental Procedure

An outstanding feature of the apparatus employed in this work is that it provides a wall-free non-turbulent dust cloud.³ The dust cloud is a cylindrical column of particles passing downward through a chamber 8 inches in diameter fitted with windows for observation. In most experiments the diameter of the moving column was 1 inch; in a few experiments it was 2 inches. The average flow velocity (volume flow rate divided by cross-sectional area of column) was approximately 30 cm./sec. for the 1-inch column and 15 cm./sec. for the 2-inch column. The dust column may be studied in the wall-free condition or may be surrounded by an open end glass tube 1 inch or 2 inches in diameter depending upon the column size (wall-confined). The wall-free column is stabilized by a dust-free envelope of pre-mixed oxidizer gas. To eliminate particle size as a variable, lycopodium (the spore of the club moss, particle diameter *ca.* 30 μ) has been employed as the fuel. An elemental analysis of lycopodium gave the following results, expressed as per cent. by weight: C, 68.02; H, 9.60; N, 1.32; S, 0.08; and ash at 650°, 1.1.

To ignite the dust cloud, a condenser of fixed value charged to a known voltage is discharged directly (or through a resistance or inductance) across a 6 mm. gap formed by very small tungsten wires (in most cases 0.005 to 0.02 inch in diameter). The 6 mm. gap was observed in previous experiments⁴ to be the optimum distance for a particular set of conditions. The energy E on the condenser was calculated from $CV^2/2$, where C is the capacitance in farads and V is the voltage in practical volts. The circuit resistance external to the spark gap was approximately 0.2 ohm. An estimated 5% of the energy was left on the condenser after discharge.

Since the energy lost in the external circuit is unknown, the quantity $CV^2/2$ should not be regarded as the energy that went into the gap. It should, moreover, be pointed out that the spark energy that enters the gap may not be (and most likely is not) entirely utilized for ignition. Prior to ignition the spark kernel may lose energy by (a) heating the electrodes, (b) doing work of expansion and (c) radiating to the surroundings. Although the external circuit losses and factor (a) have been minimized, the term "minimum condenser energy" rather than "minimum ignition energy" is used. Factors (b) and (c) may be appreciable in these experiments. It is not the intent of this paper to furnish "absolute" minimum ignition energies for dust clouds.

Experiments were carried out at 1 atmosphere and 25° to determine the minimum condenser energy for ignition (at a fixed oxygen concentration and dust concentration) and to determine the minimum oxygen concentration in an oxygen-nitrogen mixture for ignition (employing a fixed condenser energy and fixed dust concentration). The criterion for ignition was a flame propagation of at least 4 inches from the spark gap. The rate and manner of introduction of the spark energy were altered by employing an inductance or various resistances. The inductance was a 1/8-inch copper tube helix, 3 inches in diameter, 12 inches long and consisted of 36 turns. It had a measured d.c. resistance of less than 0.3 ohm and an inductance, calculated from the dimensions of the coil, of 27 microhenries. The resistances were of the carbon type, ranging from 25 ohms to 10 megohms. Because of the violence of the combustion when oxygen concentrations beyond 35 mole % are used, few results were obtained for higher oxygen concentrations.

Results

Curve Characteristics.—Previous investigators in this field⁵⁻⁷ report fixed values of the minimum ignition energy or minimum oxygen concentration for ignition. Our experience with various dusts including boron, carbon and magnesium as well as lycopodium has been that these quantities are

(3) L. E. Line, Jr., and H. A. Rhodes, unpublished work.

(4) L. E. Line, Jr., W. J. Clark and J. C. Rahman, "Sixth Symposium (International) on Combustion," Reinhold Publ. Corp., New York, N. Y., 1957, p. 779.

(5) I. Hartmann, J. Nagy and H. R. Brown, U. S. Bur. Mines Rept. Invest. No. 3722, 1943.

(6) I. Hartmann, *Ind. Eng. Chem.*, **4C**, 752 (1948).

(7) I. Hartmann, *Sci. Monthly*, **79**, 37 (1954).

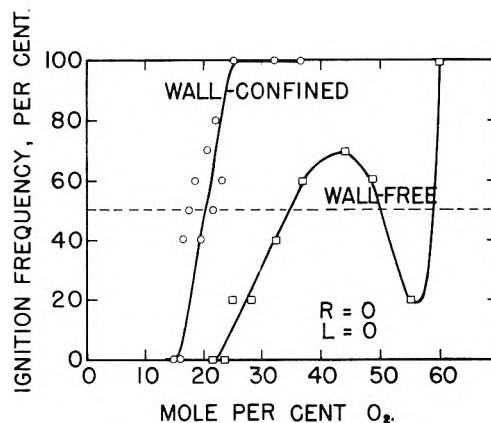


Fig. 1.—Wall effect on minimum O₂ concentration for ignition of lycopodium; no inductance; $E = 0.46$ joule; $C = 0.0023$ microfarad; dust concentration, 180 mg./l.; one inch dust column; 6 mm. spark gap.

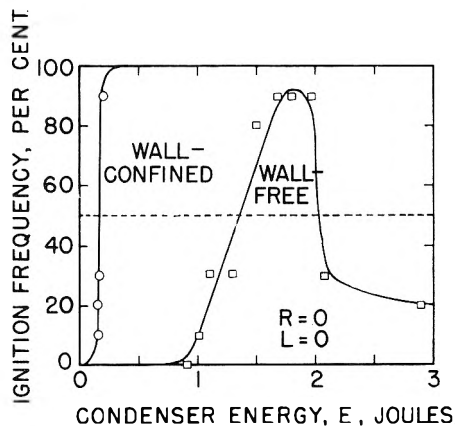


Fig. 2.—Wall effect on minimum E for ignition of lycopodium; no inductance; O₂ concentration, 23 mole %; C (wall-confined) = 0.0023 microfarad; C (wall-free) = 0.025 microfarad; dust concentration, 180 mg./l.; one inch dust column; 6-mm. spark gap.

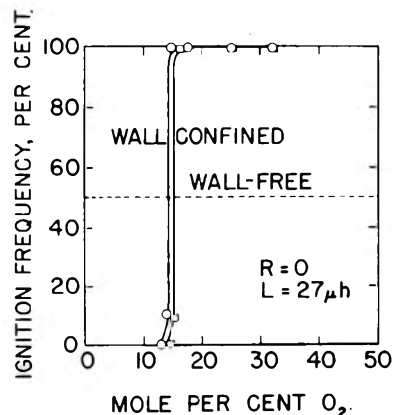


Fig. 3.—Wall effect on minimum O₂ concentration for ignition of lycopodium with inductance; $E = 0.46$ joule; $C = 0.0023$ microfarad; dust concentration, 180 mg./l.; one inch dust column; 6 mm. spark gap.

more accurately represented in terms of a range above which every trial gives ignition and below which no trial gives ignition. Within the range, ignition has only a certain probability.

Our results are reported by means of ignition frequency curves, which give the percentage of trials igniting (usually based on 10) along the ordinate

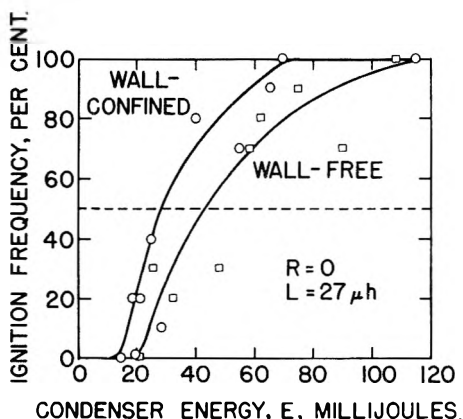


Fig. 4.—Wall effect on minimum E for ignition of lycopodium with inductance; O_2 concentration, 23 mole %; $C = 0.0008$ to 0.025 microfarad; dust concentration, 180 mg./l.; one inch dust column; 6 mm. spark gap.

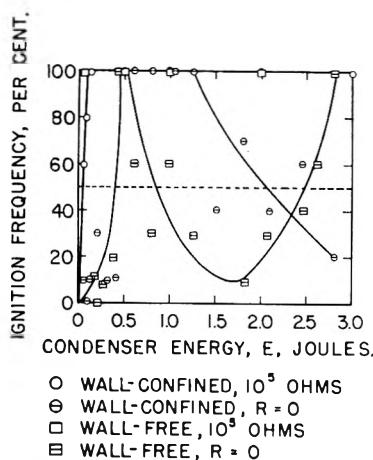


Fig. 5.—Ignition of 2 inch dust columns of lycopodium with and without resistance: O_2 concentration, 23 mole %; $C = 0.0008$ and 0.0015 microfarad for $R = 10^5$ ohms; $C = 0.0023$ and 0.025 microfarad for $R = 0$; dust concentration, 180 mg./l.; 6 mm. spark gap.

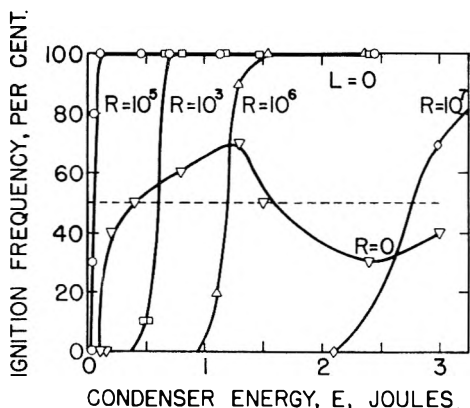


Fig. 6.—Effect of various resistances on minimum E for ignition of wall-free lycopodium dust column: O_2 concentration, 23 mole %; $C = 0.0008$ to 0.025 microfarad; dust concentration, 80 mg./l.; one inch dust column; 6 mm. spark gap.

and the stored condenser energy or oxygen concentration along the abscissa. Examples are given in Figs. 1 through 7 and in Fig. 9.

With capacitance (*i.e.*, very fast) sparks, particularly when the dust column is wall-free, the igni-

tion frequency curve is likely to be erratic or to rise more or less sharply to a maximum and drop to a low ignition frequency (Figs. 1, 2, 5, 6 and 9). For wall-confined columns, the curves are generally steeper at the beginning than for the wall-free ones, but on occasion may later decrease in ignition frequency.

With sparks moderated by added inductance L or added resistance R , the curves are of quite reasonable shape, and in general the differences between wall-free and wall-confined columns practically disappear (*cf.* Figs. 3, 4, 5, 6 and 7). It may be instructive to observe in Figs. 6, 7 and 8 that as the optimum resistance ($R = 10^5$ ohms) is approached, the slope of the ignition-frequency curve increases. Conversely, as the resistance corresponding to the first maximum ($R =$ approximately 10^2 ohms, Fig. 8) is approached, the slope of the ignition-frequency curve decreases. To some extent this tendency is suggested also by Figs. 9 and 10.

Wall Effect and Size of Dust Column.—We consider now the effect of experimental conditions on the ease of ignition. As a measure of this we take the minimum condenser energy or oxygen concentration at which 50% of the trials ignite (dashed lines), ignoring the portion of the curve beyond a maximum.

For one inch dust clouds, the environmental effect of a confining wall is striking (as much as a ninefold reduction in condenser energy and a 1.7-fold reduction in oxygen concentration) when an unmoderated spark is discharged across the gap, but slight when the optimum inductance⁴ or resistance is employed (*cf.* Figs. 1, 2, 3, 4, 6 and 7).

For 2 inch dust clouds, the results were somewhat different. As with 1 inch dust clouds the curves are of reasonable shape when a resistor of 10^5 ohms was employed, the ignition frequency rising sharply to 100% and remaining unchanged up to rather high energies. Also the minimum condenser energy was the same for the confined and unconfined condition. However, unlike the 1 inch dust cloud, the 2 inch dust cloud required about the same ignition energy (with $R = 0$) for the wall-free column as for the wall-confined one.

Spark Moderation.—Table I, obtained from the results of Figs. 1 through 4, shows that a 27-microhenry inductance reduces the condenser energy or the oxygen concentration for ignition. The reduction in required energy for the wall-free case was about thirty-fold; for the wall-confined case it was about sixfold. Corresponding reductions in required oxygen concentration were two- and 1.3-fold, respectively.

The effect of series resistances up to 10^7 ohms is summarized in Figs. 8 and 10 (from data in Figs. 6, 7 and 9). In Fig. 8 a resistance of 10^5 ohms appears to give the lowest required condenser energy, the reduction being approximately tenfold for both wall-free and wall-confined systems. A similar resistance (10^5 to 10^6 ohms) is optimum in reducing the required oxygen concentration. The reduction here is over twofold. In Fig. 10, for $E = 0.1$ joule, no ignitions were obtained in 35% oxygen for $R = 10^2, 10^3$ and 10^7 ohms; for $E = 1$ joule there were no ignitions for $R = 10^7$ ohms.

TABLE I
IGNITION OF LYCOPodium IN O₂-N₂ MIXTURES

Confinement	Added inductance, <i>L</i> , μhenries	Mole % O ₂ for 50% ignitions ^a	Condenser energy for 50% ignitions, joules ^b
Wall-free	0	34.0	1.35
Wall-free	27	14.5	0.043
Wall-confined	0	20.0	.175
Wall-confined	27	15.5	.028

^a Condenser energy, 0.46 joule. ^b 23 mole % O₂.

The initial increase in required condenser energy (branch A, Fig. 8) followed by passage through a minimum (branches B and C, Fig. 8) is a curious result which has been reported previously by Boyle and Llewellyn for magnesium and aluminum.⁸ Passage through a minimum oxygen concentration (Fig. 10) was not reported by them. In the case of the curve for *E* = 0.1 joule an initial maximum similar to that of Fig. 8 is suggested by the fact that for an oxygen concentration of 35% (the highest used) and *R* = 0, the ignition frequency was 30%; but for *R* = 10² and *R* = 10³ ohms, no ignitions were obtained, signifying that higher oxygen concentrations than for *R* = 0 would have been required.

Discussion

It is clear from the foregoing presentation that the study of one unknown (ignition of dust clouds) has been complicated by the presence of another unknown (the actual energy in a spark discharge that is available for initiating combustion). In general this latter factor needs intensive study before a proper interpretation of the spark ignition of dust clouds, or indeed of any system with high-energy sparks, can be made. Some interesting qualitative observations on the present results are nevertheless possible. They may be applicable to dust clouds of other materials.

The effect of oxygen concentration on the minimum condenser energy for ignition has been indicated in previous papers.^{4,6} A change in conditions which decreases the required gap energy for ignition or which increases the fraction of total energy utilized for ignition should result in a decrease in the oxygen concentration required for ignition.

Assuming no change in gap resistance, the insertion of a low-resistance inductance into the spark circuit (consisting only of condenser, switch, leads and spark gap) should lengthen the discharge time without materially decreasing the energy to the gap. It would appear, therefore, that a longer discharge time somehow makes ignition easier.

The addition of resistance also decreases the discharge time, but there is at the same time a decrease in the energy delivered to the gap. It is, therefore, remarkable to observe (branches B of Figs. 8 and 10) a decrease in condenser energy or oxygen concentration as the resistance was increased. In these regions the importance of the gap energy must be secondary.

Both branches A and B of Fig. 8 can be correlated with discharge time. For an *RLC* circuit (where *R* is time-independent), it can be shown that for *R*² << 4*L*/*C* the current executes damped oscillation

(8) A. R. Boyle and F. J. Llewellyn, *J. Soc. Chem. Ind. London*, **69**, 173 (1950).

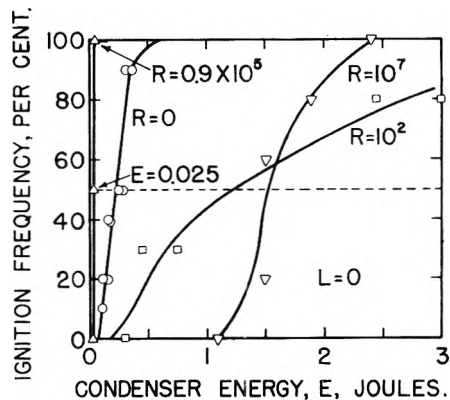


Fig. 7.—Effect of various resistances on minimum *E* for ignition of wall-confined lycopodium dust column: O₂ concentration, 23 mole %; *C* = 0.0008 to 0.025 microfarad; dust concentration, 80 mg./l.; one inch dust column; 6 mm. spark gap.

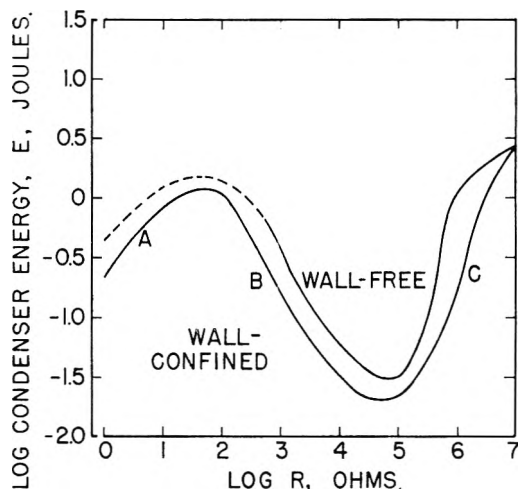


Fig. 8.—Variation of minimum *E* with resistance for ignition of lycopodium: O₂ concentration, 23 mole %; *C* = 0.0008 to 0.025 microfarad; dust concentration, 80 mg./l.; one inch dust column; 6 mm. spark gap.

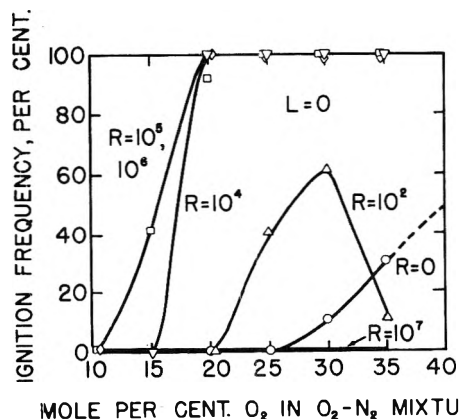


Fig. 9.—Effect of various resistances on the minimum O₂ concentration for ignition of wall-free lycopodium dust column: *E* = 1 joule; *C* = 0.025 microfarad; dust concentration, 80 mg./l.; one inch dust column; 6 mm. gap.

with a time constant for the envelope equal to 2*L*/*R*, and that for *R*² >> 4*L*/*C* the current rapidly reaches a maximum value and then decays exponentially with a time constant equal to *RC*. When one holds *L* and *C* constant (Figs. 8 and 10)

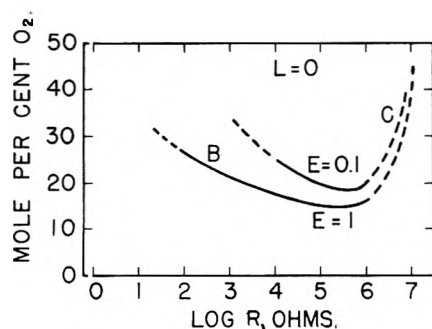


Fig. 10.—Variation of minimum O_2 concentration with resistance for ignition of lycopodium: $E = 0.1$ and 1 joule; $C = 0.0015$ and 0.025 microfarad, respectively; dust concentration, 80 mg./l.; one inch dust column; 6 mm. spark gap.

and varies R , the time constant goes through a maximum, and the value of R that will most rapidly dissipate the energy stored on the condenser is $R^2 = 4L/C$. Assuming that $L = 1$ microhenry and $C = 0.02$ microfarad, we calculated this resistance to be 14 ohms. In the assumed circuit, going to larger or smaller resistances will increase the discharge time. It is interesting that the initial peak in Fig. 8 comes at about this resistance above and below which the required condenser energy for ignition is also diminished.

Turning finally to branches C of Figs. 8 and 10, there are two possibilities for explaining these rises, both of which may be operating. One is that there is obviously some discharge time over which the spread of a very small amount of energy will not cause ignition; the other is that there should be some point at which further increase in R causes the energy losses in the external circuit to outweigh the advantage of a slow spark discharge.

Whether the effects of a resistance or inductance are due to the gap energy appearing in a more useful form (*e.g.*, short duration sparks are known to have a high efficiency for the production of visible light) or to some optimum time for the process of ignition, we cannot say for sure until further investigation can be carried out. However, we venture to suggest a tentative explanation for the differences in ignition behavior between short duration and long duration sparks. High speed motion pictures of the events following the discharge (no ignition, $R = 0$) of a condenser with 1.5 joules stored energy into a lycopodium-oxygen-nitrogen mixture show first a brilliant spark zone approximately 0.1 cc. in volume. Within 2 milliseconds the dust particles were pushed back to the extent that a nearly dust-free zone (estimated volume, 4 cc.) was created. This is due presumably to the rapid expansion of the hot spark kernel to ambient pressure (~ 1 atmosphere). Pictures show further that with a 10^5 -ohm resistor or a 27-microhenry inductance the dust column is practically undisturbed. Finally, the photographic evidence indicates that with a 10^6 -ohm resistor very little flame propagation through lycopodium occurs in the first few milliseconds after discharge.³ We suggest that ignition with fast sparks is more difficult than with slow ones for two

reasons. First, the violent expansion consumes thermal energy by doing work against the surrounding atmosphere before significant chemical reaction gets under way. Thus it is estimated that about 0.4 joule of work would be done in the expansion of 0.1 to 4 cc. against 1 atmosphere. Perhaps more important, however, is the fact that the demand for ignition energy is greatly increased by virtue of the enlarged surface area, and this demand may not be met easily by the expanded kernel. In terms of the minimum enthalpy concept,⁹ a much larger excess enthalpy would be required for flame propagation in the wave front of enlarged radius than would have been required for a wave front where little or no expansion has occurred. The minimum oxygen concentration for ignition will be reduced with increase in discharge time because of the decreasing demand for gap energy.

The above considerations account for the passing of the ignition-frequency curve through a maximum as E is increased and the absence of such behavior when the spark is suitably moderated (Figs. 2, 5 and 6).

Why with fast sparks the ignition frequency should decrease (Fig. 1) on replacement of nitrogen by oxygen (transport and thermal characteristics approximately the same) has not been explained. It is not the result of a second ignition limit, since the peak is absent when the spark is moderated (*cf.* Figs. 1 and 3; Fig. 9).

It is of further interest to speculate on the wall effect. When an unmoderated spark is passed through the wall-confined 1 inch dust column, the violent expansion of the kernel induces turbulence in the tube instead of free expansion as in the wall-free case. This turbulence should greatly increase the burning velocity,¹⁰ thereby making ignition easier than in the corresponding wall-free case. This argument has strong support in the fact that when the slower sparks are employed, it matters little whether a wall surrounds the column or not. The results with the 2 inch wall-confined column are also in accordance with the above picture. In passing from a 1 inch confined column to a 2 inch confined column, one would think that less turbulence would be induced; *i.e.*, it would become more nearly like the wall-free case. A greater ignition energy under otherwise similar conditions would therefore be required for the 2 inch confined than the 1 inch confined column, and the results (*cf.* Fig. 2 with Fig. 5) are in accordance with this prediction.

Acknowledgment.—The authors wish to thank James C. Rahman, formerly of Experiment Incorporated, for carrying out some of the experiments. This research was supported by the United States Air Force through the Air Force Office of Scientific Research of the Air Research and Development Command under Contract No. AF 18(600)-1508.

(9) G. Von Elbe, "Fourth Symposium (International) on Combustion," The Williams and Wilkins Co., Baltimore, Md., 1953, p. 13.

(10) H. M. Cassel, A. K. Das Gupta and S. Guruswamy, "Third Symposium on Combustion and Flame and Explosion Phenomena," The Williams and Wilkins Co., Baltimore, Md., 1949, p. 185.

THE VAPOR PRESSURES OF BiI_3 OVER LIQUID Bi-BiI_3 SOLUTIONS¹

BY DANIEL CUBICCIOTTI AND F. J. KENESHEA, JR.

Stanford Research Institute, Menlo Park, California

Received September 12, 1958

The vapor pressures of BiI_3 over the liquid and its mixtures with Bi were determined from 410 to 470° and over the composition range 0 to 50 mole % Bi. The vapor pressure of BiI_3 could be expressed by the equation $\log p(\text{mm.}) = -4310/T + 8.170$. The activity of the BiI_3 followed Raoult's law up to about 30 mole % added Bi and showed positive deviations for larger Bi concentrations.

Introduction

As a continuation of our study of the thermodynamics of bismuth-bismuth halide solutions² we have determined the effect of Bi additions on the vapor pressure of BiI_3 . The Bi-BiI_3 system is similar to its bromide and chloride counterparts. Phase diagram studies have shown that Bi will dissolve appreciably in liquid BiI_3 before a second phase separates.³ There is some evidence for the formation of solid BiI which melts incongruently—similar to BiBr and BiCl . The iodide system differs from the chloride and bromide in the relatively high melting point of BiI_3 .

Experimental

Method.—The vapor pressures were determined by the transpiration method described in detail earlier.² The diffusion errors and flow rate effects were essentially the same as those reported for the other systems studied.

Materials.— BiI_3 was prepared by dissolving reagent grade Bi_2O_3 in aqueous HI , evaporating to dryness and melting in a stream of dry N_2 . It was then doubly distilled in a stream of dry N_2 and finally collected in the transpiration cell.

BiI_3 has a tendency to lose I_2 ^{3b} when heated even in an inert atmosphere. Therefore, the product collected from a distillation contained I_2 in excess of stoichiometric BiI_3 . Analyses of two samples prepared in that way showed 35.20 and 35.33% Bi (35.44 theoretical). The BiI_3 thus contained a small excess of I_2 when put into the cell. During the transpiration experiments the sample evolved I_2 , so it may even have had a Bi excess (over stoichiometric BiI_3) before any Bi was added. Therefore the exact composition of the starting material was not known precisely. However, from an estimate of the amounts of material present and I_2 evolved, the excess impurity (either Bi or I_2) was certainly less than one mole per cent. during the time that the vapor pressure of "pure" BiI_3 was measured.

The melting points determined by cooling curve techniques on four samples of BiI_3 ranged from 405.9 to 406.6°. Literature values have been reported to be: 412°,^{3a} 408°,^{3b} 405°.^{3c}

The Bi and N_2 were the same as used before. Because small proportions of O_2 in the N_2 would be capable of oxidizing the iodide to I_2 , the N_2 was passed over hot Cu and then Fe filings before being exposed to the sample.

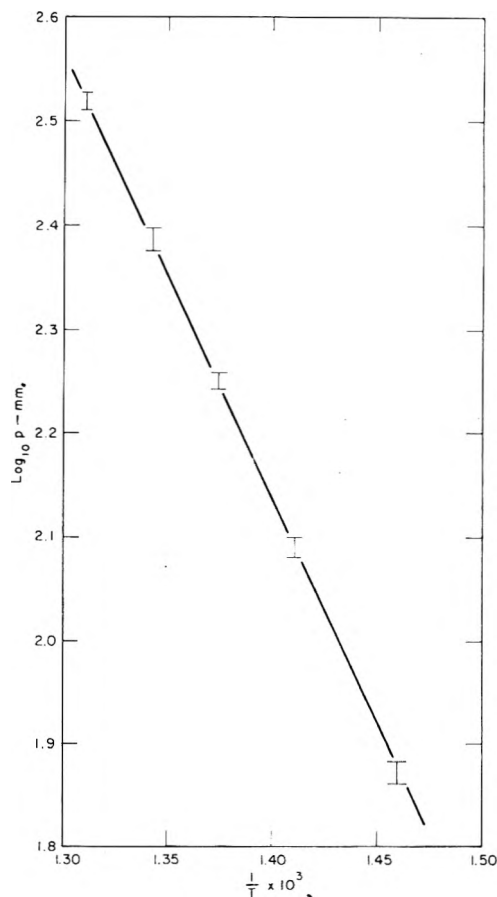
Analysis of Transported Vapor.—Since iodine was produced when the BiI_3 was heated, the proportion of "free" iodine in the collected material was determined in an attempt to establish the partial pressure of I_2 over the melt. The sample collected was dissolved in a solution of HCl and KI . The solution was titrated with 0.005 *N* thiosulfate to a starch end-point. Since iodine is produced easily by any air present, this entire procedure was performed under an N_2 atmosphere. Even so, some of the scatter of the iodine determinations probably was due to air oxidation.

To investigate the possibility of some gaseous species of lower valence, several samples of condensate were collected

from a melt with a gross composition of 70 mole % Bi. (At this composition the melt was probably a two-liquid phase system.) Analyses of those samples for Bi agreed within about one per cent. of theoretical for BiI_3 , so the fraction of any low valence bismuth iodide in the vapor was negligible for the present purposes.

Results

In each series of determinations the vapor pressure of BiI_3 was measured from 410 to 490°; then additions of Bi were made and the pressure measured at 410, 435 and 470°. Two series of determinations were made. In one, the first Bi additions were quite small; whereas in the other the Bi additions were all relatively large.

Fig. 1.—The vapor pressure of BiI_3 .

BiI_3 .—The results obtained on BiI_3 are summarized in Fig. 1. The I 's in the figure include the results obtained on three different samples. The data at each temperature extended over a range of about 6% in pressure. The curve drawn through the data was a straight line that could be represented by the equation

(1) This work was made possible by the financial support of the Research Division of the United States Atomic Energy Commission.

(2) For previous papers see: THIS JOURNAL, **62**, 463, 843 (1958).

(3) (a) L. Marino and R. Becarelli, *Atti Accad. Lincei*, **21** (5), 695 (1912); (b) H. S. van Klooster, *Z. anorg. Chem.*, **80**, 104 (1913); (c) G. G. Urazov and M. A. Sokolova, *Akad. Nauk SSSR., Inst. Obshch. Neorg. Khim., Sektor Fiz.-Khim. Anal., Izvest.*, **25**, 117 (1954).

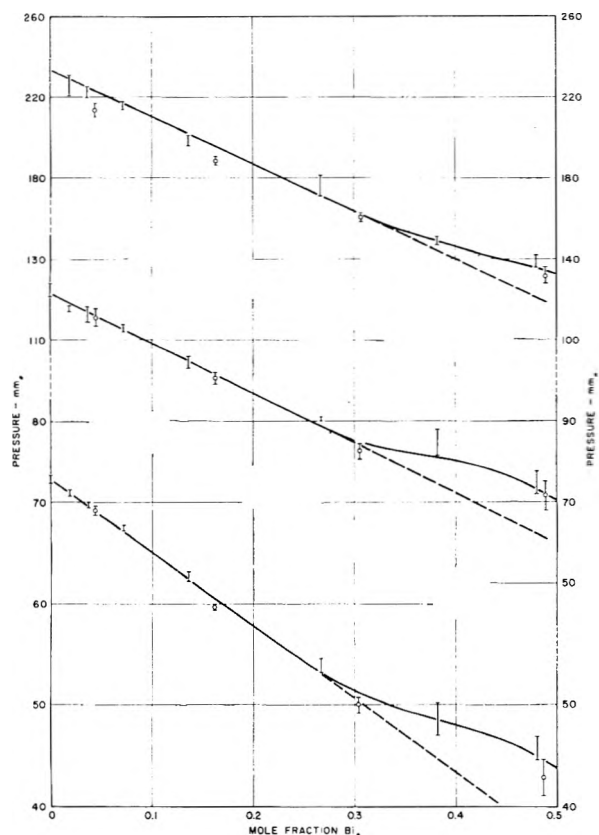


Fig. 2.—The pressure of BiI_3 as a function of added Bi at 410, 435 and 470°. The dashed lines represent Raoult's law.

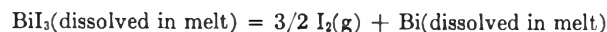
$$\log p(\text{mm.}) = -4310/T + 8.170$$

From the slope of the line, a heat of vaporization of 19.8 ± 0.5 kcal./mole was derived. The only literature value for a vapor pressure is a comment by van Klooster^{3b} that BiI_3 boiled at about 500°. The normal boiling point derived by linear extrapolation of our data is 542°.

Mixtures of Bi with BiI_3 .—The effect of Bi additions on the vapor pressure of BiI_3 is summarized in Fig. 2. Each I represents three to five determinations; and the different types of I's distinguish the different series of determinations. The curves were drawn as smoothly as possible through all three sets of points.

Iodine Pressures.—The iodine pressures observed were small compared with those of the BiI_3 and the values were somewhat erratic. The results obtained for Bi additions of from 0 to 6% in one series of determinations are shown in Fig. 3. For Bi additions greater than about 10% the iodine evolved was too small to measure.

The equilibrium governing the I_2 pressure can probably be represented by the equation



The standard free energy change for that reaction is known,⁴ and therefore the activity of the dissolved Bi can be calculated.

Such calculations indicate that the activity of the Bi in the melts was greater than its mole fraction. The values calculated are in some doubt because the exact concentration of Bi was indefinite. (As

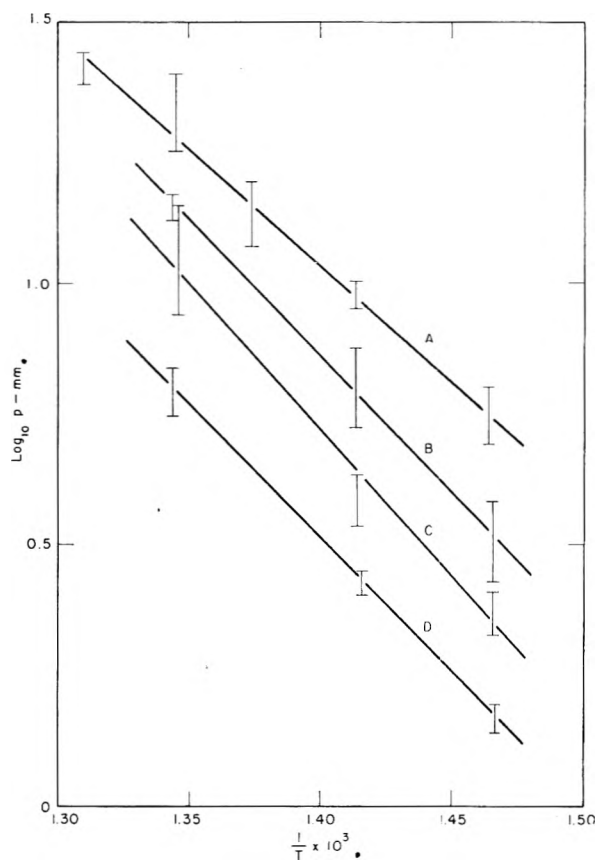


Fig. 3.—The pressure of iodine over Bi- BiI_3 mixtures: curve A, no added Bi; B, 1.7 mole % Bi; C, 3.2 mole % Bi; D, 6.3 mole % Bi.

stated above, the BiI_3 was non-stoichiometric.) The Henry's law constants determined for the Bi were of the order of five or ten. Thus, even allowing for rather large experimental errors, the constants were greater than unity.

Discussion

Perhaps the most interesting feature of this system is the long range over which the BiI_3 obeys Raoult's law. Thus, at each of the temperatures studied, over the composition range from 0 to 30 mole % added Bi, the BiI_3 followed Raoult's law (assuming Bi and BiI_3 as components). This behavior is notable in view of the very short range of compositions in which Raoult's law obtained in the bromide and chloride systems.

Beyond about 30 mole % Bi, the vapor pressure of the BiI_3 exhibited positive deviations which were almost as large as those observed in the chloride and bromide systems. The partial molal enthalpy of solution of BiI_3 was calculated from the change of its activity with temperature.² The enthalpy was zero up to 30 mole % Bi, and then rose, reaching a value of about one kcal. at about 45 mole % Bi. Up to the highest Bi concentration (50 mole %) there was no evidence for a decrease in the enthalpy as observed in the chloride and bromide systems.

(4) L. Brewer, *et al.*, "Chemistry and Metallurgy of Miscellaneous Materials," N.N.E.S. IV-19B, McGraw-Hill Book Co., Inc., New York, N.Y., 1950, p. 115.

It may be that such a decrease would occur at Bi compositions greater than those studied.

The Henry's law constants obtained above for Bi were greater than unity. That is, they indicate positive deviations from Raoult's law for the Bi in dilute solution. Thus, in this system both

components tend to show positive deviations from Raoult's law.

Acknowledgments.—The authors are indebted to Mr. William E. Robbins, who performed the experimental work, and to Dr. C. M. Kelley for fruitful discussions.

THE HEAT CAPACITY OF THE SYSTEM CARBON TETRACHLORIDE-PERFLUOROMETHYLCYCLOHEXANE THROUGH THE CRITICAL REGION

BY HARTLAND SCHMIDT, GEORGE JURA AND JOEL H. HILDEBRAND

Contribution from the Departments of Chemistry, University of California, Berkeley and Riverside, California

Received September 24, 1958

The heat content of a mixture of carbon tetrachloride and perfluoromethylcyclohexane having the critical composition has been determined through a range of temperature spanning the critical by means of an ice calorimeter. This allows time for the system to come to equilibrium at the initial temperature. Close to the critical point, several days were required. Tangents to the curve for $H_t - H_0$ vs. t give the heat capacity of the system. The heat capacity of the mixture continues to fall through some 7° above the critical point before reaching the approximate constancy of a completely homogeneous mixture. This confirms earlier, exploratory results.

The senior author,¹ in 1952 discussed the fluctuations in density occurring in two-component liquid systems just above the temperature where the meniscus disappears and suggested: (a) that the meniscus would reappear in a centrifugal field, and (b) that the volume and entropy of the system would reflect the rapid change occurring in the structure of the liquid. The former suggestion (a) was verified by Hildebrand, Alder, Beams and Dixon,² who found that in a centrifugal field with an acceleration of 10^8 cm. sec.⁻¹ the meniscus temperature of the system perfluoroheptane-2,2,4-trimethylpentane was raised 10° of which 1.9° was attributable to sedimentation of the denser component, the remainder to hydrostatic pressure. The second expectation (b) was verified by Jura, Fraga, Maki and Hildebrand,³ who found that a liquid-liquid system of the critical composition has, for many degrees above the two-phase region, a volume-temperature curve that is convex upward and a heat capacity considerably in excess of its value at still higher temperature.

Because this last investigation was exploratory only, the present one was undertaken in order to have more precise figures for this important thermodynamic quantity. We found that equilibria in the immediate supra-critical region is attained very slowly, and that stirring could affect the structure of the liquid so that it was necessary to discard the usual calorimetric method of measuring the rise in temperature following the addition of electrical energy in favor of ice calorimetry, which permitted holding the system for as long as necessary at the initial, higher temperature, with no stirring during equilibration. The differences between the heat content of the system at a series of upper temperatures and its heat content at 0° were measured. These differences were plotted

against the initial temperatures and the slope of the curve at any point gave the heat capacity. The fluorocarbon thus purified gives a critical temperature of 26.2° with carbon tetrachloride.² Higher values that have been reported for this system may have been due to traces of carbon disulfide in the carbon tetrachloride or of air in the fluorocarbon, either of which would raise the observed critical temperature.

Experimental

Crude perfluoromethylcyclohexane supplied by Du Pont Organic Chemicals and Minnesota Mining Fluorochemicals Departments was passed through a 2 meter silica column of 1 cm. i.d. This material was then refluxed for 6 hours with saturated KMnO_4 solution, washed several times with H_2SO_4 , water and 10% NaOH , and dried over "Drierite." The liquid was distilled on a packed helix column operating at about 30 theoretical plates efficiency. The boiling point range of the middle cut used was 76.38–76.45° (760 mm.)⁴ The resulting sample gave greater than 77% transmission throughout the range 208 to 290 millimicrons through 1 cm. of the C_7F_{14} . The density of the material was 1.7891 ± 0.0002 g./cc. at 25°.

The CCl_4 used was Eastman "Spectro-grade." This was dried over CaSO_4 and distilled on a Podbielniak "Hyper-Cal" column under conditions giving more than 100 theoretical plates. The boiling range of the fraction used was 0.07° and the boiling point assumed (76.75° at 760 mm.)⁴ was used to calibrate the thermocouple. The density of the CCl_4 was 1.5858 ± 0.0002 g./cc. at 25° (lit.⁵ 1.5843–1.5858), and n_D 1.4580 \pm 0.0003 (lit. 1.4576).

The Bunsen isothermal ice calorimeter was similar in design to one described and calibrated by Ginnings and Currucini.⁵ Use of an isothermal method to measure the heat content difference $H_T - H_{276.16}$ made it possible to determine the heat capacity over arbitrarily long equilibration periods. The "static" heat capacity could thus be determined without the difficulties due to heat leak, thermal equilibration and mechanical heating during stirring which have plagued previous attempts to measure heat capacities in this region by conventional adiabatic methods. The calorimeter was calibrated electrically from time to time as described by the Bureau of Standards workers⁵ and their calibration factor of 270.33 abs. joules per g. of Hg displaced was roughly (0.06% av. dev.) verified. Closer calibration

(1) J. H. Hildebrand, *J. Coll. Sci.*, **7**, 551 (1952).

(2) J. H. Hildebrand, B. J. Alder, J. W. Beams and H. M. Dixon, *THIS JOURNAL*, **58**, 577 (1954).

(3) G. Jura, D. Fraga, G. Maki and J. H. Hildebrand, *Proc. Nat. Acad. Sci.*, **39**, 19 (1953).

(4) J. Timmermans, "Physico-Chemical Constants of Pure Organic Compounds," Elsevier Publishing Co., Inc., New York, N. Y., 1950.

(5) D. D. Ginnings and R. J. Currucini, *J. Research Natl. Bur. Standards*, **38**, 583 (1947).

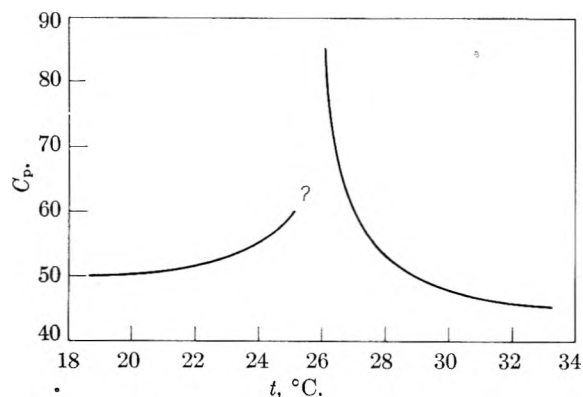


Fig. 1.

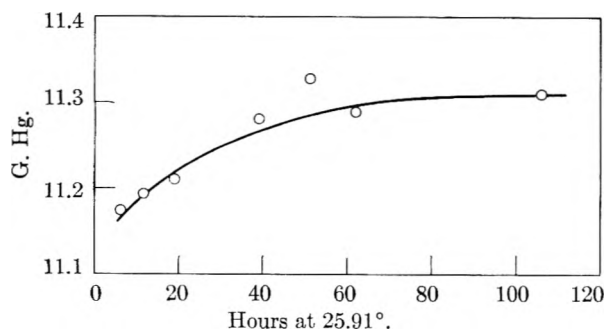


Fig. 2.

was not attempted in this series of measurements since the reproducibility of the experimental runs gave sufficient indication of the precision of the method, and greater absolute accuracy was unnecessary. A controlled flow of 0.14 cc./sec. of air dried by flow through saturated KOH solution and CaSO_4 , and chilled to the ice-point in the ice-bath surrounding the calorimeter, served to sweep moist air out of the central sample chamber and prevent dri't due to water condensation during runs. The ice mantle surrounding the sample well was formed and shaped by suspending a small copper bucket of solid CO_2 at various heights in the sample chamber, using care to see that the ice mantle extended all the way to the top of the ice-water chamber.

Great care was taken to exclude dissolved air in preparing the sample. A carefully cleaned copper sample bulb of about 60-cc. capacity, tapered to slide easily down the calorimeter well, was equipped with a metal-to-glass seal entrance tube connected to a degassing chamber. The sample bulb contained three fine mesh copper screen disks soldered horizontally for thermal conduction. The assembly was isolated under vacuum and found to leak less than 10^{-2} mm. in 24 hours. The purified components of the solution were then weighed into the degassing bulb; the assembly was linked to a vacuum line with a short piece of Tygon tubing; the solution was frozen with solid CO_2 , and the bulb was evacuated briefly. The solution was isolated, melted, refrozen and degassed several times before it was distilled over into the sample bulb. After the sample bulb was sealed off, the assembly was again weighed to see if there was an appreciable loss in weight due to the evacuation of the frozen sample. The loss indicated was 0.1% of the sample weight, and, since the two components have practically identical vapor pressures, it was assumed that the composition was not changed appreciably by this procedure. The total amount of air in the sample, including residual dissolved air and air from leakage during the six months of the measurements, should not have been more than that represented by a partial air pressure of a few mm. over the solution.

The sample was suspended by a Nylon string in a copper pipe surrounded by a 12 kg. copper block for heat ballast. This pipe was mounted to extend through a well-insulated water thermostat of about 100-liters capacity. The temperature fluctuations were recorded continuously on a 1 mv. full scale Brown recorder connected to a quick responding thermistor bridge in the water-bath. The mean tempera-

ture of the bath remained constant to 0.003° over periods of several days, and the total amplitude of the fluctuation over the thermostating cycle of about 2 minutes was of the order of 0.01° . The absolute temperature of the bath was determined on a Brooklyn Thermometer Co. certified mercury thermometer graduated to 0.01° in conjunction with two other thermometers which were used to get an average relative temperature over the interval studied. Thus, the over-all accuracy of the temperature of the sample itself was about $\pm 0.01^\circ$ while the relative temperature scale of the runs was accurate to about 0.005° . It was found by trial that the heat content became constant after six hours of thermostating at temperatures far from the observed heat capacity discontinuity, but that equilibration times were very much longer close to that temperature. The sample was always heated to about 50° and mixed thoroughly before it was suspended in the thermostat, since it was found that equilibration of the unstirred sample was attained more rapidly if the sample temperature was approached from above.

To initiate the measurement the sample was allowed to fall free into the calorimeter to within a fraction of an inch of the bottom of the sample well by release of a loop in the Nylon string. The string was then completely released to allow the sample to rest on the bottom of the well. Calculations indicated that heat losses of the sample during the fall were negligible and that possible variations in the mode of dissipation of the gravitational energy would have no detectable heat effect. Corrections for drift and changes of Hg height in the reading capillary, were less than 1% and usually less than 0.3% of the total heat effect. The heat capacity of the bulb was estimated to be 6.5 cal. deg. $^{-1}$. It contained 0.427 mole of mixture in which the mole fractions were: CCl_4 , 0.7216; C_2F_6 , 0.2784.

Results

The results expressed as calories per mole between t and 0° are shown in Table I. Each value represents the mean of at least two runs with an average deviation from the respective means of less than 0.05%. A total of 43 runs were completed of which 5 were rejected on the basis of large deviations from the mean of the other runs at that temperature. It should be noted that the temperature and heat content values given have the indicated precision only relative to other values in the set since only a crude estimate of the heat capacity of the sample bulb, assumed constant over this range of temperature, was used to obtain the net molar heat content of the sample. Figure 1 gives values of the heat capacity in calories per mole per degree obtained from a large scale plot of the data. The points in the neighborhood of 26° are somewhat uncertain on account of extreme slowness in attaining equilibrium. Figure 2 plots ΔH vs. time for repeated runs at $t = 25.90 \pm 0.01^\circ$, showing that several days seemed to be necessary for reaching a not very exactly reproducible equilibrium. This effect, observed only in this narrow region, makes it impossible to fix the shape of the peak of the λ -type curve of Fig. 1.

TABLE I

t , °C.	$H_t - H_0$, cal. mole $^{-1}$	t , °C.	$H_t - H_0$, cal. mole $^{-1}$	t , °C.	$H_t - H_0$, cal. mole $^{-1}$
19.385	970	26.014	1316	29.785	1533
24.734	1250	26.107	1322	30.869	1583
25.163	1275	26.323	1342	31.05	1593
25.439	1293	26.940	1379		
25.857	1307	28.165	1448	33.87	1730

Discussion

* The λ -shape of the C_p curve is similar to that found in the earlier study. Its most significant

feature, as in the other case, is the fact that some 7 degrees beyond the critical temperature is necessary for C_p to descend to the approximately constant value of a homogeneous liquid. Below the critical point, the system would gain entropy with rising temperature more rapidly than if the components were separate, because of the increasing disorder attending mutual penetration. Above that point, the randomness is still far from complete, as shown also by its milky appearance. The right-hand branch eventually sinks lower than the left as the randomness becomes maximum. The curve shows clearly the temperature range beyond which randomness can be regarded as virtually complete.

In studying the heat capacity of a system such as this, one would expect, even away from the critical composition, a cusp rather than a first order transition in the C_p vs. T curve when the phase boundary is crossed. The cusp rather than the typical line of a first-order transition would be observed simply because only an infinitesimal amount of one of the phases is present at the transition. We would expect the cusp to become a typical λ -curve at the critical concentration if the true C_p of the two phases below the critical temperature were known. In the data presented, the C_p 's in the two phase region represent only the gross

heat capacity of the entire contents of the calorimeter. The necessary heats of solution and dilution have not been measured. Consequently, the shape of the curve below the critical deviates from that expected from a typical λ -curve, while above this temperature the C_p curve behaves as expected.

Our data suggest that the gross C_p has a maximum just below the critical: however, the data are too meager to establish this point. We believe that if we had available all of the thermodynamic data necessary to obtain the true heat capacity, this maximum would disappear and we would obtain a typical λ -curve.

Two non-polar liquid components that are sufficiently different in internal forces as to be able to form two liquid phases dissolve in one another with expansion and absorption of heat. As the temperature rises, the rate of mutual solubility increases, making an increasing contribution to the heat capacity of the system. This accounts for the low temperature branch of the C_p curve. This was to be expected. Our interest, however, has been primarily in the upper branch, above the meniscus temperature.

Acknowledgment.—We express our appreciation to the Atomic Energy Commission and to the Research Corporation for support of this work.

NOTES

EFFECT OF MICELLAR BEHAVIOR ON ADSORPTION CHARACTERISTICS OF TWO SURFACTANTS

By W. E. BELL¹

Union Research Center, Union Oil Company of California, Brea, California

Received June 19, 1958

In the process of determining degrees of adsorption of various surfactants on mineral surfaces, it appeared that micellar behavior affected the adsorption characteristics of the surfactants. This can be illustrated by comparing the adsorption characteristics of Igepal CA-630 (an alkyl aryl polyether alcohol) and Pluronics L-44 (a condensate of ethylene oxide with propylene glycol and oxide) on silica surfaces (45-60 mesh sand) from aqueous solution. Both surfactants were commercial 100% active products containing molecular sizes following a theoretical distribution.

Figure 1 compares adsorption isotherms for the two surfactants. The Igepal solutions were analyzed by ultraviolet spectrophotometric methods and the Pluronics solutions by surface tension methods. Similar results were obtained by Hsiao and Dunning² for Igepal. The amount of Igepal

adsorbed on the sand surface reaches a maximum at a concentration of about 300 p.p.m. and remains constant as the concentration increases. On the other hand, the amount of Pluronics adsorbed continues to increase as the concentration increases. Based on the sand surface area and the amounts of

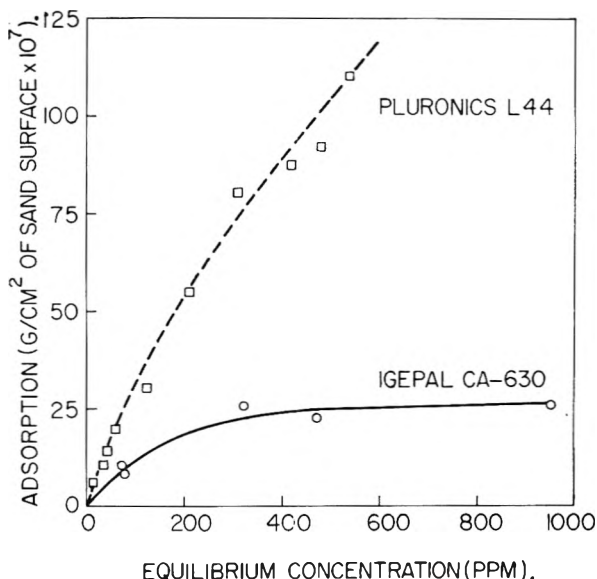


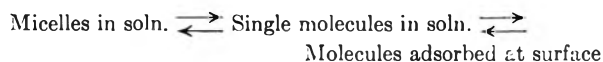
Fig. 1.—Adsorption of Pluronics L44 and Igepal CA-630 from aqueous solution by sand.

(1) John Jay Hopkins Laboratory for Pure and Applied Science, General Atomic Division of General Dynamics Corporation, San Diego, California.

(2) L. Hsiao and H. N. Dunning, *THIS JOURNAL*, **59**, 362 (1955).

each surfactant adsorbed, both Igepal and Pluronics show multilayer adsorption.

It is believed that the difference in adsorption behavior can be explained by the equilibrium suggested by Hartley³



At concentrations above the critical micelle concentration, micelles compete with surface adsorption for the surfactant molecules. In the case of Igepal, formation of micelles prevents a built-up of the concentration of single molecules in solution; therefore, the degree of adsorption changes little. In the case of Pluronics, however, there is little micelle formation to compete with the adsorption process and therefore the degree of adsorption continues to increase with concentration. As evidence for this theory, Mankowich⁴ found that the Igepal type of surfactant showed a critical micelle concentration of about 100 p.p.m. and that at concentrations appreciably above this, approximately 110 molecules aggregated together to form a micelle. The Pluronics type showed no critical micelle concentration and little, if any, indication of molecules aggregating to form micelles.

Figure 2 shows surface tension depression versus concentration curves for Igepal and Pluronics in

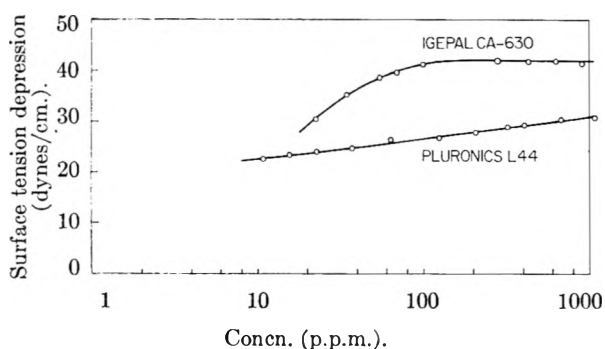


Fig. 2.—Comparison of surface tension depressions of aqueous solutions of Pluronics L44 and Igepal CA-630.

aqueous solution. Surface tensions were measured by the du Nouy method. The increase in surface tension depression with concentration is indicative of the amount of surfactant adsorbed at the water-air interface. The Igepal curve reaches a maximum at about 220 p.p.m., whereas the Pluronics curve continues to rise with increasing concentration. These curves are similar in shape to the adsorption isotherms for the two surfactants, which agrees with the postulation involving an equilibrium of micelles, single molecules, and adsorbed molecules. Above the critical micelle concentration for Igepal, the water-air interface, as did the water-sand interface, must compete with micelles for the surfactant molecules.

(3) G. S. Hartley, *Trans. Faraday Soc.*, **37**, 130 (1941).

(4) A. M. Mankowich, *This Journal*, **58**, 1027 (1954).

THE REACTION OF RECIPROCAL SALT PAIRS DURING CRYSTALLIZATION FROM THE GASEOUS PHASE¹

By HAROLD F. MASON AND FARRINGTON DANIELS

Contribution from the Chemistry Department, University of Wisconsin, Madison, Wisconsin

Received June 26, 1958

Four reciprocal salt pairs of the alkali and silver halides reacted in the gas phase at temperatures around 1000° and the gaseous products were quenched to the solid state. It was hoped to be able to study the rate of reaction between several different gaseous alkali halides. In all cases, however, the products were almost exclusively the stable salt pairs. The extent of reaction observed was far in excess of the partial conversion predicted on the basis of thermodynamics for the gas-phase reactions. It is concluded that the stable salt pair was formed during the crystallization process and that any reaction in the gas phase is obscured.

Reactant salts were vaporized into separate streams of oxygen-free dry nitrogen. The two streams of pure gaseous salts were mixed and reacted for 0.3 to 13 seconds in a tubular flow system in an electrically heated furnace. The mixture of product gases then was quenched rapidly to the solid state on a water-cooled metal surface. Product crystals showed the fine-grained habit typical of sublimates. From this fact and from visual observation of the condensation process, it is believed that crystallization took place directly from the gaseous state. After each run, the quench surface was withdrawn and the product analyzed by X-ray diffraction.

Tables I-III summarize the phases which were identified in the product mixture from the reaction of three reciprocal pairs of alkali halides. Lattice constants are given for each product phase, together with values for the pure phases.^{2,3} The number of lines present in the diffraction pattern is also given for each phase.

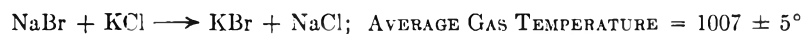
In all cases, diffraction patterns were almost exclusively those of the stable salt pairs formed by complete reaction of the reciprocal salts, plus excess reactant. The data are particularly convincing for the NaBr-KCl system (Table I). This system forms the most sensitive test of complete reaction, since the product-reactant pair KCl-KBr forms a continuous solid solution.² Thus, degree of conversion may be measured by the unit cell dimension *a* of the K(Cl,Br) phase. This is very close to the value for the pure product KBr. The results for NaI-KBr and NaI-KCl are consistent with nearly complete reaction. In these cases product and reactant species do not form continuous solid solutions, so that the extent of reaction must be estimated from the relative strengths of product and reactant patterns. Except for a single weak and questionable line observed in each of two runs, no patterns were observed for that reactant which was not originally present in stoichiometric excess. We conclude that essentially complete reaction occurred in all cases.

(1) Complete details of this research may be found in the Ph.D. thesis of Harold F. Mason, filed in the Library of the University of Wisconsin in 1954.

(2) H. F. Mason, Ph.D. thesis, Univ. of Wisconsin, 1954.

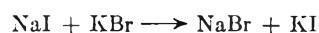
(3) Natl. Bureau of Standards Circular 539, "Standard X-Ray Diffraction Powder Patterns," Vol. I-III, U. S. Gov. Printing Office (1953-1954).

TABLE I



Experiment	Products, α , Å.	Phase	α , pure phase, Å.	No. of lines	Contact time, sec.	Excess reactant
1	6.597 \pm 0.005	KBr	6.590	6	13.0	NaBr
	5.82 \pm .02	NaCl (+NaBr)	5.640	3		
2	6.585 \pm .003	KBr	6.590	8	8.04	NaBr
	5.716 \pm .006	NaCl (+NaBr)	5.640	2		
3	6.584 \pm .003	KBr	6.590	8	5.43	NaBr
	5.717 \pm .008	NaCl (+NaBr)	5.640	3		
4	6.595 \pm .006	KBr	6.590	7	3.30	NaBr
	5.747 \pm .001	NaCl (+NaBr)	5.640	2		
5	6.581 \pm .004	KBr	6.590	8	2.41	NaBr
	5.801 \pm .011	NaCl (+NaBr)	5.640	3		
6	6.593 \pm .006	KBr	6.590	7	2.00	NaBr
	5.850 \pm .013	NaCl (+NaBr)	5.640	4		
7	6.586 \pm .005	KBr	6.590	8	1.81	NaBr
	5.728 \pm .005	NaCl (+NaBr)	5.640	2		
8	6.582 \pm .004	KBr	6.590	8	0.65	NaBr
	5.721 \pm .001	NaCl (+NaBr)	5.640	2		

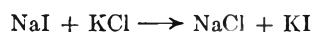
TABLE II

Average gas temperature = 957 \pm 3°

Ex-periment	Products, α , Å.	Phase	α , pure phase, Å.	No. of lines	Contact time, sec.	Molar % (NaI + KBr = 100%)
9	7.048 \pm 0.012	KI	7.063	7	2.29	45.5
	5.988 \pm .008	NaBr	5.977	3		
10	7.049 \pm .008	KI	7.063	7	0.92	49.7
	5.988 \pm .012	NaBr	5.977	2		
11	6.981 \pm .006	KI	7.063	4	.46	63.8
	6.639 \pm .012	KBr	6.590	4		
12	5.973 \pm .002	NaBr	5.977	3	.32	58.6
	(6.40)	NaI?	6.48	1?		
12	7.00 \pm .01	KI	7.063	3	.32	58.6
	6.658 \pm .010	KBr	6.590	3		
	5.989 \pm .009	NaBr	5.977	3		

TABLE III

COMPOSITION OF SALT MIXTURES CONDENSED FROM THE GAS PHASE



Average gas temperature = 1005°

Ex-periment	Products, α , Å.	Phase	α , pure phase, Å.	No. of lines	Contact time, sec.	Molar % (KCl + NaI = 100%)
13	7.061 \pm 0.001	KI	7.063	3	1.36	31.4
	5.648	NaCl	5.640	1		
14	7.068 \pm .008	KI	7.063	7	1.43	30.1
	5.655 \pm .004	NaCl	5.640	2		
	(6.23)	KCl?	6.297	1?		
	(6.46)	NaI?	6.48	1?		

In separate experiments the AgCl-KBr reaction was observed to go to completion. Although these results are handicapped by experimental difficulties, they confirm similar and more secure observations with the alkali halide pairs.

Equilibrium constants for the gas-phase reactions of the reciprocal salt pairs are summarized in Table IV. Equilibrium constants were calculated from thermodynamic data given by Brewer,⁴ Kelley,⁵⁻⁶ Latimer,⁷ and Bichowsky and Rossini.⁸

(4) L. Brewer, in L. L. Quill (ed), "The Chemistry and Metallurgy of Miscellaneous Materials: Thermodynamics," 1st ed., McGraw-Hill Book Co., New York, N. Y., 1950.

(5) K. K. Kelley, U. S. Bur. Mines Bull. 383, U. S. Gov. Printing Office, 1935.

Under the experimental conditions the free energies of formation of the reactant and product species from the elements range from 40 to 70 kcal. per mole. The free energy changes are well known and the uncertainty in the equilibrium constants is probably less than 5%.

TABLE IV

CALCULATED EQUILIBRIUM CONSTANTS, GAS PHASE DOUBLE DECOMPOSITIONS

System	1000°K.	1500°K.
NaBr + KCl \rightarrow NaCl + KBr	1.05	1.09
NaI + KBr \rightarrow NaBr + KI	1.65	1.00
NaI + KCl \rightarrow NaCl + KI	1.74	0.78
AgCl + KBr \rightarrow AgBr + KCl	53.0	7.94

^a Standard state gases at 1 atmosphere.

From the data in Table IV the equilibrium mixture of gaseous alkali halides should contain about equal amounts of reactant and product molecules (*i.e.*, about 50% forward reaction). In contrast, the quenched solid products were almost exclusively composed of the stable salt pair plus a small amount of that reactant originally present in stoichiometric excess. That is, 100% forward reaction occurred to the stable salt pair. The products are the same as those observed when the reacting salts were powdered and mixed and allowed to react for long periods of time at high temperatures.^{9,2,10} We conclude that the major chemical reaction occurred during crystallization from the gaseous state, and that the products formed by crystallization of gaseous reciprocal salt systems are identical with those obtained by complete reaction in the solid state at the crystallization temperature—namely, the stable reciprocal salt pairs.

(6) K. K. Kelley, U. S. Bur. Mines Bull. 434, U. S. Gov. Printing Office, 1941.

(7) W. M. Latimer, "The Oxidation States of the Elements and their Potentials in Aqueous Solution," Prentice-Hall Inc., New York, N. Y., 1938.

(8) F. R. Bichowsky and F. D. Rossini, "The Thermochemistry of the Chemical Substances," Reinhold Publ. Corp., New York, N. Y., 1936.

(9) H. F. Mason, THIS JOURNAL, **61**, 769, 796 (1957).

(10) L. J. Wood, *et al.*, *J. Am. Chem. Soc.*, **56**, 92 (1934); **57**, 822 (1935); **58**, 1341 (1936); **60**, 2320 (1938); **62**, 766 (1940); **66**, 1259 (1944); **74**, 727, 2355 (1952).

This conclusion should be of interest in inorganic synthesis and in geochemistry. One cannot always assume that the composition of a crystalline material condensed out from a gaseous mixture is a measure of the composition of the gas. Further, rapid reactions may take place during or after the condensation and crystallization.

Acknowledgment.—The authors are glad to acknowledge the assistance of Prof. Sturges Bailey of the Geology Department of the University of Wisconsin for help in the determination of X-ray patterns, to Prof. Marion Jackson of the Department of Soils for the use of X-ray apparatus, and to Prof. John Margrave of the Department of Chemistry, for advice on techniques in high temperature chemistry. The work was conducted in part under a fellowship from the Eastman Kodak Company and in part under a research contract with the Wright-Patterson Air Development Center.

THE PRESENCE OF THE SO_2^- RADICAL ION IN AQUEOUS SOLUTIONS OF SODIUM DITHIONITE

BY R. G. RINKER, T. P. GORDON, D. M. MASON¹ AND W. H. CORCORAN

Contribution from the Chemical Engineering Laboratory of the California Institute of Technology, Pasadena, California

Received June 18, 1958

Upon the basis of work by Dunitz,² van der Heijde,³ and Hodgson, *et al.*,⁴ it was reasonable to expect that dithionite anions ($\text{S}_2\text{O}_4^{2-}$) in aqueous solutions are in equilibrium with paramagnetic SO_2^- radical ions. Because SO_2^- appears to have a role⁵ in the air oxidation of sodium dithionite in a basic aqueous solution, an effort was made to determine its presence by use of electron paramagnetic resonance (e.p.r.).

Chemically pure sodium dithionite (Baker Chemical Company, batch No. 3712, lot JTB 6113) was further purified by three fractional crystallizations from oxygen-free aqueous solutions at 0°. The purified crystalline product then was used to make a saturated, oxygen-free alkaline solution at 0° which was 0.5 mole in sodium hydroxide to inhibit thermal decomposition of the dithionite at room temperature.

Pyrex sample tubes with outside diameters of 1 mm. and lengths of 76 mm were filled, respectively, with the saturated solution described above and also with solutions prepared by diluting the saturated solution tenfold and hundredfold. For purposes of comparison, tubes also were filled with a completely oxidized, concentrated solution of dithionite. Furthermore a set of tubes was prepared from a sodium thiosulfate solution which was saturated at room temperature and was acidified to provide a source of colloidal sulfur.

In the e.p.r. measurements, the stabilized, oxygen-free dithionite solutions showed paramagnetism, in which case sharp resonance was observed at 3.365 kilogauss with a fixed Klystron frequency of 9.453×10^9 sec.⁻¹. Neither the completely oxidized dithionite solution nor the acidified thiosulfate solution displayed paramagnetism. The width of the single resonance peak for each dithionite sample showing paramagnetism was about 2 gauss at half-peak height. A

value of 2.0051 was found for the spectroscopic splitting factor, g , which was based upon a comparison with the g -value of 2.0023 for the free electron for manganous ion in aqueous solution. The sharpness of the peak indicated that the lifetime of SO_2^- must be long compared to the free-electron relaxation time of 10^{-9} sec.

Observations on the dithionite solutions of various dilutions showed that the SO_2^- concentration varied as the square root of the dithionite concentration so that the equilibrium relationship may be written as

$$K_{\text{eq}} = \frac{(\text{SO}_2^-)^2}{(\text{S}_2\text{O}_4^{2-})}$$

The absolute concentration of SO_2^- was not determined. The limit of detection for the e.p.r. equipment with a 5-mm. cavity was estimated to be 10^{-9} mole, equivalent to a 2×10^{-6} molar solution.

Because the e.p.r. studies were conducted at only one frequency, it cannot be concluded that there is no orbital contribution to the paramagnetism. The g value, however, indicates that it probably is small. Also, even though there appeared to be slight line broadening as a function of dilution, the data were not sufficient to estimate the effects of exchange interactions on line width.

It is pertinent to this study to note that in agreement with Hodgson, *et al.*,⁴ dry $\text{Na}_2\text{S}_2\text{O}_4$ powder in e.p.r. measurements also was observed to exhibit paramagnetism. Purified $\text{Na}_2\text{S}_2\text{O}_4$ was dried at 100° *in vacuo* over P_2O_5 for several days before sampling. Ultraviolet irradiation of the dry powder for several hours did not increase the paramagnetism in an experiment carried out at room temperature.

In summary, SO_2^- appears to be present as a real species in dithionite solutions and, by taking it into account, the mechanism of the oxidation reaction may be more readily explained.

Professors H. M. McConnell and D. M. Yost and Mr. H. H. Dearman were most helpful in supplying time, facilities and thought in the e.p.r. measurements.

PROTON N.S.R. SPECTROSCOPY. III. ANNIHILATION OF NITROGEN QUADRUPOLE BROADENING BY MEANS OF STRONG MOLECULAR ELECTRIC FIELD GRADIENTS

BY G. V. D. TIERS AND F. A. BOVEY

Contribution No. 144 from the Central Research Department, Minnesota Mining and Manufacturing Company, St. Paul, Minnesota

Received July 13, 1958

The nuclear spin resonance (n.s.r.) absorption due to protons attached to N^{14} is expected to be a triplet because of interaction with the three spin states of N^{14} ($I = 1$). This has been observed for rigorously dried liquid ammonia,¹ for alkylamines in acid solution,^{2,3} and for dilute solutions (5% w./v. or less) of *n*-butylamine in trifluoroacetic acid solution⁴ and for pure liquid formamide, acetamide and *N*-methylacetamide at elevated temperatures.³ It has been demonstrated that this triplet is collapsed to a singlet^{1,3,4} when the experimental conditions are such that a fairly rapid exchange of N^{14} -H protons becomes possible. The singlet, or the components of the triplet, generally are broadened by quadrupole relaxation of the N^{14} nucleus unless the nitrogen is symmetrically substituted (as in ammonium ions) or unless proton exchange is very rapid.³⁻⁵ In symmetrically substituted

(1) Division of Chemical Engineering, Stanford University, Stanford, California.

(2) J. D. Dunitz, *Acta Cryst.*, **9**, 579 (1956).

(3) H. B. van der Heijde, *Rec. trav. chim. Pays-Bas*, **72**, 95 (1953).

(4) W. G. Hodgson, A. Neaves and C. A. Parker, *Nature*, **178**, 489 (1956).

(5) To be published.

(1) R. A. Ogg, *Disc. Faraday Soc.*, **17**, 215 (1954); *J. Chem. Phys.*, **22**, 560 (1954).

(2) E. Grunwald, A. Loewenstein and S. Meibom, *ibid.*, **27**, 630 (1957).

(3) J. D. Roberts, *J. Am. Chem. Soc.*, **78**, 4495 (1956).

(4) G. V. D. Tiers, unpublished experiments.

(5) H. S. Gutowsky and A. Saika, *J. Chem. Phys.*, **21**, 1688 (1953).

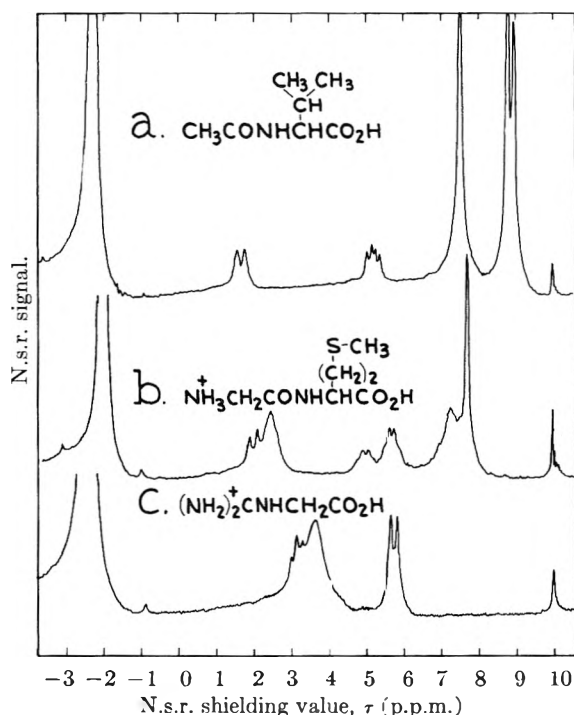


Fig. 1.—Proton n.s.r. spectra of trifluoroacetic acid solutions (20% wt./vol.) of: (a) N-acetyl-DL-valine; (b) glycyl-DL-methionine; (c) glycoeyamine.

N^{14} compounds, the electric field at the N^{14} nucleus is evidently so homogeneous that very little torque is exerted on the nucleus as the molecule rotates in solution.

It appears possible in principle^{5,6} that a very narrow singlet N^{14} -H proton n.s.r. peak should be observed *even without proton exchange* if the electric field at the N^{14} nucleus can be made very inhomogeneous by proper choice of structure. So far as we are aware, no n.s.r. spectral data have been reported for any compounds fulfilling this condition. As a part of a larger study, to be reported later, we have found that many N-substituted amides, some closely related to those reported to give a broad N-H resonance, show this dramatic narrowing, giving n.s.r. peaks in trifluoroacetic acid solution having the relatively small apparent half-height widths of 6-10 cycles-sec.⁻¹. Among these compounds are: N-acetyl-glycine, N-acetyl-DL-alanine, N-acetyl-DL-valine and N-acetyl-DL-leucine; in addition, many (but not all) of the glycol peptides of the common α -amino acids, e.g., glycyl-DL-methionine, glycyl-DL-serine, glycyl-DL-threonine, glycyl-DL-alanine and certain others. Guanidinoacetic acid (glycoeyamine) is an example of a compound which is not an amide but shows the effect clearly for the proton on the nitrogen bonded to the methylene group. Figure 1 shows the spectra (obtained with a Varian V-4300-2 40.00 Mc-sec.⁻¹ n.s.r. spectrometer, tetramethylsilane as internal reference standard,⁷ and a sweep of 220 mm. for 13 p.p.m.) of N-acetyl-DL-valine, glycyl-DL-methionine and glycoeyamine. The NH resonance at 1.72, 2.05 and 3.14 τ , respectively, is split by neighboring α -protons in the

expected manner; the α -proton peak at 5.24, 5.00 and 5.71 τ , respectively, shows an equal splitting by the N-H proton. This splitting varies from 5 to 8 cycles-sec.⁻¹ in the different compounds; it stands as proof that proton exchange is excluded as a cause of the observed narrowing.

These observations indicate that it may be possible by such means to gain useful information concerning the electric fields surrounding various types of substituent groups.

We thank George Filipovich for excellent maintenance and operation of the n.s.r. equipment.

CHRONOPOTENTIOMETRIC STUDY OF THE DISPROPORTIONATION OF URANIUM(V)

BY REYNOLD T. IWAMOTO

Department of Chemistry, University of Kansas, Lawrence, Kansas

Received July 28, 1958

Chronopotentiometry, voltammetry at constant current, has been utilized successfully by Gierst and Juliard¹⁻² and by Delahay and co-workers³⁻¹⁰ for the evaluation of physico-chemical processes preceding and accompanying electrochemical reactions. This paper describes an extension of this technique for the evaluation of disproportionation reaction rate constants.

The disproportionation of uranium(V) has been investigated polarographically by a number of workers.¹¹⁻¹⁸ Among them, Orlemann and Kern^{14,16} have obtained experimental and calculated values for the disproportionation rate constant. As with their theoretical approach, the reaction volume concept has been followed in this paper.

Experimental

Reagents.—Reagent grade chemicals were used throughout. The uranyl perchlorate solution $2.07 \times 10^{-3} M$ was prepared by converting a weighed sample of uranyl nitrate hexahydrate, through a double evaporation to dryness with perchloric acid, to the perchlorate and diluting to a known volume with 0.4 M perchloric acid. The pH of the solution was 0.83.

Apparatus.—Similar electrical equipment and cells have been described previously.¹⁹

- (1) L. Gierst and A. Juliard, Comité intern. thermodynam. et cinét. électrochim., Compt. rend., 2nd Réunion, Milan, 117, 279 (1951).
- (2) L. Gierst and A. Juliard, THIS JOURNAL, **57**, 701 (1953).
- (3) P. Delahay and T. Berzins, *J. Am. Chem. Soc.*, **75**, 2486 (1953).
- (4) T. Berzins and P. Delahay, *ibid.*, **75**, 4205 (1953).
- (5) P. Delahay and C. C. Mattax, *ibid.*, **76**, 874 (1954).
- (6) P. Delahay and C. C. Mattax, *ibid.*, **76**, 5314 (1954).
- (7) P. Delahay, C. C. Mattax and T. Berzins, *ibid.*, **76**, 5319 (1954).
- (8) P. Delahay and W. Vielstich, *ibid.*, **77**, 4955 (1955).
- (9) T. Berzins and P. Delahay, *ibid.*, **77**, 6448 (1955).
- (10) P. Delahay, *Disc. Faraday Soc.*, **17**, 205 (1954).
- (11) I. M. Kolthoff and W. E. Harris, *J. Am. Chem. Soc.*, **67**, 1484 (1945).
- (12) I. M. Kolthoff and W. E. Harris, *ibid.*, **68**, 1175 (1946).
- (13) H. G. Heal and J. Thomas, *Trans. Faraday Soc.*, **45**, 11 (1949).
- (14) D. M. H. Kern and E. F. Orlemann, *J. Am. Chem. Soc.*, **71**, 2102 (1949).
- (15) K. A. Kraus, F. Nelson and G. L. Johnson, *ibid.*, **71**, 2510 (1949).
- (16) E. F. Orlemann and D. M. H. Kern, *ibid.*, **75**, 3058 (1953).
- (17) J. Koryta and J. Koutecky, *Collection Czechoslov. Chem. Commun.*, **20**, 423 (1955).
- (18) H. Imai, *Bull. Chem. Soc. Japan*, **30**, 873 (1957).
- (19) C. N. Reilly, G. W. Everett and R. H. Johns, *Anal. Chem.*, **27**, 483 (1955).

(6) J. A. Pople, *Molecular Phys.*, **1**, 168 (1958).

(7) G. V. D. Tiers, *THIS JOURNAL*, **62**, 1151 (1958).

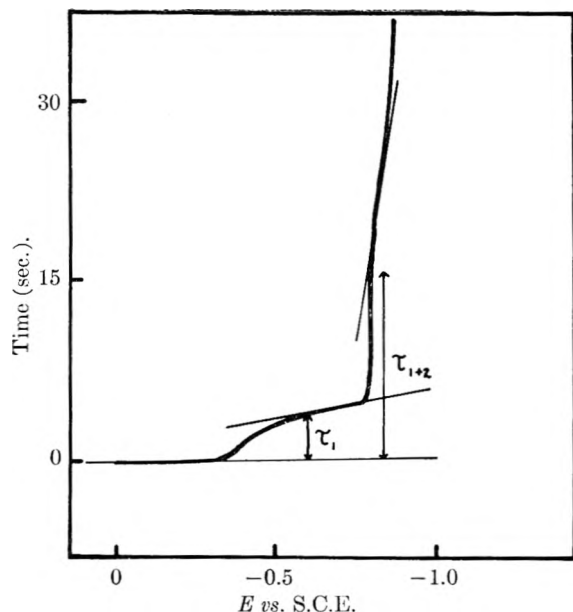


Fig. 1.—Chronopotentiogram for the reduction of uranyl ions: $2.07 \times 10^{-3} M$ uranyl perchlorate; $0.4 M$ perchloric acid; current 698 microamperes, electrode area 3.42 cm^2 .

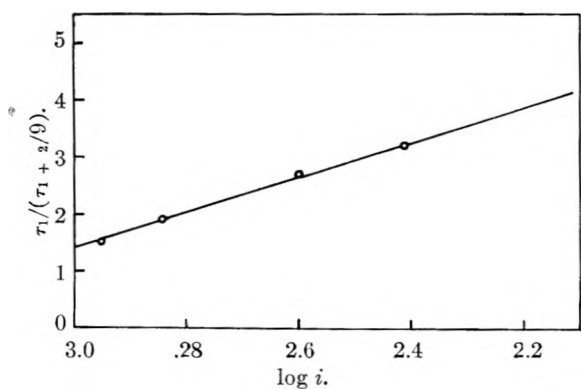
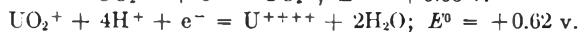


Fig. 2.—Variations of $\tau_1/(\tau_1 + \tau_2/9)$ with $\log i$

Discussion

The standard oxidation-reduction potentials



indicate the instability of uranium(V) solutions with respect to disproportionation to uranium(VI) and (IV). The disproportionation has been studied polarographically by a number of investigators,¹³⁻¹⁸ who have indicated the relationship for the process

$$\frac{d[\text{U(V)}]}{dt} = k[\text{H}^+][\text{U(V)}]^2$$

Orlemann and Kern¹⁶ have reported the successful theoretical evaluation of k based on the reaction volume concept developed by Wiesner²⁰ and Brdicka.²¹ Theoretical evaluation of k based on consideration of the problem as a simultaneous reaction and diffusion case was found to be impractical.¹⁶

In brief, the reaction volume approach involves the following considerations. In a region very close to the drop where there are uranium(VI)

species diffusing in from the bulk of the solution and uranium(VI) species being formed by disproportionation of uranium(V), all the uranium(VI) immediately is converted electrochemically to uranium(V). For a plane electrode, the approximate value of the thickness of this reaction layer is $3/2 \cdot 0.28D^{1/2}t^{1/2}$, D being the common value for the diffusion coefficient of the oxidant, D_0 , and the reductant, D_R , which are considered equal.¹⁶ The continual formation of uranium(V) is balanced by the diffusion of uranium(V) out from the reaction volume and by its disproportionation into uranium(VI) and (IV). The concentration of uranium(V), in this case, is approximated to be equal to the original concentration of uranium(VI).

A typical chronopotentiogram for the reduction of uranyl ion in $0.4 M$ perchloric acid is shown in Fig. 1.

The transition time for the first reduction wave of uranium(VI) at a mercury pool, τ_1 , is a function of current density. Close scrutiny of the dependency of transition time on current density, however, indicates that the value of $i\tau_1^{1/2}$ is not constant, but increases with decreasing current density, the result of the reduction product, uranium(V), undergoing disproportionation in the diffusion layer and regenerating uranium(VI). At high current density the deviation is less, because the resultant shorter transition time permits only a small amount of uranium(VI) to be reformed through disproportionation, whereas at low current density the deviation is greater due to the transition time being prolonged.

The constancy of $i(\tau_1 + \tau_2)^{1/2}$, Table I, indicates that the over-all transition time measured at the second wave is not affected by any kinetic process. Because $\tau^{1/2}$ is proportional to n which is 3, the first transition time, involving one electron, if unaffected by disproportionation should be $1/9$ the sum of the first and second transition times. In this case, however, besides diffusion supplying uranium(VI) species, disproportionation of the reduction product, uranium(V), also contributes uranium(VI) which prolongs the first transition time. It has been shown for a solution containing equal concentrations of electroactive substances having approximately the same diffusion coefficient and undergoing the same number of electron changes, the transition time involving both substances is 4 times that for a solution containing only one of them.⁴ The reason is that at this point equal amounts of the two species would be diffusing in toward the electrode and half the current would be required to take care of one species and half the other.

If the rate of diffusion of uranium(VI) to the electrode surface is equal to the rate of formation of uranium(VI) through disproportionation of uranium(V), assuming that all the uranium(VI) thus formed in the reaction volume is reduced immediately, the transition time would be 4 times the transition time where diffusion was the sole means of supplying uranium(VI) species. Half the current, under such a situation, would be due to the reduction of uranium(VI) formed through dispo-

(20) K. Wiesner, *Z. Elektrochem.*, **49**, 164 (1943).

(21) R. Brdicka and K. Wiesner, *Collection Czechoslov. Chem. Commun.*, **12**, 138 (1947).

TABLE I
CHRONOPOTENTIOMETRIC DATA FOR THE REDUCTION OF URANIUM(VI)^a

Run No. 1	<i>i</i> (μamp.)	τ_1 (sec.) ^b	τ_{1+2} (sec.) ^b	$i\tau_1^{1/2}$	$i\tau_{1+2}^{1/2}$	$\tau_1/\tau_{1+2}/9$	Electrode area (cm. ²)	k (moles/l.) ⁻² sec. ⁻¹
	262	48.6	136	1830	3070	3.22	3.42	54
	398	17.0	56.4	1640	2990	2.71	Temp. (°C.)	
	698	3.84	18.2	1370	2980	1.90	24.5 ± 0.5	
	897	2.10	12.6	1300	3180	1.50		
Run No. 2	86.5	14.2	55.3	326	644	2.31	Electrode area (cm. ²)	
	93.3	11.8	48.2	321	648	2.21	0.79	28
	124	5.62	31.1	294	692	1.62	Temp. (°C.)	
	177	2.66	15.0	288	685	1.59	25.0 ± 0.1	
	248	1.03	7.38	250	675	1.26		

^a 0.4 M HClO₄, μ of 0.4, pH of 0.83. ^b Represents the average of two values.

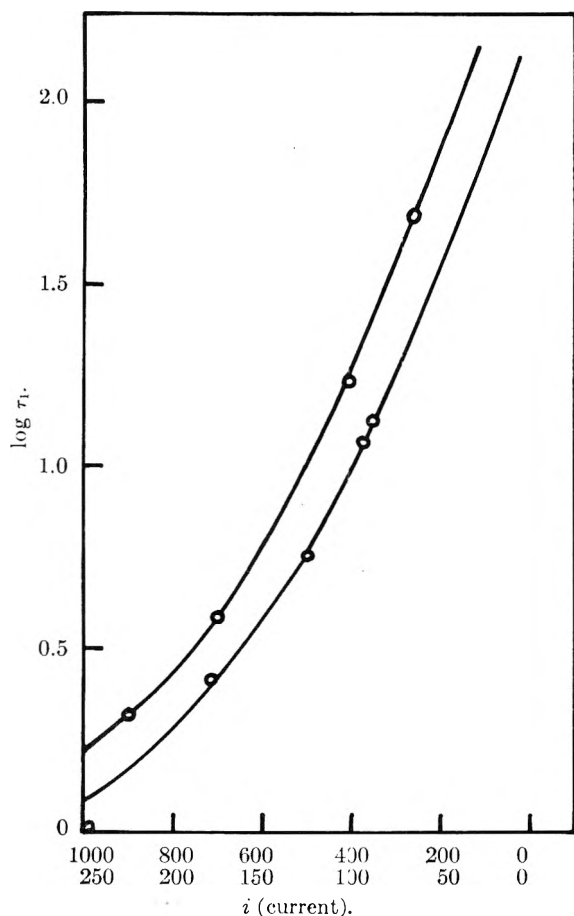


Fig. 3.—Variations of $\log \tau_1$ with current.

portionation of uranium(V). This current is $1/2$ of the current when $\tau_1/(\tau_{1+2}/9)$ equals 4 obtained from the plot of $\tau_1/(\tau_{1+2}/9)$ vs. $\log i$ (Fig. 2). Currents of 70 and 7.5 microamperes were obtained for the data in Table I.

The thickness of the reaction layer has been shown by Orlemann and Kern¹⁶ through statistical consideration to be approximately $3/2 \cdot 0.28D^{1/2}t^{1/2}$ for a plane electrode. The value of $t^{1/2}$ is obtained by plotting $\log \tau_1$ vs. i (Fig. 3). For currents of 140 and 15 microamperes, transition times of 126 and 100 seconds, respectively, were obtained. Using a value of 0.68×10^{-5} cm.² sec.⁻¹ for D , the common value for $D_{\text{UO}_2^{++}}$ and $D_{\text{UO}_2^+}$ which for pur-

pose of this calculation can be considered equal, reaction layer thicknesses of 12.2×10^{-3} cm. and 10.9×10^{-3} cm. were obtained.

For the disproportionation

$$-\frac{d[\text{U(V)}]}{dt} = \frac{2d[\text{U(VI)}]}{dt} \quad (1)$$

$$\frac{d[\text{U(VI)}]}{dt} = \frac{i_D}{FA\nu} \quad (2)$$

$$\frac{d[\text{U(V)}]}{dt} = k[\text{UO}_2^+]^2[\text{H}^+] \quad (3)$$

Combining the above equations

$$k[\text{H}^+][\text{UO}_2^{++}]^2 = \frac{2i_D}{FA\nu} \quad (4)$$

where i_D is the fraction, $1/2$, of the current used to reduce uranium(VI) formed through disproportionation of uranium(V), F is the faraday, A the area of the electrode, and ν is the reaction layer thickness.

The calculated k values of 54 and 28 (moles/l.)⁻² sec.⁻¹ agree with the theoretical and experimental values of k , 28 and 98 (moles/l.)⁻² sec.⁻¹, respectively, reported by Orlemann and Kern,¹⁶ for a 0.4 M perchlorate medium of 0.4 ionic strength.

It appears that disproportionation rate constants of the correct order of magnitude may be derived from chronopotentiometric data and application of the reaction volume concept.

OXIDATION OF SILICON CARBIDE IN THE TEMPERATURE RANGE 1200 TO 1500°

BY ROBERT F. ADAMSKY

Basic Research Branch, Research and Development Division, The Carborundum Company, Niagara Falls, New York

Received July 28, 1958

Present usage of bonded and self-bonded silicon carbide in heating elements, as electrical resistors and as a refractory material and use of single crystals for semi-conductor applications has promoted considerable interest in the evaluation of the oxidation behavior of silicon carbide. A large number of observations on the oxidation process have been reported previously and Nakatogawa,¹

(1) T. Nakatogawa, *J. Chem. Soc., Japan, Ind. Chem. Sect.*, **57**, 348 (1954).

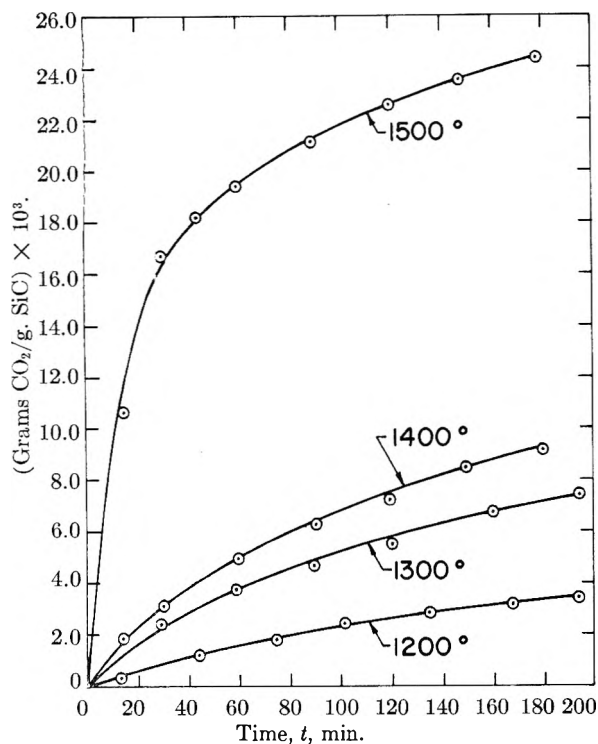


Fig. 1.

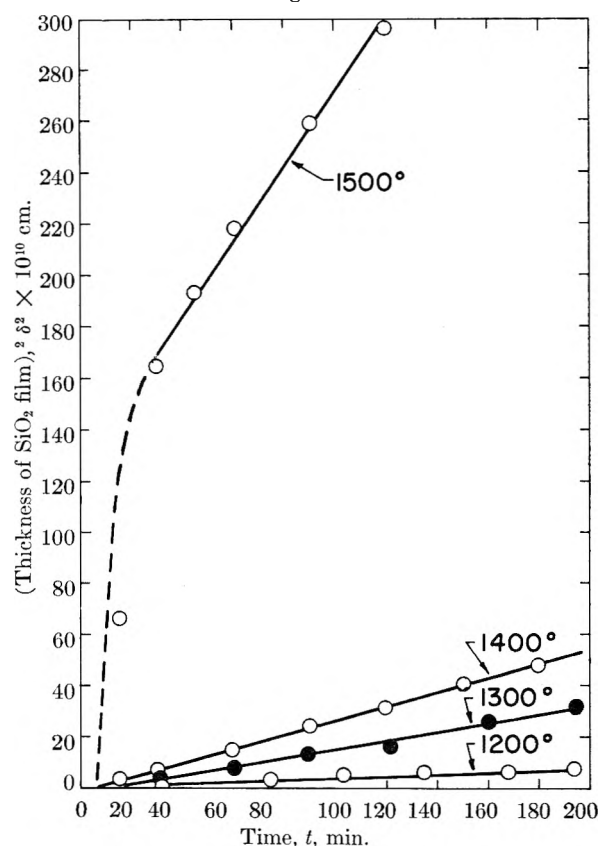


Fig. 2.

Erwin² and Suzuki,³ recently have conducted studies that parallel to some extent the present one.

(2) G. Erwin, paper presented at 59th American Ceramic Society Convention, Dallas, Texas, April 5-8, 1957.

(3) H. Suzuki, *Yogyo Kyokai Shi*, **65**, 88 (1957); *C. A.*, **51**, 17362 (1957).

The data presented here represent total oxidation rates for granular samples of silicon carbide in a moving stream of oxygen. It is intended that this work be complemented later by an investigation of the mechanism of the oxidation of single crystals of silicon carbide, in which different techniques for measuring oxidation will be employed.

Experimental Procedure

The rate of oxidation was measured indirectly by determining the weight of CO and CO₂ produced in the oxidation reaction. The CO was converted to CO₂ by oxidation over a CuO catalyst at 300°, and the total quantity of CO₂ absorbed in Ascarite-filled bulbs. Two bulbs in parallel were connected to the CuO tube by a three-way stopcock, so that periodic weighings of the Ascarite bulbs could be made while the reaction progressed. Precautions were taken to ensure that all weighings were made at constant humidity.

Oxygen was purified by passage over platinized asbestos at 300°, activated alumina, P₂O₅ and Ascarite, to remove H₂, H₂O, CO and CO₂. The oxygen flow rate was 210 cc./min. at one atmosphere pressure and was measured by a flowmeter placed in the line immediately downstream from the purification system.

The oxidation chamber was a dense alumina tube sufficiently impervious to permit evacuation to pressures below 10⁻⁵ mm. for initial degassing of the silicon carbide surfaces. Pressure was measured by a McLeod gauge. The ceramic tube was heated in a silicon carbide resistor furnace and the hot zone was 15 cm. in length. Temperature was controlled to ±10° by a West Gardsman controller and was measured by a Pt-Pt 10% Rh thermocouple located outside the alumina tube. The thermocouple was calibrated in terms of temperature inside the tube at the sample location.

The silicon carbide used for oxidation measurements was treated with a mixture of HF and HNO₃ to remove free surface Si and SiO₂; and then with fused KHSO₄ to remove other possible surface contaminants. This treated material was subjected to a slight pre-oxidation by heating to 800° in air and then exposed again to HF to remove the SiO₂. After repeated washings with distilled H₂O, the silicon carbide was dried.

The treated silicon carbide had the spectrographic analysis

B < 0.001%	Al < 0.005
Fe .008	Cu .001
Mg < .001	Ti .001
Mn < .001	Ca .001

The surface area as measured by an air permeability technique⁴ was 81 cm.²/g., and the average particle size, determined by microscopic measurement, was 200 μ. The silicon carbide particles, when examined with the petrographic microscope, appeared as predominantly colorless, irregular crystals showing conchoidal cleavage and exhibiting few plane surfaces. X-Ray examination showed the material to be essentially type 6-H (the crystallographic designation is that of Ramsdell.⁵)

A weighed sample of about two grams was placed in a shallow, porous, alumina combustion boat and inserted into the oxidation chamber. The sample was degassed at elevated temperatures and at reduced pressures prior to entry of oxygen. The degassing conditions are defined later in this paper.

Results and Discussion

The results presented in Fig. 1 are in terms of the measured weight of CO₂ per gram of SiC, as a function of time and represent averages of several determinations. The accuracy of the measurements may be indicated by the experiments at 1200°, since a large number of determinations were made at this temperature. For these experiments, the standard deviation of the measured weight of CO₂ was ±8%.

(4) B. Dubrow and M. Nieradka, *Anal. Chem.*, **27**, No. 2, 302 (1955).
 (5) L. R. Ramsdell, *Amer. Mineral.*, **32**, 64 (1947).

The initial oxidation rate was found to be markedly dependent on the degassing treatment, being higher for lower pressures and higher degassing temperatures. Because silicon carbide decomposes by loss of Si vapor, it is desirable to exceed the dissociation pressure for a given temperature of degassing. However, the dissociation pressures of silicon carbide are not known very exactly; hence, a temperature of 1300° and the somewhat high pressure of 1.5×10^{-3} mm. was adopted for degassing conditions. This pressure is in excess of the dissociation pressure of silicon carbide at 1300° estimated from reported data.⁶ With these conditions of degassing, variations in the initial oxidation rate were found with degassing time. These data suggest that strongly adsorbed layers of surface gases were affecting the oxidation of silicon carbide. After preliminary experiments, a degassing treatment was adopted which consisted of heating the sample at 1300° under 1.5×10^{-3} mm. pressure for 16 hours. This preliminary treatment was found sufficient to clean the surface of the silicon carbide so that reproducible initial rates of oxidation occurred during subsequent testing.

After oxidation, the silica formed on the surface of the silicon carbide was analyzed chemically, and the amount was found to agree to within one per cent. of that calculated from the CO and CO₂ evolution. X-Ray diffraction indicated that the product silica film was non-crystalline in nature over the entire temperature range in which the oxidation determinations were made.

The thickness δ , of the silica film was calculated from the measured weight of CO₂, assuming a uniform coverage and a constant surface area for the SiC particles. The density used for SiO₂ was that for silica glass, 2.20 g./cm.³. In Fig. 2, the square of the silica film thickness is plotted against time, and the resulting straight lines indicate that, except for early stages of the reaction at 1500°, the oxidation process obeys a rate law of the form

$$\delta^2 = kt + C$$

where k is the specific rate constant, t is time and C is a constant. A parabolic rate law for oxidation of silicon carbide in this temperature range also has been found by Nakatogawa¹ and Erwin.² By plotting the logarithm of the reaction rate against the reciprocal of the absolute temperature, an activation energy of 66 ± 8 kcal./mole is obtained. In comparison, a value of 60 kcal./mole for green silicon carbide is found by Nakatogawa.

The parabolic law indicates that the rate-determining step in the oxidation of silicon carbide is the diffusion of some species through the SiO₂ film, and the activation energy is the energy which must be present to initiate the diffusion process. The diffusing species controlling the rate is either an oxygen species, which diffuses inward to the silicon carbide-silica interface, or CO which diffuses outward to the atmosphere. The high initial oxidation rate at 1500° suggests that a very rapid surface reaction occurs between silicon carbide and oxygen, and that this reaction controls the oxidation rate until a suffi-

cient thickness of SiO₂ forms to produce a diffusion-controlled mechanism. Similar behavior may occur at the lower temperatures, but it is not evident.

The evolution of the gaseous product CO is very important in the reaction involving a granular silicon carbide sample because non-uniform oxidizing conditions may exist within the sample. CO and CO₂ can themselves oxidize silicon carbide as Lea⁷ and Erwin² have shown, and if the partial pressures of these gases become large in the neighborhood of the silicon carbide particles, the mechanism could become more complex. In addition, at the higher temperatures, sintering of the SiO₂ envelopes of adjacent silicon carbide particles is likely to alter the kinetics to some extent; hence, the rates reported herein may not be the same as for isolated particles.

Acknowledgments.—The author thanks Mr. S. D. Mark for his valuable advice, and Dr. T. Nakatogawa for translating portions of references 1.

(7) A. C. Lea, *J. Soc. Glass Tech.*, **33**, 27 (1949).

TEMPERATURE AS A VARIABLE DURING A KINETIC EXPERIMENT

BY ROBERT EARL DAVIS¹

Converse Memorial Laboratory of Harvard University, Cambridge, Mass.

Received July 28, 1958

Kinetic experiments usually are made with accurate temperature control at a constant temperature and the activation parameters of a reaction are determined in separate experiments at different temperatures. Yet temperature can be purposely a variable during a single experiment. Indeed, differential thermal analysis (DTA) has been an important method of investigation^{2,3} of many problems which are basically rate or kinetic problems such as phase transformations or dehydrations of hydrate salts. Basically, DTA involves the measurement of the temperature difference between a sample and a standard as both are heated. Borchardt and Daniels⁴ have applied DTA to measure the rate of chemical reaction in solution as a function of temperature. In their method, the amount of heat produced by the reaction is compared with a solvent blank while the entire system is being heated. The kinetic parameters of a reaction can be determined by an analysis of the slope, height and area of the DTA curve. The method also measures the heat of reaction, ΔH . Thus the rate, the order, the activation energy and the heat of chemical reaction are determined in a single, rapid experiment.

This note describes the use of the ultraviolet absorption of one reactant to follow the extent of reaction with time as the temperature is progres-

(1) (a) Public Health Service Research Fellow of the National Cancer Institute. (b) Department of Chemistry, Massachusetts Institute of Technology, Cambridge 39, Mass.

(2) C. B. Murphy, *Anal. Chem.*, **30**, 867 (1958).

(3) W. J. Smothers and Y. Chiang, "Differential Thermal Analysis," Chemical Publishing Co. Inc., New York, N. Y., 1958.

(4) H. J. Borchardt and F. Daniels, *J. Am. Chem. Soc.*, **79**, 41 (1957).

(6) O. Ruff, *Trans. Electrochem. Soc.*, **68**, 87 (1935).

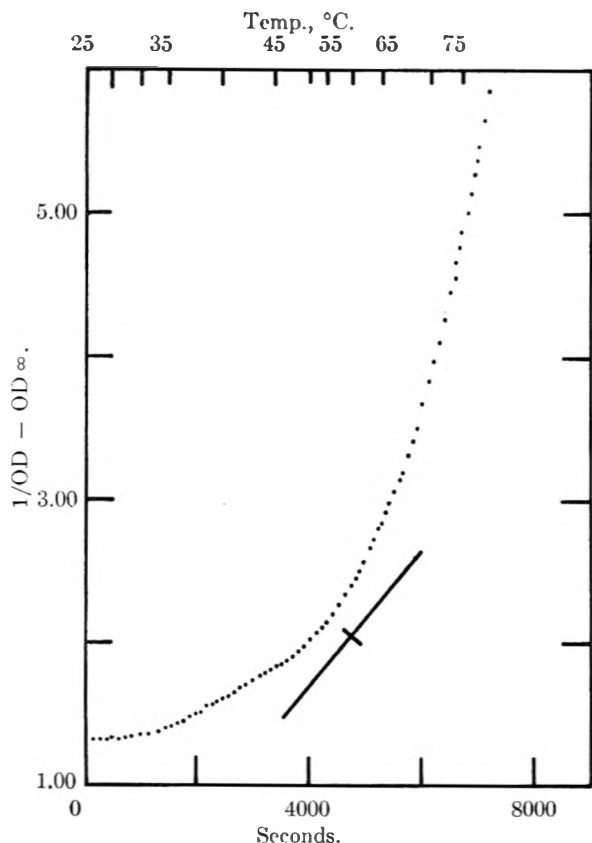


Fig. 1.—Second-order plot of the reaction of sulfur and triphenylphosphine in benzene; upper abscissa, temperature in the cell as a function of temperature. Shown is the slope determined at 55° which is then corrected +3%.

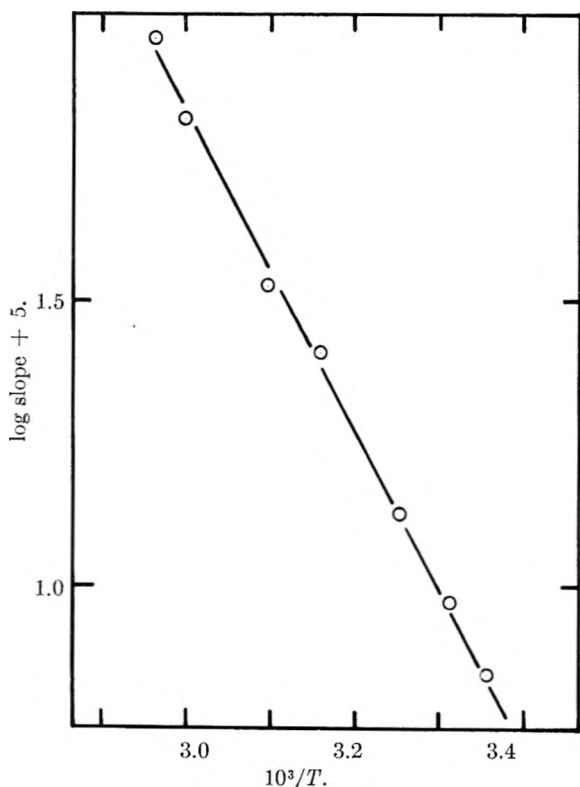


Fig. 2.—Arrhenius plot of log corrected slope determined from the curve of Fig. 1 versus $1/T$.

sively raised. This note is submitted with emphasis upon the method rather than upon the chemical reaction studied.⁵

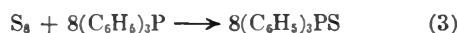
Consider the reaction



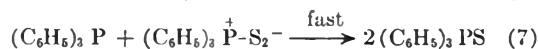
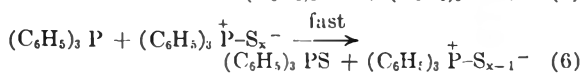
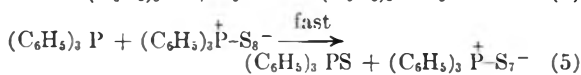
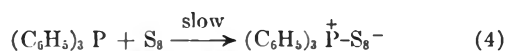
$$\text{rate} = A \exp(-E_a/RT) (X)^m (Y)^n \dots \quad (2)$$

Equation 2 can, in general, be solved completely even if T , the temperature, is not constant.⁶ The rate is a function of concentration, time and temperature. However, the most convenient method involves (i) an assumption as to the order ($m + n + \dots$) of the reaction, (ii) a plot of the derived function for that order⁷ and (iii) the determination of the slope of the derived curve at a given temperature. The slope with small corrections is proportional to the rate constant k at that temperature. The Arrhenius plot of *log corrected slope versus $1/T$* is linear if the correct assumption concerning the reaction order has been made.

The method requires a nearly continuous record of the optical density and temperature of the solution for construction of smooth curves of each with time. A continuous record of each is most desirable and provides an automatic method. The reaction chosen for study is that of octatomic sulfur and triphenylphosphine in benzene



forming the phosphine sulfide. Reaction 3 has been studied both by a titration method⁸ and by ultraviolet absorption analysis⁹ using more conventional techniques. Evidence has been presented^{8,9} that the rate-determining step is a bimolecular reaction of the phosphine with S_8 with ring opening forming a phosphonium octasulfide, $(C_6H_5)_3P^+S_8^-$. Rapid displacement reactions with the phosphine produce the phosphine sulfide and lower phosphonium polysulfides. The activation energy of the reaction



determined in separate kinetic experiments^{8,9} is 16.0 ± 0.2 kcal./mole (Table I).

Figure 1 presents an experiment in which the temperature has been raised from 23 to 77°. The concentrations of the reactants are $(S_8)_0 = 2.00 \times$

(5) It should be pointed out that the rate of change of any physical property proportional to the rate of reaction could be used to obtain the kinetic parameters.

(6) However, the reader should refer to ref. 3 for a discussion of some of the mathematical difficulties involved for a solution in closed form. The rate of heating is required for solution.

(7) First order, *log concentration versus time*. See A. A. Frost and R. G. Pearson, "Kinetics and Mechanism," John Wiley and Sons, Inc., New York, N. Y., 1953, pp. 8-25, 147-158, for other reaction orders.

(8) P. D. Bartlett and G. Meguerian, *J. Am. Chem. Soc.*, **78**, 3710 (1956).

(9) P. D. Bartlett, E. Cox and R. E. Davis, in preparation.

$10^{-3} M$ and $(C_6H_5)_3P_0 = 1.60 \times 10^{-2} M$; therefore, a plot of $1/OD-OD_\infty$, where OD is the optical density, versus time is the proper derived function for a second-order reaction with the reactants at equal equivalent concentrations.⁷ The upper abscissa has been added to show the temperature in the reaction cell as a function of time. The slope of Fig. 1 at any given temperature is then corrected for the change in density of the solvent with temperature and for a small change in the molar extinction coefficient of sulfur with temperature. The resultant Arrhenius plot (Fig. 2) of *log corrected slope versus 1/T* gives an activation energy of 16.5 ± 0.4 kcal./mole, in agreement with 16.0 ± 0.2 kcal./mole.

TABLE I

RATE CONSTANTS IN BENZENE			
Temp., °C. ^a	k_2 , l. mole ⁻¹ sec. ^{-1b}	Ref. method ^c	
7.35	7.50×10^{-4}	9	Ultraviolet
25.00	4.40×10^{-3}	8,9	Ultraviolet titr.
35.00	11.3×10^{-3}	8,9	Ultraviolet titr.

^a ± 0.02 . ^b Rate = $k_2(S_8)((C_6H_5)_3P)$. ^c Ultraviolet analysis of sulfur, titr. iodometric analysis of the phosphine.

The main requirements for the use of this method are (i) the rate of reaction is moderately slow at the lowest temperature; (ii) the temperature in the cell must be uniform; (iii) the activation energy does not vary with temperature; (iv) the boiling point of the solvent cannot be exceeded; and (v) Beer's law must be obeyed even though the molar extinction coefficient may change with temperature. Requirement (ii) restricts the size of the cell and the rate of heating. If the activation energy varies greatly with temperature one would be unable to obtain the correct order of the reaction and the rate constants. The main disadvantage of this method is that only a small percentage of reaction is used to determine the rate at any one temperature. The advantage is obtaining the rate, the order of the reaction, the frequency factor and the activation energy in a single rapid experiment.

Experimental

The purification of sulfur, triphenylphosphine and benzene has been reported previously.⁸ The use of the ultraviolet absorption spectrum of sulfur to study this reaction at a constant temperature and with conventional techniques will be subject to a forthcoming publication.⁹ The thermostated cell compartment for a Beckman DU spectrophotometer has been discussed.¹⁰ The brass jacket was carefully made to ensure good thermal contact with a square Corex cell. To the top of the cell was sealed a 7 mm. Pyrex tube (15 cm. in length) through which a multi-junction thermocouple was placed into the cell just above the light path. The output of the thermocouple was applied to a Speedomax recorder. The reactants were mixed and placed in the cell (total volume 1 to 2.6 ml). Water, circulated at the rate of one gallon per minute through the compartment, was slowly heated. Optical density measurements were manually recorded every 30 seconds at 345 m μ . The heating rate does not enter into the graphic analysis of the data but averaged 0.5 degree per minute to cover the range of 23 to 77°. Other heating rates can be used to cover only a 25° increase.

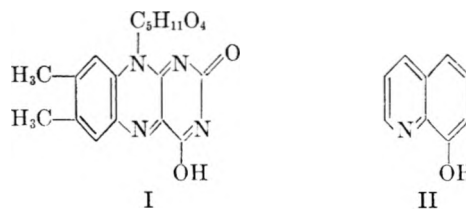
(10) P. D. Bartlett and R. E. Davis, *J. Am. Chem. Soc.*, **80**, 2513 (1958).

THE CHELATING TENDENCY OF RIBOFLAVIN¹

BY THOMAS R. HARKINS AND HENRY FREISER²

Received August 4, 1958

The structural similarity of riboflavin (I) and 8-hydroxyquinoline (II) has been noted previously by Albert³ in accounting for the ability of the riboflavin to complex various metal ions. His results indicated an unusual metal stability order in that iron(II) ($\log K_1 = 7.1$) formed a more stable complex than did copper(II) ($\log K_1 = 6.5$). Inasmuch as 8-hydroxyquinoline chelates follow the usual stability order, this result was unexpected. Of course, it is possible that the pres-



ence of a sterically hindering group in riboflavin (the fused benzene ring) would have a sufficiently greater effect on copper(II) which is smaller than iron(II). The sterically hindering group present in 2-methyl-8-hydroxyquinoline was shown to have a greater effect on the chelates of the smaller metal ions.⁴ Another interesting observation concerning metal-riboflavin complexes was made by Foye and Lange⁵ who prepared a series of such complexes whose composition corresponded to a two to one mole ratio of metal to riboflavin.

The stoichiometry and thermodynamics of the formation of metal-riboflavin reported in this paper was undertaken to evaluate these observations.

Experimental

Stock solutions of approximately 0.01 M metal ions were prepared by dissolving their reagent grade perchlorates (G. Frederick Smith Co.) in water. The copper(II) and cobalt(II) solutions were standardized by electrodeposition. The nickel(II) solution was standardized by precipitation with dimethylglyoxime. Zinc(II) was standardized gravimetrically as $ZnNH_4PO_4$. The iron(II) solution was prepared by dissolving high purity iron wire in perchloric acid under an inert atmosphere.

Riboflavin, obtained from the Nutritional Biochemicals Corp., was dried at 110°. *Anal.* Calcd. C, 54.25; H, 5.36. Found: C, 55.59; H, 4.99.

The titration apparatus and procedure have been previously described.⁶ A slight modification in preparing the solution for titration was undertaken to facilitate the dissolution of riboflavin. Fifty-five milliliters of water was added to a weighed quantity of the reagent. A small measured volume of standard base was added to bring about solution after which the perchloric acid and metal perchlorate were added and the titration proceeded in the customary

(1) Abstracted from the thesis submitted by T. R. Harkins in partial fulfillment of the requirements for the Ph.D. degree at the University of Pittsburgh, June, 1956.

(2) Department of Chemistry, University of Arizona, Tucson.

(3) A. Albert, *Biochem. J.*, **54**, 646 (1953).

(4) W. D. Johnston and H. Freiser, *Anal. Chim. Acta*, **11**, 201 (1954).

(5) W. O. Foye and W. E. Lange, *J. Am. Chem. Soc.*, **76**, 2199 (1954).

(6) H. Freiser, R. G. Charles and W. D. Johnston, *ibid.*, **74**, 1383 (1952).

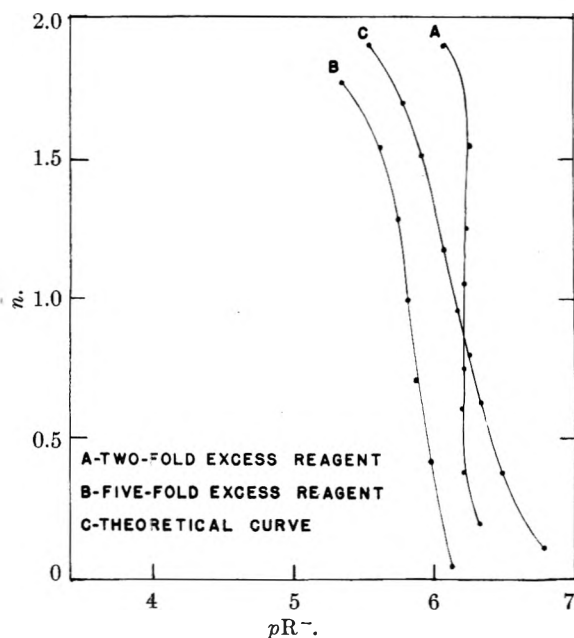


Fig. 1.—Formation curves copper(II)-riboflavin complex.

fashion. The results of the measurements at several temperatures as well as the thermodynamic quantities calculated therefrom are summarized in Table I.

TABLE I
CHELATE FORMATION DATA FOR RIBOFLAVIN IN WATER
(5:1 Ratio of Riboflavin to Metal)

Metal	Temp., °C.	Log K_1	$2 \log K_{ao}$	ΔF ,	ΔH , kcal.	ΔS , e.u.
Cu(II)	10	6.0	11.7			
	25	5.9	11.6	-15.8	-3	44
	40	5.9	11.5			
	25 ^a	6.2	12.4			
Ni(II)	10	4.2	7.8			
	25	4.2	7.8	-10.6	+3	46
	40	4.1	8.0			
Co(II)	10	4.1	7.6			
	25	4.3	7.8	-10.6	+5	52
	40	4.3	8.1			
Zn(II)	10	4.9	9.5			
	25	4.9	9.6	-13.1	+1	47
	40	4.9	9.6			
Reagent + H ⁺	10	10.02				
	25	9.69		-13.2	-8.3	16
	40	9.40				

^a 2:1 ratio of riboflavin to metal.

Discussion

Initially the titrations were carried out using a two to one mole ratio of riboflavin to metal as Albert had done.³ Under these conditions, the results for copper(II) agreed with those he reported. However, the titration curve indicated an overlap of the complex formation with hydrolysis. Further, the formation curve obtained indicated that something was amiss since its slope was too steep. In Fig. 1, curve A which represents the results of the titration with a 2 to 1 riboflavin-metal ratio is compared with curve C which has been calculated on the basis of simultaneous addition of two moles of reagent to the metal. Curve C was derived by

assuming a value for $\log K_f$ (in this case 12.3), and using the expression

$$pR = 1/2 \left\{ \log \frac{\bar{n}}{2 - \bar{n}} - \log K_f \right\}$$

to evaluate pR at various values of \bar{n} . Curve B represents the results of a titration in which the riboflavin-metal ratio is five to one. This curve has flattened to approximately the slope of curve B and is displaced in the direction of lower $\log K$ values. The remainder of the titrations were carried out at the higher riboflavin-metal ratios to avoid interference by hydrolytic phenomena. Were it not for the relatively low solubility of riboflavin, even higher ratios would have been employed.

No result is reported for iron(II) because the titration curves for this metal both in the presence and absence of riboflavin were identical. This indicated that hydrolysis is a more favorable reaction than complex formation. The stability constant previously reported³ is of doubtful validity and probably can be attributed to hydrolysis. Thus, the unusual metal stability sequence in which iron(II) appears before copper(II) may not be claimed for riboflavin.

The results reported here do show a displaced metal stability sequence reminiscent of what was found for 2-methyl-8-hydroxyquinoline.⁴ The extraordinary sensitivity of nickel to the influence of steric hindrance to chelate formation exhibited with 2-methyl-8-hydroxyquinoline would seem to account for its displacement below zinc with riboflavin whose fused benzene ring in juxtaposition to the nitrogen involved in chelation offers steric hindrance. A comparison of the ΔH values with those of 4-methyl-8-hydroxyquinoline as was made with 2-methyl-8-hydroxyquinoline⁴ reveals a similar trend of decreasing difference with increasing ionic radius of the metal. Also the ΔS values found here are very close to those observed with the 2-methyl-8-hydroxyquinoline.

The isolation of metal-riboflavin complexes in which there is a 2:1 molar ratio of metal to riboflavin could not be predicted from the data obtained in this investigation. The titration data indicate that two moles of hydrogen ion are liberated per mole of metal ion in the reaction with riboflavin. Since the metals are divalent, this would satisfy their neutralization of charge requirements. Structures corresponding to the formulas assigned to complexes isolated in basic solution by Foye and Lang⁵ (e.g., $M_2R \cdot H_2O$) would be difficult to visualize on this basis. The stoichiometry of two metal ions per riboflavin molecule might be accounted for with one metal ion chelating with the oxine type grouping and the other metal ion binding to the ribitol group. To account for a neutral species being formed, however, a negative group such as hydroxyl would have to be bound to the metal attached to the flavin portion of the molecule.

Acknowledgment.—The authors gratefully acknowledge the financial assistance of the U. S. Public Health Service.

THERMAL CONDUCTIVITY OF POLYCRYSTALLINE BORON¹

BY CLAUDE P. TALLEY

Experiment Incorporated, Richmond 2, Virginia

Received August 2, 1958

To the author's knowledge there have been no previous reports of the thermal conductivity of boron. In the course of preparing samples of boron to study its oxidation properties, cylindrical polycrystalline boron rods about 1 mm. in diameter and several centimeters long were made which contained a 0.025 mm. diameter tungsten core. Such specimens are well suited to the measurement of thermal conductivity, and it was decided to take this opportunity to obtain at least an order-of-magnitude estimate of this property for boron.

The boron rods were prepared by the reduction of boron tribromide by hydrogen near a 0.025 mm. diameter tungsten filament at about 1250°. Wet chemical analysis for total boron showed that the boron content exceeded 99% by weight. The main impurity in the rods was that due to the tungsten core, which amounted to about 0.7% by weight. Emission spectrographic analysis indicated small amounts of Ca, Fe, Cu, Mg and Si amounting to a total of 0.02% by weight.

The thermal conductivity of a polycrystalline boron rod was measured in the following manner. The tiny 0.025 mm. diameter tungsten core was heated electrically and served as the heat source. The circuit consisted of battery, variable resistor, ammeter, voltmeter and the specimen immersed in a constant temperature water-bath. At the temperatures used in these experiments the electrical conductivity of the boron was negligible, and therefore practically all the electrical current that passed through the rod flowed through the tungsten filament located in the core. Electrical contact was made to the tungsten by fusing on platinum leads at each end of the rod. Heat generated in the tungsten was conducted through the cylindrical casing of boron and into a surrounding water-bath. The temperature of the inside surface of the boron was assumed to be equal to the temperature of the tungsten.

The temperature of the tungsten was obtained by computing its resistance from the measured voltage and current supplied to the rod and comparing this resistance with a previously experimentally determined curve on the same rod, at negligible power input, of resistance versus temperature. The temperature of the outside surface of the boron was assumed equal to that of the stirred water-bath. In a typical experiment with a 1.19 mm. diameter by 27.4 mm. length rod, the power supplied to the 0.025 mm. diameter tungsten core was 0.70 cal./sec., the resistance of the tungsten corresponded to a temperature of 80°, and the temperature of the water-bath was 22°. In these preliminary experiments an average value of 0.003 cal./(sec. cm.² °C./cm.) was obtained for the thermal conductivity between 20 and 80°. The equation for the calculation of the thermal conductivity was²

$$K = \frac{Q \ln r_2/r_1}{2\pi L(T_1 - T_2)}$$

where

- K = thermal conductivity
- Q = rate of heat conduction
- r_2 = outside radius of boron rod
- r_1 = radius of the tungsten core
- L = length of boron rod
- T_1 = temperature at r_1
- T_2 = temperature at r_2

(1) This work was supported by the Office of Naval Research.

(2) W. H. McAdams, "Heat Transmission," 3rd Ed., McGraw-Hill Book Co., Inc., New York, N. Y., 1954, Chapter 2.

Heat loss at the ends of the rod was neglected because of the high length-to-diameter ratio of the rod. By electrically probing a polished cross section of a polycrystalline boron rod for electrical resistance, it was found that the tungsten filament in the center had remained essentially unaltered during deposition, and therefore r_1 was taken as equal to the starting radius of the tungsten filament. For example, at a distance of about 0.010 mm. from the center of the rod the resistance was only a few ohms, whereas at about 0.025 mm. from the center of the rod the resistance increased to about 150,000 ohms. Also the tungsten core appeared under the microscope to be a maximum of 0.035 mm. in diameter.

Using this same technique a value was obtained for the thermal conductivity of Pyrex glass rods containing a central 0.025 mm. diameter tungsten filament which agreed with published values within a factor of three. Considering that the thermal conductivity of Pyrex is about the same as obtained on polycrystalline boron and considering the accuracy of measurement of the individual quantities, the thermal conductivity value obtained for boron is thought to be accurate to within a factor of three also.

THE DESICCATION AND DENSITY OF ACETONE

BY K. S. HOWARD AND F. P. PIKE

*Department of Chemical Engineering, North Carolina State College
Raleigh, N. C.*

Received August 11, 1958

The dehydration of otherwise pure acetone has been a troublesome problem for many years. The ordinary inert desiccants, such as CaCl_2 and CaSO_4 , are extremely slow-acting¹ and are ineffective² in the complete removal of water, since small amounts of water are retained very tenaciously by the acetone phase. Formation of an addition compound between acetone and sodium iodide³ with subsequent regeneration of "anhydrous" acetone was used by Young⁴ to obtain a product with a density of 0.79053 g./ml. at 20°. Timmermans² has used P_2O_5 for dehydration, a process which involves great loss of material through condensation reactions and requires an efficient distillation column for separation of the product. Interpolation of the Timmermans data gives a density of 0.7904 g./ml. at 20°, and this value was accepted for many years as the density of anhydrous acetone. However, Thirion and Craven⁵ used desiccation by acetic anhydride, followed by distillation, to obtain a product with an average density at 20° of 0.78990 ± 0.00006 g./ml., significantly lower than these previous values. The results of Thomas and McAllister¹ confirm this lower density.

The current work was begun in an attempt to find a simple procedure, employing ordinary laboratory equipment, for complete dehydration of acetone. Use of the sodium iodide adduct was no more successful here than it had been in Young's hands.⁴ Dehydration by CaH_2 or acetic anhydride led to great material loss and separation problems. An attempt to titrate the water by modifications of the Karl Fischer technique,⁶ followed by distil-

(1) K. T. Thomas and R. A. McAllister, *A. I. Ch. E. J.*, **3**, 161 (1957).

(2) J. Timmermans, "Physico-Chemical Constants of Pure Organic Compounds," Elsevier Publ. Co., Inc., New York, N. Y., 1950, p. 354.

(3) K. Shipsey and E. A. Werner, *J. Chem. Soc.*, **103**, 1255 (1913).

(4) W. Young, *J. Soc. Chem. Ind.*, **52**, 449 (1933).

(5) P. Thirion and E. C. Craven, *J. Appl. Chem.*, **2**, 210 (1952).

(6) J. Mitchell, Jr., and D. M. Smith, "Application of the Karl Fischer Reagent to Quantitative Analyses Involving Water," Interscience Publishers, Inc., New York, N. Y., 1948.

lation of the anhydrous acetone, was unsuccessful. Use of the acetone-urea complex⁷ did not appear promising.

The authors were, however, able to obtain high yields of acetone with an average density at 20.00° of 0.78994 ± 0.00003 g./ml., using a synthetic zeolite as a desiccant, followed by distillation with ordinary equipment.

Experimental

Most reagent grade acetone is unlikely to contain significant impurities, with the exception of water; "Baker Analyzed" reagent grade material (J. T. Baker Co., Phillipsburg, N. J.) was found to be a particularly suitable starting material, with a water content of about 1.2 mole %. The synthetic zeolite Type 5A Molecular Sieve (Linde Air Products, New York, N. Y.) was regenerated by heating at 670° F. for 3 hours in an air oven; the hot material was sealed and allowed to cool. This regenerated material was added to the starting acetone in a weight ratio of 1 part Molecular Sieve to 7 parts acetone; this amount represents a 3- to 4-fold excess over the calculated capacity of the zeolite. If this operation is carried out in the flask to be used for subsequent distillation, the possibility of water contamination from the atmosphere during future transfer operations is obviated. The mixture was allowed to stand 18 to 24 hours, with occasional swirling, and then was quickly connected to a Vigreux column equipped with a straight water-cooled condenser and receiving flask, all of which had been purged with a steam of CaSO₄-dried air to remove water adsorbed on the glass surfaces. All junctions were non-lubricated ground glass joints, and the apparatus was vented through a CaSO₄ drying tube. The center cut, comprising 80 to 90% of the starting volume, was collected. This material had a density of 0.78993 g./ml. Using this sample, the entire desiccation procedure was carried out a second time, with fresh Molecular Sieve and the twice-treated distillate had a density of 0.78996 g./ml., indicating that no further drying had been effected. An additional preparation, from another sample of "Baker Analyzed" acetone, had, after one desiccation treatment, a density identical to those reported above. The refractive index of the various preparations was similarly constant.

The densities were determined using the apparatus and procedure described by Thomas and McAllister,¹ with the modification that all glass surfaces were thoroughly dried with a CaSO₄-dried air stream, and exposure of the acetone to ordinary air at any point during loading of the pycnometers was eliminated.

Refractive index measurements were made using a Bausch and Lomb precision refractometer capable of giving results accurate to ± 0.00003 unit.

TABLE I

THE DENSITY OF ANHYDROUS ACETONE	
Temp. (°C.)	Density (g./ml.)
20.00	0.78989
	.78997
	.78996
25.00	.78419
	.78426
	.78429
37.80	.76943
	.76944
50.05	.75482
	.75481

Results and Discussion

The densities of the desiccated acetone are given in Table I. Temperature control was within $\pm 0.01^\circ$. The refractive index (n_D^{25}) of this acetone was 1.35589 ± 0.00003 , which com-

pares favorably with the 1.35596 ± 0.00003 reported by Thomas and McAllister.¹

Although the reproducibility of the density results was within the precision of the method (± 0.00005 g./ml.), the accuracy of the results is claimed only to ± 0.0001 g./ml. because of the difficulty of precisely evaluating the purity of the acetone. The assumption for insignificantly low water content of the samples is based on the identity of samples prepared by the method from different starting materials, and the failure of successive repeated applications of the desiccation procedure to change the measured properties. Density and refractive index were the analytical methods for evaluating both these criteria. In addition, the assumption of the absence of any impurity other than water appears valid in view of the close correspondence of both density and refractive index values of acetone from these preparations to those reported for material prepared through processes employing more rigorous separation techniques. It seems improbable that any significant impurity would remain undetected by both analytical methods.

Acknowledgment.—This work was carried out with funds made available by the National Science Foundation, and the authors gratefully acknowledge this support and encouragement.

THE EFFECT OF DROP SIZE ON THE ACCURACY OF SURFACE TENSION DETERMINATIONS BY THE SESSILE DROP METHOD

BY EDWARD B. DISMUKES

Southern Research Institute, Birmingham 5, Alabama

Received August 12, 1958

A classical method for determining surface tension, particularly of molten metals and salts, is the sessile drop method. If a liquid drop rests on suitable flat surface and assumes an obtuse contact angle, the dimensions of the drop silhouette, namely, the maximum radius r and the distance h from the maximum diameter to the vertex, are determined by gravitational acceleration g , the liquid density d and the surface tension γ . No analytical solution of the differential equations that relate these quantities has been obtained, but the surface tension may be calculated from approximation formulas such as the Worthington formula¹

$$\gamma = \frac{1}{2} h^2 g d / (1 + 0.6094 h/r) \quad (1)$$

or from the Bashforth and Adams tables.² The use of these tables has been reviewed by Ellefson and Taylor.³

Kingery and Humenik⁴ recently pointed out that the accuracy of surface tension determinations by the sessile drop method becomes less as the drop

(1) A. M. Worthington, *Phil. Mag.*, **20**, 51 (1885).

(2) F. Bashforth and S. C. Adams, "An Attempt to Test the Theories of Capillarity," Cambridge University Press, 1883.

(3) B. S. Ellefson and N. W. Taylor, *J. Am. Ceram. Soc.*, **21**, 193 (1938).

(4) W. D. Kingery and M. Humenik, Jr., *THIS JOURNAL*, **57**, 359 (1953).

(7) W. Schlenk, Jr., *Ann.*, **565**, 204 (1949); O. Redlich, C. M. Gable, A. K. Dunlop and R. W. Millar, *J. Am. Chem. Soc.*, **72**, 4153 (1950).

becomes more spherical owing to small volume, high surface tension, or low density. Baes and Kellogg⁵ have treated quantitatively the relation between size and the error in surface tension calculated by the Bashforth and Adams method. These authors constructed a graph to show that increasing the factor r/h , which is equivalent to increasing the size of the drop, appreciably lowers the "error factor," defined as the ratio of the percentage error in the calculated surface tension value to the percentage error in the experimentally measured value of h . (The accuracy of h is a far more critical factor than the accuracy of r in calculating surface tension, as shown by equation 1.) In other words, Baes and Kellogg have shown that if a given amount of error in h is to be encountered, it is far less significant for large drops than for small drops in the Bashforth and Adams method of evaluating surface tension.

There is another question concerning accuracy: how is the amount of error in h affected by the size of the drop being studied? This question of accuracy in measurements, which must be considered before Baes and Kellogg's treatment of accuracy in calculations can have its fullest meaning, is treated in this paper.

The accuracy of the quantity h depends primarily on locating the horizontal plane in which the maximum diameter of the drop lies. This plane is located by designating the two points where the tangents to the drop are vertical, namely, the two points at the ends of the maximum diameter. Clearly, these points can be designated more accurately the greater is the curvature of the drop at these points.

Figure 1 represents segments of drop profiles near one of the points of vertical tangency. These curves do not bear direct resemblance to actual silhouettes, for the scale of horizontal coordinates has been expanded considerably relative to that of vertical coordinates. In order to plot the curves in the figure, the quantity gd/γ was arbitrarily set equal to unity, and the dimensions of the drops were obtained from Bashforth and Adams' tables. The interesting thing to note is that as the drop size increases and hence r/h increases, the drop profiles approach a limiting shape; specifically, the points (5) corresponding to $r/h = 2.18$ do not lie perceptibly off the curve (4) corresponding to $r/h = 1.51$.

Suppose that horizontal coordinates cannot be discerned with an accuracy greater than 0.001 cm., which is the distance AG. Then, for a drop having $r/h = 1.03$, the error in h may be as great as $1/2$ HH' or 0.025 cm. For a drop having $r/h = 1.51$, the error in h may be as great as $1/2$ JJ' or 0.040 cm. The absolute error in h is thus larger for the larger drop, but the magnitude of h is such that the percentage error for the larger drop is considerably smaller, 3.3% as against 7.4%. Moreover, if the drop size increased until r/h were 2.18, the absolute error in h would remain at 0.040 cm. while the percentage error would decline to 2.8%. The numerical magnitudes of error discussed here apply only

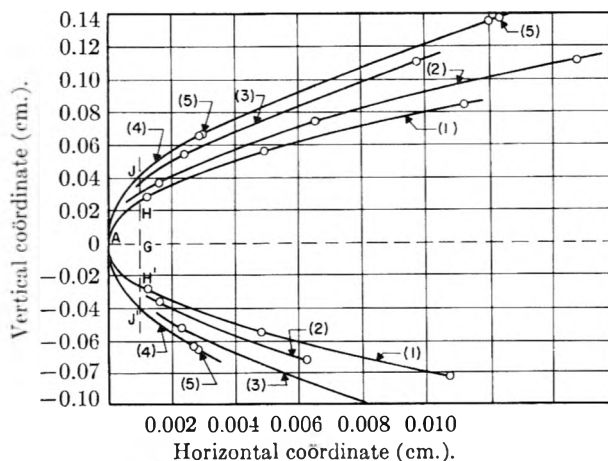


Fig. 1.—Coordinates on drop profiles measured from point A ($gd/\gamma = 1.0$): (1) $r/h = 1.03$; (2) 1.05; (3) 1.15; (4) 1.51; (5) 2.18.

to the assumption that $gd/\gamma = 1.0$, but it follows¹ that the percentage error in h decreases as the drop size increases regardless of what the physical constants of the liquid are.

The preceding discussion treats the predominant source of error in h , that is, locating the plane of the maximum diameter. It has indeed been shown that the other source of error, locating the vertical coordinate of the vertex, is relatively unimportant. If the vertex is located as the point on the silhouette immediately above the midpoint of the maximum diameter, the largest horizontal error assigned to the vertex location will be of the same approximate magnitude as the horizontal error in locating the endpoints of the maximum diameter. Curves corresponding to drop profiles near the vertex were constructed, and it was thus shown that for a drop having $r/h = 1.03$ there would not be an error in h greater than 0.001 cm. derived from mislocation of the vertex when the error in h derived from mislocation of the plane of maximum diameter is 0.025 cm. For larger drops, the error in h derived at the vertex would be even less significant in comparison with that derived at the maximum diameter.

The conclusions from this study and that of Baes and Kellogg, that large drops should be studied to obtain the greatest accuracy in measuring h and the greatest accuracy in calculating surface tension, are illustrated in Table I where the error in the surface tension of mercury is considered as a function of drop size. A modified form of Fig. 1 has been used to take into account the physical constants of mercury, assumed to be $d = 13.6$ g./cm.³ and $\gamma = 490$ dynes/cm. It has been assumed that the least discernible coordinate corresponding to AG in Fig. 1 is 0.2μ or 0.00002 cm., which is the ultimate resolution of a good light microscope. The third and fourth columns in the table list the resulting absolute and percentage errors in h , and the fifth column lists Baes and Kellogg's corresponding error factors. The final column gives the percentage errors in surface tension, obtained by multiplying the factors in the fourth and fifth columns, and demonstrates that the use of large drops is preferred.

(5) C. F. Baes, Jr., and H. H. Kellogg, *Trans. AIME*, **197**, 643 (1953).

TABLE I
ERRORS IN SURFACE TENSION CALCULATIONS FOR VARIOUS
SIZES OF MERCURY DROPS

r/h	h (cm.)	Δh (cm.)	$100 \frac{\Delta h}{h}$	Error factor ⁸	$100 \frac{\Delta \gamma}{\gamma}$
1.0269	0.06472	0.0012	1.8
1.0507	.08787	.0013	1.5
1.1547	.14701	.0016	1.1	9.0	10
1.5055	.23035	.0018	.80	3.8	3
1.8347	.26189	.0018	.70	2.9	2
2.1814	.27768	.0018	.66

Another important fact can be learned from Table I; that is, the sessile drop method is inherently subject to significant error even under optimum conditions. Even if optical resolution were the controlling uncertainty, appreciable errors would be encountered. Usually the optical system that renders an image of the drop does not render a perfect image, and experimental errors much larger than the limiting optical resolution are encountered. Various authors have discussed sources and magnitudes of experimental errors.⁶⁻⁹ In view of the magnitude of these errors it is not surprising that various laboratories have had difficulty in obtaining consistent surface tension data by the sessile drop method. Kamball,⁹ in summarizing measurements on mercury, points out that values from 438 to 515 dynes/cm. have been reported over a relatively narrow range in temperature.

Acknowledgment.—This study was carried out in connection with a research program for the United States Atomic Energy Commission (Contract AT-(40-1)-2073). The author gratefully acknowledges this financial support and also expresses his appreciation to Dr. Locke White, Jr., and Dr. W. S. Wilcox of Southern Research Institute for their helpful discussions of this work.

(6) S. G. Cook, *Phys. Rev.*, **34**, 513 (1929).

(7) R. S. Burdon, *Nature*, **128**, 456 (1931).

(8) O. L. Wheeler, H. V. Tartar and E. C. Lingafelter, *J. Am. Chem. Soc.*, **67**, 2115 (1945).

(9) C. Kamball, *Trans. Faraday Soc.*, **42**, 526 (1946).

THE POLAROGRAPHIC BEHAVIOR OF CHROMAMMINES AND CHROMIUM(III) SALTS IN AN ACETATE BUFFER

By J. A. FRIEND AND P. W. SMITH

Department of Chemistry, University of Tasmania, Hobart, Tasmania

Received August 12, 1958

Following investigations¹⁻³ of the polarographic reduction of cobaltamines, we have carried out a study of a number of chromamines, which have not received much attention so far, except for a brief comment in a paper by Holtzclaw,⁴ in which *cis*- and *trans*-(dichlorobisethylenediamine)-chromium(III) chloride were stated to be too unstable in solution for satisfactory measurements to be

(1) J. B. Willis, J. A. Friend and D. P. Mellor, *J. Am. Chem. Soc.*, **67**, 1680 (1945).

(2) H. A. Laitinen, J. C. Bailar, H. F. Holtzclaw and J. V. Quagliano, *ibid.*, **70**, 2999 (1948).

(3) (a) H. A. Laitinen, A. J. Frank and P. Kivalo, *ibid.*, **75**, 2865 (1953); (b) H. A. Laitinen and P. Kivalo, *ibid.*, **75**, 2198 (1953); (c) P. Kivalo, *ibid.*, **77**, 2678 (1955).

(4) H. F. Holtzclaw, *This Journal*, **59**, 300 (1955).

made on them. Our present work covers nine chromamines, and has necessitated a further examination of some aspects of the polarography of simple chromium(III) salts.

The supporting electrolyte finally chosen was a solution 0.1 *M* in sodium acetate and acetic acid. This had a *pH* of 4.8 and was near the *pH* found most satisfactory by Lingane and Pecsok^{5,6} in their studies of simple chromium salts in buffered CaCl_2 solutions. In our electrolyte, most of the chromamines yielded double waves, the heights of the successive steps of which were in the ratio 1:2 (approximately). This suggested a reduction proceeding through a bivalent state.

Experimental

The chromamines were prepared by standard methods, for the most part according to directions given by Palmer,⁷ but with occasional modifications to improve yields. Analyses for chromium were carried out by decomposing the complex salts by heating with a sulfuric-nitric-phosphoric acid mixture, then oxidation of the chromium to dichromate with silver nitrate and ammonium peroxydisulfate in the presence of MnSO_4 . The experimental technique followed the usual lines,⁸ but was modified for use with a 20-mg. sample. The analyses agreed well with the calculated values, except for the sample of tris(ethylene-diamine)-chromium(III) chloride, but an analysis of this compound by ignition gave a more satisfactory Cr content.

The compounds prepared and the analytical results obtained are listed below

Compound	Cr, %	
	Calcd.	Found
$[\text{Cr}(\text{NH}_3)_6](\text{NO}_3)_3 \cdot \text{HNO}_3$	12.9	12.9
$[\text{Cr}(\text{NH}_3)_5\text{Cl}]\text{Cl}_2$	21.4	21.4
$[\text{Cr}(\text{NH}_3)_5\text{H}_2\text{O}](\text{NO}_3)_3$	15.2	15.0
$[\text{Cr}(\text{NH}_3)_5\text{NO}_3](\text{NO}_3)_2$	not analyzed	
$[\text{Cr}(\text{NH}_3)_5\text{NO}_2]\text{Cl}_2$	not analyzed	
$[\text{Cr}(\text{NH}_3)_4\text{C}_2\text{O}_4](\text{NO}_3)_2 \cdot \text{H}_2\text{O}$	18.05	18.1
<i>cis</i> - $[\text{Cr}(\text{NH}_3)_4(\text{H}_2\text{O})\text{Cl}]\text{Cl}_2$	21.3	21.4
$[\text{Cr}(\text{C}_2\text{H}_8\text{N}_2)_3]\text{Cl}_3 \cdot 2\text{H}_2\text{O}$	13.9	14.3

Hexaquo-chromium(III) chloride (violet chromium chloride) was prepared by boiling an aqueous solution of "green chromium chloride," cooling rapidly in ice and salt, and saturating the solution with HCl gas.⁹ The grey precipitate was washed with cold saturated HCl and acetone and recrystallized from water by saturating with HCl gas. The product seemed to be a hemihydrate (see Recoura⁹).

Anal. Calcd. for $\text{CrCl}_3 \cdot 6.5\text{H}_2\text{O}$: Cr, 18.9; Cl, 38.6. Found: Cr, 18.6; Cl, 39.1.

Dichlorotetraquo-chromium(III) chloride "green chromium chloride" was May and Baker's "chromic chloride."

Chromium(III) Acetate.—A violet chromium acetate was prepared by treating a solution of green chromium chloride at 20° with sodium hydroxide solution in slight excess, collecting the precipitated chromium(III) hydroxide and treating it with a small excess of glacial acetic acid. After some hours, the small residue was removed by filtration, and the solution evaporated under reduced pressure at room temperature until no further volatile matter distilled. The identity of the product is uncertain, but its analysis agreed with that of a compound $\text{Cr}_2(\text{CH}_3\text{COO})_6(\text{CH}_3)_2 \cdot (\text{H}_2\text{O})_3 \cdot 9\text{H}_2\text{O}$ described by Reihlen.¹⁰ We hope to discuss this point in more detail elsewhere, but it does appear that

(5) J. J. Lingane and R. L. Pecsok, *J. Am. Chem. Soc.*, **71**, 425 (1949).

(6) R. L. Pecsok and J. J. Lingane, *ibid.*, **72**, 189 (1950).

(7) W. G. Palmer, "Experimental Inorganic Chemistry," Cambridge University Press, Cambridge, 1954.

(8) See, e.g., A. I. Vogel, "Textbook of Quantitative Analysis," 2nd Edn., Longmans, London, 1951, p. 257.

(9) A. Recoura, *Compt. rend.*, **100**, 1227 (1886); **102**, 515, 922 (1886).

(10) H. Reihlen, *Z. anorg. allgem. Chem.*, **133**, 82 (1924).

some of the nine hydrate water molecules may be included in the coordination sphere of the chromium atoms.

Anal. Calcd. for $\text{Cr}_3(\text{CH}_3\text{COO})_6(\text{OH})_3(\text{H}_2\text{O})_{12}$: Cr, 20.1. Found: Cr, 20.1.

Polarograms were recorded at 25° on a Tinsley pen-recording instrument, which did not allow the determination of half-wave potentials to better than ± 5 mv. The capillary had the following characteristics: $m^2/d^3/s = 1.86 \text{ mg.}^{2/3}/\text{sec.}^{-1/2}$, period 2.8 sec. at 50 cm. head of mercury. Potentials are quoted relative to the saturated calomel electrode (SCE).

Oxygen was removed from the solutions in the normal way with purified nitrogen. Maxima were removed where necessary with "Lissapol N" or "NX" (non-ionic detergents from I.C.I. Ltd.) at a concentration of 0.001–0.003% (w./v.). Chemicals used in buffer solutions were analytical reagent grade.

Results

Chromammines.—The half-wave potentials observed are shown in Table I.

TABLE I

HALF-WAVE POTENTIALS OF CHROMAMMINES IN ACETATE BUFFER, pH 4.8, $\mu = 0.2$ (NO MAXIMUM SUPPRESSOR)

Complex ion	$E_{1/2}$ (v.)	
	1st step	2nd step
$[\text{Cr}(\text{NH}_3)_6]^{3+}$	0.83–0.84	1.43–1.45
$[\text{Cr}(\text{NH}_3)_5\text{Cl}]^{2+}$.78	1.44
$[\text{Cr}(\text{NH}_3)_5\text{H}_2\text{O}]^{3+}$.81–0.83	1.44–1.45
$[\text{Cr}(\text{NH}_3)_5\text{NO}_3]^{2+}$.88–0.95	1.44–1.46
$[\text{Cr}(\text{NH}_3)_5\text{NO}_2]^{2+}$.92–0.94	No wave obsd.
$[\text{Cr}(\text{NH}_3)_4\text{C}_2\text{O}_4]^+$	1.07–1.08	1.45–1.48
$[\text{Cr}(\text{NH}_3)_4(\text{H}_2\text{O})\text{Cl}]^{2+}$	0.76–0.78	1.36–1.44
$[\text{Cr en}_3]^{3+}$.86–0.88	No wave obsd.
$[(\text{NH}_3)_5\text{Cr}(\text{OH})\text{Cr}(\text{NH}_3)_5]^{5+}$.95	1.55

By comparison with the cobaltammines, the half-wave potential of the first step shows much less variation from one compound to another. The second step falls at -1.45 v., with a small dependence on concentration in the range studied (0.5 – 3) $\times 10^{-3}M$. The binuclear complex $(\text{NH}_3)_5\text{Cr}(\text{OH})\text{Cr}(\text{NH}_3)_5$ is reduced only at -1.55 v., and two other complexes resist reduction in the range of potentials available before the onset of hydrogen discharge (estimated at -1.58 v. for pH 4.8¹¹). The maximum suppressor, when used, shifted the waves to more negative potentials, but did not affect the diffusion currents.

Application of the Ilkovic equation¹² to the waves of $[\text{Cr}(\text{NH}_3)_6](\text{NO}_3)_3$ gave $n = 1.03$ and 1.92 electrons for the two steps. In some cases, the values of n diverged from 1 and 2, because of the presence of small pre-waves and other irregularities. Some waves were tested for reversibility by the customary procedure of determining the slope of the plot of $\log i/(i_d - i)$ vs. potential.

In the presence of 0.002% "Lissapol N," the slopes were as follows: $[\text{Cr}(\text{NH}_3^+)_6]^{3+}$, 0.054 v.; $[\text{Cr}(\text{NH}_3)_5\text{Cl}]^{2+}$, 0.060 v. (first step). The shapes of the waves were affected by higher concentrations of suppressor; thus, in the presence of 0.003% "Lissapol N," $[\text{Cr}(\text{NH}_3)_5\text{Cl}]^{2+}$ gave a slope of 0.078 v., and $[\text{Cr en}_3]^{3+}$ one of 0.040 v. Too much reliance should not therefore be placed on the fact that the slopes approximated to the

(11) O. H. Müller, "The Polarographic Method of Analysis," 2nd Edn., Chemical Education Publishing Co., Easton, Pa., 1951, p. 116.

(12) See I. M. Kolthoff and J. J. Lingane, "Polarography," 2nd Edition, Interscience Publishers, New York, N. Y., 1952, p. 43.

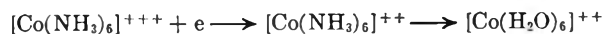
theoretical value for a reversible one-electron reduction.

In most cases, the diffusion currents and half-wave potentials remained constant over periods of up to two hours. The clearest exception was the behavior of *cis*-(chloroaquatetrammine)-chromium ion, the half-wave potentials of which changed over 16 hours steadily from -0.76 and -1.36 v. to -0.92 and -1.43 v. As the diffusion current did not change substantially at the same time, it seemed likely that this behavior was due to the formation of a hydrated chromium(III) ion.

Chromium Salts.—The results obtained are summarized in Table II. They are similar to the results reported by de Sesa, *et al.*¹³ in 1 *M* acetate buffer, pH 4.8. Although the half-wave potentials are different, the polarograms resemble those reported by other workers in different supporting electrolytes.^{6,14} We found, however, that the waves of both $\text{Cr}(\text{H}_2\text{O})_6^{3+}$ and $\text{Cr}(\text{H}_2\text{O})_4\text{Cl}_2^+$ decreased in height until after 24 hours they had almost disappeared. First-order kinetics, with $k_1 = 6.0 \times 10^{-5} \text{ sec.}^{-1}$ and $5.2 \times 10^{-5} \text{ sec.}^{-1}$, described the process (one experiment only was done on each). "Anion penetration" of complex chromium ions by acetate (and other organic anions) has been known for many years.¹⁵ In the present instance, it appears that the initial attack is on a water ligand, unless of course the observed rate constants are average values.

Both our preparation of chromium(III) acetate and a commercial sample (May and Baker's) showed only a trace of a wave at -0.9 v. This suggests that the reducible chromium aquo ions are slowly converted, in acetate solution, into an irreducible polynuclear ion such as that to which Reihlen gave the structure $[\text{Cr}_3(\text{COOCH}_3)_6(\text{OH})_2(\text{OH})_2(\text{H}_2\text{O})_2]^+$. This probably needs reformulation, as suggested by Küntzel,¹⁶ to fill the coordination spheres of the Cr atoms with H_2O when necessary, as $[\text{Cr}_3(\text{COOCH}_3)_6(\text{OH})_2(\text{H}_2\text{O})_4]^+$.

Mechanism of Reduction of Chromammines.—In the polarographic reduction of cobaltammines, it is generally accepted that the process proceeds by way of a Co(II) ammine,^{2,3,4} thus



The observed irreversibility of the first step was attributed to the change of configuration of the complex ion from $3d^24s4p^3$ to $4s4p^34d^2$. An analogous mechanism could apply in the present instance. The greater instability of the chromium complexes, together with the ability of Cr^{3+} to reduce water, could account for some of the complications in the polarographic reduction curves. The slow exchange of H_2O with $[\text{Cr}(\text{H}_2\text{O})_6]^{3+}$ found by Plane and Taube¹⁷ suggests that the configuration of the complex is $3d^24s4p^3$. Further, Hume and Stone¹⁸ have shown that the complex

(13) M. A. de Sesa, D. N. Hume, A. C. Glamm and D. D. Ford, *Anal. Chem.*, **25**, 983 (1953).

(14) J. B. Willis, *Proc. Roy. Soc. N.S.W.*, **78**, 239 (1944).

(15) Weinland and Koch, *Z. anorg. allgem. Chem.*, **39**, 256 (1904).

(16) Küntzel, quoted by C. L. Rollinson in "The Chemistry of the Co-ordination Compounds," ed. J. C. Bailar, Jr., Reinhold Publ. Corp., New York, N. Y., 1956, p. 463. *Cf. C. A.*, **43**, 6851f (1949).

(17) R. A. Plane and H. Taube, *This Journal*, **56**, 33 (1952).

TABLE II

CHARACTERISTICS OF CHROMIC SALTS IN ACETATE BUFFER,
pH 4.8, $\mu = 0.2$

Compound	Time, min.	i_d (1st wave)	$-E_{1/2}$ (1st wave), v.	$-E_{1/2}$ (2nd wave), v.
$\text{Cr}(\text{H}_2\text{O})_6 \text{Cl}_3$ 0.0015 M	18	2.9 μA	-0.84	-1.43
	37	1.9	-.84	
	107	1.0	-.84	
$\text{Cr}(\text{H}_2\text{O})_4 \text{Cl}_2 \text{Cl}$ 0.0009 M	3630	0.4	-.9	
	22	1.7	-.87	-1.45
Chromium acetate ^a	60	1.25	-.87	-1.45
	20	0.2	-.9	
Chromium acetate ^b		0.2	-.9	

^a This was the salt prepared as described in this paper. Its concentration was 0.37% (w./v.); assuming the formula for the non-electrolyte, this is approximately 0.00048 M.
^b May and Baker's "Chromium acetate," the concentration was 0.27% (w./v.).

of Cr(II) with ethylenediamine has a magnetic moment of 4.4–4.5 Bohr magnetons, corresponding to four unpaired electrons. This means that a change of configuration similar to that postulated for cobalt would attend the reduction of a chromium complex.

The standard reduction potential for $\text{Cr}(\text{NH}_3)_6^{+++} \rightarrow \text{Cr}(\text{NH}_3)_6^{++}$ is not known, but it has been estimated¹⁹ that it lies at about -0.7 v. (*i.e.*, at about -0.95 v. with respect to the SCE). The hexaquo chromium(III) ion has a standard reduction potential of -0.414 v. (-0.66 v. *vs.* SCE). Our observations, however, indicate that the hexaquo chromium ion has approximately the same reduction potential as the hexamine under the conditions of our experiments, *viz.*, -0.84 v. *vs.* the SCE at a concentration of about 10^{-3} M.

(18) D. N. Humé and H. W. Stone, *J. Am. Chem. Soc.*, **63**, 1200 (1941).

(19) R. N. Keller and R. W. Parry in "The Chemistry of the Coordination Compounds," ed. J. C. Bailar, Jr., Reinhold Publ. Corp., New York, N. Y., 1956, p. 186.

THE SYSTEM MAGNESIUM BROMIDE, AMMONIUM BROMIDE AND WATER AT 25^o

BY JACK ALLEN CAMPBELL AND FREDERICK L. MARSH

Contribution from the Department of Chemistry, Blackburn College, Carlinville, Illinois

Received August 18, 1958

A compound, $\text{MgBr}_2 \cdot \text{NH}_4\text{Br} \cdot 6\text{H}_2\text{O}$, analogous to carnallite, was described by de Schulten,² but there seems to have been no systematic phase study made of the three component system.

Experimental

The best commercially available grades of ammonium bromide and magnesium bromide hexahydrate were mixed in varying proportions with water and slowly rocked in a bath maintained at $25 \pm 0.02^\circ$ until equilibrium was reached, usually for 48 hours. Both the liquid phases and wet solids were analyzed for ammonia and bromine. The former was determined by releasing the ammonia with caustic and distilling it into 4% boric acid where it was

(1) Presented before the Ninth Annual Undergraduate Chemistry Symposium, Loyola University, Chicago, Illinois, May 17, 1958.

(2) M. A. de Schulten, *Bull. soc. chim.*, **17**, 167 (1897).

titrated with standard hydrochloric acid, using equal parts of brom cresol green and methyl red as an indicator. Bromine was determined by the familiar Volhard method.

TABLE I

THE SYSTEM $\text{MgBr}_2\text{-NH}_4\text{Br-E}_2\text{O}$

Solution %		Wet solid %		Solid phase in Equilibrium
MgBr_2	NH_4Br	MgBr_2	NH_4Br	
50.31 ^a	0			$\text{MgBr}_2 \cdot 6\text{H}_2\text{O}$
50.28 ^a	0.14 ^a			$\text{MgBr}_2 \cdot 6\text{H}_2\text{O} - \text{MgBr}_2 \cdot \text{NH}_4\text{Br} \cdot 6\text{H}_2\text{O}$
42.22	3.75	43.60	12.00	$\text{MgBr}_2 \cdot \text{NH}_4\text{Br} \cdot 6\text{H}_2\text{O}$
37.40	8.13	44.50	20.15	$\text{MgBr}_2 \cdot \text{NH}_4\text{Br} \cdot 6\text{H}_2\text{O}$
36.44 ^a	9.20 ^a			$\text{MgBr}_2 \cdot \text{NH}_4\text{Br} \cdot 6\text{H}_2\text{O} - \text{NH}_4\text{Br}$
28.37	14.95	20.36	38.73	NH_4Br
13.91	28.25	5.67	72.45	NH_4Br
5.65	37.80	2.95	69.20	NH_4Br
0	44.08 ^a			NH_4Br

^a Mean of several determinations.

Results and Discussion

The results obtained from this study are presented in Table I and Fig. 1 where all percentages

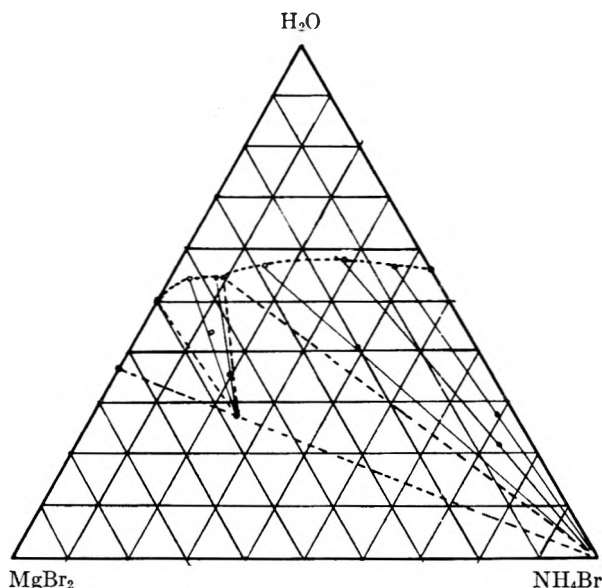


Fig. 1.—Schreinemakers diagram of data exhibited in Table I. Coexisting solid and liquid phases are joined by solid lines, while regions are delineated by dotted lines.

are on a weight basis. The solubility of magnesium bromide was found to be 50.31% which compares favorably with 50.68% reported by Getman.³ The solubility of 44.08% obtained for ammonium bromide may be compared with the value 43.86% obtained by Scott and Durham.⁴ Confirming the work of de Schulten² the single double salt which was observed was found to have a composition conforming to $\text{MgBr}_2 \cdot \text{NH}_4\text{Br} \cdot 6\text{H}_2\text{O}$. The invariant solutions were found to have compositions of 50.28% MgBr_2 and 0.14% NH_4Br in equilibrium with compound and magnesium bromide hexahydrate, while compound and ammonium bromide were in equilibrium with a solution containing 36.44% MgBr_2 and 9.20% ammonium bromide.

(3) F. H. Getman, *Rec. trav. chim.*, **54**, 866 (1935).

(4) A. F. Scott and E. J. Durham, *THIS JOURNAL*, **34**, 535 (1930).

The compound resembles carnallite in that it is an incongruently saturating type of double salt. Water decomposes it into ammonium bromide and a solution richer in magnesium bromide.

THE EFFECT OF EXCESS SALT ON MINIMA OBSERVED IN $\gamma/\log C$ CURVES FOR SURFACE ACTIVE AGENTS

By S. P. HARROLD

Basic Research Department, Thomas Healey & Co. Ltd., Newcastle upon Tyne, 1, England

Received July 25, 1958

The minimum which occurs in the surface tension (γ)/concentration (C) curves of surface active agents has been variously explained as due to metal ions in the water,¹ impurities in the chemical compounds examined² or to time effects.³ The most likely explanation is the presence of other components since it is possible^{4,5} to remove the minimum by successive purification processes, and to produce one by the addition of a third component.⁶ It has been observed that the addition of excess salt with a common ion removes the minimum in the $\gamma/\log C$ curve for several anionic detergents.

Experimental

Surface tensions were measured by the du Noüy tensiometer with appropriate corrections.⁷ Sodium alkylbenzene sulfonate (ABS) was prepared by direct sulfonation of tetrapropylene benzene, boiling range 284–294°, with SO_3 .⁸ The material was found to be 96.7% pure (dry weight basis) by the method of Epton⁹ based on cetylpyridinium bromide referred to dichromate.

Sodium lauryl sulfate (SDS) was synthesized by condensation of lauryl alcohol with chlorosulfonic acid in ether. (Calcd. for $\text{C}_{12}\text{H}_{25}\text{SO}_4\text{Na}$: C, 50.0; H, 8.7; S, 11.1. Found: C, 49.7; H, 8.5; S, 11.2.) Soxhlet extraction with light petroleum was used to reduce the minimum in the curve of surface tension with concentration.

Sodium *p*-nonylbenzene sulfonate was prepared by synthesis from pelargonyl chloride by Friedel–Crafts condensation with benzene followed by reduction with hydrazine and sulfonation. (Calcd.: C, 58.8; H, 7.5. Found: C, 57.95; H, 8.3.) It was purified by recrystallization from ethanol.

A.R. grade NaCl was used at a constant concentration of 0.2 *M*, and solutions were made in distilled water which had been passed over a fresh bed of Bio-deminolit.

Results and Discussion

Sodium *p*-nonylbenzene sulfonate had no minimum in its $\gamma/\log C$ curve after purification (Fig. 1, I). The addition of 0.5% of a third component, lauryl alcohol, resulted in the appearance of a pronounced minimum (Fig. 1, II). Repetition of the experiment with added alcohol in 0.2 *M* sodium chloride essentially removed the minimum (Fig. 1, III).

The absence of a minimum in the presence of salt

(1) C. Robinson in, "Wetting & Detergency," Harvey, London, 1937, p. 137.

(2) D. Reichenberg, *Trans. Faraday Soc.*, **43**, 467 (1947).

(3) E. J. Clayfield and J. B. Matthews, "Proc. 2nd Internat. Cong. Surface Activity," Butterworth, London, 1957, Vol. 1, p. 172.

(4) A. P. Brady, *THIS JOURNAL*, **53**, 56 (1949).

(5) E. F. Williams, N. T. Woodberry and J. K. Dixon, *J. Colloid Sci.*, **12**, 452 (1957).

(6) J. D. Miles and L. Shedlovsky, *THIS JOURNAL*, **48**, 57 (1944).

(7) W. D. Harkins and H. F. Jordan, *J. Am. Chem. Soc.*, **52**, 1751 (1930).

(8) G. K. Ashforth, private communication.

(9) S. R. Epton, *Trans. Faraday Soc.*, **44**, 226 (1948).



Fig. 1.—Surface tension of *p*-nonylbenzene sulfonate: I, alone in distilled water at 20°; II, plus 0.5% by weight lauryl alcohol; III, plus 0.5% lauryl alcohol in 0.2 *M* NaCl

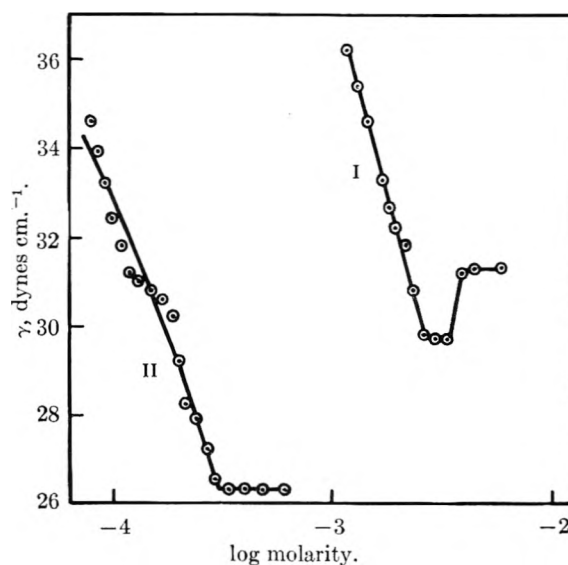


Fig. 2.—Surface tension of sodium tetrapropylene benzene sulfonate: I, in distilled water at 20°; II, in 0.2 *M* NaCl

was also found for ABS (Fig. 2) where the minimum without salt is probably due to the presence of several closely related alkyl benzenes, and for SDS (Fig. 3) where the minimum without salt is probably due to traces of lauryl alcohol. An explanation is offered based on the treatment of adsorption at the fluid/water interface given by Reichenberg.²

No Salt.—The Gibbs equation for adsorption at the air/water interface for an ionized surface active agent (det.) containing a small amount of impurity, e.g., lauryl alcohol (alc.) may be written

$$-d\gamma = \Gamma_{\text{det}} d\mu_{\text{det}^-} + \Gamma_{\text{Na}^+} d\mu_{\text{Na}^+} + \Gamma_{\text{alc}} d\mu_{\text{alc}} + \Gamma_{\text{OH}^-} d\mu_{\text{OH}^-} + \Gamma_{\text{H}_2\text{O}} d\mu_{\text{H}_2\text{O}} \quad (1)$$

where γ is the surface tension and Γ the surface

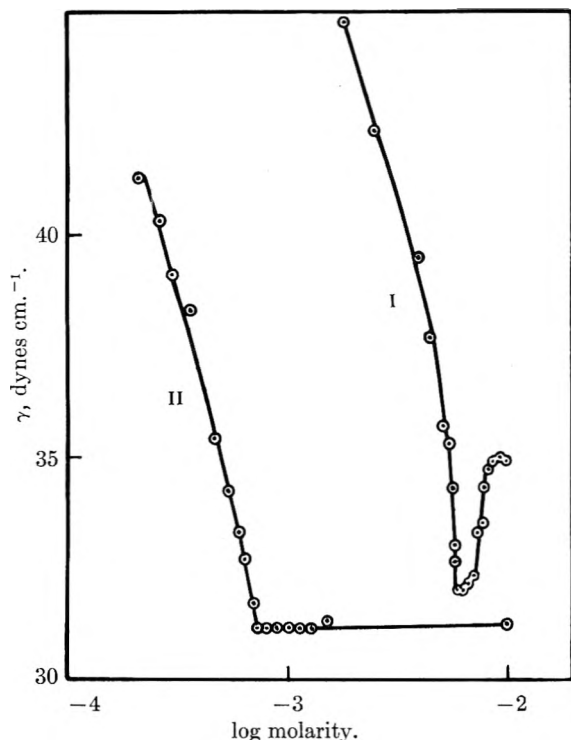


Fig. 3.—Surface tension of sodium dodecyl sulfate: I, in distilled water at 20°; II, in 0.2 *M* NaCl.

excess of the individual components, chemical potential μ

$$d\mu_{OH^-} + d\mu_{H_3O^+} = d\mu \approx 0$$

in the dilute solutions we are considering. It is not generally true, as Pethica¹⁰ points out, that $\Gamma_{det^-} = \Gamma_{Na^+}$, so we must write

$$-d\gamma = \Gamma_{det^-}d\mu_{det^-} + \Gamma_{alc}d\mu_{alc}$$

where $d\mu_{det^-} = nRT d \ln f_{\pm det^-} C_{det^-}$, the value of n not being precisely known. f_{\pm} is the mean activity coefficient of the det^- , concentration C . Thus,

$$-d\gamma = \Gamma_{det^-} nRT d \ln f_{\pm det^-} C_{det^-} + \Gamma_{alc} nRT d \ln C_{det^-} + \Gamma_{alc} d\mu_{alc} \quad (3)$$

or

$$\frac{-d\gamma}{d \ln C_{det^-}} = \Gamma_{det^-} nRT \left[1 + \frac{d \ln f_{\pm det^-}}{d \ln C_{det^-}} \right] + \frac{\Gamma_{alc} d\mu_{alc}}{d \ln C_{det^-}} \quad (4)$$

Now $f_{\pm det^-}$ decreases with increasing C_{det^-} and will decrease sharply at the critical micelle concentration (c.m.c.). Before the c.m.c. $d\mu_{alc}/d \ln C_{det^-}$ will be $+ve$: as Sawyer and Fowkes¹¹ show, up to 90% of the surface may be preferentially covered with the long chain alcohol.

Above the c.m.c., where alcohol has been shown to desorb from the air/water interface,¹² $d\mu_{alc}/d \ln C_{det^-}$ becomes $-ve$ at the same time as $f_{\pm det^-}$ is much smaller and so the R.H.S. of eq. 4 may become $-ve$, accounting for the change in slope of the $\gamma/\log C$ curve to give a minimum.

Excess Salt with Common Ion.—Consider the addition of impure anionic detergent added to a solution containing excess salt

$$-d\gamma = \Gamma_{Na^+}d\mu_{Na^+} + \Gamma_{Cl^-}d\mu_{Cl^-} + \Gamma_{OH^-}d\mu_{OH^-} + \Gamma_{H_3O^+}d\mu_{H_3O^+} + \Gamma_{det^-}d\mu_{det^-} + \Gamma_{alc}d\mu_{alc} \quad (5)$$

As before, $d\mu_{H_2O} \approx 0$; $d\mu_{Cl^-}$ will approximate to zero too since no more will be added and $d\mu_{Na^+}$ can be neglected since the concentration of Na^+ will already be determined by the excess salt. Therefore

$$-d\gamma = \Gamma_{det^-}d\mu_{det^-} + \Gamma_{alc}d\mu_{alc} \quad (6)$$

and

$$\frac{-d\gamma}{d \ln C_{det^-}} = \Gamma_{det^-} nRT \left[1 + \frac{d \ln f_{det^-}}{d \ln C_{det^-}} \right] + \frac{\Gamma_{alc} d\mu_{alc}}{d \ln C_{det^-}} \quad (7)$$

In this case $n = 1$, as shown by Pethica,¹⁰ and f_{det^-} will be constant in the presence of excess salt with a common ion.¹³ The first term on the R.H.S. of eq. 7 does not decrease. The experiments show $d\gamma/d \ln C_{det^-}$ does not change sign, hence the contribution of the activity term to the equilibrium must be significantly greater than that due to the change in chemical potential and surface excess of the additive.

It is well known that the presence of excess salt lowers the critical micelle concentration and thus the bulk concentration at which Γ_{det^-} approaches saturation (reduction in double layer repulsion and solvation effects). It may be that this will increase the proportion of det^- in the surface at the expense of alc so that Γ_{alc} may be less, reducing the contribution of the second term in this instance.

Acknowledgment.—The author wishes gratefully to acknowledge the advice of his colleagues and in particular Dr. J. F. Goodman.

(13) H. S. Harned and B. B. Owen, "Physical Chemistry of Electrolytic Solutions," Reinhold Publ. Corp., New York, N. Y., 2nd Edn., 1950, Ch. 14.

SOLUBILITIES IN 2-METHOXYETHANOL. I. 1-1 ALKALI METAL SALTS¹

BY R. F. TRIMBLE, JR.

Department of Chemistry, Southern Illinois University, Carbondale, Illinois

Received September 8, 1958

Although 2-methoxyethanol is widely used as a solvent for organic materials little attention has been given it as a solvent for inorganic salts. Kobe and Motsch² determined the solubilities of $Ca(NO_3)_2$ and $Sr(NO_3)_2$ in various glycol ethers, 2-methoxyethanol among them. Apparently no other solubility determinations of inorganic salts have been published. Because of the theoretical and practical interest such data would have, a survey of the solubilities of some inorganic salts in this solvent is warranted.

Experimental

In order to simplify the apparatus and the procedure high precision was not sought. Ordinary reagent grade salts were used without further purification. Technical grade 2-methoxyethanol (Methyl Cellosolve) was distilled and the first 15% and the final 10% discarded. This procedure effectively eliminates water.

(10) B. A. Pethica, *Trans Faraday Soc.*, **50**, 413 (1954).

(11) W. M. Sawyer and F. M. Fowkes, *THIS JOURNAL*, **62**, 159 (1958).

(12) G. Nilsson, *ibid.*, **61**, 1135 (1957).

(1) This paper was in part presented as a talk to the Division of Chemistry Section A at the 51st annual meeting of the Illinois State Academy of Science, Urbana, Ill., May 9, 1958.

(2) K. A. Kobe and W. L. Motsch, *THIS JOURNAL*, **56**, 185 (1952).

TABLE I
 SOLUBILITIES IN 2-METHOXYETHANOL

Salt	30°		35°		40°		45°	
	g./100 g. solvent	molal	g./100 g. solvent	molal	g./100 g. solvent	molal	g./100 g. solvent	molal
LiCl	33.4	7.89	—	—	—	—	32.4	7.66
NaCl	0.789	0.136	0.699	0.120	0.612	0.105	0.567	0.0970
KCl	0.416	.0558	0.407	.0546	0.396	.0531	0.384	.0515
RbCl	1.45	.120	1.39	.115	1.35	.112	1.30	.108
CsCl	3.90	.232	3.83	.227	3.75	.223	3.70	.220
KBr	3.96	.333	3.75	.315	3.56	.299	3.41	.286
KI	34.2	2.06	33.4	2.01	32.7	1.97	32.1	1.93
KNO ₃	1.03	0.102	1.04	0.103	1.06	0.105	1.05	0.104
KClO ₄	0.868	0.0626	0.875	0.0631	0.883	0.0637	0.898	0.0648

One or two grams of the salt in a small glass stoppered bottle was dried at 180–200° overnight. About 50 ml. of solvent was added and the bottle attached to a paddle wheel in a constant temperature bath ($\pm 0.05^\circ$). In sampling, the bottle was removed from the bath, dried, and 2–5 ml. of the solution pipetted into a weighing bottle. When necessary the sample was withdrawn through a glass wool filter. There was no difficulty with precipitation in the pipet. The weighed samples were evaporated to dryness in an oven at 120°, just below the boiling point of the solvent (124°). No charring was observed in any case, although attempts to carry out the evaporation on a hot plate often resulted in charring.

Equilibrium usually was reached within 24 hours, but in any case samples were taken until constant values were obtained. Each solution was sampled at 30, 35, 40 and 45°. The results reported are the averages of at least two independent runs except in the case of LiCl.

The analytical procedure was capable of giving results with a standard deviation of $\pm 0.2\%$. This precision was achieved with the very soluble salts CsCl, KBr and KI. With the less soluble salts the precision was limited by the weighing error and ran about 0.5–0.8%. However, the results from different runs of the same salt had a standard deviation of about $\pm 2\%$.

The lowest temperature was set at 30° to eliminate cooling coils from the constant temperature bath and because Kobe and Motsch report that below this temperature they found equilibrium was reached only very slowly. The highest temperature studied was limited to 45° by the thermal sensitivity of the hand.

In order to determine whether solvates form at room temperature samples of dried salt were shaken for 24 hours with the solvent. The salt was then filtered off, washed with a small amount of ethanol followed by ether and weighed. It was reweighed after heating at 124° for 10–12 hours and the loss of weight attributed to a loss of 2-methoxyethanol of solvation.

Discussion

The solubilities are shown in Table I. These values should be considered to have a standard deviation of $\pm 2\%$ except in the case of LiCl. The LiCl solution was extremely viscous, which makes it doubtful whether equilibrium really was attained, and contained colloidal LiCl. Only a single run was made with LiCl and the values given should be taken as estimates only.

Except for KNO₃ and KClO₄ all of the salts are less soluble at higher temperatures. Kobe and Motsch found that in various glycol ethers Ca(NO₃)₂ and Sr(NO₃)₂ had positive temperature coefficients of solubility when they were solvated. However, no solvation was observed at room temperature in the present study (LiCl was not run). It is possible that the alcohol-ether wash decomposed some solvates of low stability.

The variation in solubility from run to run for a given salt undoubtedly is caused by variations in the amount of absorbed water. This factor is

difficult to control and is probably the major reason for the wide variations in the solubilities reported for salts in methanol and ethanol.³

The solubilities at 25° were estimated graphically in order to compare 2-methoxyethanol with methanol and ethanol. The results are shown in Table II. The solubilities in methanol and ethanol were chosen, when a choice was available, as representative and consistent values. No effort was made to evaluate the original papers and report a "best" value.

 TABLE II
 COMPARISON OF MOLAL SOLUBILITIES AT 25°

Salt	CH ₃ OH	CH ₃ OCH ₂ H ₂ OH ^a	C ₂ H ₅ OH
LiCl	9.68 ^b	7.97	5.81 ^{c,f}
NaCl	0.239 ^b	0.149	0.011 ^c
KCl	.071 ^b	.0567	.0029 ^c
RbCl	.111 ^b	.124	.0064 ^c
CsCl	.179 ^b	.234	...
KBr	.177 ^b	.344	.0119 ^e
KI	1.02 ^b	2.09	.115 ^e
KNO ₃	0.043 ^c	0.101	.015 ^c
KClO ₄	0.00761 ^d	0.0621	.00087 ^d

^a Estimated, see text. ^b T. Pavlopoulos and H. Strehlow, *Z. physik. Chem.*, **202**, 474 (1954). ^c F. A. H. Schreinemakers, *ibid.*, **65**, 575 (1909). These values are for 98% methanol and 92% ethanol, both at 30°. ^d H. H. Willard and G. F. Smith, *J. Am. Chem. Soc.*, **45**, 286 (1923). ^e W. E. S. Turner and C. C. Bissett, *J. Chem. Soc. (London)*, **103**, 1904 (1913). ^f Interpolated. ^g P. T. Walden, *Z. physik. Chem.*, **55**, 712 (1906).

The fact that 2-methoxyethanol resembles methanol so closely in solvent power is somewhat surprising. On the basis of its low dielectric constant, 16.0, one would expect it to be a much poorer solvent than either methanol or ethanol with dielectric constants of 24.3 and 32.63, respectively. For salts with very large ions, Rb⁺, Cs⁺, Br⁻, I⁻, NO₃⁻ and ClO₄⁻, 2-methoxyethanol even surpasses methanol as a solvent. This enhanced solvent action may result from the large dipole moment of 2-methoxyethanol, 2.04 *D* as compared to 1.664 *D* for methanol and 1.68 *D* for ethanol (vapor).⁴

A negative temperature coefficient of solubility is a common feature of LiCl, NaCl and KCl in

(3) A. Seidell, "Solubilities of Inorganic and Metal Organic Compounds," 3rd ed. and suppl., D. Van Nostrand Co., New York, N. Y., 1940, 1952. The reported solubilities of KCl in ethanol at 25° vary from 0.00288 to 0.011 molal, and those of KBr in methanol at 25° from 0.142 to 0.214 molal.

(4) J. A. Riddick and E. E. Toops, Jr., "Organic Solvents," 2nd ed., "Techniques of Organic Chemistry," Vol. VII, Interscience Publishers, Inc., New York, N. Y., 1955.

methanol and ethanol.⁵⁻⁷ LiCl, NaCl and KCl in methanol all have a maximum solubility somewhere between 30 and 50° and it may be that such a maximum occurs in 2-methoxyethanol solutions somewhere below 30°. On the basis of some preliminary work with solutions at the boiling point it appears unlikely that any of the salts studied show a minimum solubility above 45°.

The author acknowledges the aid of Miss Hanlin Hwang, and the financial assistance of the Graduate Council of Southern Illinois University.

(5) E. Lloyd, C. B. Brown, D. Glynwyn, R. Bonnel and W. J. Jones, *J. Chem. Soc.*, 658 (1928).

(6) E. R. Kirn and H. L. Dunlop, *J. Am. Chem. Soc.*, **53**, 391 (1931).

(7) W. E. S. Turner and C. C. Bissett, *J. Chem. Soc.*, **103**, 1904 (1913).

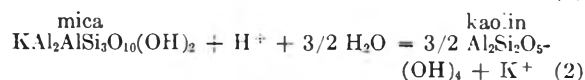
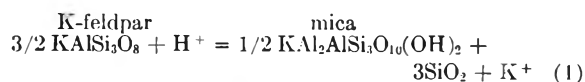
HYDROLYSIS OF K-FELDSPAR AND MICA AT ELEVATED TEMPERATURES AND PRESSURES

By J. J. HEMLEY¹

University of California, Berkeley, Cal.

Received September 19, 1958

A study of the hydrolysis equilibria of K-feldspar and K-mica (muscovite) was conducted at elevated temperatures and pressures in acid chloride solutions. The occurrence and the reversibility of these reactions was demonstrated



Equilibration experiments were then conducted in the same manner. A small amount of aqueous charge of appropriate normality in KCl and HCl was placed in the platinum tubes together with a considerable excess of the particular mineral assemblage under investigation. The tubes were placed under pressure and the bombs heated to temperature. Temperature was controlled within $\pm 5^\circ$. At the cessation of the run of a few weeks duration the bombs were quenched rapidly in a mercury plus ice-water bath, and the contents of the tubes quickly extracted for study. Equilibrium was approached from both directions. Most of the experimentation was conducted at a total solution pressure of 15000 p.s.i. and at temperatures from 200 to 500°.

Above about 350° the mica-kaolinite assemblage changes to mica-pyrophyllite-boehmite because of the thermal instability of kaolinite above this temperature. At still higher temperatures other mineral assemblages are developed.

The reactions are exothermic and the equilibria shift to higher acidities with increasing temperatures. Because of the lack of appropriate thermodynamic data at elevated temperatures and pressures, the experimental results cannot be treated rigorously. On the basis of data available it is concluded that the experimental equilibrium quotients of the reactions, $m_{\text{KCl}}/m_{\text{HCl}}$, do not differ from the corresponding equilibrium constants by more than a factor of 5 up to 350° or higher. The consistency of the experimental results using KCl solutions of varied concentration (0.65 to 4*m*) indicates a relatively small experimental error.

Standard free energies for reactions 1 and 2 are shown in the Table I. The experimental reproducibility is indicated for each. The effect of a change in solution pressure (5000 to 35000 p.s.i.) on the stability fields of these minerals was shown to be relatively small as compared to the effect of temperature and the K^+/H^+ ratio. The hydrolysis process is favored by an increase in solution pressure.

Acknowledgments.—Financial support of this

TABLE I
STANDARD FREE ENERGY OF REACTION
15000 p.s.i., kcal./mole H^+

	200°	300°	400°	500°
Reaction 1	-10.6 ± 0.43	-9.30 ± 0.52	-8.31 ± 0.61	-7.42 ± 0.71
Reaction 2	-6.7 ± 0.43	-5.24 ± 0.52	-4.00 ± 0.61	-2.83 ± 0.71

The experiments were conducted using scaled platinum tubes housed in cold-seal rod bombs. Pressure vessels of this type have been described by Tuttle.²

(1) U. S. Geological Survey, Denver, Colo.

(2) O. F. Tuttle, *Bull. Geol. Soc. Am.*, **60**, 1727 (1949).

work was rendered by the National Science Foundation and by the American Research Institute. The writer is grateful for the assistance of Professor Charles Meyer of the Department of Geology and Professor Leo Brewer of the Department of Chemistry, University of California, Berkeley.

INDEXES

PUBLISHED BY THE
**AMERICAN
CHEMICAL
SOCIETY**

27-Year Collective Formula Index to Chemical Abstracts

Over half a million organic and inorganic compounds listed and thoroughly cross referenced for 1920-1946. In 2 volumes of about 1000 pages each.

Paper bound \$100.00 Cloth bound \$120.00

10-Year Numerical Patent Index to Chemical Abstracts

Over 143,000 entries classified by countries in numerical order with volume and page references to Chemical Abstracts for 1937-1946. Contains 182 pages.

Cloth bound \$10.00

Decennial Indexes to Chemical Abstracts

Complete subject and author indexes to Chemical Abstracts for the 10-year periods of 1917-1926, 1927-1936 and 1937-1946.

2nd Decennial Index (1917-1926). Paper bound. \$125.00

3rd Decennial Index (1927-1936). Paper bound. \$175.00

4th Decennial Index (1937-1946). Paper bound. \$200.00
(Foreign postage on the Decennial Indexes is extra.)

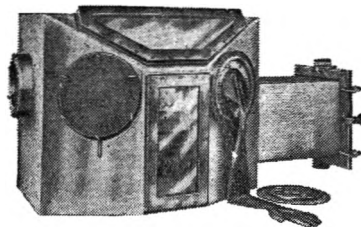
Order from:

Special Issues Sales

American Chemical Society

1155 16th St., N.W.

Washington 6, D.C.



BLICKMAN VACUUM DRY BOX

Designed for safe handling of radio-isotopes, reactor fuel containing Plutonium or U233 and other hazardous substances. With air-lock, it can be sealed to create a vacuum. Fabricated of stainless steel plate—34" long x 26" high x 24" wide at base. Air-lock measures 18" x 12". Send for Technical Bulletin A-2. S. Blickman Inc. 9002 Gregory Ave., Weehawken, N. J.

BLICKMAN
LABORATORY EQUIPMENT

Look for this symbol of quality



Literature Resources for Chemical Process Industries

Designed To Help Both The *New* And
The *Experienced* Searcher Of Literature
Find What He Wants

Discusses various information sources with
13 articles on market research, 7 on resins
and plastics, 6 on textile chemistry, 10 on
the food industry, 10 on petroleum, and
13 on general topics, plus 34 pages of index.

order from:

Special Issue Sales

American Chemical Society

1155 Sixteenth Street, N.W.

Washington 6, D.C.

Number 10 in

Advances in Chemistry Series

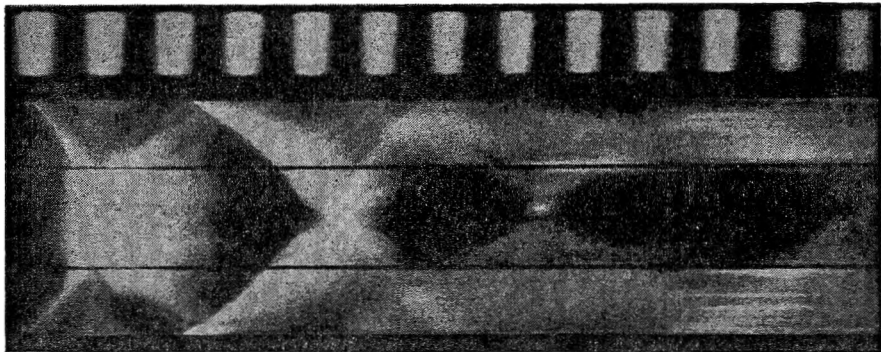
edited by the staff of

Industrial and Engineering Chemistry

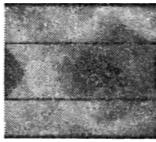
582 pages—paper bound—\$7.50 per copy



REPORT ON *Plasma Propulsion
at Republic Aviation*



Space-Time Trace: With space as ordinate and time as abscissa, photograph shows development of pinch effect in plasma, followed by shock waves. Picture was obtained with special streak camera — part of the instrumentation devised for Republic's experimental Plasma Propulsion program. Each space at top measures an interval of 10 microseconds.



An experimental Plasma Propulsion System under test at Republic Aviation gives promise of a power plant ideally suited to space vehicles. The system generates plasma from a heavy gas and subjects it to magnetic acceleration to produce thrust at high exhaust velocity.

Research and Development in Plasma Propulsion and in a number of branches of Hydromagnetics and Plasma Physics is being sharply expanded as part of Republic's new \$35,000,000 Research and Development Program. Investigations currently in progress include studies of plasma generation of electricity and the application of Hydromagnetics to Hypersonics.

Opportunities to Lead Theoretical and Experimental Research

The Scientific Research Staff welcomes the affiliation of scientists and engineers of stature in the following fields:

- | | |
|--|---|
| HYDROMAGNETICS | PLASMA PHYSICS |
| GASEOUS ELECTRONICS | COMBUSTION AND
DETONATION |
| HYPERSONICS AND
SHOCK PHENOMENA | INSTRUMENTATION |
| PHYSICAL CHEMISTRY | HIGH POWER PULSE
ELECTRONICS |

Salaries commensurate with the high degree of talent and creativity required. You work with stimulating associates in a laboratory atmosphere. \$14,000,000 of additional facilities now being built for Republic's new Research Center in suburban Long Island.

Write in confidence directly to:

DR. THEODORE THEODORSEN, Director of Scientific Research



REPUBLIC AVIATION

FARMINGDALE, LONG ISLAND, NEW YORK

